Probing the star formation history of early-type galaxies in clusters

Terlevich, Alejandro Ivan

Probing the star formation history of early-type galaxies in clusters

by Alejandro Ivan Terlevich

A thesis submitted to the University of Durham
in accordance with the regulations for
admittance to the Degree of Doctor of Philosophy.

Department of Physics
University of Durham
October 7, 1998

Preface

The work described in this thesis was undertaken between 1994 and 1998 whilst the author was a research student under the supervision of Dr Richard Bower in the Department of Physics at the University of Durham.

Some of the work was carried out in collaboration with the following staff: Dr. Richard Bower, Dr. N. Caldwell (Of the Steward Observatory, Tucson, Arizona) (Chapter 2); Dr T. Kodama (of the Institute of Astronomy, Cambridge), Dr R. G. Bower (Chapter 4); Dr Harald Kuntschner, Dr. R. G. Bower (Chapter 5); Dr R. G. Bower (Chapter 6). The major part of the work presented is, however, the author's own work. This work has not been submitted for any other degree at the University of Durham or at any other University.

Certain results have appeared in the following paper:

Bower, R. G., Kodama, T., Terlevich, A. I., 1998, MNRAS, 299, 1193

Abstract

Probing the Star Formation History of Early Type Galaxies in Clusters

by Alejandro Ivan Terlevich

In this thesis, we present a new photometric catalogue of the local Coma galaxy cluster in the Johnson U- and V- bands. We cover an area of 3360arcmin^2 of sky, to a depth of $V = 20$mag in a 13 arcsec diameter aperture, and produce magnitudes for $\sim$ 1400 extended objects in metric apertures from 8.8 to 26arcsec diameters. The mean internal RMS scatter in the photometry is 0.014mag in V, and 0.026mag in U, for $V_{13} < 17$mag.

We use this photometric catalogue to place limits on the levels of scatter in the colour–magnitude relation (CMR) in the Coma cluster. We subdivide the galaxy population by morphology, luminosity and position on the sky, and analyse the CMR in each of them. The lowest levels of scatter are found in the elliptical galaxies, and the late type galaxies have the highest numbers of galaxies blue-wards of the CMR. We finds signs of *decreased* scatter and systematically bluer galaxy colours with increasing projected radius from the center of the cluster, and attribute it to a mean galactic age gradient.

We find that the typical mass of galaxies within clusters can increase by a factor of two through dissipationless merging without destroying the CMR.

We compare the spectral line indices of galaxies in the Coma cluster with their deviation from the mean colour-magnitude relation (CMR). We find that the CMR in Coma is driven primarily by a luminosity–metallicity correlation, however we cannot rule out a contribution from age effects. Colour deviations blue-ward of the mean relation are strongly correlated with the Hydrogen Balmer line series absorption, indicating the presence of a young stellar population in these blue galaxies.

We use a wavelet code to suggest an association between X-ray cluster substructure and 'E+A' galaxy activity in high redshift clusters.

Acknowledgements

I would like to express my sincere thanks to Richard Bower for being the best supervisor in the world ever. Without his incisive thoughts and guidance, this thesis could never have been. I am especially indebted to his superhuman powers of encouragement, even in the face of insurmountable pessimism. I would also like to thank Nelson Caldwell, for showing me what a telescope is, and my other collaborators, Jim Rose, Taddy Kodama and Harald Kuntschner for many invaluable conversations. Others whom I have had invaluable interactions with include Scott Croom, Carlton Baugh and John Lucey. I feel Ian Smail is owed a special vote of thanks. His knowledge of astronomy is surpassed only by his grasp of astronomical politics. I also owe him several pints for what I can only imagine must have been a superbly imaginative letter of recommendation.

All work for this thesis was produced on STARLINK computer equipment installed and maintained by Alan Lotts. Much use was made of the NASA/IPAC Extragalactic database (NED), the Babbage e-print server, and the NASA Astrophysics Data System Abstract Service.

The people who have made the last four years more fun than they had any right to be include Karen Haigh, Geraint Lewis, Steve Hatton, Simon Shaw Scott Kay and Andrew Benson (aka. Terrance and Phillip), Mike Beasley, Dodgy Doddson, Dug Burke, Mike McCartney, Bill Ballinger, Andy Taylor, Frossie Economou, Scary Rachel Johnson, Clanger Chang, Fiona Hoyle, Claire Halliday, Eric Bell, Russell Smith, James Turner, Ed Totten, Karen Brazier, Frazer Pierce, Ana Campos, Michelle Felton, Dave 'pastie' Lee, Roger 'organic' Haynes, Jane Chapman. An extra special thanks is due to Kaff and especially Hayley, for keeping me fed and sane.

My parents hold ultimate responsibility for my actions, and so I'd like to thank them for being brought up properly. I'd especially like to thank them for not sending me too many socks, jumpers or sausages despite the horrid cold weather in the North of Britain, and for not visiting as often as they threatened. I'd also like to congratulate my sister for becoming a doctor before I did. I know she seems to think it's funny.

Contents

Chapter 1

Introduction

Elliptical galaxies and the bulges of lenticular and spiral galaxies are the most fundamental objects in the universe (apart maybe from stars), yet there is no formation scenario which successfully accounts for their properties.

The 'classical' formation scenario put forward by, e.g., Eggen, Lynden-Bell, & Sandage (1962), Searle, Sargent, & Bagnuolo (1973) and Tinsley & Gunn (1976) proposes that the stars were formed in a single high redshift burst, and have been evolving passively to the present day. This model reflects the 'classical' view of elliptical galaxies, as being made up entirely of old, metal-rich stars.

Much evidence has recently been amassed to support the case not just for the old ages of the stellar populations, but also for their having formed in situ within their present galaxy. The colour–magnitude relation (CMR) for early type galaxies (Faber 1973, Visvanathan & Sandage 1977, Frogel et al. 1978, Persson, Frogel, & Aaronson 1979, Bower, Lucey, & Ellis 1992a, Bower, Lucey, & Ellis 1992b) forms a scaling relation between a galaxy's colour and its luminosity, with the more luminous galaxies having redder colours than the less luminous ones. Using models for galaxy evolution which predicted empirically calibrated line strength indices and colours, Worthey (1994) formulated his '2/3' law ($\Delta[\mathrm{Fe/H}] \sim \frac{2}{3}\Delta log(t)$), which shows how age and metallicity have a degenerate effect on integrated galaxy colours. This means that the CMR could equally well be driven by age or metallicity effects. Observations of the CMR in high redshift ($z \sim 0.5$) clusters, however, show the cluster CMR must be attributed to a mass metallicity relationship (Dressler 1984, Vader 1986, Kodama 1997, Ellis et al. 1997, Stanford, Eisenhardt, & Dickinson 1998).

The origin of this mass metallicity sequence arises as a natural consequence of the single burst galaxy formation model, when coupled with galactic winds (Larson 1974, Arimoto & Yoshii 1987, Franx & Illingworth 1990). In brief, the amount of metals in a galaxy depends solely on the amount of gas it has processed. If elliptical galaxies formed all of their gas into stars, they should all contain equal amounts of metals (Tinsley 1980, Pei & Fall 1995). What the galactic (or supernova driven) wind models achieve, is to remove the remaining gas in a galaxy using the energy injected into the inter stellar medium (ISM) mainly by the supernovae. Once the energy injected into the ISM is sufficient to overcome the gravitational potential of the galaxy, the gas is blown away and star formation ceases. This point is reached faster for less massive galaxies, than for more massive galaxies. The supernovae do not just inject energy into the ISM, they also enrich it with metals, thus the more massive galaxies which can hold on to their gas reservoirs for longer during their star formation burst, end up having higher metallicities than the less massive galaxies, and therefore redder colours.

About one third of local cluster elliptical galaxies exhibit peculiarities (for an early type galaxy) such as dust lanes, shells, kinematically decoupled cores or tidal tails (Kormendy & Djorgovski 1989). Additionally, the colours of early type galaxies become bluer, and the equivalent width of $H\beta$ absorption increases with these signs of disturbance (Schweizer et al. 1990, Schweizer & Seitzer 1992). These signs of morphological disturbances in local early type galaxies justify a second class of formation scenario, where early type galaxies form out of the dissipative merger of late type galaxies (Toomre & Toomre 1972, White 1979, Barnes 1988). These scenarios are supported by the hierarchical galaxy formation models (e.g. White & Frenk 1991, Kauffmann, White, & Guiderdoni 1993, Cole et al. 1994 and subsequent papers). These semi-analytic models use extended Press-Schecter theory (Press & Schecter 1974, Bower 1991, Bond et al. 1991) to calculate the evolution of dark matter haloes within a CDM cosmology. They then use simple prescriptions for gas hydrodynamics, stellar evolution, and gas feedback from the stellar component, to model the evolution of a dense gas component (galaxies) within the dark matter haloes. In these models, the morphology of a galaxy is not predefined from the formation of the galaxy (as in the 'classical' model), but depends on the evolutionary history of the galaxy. Such models predict that large galaxies formed relatively recently ($z \leq 2$) from the gradual merger of smaller galaxies, but their constituent stars form before the final galaxy is assembled, so can be old. The constraints from the slope and scatter in the CM relation (see below) are somewhat loosened by the fact that these models tend to form large galaxies from mergers of large fragments, rather than from a random selection of the fragments available at the earlier epoch (Kauffmann 1996).

In addition to the dynamical evidence for galaxy interactions presented above, there is strong evidence for the evolution of galaxy stellar populations over and above what is allowed by the passively evolving 'classical' elliptical galaxies. High redshift clusters are known to have a higher proportion of blue galaxies than do local clusters (Butcher & Oemler 1978, Butcher & Oemler 1984, Couch & Newell 1984). Subsequent spectroscopic studies of these 'Butcher-Oemler' galaxies (e.g., Dressler & Gunn 1983, Couch & Sharples 1987, Barger et al. 1996) showed that many of them appeared to have spectra characteristic of the old stellar populations found in ellipticals, with the addition of strong Balmer absorption lines, characteristic of hot, young A stars. These spectra could be modeled by superposing an old stellar population, with a young burst population consisting of no more than 15% of the host galaxy mass, and having an age of not more than 2Gyr. Additionally, Barger et al. (1996) calculated that as many as 30% of the galaxies in their clusters would have undergone one of these bursts in their lifetime. High resolution HST imaging of Butcher–Oemler clusters, has revealed that the blue population is in fact dominated by spheroidal systems, about half of which show signs of recent or ongoing interactions with other galaxies (Couch et al. 1994, Smail et al. 1997, Couch et al. 1998).

A population of these 'E+A' galaxies has been identified in the local Coma and ACO 3125/3128 clusters (Caldwell et al. 1993, Caldwell et al. 1996), although the burst size is much smaller than that in the higher redshift Butcher-Oemler clusters. In Coma, Caldwell et al. associate the 'E+A' galaxies with a group of galaxies around NGC4839 and suggest that their starburst activity was triggered by the passage of the group through the main cluster. Others suggest however that this group has not yet fallen through the Coma cluster (Colless & Dunn 1996), and that its fraction of 'E+A' galaxies is similar to that seen in local galaxy groups (Zabludoff et al. 1996).

Like the other scaling relations of early type galaxies, i.e. the 'fundamental plane' (Dressler et al. 1987, Djorgovski & Davis 1987, Bender, Burstein, & Faber 1992, Saglia, Bender, & Dressler 1993, Jorgensen, Franx, & Kjaergaard 1993, Pahre, Djorgovski, & De Carvalho 1995), the CMR has very low levels of scatter. These low levels of scatter have been used to place constraints on the ages of the stellar populations in the galaxies (Bower, Lucey, & Ellis 1992b, Bender, Burstein, & Faber 1993, Renzini & Ciotti 1993, Bower, Kodama, & Terlevich 1998). In the case of the CMR, it is assumed that the relation primarily reflects variations in mean galactic metallicity with luminosity, and that the scatter about the relation is caused primarily by age effects. Bower, Lucey, & Ellis (1992b) considered the constraints imposed upon the single burst galaxy formation model by the observed levels of scatter in local cluster cores (RMS scatter for $(V, U - V)$ CMR $\sim$ 0.035mag in the Coma cluster (Bower, Lucey, & Ellis 1992a)). Immediately after its creation, a stellar population is extremely blue, but it quickly reddens asymptotically to the colours of its reddest stars. The rate of change of the colour monotonically decreases, but never reaches zero, such that the colour of a stellar population always depends on its age, but its sensitivity declines with time. It therefore follows that there are two ways of creating a population of (single burst) galaxies with low colour scatter. Either they all formed at the same time, or they are very old. Bower, Lucey, & Ellis considered the first possibility highly unlikely, and so characterised the spread of age in the galaxies by their characteristic collapse times. They concluded that the bulk of stars in these galaxies must have formed by a lookback time of 10Gyr, corresponding to a median redshift of $z \sim 2$. Interestingly, in a subsequent paper, Bower, Kodama, & Terlevich (1998) used more realistic models for the star formation histories of cluster galaxies, using exponentially decreasing star formation rates, and realistic timescales for the truncation of that star formation as the galaxies fell into 'clusters'. They found that star formation was permitted at look back times as late as 3Gyr ago, but that the models were still constrained to have formed the bulk of their stars at large look back times, i.e. the bulk of stars in most of the galaxies are still old, but some of the galaxies can contain stellar populations as young as 3Gyrs.

In addition to constraining the star formation history, the CMR also constrains the merging history of elliptical galaxies. As noted by Ostriker (1980), dissipationless merging of galaxies tends to average out the colours, thus destroying the slope of the CMR. Dissipative mergers however, could well violate the constraints set up by the CMR scatter, by forming enough new stars in the new potential well formed by the merger, these new stars will have higher metallicities, and hence redder colours than the stars in the merged fragments. Hierarchical models circumvent this problem by forming a correlation between the mass of a galaxy, and the mass of its progenitors (Kauffmann & Charlot 1998), thus preserving the CMR slope even through dissipationless mergers.

Most of these studies have concentrated on early type galaxies in the cores of rich clusters. Bower, Lucey, & Ellis (1992b) have shown that the colour magnitude relation on the cores of the Coma and Virgo clusters are identical to within observational uncertainties, however studies of the CMR in Hickson compact groups (Zepf, Whitmore, & Levison 1991) show increased scatter, as do studies of field ellipticals (Larson, Tinsley, & Caldwell 1980). Guzman et al. (1992) claim to find a difference in the zero-point of the $Mg_2 - \sigma$ relation between the core of the Coma cluster, and a 'halo' population ($> 1°$ from the core). Abraham et al. (1996) find a $b - r$ colour gradient (using CMR corrected colours) with projected cluster radius in the $z = 0.23$ cluster Abell 2390, in the sense that the outer galaxies have bluer colours than the inner galaxies. González used the Worthey (1994) models, to investigate a population of local field ellipticals, and found a striking result: His galaxies have a small range in metallicity, but a large spread in luminosity weighted mean age. This is just the opposite of what is found in similar spectroscopic studies of local rich clusters such as Virgo and Coma (Kuntschner 1998, Kuntschner & Davies 1998, Mehlert et al. 1998), where the cluster ellipticals seem to be uniformly old and span a range in metallicities. Clearly there is evidence for environmental influence upon the star formation histories of early type galaxies.

In this thesis, we will address the question of environmental effects on the CMR, and on early type galaxy evolution in general. The questions which we wish to address are

1. Can we find any environmental dependence of the CMR within the Coma cluster?

2. How accurate is the suggestion that dissipationless mergers would violate the CMR (Ostriker 1980) in the light of modern 'hierarchical' models for the evolution of structure, which predict much merging of galaxies?

3. If both $(U - V)$ colour and Hydrogen Balmer line strength are sensitive to the age of the stellar populations, can we see this correlation in a sample of galaxies?

4. Is there any correlation between the cluster environment as shown by X-ray images, and the Butcher-Oemler effect?

In chapter 2, we present a new photometric catalogue of the Coma cluster, in the U- and V- bands. The $(U - V)$ colour is sensitive to the presence of young stellar populations. We have a fainter luminosity limit than Bower, Lucey, & Ellis (1992a), and extend out to over half a degree from the center of the cluster.

We address question 2 in chapter 3 by subdividing the photometry of chapter 2 by morphology, luminosity and position on the sky, and analysing the properties of the CMR in each of them.

In chapter 4 we use the hierarchical merging history from Baugh et al. (1998) and a random merging history model of our own, to attempt to answer question 2.

In chapter 5, we use the spectra of Caldwell et al. (1993) in conjunction with the model grids of Worthey (1994) and Worthey & Ottaviani and our photometry from chapter 2 to investigate question 3. We also look at the feasibility of quick and dirty searches for E+A galaxies using U-V colours.

In chapter 6 we use the galaxy classifications of Couch & Sharples (1987), with our own ROSAT HRI X-ray images, to investigate correlations between cluster X-ray structure and Butcher-Oemler activity in the $z \sim 0.3$ clusters AC114 and AC118.

Conclusions are summarised in chapter 7, where we also discuss possible future work.

Throughout this work, we will assume a value of the Hubble Constant of $H_0 = 100 kms^{-1} Mpc^{-1}$.

References

Abraham R. G. et al., 1996, ApJ, 471, 694

Arimoto N., Yoshii Y., 1987, A&A, 173, 23

Barger A. J., Aragon-Salamanca A., Ellis R. S., Couch W. J., Smail I., Sharples R. M., 1996, MNRAS, 279, 1

Barnes J. E., 1988, ApJ, 331, 699

Baugh C. M., Cole S., Frenk C. S., Lacey C. G., 1998, ApJ, 498, 504

Bender R., Burstein D., Faber S. M., 1992, ApJ, 399, 462

Bender R., Burstein D., Faber S. M., 1993, ApJ, 411, 153

Bond J. R., Kaiser N., Cole S., Efstathiou G., 1991, ApJ, 379, 440

Bower R. G., 1991, MNRAS, 248, 332

Bower R. G., Kodama T., Terlevich A. I., 1998, MNRAS, 299, 1193, astro-ph/9805290

Bower R. G., Lucey J. R., Ellis R. S., 1992a, MNRAS, 254, 589

Bower R. G., Lucey J. R., Ellis R. S., 1992b, MNRAS, 254, 601

Butcher H., Oemler J., A., 1978, ApJ, 226, 559

Butcher H., Oemler J., A., 1984, ApJ, 285, 426

Caldwell N., Rose J. A., Franx M., Leonardi A. J., 1996, AJ, 111, 78

Caldwell N., Rose J. A., Sharples R. M., Ellis R. S., Bower R. G., 1993, AJ, 106, 473

Cole S., Aragon-Salamanca A., Frenk C. S., Navarro J. F., Zepf S. E., 1994, MNRAS, 271, 781

Colless M., Dunn A. M., 1996, ApJ, 458, 435

Couch W. J., Barger A. J., Smail I., Ellis R. S., Sharples R. M., 1998, ApJ, 497, 188

Couch W. J., Ellis R. S., Sharples R. M., Smail I., 1994, ApJ, 430, 121

Couch W. J., Newell E. B., 1984, ApJS, 56, 143

Couch W. J., Sharples R. M., 1987, MNRAS, 229, 423

Djorgovski S., Davis M., 1987, ApJ, 313, 59

Dressler A., 1984, ApJ, 281, 512

Dressler A., Gunn J. E., 1983, ApJ, 270, 7

Dressler A., Lynden-Bell D., Burstein D., Davies R. L., Faber S. M., Terlevich R., Wegner G., 1987, ApJ, 313, 42

Eggen O. J., Lynden-Bell D., Sandage A. R., 1962, ApJ, 136, 748

Ellis R. S., Smail I., Dressler A., Couch W. J., Oemler J., Augustus, Butcher H., Sharples R. M., 1997, ApJ, 483, 582

Faber S. M., 1973, ApJ, 179, 731

Franx M., Illingworth G., 1990, ApJ, 359, L41

Frogel J. A., Persson S. E., Matthews K., Aaronson M., 1978, ApJ, 220, 75

González J. J., 1993, Ph.D. thesis, Univ. California, Santa Cruz

Guzman R., Lucey J. R., Carter D., Terlevich R. J., 1992, MNRAS, 257, 187

Jorgensen I., Franx M., Kjaergaard P., 1993, ApJ, 411, 34

Kauffmann G., 1996, MNRAS, 281, 487

Kauffmann G., Charlot S., 1998, MNRAS, 294, 705

Kauffmann G., White S. D. M., Guiderdoni B., 1993, MNRAS, 264, 201

Kodama T., 1997, Ph.D. thesis, Institute of Astronomy, University of Tokyo

Kormendy J., Djorgovski S., 1989, ARA&A, 27, 235

Kuntschner H., 1998, Ph.D. thesis, Department of Physics, University of Durham

Kuntschner H., Davies R. L., 1998, MNRAS, 295, L29

Larson R. B., 1974, MNRAS, 169, 229

Larson R. B., Tinsley B. M., Caldwell C. N., 1980, ApJ, 237, 692

Mehlert D., Bender R., Saglia R. P., Wegner G., 1998, in Untangling Coma Berenices: A New Vision of an Old Cluster, p. 107

Ostriker J., 1980, Comments on Astrophysics, 8, 177

Pahre M. A., Djorgovski S. G., De Carvalho R. R., 1995, ApJ, 453, L17

Pei Y. C., Fall S. M., 1995, ApJ, 454, 69

Persson S. E., Frogel J. A., Aaronson M., 1979, ApJS, 39, 61

Press W. H., Schecter P., 1974, ApJ, 187, 425

Renzini A., Ciotti L., 1993, ApJ, 416, L49

Saglia R. P., Bender R., Dressler A., 1993, A&A, 279, 75

Schweizer F., Seitzer P., 1992, AJ, 104, 1039

Schweizer F., Seitzer P., Faber S. M., Burstein D., Dalle Ore C. M., Gonzalez J. J., 1990, ApJ, 364, L33

Searle L., Sargent W. L. W., Bagnuolo W. G., 1973, ApJ, 179, 427

Smail I., Dressler A., Couch W. J., Ellis R. S., Oemler J., Augustus, Butcher H., Sharples R. M., 1997, ApJS, 110, 213

Stanford S. A., Eisenhardt P. R., Dickinson M., 1998, ApJ, 492, 461

Tinsley B. M., 1980, ApJ, 241, 41

Tinsley B. M., Gunn J. E., 1976, ApJ, 203, 52

Toomre A., Toomre J., 1972, ApJ, 178, 623

Vader J. P., 1986, ApJ, 306, 390

Visvanathan N., Sandage A., 1977, ApJ, 216, 214

White S. D. M., 1979, MNRAS, 189, 831

White S. D. M., Frenk C. S., 1991, ApJ, 379, 52

Worthey G., 1994, ApJS, 95, 107

Worthey G., Ottaviani D. L., 1997, ApJS, 111, 377

Zabludoff A. I., Zaritsky D., Lin H., Tucker D., Hashimoto Y., Shectman S. A., Oemler A., Kirshner R. P., 1996, ApJ, 466, 104

Zepf S. E., Whitmore B. C., Levison H. F., 1991, ApJ, 383, 524

Chapter 2

Photometry of Galaxies in the Coma Cluster.

Abstract. In this chapter, we present a new photometric catalogue of the local Coma galaxy cluster in the Johnson U- and V- bands. We cover an area of 3360arcmin^2 of sky, to a depth of $V = 20$mag in a 13 arcsec diameter aperture, and produce magnitudes for ~ 1400 extended objects in metric apertures from 8.8 to 26arcsec diameters. The mean internal RMS scatter in the photometry is 0.014mag in V, and 0.026mag in U, for $V_{13} < 17$mag.

2.1 Introduction

For this project we have chosen to study the $(U - V)$ colours of early type galaxies both in the core and in the outskirts of the Coma cluster. Although the colours of the galaxies in Coma have been studied before, both in a wide area (e.g. Dressler (1980); Godwin, Metcalfe, & Peach (1983)) and with high precision U and V band CCD data (Bower, Lucey, & Ellis [BLE]), there have been no wide area high precision U and V band studies of the galaxies in Coma. We therefore plan to extend the photometry of BLE to approximately double the distance from the cluster core (taken as being NGC4874), and to fainter limiting magnitudes. The extra coverage and depth will enable us to obtain colours for the abnormal spectrum 'E+A' galaxies of Caldwell et al. (1993) and Caldwell et al. (1996), many of which are to be found in the South West corner of the cluster around a group of galaxies dynamically associated with NGC4839 (Baier 1984, Escalera, Slezak, & Mazure 1992, Colless & Dunn 1996).

Significant advances in detector technology since the work of BLE, allows us to use much larger CCD chips. We have therefore taken tiled images across the coma cluster, giving us almost continuous coverage of the area of the cluster we are interested in. In contrast, BLE targeted individual galaxies. Because of the continuous coverage, our sample of galaxies is more complete than that of BLE, including all of the Godwin, Metcalfe, & Peach galaxies within our area of sky, but with significantly higher accuracy than the Godwin, Metcalfe, & Peach data.

We chose to use the Johnson (Johnson & Morgan 1953) U and V filters because they straddle the 4000Å break in the spectra of galaxies at low redshift, and are thus very sensitive to the ages of the stellar populations. They are especially sensitive to recent bursts of star formation (e.g. Worthey 1994, Charlot & Silk 1994)

The photometric data described in this chapter will be used to produce checks on the universality of the colour-magnitude relation (CMR) across the cluster, not just in the core (chapter 3). Its slope and scatter for all morphological types will be used in chapter 4 to place constraints on the merging history of local rich cluster galaxies, and the deviations from the CMR of individual galaxies will be compared to spectral features in chapter 5.

2.2 Observations

The observing runs which provided data for use in this project are summarised in table 2.1. U and V-band observations were obtained in two successive years at the SAO 1.2m on Mt Hopkins, Arizona. The detector used was a thinned, back-side illuminated, AR coated 2048×2048 Loral CCD, giving us a 10 arcmin ($192h^{-1}kpc$) field of view. The chip had a read noise of 7 electrons, and a gain of 2.3 electrons per ADU. Because the chip was thinned, it had a very high quantum efficiency in the U band (see figure 2.1). We ran the chip in 2×2 binning mode, effectively re binning four pixels into one on reading out the chip. This introduces no extra noise, nor cuts down on the area of sky covered by the chip, which just behaves as a 1024×1024 device. Although the pixel scale doubles to 0.63 arcsec pixel^{-1}, the chip can be read out four times faster, and the larger pixel size is still small enough to oversample our stellar point spread function, whose FWHM never fell below 1.7″ for any of our images (figure 2.7). Figure 2.1 shows the response of the camera (filter + CCD) for our wavelength range. The quantum efficiency of the CCD stays high and almost constant right across the U band, giving effective filter responses which approximate the standard shape. The same setup was used for all observations to maintain a common photometric system for the whole dataset.

The observations cover a continuous region covering the South West group around NGC4839, the central parts around NGC4874 and NGC4889 and also a large amount of the North East of the cluster (see figure 2.2). The observations were also designed to cover all of the (Caldwell et al. 1993) and (Caldwell et al. 1996) abnormal spectra galaxies, however inclement weather meant that some were missed towards the extreme SW and NE. The presence of a seventh magnitude star just north of the center of the cluster means that there is a hole in our data there too.

The aims of this project require that we are able to photometer galaxies as faint as 17.5mag to better than 0.02mag in both the U and V bands within a 13 arcsec diameter metric aperture. We set this limit to obtain data of comparable quality to that of BLE. These requirements translate to a signal to noise ratio for a 17.5mag galaxy in a 13 arcsec aperture of 50. To add a safety margin, we aimed to achieve a signal to noise of 100 for a $V = 17.5$ galaxy in a 5" diameter aperture. We used a modified version of the `signal95` program to calculate exposure times of 400s and 2700s minutes for V and U band exposures respectively. The `signal95` program was modified to take into account the detector characteristics of the Loral CCD camera on the SAO 1.2m. The 400s V band exposures are short enough that cosmic ray hits on the detector are not a severe problem, but for the 2700s U band exposure, the cosmic ray flux would make taking a single exposure unacceptable. Instead we took three 900 second exposures which were co-added later. Even in these shorter 900s exposures, the sky level was much higher than the read noise, so we suffered no increase in the noise levels by taking multiple images. To reduce any systematic differences in the photometry between parts of the cluster, observations of the central and SW regions were interleaved during the observing runs.

Before sunset on each night, we took a series of 20 to 30 bias frames. These are zero length exposures used to subtract the bias current produced by the CCD pre-amplifier. Each bias image is noisy due to the readout noise of the CCD, so we create a master bias image by averaging together all of the individual bias frames. Because the CCD is read out one row at a time, the bias current tends to change slightly along rows, but not down columns, so we reduced the noise in the bias image even further by averaging together all of the rows. This produces an map of how the bias current changes across the CCD. In addition to the bias current, a CCD can also have 'dark current', where charge builds up in the pixels over time, even without being exposed to light. The CCD we used has an overscan strip of two columns of pixels at the edge of the detector which are never exposed to light, even with the shutter open. This strip can be used to measure the dark current during each exposure.

The QE of the detector is not constant across its surface. A map of its variation (known as flatfield images) can easily be measured by taking an exposure of a spatially uniform source of light, usually a de-focussed image of the inside of the dome, or the twilight sky. Before sunset on each night, we took dome flats using a tungsten lamp which illuminated a white cloth screen attached to the inside of the dome. During twilight each night, we took sky flats by taking about 15 snapshots of different parts of the sky, and calculating their median to remove any stars from the images. Flats were taken for both the U and V filters. The sky flats were found to be a better match to the variations seen in the actual night sky exposures, so these were used.

During the night, immediately after dusk and before twilight, standard stars from Landolt (1992) were observed over a wide range in airmass. Care was taken to ensure the colours of the stars matched those of our galaxies, typically $0 \leq (U - V) \leq 2$. With our large field of view it was possible to observe many standards simultaneously. To have additional checks on the overall homogeneity of the final photometry, we used large overlaps of ~ 1 arcmin between the actual Coma cluster images, ensuring that the objects in this overlap region were observed in both images. We also took shorter (300s and 100s for U and V respectively) repeated observations of the central parts of the cluster, thus using the galaxies there as 'standard' galaxies. This is particularly important for the U band, as the spectral energy distribution of the standard stars is different from that of the early type galaxies.

Dates	Observer(s)	Usable Nights
20–21 March, 1996	Caldwell	1.5
11–14 April, 1996	Caldwell & Terlevich	4
9–11 May, 1996	Caldwell	4
1–5 April, 1997	Caldwell & Terlevich	1.5

Table 2.1. Summary of observing time.

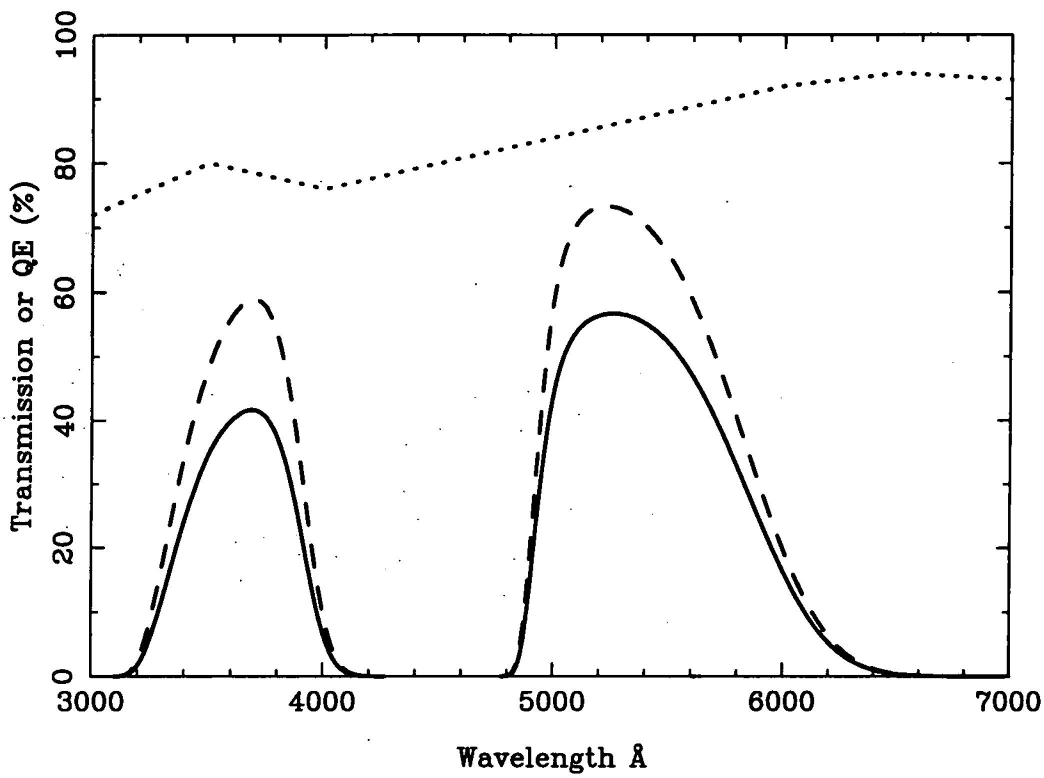

Figure 2.1: Camera spectral response. The dotted line shows the Loral CCD quantum efficiency, the dashed line shows the transmission of the U and V filters. The solid line is the combination of both, showing the effective spectral response of the Loral CCD plus the filters. Because of the relatively flat QE of the CCD, unlike the RCA CCD used by Bower, Lucey, & Ellis (1992a) which drops off rapidly blue-wards of ~ 3800Å, the overall response in the U of the system is very close to the ideal shape of the filter.

2.2.1 Photometric Conditions

To calculate the photometric system we used a 4 term transformation equation:-

$$mU = U + u1 + u2 \times XU + u3 \times (U - V) + u4 \times TU$$

$$mV = V + v1 + v2 \times XV + v3 \times (U - V) + v4 \times TV$$

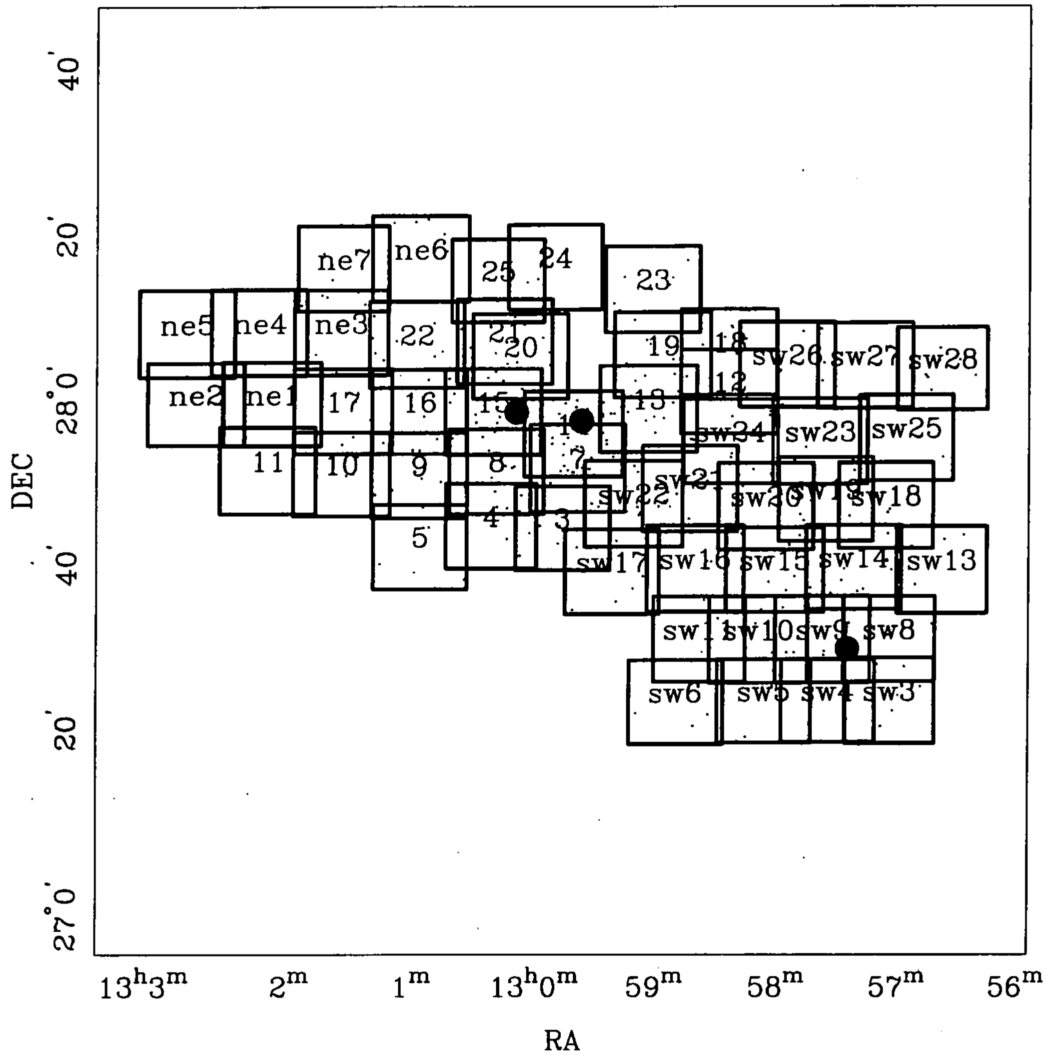

Figure 2.2: The distribution of observed images across Coma. All observed galaxies with $V_{16} > 18$ are shown as a dot. The large dots show, from left to tight, the positions of NGC4889, NGC4874 and NGC4839 respectively. The dynamical center of the Coma cluster is somewhere between NGC4889 and NGC4874, while the dynamical center of the substructure in the SW corner is NGC4839.

where mU and mV are the measured V and U magnitudes respectively, U and V are the Landolt U and V magnitudes respectively, $u1, u2, u3, u4, v1, v2, v3, v4$ are the fit parameters, and TU, TV, XU and XV are the observation time and airmass for the U and V images respectively. We found that by taking out a systematic drift in the photometric zero point with time (the u4 and v4 terms in the transform equations), we could reduce the residuals of the V fit to below 0.007mag, however the U band residuals were as high as $0.03mag$. This indicated that none of the data was sufficiently photometric for this project, an indication which was confirmed through the examination of the standard

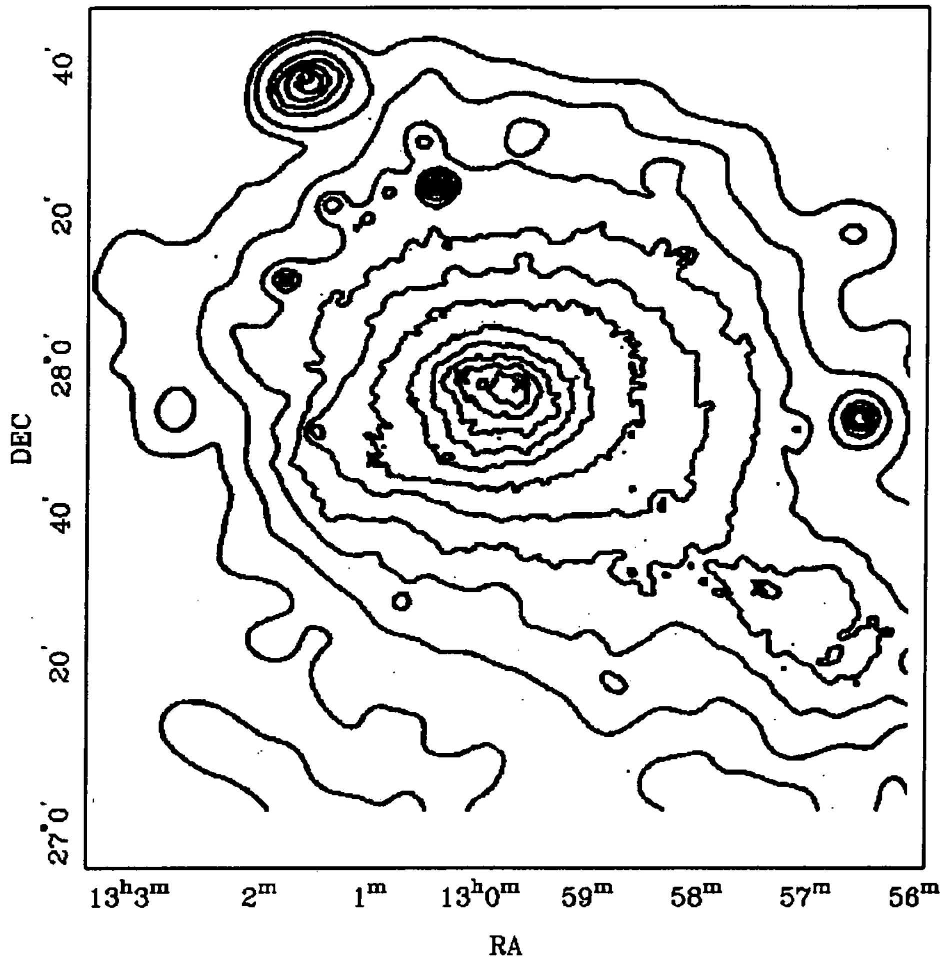

Figure 2.3: ROSAT PSPC X-ray image of the Coma cluster from White, Briel, & Henry (1993) on the same axes as figure 2.2.

galaxy observations. We found that after the photometric transformation defined by the standard stars had been applied, there was still a systematic offset in the standard galaxy photometry observed on different nights, and sometimes even on the same nights of up to $0.^{m}02$. The method we used to remove these offsets is described in section 2.3.3

Figure 2.4: A mosaic of most of our images of the Coma cluster. We have used the U images as the blue component of the image, the V images as the red component, and the mean of the two as the green component.

2.3 Data reduction

The reduction of the CCD images was carried out using the `IRAF ccdproc` program. This program automatically subtracts the readout bias, which it calculates from the bias strip in the image, from the science exposures, the flat field images and the bias images. It then subtracts the bias image from the science image to remove any remaining zero level bias and divides by the normalised flat field image for each filter to calibrate for the relative detector pixel response.

Cosmic ray hits on the CCD detector leave blemishes on the image. Depending on the angle of incidence of the cosmic ray, they either leave a spot or streak of a few or even just one pixel. Because they are formed by a single particle, the pattern of charge they leave on the CCD is very sharp, and easily distinguished from the images of astronomical objects (assuming the pixel scale is properly oversampling the point spread function). We use this sharpness property of the cosmic ray hit to automatically remove them from the images, using the 'qzap' IRAF procedure, written by Mark Dickinson. Firstly the program finds all pixels in an image which are more than five standard deviations deviant from the background level of the image. Cosmic ray hits are then separated from astronomical objects by performing a 'flux ratio' test; If the flux in a pixel is higher than that in its neighbours by more than a given ratio (the flux ratio, ~ 10), it is marked as a cosmic ray, and removed by interpolation. Routines such as this should always be used with extreme caution, if the parameters used by the program (specifically the flux ratio) are chosen without due care, the routine will quietly either remove from the image any sharp object such as the cores of stars, or alternatively, will not remove the fainter cosmic rays. To guard against these possibilities, we checked each image after removing the cosmic rays. We subtracted the cleaned image from the original image to leave a map of what was removed. By comparing this map with the original image, we could tune the flux ratio such that as many of the cosmic ray hits were removed as possible without touching the stars.

The three $900sec$ U band exposures were combined into a single image by simply taking the average of the three. The `IRAF imcombine` task has many features for rejecting parts of an image which do not appear in all of the exposures, presumably a cosmic ray hit. However, if as is the case with our data, the seeing conditions vary even slightly during the exposures, then the flux in the cores of stellar images can vary greatly between exposures, so much so that the flux in the core of the star with the best seeing will get rejected. We found that in every case, the approach outlined above using the qzap routine was more efficient at removing cosmic rays than the imcombine task.

Where the qzap routine finds a cosmic ray. it interpolates the surrounding pixels across it. This works well when the cosmic ray is either in an area of background, or in a smooth gradient, however if the cosmic ray happens to hit too near the center of a star or galaxy, the interpolation will not work properly, and we mark the object as being suspect during subsequent reduction.

The chip used had a number of cosmetic defects, such as bad columns. A list of the known defects is kept at the observatory and we added some minor ones to it. We removed the defects by interpolating across their smallest dimension. This has the same drawbacks as the removal of cosmic rays, in that it works well in an area of background, or in a smooth gradient, but not otherwise. We therefore also mark objects within 5 pixels of a defect as suspect in the subsequent reduction procedures.

2.3.1 *Galaxy identification, photometry and astrometry*

Lists of candidate objects were produced using the Sextractor1.2b10 program (Bertin & Arnouts 1996). It was run on each V image to produce a list of positions, a `CLASS_STAR` index, describing whether the object is a point source or extended, and a rough (uncalibrated) magnitude. To produce the `CLASS_STAR` index, Sextractor needs to know the rough seeing FWHM for the image, so this was measured for about 5 stars on each image using the `IRAF imexam` program prior to running Sextractor. The rough magnitude produced by Sextractor was then used to reject the faintest objects, to avoid confusion and crowding problems later on in the reduction procedure. All objects within 15 pixels (9.45 arcsec) of an edge of the CCD were also rejected. In order to avoid confusion and crowding problems later, the rough magnitude produced by Sextractor was used to reject the faintest objects, along with all the objects within 15 pixels of the edge of the CCD. This gives rise to the sharp cutoff in the V magnitude distribution seen in figure 2.5.

The list of positions for the galaxies in each image was used by the IRAF `phot` package to generate fixed aperture magnitudes in a range from $7 - 24$ pixel radii, corresponding to $8.8'' - 30''$ diameter apertures. Phot takes the position of the object given to it, and recalculates the centroid of the object before positioning an aperture around it, thus we were able to use the same positions for both the V and U images in most cases, and if the position was slightly out, phot would automatically correct it. This approach worked well in most cases, but for some pairs of U and V images where the centroids of the objects in the images differed by more than three pixels, an x–y offset between the images was

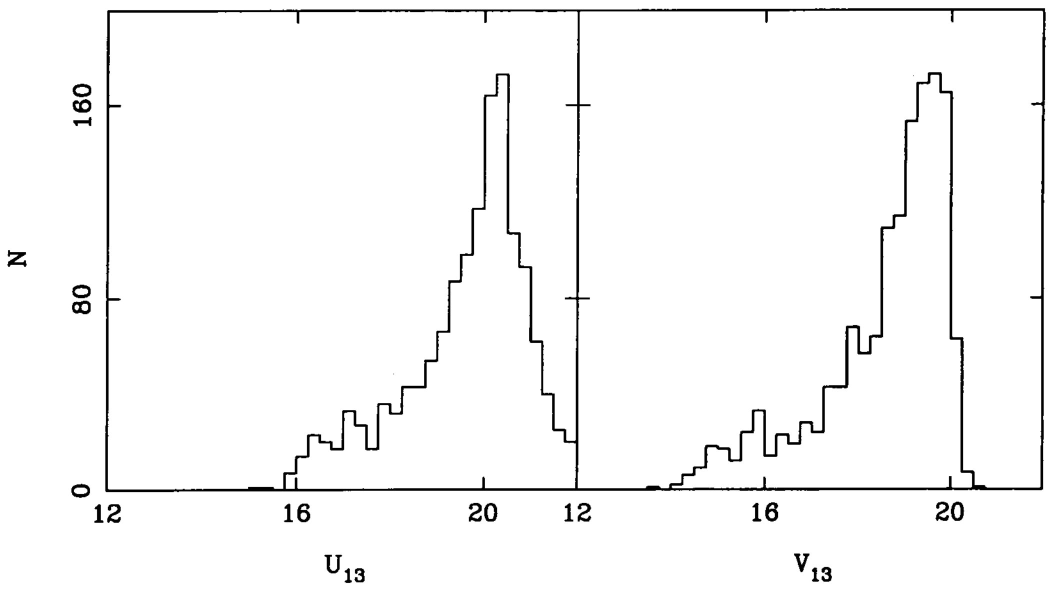

Figure 2.5: The 13″ diameter aperture magnitude distribution for all the galaxies in our sample for both the U and V bands. When making the list of targets using Sextractor (see section 2.3.1 in main text) we applied a magnitude limit. Although the magnitudes had not been calibrated using the standard stars, and the same magnitude offset was used for each V band image, we still get a sharp cutoff in the V band magnitude distribution of the final calibrated V-band magnitudes.

calculated and applied prior to the U band photometry. The background was measured individually for each object. We used annuli with both 40 and 120 pixel inner radii, and a width of 10 pixels. The background for a galaxy was taken as the median of the pixels within its annulus.

Astrometry for the frames was calculated using the HST guide star catalogue as a source of reference stars. These were identified on our U and V band images, and a plate solution was calculated using the `IRAF immatch` package. The Guide star catalogue only contains on average about five objects in each of our images, so the RMS scatter in our astrometry was approximately 1 arcsec in each image. This was considered good enough for our purposes.

2.3.2 Seeing corrections

In this discussion, we restrict ourselves to a circularly symmetric PSF. All our measured properties are circularly averaged, so any non spherical symmetry in the PSF, due maybe to poor tracking or focus, would cause only second order effects (Saglia et al. 1993).

The Fourier transform of the PSF can be predicted using atmospheric turbulence theory to be $exp[-(kb)^{5/3}]$ (Fried 1966, Woolf 1982), where the scaling parameter $b = FWHM/2.9207006$. As done by Saglia et al. (1993), we generalise this to

$$\hat{p}_{\gamma}(k) = exp\left[-(kb)^{\gamma}\right] \tag{2.1}$$

where γ controls the amount of light in the wings of the PSF. $\gamma = 2$ corresponds to a Gaussian profile, while the theoretically predicted value of $\gamma = 5/3$ gives a more wingy PSF. Lower values of γ produce even larger wings.

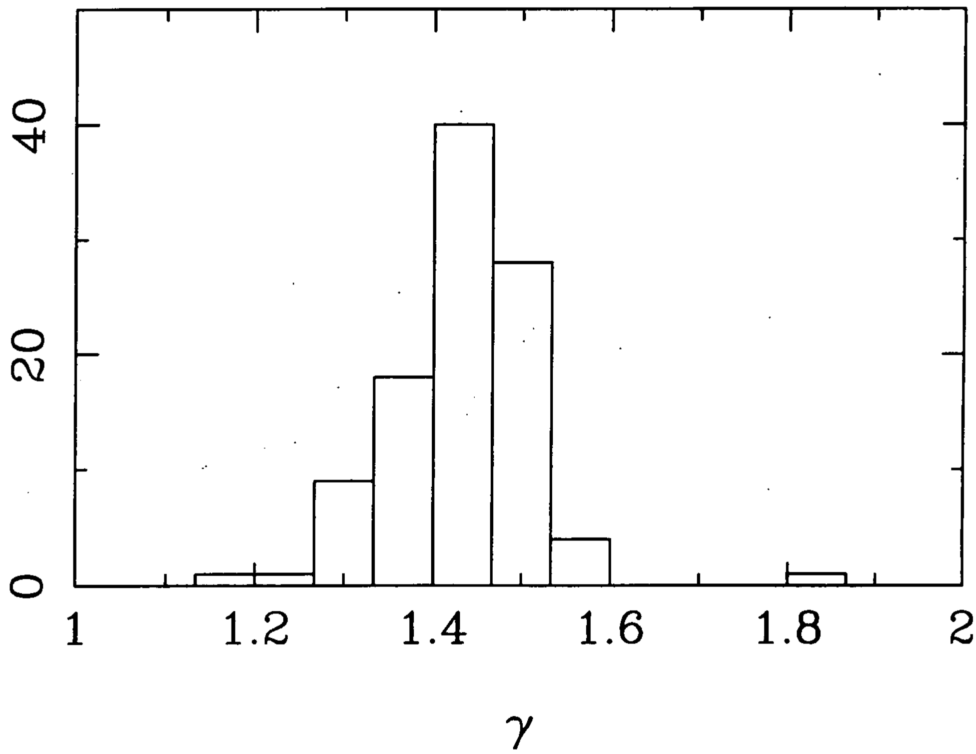

Figure 2.6: The distributions of γ parameters obtained by least squares fitting of the profile of the brightest stars in each image to the theoretical seeing PSF described in equation 2.1. γ controls the amount of light in the wings of the PSF. $\gamma = 2$ corresponds to a Gaussian profile, while the theoretically predicted value of $\gamma = 5/3$ gives a more wingy PSF. Lower values of γ produce even larger wings.

We used least square fits of the brightest stellar objects in each image to obtain both γ and b (or the FWHM) for each exposure. Figures 2.6 and 2.7 show a histograms of the distributions of γ and the FWHM respectively for all of the images. Although the values of γ vary from 1.2 to 1.8, there is very little variation between stars in the same exposure, so we adopt a different γ for each image.

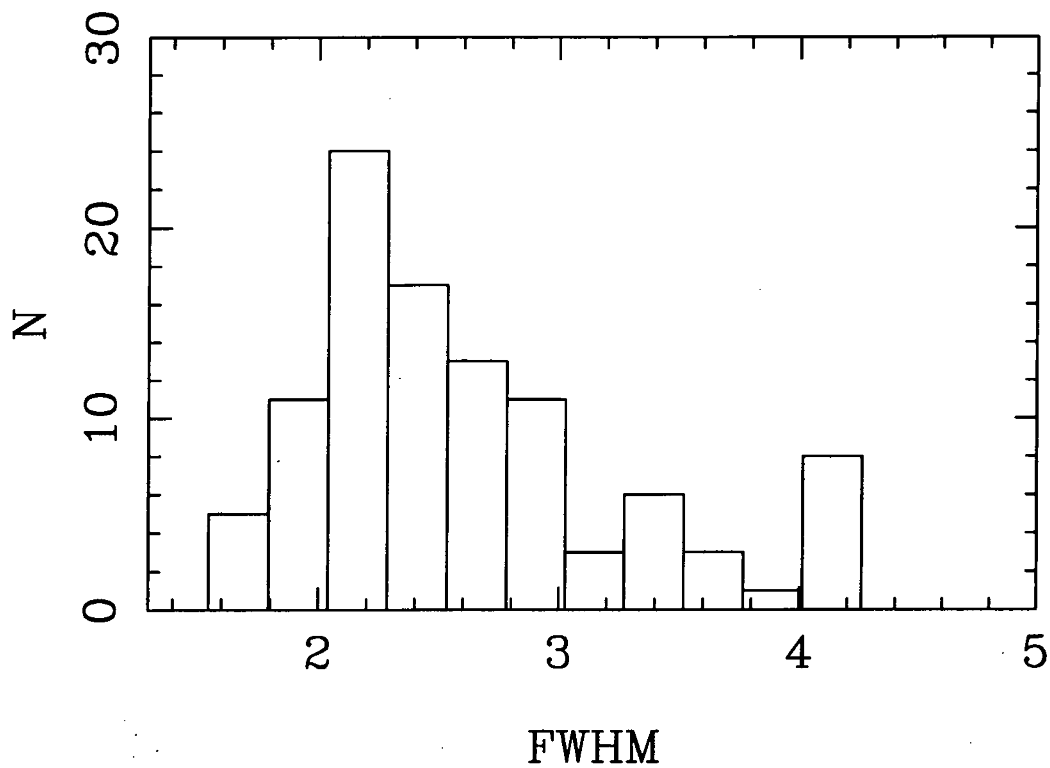

Figure 2.7: The distributions of the seeing FWHM obtained by least squares fitting of the profile of the brightest stars in each image to the theoretical seeing PSF described in equation 2.1.

The Intensity at a radius R from a source ($I(R)$), is then given by the convolution of the surface brightness distribution of the object in the sky ($I^s(R)$) with the PSF ($p_\gamma(R)$).

$$I(R) = I^s(R) \otimes p_\gamma(R) \tag{2.2}$$

For stellar objects, we simply take the intensity distribution on the sky to be a delta function, and for galaxies, we use the canonical deVaucoleurs $R^{1/4}$ law.

$$I^s(R) = \begin{cases} I_e exp\left\{-7.669\left[\left(\frac{R}{R_e}\right)^{1/4} - 1\right]\right\} & , \text{ galaxy} \\ L\delta_D(R) & , \text{ star} \end{cases}$$

where R_e is the half light radius, at which $F(R_e) = F(\infty)/2$, $I_e = I(R_e)$, $\delta_D(R)$ is the Dirac delta and L is the luminosity of the star.

To convert the luminosity distributions of an object in the sky into the luminosity distribution of the object on the detector we must convolve with the PSF (equation 2.2).

To seeing correct our objects we require the difference, in magnitudes, of the flux of an object as measured within an aperture of radius R on our detector ($F(R)$), and its flux as measured within the same aperture on the sky ($F^s(R)$). To find the flux inside an aperture of radius R, we simply integrate the required luminosity distribution,

$$F(R) = \int_0^R 2\pi R' I(R') dR'$$
$$F^s(R) = \int_0^R 2\pi R' I^s(R') dR'$$

The seeing correction is then simply $-2.5 \times log[F^s(R)/F(R)]$ (for stars $F^s(R) \equiv L$). As can be seen from figure 2.8, the value of R_e has little effect on the seeing correction, so we simply use $R_e = 5''$ for all of our galaxies.

We use numerical integration techniques to perform both the integrations and the convolutions. The results of which, for a variety of apertures and seeing FWHM are shown in tables 2.2 and 2.3. Both of these tables assume $\gamma = 1.47$, the average value for our observations (see figure 2.6).

seeing	Aperture diameter (arcsec)										
FWHM	4	6	8	10	13	16	20	25	32	40	50	60
4.50	0.909	0.564	0.376	0.268	0.176	0.126	0.087	0.060	0.039	0.027	0.018	0.014
4.00	0.789	0.476	0.314	0.222	0.146	0.104	0.072	0.050	0.033	0.022	0.015	0.011
3.50	0.667	0.391	0.254	0.180	0.118	0.085	0.059	0.041	0.027	0.018	0.012	0.009
3.00	0.542	0.309	0.200	0.141	0.093	0.067	0.046	0.032	0.021	0.014	0.010	0.007
2.50	0.418	0.233	0.150	0.106	0.070	0.050	0.035	0.024	0.016	0.011	0.007	0.005
2.00	0.300	0.165	0.106	0.075	0.050	0.036	0.025	0.017	0.011	0.008	0.005	0.004
1.50	0.193	0.106	0.068	0.049	0.032	0.023	0.016	0.011	0.007	0.005	0.003	0.002
1.00	0.104	0.057	0.037	0.027	0.018	0.013	0.009	0.006	0.004	0.002	0.001	0.001

Table 2.2. Table of galaxy seeing corrections based on a galaxy with $R_e = 5$arcsec. To obtain the seeing corrected value, the seeing correction is subtracted from the observed aperture magnitude. We parameterise the profile of the PSF using $\gamma = 1.47$, the average γ for our observations. Corrections are show for circular apertures ranging from 4 to 60arcsec diameters. When seeing correcting our data, we calculated a correction for each image by fitting a FWHM and γ to it from the bright stars.

2.3.3 Photometric Calibration

Upon inspection of the standard stars it became apparent that the conditions during most of the observations were not adequate for high accuracy photometry (see section 2.2.1). Particularly evident when examining the large overlap regions between images and the

seeing	Aperture diameter (arcsec)										
FWHM	4	6	8	10	13	16	20	25	32	40	50	60
4.50	1.093	0.573	0.332	0.214	0.129	0.088	0.060	0.041	0.028	0.020	0.014	0.011
4.00	0.922	0.461	0.263	0.170	0.104	0.072	0.049	0.034	0.023	0.016	0.012	0.009
3.50	0.746	0.357	0.202	0.132	0.082	0.057	0.040	0.028	0.019	0.013	0.010	0.007
3.00	0.573	0.263	0.150	0.099	0.063	0.044	0.031	0.022	0.015	0.011	0.008	0.006
2.50	0.408	0.184	0.107	0.072	0.046	0.033	0.023	0.016	0.011	0.008	0.006	0.004
2.00	0.263	0.120	0.072	0.049	0.032	0.023	0.016	0.012	0.008	0.006	0.004	0.003
1.50	0.150	0.072	0.044	0.031	0.020	0.015	0.011	0.008	0.005	0.004	0.003	0.002
1.00	0.072	0.037	0.023	0.016	0.011	0.008	0.006	0.004	0.003	0.002	0.001	0.001

Table 2.3. Table of stellar seeing corrections. To obtain the seeing corrected value, the seeing correction are subtracted from the observed aperture magnitude. We parameterise the profile of the PSF using $\gamma = 1.47$, the average γ for our observations. Corrections are show for circular apertures ranging from 4 to 60arcsec diameters. When seeing correcting our data, we calculated a correction for each image by fitting a FWHM and γ to it from the bright stars.

repeated observations of certain fields, was a systematic drift in the photometric zero point of up to $.2mag$ between images. As these offsets were so readily measurable, we used them to correct the zero points of the individual images to create a consistent photometric system.

The method we used to generate this system is very similar to that used in Maddox, Efstathiou, & Sutherland (1990) to homogenise the APM galaxy catalogue, however, due to our detector's far smaller size, and its linearity, the assumption that a homogeneous photometric system can be generated merely by adjusting the zero points of each plate individually is more valid. We will now outline our calibration method.

To calculate a set of zero-point offsets for each image the regions of overlap between each pair of images was examined. An object positioned in an area where frames i and j overlap will have magnitudes m_i and m_j as measured from frames i and j respectively. The actual magnitude for this object is m_0, and in the absence of observational errors, these three quantities can be related to each other thus,

$$m_0 = m_i + C_i = m_j + C_j \qquad (2.3)$$

where C_i is the correction applied to the zero point of image i. If we define

$$T_{ij} = m_i - m_j = C_j - C_i$$

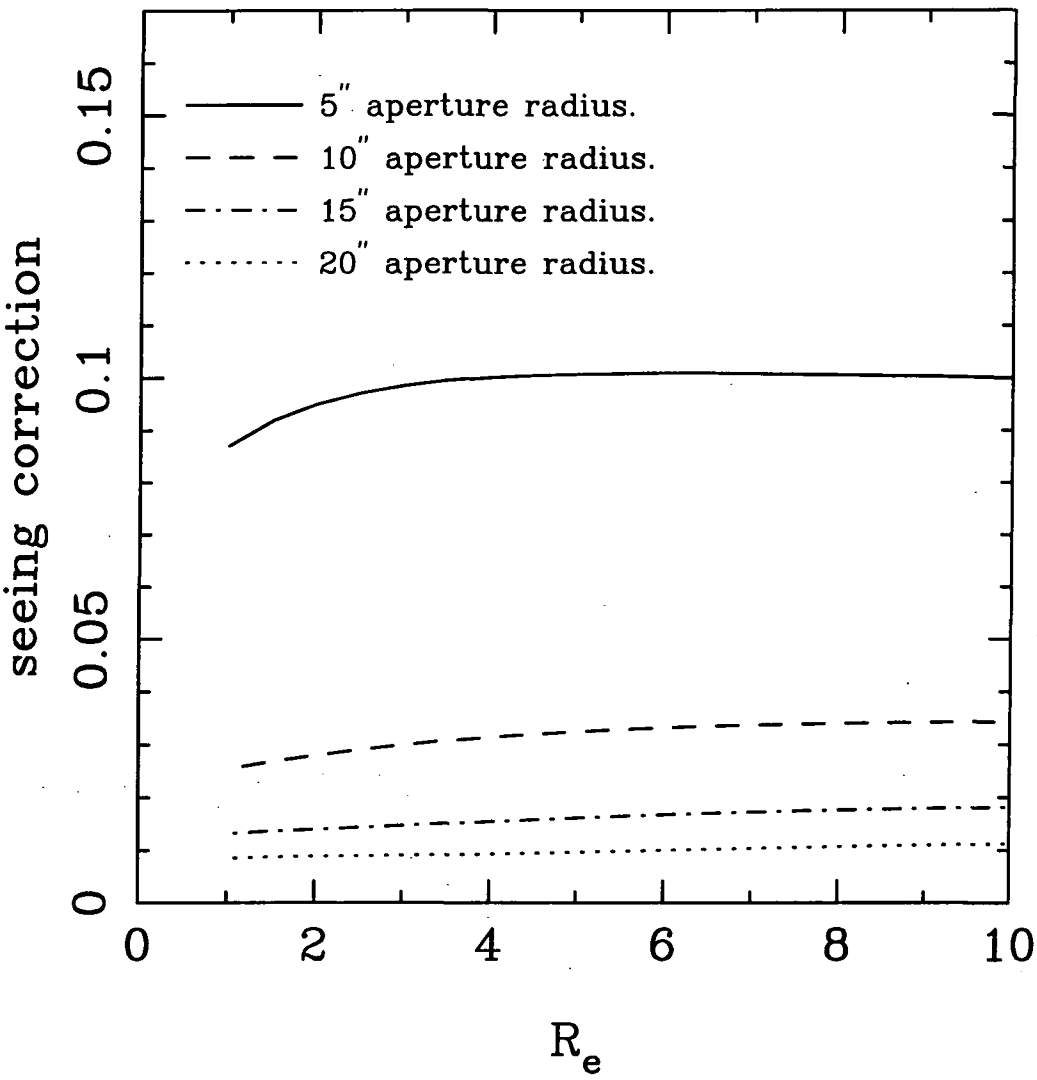

Figure 2.8: The effect of seeing correcting galaxies of different R_e in various apertures. The calculation uses a seeing FWHM of 2.5″ and a γ of 1.47 (the average γ for our observations). The effect of Re on the seeing correction can be seen to be relatively unimportant.

as the overlap difference between i and j, then the offset correction for any image can be calculated from the overlap differences and offset corrections of any adjacent overlapping image.

$$C_{i_j} = C_j + T_{ij}, \forall j \subset i$$

where $j \subset i$ denotes any pair of images i,j with a valid overlap region, and C_{i_j} denotes the C_i as calculated from image j. In the absence of observational errors,

$$C_i = C_{i_j}$$

However we do have observational errors, so we must apply an iterational approach to determine the C_i. Firstly we construct an observed estimate of the T_{ij}.

$$T^e_{ij} = \frac{\sum_{n=1..N_{ij}}(m_{n_i} - m_{n_j})}{N_{ij}}$$

where N_{ij} is the number of bright objects in the region of overlap between images i and j, and the m_{n_i} and m_{n_j} are the measured magnitudes of object n in images i and j respectively.

Now we can use a weighted mean of the T^e_{ij} to find a value for the photometric offsets :-

$$C^{n+1}_i = \frac{C^n_i W_i + \sum_{j \subset i} W_{ij} C^n_{ij}}{W_i + \sum_{j \subset i} W_{ij}}$$

or

$$C^{n+1}_i = \frac{\left(C^n_i W_i + \sum_{i \subset j}(C^n_j + T^e_{ij})W_{ij}\right)}{\left(W_i + \sum_{j \subset i} W_{ij}\right)} \qquad (2.4)$$

where the C^n_i are the C_i calculated in iteration n, W_i is the mean of the weights, W_{ij}. These weights were chosen to be proportional to the number of objects used to calculate the T^e_{ij}, and normalised to be in the range zero to one. :-

$$W_{ij} = N_{ij}/35$$

We chose to use the number in the overlap (N_{ij}), rather than the inverse of the scatter in the $(m_{n_i} - m_{n_j})$. With the low number of objects present in our overlaps, the scatter is not always well determined, and can be artificially low for overlaps with low N_{ij}, just the opposite of the required behaviour.

This iterative method does not constrain the total photometric offset, it merely ensures the best possible relative photometry of the system by removing as much of the drift in the zero point between images as is possible in a self consistent manner. We therefore arbitrarily re-normalise the C_i after every iteration so that they have zero mean.

Equation 2.4 was iterated to find the best set of C_i. To measure the progress of the iterations, we construct a measure of the homogeneity of the system after iteration n,

$$E^n = \sum_{i=1..N} \sum_{i \subset j} W_{ij}(T_{ij} + C^n_i - C^n_j)^2 \qquad (2.5)$$

where N is the total number of images for which we are trying to ascertain the C_is.

We start off with the photometric transformation as defined by the standard stars for the photometric nights (see section 2.2.1), and use these same parameters for the non photometric data. For the V band photometry, setting the $C_i^{n=0} = 0$, we get $E^{n=0} = 0.39$, while after 7000 iterations $E^{n=7000} = 0.0004$. The U band data started off with $E^{n=0} = 0.6$, and after 7000 iterations, $E^{n=7000} = 0.0006$. After about 7000 iterations, the rate of change of E^n has slowed to less than $E^n/1000$ per iteration.

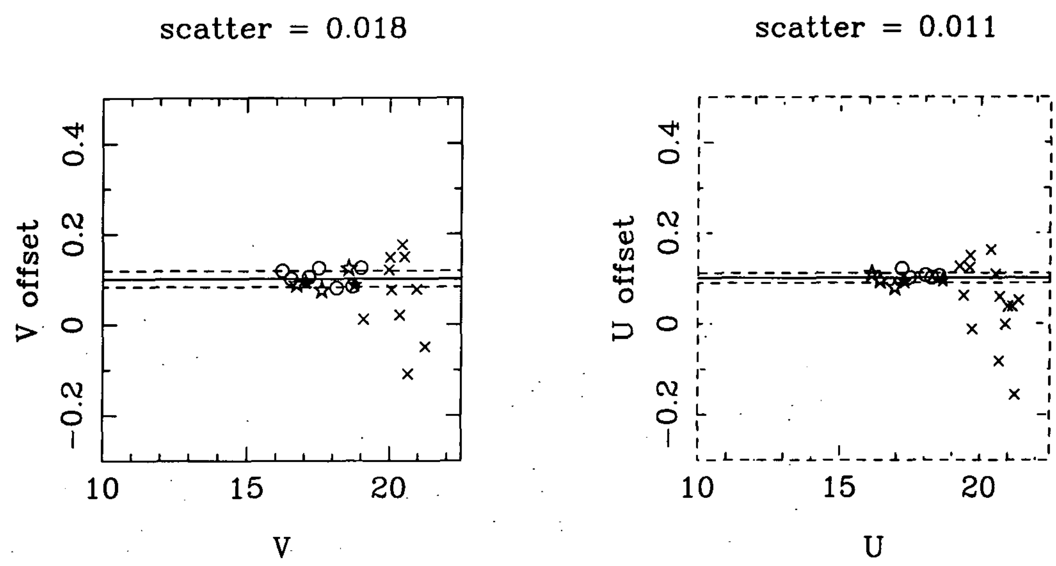

Figure 2.9: The V and U offsets ($m_{n_i} - m_{n_j}$) of objects in a region where two images overlap as a function of magnitude (m_i). The offset of each point is the difference between the 13″ aperture magnitude of that object after seeing correction, as measured from two overlapping images. The T_{ij}^e for this pair of images is then calculated as the mean of the ($m_i - m_j$). Circles represent extended objects, while the stars represent point sources. Open symbols lie within 5″ of a known defect on the CCD, or within 40 pixels (25.2″) of the edge of the detector. Crossed symbols are not used in the calculation of the T_{ij}^e value, or the RMS scatter about it. The RMS scatters for the U and V images shown here are consistent with the photometric errors. The V band images have seeing FWHM of 3.4 and 2.1, whilst the U images have seeing FWHM of 2.8 and 2.4, so the lack of difference between the offsets as measured by the point and extended objects, especially in the V band images indicates that the seeing correction (sec. 2.3.2) has worked well.

Obviously much care has to be taken in the measurement of the T_{ij}^e. We must ensure that effects such as different seeing conditions on the two overlapping images do not cause any systematic offsets. Although seeing conditions are taken into account for each object when measuring the m_i (see section 2.3.2), the effect of seeing on objects adjacent to the aperture are not corrected for i.e. more light from an adjacent object will enter the aperture for images with worse seeing. We therefore measured the m_i in various sized apertures, from 8.8″ to 26″ diameter, and using background annuli from 20″ to 100″ diameter with 25″ and 3.2″ widths. If the T_{ij} are well behaved under all measuring conditions, then we simply take the median value. If they are not well behaved, we inspect the region more carefully to ascertain the cause, or we mark the T_{ij} as unreliable. Figure 2.9 shows the V and U offsets ($m_{n_i} - m_{n_j}$) of objects in a region where two images overlap as a function of magnitude (m_i). The T^e_{ij} measured from these offsets are shown as solid lines. Extended sources are shown as circles, while point sources are shown as star symbols. The fact that both types of symbols lie on top of each other shows that the seeing correction works well, especially in the V images. One V image has poor seeing (3.4 arcsec FWHM) while the other has moderate seeing (2.1 arcsec FWHM).

To summarise, we can now construct a homogeneous dataset by adding to each magnitude m_i, the offset correction for the image in which it was measured (C_i) to obtain the object's corrected magnitude m_0 (see equation 2.3). This homogeneous photometric system however is only relative. To set the overall photometric offset, we use the fixed aperture magnitudes of BLE. We have new observations of all of the BLE sample, so using these galaxies we can define a transformation between our corrected aperture magnitudes, and theirs,

$$\begin{aligned}
V_{BLE} &= V + C_{V1} + (U - V)C_{V2} \\
U_{BLE} &= U + C_{U1} + (U - V)C_{U2} \\
C_{V1} &= -1.272 \\
C_{V2} &= 0.006 \\
C_{U1} &= -0.884 \\
C_{U2} &= 0.072
\end{aligned}$$

where U_{BLE},V_{BLE},U and V are the BLE92a magnitudes, and our magnitudes respectively. the Cs are the fit parameters, and were determined using 16arcsec diameter aperture photometry for both our magnitudes and those of BLE. While C_{V1} and C_{U1} simply fix our photometric zero point to that of BLE, the C_{V2} and C_{U2} define a colour term, and show how our filters differ from theirs. From the low value of C_{V2}, we can conclude that our V band response is similar to that of BLE, but the larger value of the C_{U2} parameter indicates that our U band response is not such a good match, probably due to our increased sensitivity to the blue portion of the U bandpass (see fig. 2.1).

2.3.4 *Summary of reduction procedure*

In the previous sections we have described in detail the steps taken to reduce the data from raw images to corrected magnitudes, however, the overall procedure used is difficult to follow due to the highly detailed nature of the sections. We therefore briefly describe the overall procedure in a less detailed manner below.

- The raw images were bias subtracted and flatfielded.
- Cosmic ray hits were removed from the images.
- Cosmetic defects on the CCD were removed by interpolating across them.
- We co-added the U band exposures into single images.
- Solutions to the photometric transformations were found for the most photometric nights.
- `Sextractor` was used to find positions for the objects in the images. Objects close to the edges and faint objects were not included in the position lists.
- The seeing conditions for each image were measured from the brightest stars stars in that image.
- We used the `IRAF phot` package to obtain photometry in $8.8, 13, 60, 20.2, 25.2$ and 26arcsec diameter apertures, with 40 and 120arcsec inner radii background annuli.
- The photometry was corrected for seeing.
- We used the HST Guide Star Catalogue to calculate plate solutions for each image.
- We measured photometric zero point differences between each pair of images with overlapping areas of sky in both the U and V bands. These offsets were used to construct a homogeneous photometric system.

– We compared our photometry with that of BLE to place our photometry into their photometric system.

2.4 Quantifying the photometric errors

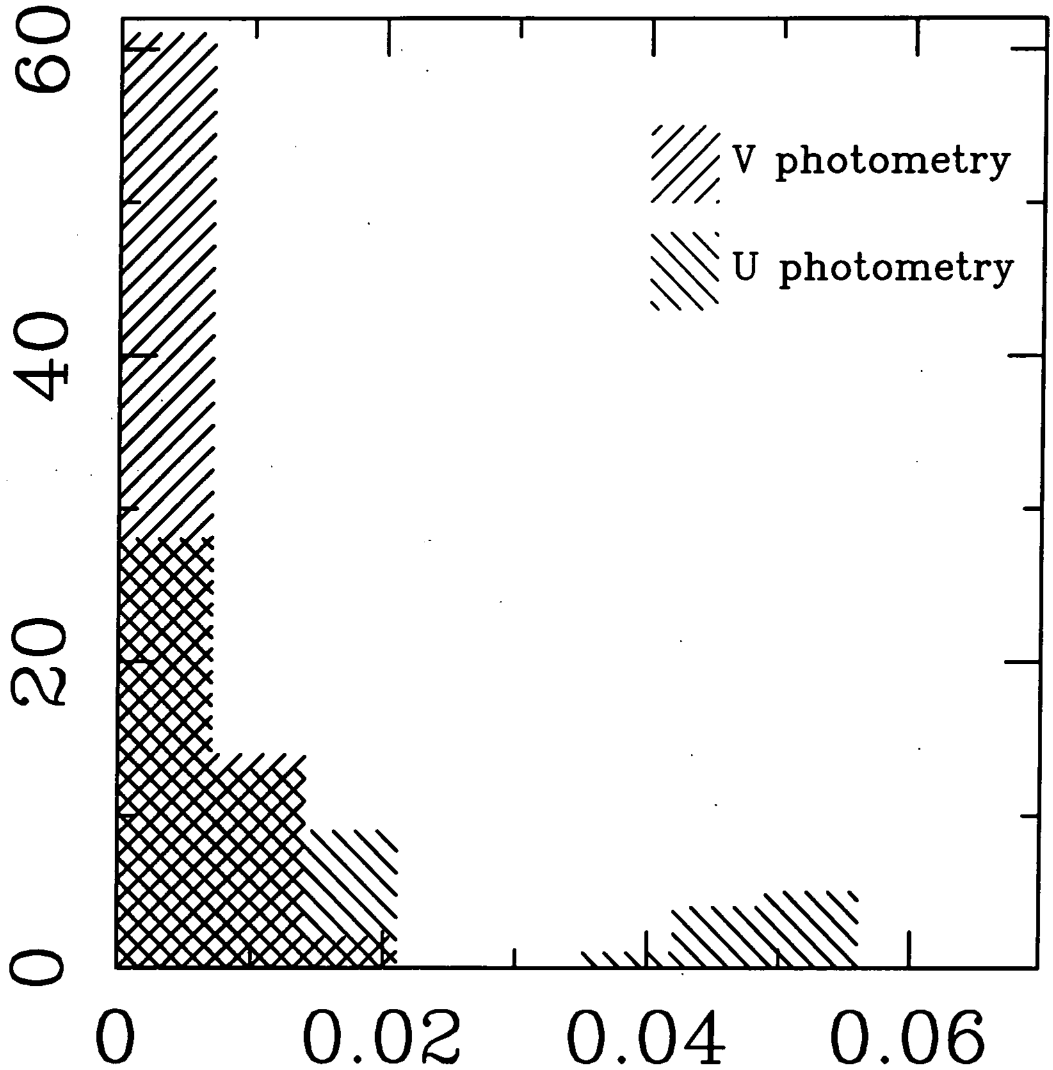

Figure 2.10: Histogram of the absolute values of the sums of all the closed loops of T_{ij} with less than five elements, for both the V and U images (see section 2.4 for details). Under perfect conditions, these loops should all sum to zero, so we use their deviation from zero to measure the level of internal inconsistency of our photometric system. Apart from a small crop of loops in the U photometry with sums around $0.05mag$, due to a single image in the SW (sw8) which had problems with scattered light, all of the loops have sums with values of the order of our estimated photometric errors (see figure 2.11).

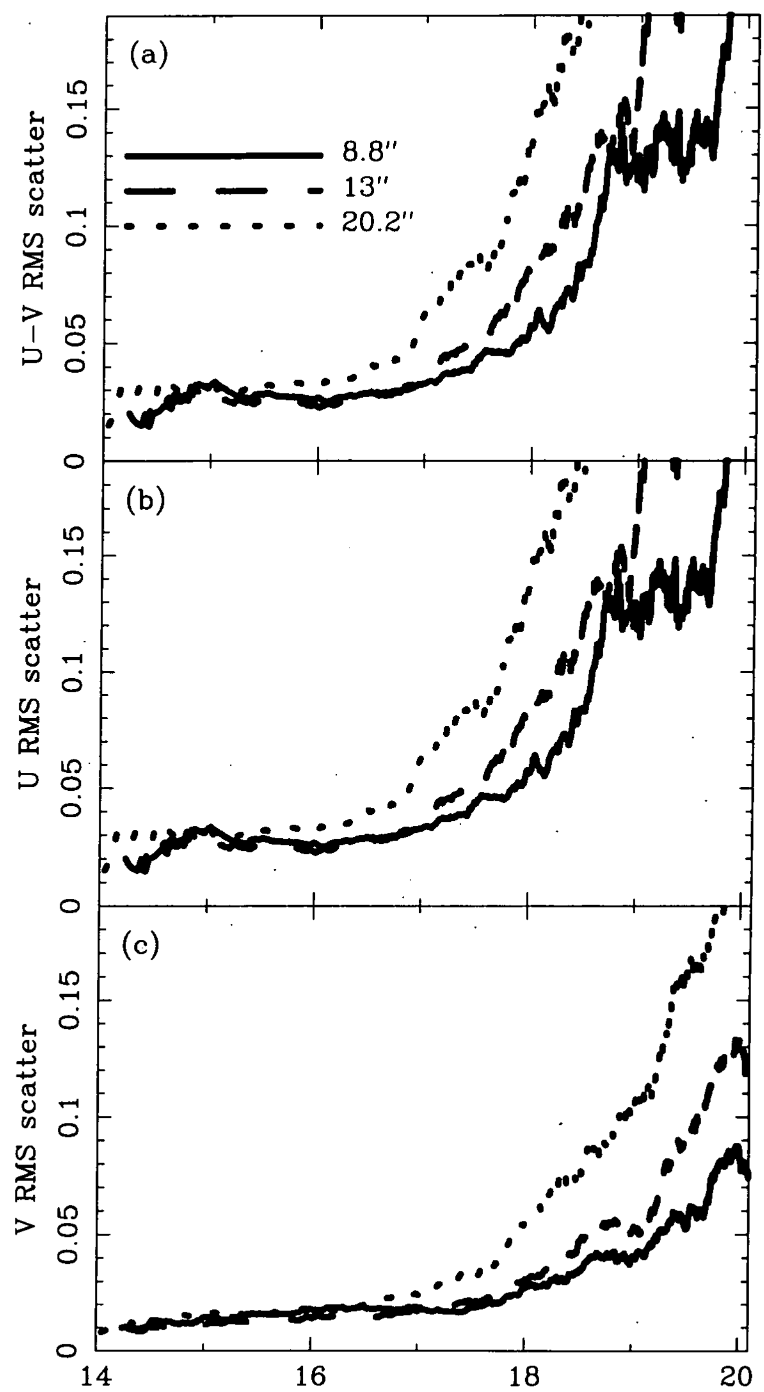

Figure 2.11: In the three panels, we plot the running mean biweight scatter as a function of V_{13} magnitude, from repeated observations of galaxies in overlapping regions, of our U and V photometry (panels b and c) as measured through circular apertures of 8.8″,13″ and 20.2″ diameter. We also plot the scatter in our $(U - V)$ colours (panel a), calculated by adding the scatter from the U and V photometry in quadrature. A bin size of 60 observations was used in calculating the running mean, except at the bright end of the magnitude range, where it was allowed to go down to 6 so as to get values at these extremes. This explains the decreased smoothness of the line at the bright end. These plots show that most of the scatter in our colours comes from the U band photometry. Table 2.4 lists the mean RMS scatter down to $V_{13} = 17$mag for all of our apertures.

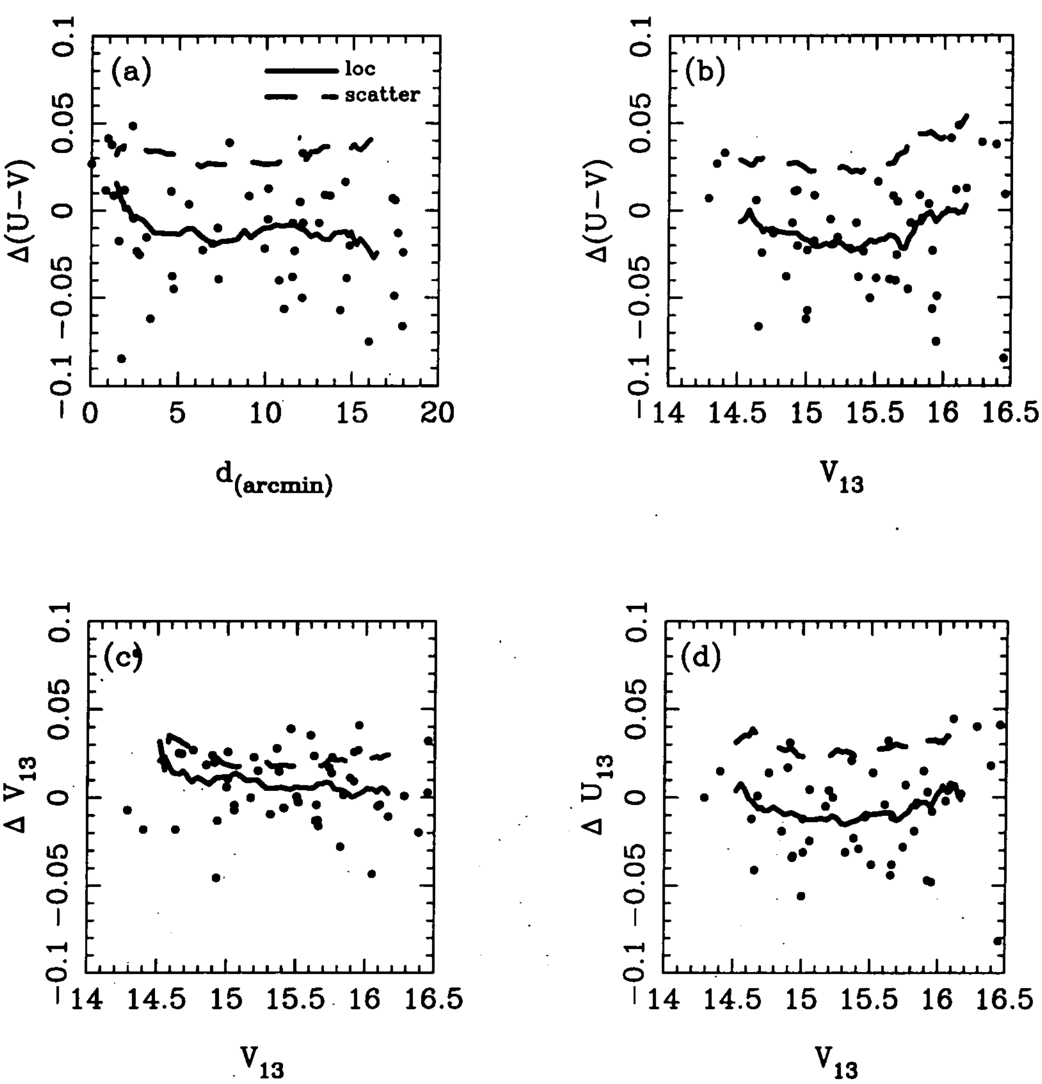

Figure 2.12: The four panels show the behaviour of the residuals between our 13arcsec diameter aperture photometry and that of BLE. In all cases, the residuals are calculated by subtracting the BLE data from ours, for example, a negative $\Delta(U-V)$ indicates that our colour for a galaxy is bluer than the BLE colour. The Solid and dashed lines show running biweight location and scatter indicators (see appendix B). The running biweights have a bin size of 20, but this reduces to 10 towards the ends of the lines. In all of the panels, the levels of scatter between our data and that of BLE is entirely consistent with the levels of observational error in both datasets. Panel (a) shows the difference between the $(U-V)_{13}$ colours obtained in this paper and those of BLE, as a function of distance from NGC4874. The overall scatter between our colours and theirs is 0.034mag. This is of the order of both our photometric errors (see figure 2.11) and theirs. Panel (b) shows how our colours compare to the BLE colours as a function of luminosity. Panels (c) and (d) show how our U and V band magnitudes compared with those of BLE. The overall RMS scatter in the residuals for these panels are 0.032 and 0.022mag respectively. It is important to note that we have only used the BLE data to set an overall photometric offset and colour term for all of our galaxies, neither of which could reduce the level of scatter between the two datasets to these levels if there was something seriously wrong with our dataset. It is also worth noting that the mean difference between our colours and the BLE colours does not depend on the distance from the center of the cluster, indicating that at least out to the maximum radius of the BLE dataset, our photometry has no anomalous drift in the photometric zero point.

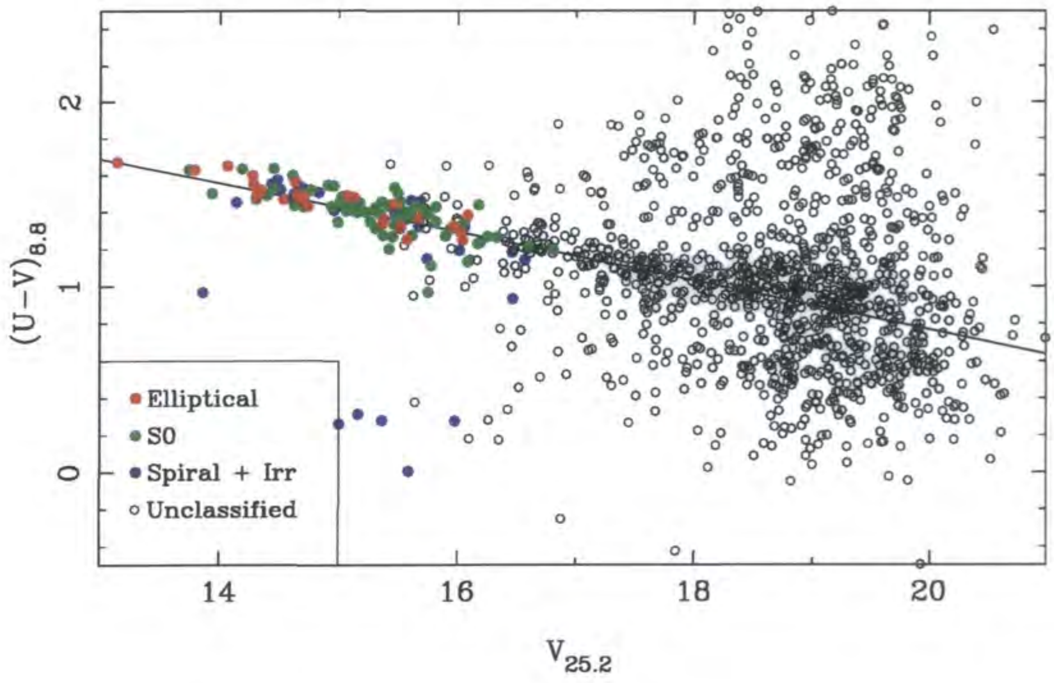

Figure 2.13: The (U, V) colour magnitude relation for all objects detected for which Sextractor gives a CLASS_STAR ≤ 0.2. The V are taken from the $25.2''$ diameter aperture, as it is more complete than the $26''$ aperture. In order to increase the signal to noise in the colour term, the $(U-V)$ are taken from the smallest aperture, the $8.8''$ diameter aperture. The colours represent the morphological types of the galaxies from Andreon et al. (1996) and Andreon, Davoust, & Poulain (1997). Open symbols have no morphological information. The line is a straight forward biweight fit (see Appendix B) to the whole dataset, and follows the ridge-line of the CMR which can be seen to extend down to $m_{V25.2} \sim 19.5$.

It is vital that, having used observations taken in mostly non-photometric conditions to construct a photometric dataset, that we can independently check the validity of this system. A natural consequence of the image overlap method we used to construct the homogeneous photometric system (sec. 2.3.3) is that we can use the T_{ij} as measured from the overlaps to test for self consistency. We use the fact that, in the absence of observational errors, if we construct a closed loop around several images in the sky, and sum up the T_{ij} offsets from the overlaps around the loop, then the this sum must be zero for any closed loop.

$$\begin{aligned} T_{ab} + T_{bc} + ... + T_{na} &= C_b - C_a + C_c - C_b + ... + C_a - C_n \\ &= 0 \end{aligned}$$

As an example, a closed loop around the images shown in figure 2.2 could be

$$T_{15\rightarrow16} + T_{16\rightarrow9} + T_{9\rightarrow8} + T_{8\rightarrow15}$$

These loops are not allowed to go back on themselves for the obvious reason that $T_{ij} \equiv -T_{ji}$, so the smallest possible loop has three elements, i.e. $T_{15\rightarrow16} + T_{16\rightarrow9} + T_{9\rightarrow15}$ However these loops may suffer from increased scatter owing to the reduced number of objects in overlapping corners (i.e. $T_{9\rightarrow15}$) compared to overlapping edges (i.e. $T_{16\rightarrow15}$). Under perfect conditions, these closed loops would always sum up to zero, so the deviation from zero of the sum gives shows the level at which the T_{ij} are not self consistent. It is important to note that the T_{ij} are measured directly from the raw data, and the iterative procedure outlined in section 2.3.3 does not alter them (it alters the C_i). Therefore these loops give a measure of the quality of the data independent of the photometric calibration procedure.

Figure 2.10 shows the distribution of the absolute values of the sums around all of the closed loops with less than 5 elements for both the U and the V band images. Almost all of the loops come below the 0.02mag level for both U and V, this level of inconsistency is lower than the level of scatter in the photometry as measured from repeated observations (see fig. 2.11 and below). The small cluster of U loops between 0.04 and 0.06 are due to a single U-band image in the SW corner (sw8) which had problems with what appeared to be scattered light getting around the filter. Although we attempted to remove this as a constant gradient in the image background, it obviously did not work perfectly. The T_{ij} for all of the overlap regions involving this image were given very low weights, so that we could still calculate some sort of calibration for the image, but the non consistency in this image did not propagate to the photometry of the neighbouring images during the iterative procedure of section 2.3.3.

We have shown that we have a self consistent set of T_{ij}, but we have not shown what the overall error in our final photometry is. We can use the large number of multiply observed objects (mostly from our overlap regions) to constrain our observational errors. Table 2.4 lists the mean RMS scatter for all objects with $V_{13} < 17$mag in all of our apertures, and Figure 2.11) shows how the scatter in the observations of multiply observed objects increases with magnitude for the 8.8,13 and 20.2arcsec diameter apertures. The scatter was computed using a running biweight scatter indicator (see appendix B and chapter 3) with a maximum bin size of 60 observations, and a minimum bin size (at the bright end of the dataset) of 6. The levels of scatter in out 13arcsec apertures are the same as those

Aperture diameter	RMS scatter		
(arcsec)	U	V	$(U-V)$
8.8	0.02303	0.01619	0.02829
12.6	0.02124	0.01364	0.02532
13	0.02258	0.01352	0.0264
16	0.0277	0.01478	0.03145
20.2	0.03036	0.01727	0.035
25.2	0.0359	0.02076	0.04154
26	0.04805	0.02706	0.05528

Table 2.4. This table lists the RMS errors in our photometry for all of our apertures. It was generated using the repeated observations of both stars and galaxies. mostly in the regions of overlap between images. Figure 2.11 shows how the RMS errors vary with magnitude for the 8.8,13 and 20.2 arcsec diameter apertures. The RMS internal scatter quoted by BLE for their 13″ photometry, which only reaches a magnitude of $V_{13} = 16.5$ is 0.025 and 0.015mag for U and V respectively.

quoted by BLE (0.025 and 0.015mag for U and V respectively), and they stay constantly low down to $V_{13} \sim 17$mag. It should be noted that although table 2.4 shows that the 12.6″ aperture has the lowest RMS scatter in both U and V bands, figure 2.11 shows that fainter than $V_{13} \sim 17$, it is quickly overtaken by the 8.8″ aperture, which is better suited to the smaller sizes of the fainter galaxies.

As a final check on the validity of the calibration, we have compared our photometry with that of BLE (see fig. 2.12). The BLE dataset goes down to $V_{13} = 16.5mag$, and they quote an RMS internal scatter of 0.025 and 0.015 for the U and V-band photometry respectively. The scatter between our colours and theirs is 0.034mag, while the scatter between our photometry and theirs is 0.022 and 0.032mag for the V and U-bands respectively. This is almost exactly what we expect simply by adding the rms internal scatters of our data and theirs in quadrature, and shows that we need no extra source of scatter in our photometry other than that measured through repeated observations of objects. Equally important, given the method used to obtain a uniform photometric system for our data, is the fact that the mean colour difference does not vary as a function of distance from NGC4874 (figure 2.12, panel a), although the BLE data goes out to a much smaller radius than our new data, so we cannot rule out any effects further away from the center.

2.5 Estimated total magnitudes

It will be useful for the analysis we perform in chapter 4 to have total V-band magnitudes for our photometry. This does not have to be as accurate as the colours, so we chose to estimate them by comparison with the BLE total magnitudes. The transformation we used was

$$log_{10}(V_{25.2} - V_T) = a - bV_{25.2}$$

where the $V_{25.2}$ are our V-band 25.2 arcsec diameter aperture magnitudes, the V_T are the BLE total V-band magnitudes and a and b are the fit parameters. The form of this function was not determined using any analytical prescription for the total magnitude of a galaxy given an aperture magnitude, but simply by visual inspection of the data. We used least squares minimisation to find the best fit parameters ($a = 2.65$ and $b = -0.2$), which gave an RMS scatter in the fit of 0.12mag. The residuals of the fit are shown in figure 2.14.

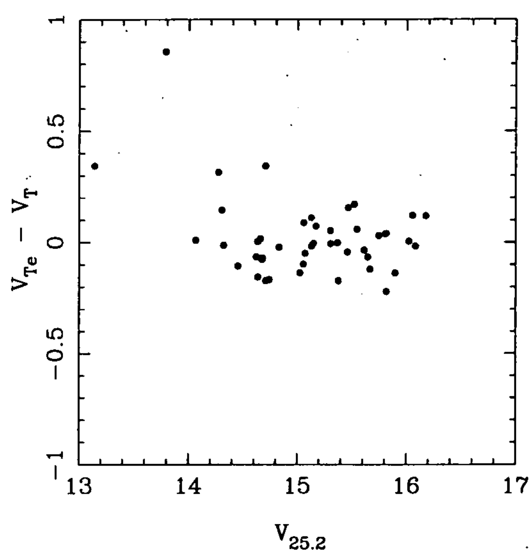

Figure 2.14: The residuals of the fit between our 25.2arcsec V-band magnitudes ($V_{25.2}$), and the BLE V-band total magnitudes (V_T). We use this fit to estimate total magnitudes (V_{Te}) from our 25.2arcsec V-band magnitudes (see text for details).

2.6 Summary

– We have obtained images of the Coma cluster which cover 3360arcmin^2 in both Johnson U and V bands.

- Although most of the images were not taken in photometric conditions, we have managed to combine them into a single homogeneous photometric system by using the multiple observations of objects in the large overlap regions we allowed ourselves between the images.

- We find the rms internal scatter the photometry of multiply observed objects with $V_{13} < 17$mag to be 0.014mag and 0.026mag for the V and U-band photometry in 13″ diameter apertures respectively. This is almost exactly the same as the scatter obtained by BLE

- We find no systematic drift in colour between our data and that of BLE with increasing distance from the cluster center

- We have constructed a homogeneous, wide area, high precision photometric dataset with which to investigate the colour-magnitude relation (see figure 2.13) in the Coma cluster.

References

Andreon S., Davoust E., Michard R., Nieto J. L., Poulain P., 1996, Astronomy and Astrophysics Supplement Series, 116, 429

Andreon S., Davoust E., Poulain P., 1997, Astronomy and Astrophysics Supplement Series, 126, 67

Baier F. W., 1984, Astronomische Nachrichten, 305, 175

Bertin E., Arnouts S., 1996, Astronomy and Astrophysics Supplement Series, 117, 393

Bower R. G., Lucey J. R., Ellis R. S., 1992, MNRAS, 254, 589

Caldwell N., Rose J. A., Franx M., Leonardi A. J., 1996, AJ, 111, 78

Caldwell N., Rose J. A., Sharples R. M., Ellis R. S., Bower R. G., 1993, AJ, 106, 473

Charlot S., Silk J., 1994, ApJ, 432, 453

Colless M., Dunn A. M., 1996, ApJ, 458, 435

Dressler A., 1980, ApJS, 42, 565

Escalera E., Slezak E., Mazure A., 1992, A&A, 264, 379

Fried D. L., 1966, J. Opt. Soc. Am., 56, 1372

Godwin J. G., Metcalfe N., Peach J. V., 1983, MNRAS, 202, 113

Johnson H. L., Morgan W. W., 1953, ApJ, 117, 313

Landolt A. U., 1992, AJ, 104, 340

Maddox S. J., Efstathiou G., Sutherland W. J., 1990, MNRAS, 246, 433

Saglia R. P., Bertschinger E., Baggley G., Burstein D., Colless M., Davies R. L., McMahan J., R. K., Wegner G., 1993, MNRAS, 264, 961

White S. D. M., Briel U. G., Henry J. P., 1993, MNRAS, 261, L8

Woolf N. J., 1982, ARA&A, 20, 367

Worthey G., 1994, ApJS, 95, 107

Chapter 3

Environmental Dependence of the Colour-Magnitude Relation.

Abstract. In this chapter we place limits on the levels of scatter in the colour–magnitude relation (CMR) in the Coma cluster. We subdivide the galaxy population by morphology, luminosity and position on the sky, and analyse the CMR in each of them. The lowest levels of scatter are found in the elliptical galaxies, and the late type galaxies have the highest numbers of galaxies bluewards of the CMR. We finds signs of *decreased* scatter and systematically bluer galaxy colours with increasing projected radius from the center of the cluster, and conclude it to be due to a gradient in the mean galactic ages with projected radius.

3.1 Introduction

The overriding feature of early type galaxies in the cores of clusters is their uniformity. Structurally, early type galaxies are very simple. They can be parametrised using an $R^{1/4}$ profile, with an added exponential disk (e.g. Saglia et al., 1997). They obey a set of simple 'scaling relations' which allow their properties to be scaled between galaxies of different luminosities. The 'fundamental plane' (FP) correlations (Dressler et al. 1987, Djorgovski & Davis 1987, Bender, Burstein, & Faber 1992, Saglia, Bender, & Dressler 1993, Jorgensen, Franx, & Kjaergaard 1993, Pahre, Djorgovski, & De Carvalho 1995) of luminosity, velocity dispersion and effective radius connects a galaxy's overall structure with its dynamics, and has its origin in the virial relation, but departs from the form predicted by the ideal relation by having a shallower slope. The progressive reddening of the integrated colours of elliptical galaxies with increasing luminosity is known as the colour-magnitude relation (CMR) (Faber 1973, Visvanathan & Sandage 1977, Frogel et al. 1978, Persson, Frogel, & Aaronson 1979, Bower, Lucey, & Ellis 1992a, Bower, Lucey, & Ellis 1992b), despite its being a far simpler relation than the FP (a univariate rather than a bivariate relation), it nonetheless has similarly small levels of scatter.

In this chapter, I will use the high precision wide area photometry presented in chapter 2 to investigate the CMR across a single cluster. Bower, Lucey, & Ellis (1992b) have shown that the colour magnitude relation on the cores of the Coma and Virgo clusters are identical to within observational uncertainties, however studies of the CMR in Hickson compact groups (Zepf, Whitmore, & Levison 1991) show increased scatter, as do studies of field ellipticals (Larson, Tinsley, & Caldwell 1980). It must be noted that these group and field galaxy samples contain data from many disparate sources, therefore there must be an added source of scatter in matching the various photometric datasets onto a single photometric system. Despite this, at least in the sample of Larson, Tinsley, & Caldwell, the extra scatter seems too large to be accounted by increased observational uncertainties alone, and therefore must be real. In a large area study of the $z = 0.228$ cluster A2390, Abraham et al. (1996) detect a gradient in colour, and spectral properties of the galaxies with projected radius, which they attribute to a decrease in the mean age of cluster galaxies with radius.

Further evidence for an environmental dependence of the CMR comes from studies of spectral line indices. Broadband colours are notoriously inefficient at separating the effects of age and metallicity on a stellar population, a degeneracy neatly summarised by Worthey (1994) in his '2/3' law ($\Delta[Fe/H] \sim \frac{2}{3}\Delta log(t)$). This has led to studies of the stellar populations of early type galaxies in the cores of clusters using spectral line indices chosen to break this degeneracy and disentangle the effects of age and metallicity. Such studies (e.g. (Mehlert et al. 1998, Kuntschner 1998, Kuntschner & Davies 1998)) show that the CMR is driven by metallicity variations with galaxy luminosity, rather than age, a result supported by photometric studies of the CMR in high redshift clusters

(Ellis et al. 1997, Kodama & Arimoto 1997, Kodama 1997, Kodama et al. 1998). These studies all point towards the galaxies which make up the CMR in the cores of rich clusters being primarily constituted of uniformly old stellar populations. When González (1993) used these same spectroscopic techniques on early type galaxies in the field, the results were almost exactly the opposite. Rather than a coeval population of galaxies spanning a metallicity range, González found a population with similar metallicity, but with variations of several Gyrs in the luminosity weighted mean age of the stellar populations.

The data presented in chapter 2 extends out to almost the virial radius of the cluster. We therefore expect that on the outer part of the dataset, the galaxies will have only recently fallen into the cluster from the field. Additionally, we also have photometry for the SW corner around the galaxy NGC4839. This group of galaxies has been shown to be dynamically separate from the main cluster (Baier 1984, Escalera, Slezak, & Mazure 1992, Colless & Dunn 1996) with an associated peak in the X-ray profile of the cluster (Briel, Henry, & Boehringer 1992, White, Briel, & Henry 1993, Vikhlinin, Forman, & Jones 1994). Whether or not the group has already made one pass through the Coma cluster (e.g. Biviano et al., 1996) or is falling in for the first time (e.g. Colless & Dunn, 1996), it still retains a large number of 'post-starburst' or 'E+A' galaxies (Caldwell et al. 1993, Caldwell et al. 1996), more consistent with a group, or field population (Zabludoff et al. 1996) than the main body of the cluster.

By measuring the CMR in the three 'environments' of the cluster core, the outer parts of the cluster, and the NGC4839 group, we will be able to determine whether the CMR does have an environmental dependence. Because our entire dataset comprises of overlapping interleaved observations which have been placed into a single photometric system (see chapter 2) we will not encounter the problems of disparate datasets adding to the noise in the data.

3.2 Analysis technique

We ascertained cluster membership using recessional velocities from the NASA/IPAC Extragalactic Database[1] (NED). Most of the velocities can be attributed to Colless & Dunn (1996). Galaxies having velocities between $4000 kms^{-1}$ and $10000 kms^{-1}$ were taken as confirmed members. From this sample we then removed galaxies with 'bad' photometry. Galaxies were seemed bad, and thus rejected if

- Emission from a nearby object entered the $13''$ diameter aperture used throughout this chapter.

- One of the CCD bad columns passes through the galaxy.

- A cosmic ray was removed from part of the galaxy in the V image (Cosmic rays in the U images were less of a problem due to the image being composed of multiple exposures).

figure 3.1 shows snapshots of the V band images of the rejected galaxies. Figures 3.12, 3.13, 3.14, 3.15 and 3.16 show snapshots of the V band images of the member galaxies that remain. In all these snapshots, the circle represents our 13arcsec diameter aperture.

Due to the variable conditions encountered throughout the observing runs, we have not attempted to morphologically type our galaxies, but have instead relied upon the morphological classification of Andreon et al. (1996) and Andreon, Davoust, & Poulain (1997). Even with good conditions, we would not have been able to extend morphological classifications with any accuracy to fainter galaxies. The different colours of the symbols in figures 3.3, 3.4, 3.5 and 3.6 correspond to the broad morphological type of the galaxy. The actual morphological types used in these broad classifications are shown in table 3.1, and their frequency in our data is given in table 3.2.

Regression analysis of the colour magnitude relation was performed using the biweight estimator (see appendix B) due to its robustness and resistance in the case of non Gaussian distributions (Beers, Flynn, & Gebhardt 1990). In this case we are interested in the scatter of the ridge line of the CMR, and do not want to be unduly influenced by the odd blue

[1] The NASA/IPAC Extragalactic Database (NED) is operated by the Jet Propulsion Laboratory, California Institute of Technology, under contract with the National Aeronautics and Space Administration.

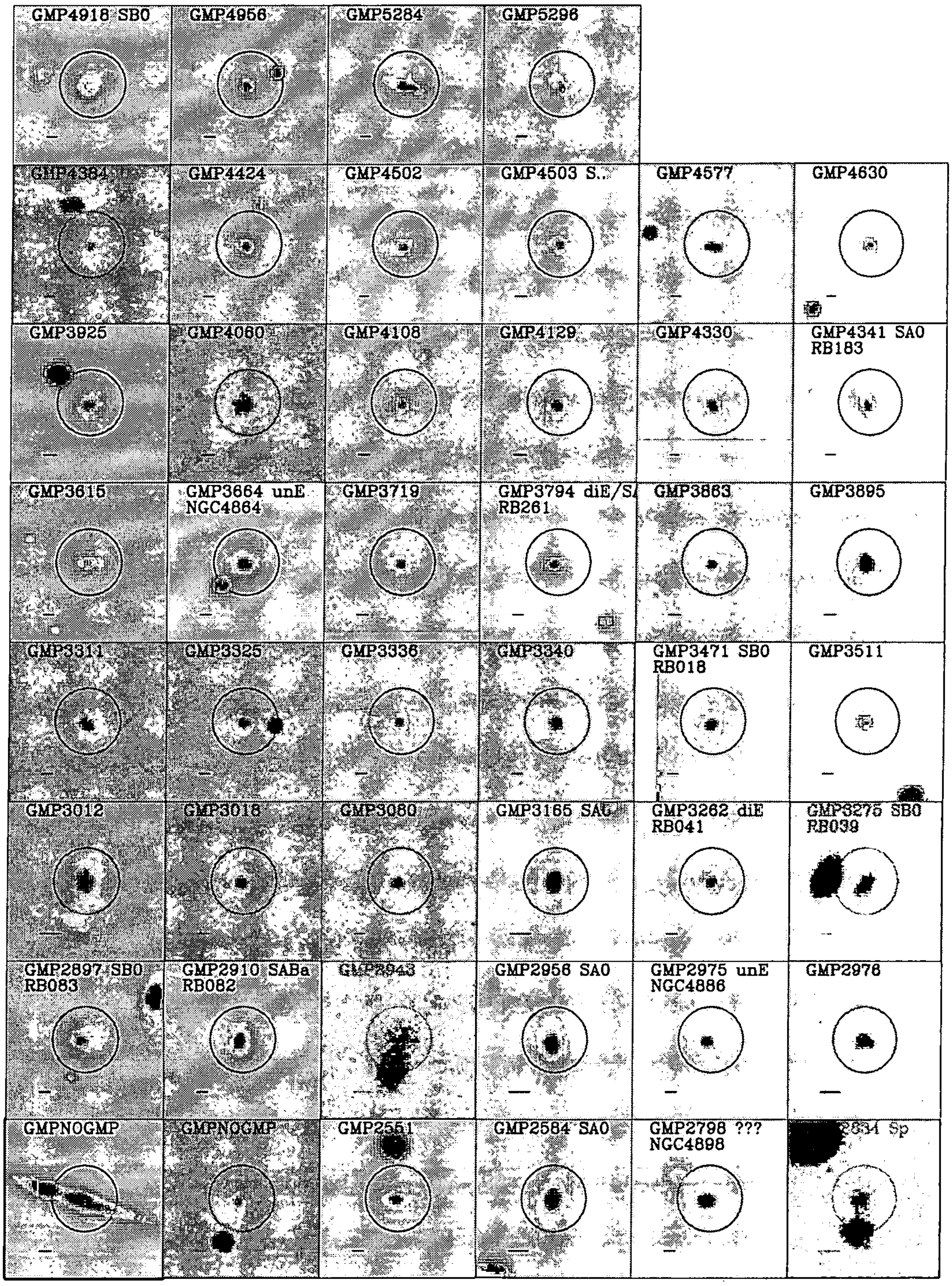

Figure 3.1: The V band images of the galaxies whose radial velocity puts them within the Coma cluster, but which have been rejected for some reason or another from our sample.The main reason for rejection is from overly close companions. Other reasons include a bad column in the CCD (as in GMP5296), or a cosmic ray, too close to the core of the galaxy to be properly removed. The text in each panel gives the GMP number of each galaxy, and its morphological type (if it has one). The next line gives any other name the galaxy might have as given by NED. If a galaxy has more than one name in NED, only the first one is given. The circle represents the 13$''$ diameter aperture used to measure the colours and magnitudes throughout this chapter, and the line at the bottom of each panel gives the width of the seeing disk for that image.

Dataset	Morphological types
(5) S0 morph	SA0 SAB0 SB0 diE/SA0 diE/SAB0 unE/SA0
(6) E morph	Epec boE diE unE
(7) Sp morph	SA0/a SB0/a SAB0/a SAB0p SABa S.. Sp SBa Sa

Table 3.1. This table shows what morphological types make up our different morphological datasets. The morphology types are those from Andreon et al. (1996) and Andreon, Davoust, & Poulain (1997). Table 3.2 shows the frequency of each morphological type in the whole dataset. The datasets that are not shown here (i.e. (iv) E & S0 morph) are simply made up by adding the above datasets. Some morphological types (i.e. Andreon's '???' category) aren't in any dataset.

outlier. The biweight is a robust, resistant and efficient location and scale indicator, as is apparent from table 3.4. Here the results of measuring the scatter in various subsamples of the cluster members (see section 3.3) using a straight forward biweight technique are compared to the results of using a biweight technique in conjunction with a single 3σ initial clip of the dataset. The difference in every case is within the 1σ error estimate of the un-clipped method. Using both the clipped, and the unclipped biweight, we can investigate the properties of subsamples of galaxies such as the late type subsample (dataset 7; defined in section 3.3), where we clearly see a well defined CMR ridge-line, but also many blue galaxies. The difference between the clipped and unclipped biweight clearly shows this (see table 3.4).

We not only used the biweight estimator to measure the scatter in the CMR, but by minimising the biweight scatter of the colour residuals, we used it to obtain a best fit CMR to the data (see appendix B for details).

The errors in the best fit relation were calculated by bootstrap resampling of the data. The observational uncertainties in the colour as a function of galaxy luminosity ($O_c(L)$) are well known for this dataset (see fig. 2.11), so in order to make an estimate of how much of the measured scatter in the CMR is due to observational errors, we defined a mean observational colour scatter thus,

$$\bar{O}_c = \frac{\sum O_c(L_i)}{N}$$

Morphological type	Number of galaxies
No morph	147
???	1
Sp	11
S..	5
SBa	1
Sa	3
SA0/a	6
SB0/a	2
SAB0/a	3
SAB0p	1
Total late type galaxies	32
SA0	42
SAB0	7
SB0	15
diE/SA0	4
diE/SAB0	1
unE/SA0	2
Total S0 type galaxies	71
Epec	1
boE	5
diE	10
unE	10
Total early type galaxies	26

Table 3.2. The frequency of each morphological type in dataset 1 (see table 3.3. This dataset is effectively all confirmed cluster members minus the galaxies deemed 'bad' (see section 3.2. About half of the galaxies have no morphological information. The four subdivisions in this table separate the galaxies into the gross morphological types used throughout this chapter, i.e. no morphology, late type (spiral), S0 and elliptical. When we refer to early type galaxies, we are referring to the S0 and elliptical galaxies grouped together.

where the L_i are the luminosities of the galaxies in the dataset, and N is the number of galaxies. Using this value for the observational errors, a value for the intrinsic scatter in the CMR can be calculated.

$$I = \sqrt{\sigma^2 - \bar{O}_c^2} \tag{3.1}$$

where σ is the observed scatter of the CMR. The intrinsic scatter as a function of observed scatter, both normalised by the observational errors is shown in figure 3.2.

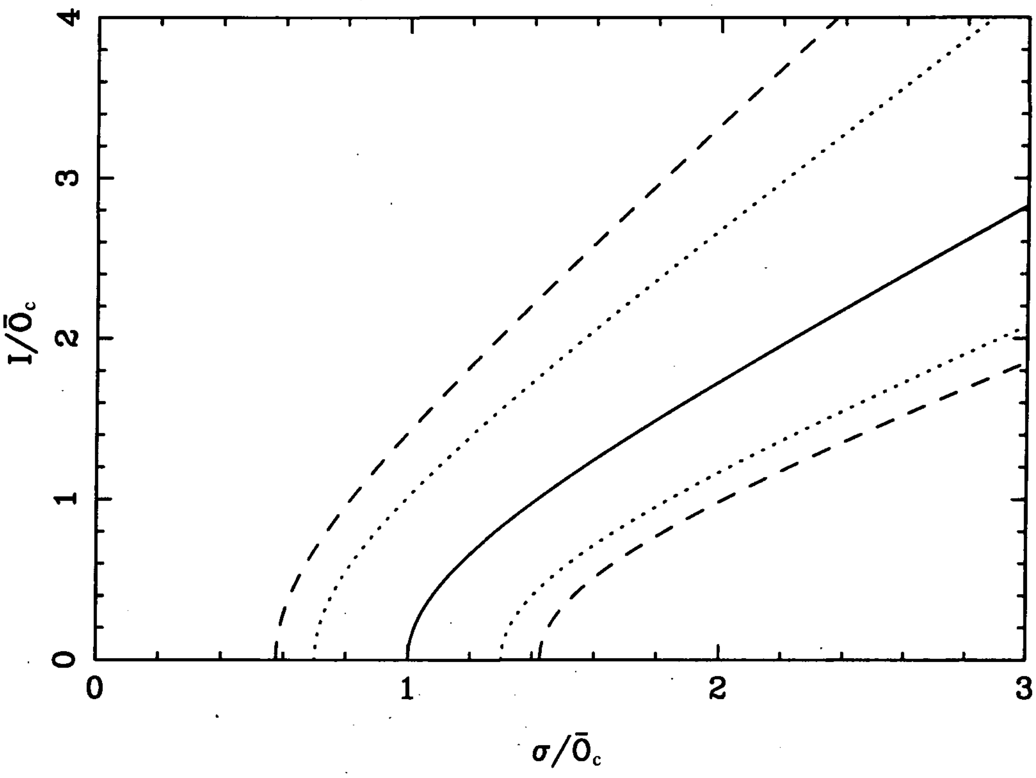

Figure 3.2: The intrinsic scatter (I) as a function of observed scatter (σ) in the CMR (the solid line, see equation 3.1). Both quantities are normalised by the observational errors ($\bar{O}_c$). The dashed and dotted lines are the 3σ limits for the cases where the CMR scatter is measured using 25 and 50 galaxies respectively (see equation 3.2).

We are measuring the scatter using N samplings of the distribution, which introduces an extra uncertainty over and above the uncertainty in the fit itself. We constructed a simulation in which we use the same techniques as used for the real data, i.e. specifically using biweight estimators, to ascertain the scatter of a simulated CMR with N galaxies. This simulation was repeated 1000 times for a series of N between 10 and 150. The results were used to derive the following expression for the limits on the intrinsic scatter (I) given a mean observational error in the colours ($\bar{O}_c$) and measured scatter σ

$$\sqrt{\frac{\sigma^2}{1 \pm \frac{n^2}{2(N-2)}} - \bar{O}_c^2} \tag{3.2}$$

where N is the number of galaxies in the CMR, and n is the significance of the limits. The 3σ ($n = 3$) limits for the cases of $N = 25$ and $N = 50$ are shown in figure 3.2.

For example, if we measure the scatter in the CMR (σ) to be ~ 1.3 times larger than the observational colour errors ($\bar{O}_c$), then the intrinsic scatter is about equal to the observational errors. If we have measured this scatter using 50 points, then the lower limit for the intrinsic scatter is ~ 0.2 times the observational error, however if we measured the scatter using only 25 points, we have no lower constraint on the intrinsic scatter. It should also be noted that the upper and lower limits are not symmetrical about the intrinsic scatter.

3.3 Environmental and morphological variations

Figure 2.13 shows the colour magnitude relation for every extended object in the photometric catalogue outlined in chapter 2. Many of the objects shown will not be members of the Coma cluster, yet despite this, the CMR is clearly visible down to $V_{25.2} = 19.5$mag. In this chapter, we are interested in measuring changes in the CMR, such as in its scatter or slope, in different parts of the cluster, in different subsets of galaxy morphology, and for different luminosities. We therefore concentrate solely on those galaxies identified as members of the cluster from their recessional velocity, which were not marked as 'bad' (see section 3.2). We have used the galaxies properties, such as morphology, luminosity and position, to define 14 subsets of these 275 member galaxies (see table 3.3 for details).

Figure 3.3 shows the CMR for dataset 1 (all cluster members). The overriding feature of this diagram is the strength of the CMR, it is made up of galaxies of differing morphological types, and from every part of the cluster, yet it extends for almost five magnitudes without deviating from a straight line. Figure 2.13 shows that the CMR actually extends fainter than this in our data, but we have no redshifts for these faint galaxies. Secker, Harris, & Plummer (1997) have shown that the $(B, B-R)$ CMR in dwarf ellipticals in Coma, actually continues down to at least $B \sim 21.5$. Another important aspect of figure 3.3 is in the direction of scatter. There is almost no scatter red-ward of the CMR ridge line, not even at the faint end where the observational errors are greatest, there is however significant blue-ward scatter, most of which is due to the late type population.

In the following sections, we investigate the properties of the CMR in each of the datasets (see figures 3.4, 3.5 and 3.6). We use the techniques described in section 3.2 to ascertain the scatter about the main ridge line of the CMR, as well as the scatter in the total sample. Throughout this chapter we will be using the 13arcsec diameter aperture

Dataset	Description
1	Confirmed members: After rejecting the 'bad' galaxies (see section 3.2), we classify all galaxies from $4000kms^{-1}$ to $10000kms^{-1}$ as members of the cluster. The velocities were obtained from the NASA/IPAC Extragalactic Database (NED). Most of the velocities can be attributed to Colless & Dunn (1996). Figures 3.12, 3.13, 3.14, 3.15 and 3.16 show snapshots of the V band images of these galaxies. All of the datasets in this table are subsamples of this dataset.
2	Confirmed members with $V_{13} < 17$: A subsample of confirmed members (dataset 1) with the faint tail cut off at the point where the measurement errors in the colours starts to increase (see figure 2.11).
3	All with morphology: All member galaxies with a morphology from Andreon et al. (1996) and Andreon, Davoust, & Poulain (1997) (see table 3.1).
4	E&S0 morphology: All member galaxies with an elliptical or S0 morphological type (Early type galaxies) (see table 3.1).
5	S0 morphology: All member galaxies with S0 morphology (see table 3.1).
6	Elliptical morphology: All member galaxies with Elliptical morphology (see table 3.1).
7	Late type morphologies: All member galaxies with late type (spiral and irregular) morphology (see table 3.1).
8	E&S0 center: Early type galaxies closer to NGC4839 than NGC4874.
9	E&S0 SW: Early type galaxies closer to NGC4874 than NGC4839.
10	E&S0 inner: Early type galaxies within 15′ of either NGC4874 or NGC3849.
11	E&S0 outer: Early type galaxies further than 15′ from both NGC4874 and NGC4839.
12	E&S0 bright: The bright half of dataset 4
13	E&S0 faint: The faint half of dataset 4
14	Members bright: The bright half of dataset 1
15	Members faint: The faint half of dataset 1

Table 3.3. This table describes how the galaxies in each dataset were selected. All datasets are a subset of dataset 1.

magnitudes and colours from chapter 2, due to their low photometric errors. The CMR fits to this data are summarised in table 3.4. Table 3.5 shows the results of using the estimated total V-band magnitudes from chapter 2. The results will be necessary for the analysis in chapter 4, but will not be used in this chapter.

Table 3.4. Results of regression analysis. For a complete description of each dataset see the main text. The 'full' and 'clip' columns refer to whether a sigma clipping iteration was added to the regression analysis or not. The 'full' dataset has no clipping applied, while the 'clip' datasets take the results from the regression analysis on the 'full' dataset, apply a 3σ clip and recalculate the regression results. This leads to better rejection of many of the 'blue' galaxies which lie well away from the colour magnitude relation, but these objects should not overly affect the biweight scatter indicator used here anyway, so we show both results. The errors quoted for the slope, intercept and observed scatter, are 1σ bootstrap errors. The mean obs. scatter ($\bar{O}_c$) is used in calculating the intrinsic scatter (see main text). It is a measure of the mean observational scatter in a dataset given that dataset's luminosity function and the luminosity dependence of the observational errors (see fig. 2.11). The upper and lower limits on the intrinsic scatter are 1σ limits, and are based on the observed scatter, the mean observational scatter and the number of galaxies in the dataset.

Dataset	Number		Slope	Intercept	Observed scatter (σ)		$\bar{O}_c$	Intrinsic scatter (I)		lower limit		upper limit	
	full	clip	clip	clip	full	clip		full	clip	full	clip	full	clip
(1) All members	275	245	-0.129 ± 0.001	3.39 ± 0.09	0.0744 ± 0.008	0.064 ± 0.005	0.029	0.069	0.057	0.065	0.054	0.072	0.061
(2) $V_{13} < 17$	175	159	-0.138 ± 0.003	3.52 ± 0.2	0.0674 ± 0.009	0.0608 ± 0.006	0.025	0.063	0.055	0.059	0.052	0.067	0.059
(3) All with morph	129	120	-0.143 ± 0.004	3.6 ± 0.3	0.0599 ± 0.008	0.055 ± 0.006	0.024	0.055	0.049	0.051	0.046	0.059	0.054
(4) E&S0 morph	97	95	-0.135 ± 0.005	3.48 ± 0.3	0.0552 ± 0.009	0.0536 ± 0.007	0.024	0.05	0.048	0.046	0.044	0.054	0.053
(5) S0 morph	71	69	-0.126 ± 0.006	3.34 ± 0.4	0.0583 ± 0.01	0.0557 ± 0.009	0.023	0.053	0.051	0.048	0.046	0.059	0.056
(6) E morph	26	26	-0.164 ± 0.006	3.91 ± 0.5	0.0438 ± 0.01	0.0438 ± 0.01	0.025	0.036	0.036	0.029	0.029	0.045	0.045
(7) Sp morph	32	25	-0.173 ± 0.01	4.08 ± 0.8	0.0778 ± 0.03	0.0576 ± 0.02	0.025	0.074	0.052	0.064	0.043	0.086	0.063
(8) E&S0 center	78	78	-0.132 ± 0.004	3.43 ± 0.3	0.0517 ± 0.008	0.0517 ± 0.007	0.024	0.046	0.046	0.041	0.041	0.051	0.051
(9) E&S0 SW	19	17	-0.153 ± 0.009	3.77 ± 0.8	0.0735 ± 0.06	0.0576 ± 0.03	0.024	0.069	0.052	0.058	0.042	0.086	0.067
(10) E&S0 inner	55	55	-0.149 ± 0.006	3.71 ± 0.3	0.0542 ± 0.01	0.0542 ± 0.01	0.024	0.049	0.049	0.043	0.043	0.055	0.055
(11) E&S0 outer	42	40	-0.12 ± 0.004	3.23 ± 0.3	0.0412 ± 0.01	0.0399 ± 0.01	0.024	0.033	0.032	0.028	0.026	0.04	0.038
(12) E&S0 bright	49	49	-0.135 ± 0.006	3.49 ± 0.6	0.0461 ± 0.009	0.0461 ± 0.008	0.025	0.039	0.039	0.033	0.033	0.045	0.045
(13) E&S0 faint	49	47	-0.132 ± 0.01	3.42 ± 0.8	0.065 ± 0.02	0.0612 ± 0.01	0.023	0.061	0.057	0.054	0.05	0.069	0.065
(14) members bright	140	128	-0.144 ± 0.004	3.62 ± 0.3	0.0657 ± 0.01	0.0589 ± 0.006	0.024	0.061	0.054	0.057	0.05	0.066	0.058
(15) members faint	136	118	-0.116 ± 0.005	3.16 ± 0.3	0.086 ± 0.02	0.0682 ± 0.008	0.054	0.067	0.042	0.061	0.035	0.074	0.049

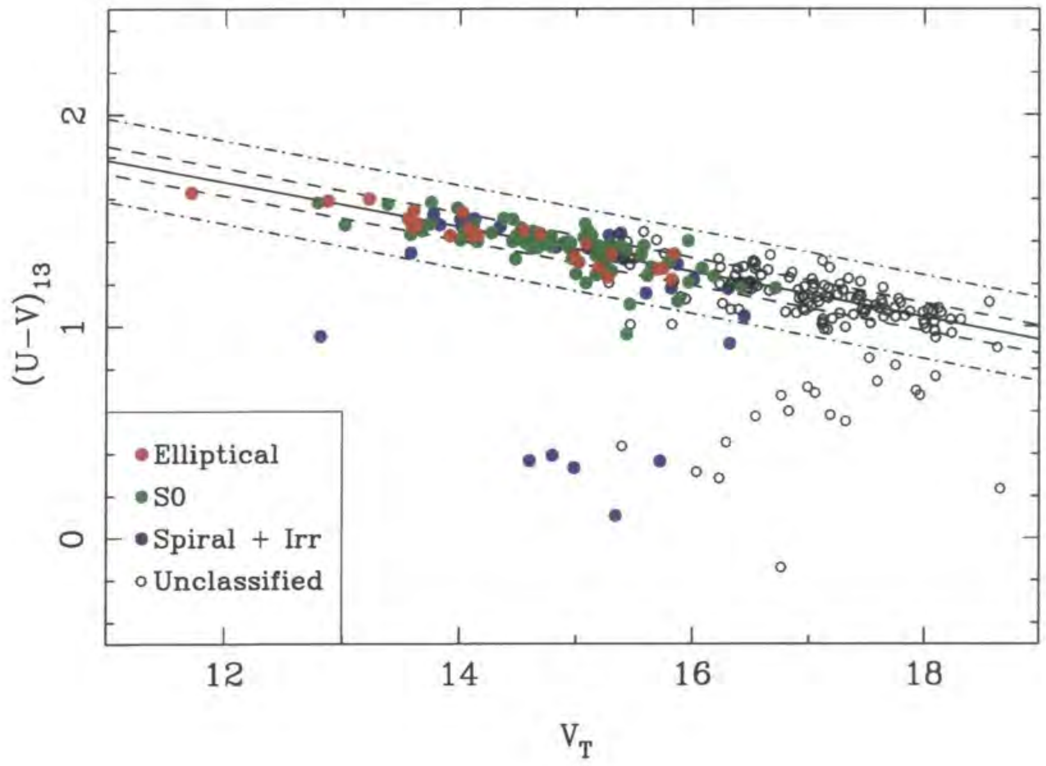

Figure 3.3: The colour magnitude relation for all galaxies determined as members of the Coma cluster through having a recessional velocity within $3000kms^{-1}$ of $7000Kms^{-1}$ (dataset (i)). The magnitudes are estimated total V magnitudes (V_T), whereas the colours are taken from $13''$ diameter apertures.Different colour symbols represent different morphological types as determined from Andreon et al. (1996) and Andreon, Davoust, & Poulain (1997). The solid line shows the best fit to the data using the biweight minimisation technique (see text). The solid line is a best fit to all the data points. The dashed lines show the 1σ and 3σ scatter after a single 3 sigma sigma clipping operation.

3.3.1 Morphological dependence of the CMR

In this section we examine variations in the CMR of galaxies of different morphological types. We use the broad morphological types defined in table 3.1. The dividing lines between the various types is somewhat arbitrary, and we err towards the later morphological types, i.e. we classify a galaxy of type diE/SA0 as S0, and one of type SA0/a as spiral. Because we have both a clipped and unclipped scatter indicator, we can investigate the scatter of the main ridge line of the CMR, and the amount of blue-ward scattering separately. Initially we shall concentrate on the ridge line, using the clipped scatter indicator. Looking at the morphologically segregated datasets (3,4,5,6 and 7) in table 3.4, they all have levels of intrinsic scatter indistinguishable within the measurement errors

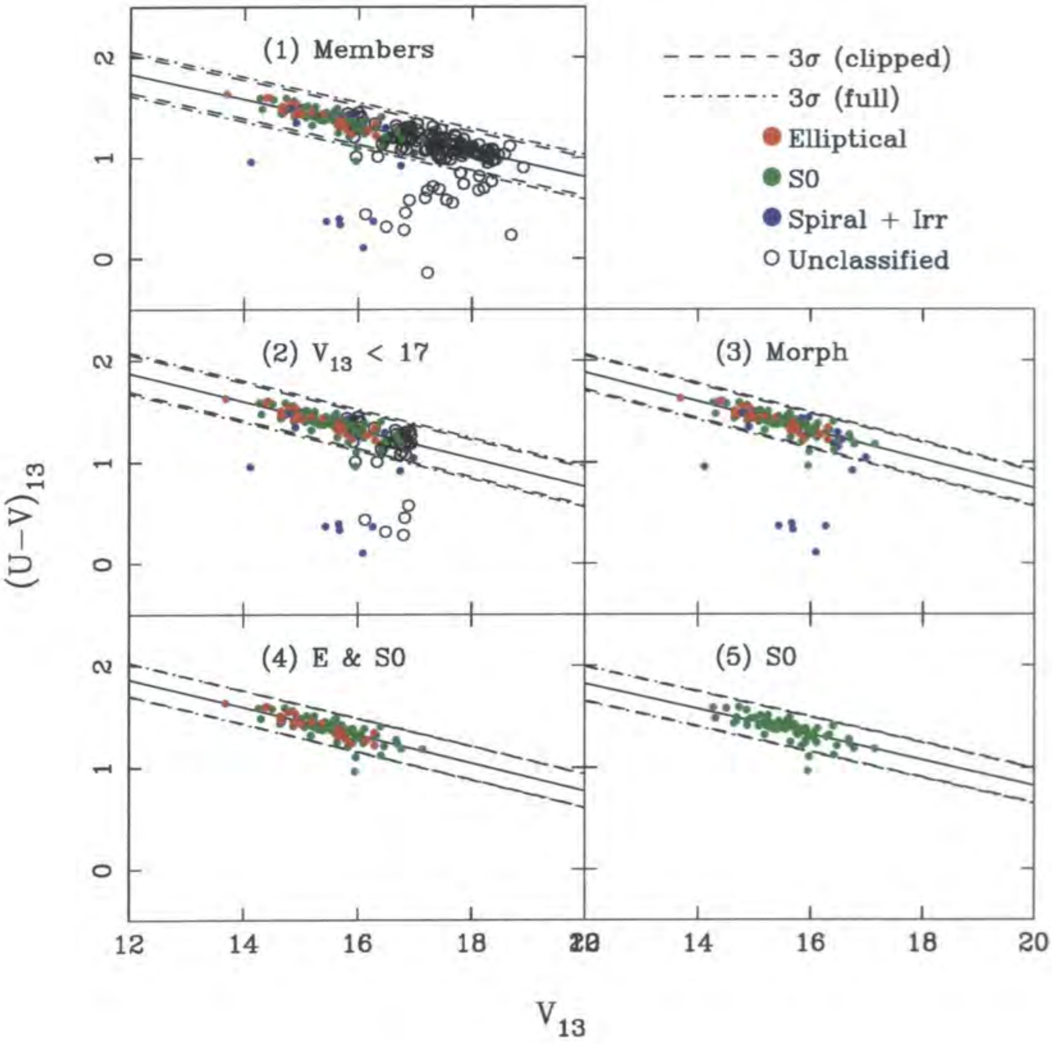

Figure 3.4: This figure, together with figures 3.5 and 3.6 show the CMRs for each of the datasets defined in the main text. The symbols are the same as those used in figure 3.3, however the dashed lines in these plots are different. They represent the 3σ scatter of the galaxies about the best fit line for the full dataset and for the clipped dataset. Because of the efficiency of the biweight scale indicator used (Beers, Flynn, & Gebhardt 1990) when dealing with outliers in non-Gaussian distributions, the clipped and non clipped datasets have similar measured levels of scatter for the most part.

($\sim$ 0.05mag), except for the elliptical galaxies (dataset 6) which has significantly lower levels of scatter ($0.036 mag$). It is worth noting that our late type galaxy dataset (7), has an indistinguishable CMR ridge-line from the S0 types. Figure 3.8 shows snapshots of the V band images of these 'red' spirals. All of the galaxies in figure 3.8 are within 3σ of the best fit CMR for dataset 6, so are included in the clip. Some of the galaxies are borderline SA0/a, however they are the minority, and cannot in themselves explain the low scatter. All of the 'red' spiral galaxies have fainter disks compared to the 'blue'

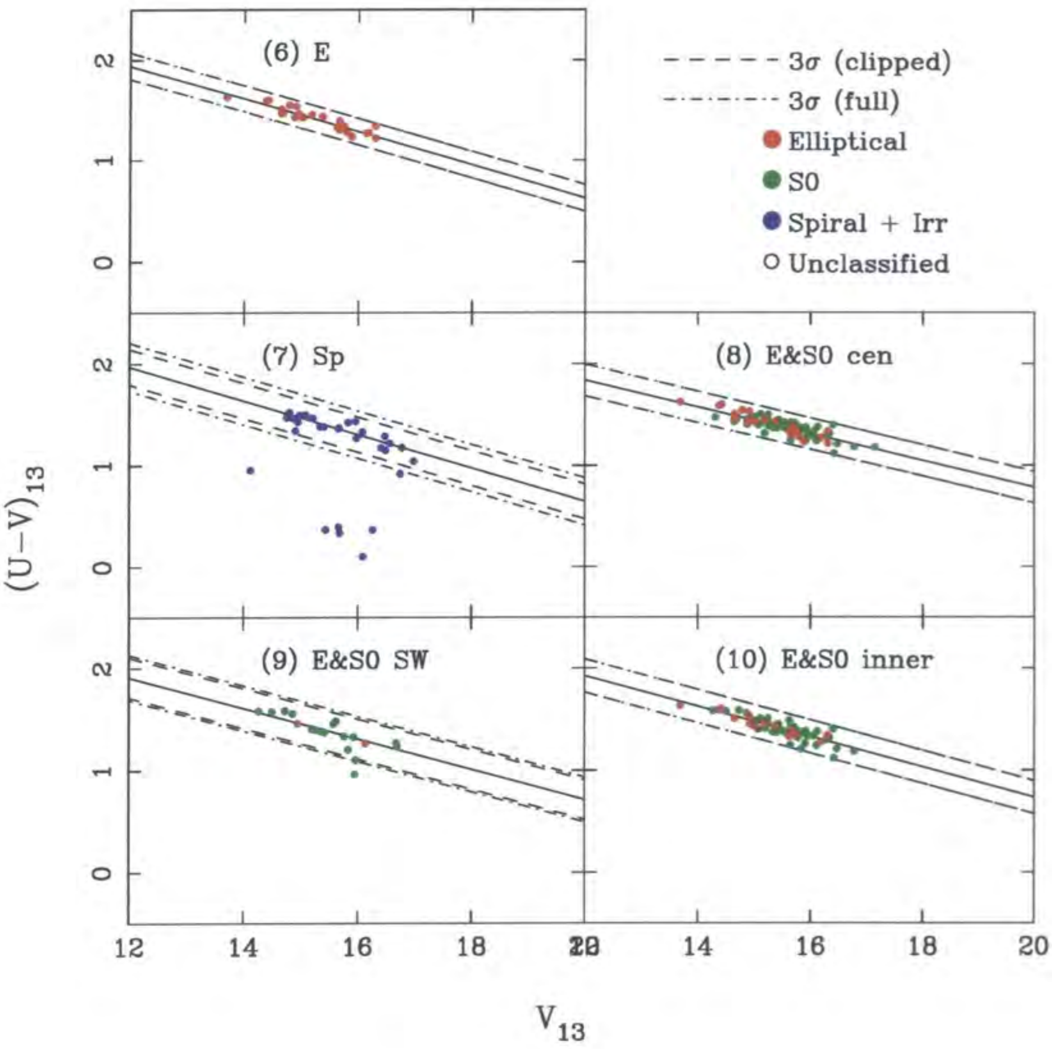

Figure 3.5: See figure 3.4

spirals in figure 3.7. The 'blue' spirals also seem to be more compact, thus more of the disk component appears in the 13″ aperture marked in the figures. We conclude that these 'red' spirals are 'anemic' (e.g. Van Den Burgh, 1991), and that they have lost their H_I gas through interactions with the intra cluster medium.

When we look at the results for the unclipped datasets, a difference between the morphological types appears. The ellipticals are unaffected, having had no galaxies removed by the clipping algorithm, and they still have the lowest intrinsic scatter. The S0 galaxies only had two galaxies clipped (GMP4945 and GMP4974), so their intrinsic scatter is only marginally increased to 0.053mag by their presence. The late type galaxies however, had seven galaxies clipped, six of which are very blue compared to the CMR ridge-line. The inclusion of these seven galaxies takes their intrinsic scatter to 0.074mag, however

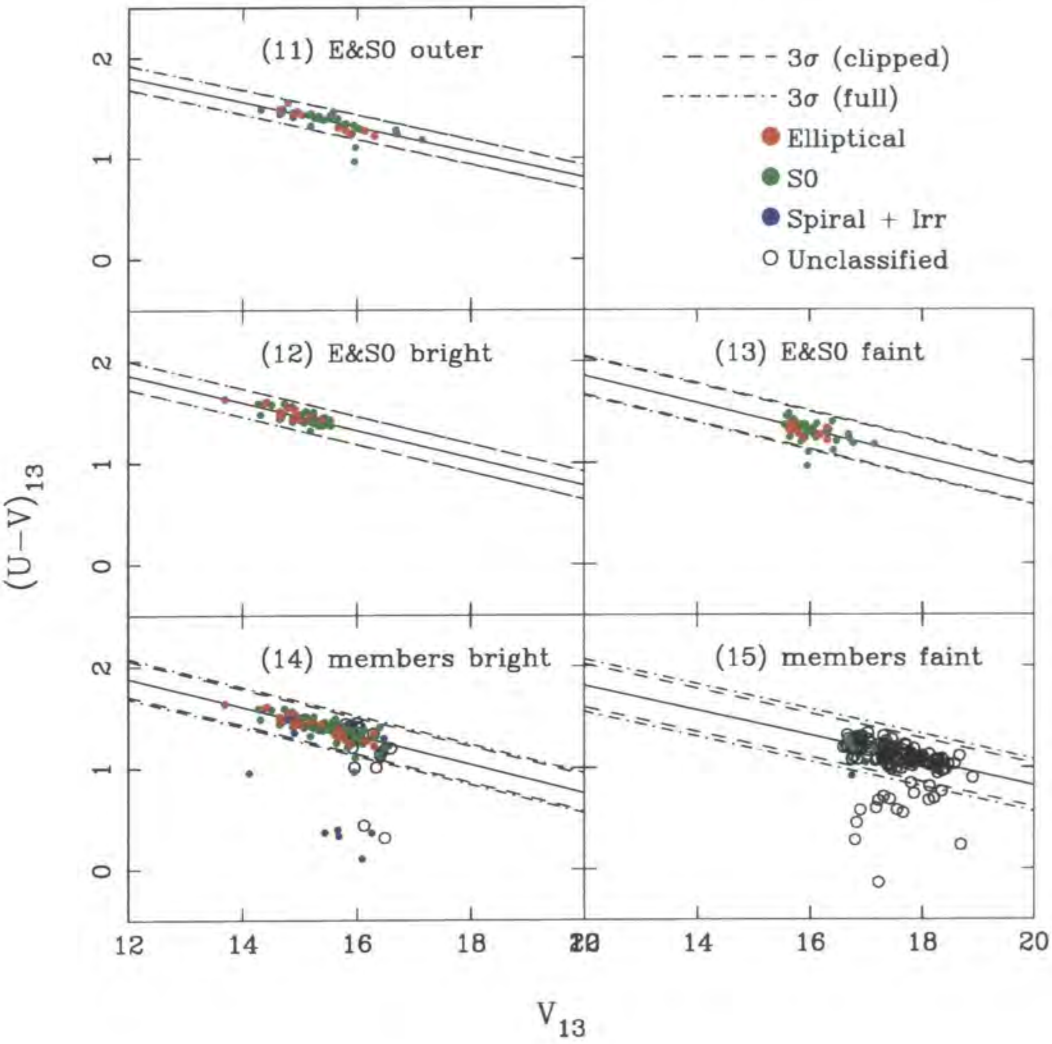

Figure 3.6: See figure 3.4

the presence of these blue galaxies is not surprising, as spiral galaxies are almost by definition actively star forming objects. Figure 3.7 shows snapshots of the V band images of these blue spirals, which even with our poor spatial resolution, can be made out to be very obviously late type. Perhaps the most surprising aspect of these galaxies, is not their presence, but the fact that there are only seven of them, out of the 32 late types in our sample.

The only other dataset with large numbers of 'blue' galaxies, is dataset 1 (all cluster members). These blue galaxies are, in addition to the late type galaxies noted above, morphologically untyped. Figure 3.9 shows V band images of all of the galaxies which deviate from the CMR ridge line for dataset 1 by more than 5σ. It is immediately obvious

Dataset	Number		Slope	Intercept	Observed scatter (σ)	
	full	clip	clip	clip	full	clip
(1) All members	267	237	-0.108 ± 0.001	2.98 ± 0.08	0.0774 ± 0.009	0.0665 ± 0.006
(2) $V_{13} < 17$	199	178	-0.107 ± 0.002	2.96 ± 0.1	0.0736 ± 0.009	0.0651 ± 0.007
(3) All with morph	127	117	-0.108 ± 0.003	2.98 ± 0.2	0.0643 ± 0.01	0.0585 ± 0.007
(4) E&S0 morph	95	93	-0.103 ± 0.002	2.9 ± 0.2	0.0589 ± 0.01	0.0572 ± 0.008
(5) S0 morph	69	67	-0.1 ± 0.004	2.87 ± 0.3	0.0635 ± 0.01	0.061 ± 0.01
(6) E morph	26	26	-0.111 ± 0.005	3.02 ± 0.3	0.0468 ± 0.01	0.0468 ± 0.01
(7) Sp morph	32	24	-0.139 ± 0.007	3.45 ± 0.6	0.0846 ± 0.07	0.0546 ± 0.03
(8) E&S0 center	76	75	-0.0997 ± 0.003	2.85 ± 0.2	0.0553 ± 0.008	0.0533 ± 0.007
(10) E&S0 inner	53	51	-0.103 ± 0.004	2.93 ± 0.3	0.0597 ± 0.01	0.054 ± 0.008
(11) E&S0 outer	42	39	-0.0987 ± 0.002	2.82 ± 0.2	0.0453 ± 0.01	0.0394 ± 0.008
(12) E&S0 bright	48	48	-0.0905 ± 0.003	2.73 ± 0.3	0.0452 ± 0.008	0.0452 ± 0.009
(13) E&S0 faint	48	47	-0.0958 ± 0.01	2.79 ± 0.7	0.0748 ± 0.02	0.072 ± 0.01
(14) members bright	138	126	-0.104 ± 0.004	2.92 ± 0.2	0.0713 ± 0.01	0.0643 ± 0.009
(15) members faint	130	112	-0.105 ± 0.003	2.92 ± 0.3	0.0859 ± 0.02	0.0684 ± 0.009

Table 3.5. This table shows the regression calculation, using the same method as table 3.4 but using the estimated total V magnitudes (see chapter 2. We have not attempted to calculate the intrinsic scatter, as the errors on the estimated total magnitude are not well defined. These values are not used further in this chapter, but are needed by the analysis of the CMR presented in chapter 4.

that they are predominantly of late type (e.g. GMP4570), although in some cases it is difficult to tell (e.g. GMP3848).

3.3.2 Luminosity dependence of CMR

The last set of datasets are the ones where we segregated the galaxies according to their luminosity (12,13,14 and 15). We have separated the early type galaxies dataset (4) into two halves of equal numbers, with the bright half of the galaxies in dataset 12, and the faint half in dataset 13.Because the members dataset (1) spans a much larger range in luminosity than do the datasets with only morphologically typed galaxies, we split that into two halves too (datasets 14 and 15).

The bright and faint early type galaxies have indistinguishable slope and intercept, however the bright sample has lower intrinsic scatter. This seems to be related to the lower scatter of the outer early type galaxies (dataset 11) compared to the inner (dataset 10), which has more faint galaxies. We cannot tell however, whether the inner galaxies

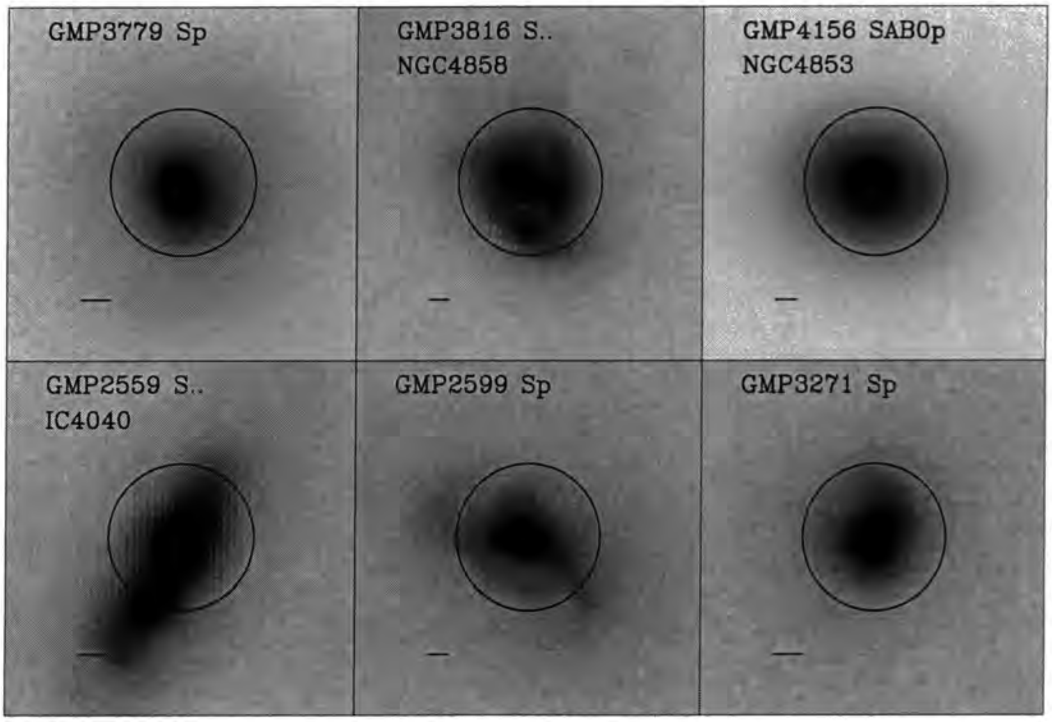

Figure 3.7: V band images of the spiral type galaxies which lie blue-wards of the measured CMR for spiral galaxies (dataset 7) by more than $5\sigma_{clip}$. The circle represents the $13''$ diameter aperture used in the measurements of both the colours and the magnitudes for the results in table 3.4. The line in the lower left of each panel shows the width of the seeing disk in each image.

have more scatter because they contain a larger number of faint galaxies, or whether the faint galaxies (dataset 13) have more scatter because they contain more inner galaxies.

The two halves of the complete members dataset, have differing slopes, but this seems to be nothing more than an aperture effect, as the slopes are indistinguishable when measured using the estimated total magnitudes (table 3.5). Although the observed scatter in the faint sample is larger than that of the bright sample, it has twice the mean observational error ($\bar{O}_c$). Once the difference in the observational errors is taken into account, both the bright and the faint samples have similar values for the intrinsic scatter.

3.3.3 Environmental dependence of the CMR

We have also defined subsamples of the cluster members according to their position in the sky. Datasets 10 and 11 contain galaxies which are either within 15arcmin of NGC4874 or not, respectively, while datasets 8 and 9 contain galaxies which are either nearer to NGC4874 or NGC4839 respectively (see table 3.3). We have restricted ourselves to

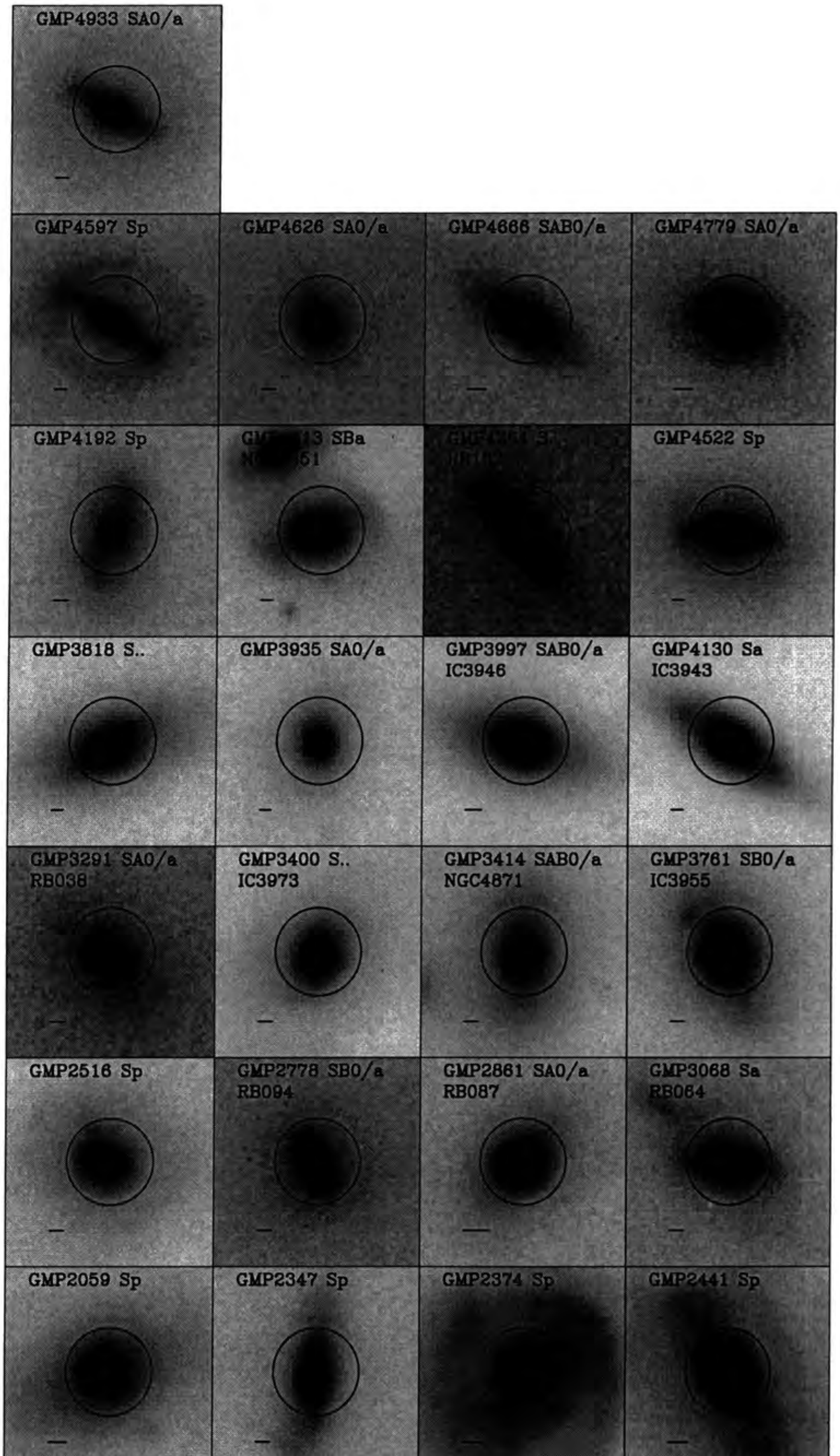

Figure 3.8: V band images of the spiral type galaxies which lie within $3\sigma_{clip}$ of the CMR for spiral galaxies (dataset 7). The circle represents the $13''$ diameter aperture used in the measurements of both the colours and the magnitudes for the results in table 3.4. The line in the lower left of each panel shows the width of the seeing disk in each image.

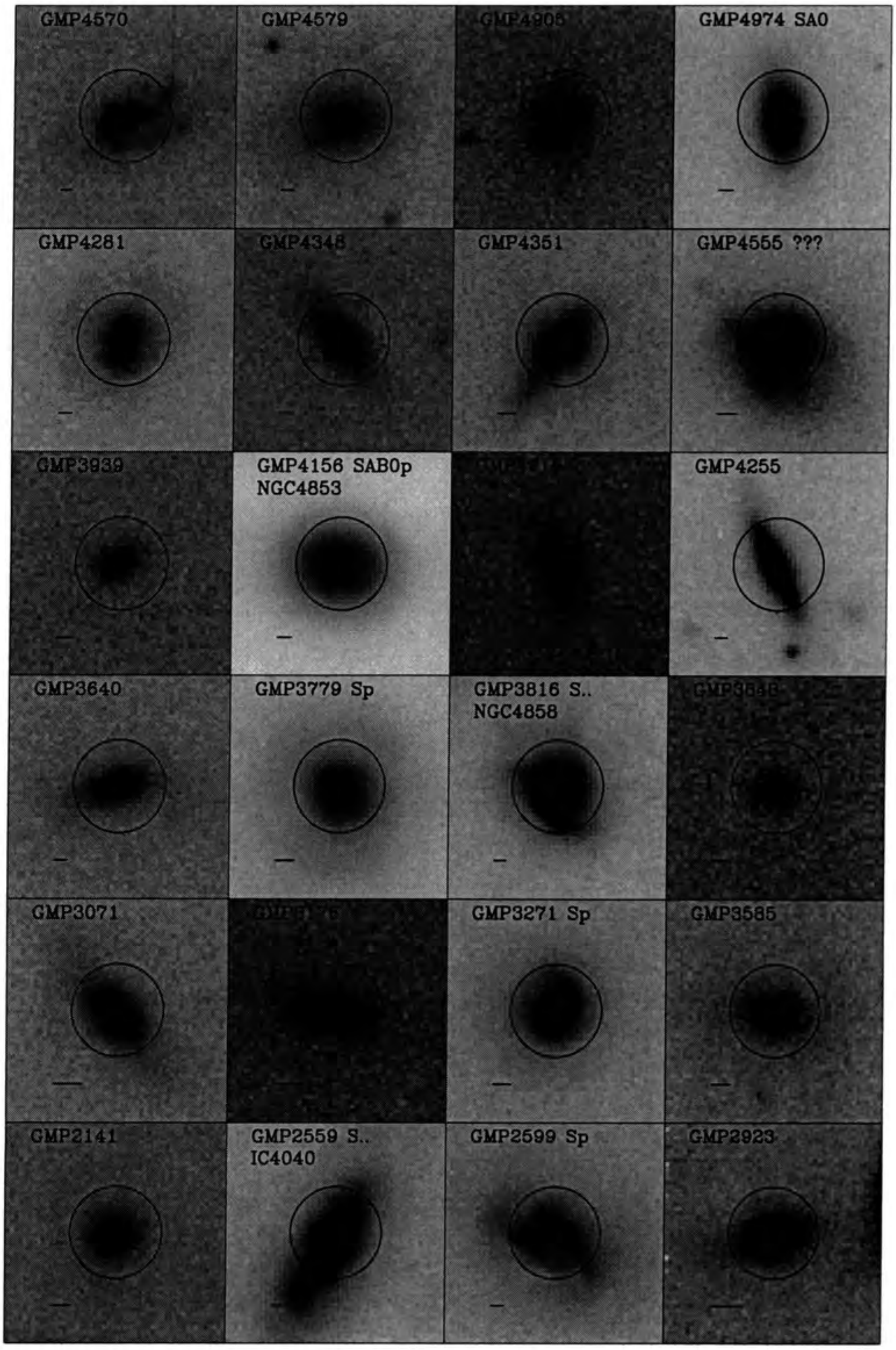

Figure 3.9: V band images of all of the galaxies which lie more than $5\sigma_{clip}$ blue-ward of the CMR for the members dataset (dataset 1). Text and symbols in the plot are as for figure 3.1. Of the galaxies that have morphologies, most are of spiral type, with only one SAO galaxy. Many of the galaxies without morphologies, also exhibit signs of late morphological types.

early type galaxies (ellipticals and S0s) to avoid as much as possible any bias arising from the morphology–density relation within the cluster, although section 3.3.1 showed there to be little variation in the properties of the CMR ridge-line between the different morphological types. The low number of galaxies in the SW sample make it very difficult to measure its scatter, the measured scatter in the full dataset is 0.07 ± 0.06, so we instead concentrate on the scatter in the central and outer samples (datasets 10 and 11). Here we see something unexpected. The outer dataset has less scatter (both observed and intrinsic) than the inner dataset. Although it is only marginally significant, it is just the opposite of what we would expect. Figures 3.5 and 3.6 show the CMRs for these datasets. From them we can see that they both have similar numbers of elliptical and S0 galaxies. There are too few elliptical galaxies in each dataset to be able to measure the scatter reliably for just the ellipticals in each one, but it is possible for the S0 galaxies. This shows the effect to be unrelated to morphology, with the 41 inner S0 galaxies having an unclipped observed scatter of 0.0597 ± 0.02 and the 30 outer galaxies having an unclipped observed scatter of 0.0377 ± 0.01. Figure 3.10 shows the luminosity function for both datasets. It shows that the inner dataset has more faint galaxies than does the outer one, but the majority of the galaxies are still in the magnitude range where the photometric errors stay almost constant (see figure 2.11). This is reflected in both datasets having the same mean observational errors (table 3.4).

3.3.4 Gradients

We have used a running biweight to attempt to determine whether the CMR scatter really does decrease towards the outer parts of the cluster. Firstly we excluded the galaxies around NGC4839 group, then we ordered the galaxies according to their projected distance from NGC4874, and calculated running biweight location and scale indicators for the residuals from the CMR ridge line for three datasets, the full dataset (1), the early type galaxy dataset (4) and a dataset of just the S0 galaxies (see figure 3.11). In all three panels, the $(U-V)$ residuals are calculated using the best fit CMR to the whole data, i.e.

$$\Delta(U-V) = (U-V) - (mV + c)$$

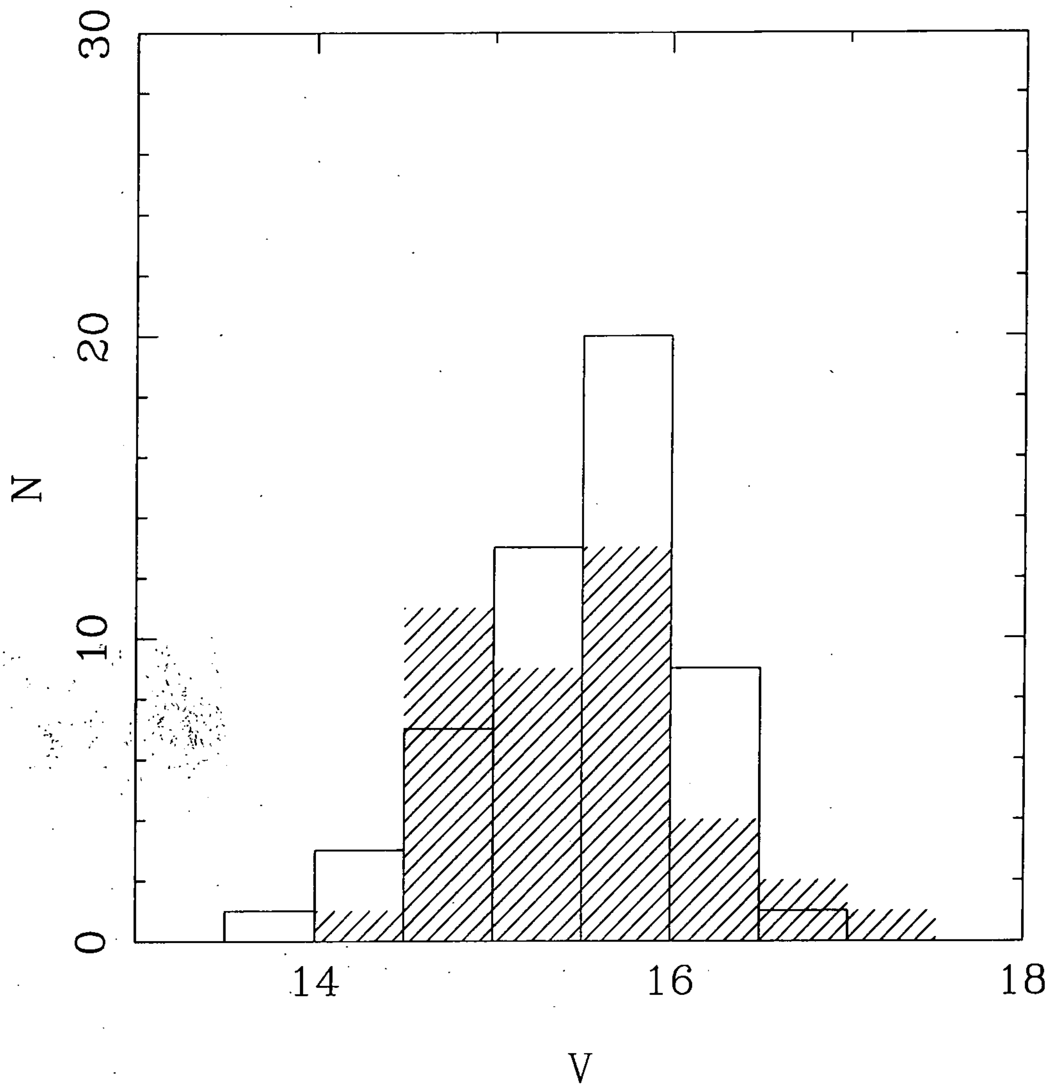

Figure 3.10: The luminosity functions for the inner and outer E+S0 datasets (10 and 11). The lined histogram represents the luminosity function for the outer dataset (11) and the outlined histogram represents the luminosity function of the inner dataset (10). Although the inner dataset has more faint objects than does the outer dataset, it is over a region where the observational errors in the photometry are hardly increasing at all, hence the mean observational errors for both datasets is the same (see table 3.4).

such that negative values of $\Delta(U-V)$ imply a galaxy is positioned to the blue side of the CMR ridge line. The m and c above are the slope and intercept of the solution from table 3.4. The first panel, using all the cluster members shows a slight increase in scatter with radius, however this could simply be due to the larger number of blue late types on the outer parts of the cluster. In order to avoid this, we used the early type galaxies dataset. This gets around the problem of faint galaxies by not including any, and similarly avoid the problem of blue late types. This time the scatter remains almost constant, with a

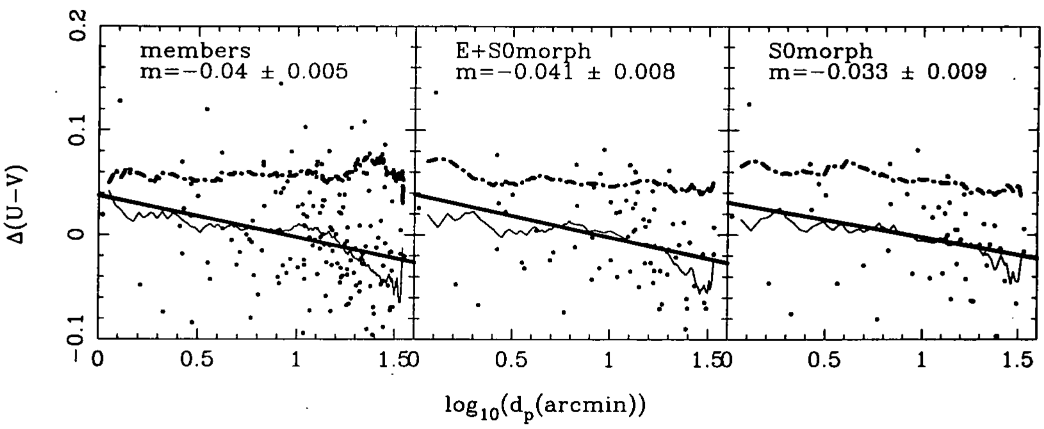

Figure 3.11: The residuals $(U - V) - (mV + c)$ of each galaxy from the best fit CM relation plotted against $\log_{10}$ projected distance from NGC4874 in arc minutes for three of the datasets described in the text. Objects around NGC4839 have been discarded. The thin line shows the running biweight location indicator and the thick line shows the running scale indicator. Both indicators have a maximum binsize of 40. This reduces to 10 at both ends. The solid straight line is a biweight fit to all of the data, the slope of which (m), and its 1σ bootstrap error is shown in each panel. The data extends out to $\sim 30arcmin$ from NGC4874. There is some evidence for decreasing scatter with distance in the E+S0 and the S0 panels, however it is only marginal and does not seem to be present in the complete cluster members dataset. Both the location indicator and the simple linear biweight fit show a progressive blueing of the residuals from the best fit CMR with increasing projected cluster-centric distance for all three datasets.

very small downward gradient. All three panels also show that the residuals from the CMR seem to getting systematically bluer towards the edges of the cluster. It seems unlikely that this could be an age effect without also incurring an increase in the scatter of the CMR, which leaves two possibilities. Firstly it could simply be a radial drift in our photometric zero points. Although we checked for this against the data of Bower, Lucey, & Ellis (see figure 2.12), it only extends out to a radius of 15 arc minutes, which is also where this effect begins to be noticeable. We can however make a quick estimate of the expected drift in our photometry. We have on average 20 objects in the overlap regions, with rms photometric errors of 0.026mag (see table 2.4), which gives an rms colour error between images of $0.026/\sqrt{20}$. Now to get to a radius of 30arcmin, we need to traverse at least 3 image boundaries, so the error accumulated is $\sqrt{3} \times 0.026/\sqrt{20} = 0.01$mag. However, the radius can be calculated in may different directions, and the photometric zero point for each image was indeed calculated in an iterative way such that any errors would dissipate in a two dimensional manner, so the value of 0.01mag (much smaller than the value of the colour gradient) can be regarded as an upper limit.

An alternative explanation could be that the galaxies in the center of the cluster are being reddened due to intercluster dust. The upper limit on the reddening through dust in the core of Coma, as compared to the field is $E(U-V) \leq 0.08$mag Ferguson (1993). could account for this amount of reddening, it could also add an extra source of scatter to the central parts of the cluster not present in the outer parts. Galaxies behind the cluster would appear both fainter and redder than an identical galaxy in front of the cluster. This would in effect increase the scatter in the CMR, but only in the central parts.

We can make a quick estimate for the contribution of this dust to the scatter in the core of the cluster. Firstly, we imagine we are looking at the core of the cluster down a pencil beam, and we define r as the distance from the core of the cluster down the beam, such that $r = -d/2$ is the front of the cluster, and $r = d/2$ is the rear of the cluster. d is the width of the cluster, and is somewhat arbitrary. We also assume that the galaxies and dust have the same isothermal density distribution:

$$\delta(r) = \frac{1}{1 + \left(\frac{r}{r_c}\right)^2}$$

where r_c is the core radius. The amount by which a galaxy at $r = x$ is reddened, is then

$$R(x) = \alpha \int_{-d/2}^{x} \delta(r)dr = \alpha r_c \left[arctan\left(\frac{r}{r_c}\right) + arctan\left(\frac{d}{2r_c}\right)\right]$$

α is a constant, which we chose in ordrer to satisfy our boundary condition, that we get the required reddening in the center of the cluster, i.e. $R(0) = 0.08mag$ (Ferguson 1993):

$$\alpha = \frac{0.08}{r_c\left[arctan\left(\frac{d}{2r_c}\right)\right]}$$

We then calculate the first and second moments of the distribution of $R(r)$:

$$\bar{R} = \frac{\int_{-d/2}^{d/2} R(r)\delta(r)dr}{\int_{-d/2}^{d/2} \delta(r)dr} = \alpha r_c arctan\left(\frac{d}{2r_c}\right)$$

and

$$\bar{R^2} = \frac{\int_{d/2}^{-d/2} R^2(r)\delta(r)dr}{\int_{-d/2}^{d/2} \delta(r)dr} = \frac{4}{3}\alpha^2 r_c^2 arctan^2\left(\frac{d}{2r_c}\right)$$

The standard deviation of $R(r)$ is then

$$SD(R) = \sqrt{\bar{R^2} - \bar{R}^2} = \frac{\alpha r_c arctan\left(\frac{d}{2r_c}\right)}{\sqrt{3}} = \frac{0.08mag}{\sqrt{3}} = 0.046mag$$

It should be remembered that this is a very rough model for the distribution of dust and galaxies in the cluster. The distribution of dust especially is very poorly known. Clearly from the fact that the levels of scatter in this model is greater that that measured for elliptical galaxies, we can say that the dust is either not distributed as an isothermal sphere, or that the limit for dust in the core is lower than the number quoted by Ferguson (1993).

The other possibility for the blueing towards the edges, is a difference in mean galactic age. Using the models for a single burst stellar population of age 10Gyr from Bower, Kodama, & Terlevich (1998), we find that $d(U-V)/dt \sim 0.03\text{mag/Gyr}$. This would make the outer galaxies approximately 2Gyr younger than the central galaxies. Assuming younger ages for the galaxy population, would make the difference in age between the inside and the outside smaller, i.e. if the galaxies are only 5Gyr old, the difference in age between the inner and outer galaxies is only 1Gyr. Abraham et al. (1996) find a $(g-r)$ colour gradient with projected radius in the $z = 0.23$ cluster Abell 2390 of $m = -0.08mag\ log10(r_p)^{-1}$, which they attribute to an age trend. To compare the Coma colour gradient with that of A2390, we used template early type galaxy spectra to K correct the Coma colours to the redshift of Abell 2390, and to convert them from $U-V$ to $g-r$. We find that the gradient shown in figure 3.11 for early type galaxies, is transformed into $m = -0.024mag\ log10(r_p)^{-1}$, a third of that measured in A2390.

A similar argument to the one above for the increased scatter in the core due to dust also applies in this case. When we look at the core, we also include galaxies in the foreground and background which are not in the cluster core, so are bluer than the core galaxies. This effect is not as large as the dust effect however, because the galaxies behind the cluster are just as blue as galaxies in front of it.

3.4 Discussion

We have placed new limits on the levels of scatter in the (U, V) CMR of the Coma cluster. The cluster members were split into groups depending on their morphology, luminosity or position on the sky, and the CMR was studied in each of them. We found the properties

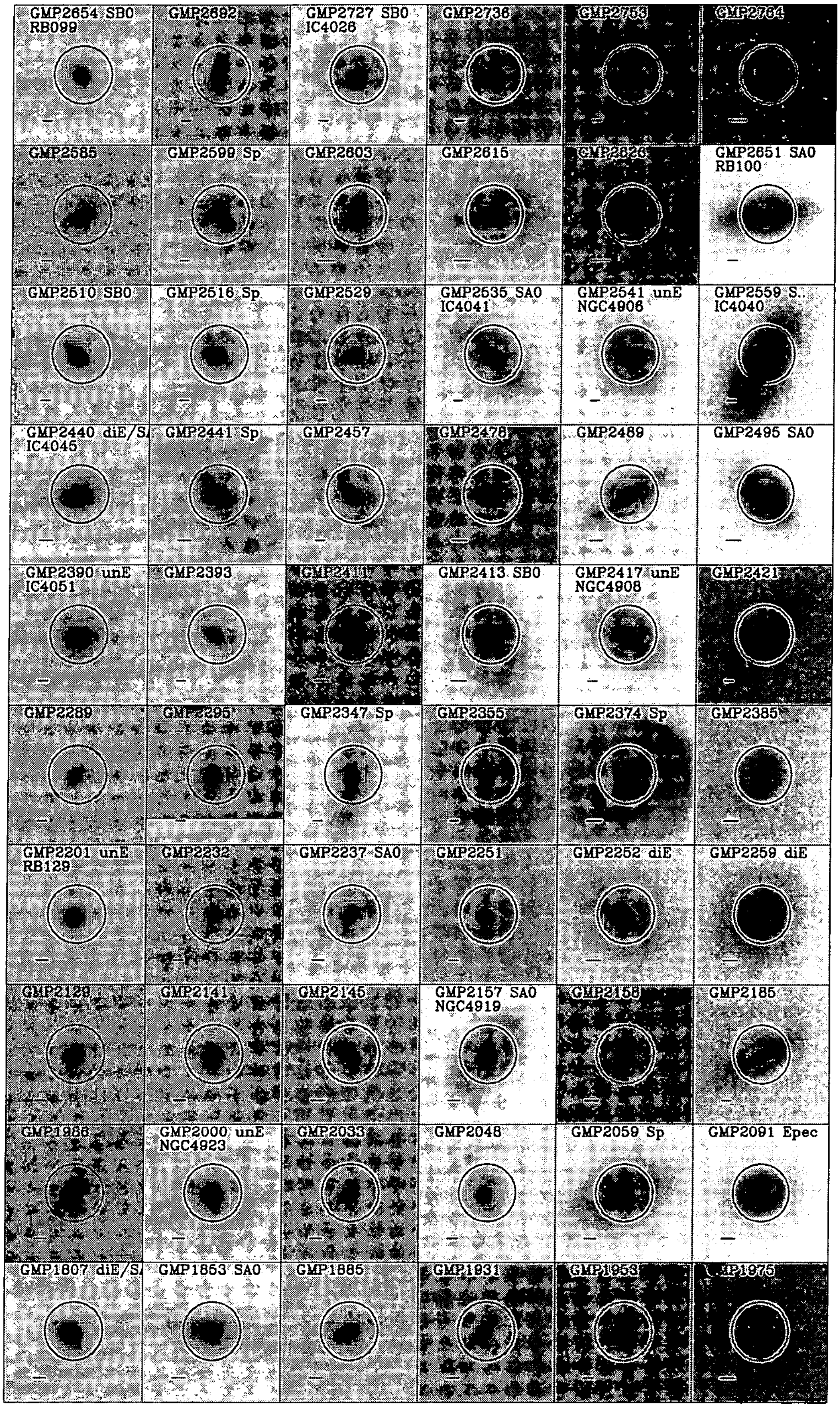

Figure 3.12: This figure, together with figures 3.13, 3.14, 3.15 and 3.16 show V band images of all of the confirmed member galaxies which have not been rejected (dataset (i)). The galaxies which have been rejected are shown in figure 3.1. The symbols and text in the panels are as in figure 3.1.

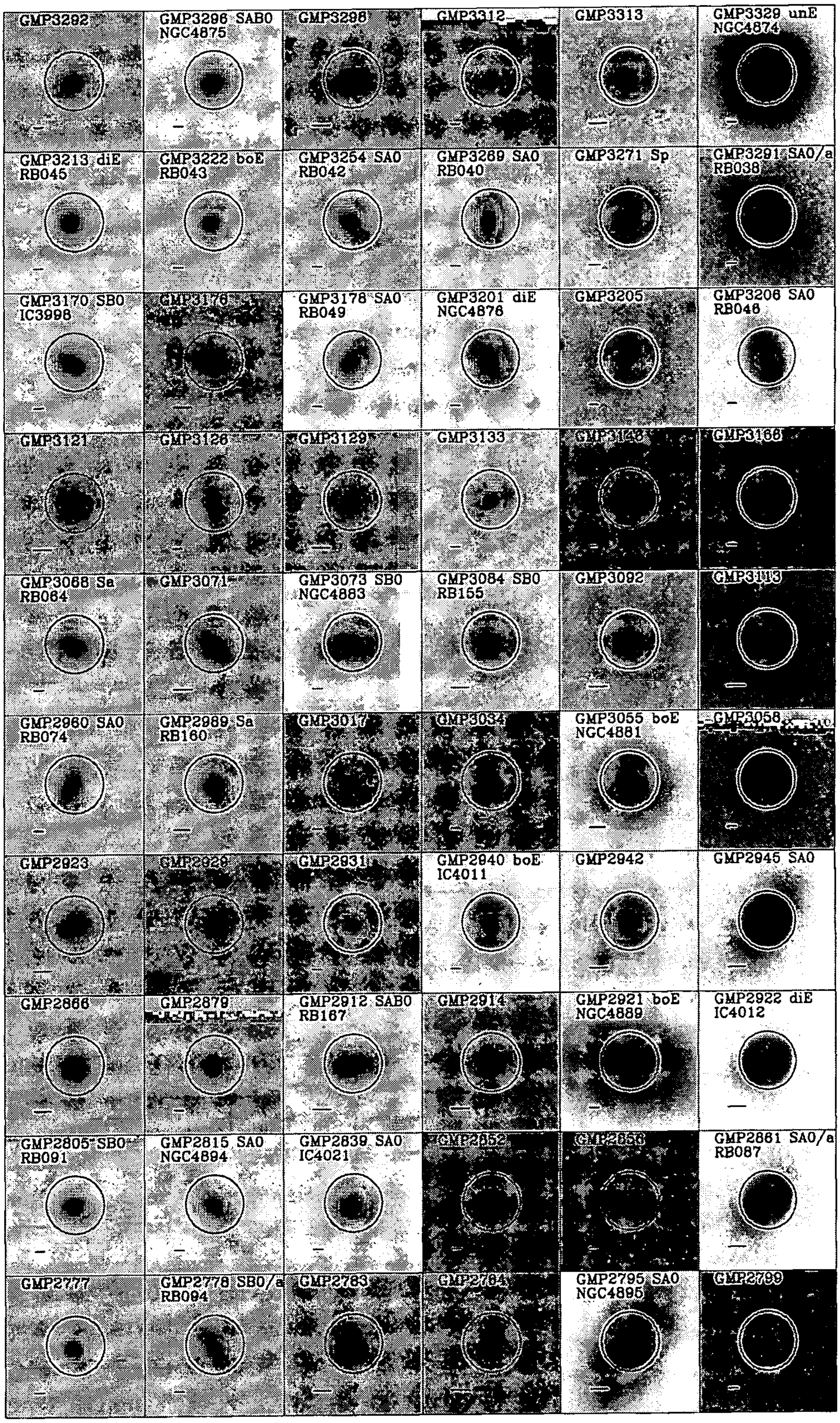

Figure 3.13: see figure 3.12

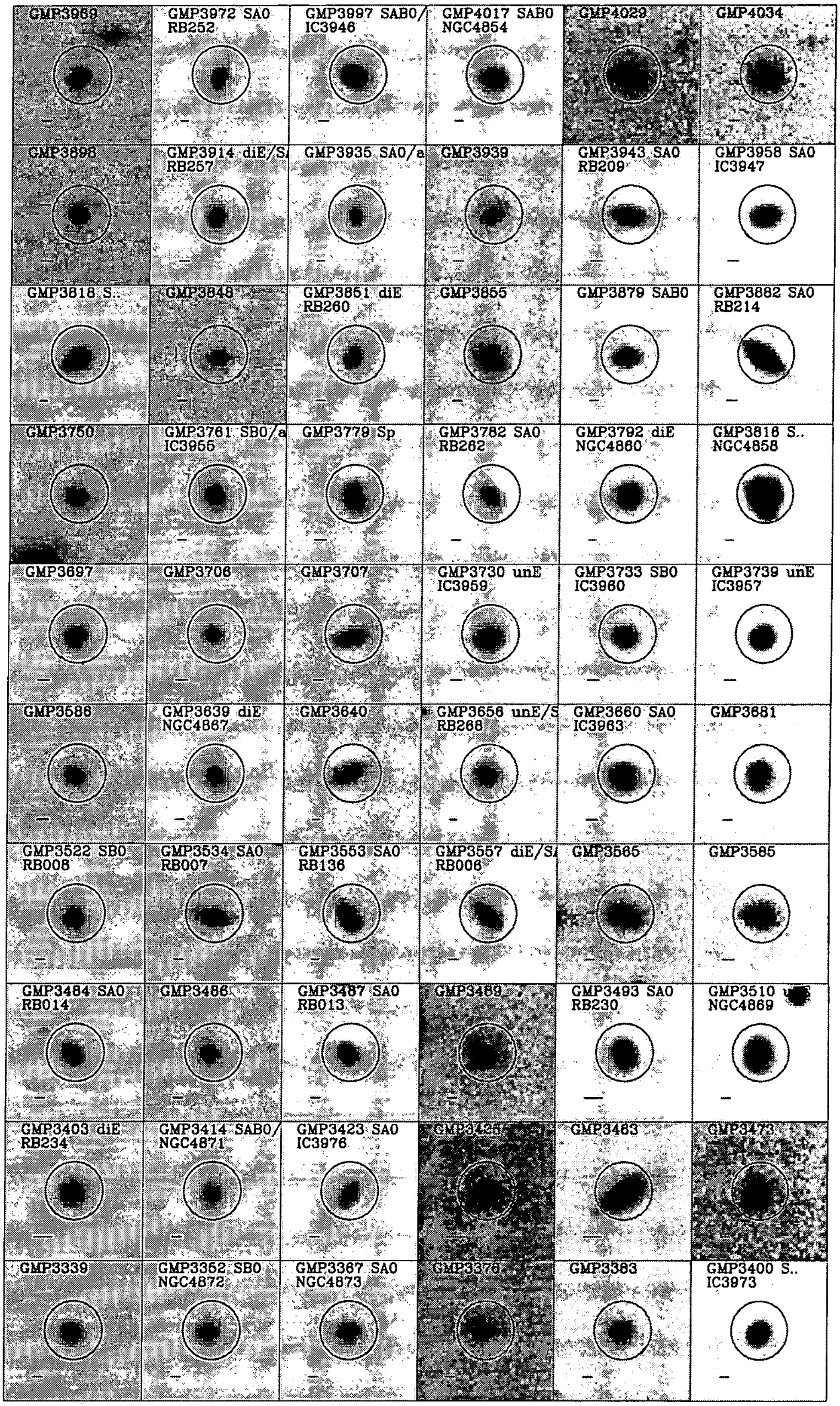

Figure 3.14: see figure 3.12

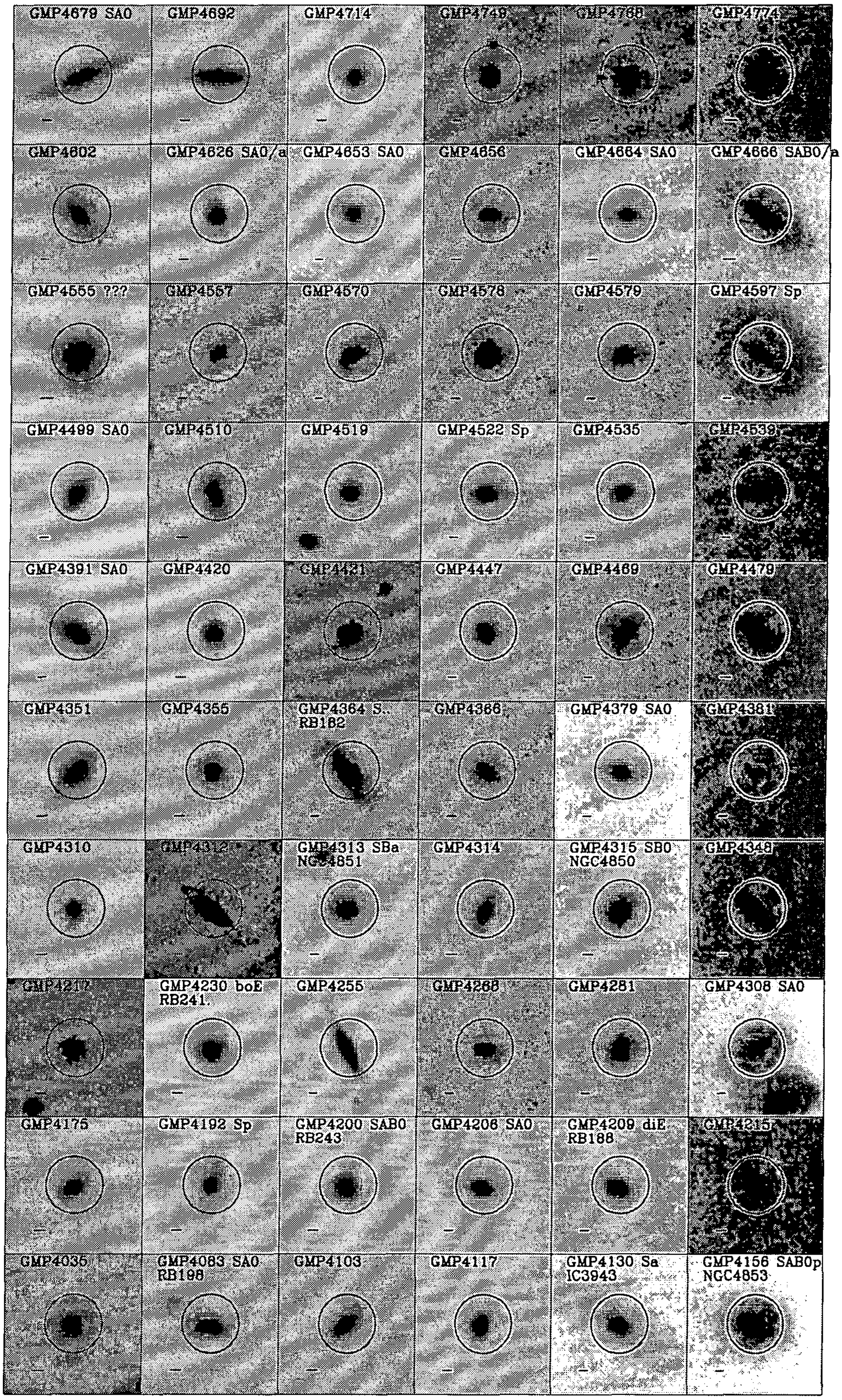

Figure 3.15: see figure 3.12

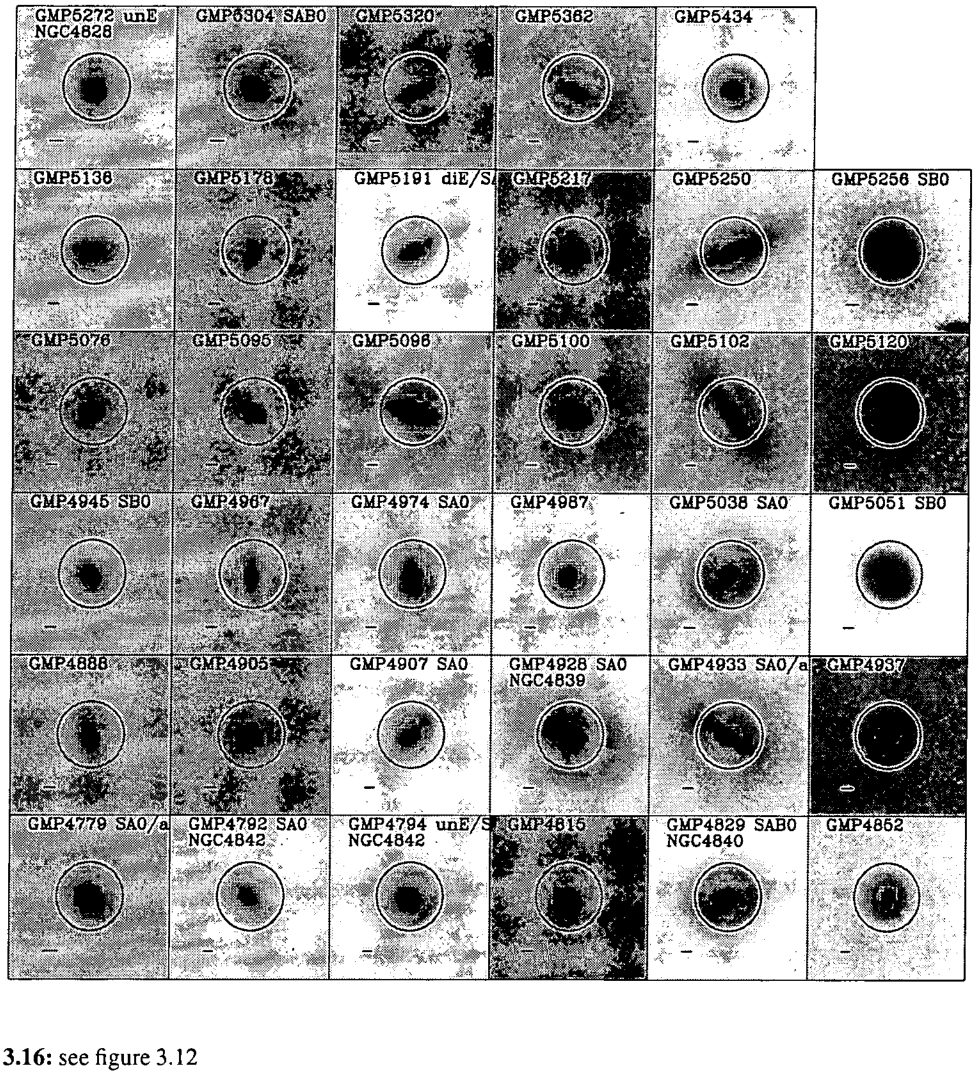

Figure 3.16: see figure 3.12

of the ridge-line to be surprisingly consistent between all of these groups. We have also calculated upper and lower limits for the intrinsic scatter in each galaxy sample, taking into account the low number statistics that we are dealing with for some of them. The results are presented in tables 3.4 and 3.5.

We find no variation in the slope of the CMR ridge-line between most of the different morphological types, apart from the late type galaxy sample, which has a marginally steeper slope, even when using estimated total magnitudes (table 3.5). This could be connected to the increased blue scatter we find towards the faint end of the CMR. In the galaxies for which we have morphological types, all of these very blue galaxies are late types. Figure 3.9 shows that even with our poor spatial resolution, which tends to make galaxies look of an earlier type, many of the unclassified blue galaxies are also of late type. The slope also remains constant with luminosity when using estimated total magnitudes, and with position of the galaxies within the cluster, indicating a universal metallicity/mass ratio.

The presence of such a large fraction of early type galaxies on the CMR ridge line, with no increase in the CMR scatter, is at first worrisome, but figure 3.8 shows that our 13arcsec aperture is dominated by bulge light, and that in every case, the galaxies possess only a very faint disk. This could be a low redshift analogue of the trend seen in high redshift clusters by Dressler et al. (1997) who conclude that ellipticals predate the cluster virialisation, but that late type galaxies turn into S0 galaxies upon encountering the cluster.

We find evidence for a colour gradient in the CMR corrected colours with projected cluster distance. Using a naive calculation for the expected slope in the photometric zero points, we conclude that it is at least a 6σ result. The slope of the gradient is approximately one third the size of that found by Abraham et al. (1996) in the $z = 0.23$ cluster Abell 2390, who attributed this to a gradient in the mean ages of the galaxies. We also find some evidence for decreasing scatter in the early type galaxies towards the outskirts of the cluster as compared with the central parts. The upper limit for $E(U-V)$ (Ferguson 1993) in the cluster core is approximately equal to the $U-V$ colour gradient observed, however we calculated the increased scatter produced in the CMR by the presence of enough dust in the cluster core to account for the colour gradient, and found that it was greater than the scatter observed in the elliptical galaxies. We therefore conclude that there cannot be sufficient dust in the cluster core to account for the entire gradient, and some must be due to age.

By comparing the colours with the stellar evolution models of Bower, Kodama, & Terlevich (1998), we estimate that the maximum age difference between the galaxies in the center of the cluster, and in the outskirts is 2Gyr. Although younger galaxies have more scatter in their CMRs than old galaxies (Bower, Lucey, & Ellis 1992b, Bower, Kodama, & Terlevich 1998), when we look at the core of the cluster, we are also being contaminated by young galaxies in front and behind the cluster.

3.5 Summary

- We place new limits on the intrinsic scatter of the CMR for elliptical galaxies in the core of the Coma cluster. We find the intrinsic scatter to be 0.036mag, with a lower limit of 0.029mag and an upper limit of 0.045mag.

- We have found no significant variations in the slope of the CMR between different morphological types of galaxy in the Coma cluster,apart from the late morphological type sample, which has a marginally steeper slope.

- We have found no significant variations in the slope of the CMR between different areas of the cluster, i.e galaxies within or without the central 15 arc minutes, and galaxies around the substructure associated with NGC4339 in the SW.

- We find no evidence for a variation of the CMR slope along its length, so long as the magnitude is a total one. When measured from a small aperture, the CMR slope increases at the bright end. We also find no evidence for an increase in the scatter of the CMR ridge-line with decreasing luminosity.

- Most of the galaxies bluewards of the CMR are either known late type galaxies (Andreon et al. 1996, Andreon, Davoust, & Poulain 1997), or seem to have late type morphologies (see figure 3.9).

- The intrinsic scatter of the CMR ridge-line is the same for S0 and for late type galaxies ($\sim$ 0.05mag). The elliptical galaxies have smaller scatter ($\sim$ 0.035mag).

– We find the scatter for the early type galaxies in the outskirts of the cluster to be marginally smaller than for the early type galaxies in the center. We also find a significant trend for the residuals about the CMR to become bluer with increasing distance from NGC4874. We rule out intra cluster dust as the sole effect, and conclude that there must be a radial gradient in the mean ages of the galaxies.

References

Abraham R. G. et al., 1996, ApJ, 471, 694

Andreon S., Davoust E., Michard R., Nieto J. L., Poulain P., 1996, Astronomy and Astrophysics Supplement Series, 116, 429

Andreon S., Davoust E., Poulain P., 1997, Astronomy and Astrophysics Supplement Series, 126, 67

Baier F. W., 1984, Astronomische Nachrichten, 305, 175

Beers T. C., Flynn K., Gebhardt K., 1990, AJ, 100, 32

Bender R., Burstein D., Faber S. M., 1992, ApJ, 399, 462

Biviano A., Durret F., Gerbal D., Le Fevre O., Lobo C., Mazure A., Slezak E., 1996, A&A, 311, 95

Bower R. G., Kodama T., Terlevich A. I., 1998, MNRAS, 299, 1193, astro-ph/9805290

Bower R. G., Lucey J. R., Ellis R. S., 1992a, MNRAS, 254, 589

Bower R. G., Lucey J. R., Ellis R. S., 1992b, MNRAS, 254, 601

Briel U. G., Henry J. P., Boehringer H., 1992, A&A, 259, L31

Caldwell N., Rose J. A., Franx M., Leonardi A. J., 1996, AJ, 111, 78

Caldwell N., Rose J. A., Sharples R. M., Ellis R. S., Bower R. G., 1993, AJ, 106, 473

Colless M., Dunn A. M., 1996, ApJ, 458, 435

Djorgovski S., Davis M., 1987, ApJ, 313, 59

Dressler A., Lynden-Bell D., Burstein D., Davies R. L., Faber S. M., Terlevich R., Wegner G., 1987, ApJ, 313, 42

Dressler A. et al., 1997, ApJ, 490, 577

Ellis R. S., Smail I., Dressler A., Couch W. J., Oemler J., Augustus, Butcher H., Sharples R. M., 1997, ApJ, 483, 582

Escalera E., Slezak E., Mazure A., 1992, A&A, 264, 379

Faber S. M., 1973, ApJ, 179, 731

Ferguson H. C., 1993, MNRAS, 263, 343

Frogel J. A., Persson S. E., Matthews K., Aaronson M., 1978, ApJ, 220, 75

González J. J., 1993, Ph.D. thesis, Univ. California, Santa Cruz

Jorgensen I., Franx M., Kjaergaard P., 1993, ApJ, 411, 34

Kodama T., 1997, Ph.D. thesis, Institute of Astronomy, University of Tokyo

Kodama T., Arimoto N., 1997, A&A, 320, 41

Kodama T., Arimoto N., Barger A. J., Arag'On-Salamanca A., 1998, A&A, 334, 99

Kuntschner H., 1998, Ph.D. thesis, Department of Physics, University of Durham

Kuntschner H., Davies R. L., 1998, MNRAS, 295, L29

Larson R. B., Tinsley B. M., Caldwell C. N., 1980, ApJ, 237, 692

Mehlert D., Bender R., Saglia R. P., Wegner G., 1998, in Untangling Coma Berenices: A New Vision of an Old Cluster, p. 107

Pahre M. A., Djorgovski S. G., De Carvalho R. R., 1995, ApJ, 453, L17

Persson S. E., Frogel J. A., Aaronson M., 1979, ApJS, 39, 61

Saglia R. P., Bender R., Dressler A., 1993, A&A, 279, 75

Saglia R. P., Burstein D., Baggley G., Bertschinger E., Colless M. M., Davies R. L., McMahan J., Robert K., Wegner G., 1997, MNRAS, 292, 499

Secker J., Harris W. E., Plummer J. D., 1997, PASP, 109, 1377

Van Den Burgh S., 1991, PASP, 103, 390

Vikhlinin A., Forman W., Jones C., 1994, ApJ, 435, 162

Visvanathan N., Sandage A., 1977, ApJ, 216, 214

White S. D. M., Briel U. G., Henry J. P., 1993, MNRAS, 261, L8

Worthey G., 1994, ApJS, 95, 107

Zabludoff A. I., Zaritsky D., Lin H., Tucker D., Hashimoto Y., Shectman S. A., Oemler A., Kirshner R. P., 1996, ApJ, 466, 104

Zepf S. E., Whitmore B. C., Levison H. F., 1991, ApJ, 383, 524

Chapter 4

Evolution of the Colour Magnitude relation through mergers.

Abstract. In this chapter, we address the question of whether the present day galaxies can have formed the bulk of their stars in smaller units, which subsequently merged. We use models based both on random and hierarchical merger scenarios to place limits on the amount of merging that can take place before the scatter in the CMR grows to unacceptable levels. We find that regardless of the model used for merging scenario, the CMR scatter does not increase to unacceptable levels so long as the merging within the cluster does not increase the mass of a 'typical' galaxy by more than a factor of two.

4.1 Introduction

The low levels of scatter in the colour magnitude relation can be used to place important constraints on the star formation histories of its constituent galaxies (e.g. see chapter 5). In the single burst model of galaxy formation, all the stars which will eventually form a galaxy in the present day, form in situ in a single burst. The star formation goes on unchecked until the most massive stars evolve to the supernova phase, injecting energy (and metals) into the inter stellar medium. The amount of time for which this enrichment phase continues depends on the size of the dark matter halo in which the galaxy sits. More massive dark matter haloes can contain the SN ejecta for longer than can low mass haloes, so the reprocessing of the ISM goes on for longer, building up higher metallicities. This supernova driven wind (or galactic wind) model (Larson 1974, Arimoto & Yoshii 1987) naturally explains the slope of the CMR as a trend of the mean stellar metallicity as a function of galactic mass.

The young stellar populations start off with very blue colours, but rapidly redden as the hot blue stars evolve off the main sequence. The colour of the population asymptotically approaches the colour of the reddest stars in the galaxy, making the colours of stellar populations are far more sensitive to their age for younger populations than for old ones. It follows that the only way of obtaining a small scatter in the CMR in such models is for either the formation of all of the galaxies to have occurred in some coordinated event, or for all of the galaxies to be so old that the differences in their ages no longer contributes overly to the scatter in the CMR. Bower, Lucey, & Ellis (1992b) used such a single burst model, together with stellar synthesis models for the evolution of the colours of single burst stellar populations (Bruzual A. 1983). They claimed that the bulk of stars in early type galaxies must have formed over 10Gyrs ago if their formation was only loosely coordinated, i.e. the spread in galaxy formation times was comparable to the characteristic collapse time scale at the epoch of formation. This constraint is not really loosened through the use of more realistic star formation histories, such as ones where the star formation rate (SFR) exponentially decays. Bower, Kodama, & Terlevich (1998) used the scatter in the CMR to place constraints on such exponentially decaying SFR models. They found that the CMR scatter only weakly constrains the epoch at which star formation ceases, but still requires the bulk of the stars to have formed at large look back times.

Differential evolution of the galaxy colours is not the only mechanism which increases scatter in the colour magnitude relation. About one third of local ellipticals have peculiarities, possibly associated with mergers/interactions (see Kormendy & Djorgovski (1989)). There is evidence for secondary bursts of star formation in high redshift clusters (e.g. Butcher & Oemler 1978, Butcher & Oemler 1984, Couch & Newell 1984, Couch & Sharples 1987, Barger et al. 1996), and also in local clusters (albeit much weaker than their higher redshift counterparts) (Caldwell et al. 1993, Caldwell et al. 1996). The UBV colours and $H\beta$ line strengths of local ellipticals are also correlated with the fine structure index, which measures the amount of dynamical disturbances in the galaxy (Schweizer et al. 1990, Schweizer & Seitzer 1992). This all points to galaxy interactions and mergers playing an important role in the recent history of early type galaxies in local clusters. It is important here that we distinguish between mergers in which substantial star formation takes place and those that take place between systems consisting only of stars, termed dissipationless merging by Bender, Burstein, & Faber (1992). Dissipationless merging between galaxies of different mass (and hence colour) will tend to average out the colours of the resultant galaxy, reducing the slope in the CMR. Because galaxies of the same final mass which formed out of a different distribution of fragment masses will have different final colours, dissipationless mergers also increase the CMR scatter. If the merging fragments contain gas, they can form stars in a burst during the merger. This burst will feel the potential of the new galaxy, so as with the supernova wind model above, the new stars will have metallicities (and hence colours) corresponding to the new galaxy's mass. Once this new stellar population ages, they will become redder than the stellar populations of the progenitors, thus reducing the destructive effect of the merger on the CMR. If enough gas is present in the merging fragments, and the merging takes place early enough in the evolution of the cluster (the differential evolution of the stellar population colours still constrains the bulk of the stars to be old), then the CMR will be preserved.

Extended Press-Schecter theory (Press & Schecter 1974, Bower 1991, Bond et al. 1991) gives a formalism for the merger history of dark matter haloes of the galaxies which end up in a given environment in the present day. By taking this gravitational framework and adding to it simple schemes for gas cooling, star formation and energy and gas feedback from supernova winds, White & Frenk (1991), Kauffmann, White, & Guiderdoni (1993), Cole et al. (1994) (and subsequent papers) have developed semi-analytical models for the formation of galaxies. Kauffmann (1996) and Kauffmann & Charlot (1998) are able to reproduce both the slope and scatter of the CMR in local rich clusters, despite the fact that considerable merging occurs between stellar components to form the final galaxies. This is due to the correlation between a galaxy's final mass, and the mass of its progenitors. In their model, larger galaxies form from systematically larger fragments than do smaller galaxies, thus preserving the CMR through the merging process.

One of the problems with these semi-analytical models for the formation of structure, is the lack of knowledge we have of many of the processes involved. The least uncertain of the processes involved are the dynamical evolution of the dark matter haloes, and the evolution of the stellar populations. The dynamical behaviour of the gas, and the feedback loops produced through the injection of energy, mass and metals into the gas by the stars is poorly understood, and the results of the models can be greatly modified through a large number of initial parameters which can at the moment only be determined through plausibility arguments.

In this chapter, we will attempt to construct a model for how the CMR evolves through merging in as simple a way as possible. The case in which mergers promote star formation cannot be considered in general terms and a specific model for star formation in galaxy mergers, and the conversion between hot and cold gas phases is required (eg., Kauffmann & Charlot (1998), Baugh et al. (1998) [BCFL]). So instead, we bypass the poorly understood area of star formation, feedback and gas dynamics by concentrating entirely on dissipationless mergers, and construct our models, where possible, to be insensitive to the choice of any initial parameters we introduce. By investigating the effects of dissipationless mergers upon the CMR we shall attempt to illuminate the general constraints that can be derived regardless of the specific star formation model, and thus determine whether the hierarchical models really do produce low scatter CMRs through their correlated merger histories, or through fine tuning of their star formation processes.

4.2 Models for the Merger Histories of Galaxies

In order to model how the CMR evolves through dissipationless mergers, we allocate galaxies to an initial 'primordial' colour magnitude relation. We assume that the initial relation is exact and that there is no differential evolution of galaxy luminosities and colours. This is clearly an over simplification, but it distinctly separates the effects of the evolution of the stellar population from those due to the merging of galaxies. Under these conditions, the slope of the initial relation is the only parameter connecting the galaxy mass with its colour. We emphasise that this scaling is arbitrary, and that choice of a steeper initial slope simply re scales the final slope and the final scatter. The key parameter that must be matched is the ratio between the scatter about the average CMR and its slope.

$$\mathrm{R} = \frac{scatter}{final\ slope}$$

This ratio is independent of the initial slope in the model. Thus, without knowing the initial slope of the relation, we can use R to place an upper-limit on the importance of dissipationless mergers.

The primordial CMR is evolved to the present day using a merging model. To correctly account for the gravitational evolution of the galaxies' dark matter haloes, and to calibrate the evolution onto a (model dependent) redshift scale, we evolve our pseudo CMRs using merger histories as defined by the simulations of BCFL, we will refer to this as the 'hierarchical' merger model. In order to test the significance of the correlations in the hierarchical model (Kauffmann 1996, Kauffmann & Charlot 1998), and to test for model dependence of the results, we have also formulated a 'random' merger model in which we remove any mass correlations in the merger history trees.

4.2.1 Hierarchical clustering

In order to generate galaxy merging histories, we use the formalism described in BCFL. This first generates a tree of merging haloes using the Monte-Carlo prescription outlined in Lacey & Cole (1993). In order to follow the merging history of galaxies, an additional ingredient is required: the merging of galaxies within a common halo. BCFL use the merger time-scales as parameterised by Cole et al. (1994), who argue that the two most important factors governing the probability of a collision between two galaxies occurring within a dark matter halo are:

- Dynamical friction, A galaxy orbiting in a dark matter halo experiences a drag force, causing its orbit to decay and increasing the probability that it will undergo a collision. This process has a time-scale which decreases as the galaxy's mass increases.

- The probability of a merger between two galaxies which do collide, increases with increasing ratio between the internal velocity dispersion of the galaxies involved, to the encounter velocity (White 1976, Aarseth & Fall 1980), and also to M_{sat}/M_{halo}, where M_{halo} is the mass of the dark matter halo in which the galaxies collide, and M_{sat} is the initial mass of the halo around the infalling galaxy.

Cole et al. (1994) therefore parameterise the merger time-scale (τ_{mrg}) as a simple scaling law

$$\tau_{mrg} = \tau^0_{mrg}(M_{halo}/M_{sat})^{\alpha_{mrg}} \quad (4.1)$$

and fix the free parameters (α_{mrg} and τ^0_{mrg}) using N-body/hydrodynamic simulations (Navarro, Frenk, & White 1995) to $\alpha_{mrg} = 0.25$ and $\tau^0_{mrg}/\tau_{dyn} = 0.5$, where τ_{dyn} is the dynamical time scale of the halo, defined as half the age of the universe at the time when the halo forms.

Galaxies that have dynamical friction time scales less than the merger time scale of the halo are assumed to merge with the dominant galaxy. Since the dynamical friction time scale is shorter for more massive galaxies, this naturally generates a tendency for large galaxies to form from mergers of massive galaxies. This approach is generic to all hierarchical galaxy formation codes. We use the code of BCFL to produce a list of galaxy fragments and their evolution as a function of redshift. We emphasise that this is only used to produce the initial CMR and to select galaxies to be merged; BCFL's parameterisation of the star formation process is ignored in what follows.

To allow a comparison with local rich cluster CMR data, it is important that we only select merger histories corresponding to galaxies that are found in rich clusters at the final time. We incorporate this requirement by only constructing merger trees for objects bound into a dark matter halo with circular velocity greater than 1000 km/s at the final time. In order to reduce computational overhead, also require that the final galaxy has absolute V-magnitude brighter than -19 in BCFL's simulations. The final results are unaffected by the cut off since we determine the slope and scatter over only the brightest 4 magnitudes of the simulated CMR (see section 4.3)). We ran some models without the $V = -19$ cutoff to verify this.

Once the galaxy merger tree has been constructed, our approach diverges from the modelling of BCFL. We start by selecting an initial epoch (z_{form}). The galaxy fragments present in the tree $z = z_{form}$ are given a magnitude scaled to the log of their total baryonic mass, and a colour according to an initial 'perfect' CMR (ie., colour =

slope × magnitude + offset). As we have already emphasised, the 'colour' we calculate is purely illustrative and serves only to show the effect of mixing the stellar populations. We make no attempt to justify the initial zero-point or slope that is applied. The evolution can then be followed by simply combining the magnitudes and colours of the fragments as they merge to form the final galaxies at $z = 0$. At some points in the tree the proto-galaxies merge with 'new' fragments (fragments with progenitors that are below the mass resolution of the merger code); in order to be consistent with our dissipationless phenomenology, we do not incorporate these objects in to the merger scheme. In any case, the treatment of these objects is only significant if $z_{form} > 2.5$; At later times, most of the mass which will form the galaxies in the final time step is already present in the merger tree. Each tree leads to the formation of a single galaxy at the present epoch. In order to match the numbers of galaxies in our observational sample the process is repeated in order to generate a realisation of the CMR.

Panels a, b & c of Figure 4.1 show examples of the present-day CMRs that we derive by this approach. If the relation is established at relatively low redshift, the amount of merging is low enough that little evolution of the initial slope occurs. By contrast, a relation that is established at higher redshift is considerably weakened due to the large number of mergers that have taken place. Despite this, a discernible CMR exists at the present-day even if the initial relation is established at $z > 2.5$. We fitted the CMR of the brightest four magnitudes of the relation by using the same biweight scale minimisation method as used for the Coma cluster CMR in chapter 3 (see appendix B for a description of the method). This is shown by a solid line in each of the panels. The robustness of the CMR to merging is surprising. As we show below it is due to the slow rate of mass growth in the hierarchical merger tree at late times.

4.2.2 Random mergers

In order to test the importance of the merger correlations in the hierarchical model, we repeated the Monte Carlo process using randomised merger trees. In order to be able to compare our results directly, we have based the simulation on the same galaxy merger trees used in the hierarchical model to imprint the initial CMR at $z = z_{form}$. However, rather than merging the fragments as ordered by the hierarchical tree, random

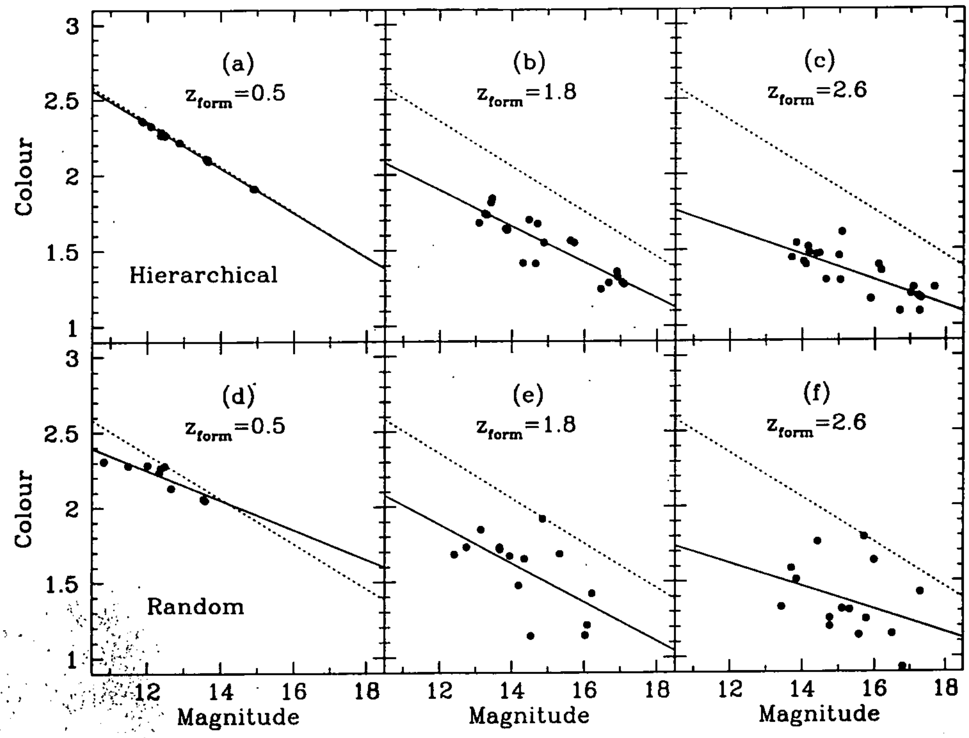

Figure 4.1: Example Monte-Carlo realisations of the present-day colour-magnitude relations produced by the hierarchical clustering model (top row) and the random merging model (bottom row). Details of the procedures used to generate these relations are given in the text. The solid line shows the mean CMR fitted by minimising the bi-weight scatter of the residuals, while the dashed line shows the initial relation, which is the same in all the panels. The three columns correspond to different redshifts at which the initial model CMR is implemented $z_{form} = 0.5, 1.8, 2.6$ respectively. As can be seen the slope of the relation weakens and the scatter increases as the degree of merging between the initial epochs and the present-day increases. The effect is more marked for a random merging process than for the hierarchical merger model.

fragment pairs (possibly from different trees) are selected at each branch of the original tree. Fragments without progenitors in the hierarchical tree also have no progenitor in the random tree. This approach preserves both the initial mass distribution and number weighted merger rates, but essentially randomises what present day galaxy an object at $z = z_{form}$ will end up in, thus destroying the mass correlations present in the original trees.

As can be seen from Panels d, e & f of Figure 4.1, the effect of the random mergers is to more rapidly reduce the slope of the initial tree and to rapidly increase the scatter of the CMR. Although a best fit line can be defined for these models, the slope varies considerably between different realisations. The data used below have been averaged over thirty realisations of the random merger trees.

4.3 Comparison with Observational Data

We use the scatter in the present day CMR to constrain its formation history, however the scatter that we measure in the simulated CMRs can be made arbitrarily small by reducing the slope of the relation. For example, because we assume a coeval population and no differential colour evolution, initially allocating all galaxies the same colour will lead to a final CMR with zero scatter but also zero slope. The key requirement is therefore that the merging process is able to maintain the ratio between the scatter and slope (R) at or below the observed ratio. This is independent of our initial CMR, and allows us to compare both the models to each other and to real data.

Figure 4.2 summarises how the ratio R varies with z_{form}. In both random and hierarchical models R increases monotonically, however the hierarchical clustering model has a much slower increase of R with z_{form}. We compare these results with our data from the Coma cluster, presented in chapters 2 and 3. The observed $U - V$ scatter is 0.059 (all galaxies, $V_T < 17$, see table 3.5) and the observed CMR slope, measured using $U - V$ colours in a metric (13″) aperture and estimated total V magnitudes, is -0.1. This gives a ratio of ~ 0.6. It is important to use the slope referenced to a total magnitude rather than an aperture measurement so that this quantity is conserved during the mergers as in the model calculation. However, to preserve a high signal to noise in the data, the colours that we use are taken from fixed size metric apertures, such that larger galaxies will have their colours measured in a smaller (relative to r_e) effective aperture than will small galaxies. Galaxies become bluer with increasing distance from the center, so this effect will tend to make smaller galaxies artificially bluer than large galaxies, adding to the CMR slope. We take the correction for this effect from Bower, Kodama, & Terlevich, who estimate the size of this effect using the elliptical galaxy colour gradients measured by Peletier et al. (1990) (although not all of their early type galaxies are in the cores of rich clusters). Their mean colour gradient is measured in $U - R$ and $U - B$, but it can be converted to a gradient in $U - V$ using the late type stellar colours from Gunn & Stryker, 1983. BKT find $\Delta(\mu_U - \mu_V)/\Delta \log r = -0.178\,\mathrm{mag/dex}$. This can be converted to a change in aperture colour as a function of radius by integrating over the de Vaucouleurs $r^{1/4}$ profile, giving a change in colour of $-0.134\,\mathrm{mag/dex}$. In order to assess the effect of this colour gradient, it is simplest to compare with the observed slope of the colour-magnitude relation plotted in $U - V$ vs. D_V coordinates (D_V measures the size of the galaxy within which the mean surface brightness is 19.80 mag arcsec^{-2}, Lucey et al., 1991). The observed slope in this parameter space is $0.46\,\mathrm{mag/dex}$ (BLE), which should be compared with the effect expected due to colour gradients of 0.134 (the aperture used to measure the colour remains fixed and therefore the relative size of the aperture is inversely proportional to D_V). Thus the colour gradient effect accounts for about 30% of the CMR slope. Including this correction raises the ratio of observed scatter to slope to 0.8.

We can compare this limit with the simulated models. For the random model, the ratio R is already too large for $z_{form} \geq 0.9$. For the hierarchical model, R increases less rapidly, so that the constraint on z_{form} is correspondingly weakened, and the observed limit on R only conflicts with the model strongly for $z_{form} \geq 2$ (although there is little room for additional sources of scatter once $z_{form} \geq 1.4$). Quoting these results in terms of redshift is, however, a little unsatisfactory as the redshift evolution of the objects mass is tied to the specific model for dynamical friction and the merger time scale adopted by BCFL in generating the galaxy merger tree. A more useful classification is the factor by which the masses of 'typical' galaxies have increased over the time scale of the simulation. We use the ratio of the mass-weighted mean mass (MWMM) between the final CMR and the 'primordial' CMR as a measure of the amount of mass growth.

We calculate the MWMM as

$$\mathrm{MWMM} = \sum M_{gal}^2 / \sum M_{gal}$$

for all the galaxies in the model, where M_{gal} is the baryonic mass of each galaxy. We experimented with imposing 'magnitude' limits, but found them to have minimal effect on the results. Thus, the MWMM ratio is simply $\mathrm{MWMM}_{z=0}/\mathrm{MWMM}_{z=z_{form}}$

The MWMM is analogous to M_* of the Press-Schechter mass function, and provides a measure of the 'typical' stellar mass of the model galaxy population. When setting up the primordial CMR, we assumed a constant mass-to-light along the sequence, so in these models mass and luminosity are directly proportional. It is therefore possible, by

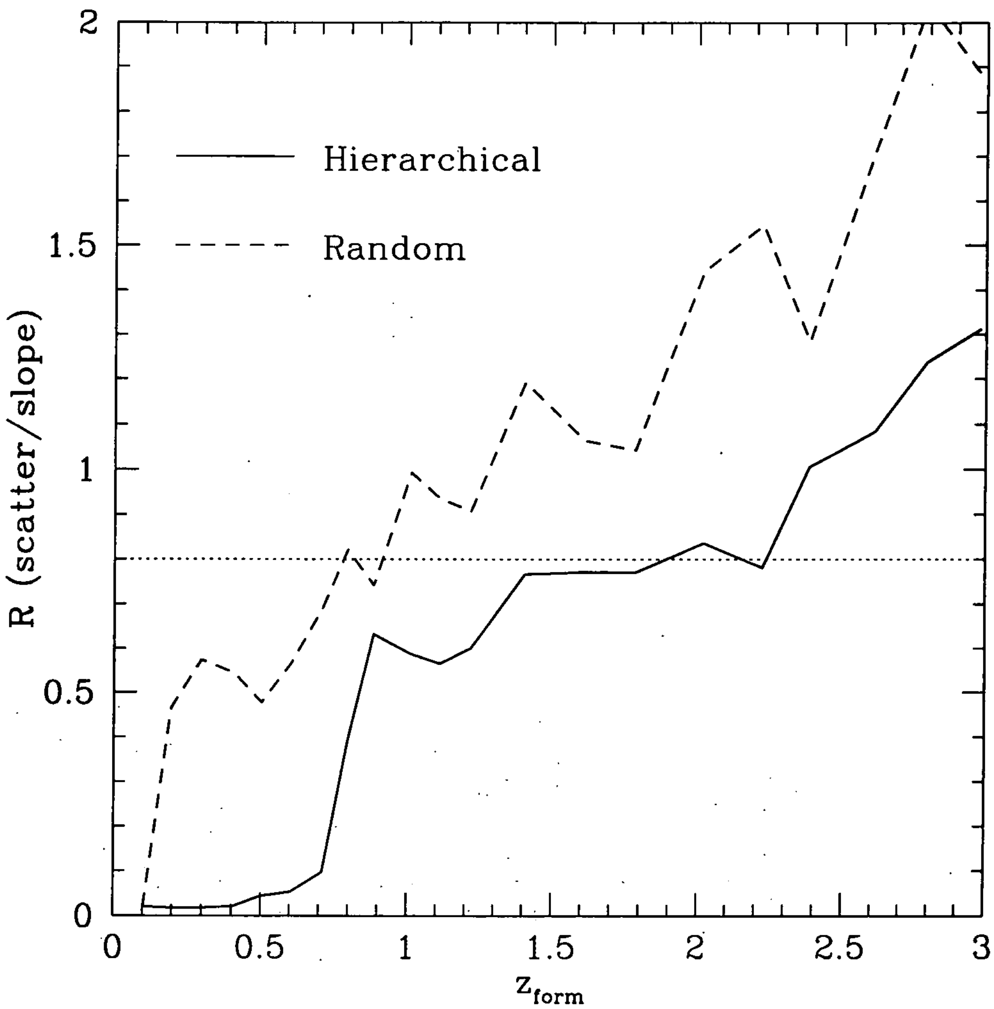

Figure 4.2: The effect of mergers in a hierarchical clustering scenario. The solid line shows the how the ratio between present-day CMR scatter and slope (R) depends on the redshift z_{form} at which test galaxies are assigned colours according to an exact correlation between colour and magnitude (the 'primordial' CMR). The effect of mergers in an equivalent random merging model is shown by the dashed line. The dotted line shows the present day value of R as measured form the Coma cluster photometry in chapters 2 and 3. See main text for details of how this was corrected for total magnitudes and colour gradients.

assuming a particular M/L ratio for the stellar population, to convert the MWMM into an equivalent luminosity, however, this is not required for the comparison we wish to make. The evolution of the MWMM ratio provides a simple measure of the mass a typical galaxy has gained in the merger process. In the hierarchical tree, this is not equivalent to the number of mergers: as we will see, the mergers at late times (low redshifts) are dominated by the accretion of small objects, which have little effect on the MWMM.

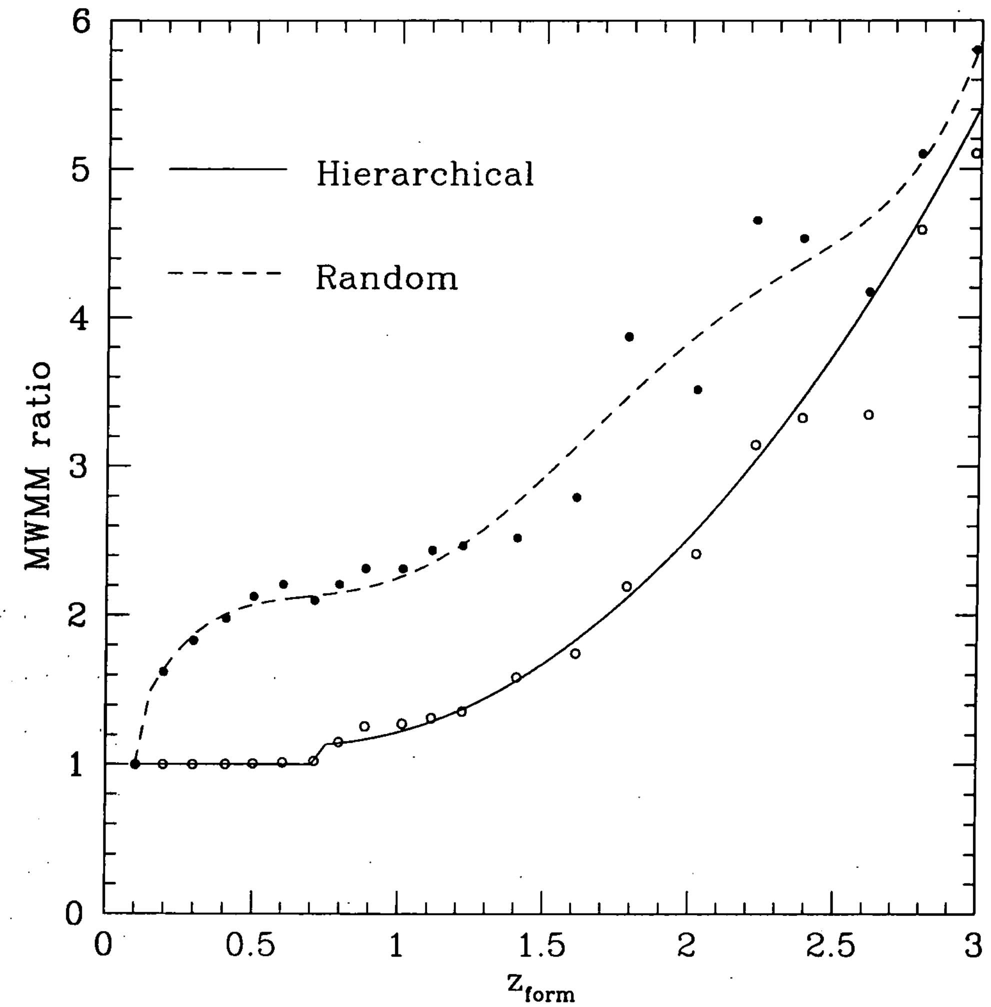

Figure 4.3: The evolution of the MWMM, expressed relative to the $z = 0$ value, as a function the formation redshift z_{form} for the a hierarchical merging model (open dots) and the random merging model (filled dots). Details of the models are given in the text. The lines are fits to the model results. They are used in figure 4.4 to convert from z_{form} to MWMM ratio

Figure 4.3 shows how the MWMM evolves as a function of redshift for the hierarchical and random models. We first consider the hierarchical case. At low z_{form}, the MWMM ratio evolves only slowly: At these redshifts, a massive cluster has formed with a large dark matter halo, effectively quashing all merging within it (see equation 4.1). While there are still many mergers taking place at $z < 0.5$, in the hierarchical merging models, these tend to be mergers which take place in small groups of galaxies which have not yet fallen into the main cluster, so tend to be between two or more small objects, or a large object with a small object. Neither of these processes significantly affect the MWMM. At higher

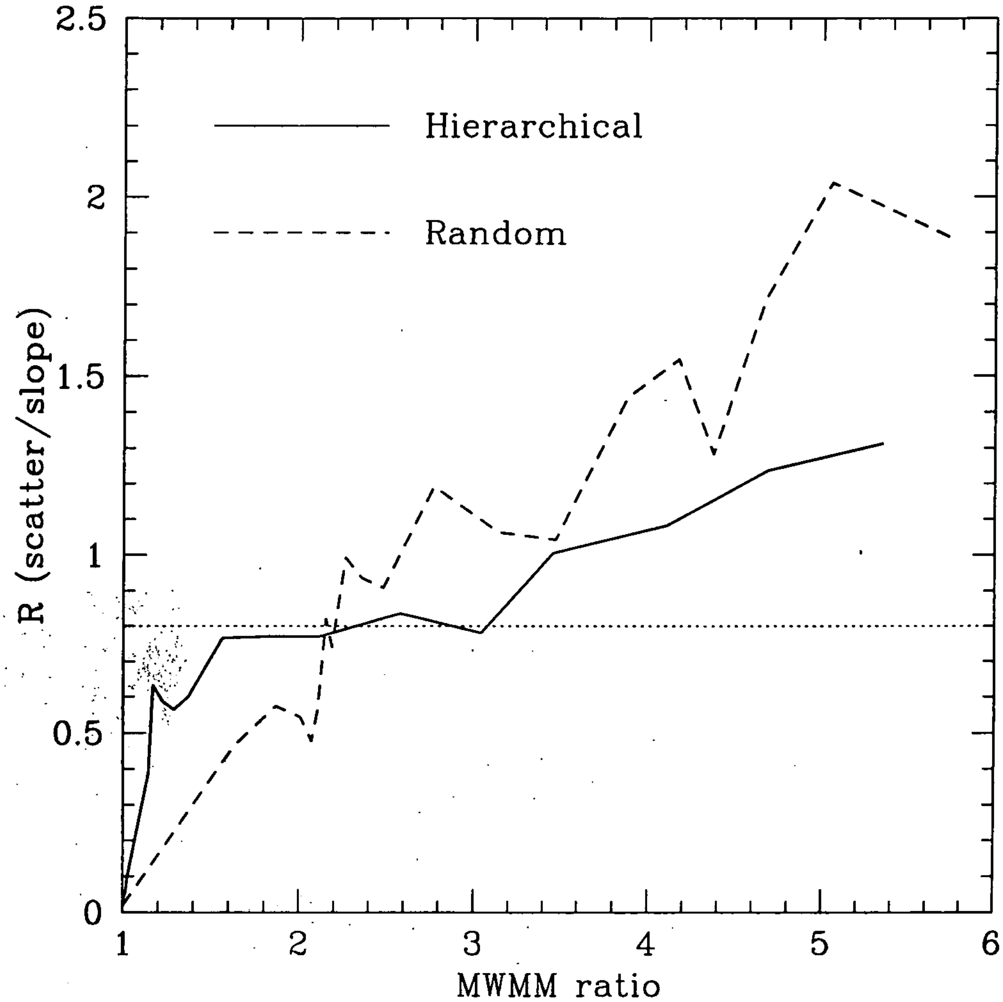

Figure 4.4: The evolution of the ratio between CMR scatter and slope (R) for the hierarchical galaxy merger model (solid line) and the random galaxy merger model (dashed line). Details of the models are given in the text. This figure is in effect the same as figure 4.2 but with the z_{form} axis converted into the ratio of the mass weighted mean mass (MWMM) at $z = 0$ to the MWMM at $z = z_{form}$, using the functions plotted in figure 4.3. The MWMM ratio gives a more model independent measure of how R evolves, as unlike z, it does not depend on the dynamical friction and merger time scales used by BCFL in constructing their merger trees. The observed value of R is shown as a dotted horizontal line. It can be seen that both models cross the observed line at similar values of the MWMM ratio.

z_{form}, the dynamics is no longer dominated by a single large dark matter halo, and so equation 4.1 allows merging to take place between more of the objects, and the MWMM evolves far more rapidly.

By contrast, the evolution of the MWMM of the random model is more sensitive to the choice of z_{form}. This is a result of the way in which the random model is constructed from the same galaxy fragments as present in the hierarchical model at the initial epoch.

At low z_{form}, the distribution of fragments is dominated by large objects. While in the hierarchical case, the presence of a massive cluster halo prevents the massive galaxies within it from merging, this is not the case with the random model. Indeed the increased fraction of massive objects at lower z_{form} encourages mergers between them, contributing heavily to the evolution of the MWMM of the population. It is important to note that Figure 4.3 does not show the evolution of the MWMM for a single realisation, but rather the effect of different starting points for the random merger tree.

To quantify the mass growth factor, both datasets have been interpolated by a smooth relation shown by the thin lines in Figure 4.3. We use this conversion to compare the evolution of the CMR as a function of mass growth. This is shown in Figure 4.4. Despite the large differences in the rate of mass growth, the evolution of the slope to scatter ratio, R, is similar for both the random and hierarchical merger trees. Both curves show steps in the R that result from the non-linear behaviour of the bi-weight scatter estimator. Although the overall impression is one of similarity, the correlations between a galaxy's mass and the mass of its progenitors, inherent in the hierarchical merging model, result in the slightly shallower overall slope of the hierarchical line in figure 4.4. Nevertheless, when compared to the observed value of R, both models set similar limits on the mass growth factor. Although the CMR can be imprinted at higher redshift in the hierarchical tree, this is compensated by the slower growth of mass in this model.

4.4 Discussion

The existence of a strong colour-magnitude correlation in present day clusters (see chapter 3) rules out the possibility that typical cluster galaxies can have grown in mass by a large factor since the formation of the bulk of their stars. Furthermore, the factor of 2-3 that we estimate probably represents an upper limit to the role of dissipationless mergers in the formation of (the majority of) present-day luminous cluster galaxies. It is extremely unlikely that the initial CMR will be completely perfect. Furthermore, we have not allowed for the differential evolution of galaxy colours due to a range in formation epochs and metallicities of the galaxy fragments in the primordial CMR. These effects will tend to make the limit on the degree of merging still more stringent. The constraint can however be weakened if the mergers are not purely dissipationless and are associated with significant star formation and consequent metal enrichment. This then conflicts with our initial parameterisation of the CMR.

Random merging of the galaxy fragments quickly increases the ratio of scatter to slope to unacceptable levels, meaning that the bulk of stars in these galaxies must have formed at redshifts below unity. Random merging however is not a good description of the evolution of galaxies in clusters. Because the dynamical friction time scale is strongly mass dependant, large galaxies tend to be formed from the merges of other large galaxies. We have incorporated this into our models by using the galaxy merger trees of BCFL, substantially increasing the robustness of the CMR to merging processes. In our hierarchical models, a primordial CMR can be evolved from formation redshifts as high as $z_{form} = 2$ without increasing the ratio of scatter to slope of the CMR above what is observed in rich clusters today, however this more due to the lack of significant merging within the cluster halo at late times (see figure 4.3), than to the correlations of galaxy mass with its progenitor mass. Correlation effects can be seen in figure 4.4, as a slightly shallower slope of the hierarchical model as compared to the random model. It would therefore be an interesting exercise to investigate the predictions of the semi–analytic hierarchical models for the CMR of group and field galaxies, where merging is still prevalent.

We can compare our results with those which examine the evolution of the CMR scatter due to differential evolution of the stellar populations (e.g. Bower, Lucey, & Ellis (1992b),Bower, Kodama, & Terlevich (1998)), which find that the bulk of stars must have formed at look-back times greater than $\sim$ 10Gyr. This is incompatible with the random merger model, where the CMR must have formed after $z \sim 1$, and therefore so must the bulk of its stars. The stellar evolution predictions can, however, be accommodated within the hierarchical merger model. If the bulk of stars formed at high redshift, as required by the stellar evolution models, the galaxies can still have undergone a history of mergers to produce a CMR at low redshift with acceptable levels of scatter.

4.5 Summary

– We place an upper limit on the role of dissipationless mergers upon the evolution of the CMR. We find that, regardless of the model used for galaxy merging, the typical mass of the galaxies in the cluster cannot increase by more than a factor of ~ 2, without disturbing the CMR to an extent ruled out by observations of local clusters.

- We find that a model which uses an extended Press–Schecter formalism to calculate the merging history of dark matter haloes, coupled with dynamical friction time-scales to model the mergers of galaxies embedded within those haloes, can indeed preserve the CMR from $z \sim 2$ through to the present day, even using purely dissipationless merging. This is mainly due to the lack of major merging events in the cores of rich clusters, so that most of the merging in these models occurs at large look-back times, when the fragments were in small groups.

- We find that the correlations of a galaxy's mass, with the mass of its progenitors, present in the hierarchical models, affects the evolution of the CMR scatter only minimally.

References

Aarseth S. J., Fall S. M., 1980, ApJ, 236, 43

Arimoto N., Yoshii Y., 1987, A&A, 173, 23

Barger A. J., Aragon-Salamanca A., Ellis R. S., Couch W. J., Smail I., Sharples R. M., 1996, MNRAS, 279, 1

Baugh C. M., Cole S., Frenk C. S., Lacey C. G., 1998, ApJ, 498, 504

Bender R., Burstein D., Faber S. M., 1992, ApJ, 399, 462

Bond J. R., Kaiser N., Cole S., Efstathiou G., 1991, ApJ, 379, 440

Bower R. G., 1991, MNRAS, 248, 332

Bower R. G., Kodama T., Terlevich A. I., 1998, MNRAS, 299, 1193, astro-ph/9805290

Bower R. G., Lucey J. R., Ellis R. S., 1992, MNRAS, 254, 601

Bruzual A. G., 1983, ApJ, 273, 105

Butcher H., Oemler J., A., 1978, ApJ, 226, 559

Butcher H., Oemler J., A., 1984, ApJ, 285, 426

Caldwell N., Rose J. A., Franx M., Leonardi A. J., 1996, AJ, 111, 78

Caldwell N., Rose J. A., Sharples R. M., Ellis R. S., Bower R. G., 1993, AJ, 106, 473

Cole S., Aragon-Salamanca A., Frenk C. S., Navarro J. F., Zepf S. E., 1994, MNRAS, 271, 781

Couch W. J., Newell E. B., 1984, ApJS, 56, 143

Couch W. J., Sharples R. M., 1987, MNRAS, 229, 423

Kauffmann G., 1996, MNRAS, 281, 487

Kauffmann G., Charlot S., 1998, MNRAS, 294, 705

Kauffmann G., White S. D. M., Guiderdoni B., 1993, MNRAS, 264, 201

Kormendy J., Djorgovski S., 1989, ARA&A, 27, 235

Lacey C., Cole S., 1993, MNRAS, 262, 627

Larson R. B., 1974, MNRAS, 169, 229

Navarro J. F., Frenk C. S., White S. D. M., 1995, MNRAS, 275, 56

Press W. H., Schecter P., 1974, ApJ, 187, 425

Schweizer F., Seitzer P., 1992, AJ, 104, 1039

Schweizer F., Seitzer P., Faber S. M., Burstein D., Dalle Ore C. M., Gonzalez J. J., 1990, ApJ, 364, L33

White S. D. M., 1976, MNRAS, 177, 717

White S. D. M., Frenk C. S., 1991, ApJ, 379, 52

Chapter 5

The Relation Between the Colour Magnitude Relation and Spectral Line Strengths.

Abstract. We compare the spectral line indices of galaxies in the Coma cluster with their deviation from the mean colour-magnitude relation (CMR). We find that the CMR in Coma is driven primarily by a luminosity–metallicity correlation, however we cannot rule out a contribution from age effects. Colour deviations blueward of the mean relation are strongly correlated with the Hydrogen Balmer line series absorption, indicating the presence of a young stellar population in these blue galaxies, possibly the result of a burst of star formation in the past 2Gyr. We also conclude that the CMR corrected $U - V$ colours are an efficient way to search for galaxies with strong Balmer absorption features.

5.1 Introduction

It has been long understood that the colours of early type galaxies are governed primarily by the effects of age and metallicity, which when increased, cause the spectral energy distribution (SED) of a single stellar population to become redder (Renzini & Buzzoni 1986, Buzzoni, Gariboldi, & Mantegazza 1992, Buzzoni, Chincarini, & Molinari 1993, Worthey 1994, Charlot & Silk 1994). In his '2/3' law (Δ[Fe/H] $\sim$ $\frac{2}{3}\Delta log(t)$), Worthey (1994) demonstrated how age and metallicity have a degenerate effect on galaxy colours. The colour–magnitude relation (CMR), in which the colours of galaxies become progressively redder with increasing luminosity, and hence increasing mass of the galaxy (Visvanathan & Sandage 1977) is seen in the cores of rich clusters, in groups, and even seems to be present in field ellipticals (Larson, Tinsley, & Caldwell 1980). Traditionally, the slope seen in the CMR has been attributed to a mass–metallicity sequence (Dressler 1984, Vader 1986), with the massive galaxies being more metal rich, and thus redder, than the less massive ones. This tendency can naturally be explained by a supernova driven wind model (Larson 1974, Arimoto & Yoshii 1987), in which more massive galaxies can retain their supernova ejecta for longer than can smaller galaxies, thus being able to process a larger fraction of their gas before it is expelled from the galaxy. Given the degeneracy between the metallicity and age of a stellar population in its broad band colours, it is also possible that the CMR be an age driven sequence, with the smaller galaxies being bluer due to a younger mean age of their stellar populations. An age dependant CMR however neither preserves its slope, nor its magnitude range with time (Kodama 1997, Kodama & Arimoto 1997). Studies of the CMR in high redshift clusters find that it has a slope comparable to that of the local cluster CMR and there is no sign of a change in its magnitude range (Ellis et al. 1997, Stanford, Eisenhardt, & Dickinson 1998). This makes an age dependant CMR in clusters highly unlikely. The low levels of scatter in the CMR of cluster cores implies that the galaxies are made up from old stellar populations (Bower, Lucey, & Ellis 1992, Bower, Kodama, & Terlevich 1998), as even small variations in the ages of the galaxies would lead to unacceptable levels of scatter in young stellar populations, whereas old stellar populations have a much smaller age dependency in their colours.

So, we have the photometric view of the CMR in clusters. The CMR is a mass–metallicity relation, and the majority of the stars within the galaxies formed at high redshift.

The picture begins to look remarkably different when spectroscopy is used. At high redshifts, the fraction of blue galaxies in many of the clusters increases (Butcher & Oemler 1978, Butcher & Oemler 1984). Couch & Sharples spectroscopically investigated the galaxies in some of these 'Butcher–Oemler' clusters. They split their sample into blue and red galaxies depending on whether they lie on the cluster CMR or not, and associate increased fraction of blue galaxies with either ongoing or recent star formation in early type galaxies. They also found that 11 out of their 73 red galaxies showed enhanced Balmer absorption lines, also indicative of recent star formation, although it is possible that the red Hδ strong galaxies can be formed by the truncation of star formation in spiral galaxies.

Spectroscopic studies of early type galaxies in local rich clusters (Caldwell et al. 1993, Caldwell et al. 1996) have shown there to be a population of galaxies with abnormal spectra. They exhibit enhanced Balmer absorption lines, or emission lines, indicative of recent star formation, but with too weak an [OII] line to be classified simply as spiral galaxies. They note the similarity of these spectra with the 'red' Hδ-strong galaxies of Couch & Sharples (1987), and find that of the galaxies associated with the dynamically separate group of galaxies centered on NGC4839 in the SW of the Coma cluster (Baier 1984, Escalera, Slezak, & Mazure 1992, Colless & Dunn 1996 and figure 2.3), about $1/3$ have abnormal spectra. So spectroscopic studies of local and distant clusters have shown there to be a population of galaxies which appear photometrically old, but which have been forming significant quantities of stars in their recent past (possibly in a massive starburst). In an effort to disentangle age and metallicity effects on stellar populations, Worthey (1994) developed a series of stellar population spectral synthesis models, to show the dependence on age and metallicity of certain spectral features such as the Balmer lines, and various metal lines. In a study of galaxies in the Fornax cluster, Kuntschner & Davies (1998) used the Worthey (1994) models to show that the elliptical galaxies in the Fornax cluster were uniformly old, and spanned a range in metallicities, however studies of field spheroidals (González 1993, Trager 1997) seem to show just the opposite, with field spheroidals seeming to have a uniform metallicity, but spanning a range in ages, yet still forming a well defined CMR.

In chapter 3 we showed that there exists a possibility that the CMR in the outer parts of the Coma cluster exhibits a systematic blue shift, compared to the CMR in the core, but we could not ascertain whether this was due to cluster dust in the core, or an older mean stellar population in the core galaxies. In this chapter we will look at spectral line indices and deviations from the CMR in the Coma cluster, using both the Worthey (1994) and Worthey & Ottaviani (1997) spectro-photometric evolution models and the spectra of Coma cluster galaxies of Caldwell et al. (1993).

5.2 The Data

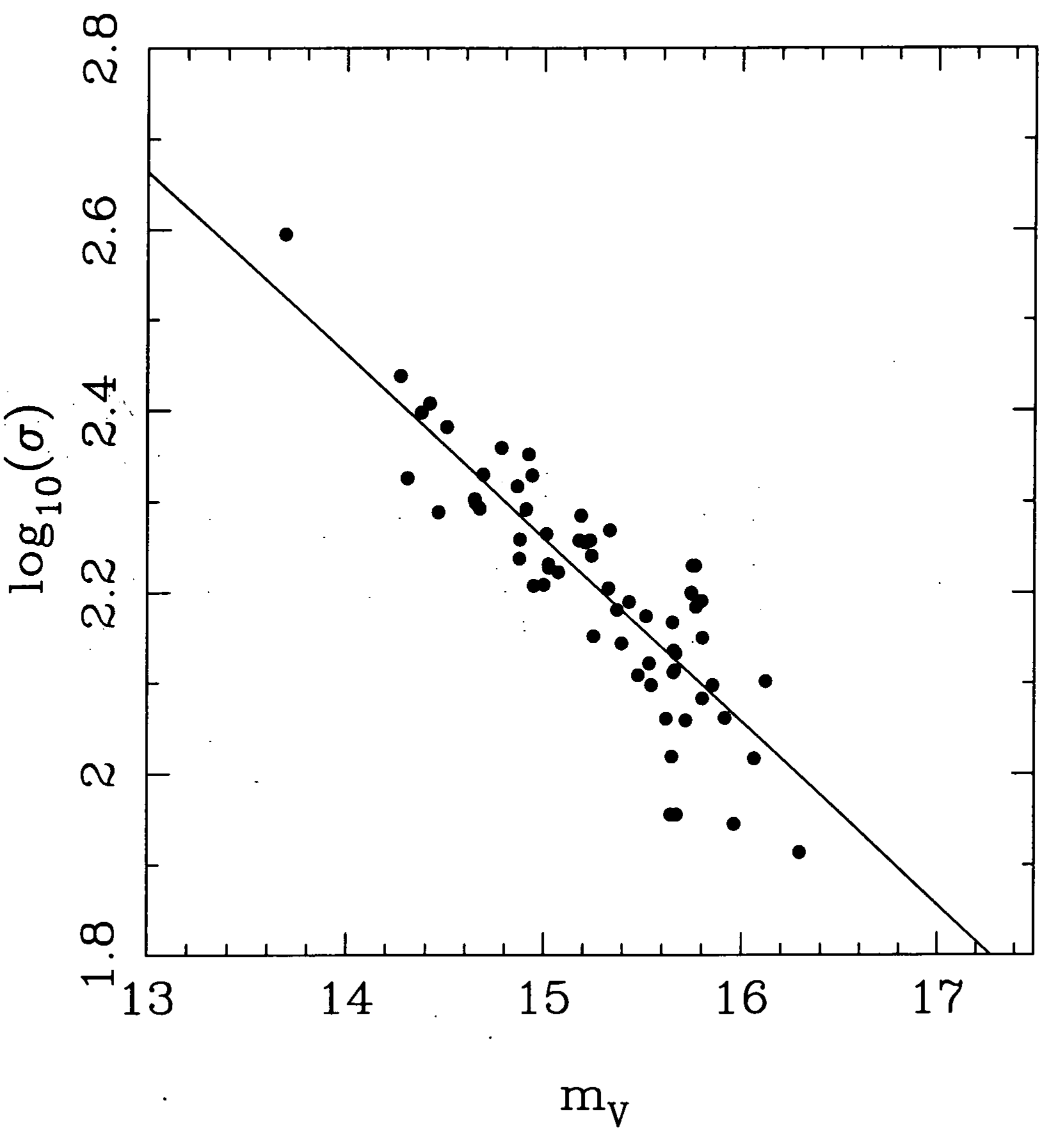

Figure 5.1: The least squares fit between the Coma galaxies' velocity dispersions from Lucey et al. 1997, and the 13″ aperture V magnitudes from chapter 2. When correcting the line strengths in this chapter for velocity dispersion, those galaxies without a measured value for σ can have one estimated using their 13″ aperture V magnitudes.

For this chapter, we have used spectra from Caldwell et al. (1993), which we re-sampled to place them into the Lick/IDS system so that we could compare them with the Worthey stellar population models (Worthey 1994, Worthey & Ottaviani 1997). Caldwell et al. selected the galaxies from the extensive catalogue of Godwin, Metcalfe, & Peach (1983), which is drawn from a 2.6 degree square field, centered on the Coma cluster, and is considered complete to $B = 20$, corresponding to $M_B < -14$. Caldwell et al. (1993) used two criteria to select early type galaxies from the Godwin, Metcalfe, & Peach (1983) sample. Firstly they fitted the $(b, b-r)$ colour magnitude relation and selected all galaxies whose colours lay within $\pm 0.15 mag$ of the fit. Secondly, they obtained independent morphologies using KPNO 4m and Palomar Sky Survey plates. Using these morphologies, and those of Dressler (1980) they removed morphologically late type systems from the list, and added some (~ 25) clearly early type galaxies which had failed to be included after the colour cut.

Finally they rejected all galaxies brighter than $B = 14.3$, as the large velocity dispersion in these more massive galaxies would make their spectroscopic analysis of the weak lines impossible.

Table 5.1 shows the distribution of Andreon et al. (1996) and Andreon, Davoust, & Poulain (1997) morphological types for the Caldwell et al. galaxies. Immediately obvious is the fact that 13 of the Caldwell early type galaxies are in fact late types according to Andreon et al. It is hardly surprising they slipped through the net though, as can be seen from figure 5.2, only one of the spiral galaxies lies more than one standard deviation bluewards of the CMR ridge line. It must be noted however that we do not have morphological information for the fainter galaxies in the sample, which is where most of the very blue galaxies reside, however out of the 7 very blue galaxies, only 3 have no morphologies.

5.2.1 Spectroscopy

The Caldwell et al. (1993) spectra were all taken on the KPNO 4m, using the HYDRA multi-fibre positioner. They have a spectral resolution of 3.8Å FWHM. The fibre aperture is $2''$. In order to compare the spectra with Worthey stellar population models (Worthey 1994, Worthey & Ottaviani 1997), the spectra were re-sampled into the Lick/IDS system by Harald Kuntshner (HK), using calibrations from observations of his on the AAT RGO spectrograph (Kuntschner 1998). This was achieved by artificially

Morphological type	Number of galaxies
No morph	26
???	1
Sp	3
S..	2
SBa	0
Sa	1
SA0/a	4
SB0/a	1
SAB0/a	2
SAB0p	0
SA0	27
SAB0	6
SB0	12
diE/SA0	1
diE/SAB0	0
unE/SA0	2
Epec	0
boE	1
diE	3
unE	6

Table 5.1. The Andreon et al. (1996) morphological types for the Caldwell et al. (1993) galaxies, split into the four coarse morphological types used in chapter 3, i.e. unclassified, spiral, S0 and elliptical. As can be seen, by far the largest group of galaxies is the S0s (48 galaxies) followed by the unclassified (27 galaxies) followed by the late types (13 galaxies) followed by the ellipticals (10 galaxies).

broadening the fluxed spectra using a Gaussian of wavelength dependant width. Because the Caldwell et al. (1993) data does not include any observations of stars in common with the Lick/IDS, the Gaussian used was that of Kuntschner (1998) who used it to correct his 4.5Å FWHM resolution AAT data to the Lick/IDS system. Both the Kuntschner and the Caldwell et al. spectra cover a similar wavelength range, and unlike the Lick/IDS spectra,

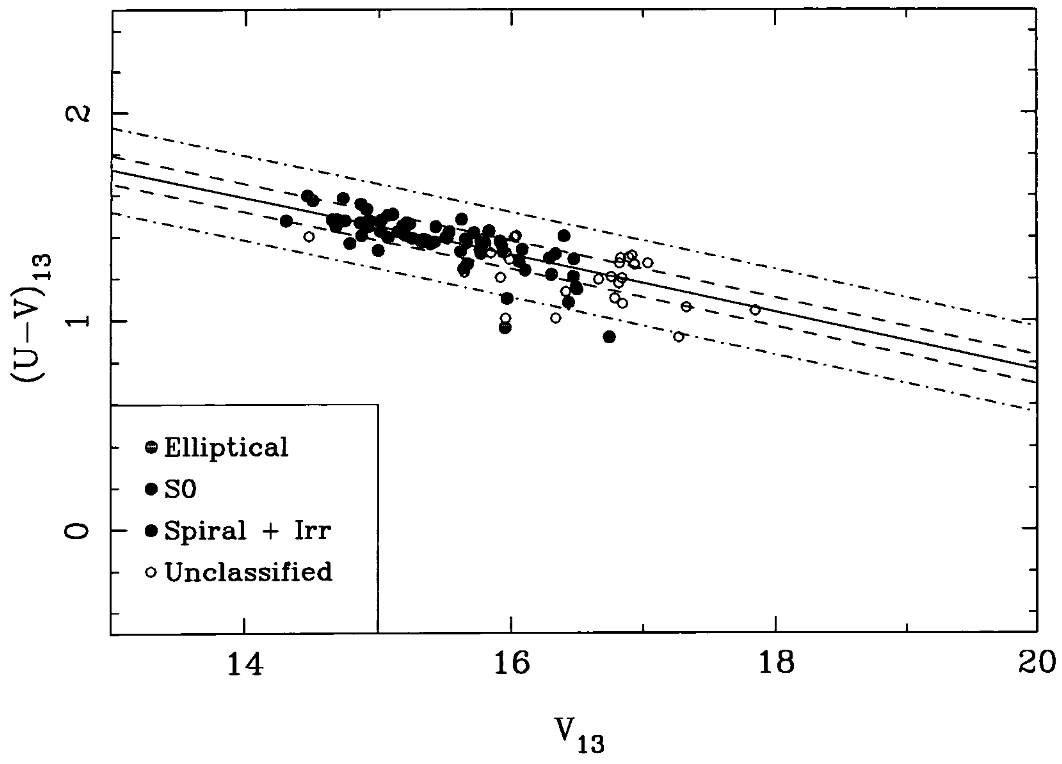

Figure 5.2: The colour magnitude relation for the Caldwell et al. galaxies, plotted in the same style as the CMR plots of Chapter 3 using 13″ diameter apertures. The colour of the symbols represents the morphological type of a galaxy as defined by Andreon et al. (1996) and Andreon, Davoust, & Poulain (1997). As can be seen from this figure, and from table 5.1, there are quite a few late type galaxies in the early Caldwell et al. sample, however, only one late type galaxy has colours which place it more than one standard deviation bluewards of the CMR ridgeline. The dashed, and dot–dashed lines represent the σ and 3σ of the data as calculated using an unclipped biweight scale estimator (see Appendix B and Chapter 3). Note that some of the galaxies in this figure were rejected from the datasets of chapter 3.

whose spectral resolution degrades notably towards the blue (see Worthey & Ottaviani (1997) fig. 7) they have a constant spectral resolution over their entire range. HK estimated the errors on the indices from the photon noise of the spectra, so they are likely to be a lower limit. They specifically do not take into account any systematics introduced through the assumptions made in the resampling of the data into the Lick/IDS system, specifically that the KPNO 4m fibre spectrograph has a similar enough spectral response to the AAT RGO long slit spectrograph.

The final step necessary to place the line indices into the Lick/IDS system is to correct the galaxy spectra for velocity dispersion. Velocity dispersion corrections for individual line indices were obtained from Kuntschner (1998), who calculated them by artificially broadening stellar spectra (e.g. Davies, Sadler, & Peletier (1993)).

The (Caldwell et al. 1993) spectra are not of sufficient resolution to calculate velocity dispersions for our galaxies, so instead we construct a 'Faber–Jackson' relation (Faber & Jackson 1976) between our our V band 13″ diameter aperture magnitudes m_{V13}, and the velocity dispersions (σ) of Lucey et al. (1997). Figure 5.1 shows the correlation between this σ and m_{V13}, which gives a relation of

$$log_{10}(\sigma) = 5.29 - 0.202 m_{V13}$$

We then used this relation to find values of σ for those galaxies in the Caldwell et al. sample which were not present in the Lucey et al. data.

We use the $H\gamma_A$ and $H\delta_A$ Balmer line indices (Worthey & Ottaviani 1997) as age sensitive spectral features. While $H\beta$ is more sensitive to age, it is also affected by nebular emission, which can rapidly fill the absorption feature (González 1993). Higher order Balmer lines are much less sensitive to emission from ionised gas (Osterbrock 1989), making an accurate measurement of the true stellar absorption easier. In order to increase the signal to noise, I have used $H\delta_A + H\gamma_A$ in the final analysis. The $C_2$4668 feature is identified by Worthey & Ottaviani (1997) as a particularly sensitive metallicity feature, however it it is possible that is suffers from over abundance problems in the larger, higher metallicity systems (Kuntschner 1998). Figure 5.3 shows both the relation between $C_2$4668 and Fe4383 for the Coma galaxies, and the theoretical relation from the Worthey models. Above a value of $\sim$ 6, the $C_2$4668 index deviates from the straight line model predictions. A similar effect is seen by Kuntschner (1998) for galaxies in Fornax. However in our data, the Fe4383 index has poorer signal to noise than the $C_2$4668 index, so we will use both, noting however the discrepancy for the high metallicity galaxies.

5.2.2 The photometry

In order to match the 2 arcsec diameter of the HYDRA fibres used for the spectra, the photometry used the smallest available aperture from the photometry outlined in Chapter 2. The 8.8 arcsec diameter aperture was the smallest aperture which was reliably seeing corrected, i.e. it showed no measurable systematic difference between stellar and galactic magnitudes when measured using differing seeing conditions. It is important to get as good a match as possible between the photometric and spectroscopic apertures, so that

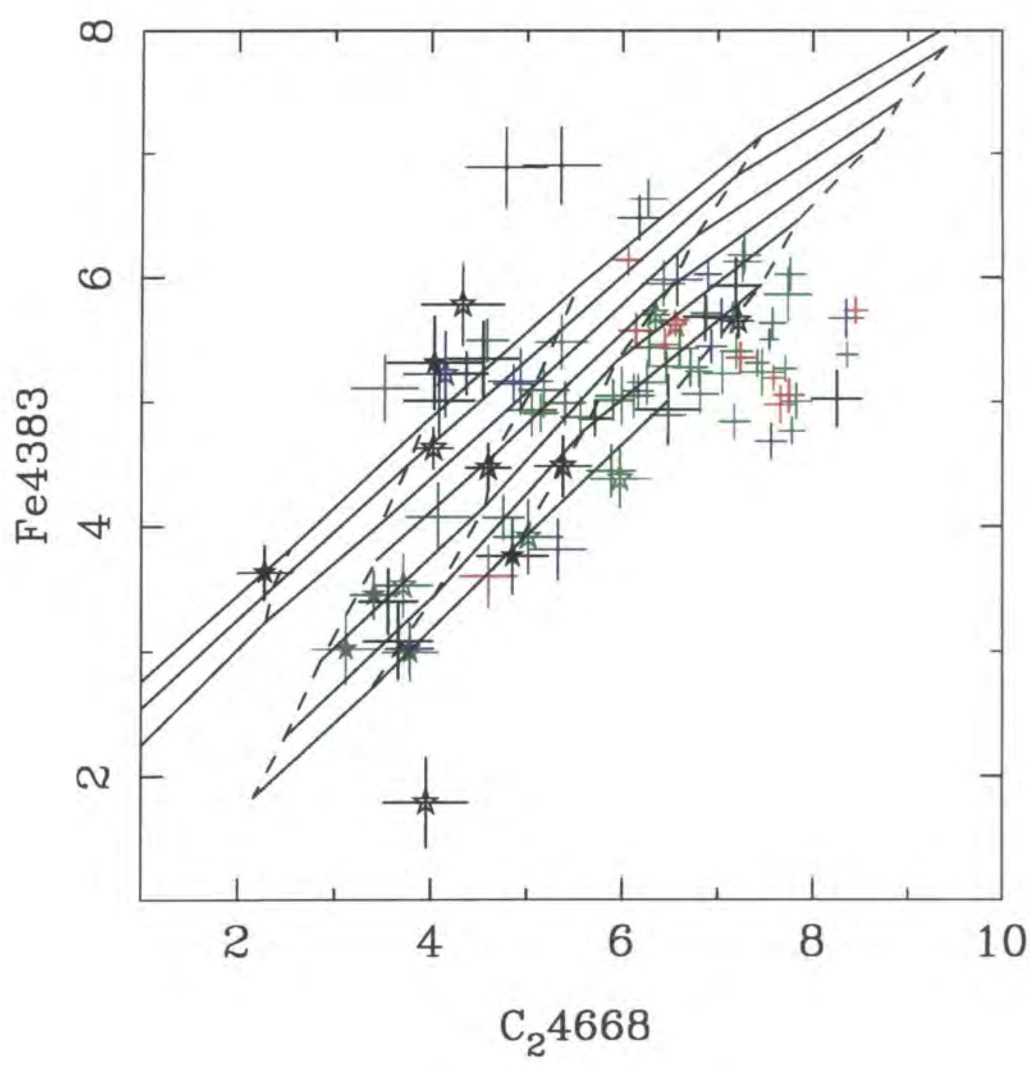

Figure 5.3: The relation between the two metal line indices used in this chapter for the Coma galaxies. The $C_2 4668$ line is easier to measure than the Fe4383 line, however it does seem to suffer from problems of overabundance in the more massive galaxies. This can be seen by the deviation of the galaxies from the theoretical relation for values of $C_2 4668 > 6$. Different symbols correspond to galaxies with different values of $\Delta(U - V)$, see figure 5.4 for details.

both are measuring the same part of the galaxy. In the case, for instance, of localised bursts of star formation occurring in the galaxy, the large photometric aperture and the small spectroscopic one, could well both be measuring different mixes of stellar populations. This is not a problem for the σ estimates, so 13 arcsec diameter aperture was used for the velocity dispersion correction because it gave the smallest residuals in the fit.

Throughout this chapter, the biweight minimising technique, outlined in appendix B and used extensively in Chapter 3, was used to fit simple straight lines to the data. It was used for its resistance to outlying data points, and its robustness against non-Gaussian data. This can be seen best in fig. 5.8, the biweight minimisation fit ignores the high $H\delta_A + H\gamma_A$ points, and fits the mean relation. A least–squares regression fit would have been heavily skewed towards the high $H\delta_A + H\gamma_A$ points, thus reducing their residuals ($\Delta(H\delta_A + H\gamma_A)$). In the case of fig. 5.8, these residuals are simply calculated as

$$\Delta(H\delta_A + H\gamma_A) = (H\delta_A + H\gamma_A) - (m \times m_V + c)$$

where m and c are the slope and intercept of the biweight fit respectively.

5.3 The colour magnitude relation

This dataset was primarily selected using its $(B, B-V)$ colour magnitude relation (see (Caldwell et al. 1993), figure 1). Figure 5.4 shows, unsurprisingly, that the colour magnitude relation is also present in our $(V, U-V)$ dataset. What our dataset also shows, is a large number of galaxies deviating blueward of the mean relation towards the faint end, an effect not seen in the $(B, B-V)$ relation of Caldwell et al. In order to trace the position of these blue galaxies in the subsequent figures of this chapter, we adopt a common labelling convention. The symbols used throughout the plots in this chapter reflect a galaxy's position in figure 5.4. No symbols (just error bars) correspond to galaxies that lie either red-ward of the colour-magnitude relation, or are within 1σ of it (see below for the value of σ). Open stars lie between 1σ and 2σ blueward of the relation, and filled stars lie more that 2σ blueward of the relation. Throughout this chapter, unless otherwise stated, when we refer to 'blue' galaxies we are referring to the objects plotted as both open and closed star symbols in figure 5.4, and'red' galaxies are the objects shown only with error bars in figure 5.4. To confuse matters further, where colour symbols are used, the colours refer to the galaxy's morphological type as taken from Andreon et al. (1996) and Andreon, Davoust, & Poulain (1997), and as defined in figure 5.2. I.e. red symbols represent ellipticals, green symbols represent S0s, blue symbols represent late types, and black symbols have no morphological classification.

The standard deviation of the relation in fig. 5.4 is $\sigma = 0.07 \pm 0.01$mag. When using the same $13''$ diameter aperture photometry as that used to calculate the scatter in chapter 3 (table 3.4), the scatter in the Caldwell galaxies is reduced to 0.066 ± 0.01mag. This

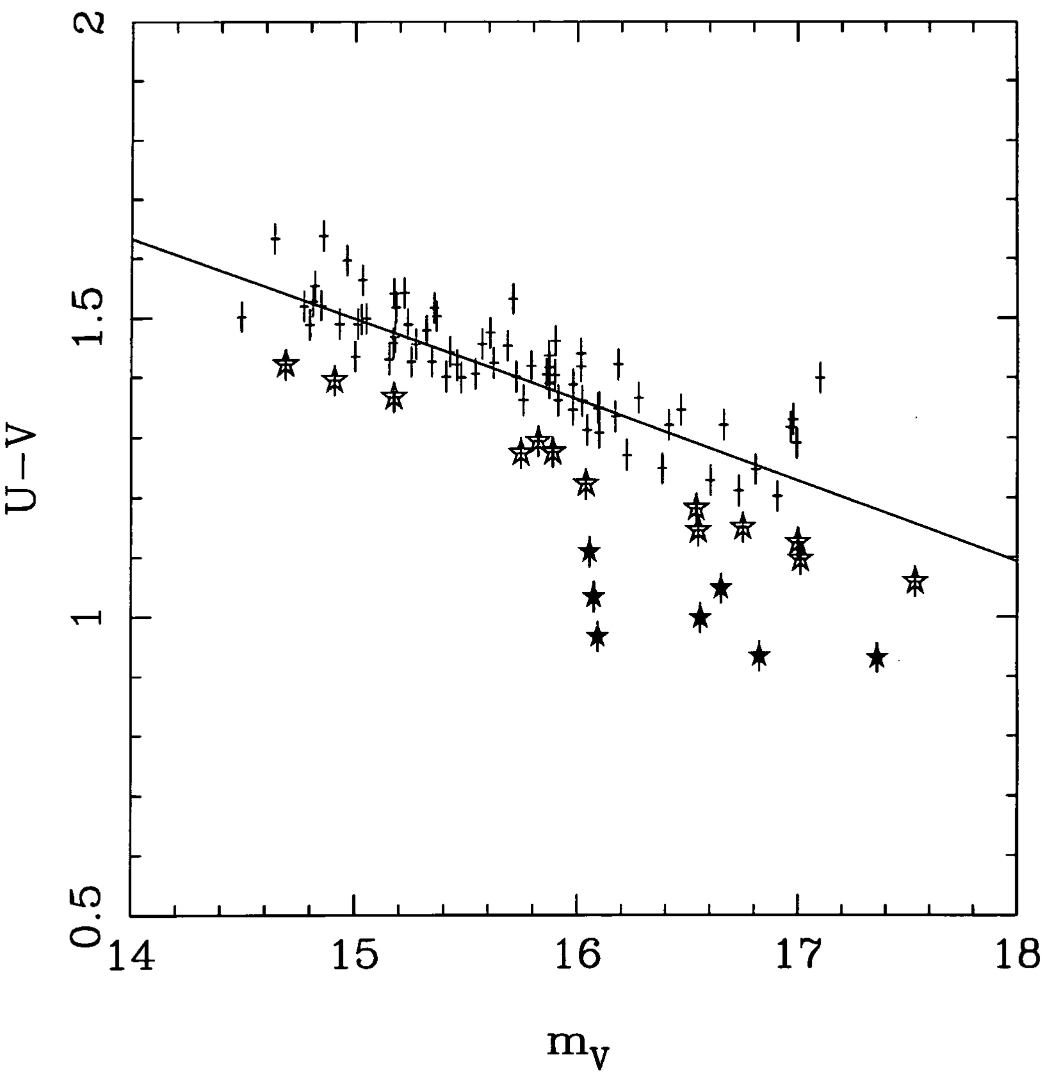

Figure 5.4: The colour-magnitude relation for the galaxies for which we have the highest S/N spectra, both colours and magnitudes are taken using the 8.8″ diameter apertures. Galaxies which lie between 1 and 2 σ blueward of the mean relation are plotted as open stars, while galaxies which lie more than 2σ blueward of the relation are plotted as filled stars. These symbols are used for the same galaxies in all subsequent plots in this chapter. The solid line shows the regression fit to the data, and is used to calculate the $\Delta(U-V)$ index.

is slightly larger than the scatter in the relation for the early type galaxies obtained in chapter 3, but not significantly so.

5.3.1 The origin of the colour magnitude relation

Although the Caldwell et al. spectra are not ideal for comparing with the Worthey stellar population synthesis models, due to the non ideal way the spectra were resampled into the Lick/IDS system (see section 5.2.1), we have attempted such a comparison using our two

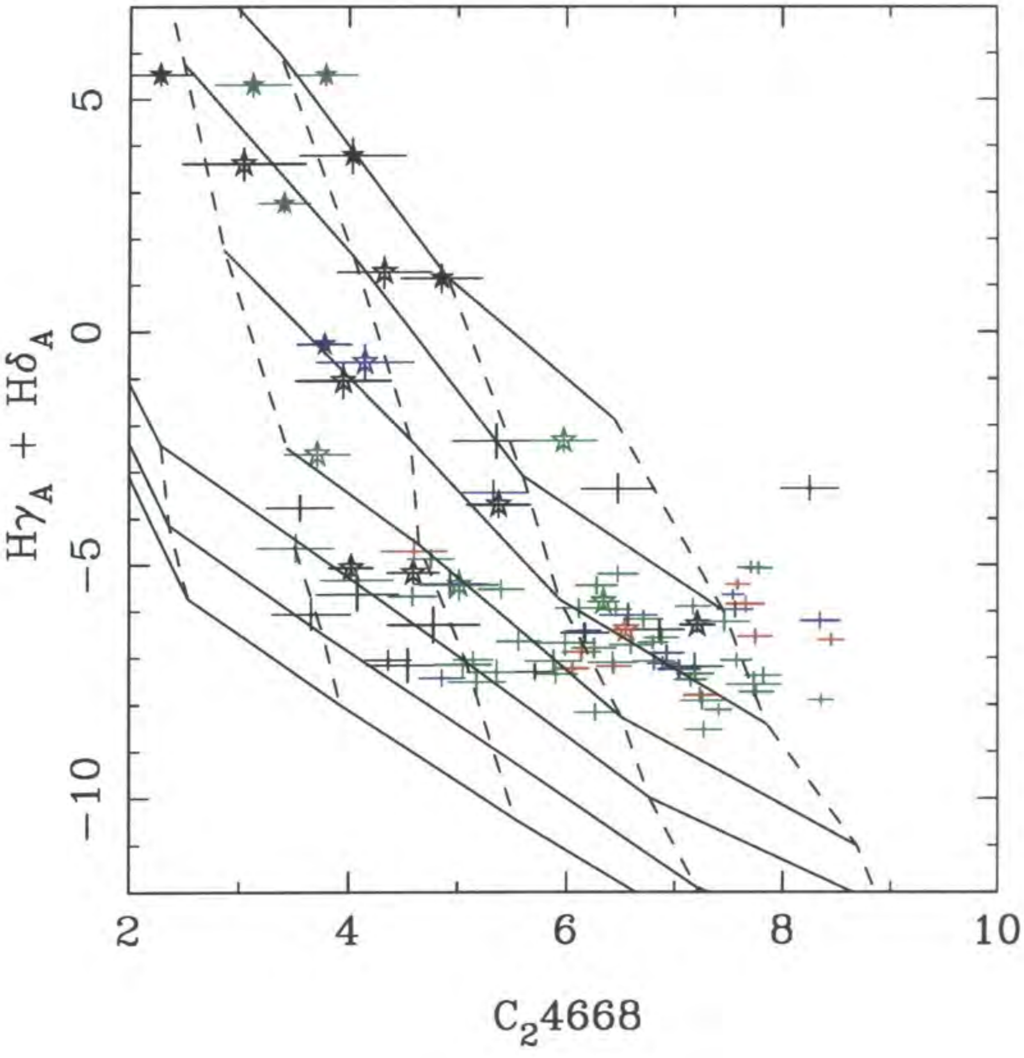

Figure 5.5: The distribution of galaxies in the (C_24668, $H\delta_A$ + $H\gamma_A$) plane, with a model grid of single stellar population models from Worthey (1994,1997). Solid lines trace loci of constant age, from 1.5 to 17 Gyrs. Dashed lines trace loci of constant $[Fe/H]$ from -2 to 0.5. The different symbols correspond to the degree of offset from the colour magnitude relation as shown in figure 5.4. Filled stars represent objects with $\Delta(U-V) < 2\sigma$, open stars represent objects with $2\sigma \leq \Delta(U-V) < \sigma$, and objects with no symbol represent objects that lie within 1σ of the best fit colour magnitude relation where σ is the standard distribution of the $\Delta(U-V)$. The different symbol colours represent the morphological type of the galaxy as taken from Andreon et al. (1996) and (Andreon, Davoust, & Poulain 1997) (1997), and as defined in figure 5.2.

most promising metallicity indicators, Fe4383 and C_24668. Figures 5.5 and 5.6 show how the galaxies lie on Worthey model grids. In both cases, the blue galaxies which deviate by more than 2σ from the CM relation in fig. 5.4 tend to populate the the low age portion of the grid. This area is entirely populated by star symbols, i.e. blue galaxies, while only six out of the 20 blue galaxies lie on the same part of the Worthey grid populated by the red

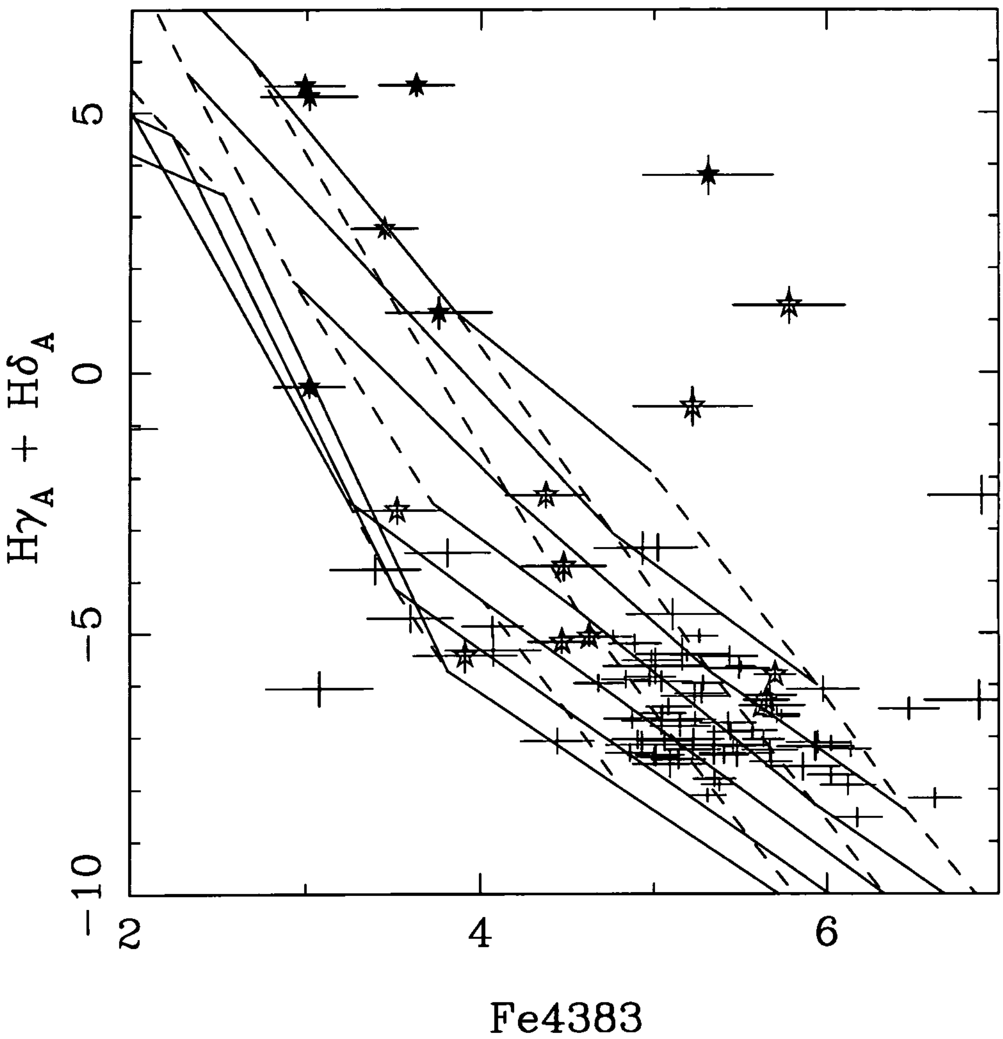

Figure 5.6: The distribution of galaxies in the (Fe4383, $H\delta_A + H\gamma_A$) plane, with a model grid of single stellar population models from Worthey (1994,1997). Solid lines trace loci of constant age, from 1.5 to 17 Gyrs. Dashed lines trace loci of constant $[Fe/H]$ from -2 to 0.5. The different symbols correspond to the degree of offset from the colour magnitude relation as shown in figure 5.4. Filled stars represent objects with $\Delta(U-V) < 2\sigma$, open stars represent objects with $2\sigma \leq \Delta(U-V) < \sigma$, and objects with no symbol represent objects that lie within 1σ of the best fit colour magnitude relation where σ is the standard distribution of the $\Delta(U-V)$.The different symbol colours represent the morphological type of the galaxy as taken from Andreon et al. (1996) and (Andreon, Davoust, & Poulain 1997) (1997), and as defined in figure 5.2.

galaxies. Both figures 5.5 and 5.6 imply a young age for the blue galaxies (an effect driven mainly by the $H\delta_A + H\gamma_A$ index), but they seem to say different things about metallicity effects, especially for the red galaxies which make up the main CM relation. The red galaxies in figure 5.5 appear to span a range both in metallicity and in age, implying a far from simple formation scenario, especially as the more massive galaxies appear to have the younger ages. We must remember however, that the model grids at these high metallicities are far from secure. Added to this, as discussed above, there appears to be an overabundance problem in the models for galaxies with $C_2$4668 > 6 (cf. fig 5.3). If we ignore these galaxies, the span in age and metallicity of the red galaxies is reduced.

Fe4383 does not suffer from the same overabundance effects as $C_2$4668, however it also has more of an age dependence, producing slightly more degenerate model grids, and has larger errors in our spectra. In figure 5.6, we can see again that the blue galaxies have younger ages than do the red ones, however they no longer exclusively populate the low metallicity portion of the grid. Some of the galaxies are in parts of the plot completely outside the parameter space covered by the model grid, although these are the galaxies with the largest error bars in the Fe4383 data. The red galaxies have a lower spread in metal line strength than they do in figure 5.5, and they do not follow the same trend in age as they did in figure 5.5, however, due to the increased scatter in the Fe4383 data, and the increased degeneracy in the model grid, it is still not possible to say that they follow a single age population model line. This may be due to the lower signal to noise of the Fe4383 index.

It is worth noting that there is some very feeble evidence for morphological segregation in figures 5.5 and 5.6. In both figures all of the elliptical galaxies populate the old portion of the model grids, while the S0s and late type galaxies are spread over the grid. I.e. there are both old and young S0 and late type galaxies, but only old ellipticals.

5.3.2 Colour offsets and line strengths

In section 5.3.1, we showed that the blue galaxies which deviate from the mean CMR have younger luminosity weighted ages than do the red galaxies, giving them enhanced Balmer absorption lines. This poses the question of how effective are photometric searches for galaxies with unusual spectral features, such as increased Balmer absorption in this case.

The three spectral lines we investigate all correlate with host galaxy magnitude (see figures 5.7, 5.9 and 5.8). Therefore, we would expect our blue galaxies to exhibit line strengths which differ from the average simply because they lie predominantly at the faint end of our galaxy distribution. We have eliminated this feature by fitting a simple linear relation between the spectral line strength and luminosity of a galaxy (see figures 5.7,

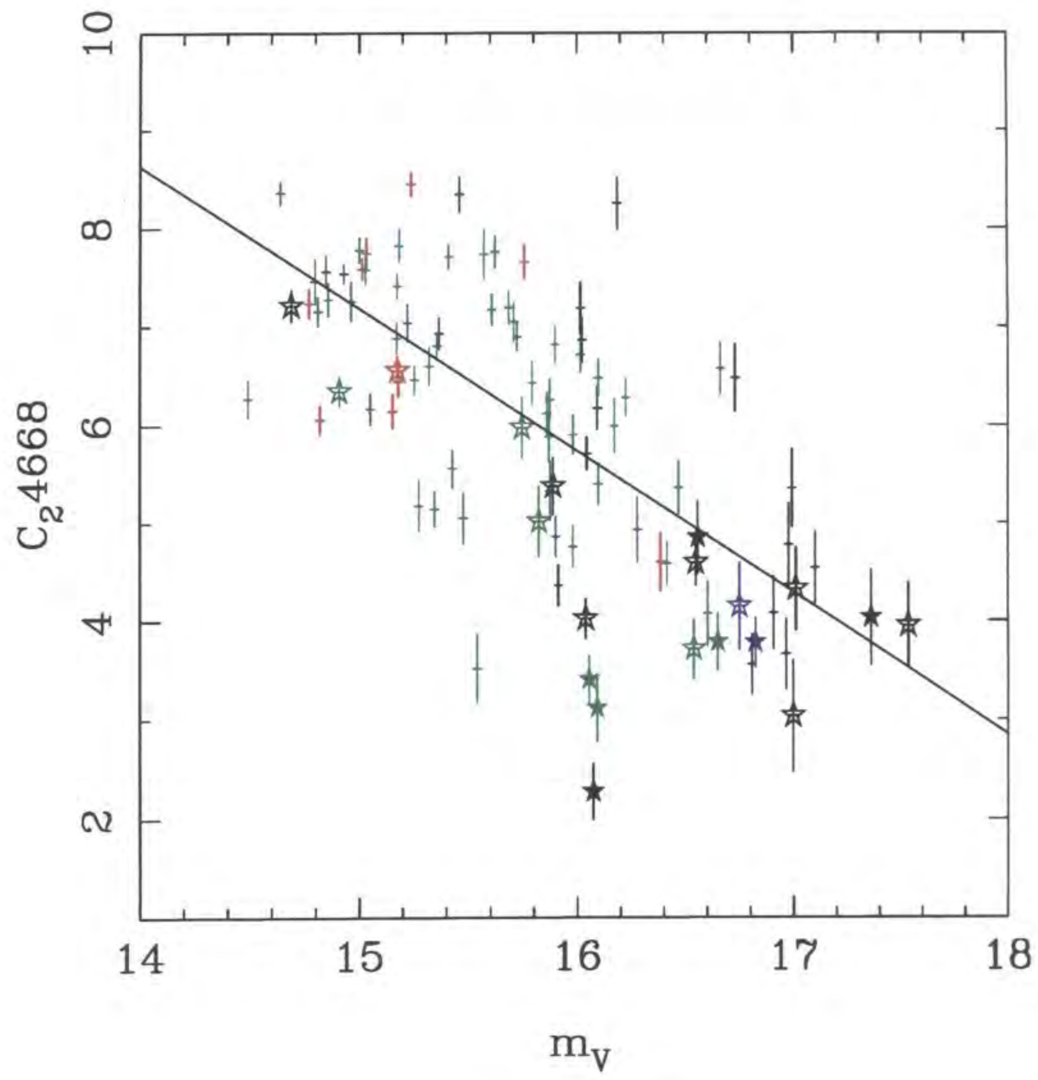

Figure 5.7: The relation between $C_2$4668 and V magnitude. The line shows the regression fit used to calculate Δ($C_2$4668). Filled stars represent objects with $\Delta(U-V) < 2\sigma$, while open stars represent objects with $2\sigma \leq \Delta(U-V) < \sigma$, where σ is the standard distribution of the $\Delta(U-V)$.

5.9 and 5.8). This relation can then be used to investigate how individual galaxies' line strength indices differ from the norm at a given luminosity. This approach is directly analogous to that taken with the colour-magnitude relation in chapter 3, and earlier in this chapter, where the $\Delta(U-V)$ measure was introduced. We therefore define

$$\Delta(X) = X - (C_X + M_X \times m_V)$$

where X is the line index ($C_2$4886,Fe4383 or $H\delta_A + H\gamma_A$), M_X and C_X are the slope and intercept of the best fit relation, and m_V is the V magnitude. Therefore, by comparing

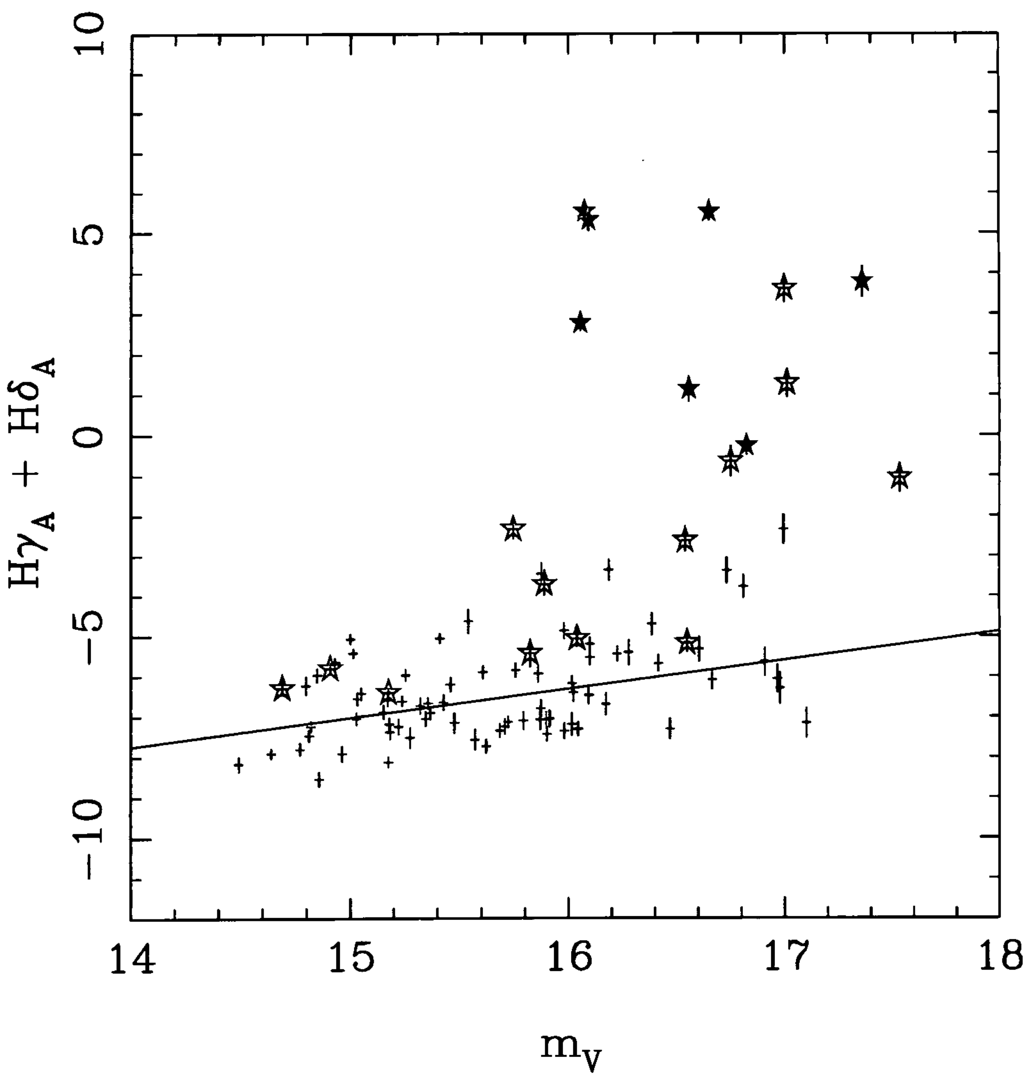

Figure 5.8: The relation between $H\delta_A + H\gamma_A$ and V magnitude. The line shows the regression fit used to calculate the $\Delta(H\delta_A + H\gamma_A)$ index. Filled stars represent objects with $\Delta(U - V) < 2\sigma$, while open stars represent objects with $2\sigma \leq \Delta(U - V) < \sigma$, where σ is the standard distribution of the $\Delta(U - V)$.

$\Delta(U - V)$ with $\Delta(X)$, we can compare a galaxy's colour offset with its spectral line strength offset.

The C_24668 relation (fig. 5.7 has a large amount of scatter about the best fit line, however there is still obviously a trend towards higher C_24668 for brighter galaxies. The $H\delta_A + H\gamma_A$ relation (fig. 5.8) also works well. The red galaxies make up a relation of increasing $H\delta_A + H\gamma_A$ with magnitude, while most of the the blue galaxies are deviant from this relation. The best fit was actually calculated using all of the data, but the biweight minimisation algorithm is very good at disregarding the 'tail' of the distribution effectively made up by the blue galaxies. Whether a satisfactory fit can be

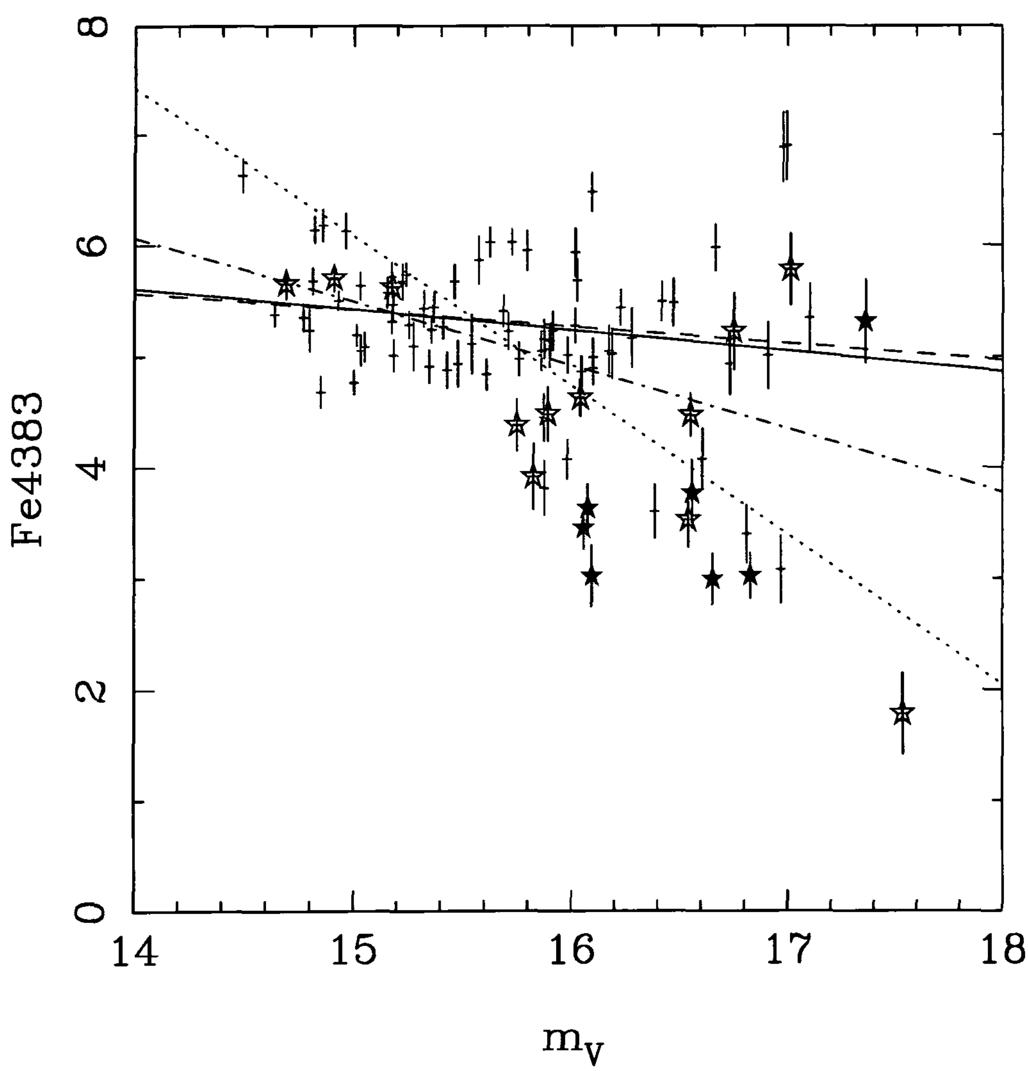

Figure 5.9: The relation between Fe4383 and V magnitude. Filled stars represent objects with $\Delta(U-V) < 2\sigma$, while open stars represent objects with $2\sigma \leq \Delta(U-V) < \sigma$, where σ is the standard distribution of the $\Delta(U-V)$.The solid line is the biweight scatter minimisation fit to all the data. The dashed line is the biweight scatter minimisation fit to only the blue galaxies, the dot-dash line shows the biweight scatter minimisation fit to galaxies with $m_V < 16$, and the dotted line shows the fit to all the data, using an OLS bisector method (see main text).

made to Fe4383 is more debatable (fig. 5.9). While there is a trend towards higher Fe4383 for the more luminous galaxies, this trend seems to bifurcate at $m_V = 16$. This leads to an uncertainty in the slope of the fit of $\sim 30\%$. Figure 5.9 shows some examples of different fits to the data. The solid line is the biweight scatter minimisation fit to all the data. The dashed line is the biweight scatter minimisation fit to only the 'normal' CMR galaxies, the dot-dash line shows the biweight scatter minimisation fit to galaxies with $m_V < 16$, and the dotted line shows the fit to all the data, using a method which

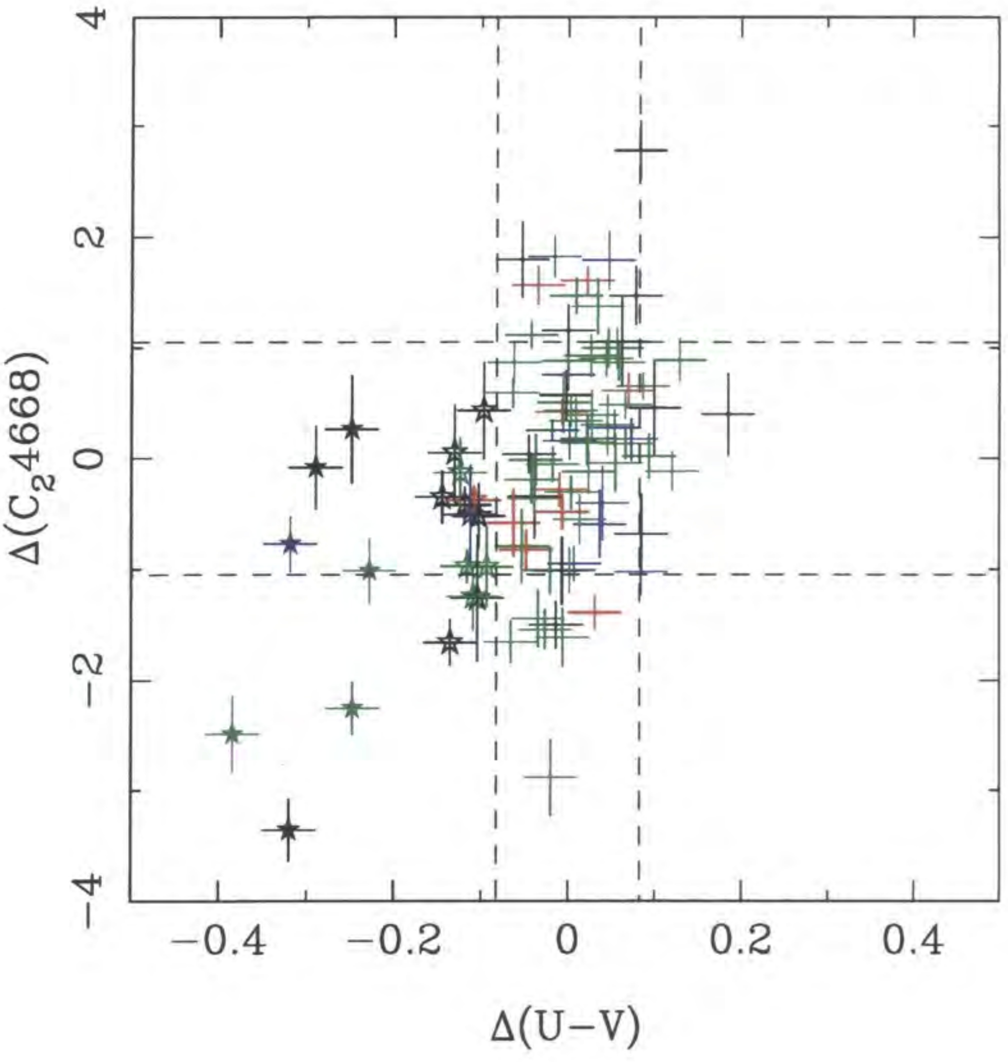

Figure 5.10: The residuals of each galaxy from the best fit colour magnitude relation, $\Delta(U-V)$, as calculated using the regression line in figure 5.4, against the $C_2$4668 line index. Filled stars represent objects with $\Delta(U-V) < 2\sigma$, while open stars represent objects with $2\sigma \leq \Delta(U-V) < \sigma$, where σ is the standard distribution of the $\Delta(U-V)$. The dashed lines represent the $\pm1\sigma$ dispersion of the $\Delta(U-V)$ and the $\Delta(C_2 4668)$.The different symbol colours represent the morphological type of the galaxy as taken from Andreon et al. (1996) and (Andreon, Davoust, & Poulain 1997) (1997), and as defined in figure 5.2.

bisects the ordinary least squares fits made by minimising the X and the Y residuals (Isobe et al. 1990, Feigelson & Babu 1992). It is not possible to say, as was the case with $H\delta_A + H\gamma_A$ in figure 5.8, that all of the 'blue' galaxies lie away from the main relation defined by the normal galaxies, as both the high and low Fe4383 branches contain 'blue' and normal galaxies. However, in these models, the Fe4383 index does have a higher dependence on age than does the $C_2$4668 index. Only one out of the seven galaxies with

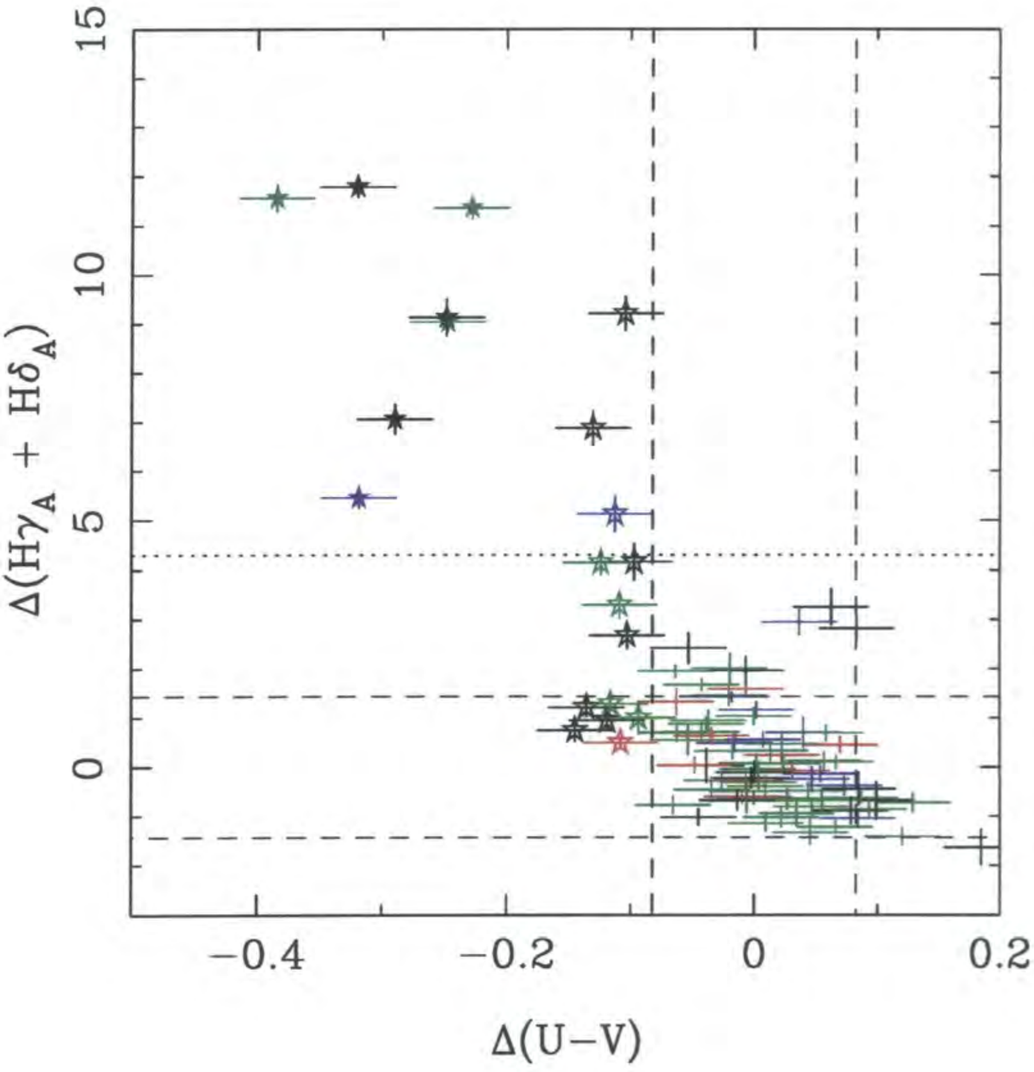

Figure 5.11: The residuals of each galaxy from the best fit colour magnitude relation, $\Delta(U-V)$, as calculated using the regression line in figure 5.4, against the $H\delta_A + H\gamma_A$line index. Filled stars represent objects with $\Delta(U-V) < 2\sigma$, while open stars represent objects with $2\sigma \leq \Delta(U-V) < \sigma$, where σ is the standard distribution of the $\Delta(U-V)$. The dashed lines represent the $\pm 1\sigma$ dispersion of the $\Delta(U-V)$ and the $\Delta(H\delta_A + H\gamma_A)$, and the dotted line shows the 3σ deviation from the mean $\Delta(H\delta_A + H\gamma_A)$ value. The different symbol colours represent the morphological type of the galaxy as taken from Andreon et al. (1996) and (Andreon, Davoust, & Poulain 1997) (1997), and as defined in figure 5.2.

$\Delta(U-V) < -2\sigma$ (filled symbols) does not lie on the lower branch, and it is the faintest one, with the largest measurement and systematic errors. It is also the galaxy furthest from the model grid in figure 5.6. We therefore conclude that the lower branch is primarily an age effect, similar to that seen in figure 5.8.

Figure 5.10 shows how the galaxies' deviation from 'normal' C_24668 line strength and 'normal' colour correlate. Only three of the $\Delta(U-V) < -2\sigma$ galaxies have ΔC_24668

values which lie outside the $\pm 1\sigma$ range indicated by the dashed lines, The other four filled symbol galaxies lie within $\pm 1\sigma$ of the mean $\Delta C_2 4668$.

The situation with $\Delta(H\delta_A + H\gamma_A)$ is very different. Figure 5.11 shows that all of the filled symbol 'blue' galaxies deviate from the mean $\Delta(H\delta_A + H\gamma_A)$ by more than 3σ. The open symbol 'blue' galaxies span a large range in $\Delta(H\delta_A + H\gamma_A)$, just over half of them deviate from the mean of the population by over 1σ, and three of them deviate by over 3σ. The open symbol galaxies which have a $\Delta(H\delta_A + H\gamma_A) < 1\sigma$ are spread uniformly along the CMR, however all of the galaxies with $\Delta(H\delta_A + H\gamma_A) > 1\sigma$ lie at the faint end ($m_V > 15.8$).

In summary if we take the population of galaxies whose colour deviates by more than 2σ from the mean CMR (the filled symbols), they all have $H\delta_A + H\gamma_A$ line strengths which deviate by over 3σ from the mean population. Additionally, all galaxies which deviate by over 3σ in $H\delta_A + H\gamma_A$ from the mean population, lie at least 1σ blue-wards of the mean CMR. This is not true of the $C_2 4668$ line. Only three of the galaxies with filled symbols deviate in $\Delta C_2 4668$ by more than 1σ from the mean.

Figure 5.11 is similar to figures of colour against Hδ line equivalent width, used by Couch & Sharples (1987) and Barger et al. (1996) for the high redshift clusters AC114, AC118 and AC103.. They modelled how a short burst of star formation, which converted about 15% of a galaxy's mass into stars and lasted about 0.1Gyr, would affect its $B - R$ colour, and $(H\delta)$ equivalent line width. They found that at first, during the starburst phase, the colours become bluer and emission fills the $H\delta$ lines (this would move a galaxy towards the bottom left corner of figure 5.11). Once the star formation ceases, the $H\delta$ emission rapidly turns into strong absorption, but the colours remain very blue (this would move the galaxy upwards, towards the top left hand corner of figure 5.11). Barger et al. (1996) referred to this stage as the post-starburst galaxy (PSG) stage, which lasts about $1Gyr$ depending on the exact model. All the time the $EW(H\delta)$ diminishes, and the colours become redder, until the galaxy returns to its original position in the $[(B - R), EW(H\delta)]$ plane after about 2Gyr.

Although we use $H\delta_A + H\gamma_A$ instead of simply using $H\delta$, and $U - V$ colours instead of $B - R$, the gross description of how a galaxy would move in figure 5.11 given above is still valid. In addition, we have corrected our colours and $H\delta_A + H\gamma_A$ for their correlation with luminosity, which should remove some of the scatter in the diagram as seen by Couch & Sharples (1987), and make it look slightly more like the theoretical predictions of Barger et al. (1996). What we find, is that there are no galaxies in our sample currently undergoing a burst of star formation ($H\delta_A + H\gamma_A$ in emission, and blue colours), however, the blue galaxy sample, sits in a the post–starburst portion of the diagram, (blue colours and strong $H\delta_A + H\gamma_A$ absorption), which ties in with section 5.3.1, and the original results of Caldwell et al. (1993).

5.4 Discussion

We have shown using both the Fe4383 and the $C_2$4668 indices, that the 'red' galaxies which make up the colour–magnitude relation in the Coma cluster, span a range of metallicities. Whether this is the sole driving force behind the CMR, or whether there is also a correlation between age and mass, we cannot say due to the high noise in the Caldwell et al. spectroscopy, and possible systematics in the way it was calibrated to the Lick/IDS system. We do note however, that if there is a correlation between age and luminosity, our data implies that it is in the sense of the larger galaxies having systematically younger ages. This is the opposite of the trend required to construct a CMR from an luminosity–age correlation, and would require the luminosity–metallicity trend to over compensate for the blue colours from the younger stellar populations in the more massive galaxies. Certainly age variations seem to be ruled out as the sole driving force behind the CMR in the cluster core. It should be noted however, that any trend in age comes form the $C_2$4668 index, at strengths where overabundance effects mean that it is no longer properly predicted by the Worthey models (see figure 5.3 and Vazdekis et al. 1996, Vazdekis et al. 1997).

Despite the attempts of Caldwell et al. to reject late type galaxies from their sample, a few still seem to have slipped in. We found that the S0 and late type galaxies span a range in ages, but all elliptical galaxies are old. Of the galaxies which lie on the CMR (the red galaxies) we found no obvious difference between the ages of the early and late types, all of them have old luminosity weighted mean stellar ages. Surprisingly, this includes 11 out of the 13 late type galaxies in the sample, however it must be remembered that the spectra are taken from a 2″ diameter aperture on the core of the galaxy, so any star formation activity in the disk of the galaxy is not likely to have much effect on the spectrum.

By comparing our CMR–corrected colour–Balmer line strength plot (figure 5.11), with those of Barger et al. (1996), we can construct an evolutionary history of the galaxies in our sample. We have used different colours and Balmer lines to those of Barger et al., so we cannot directly compare our plot with their models, however the relative shape of the evolutionary track of a galaxy during and after a starburst should remain similar. If we associate the red galaxies in figure 5.11 with the E galaxies in figure 4 (panel a) of Barger et al. (1996), then we can say that our blue galaxies lie in the post-starburst portion of the plot, and that they may have undergone a burst of star formation of up to 10% of the galaxy mass in the last 2Gyr. This is in agreement with the results of Caldwell et al. (1993).

We have also demonstrated that the use of CMR corrected $(U - V)$ colours is an efficient way of searching for post–starburst galaxies. The $(B, B - V)$ CMR constructed by Caldwell et al. (1993) for these same objects, shows no sign of our blue galaxies, however we find that only our blue objects have strong Balmer absorption features. In fact all our very blue objects, which deviate bluewards by more than two standard deviations from the CMR colour, have Balmer line strengths that deviate by more than three standard deviations from the red galaxies. If we were to search for the PSB galaxies from scratch, and made a colour cut one standard deviation redward of the CMR, we would find that half of our galaxies had Balmer line strengths that deviate by more than three standard deviations from the mean.

5.5 Summary

- The colour–magnitude relation in the Coma cluster is primarily a metallicity–mass sequence.

- We can find no age contribution to the CMR, however our spectroscopic data is not ideal for this test.

- Elliptical galaxies are old, but the spiral and S0 types span a range in ages. Most of the galaxies in the sample however, are old, no matter what their morphological type.

- The blue galaxies identified from the $(V, U - V)$ colour–magnitude relation are the only ones which have significantly younger stellar populations. They are mainly of S0, late or unclassified morphology.

- The lack of $H\delta_A + H\gamma_A$ in emission leads us to conclude that none of the blue galaxies seem to be currently undergoing a star formation burst, but most of them could have undergone a burst of star formation within the last 2Gyr.

- The use of the $(V, U - V)$ CMR is a very efficient method for finding cluster galaxies with enhanced Balmer absorption lines, however it is poor at finding galaxies with enhanced metal lines.

References

Andreon S., Davoust E., Michard R., Nieto J. L., Poulain P., 1996, Astronomy and Astrophysics Supplement Series, 116, 429

Andreon S., Davoust E., Poulain P., 1997, Astronomy and Astrophysics Supplement Series, 126, 67

Arimoto N., Yoshii Y., 1987, A&A, 173, 23

Baier F. W., 1984, Astronomische Nachrichten, 305, 175

Barger A. J., Aragon-Salamanca A., Ellis R. S., Couch W. J., Smail I., Sharples R. M., 1996, MNRAS, 279, 1

Bower R. G., Kodama T., Terlevich A. I., 1998, MNRAS, 299, 1193, astro-ph/9805290

Bower R. G., Lucey J. R., Ellis R. S., 1992, MNRAS, 254, 601

Butcher H., Oemler J., A., 1978, ApJ, 226, 559

Butcher H., Oemler J., A., 1984, ApJ, 285, 426

Buzzoni A., Chincarini G., Molinari E., 1993, ApJ, 410, 499

Buzzoni A., Gariboldi G., Mantegazza L., 1992, AJ, 103, 1814

Caldwell N., Rose J. A., Franx M., Leonardi A. J., 1996, AJ, 111, 78

Caldwell N., Rose J. A., Sharples R. M., Ellis R. S., Bower R. G., 1993, AJ, 106, 473

Charlot S., Silk J., 1994, ApJ, 432, 453

Colless M., Dunn A. M., 1996, ApJ, 458, 435

Couch W. J., Sharples R. M., 1987, MNRAS, 229, 423

Davies R. L., Sadler E. M., Peletier R. F., 1993, MNRAS, 262, 650

Dressler A., 1980, ApJS, 42, 565

Dressler A., 1984, ApJ, 281, 512

Ellis R. S., Smail I., Dressler A., Couch W. J., Oemler J., Augustus, Butcher H., Sharples R. M., 1997, ApJ, 483, 582

Escalera E., Slezak E., Mazure A., 1992, A&A, 264, 379

Faber S. M., Jackson R. E., 1976, ApJ, 204, 668

Feigelson E. D., Babu G. J., 1992, ApJ, 397, 55

Godwin J. G., Metcalfe N., Peach J. V., 1983, MNRAS, 202, 113

González J. J., 1993, Ph.D. thesis, Univ. California, Santa Cruz

Isobe T., Feigelson E. D., Akritas M. G., Babu G. J., 1990, ApJ, 364, 104

Kodama T., 1997, Ph.D. thesis, Institute of Astronomy, University of Tokyo

Kodama T., Arimoto N., 1997, A&A, 320, 41

Kuntschner H., 1998, Ph.D. thesis, Department of Physics, University of Durham

Kuntschner H., Davies R. L., 1998, MNRAS, 295, L29

Larson R. B., 1974, MNRAS, 169, 229

Larson R. B., Tinsley B. M., Caldwell C. N., 1980, ApJ, 237, 692

Lucey J. R., Guzman R., Steel J., Carter D., 1997, MNRAS, 287, 899L

Osterbrock D. E., 1989, in Published by University Science Books, 648 Broadway, Suite 902, New York, NY 10012, 1989.

Renzini A., Buzzoni A., 1986, in Spectral Evolution of Galaxies, p. 195

Stanford S. A., Eisenhardt P. R., Dickinson M., 1998, ApJ, 492, 461

Trager S. C., 1997, Ph.D. thesis, Univ. California, Santa Cruz

Vader J. P., 1986, ApJ, 306, 390

Vazdekis A., Casuso E., Peletier R. F., Beckman J. E., 1996, ApJS, 106, 307

Vazdekis A., Peletier R. F., Beckman J. E., Casuso E., 1997, ApJS, 111, 203

Visvanathan N., Sandage A., 1977, ApJ, 216, 214

Worthey G., 1994, ApJS, 95, 107

Worthey G., Ottaviani D. L., 1997, ApJS, 111, 377

Chapter 6

Butcher Oemler Galaxies and Cluster X-ray Sub-structure.

Abstract. We use a wavelet code to suggest an association between X-ray cluster substructure and 'E+A' galaxy activity in high redshift clusters.

6.1 Introduction

The clusters AC114 and AC118 were targeted by Couch and Sharples (Couch & Sharples 1987)(CS) for their spectroscopic study of the Butcher-Oemler effect in clusters at redshift 0.3. As originally stated, the Butcher-Oemler effect (Butcher & Oemler 1978, Butcher & Oemler 1984) relates to the increased fraction of blue galaxies in high and moderate redshift clusters. However, spectroscopic studies of high redshift clusters (Couch & Sharples 1987, Dressler & Gunn 1983) have subsequently been expanded to also include the appearance, in clusters, of galaxies with unusually high levels of star formation activity or abnormally strong Balmer absorption lines. The latter are commonly referred to as E+A galaxies, since their spectra are well reproduced by adding 10–20% of A-star light to a normal elliptical galaxy spectrum.

It is tempting to suggest that we are witnessing, in these distant clusters, the epoch at which E galaxies are formed from spirals, or at which star formation in spirals has just begun to fade, converting themselves into S0 types (e.g. Balogh et al., 1998). Unfortunately, this scenario has a number of problems. For example, some of the anomalous spectra are not consistent with the passive fading of a spiral galaxy and require the star formation to terminate in a strong burst (Poggianti et al. 1999). By combining the colours of the galaxies with their spectroscopic $H\delta$ line strengths, CS were able to plot the evolutionary tracks of the star burst and post starburst galaxies, and thus to classify the galaxies as normal spirals and elliptical, galaxies caught during the starburst phase and post-starburst (PSB) galaxies.

In this chapter, we present high resolution X-ray observations of these clusters. The motivation for these observations is to look at the dynamical state of these clusters. One appealing explanation of the Butcher-Oemler effect is that the population of starburst galaxies is created when a large group of gas rich galaxies is swallowed by the cluster. Possibly the tidal distortion experienced by the group results in frequent interactions between galaxies. These interactions are then likely to result in bursts of star formation. This scenario has a number of appealing features. The fraction of anomalous galaxies in the high-redshift clusters is uncomfortably high given that their unusual spectra and blue colours are short lived ($\sim$ 1 Gyr). If the rate of their creation is approximately constant, then 50% of the present-epoch early-type galaxy population would have been produced since a red-shift of 0.4. Such a high fraction of 'young' early-type galaxies appears inconsistent with the existence of a well-defined colour–magnitude relation (Bower, Lucey, & Ellis 1992). This problem could be considerably reduced if the occurrence of bursts was linked to the infall of galaxy groups and thus sporadic in nature (Abraham et al. 1996) and, perhaps, strongly dependent on redshift. Furthermore, the intermittent infall of the groups could explaining the wide variation in the fraction of blue galaxies between different high-redshift clusters. For example, the 0016+16 cluster (Koo, 1981) shows no excess fraction of blue galaxies, but does have a large population of spectroscopically identified post-starburst (E+A) galaxies (Dressler & Gunn 1992).

This chapter can be outlined as follows. Both of the clusters AC114 and AC118 show significant numbers of galaxies that are either caught in the midst of a burst of star formation, or in which star formation has only recently terminated. If it is the case that the Butcher-Oemler effect occurs in sporadic episodes associated with the infall of a large group of gas rich galaxies, then we should still expect to see evidence of the disturbance in the X-ray morphology of the cluster. The test has two stages. Firstly, we wish to establish whether the clusters have smooth, relaxed X-ray profiles without significant substructure. If the X-ray images reveal the cluster to have multiple components, then we wish to determine whether they are still physically separate systems, or whether they are interacting. In their analysis of the NGC 4839 sub-component of the Coma cluster, Burns et al. (1994) demonstrated that the presence of tails and plumes of gas were signatures of a sub-clump being broken up (and subsequently 'swallowed') by its interaction with the main cluster. We will search for the presence of such features using the wavelet transformation (eg., Grebenev et al., 1995 and references therein). The ability of the transform to separate structures with different spatial scales provides us with a quantitative method for classifying the diffuse structure of these distant clusters.

Finally, we should comment that the data we present here is part of a long term strategy of similar observations of a wide sample of high-redshift galaxy clusters. The reader is cautioned that the conclusions we draw in this chapter are based on observations of only two clusters. Observations of a much wider sample are needed in order to derive general conclusions about the X-ray structure of Butcher-Oemler clusters.

6.2 Data Analysis

The ability to decompose a signal both into spatial and frequency components makes the wavelet transform an ideal tool for analysing structures in the spatial and velocity distribution of galaxies (Slezak, Bijaoui, & Mars 1990, Escalera & Mazure 1992, Slezak, De Lapparent, & Bijaoui 1993, Lega et al. 1995) and in the distribution of X-ray emitting gas in clusters (Grebenev et al. 1995, Rosati et al. 1995, Slezak, Durret, & Gerbal 1994, Biviano et al. 1996). The reader is referred to the above papers for a detailed explanation of the method. We only include here what is either directly relevant to or different about our analysis of the data.

A wavelet transform is just a convolution of the signal $s(x, y)$ (in this case our image) with a wavelet of a specified scale, $g(x/a, y/a)$. For our case we use a radially symmetric wavelet, so the transformation at scale a can be written as

$$w(a, x, y) = s(x, y) \otimes \frac{1}{a} g\left(\frac{r}{a}\right)$$

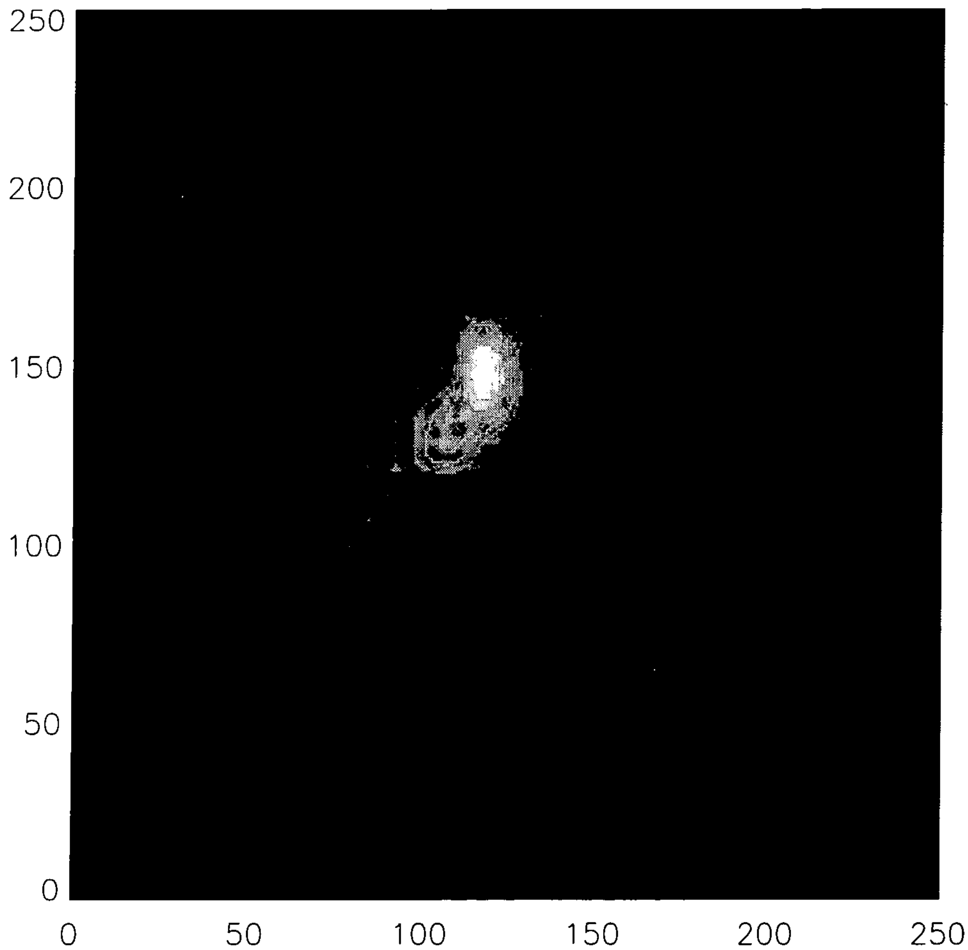

Figure 6.1: ROSAT HRI image of AC114. This image was smoothed with a $\sigma = 10''$ gaussian filter. The axes are in pixels. The scale is $2''/pixel$ which corresponds to $5.5h^{-1}$ kpc/$pixel$

There are an infinite choice of possible wavelets to use, but we have chosen the radial mexican hat, given by

$$g\left(\frac{r}{a}\right) = \left(2 - \frac{r^2}{a^2}\right) e^{-r^2/2a^2}$$

for its insensitivity to gradients and its ability to remove flat components (e.g. Slezak, Bijaoui, & Mars 1990, Grebenev et al. 1995).

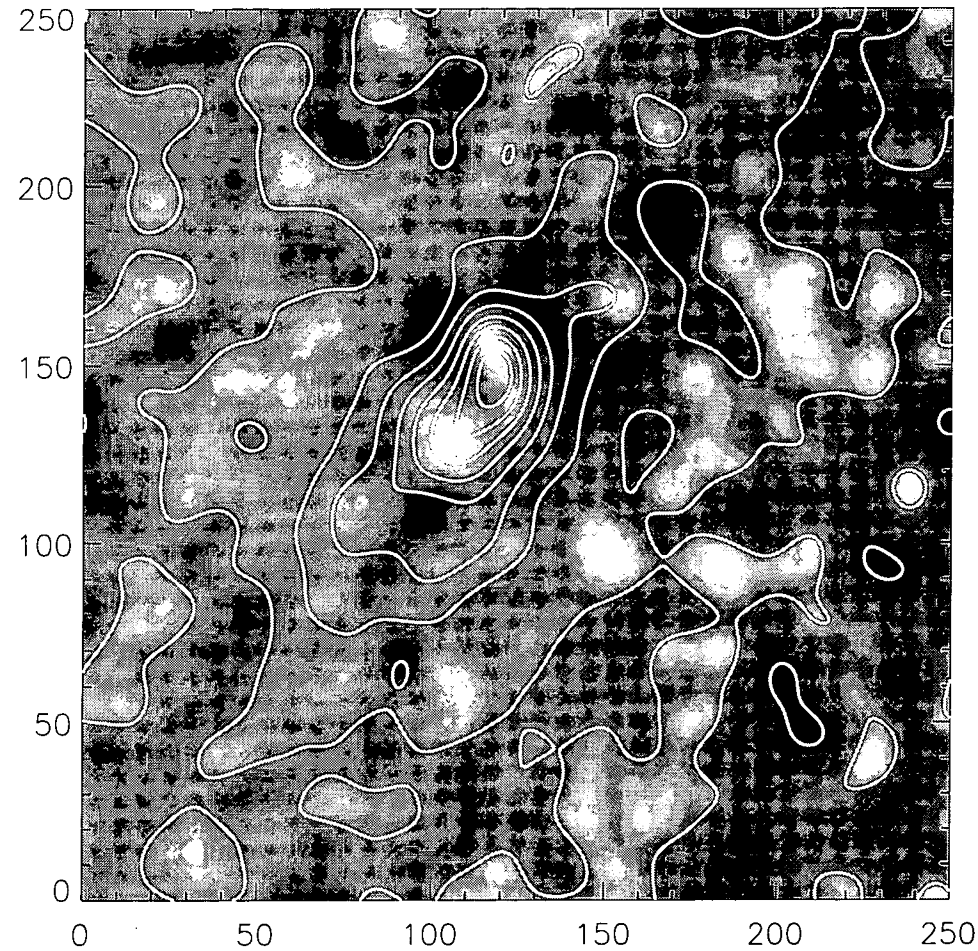

Figure 6.2: The smoothed X-ray image of AC114 after having the wavelet reconstructed model subtracted. The background appears noisier than in figure 6.1 due to renormalisation of the colourmap after removing the extended emission. The contours show the original data as seen in figure 6.1. Point sources are clearly visible where the core of the cluster used to be.

6.2.1 Reconstruction of the source

In order to allow us to create a reconstruction of the X-ray image, it is first decomposed into a set of wavelet space images corresponding to discrete scale values (i.e. a $2a$ $4a$ etc...) (See figure 6.5).

The wavelet transform transfers scale information in the source image into wavelet coefficient value in the transformed image. If we assume the source is made up from a superposition of Gaussians, then each if these Gaussians is transformed into a three

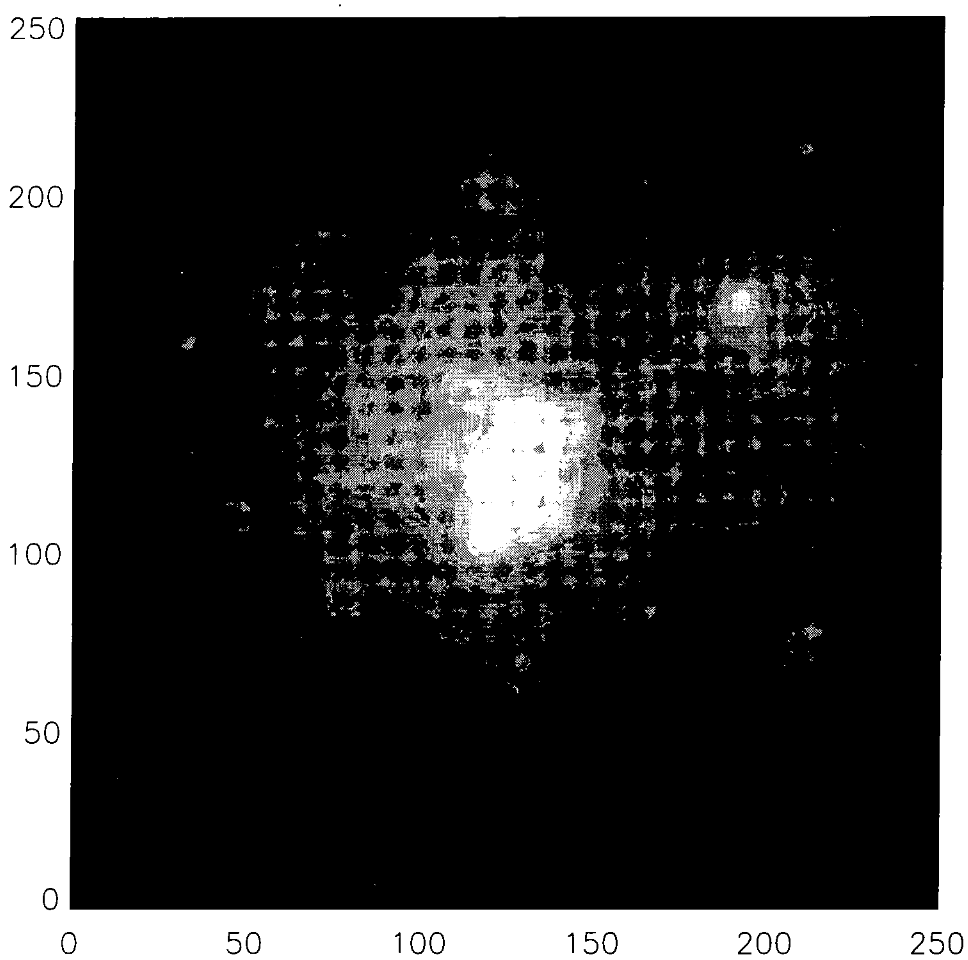

Figure 6.3: ROSAT HRI image of AC118.. This image was smoothed with a $\sigma = 10''$ gaussian filter. The axes are in pixels. The scale is $2''/pixel$ which corresponds to $5.5h^{-1}$ kpc$/pixel$

dimensional 'ellipsoid' in wavelet space, having a maximum wavelet coefficient (w_{max}) at ($a_{max}, x_{max}, y_{max}$).

The values of w_{max},a_{max},x_{max} and y_{max} can be found simply due to the very weak dependance of x_{max} and y_{max} on a_{max}. Initially we have a very sparse sampling of wavelet space in a (only $a = 30'', 80'', 130''$ and $170''$) but that is enough to get initial values for a_{max},x_{max} and y_{max}, then fixing x_{max} and y_{max} reduces the problem to the simple task of maximising the one dimensional function $w(a, x_{max}, y_{max})$. The ellipticity of the Gaussian component in the source image and its position angle (e_s,a_s) can also

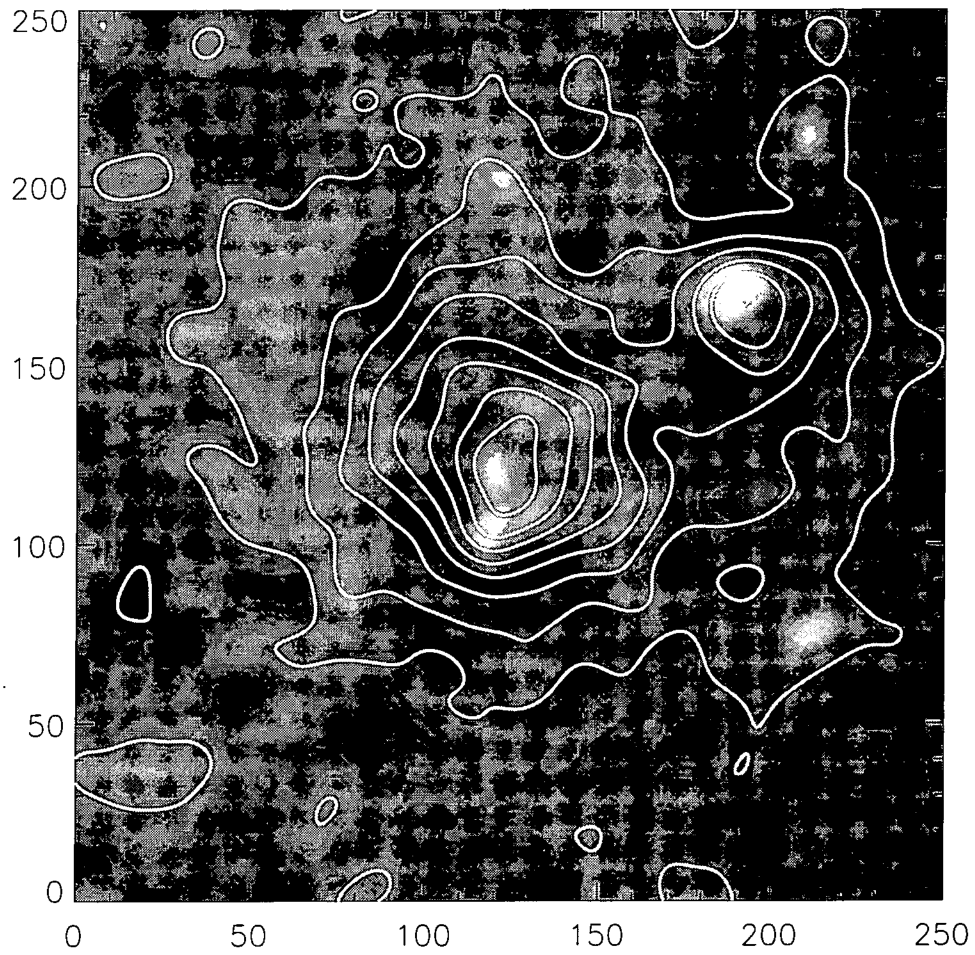

Figure 6.4: As figure 6.2 but showing AC118.

be estimated from the ellipticity and position angle of the wavelet coefficients in the $a = a_{max}$ plane (e_w,a_w).

The response of w_{max},a_{max},x_{max},y_{max}, e_w and a_w was determined empirically from synthetic source images containing single Gaussian whose parameters spanned the whole range on interest. This response function was then inverted and fitted to a simple polynomial to allow the actual source parameters to be determined from the wavelet space parameters.

As the real data is not simply made up of a single Gaussian, an iterative procedure is utilised whereby the Gaussian corresponding to the greatest maximum in wavelet space

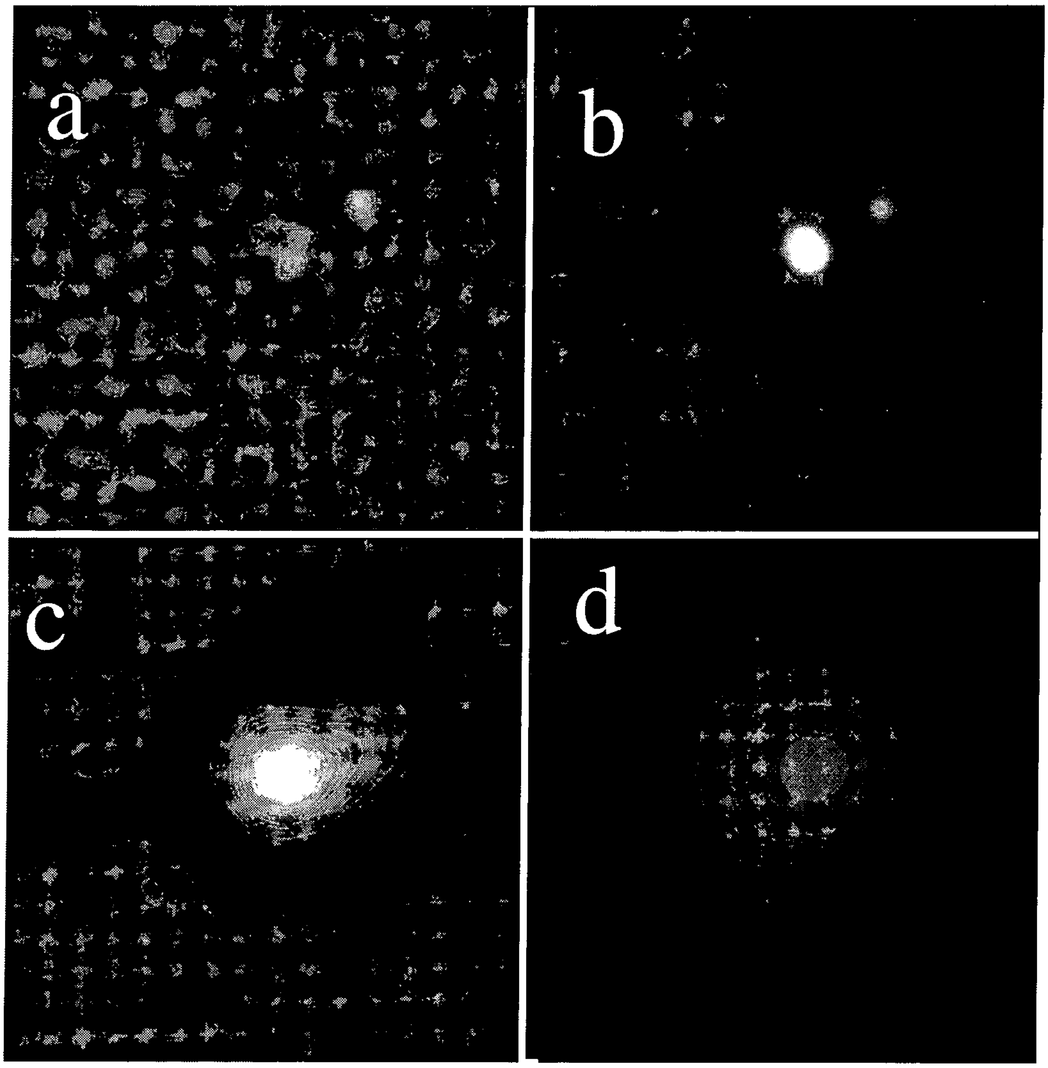

Figure 6.5: The transformations of the X-ray image of ac118 obtained using the ROSAT HRI into wavelet space. The scale of the wavelet used in each case is $a = 20'', 40'', 80''$ and $160''$ respectively.

is subtracted from the source image, which is then reprocessed to find further subcomponents.

To generate confidence intervals for the models we use the C statistic of Cash (1979) to form a likelihood ratio.

$$C = 2\sum_{i=1}^{N}(e_i - n_i\, ln\, e_i)$$

Here e_i is the expected number of counts and n_i is the actual number of counts in detector i. The model is simply a function of the parameters of the Gaussians, $\theta_1, ..., \theta_p$. The term $(C_{min})_p$ is found by varying all parameters $\theta_1, ..., \theta_p$ until a minimum C is found. Similarly $(C_{min})^T_{p-q}$ is calculated by setting $\theta_1, ..., \theta_q$ to their 'true' values, $\theta^T_1, ..., \theta^T_q$ and allowing $\theta_{q+1}, ..., \theta_p$ to vary until a minimum value of C is found.

$$\Delta C = (C_{min})^T_{p-q} - (C_{min})_p$$

is then distributed as χ^2 with q degrees of freedom. This allows us to place our detected Gaussians into order of significance.

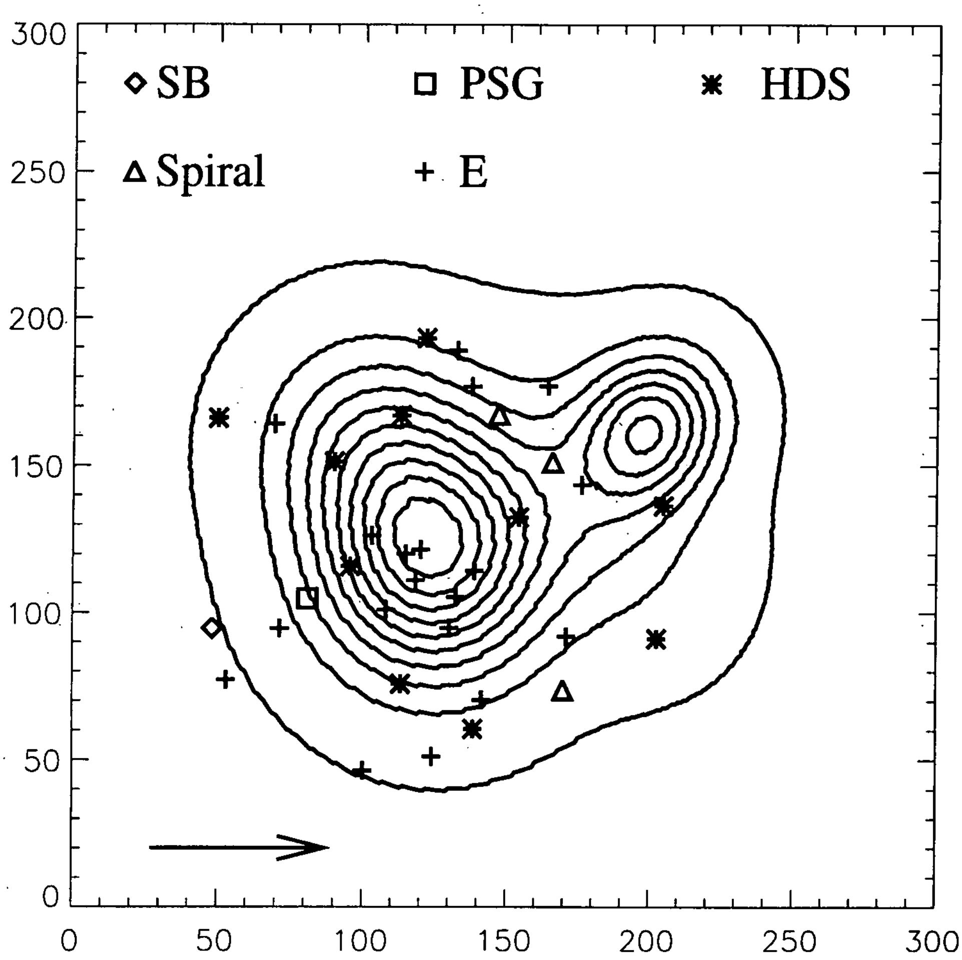

Figure 6.6: The positions of the CS galaxies superposed upon the wavelet reconstruction of the X-ray image of AC118. The axes are in 2″ pixels.

The X-ray images of AC114 and AC118 are shown in Figures 6.1 and 6.3 respectively. Figures 6.6 and 6.7 show the wavelet reconstructions of the X-ray images for AC118 and AC114 respectively with the positions of the galaxies identified by CS superposed. It is immediately obvious that both systems do not conform to a simple ellipsoidal shape. In the

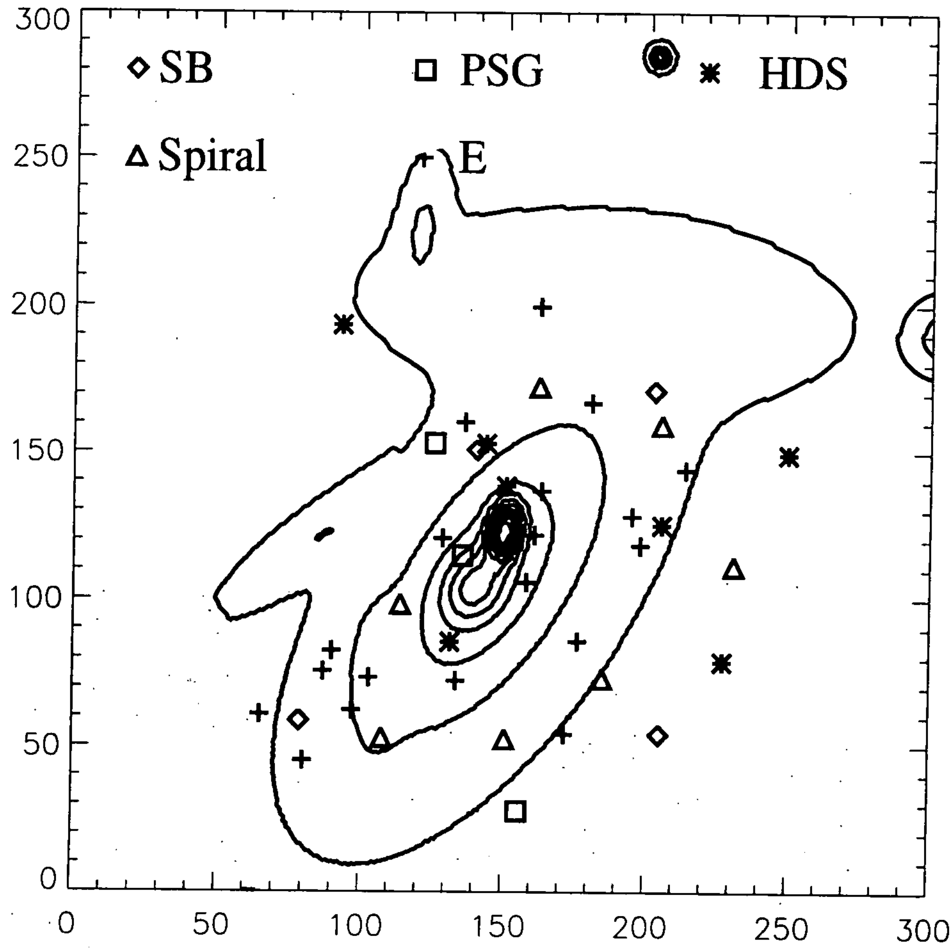

Figure 6.7: The positions of the CS galaxies superposed upon the wavelet reconstruction of the X-ray image of AC114. The axes are in 2″ pixels.

Component	X (pixels)	Y (pixels)	Flux (photons)	2σ (2″pixels)	e	Angle (degrees)
A	124.1	123.0	3991	25.2	0.39	172.6
B	199.0	163.0	1455	15.2	0.50	38.7
C	101.8	161.4	3228	22.7	0.07	162.9
D	181.3	139.0	3300	22.9	0.64	148.9

Table 6.1. Model components of the most significant large structures found in AC118. The positions of the elements are in 2″ pixels and refer to positions in figure 6.6.

Component	X (pixels)	Y (pixels)	Flux (photons)	2σ (2″pixels)	e	Angle (degrees)
A	122.4	145.0	2119.1	18.4	0.89	32.4
B	126.0	151.0	267.2	6.5	0.79	60.5
C	151.8	237.5	2531.1	20.1	0.92	93.5
D	79.6	111.0	701.3	10.6	0.97	176.6
E	32.3	148.8	242.3	6.2	0.97	139.1

Table 6.2. Model components of the most significant large structures found in AC114. The positions of the elements are in 2″ pixels and refer to positions in figure 6.7

case of AC114, there is a main center to the cluster structure (though this could be mainly due to the point sources visible in figure 6.2), but unsymmetric lower surface brightness features can be seen to extend to the North West and South East. Table 6.2 shows that the components of the wavelet transform that make up the reconstructed image all have high ellipticities The features are strongly suggestive of plumes of gas ejected in a cluster merger.

The morphology of the AC118 cluster is very different. There are two clearly defined peaks of X-ray emission separated by 154″ ($424h^{-1}$ kpc) (see table 6.1). While this clearly indicates that the cluster is a binary system, each of the peaks appears to be individually relaxed, with low values for their ellipticity (table 6.1). The bridge of emission which appears to connect the two components is not picked up by the wavelet transform, figure 6.4 shows what is left of the X-ray image after subtraction of the wavelet reconstructed image shown in figure 6.6, there is no emission between the two maxima. We therefore conclude that the two structures are not yet interacting. There is however some extended emission to the North_East, and South_West of the largest X-ray peak (see table 6.1).

6.3 Comparison with galaxy population

Figures 6.6 and 6.7 show the wavelet reconstructions of the X-ray images for AC118 and AC114 respectively with the positions of the galaxies identified by CS superposed. The CS spectra only cover the central parts of the cluster. They do not even cover the entire area of X-ray emission detected by the HRI, despite its high background noise. There are no galaxies at all covering the NW substructure in AC118, which is unfortunate given the resemblance the X-ray image has to the local Coma cluster, where Caldwell et al. (1993) associate an enhanced number of 'E+A' galaxies with substructure associated with NGC4339, and visible in the cluster X-ray image (White, Briel, & Henry 1993; see figure 2.3)

With Caldwell et al. (1993) in mind, we have labelled positions of the cluster galaxies from CS with points showing the classification of the spectra as defined by Barger et al. (1996). They model old elliptical populations which undergo a short (0.1Gyr) burst of star formation, consuming $\sim$ 10% of the galaxy mass, and younger spiral populations which undergo a stronger 20% burst. About 0.2Gyr after the onset of the burst, they classify the galaxy as a post–starburst galaxy (PSB), and after roughly 0.7Gyr they are classified as $H\delta$ strong (HDS).

Galaxies can still be in the HDS phase upto 2Gyr after the truncation of star formation. Assuming the incoming galaxies have coherent velocity dispersions of the same order as that of the main cluster ($1947Kms^{-1} \sim 2MpcGyr^{-1}$ for AC118 (CS)) any infalling groups could have been scattered about the main cluster while still being classified as an HDS galaxy. However, Galaxies are classified as SB, or PSB for a much shorted period of time. The arrow in figure 6.6 is $\sim 400h^{-1}Kpc$ long, and so shows the maximum possible distance travelled by a SB galaxy. It must be said however that the velocity dispersion of AC118 is very high (c.f. Coma of $\sim 900kms^{-1}$), so in many cases, galaxies will move far less than the length of this arrow in $.2Gyr$.

In the case of AC118, the single SB galaxy is further from the NW substructure than the length of the arrow, and so, assuming that the structures are not connected, the galaxy cannot be associated with it. In AC114 (figure 6.7), the SB galaxies are distributed all over the cluster, and could be associated with any of the substructures listed in table 6.2, however the numbers of SB and PSB galaxies in AC114 is much higher (7) than the number in AC118 (2). This is possibly associated with the increased amount of substructure and signs of disturbance in AC114.

6.4 Discussion

The wavelet decomposition of the X-ray gas shows signs of substructure in both clusters: they are not simple relaxed systems. AC118 shows immediate evidence of binary structure. AC114 also has a disturbed morphology. But, can we conclude that the Butcher-Oemler effect is caused by the infall of a large group? Disturbance and plumes seen in AC114, together with its increased number of SB and PSB galaxies are certainly consistent with this picture. The two systems seen in AC118 show little sign of disturbance. This suggests that they have only recently encountered each other, or even that they are quite distant from each other, and only appear close in projection.

It is possibly however, that as in the Coma cluster, AC118 has a population of PSB/SB galaxies associated with the second peak, which we do not see in the CS data.

Clearly, a larger dataset is needed before we can answer the questions posed in this chapter. In chapter 7 we describe an ongoing project to produce $\sim$ 500 spectra for Abell 1758 ($z = 0.28$), covering an area of 10×10arcmin, which corresponds to $1.5 \times 1.5h^{-1}Mpc$.

6.5 Summary

- We develop a method to break down X-ray cluster images into Gaussian subcomponents, which we can use to analyse their substructure.

- We attempt to correlate the X-ray substructure in two Butcher–Oemler clusters, AC114 and AC118, with their population of starburst and post–starburst galaxies as observed by Couch & Sharples (1987). Although we note that the cluster with the most disturbed morphology, and the most signs of substructure also has the most SB and PSB galaxies, we cannot correlate any galaxies with any single cluster subcomponent.

References

Abraham R. G. et al., 1996, ApJ, 471, 694

Balogh M. L., Schade D., Morris S. L., Yee H. K. C., Carlberg R. G., Ellingson E., 1998, ApJ, 504, L75

Barger A. J., Aragon-Salamanca A., Ellis R. S., Couch W. J., Smail I., Sharples R. M., 1996, MNRAS, 279, 1

Biviano A., Durret F., Gerbal D., Le Fevre O., Lobo C., Mazure A., Slezak E., 1996, A&A, 311, 95

Bower R. G., Lucey J. R., Ellis R. S., 1992, MNRAS, 254, 601

Butcher H., Oemler J., A., 1978, ApJ, 226, 559

Butcher H., Oemler J., A., 1984, ApJ, 285, 426

Caldwell N., Rose J. A., Sharples R. M., Ellis R. S., Bower R. G., 1993, AJ, 106, 473

Cash W., 1979, ApJ, 228, 939

Couch W. J., Sharples R. M., 1987, MNRAS, 229, 423

Dressler A., Gunn J. E., 1983, ApJ, 270, 7

Dressler A., Gunn J. E., 1992, ApJS, 78, 1

Escalera E., Mazure A., 1992, ApJ, 388, 23

Grebenev S. A., Forman W., Jones C., Murray S., 1995, ApJ, 445, 607

Lega E., Scholl H., Alimi J.-M., Bijaoui A., Bury P., 1995, Parallel Computing, 21, 265

Poggianti B., Smail I. R., Dressler A., Couch W., Barger A., Butcher H., Ellis R. S., Oemler A., 1999, ApJ, in press, (astro-ph/9901264)

Rosati P., Della Ceca R., Burg R., Norman C., Giacconi R., 1995, ApJ, 445, L11

Slezak E., Bijaoui A., Mars G., 1990, A&A, 227, 301

Slezak E., De Lapparent V., Bijaoui A., 1993, ApJ, 409, 517

Slezak E., Durret F., Gerbal D., 1994, AJ, 108, 1996

White S. D. M., Briel U. G., Henry J. P., 1993, MNRAS, 261, L8

Chapter 7

Conclusions and Further Work

In this thesis, we have investigated the star formation history in early type galaxies based on their photometric and spectroscopic properties.

We find the following answers to the questions posed in chapter 1.

1. We find a radial dependence of the CMR corrected colours with projected cluster radius. If interpreted as a gradient in the mean age of the galaxies with projected radius, we conclude that galaxies at a radius of $0.58h^{-1}Mpc$ are on average 1 – 2Gyr younger than those in the cluster core. We calculated the increased scatter produced in the CMR by the presence of enough dust in the cluster core to account for the colour gradient, and found that it was greater than the scatter observed in the elliptical galaxies. We therefore conclude that there cannot be sufficient dust in the cluster core to account for the entire gradient, and some must be due to age. Guzman et al. (1992) also concluded that galaxies in the 'halo' of the Coma cluster had younger mean stellar ages than those in the core, from an offset in their $Mg - \sigma$ relation.

   We find no dependence of the CMR slope or scatter on galaxy luminosity, implying a constant mass to metallicity ratio for all galaxies.

2. Dissipationless mergers do not destroy the CMR, regardless of the precise merger scenario employed, so long as the typical mass of a galaxy does not increase by more than a factor of ~ 2. We find that hierarchical clustering models can preserve an initial CMR formed before $z = 2$, however this is due mainly to the lack of mergers in the models once a large cluster dark matter halo forms, rather than to correlations

between a the mass of a galaxy, and the mass of its progenitors (Kauffmann 1996). This result means that it is still possible to construct elliptical galaxies out of stars which formed at high redshift (as is required by the differential colour evolution models , e.g. Bower, Lucey, & Ellis 1992), but still have the galaxies merge as is required by models of the evolution of structure in the universe.

3. We find that the CMR corrected $U - V$ colour and hydrogen Balmer line absorption correlate well in our sample, and leads us to two conclusions. Firstly, there are no currently star–bursting galaxies in our Coma sample (using the definition of Barger et al. (1996)). Secondly, the use of $(U - V)$ colours is an efficient way to find galaxies with enhanced Balmer absorption features.

   We note that the blue galaxies identified in chapter 5 are also the galaxies with the youngest ages as identified by Worthey (1994) models, and are either S0 or late type systems. All of the elliptical galaxies are old. We also confirm that the CMR in the Coma cluster spans a range in metallicity, but we cannot rule out some correlation between galaxy mass and age (Bressan, Chiosi, & Tantalo 1996).

4. We find little correlation between the X-ray substructure of AC114 and AC118 with their starburst (SB) and post–starburst (PSB) galaxy population. Although AC114, with more substructure, has more SB and PSB galaxies, the low numbers of galaxies involved, and their lack of spatial coverage, mean that we cannot attribute any significance to it. We plan to address this situation with future observations (see below).

In conclusion, elliptical galaxies in clusters are old, and formed the bulk of their stars in smaller systems, which then merged before the galaxies fell into the clusters in which we now see them. The galaxies on the outer parts of clusters are on average younger than the galaxies in the cores of clusters. From both the properties of the CMR, and the distributions in age and metallicity, S0 galaxies would seem to be more similar to the bulges of late type galaxies in cluster cores than to elliptical galaxies. This could be indicative of a shared evolutionary path (Dressler et al. 1997).

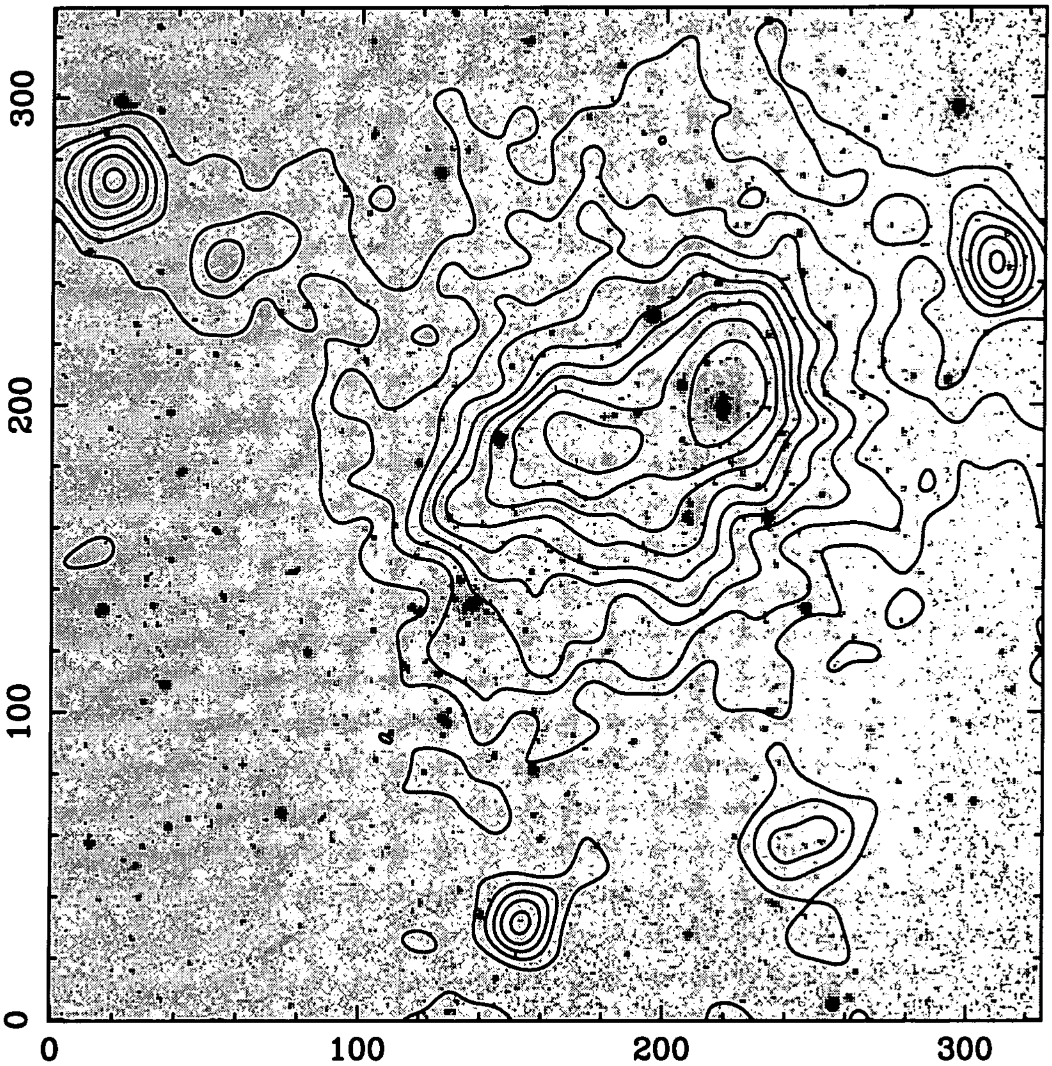

Figure 7.1: Our 28Ksec ROSAT HRI exposure of Abell 1758 superposed upon an I band image from Smail et al. (1998). The image is 9.7′ on each side. While both the X-ray and optical images display a binary structure,it can be seen from the fact that the SE galaxy concentration does not correspond to the SE X-ray maximum, but instead seems to be associated with a plume of X-ray emission, that this cluster is in a very disturbed state. This is probably the result of recent large-scale merging.

7.1 Further work

To expand upon the work presented in chapter 6, we propose to observe moderate redshift ($z \sim 0.3$) clusters to obtain both photometry and spectroscopy of large numbers of galaxies out to the virial radius. In order to quantify the role of the overall cluster environment upon the evolution of the individual cluster galaxies, it is vital to use a sample of clusters with a wide variety of X-ray morphologies, from the relatively relaxed (i.e. AC118) to the obviously disturbed (i.e. A1758, see figure 7.1). A large number of spectra over the wide area of the cluster can be used to identify member galaxies, and by placing each galaxy on a colour–H_δ line strength plane (e.g. Couch & Sharples 1987, Barger et al. 1996), their position in the star formation cycle can be identified, as well as the length of time since the last star formation event.

In their wide area survey of the relaxed cluster A2390, Abraham et al. (1996) show in there to be too few currently star-forming galaxies by a factor of two, to sustain its large population of H_δ strong (HDS) galaxies. Observations of clusters with a more disturbed X-ray morphology, including clusters which still retain signs of recent major mergers, will provide direct evidence for the relative importance of at least one triggering mechanism. A surfeit of starbursting galaxies relative to the HDS population in these disturbed clusters would be direct evidence for the role of the overall cluster environment in the triggering of Butcher-Oemler galaxies. Additionally, unless there is a significant delay between the cluster being disturbed and the appearance of starbursts within galaxies, the X-ray substructure in the cluster will also be identifiable with hot-spots of starbursting galaxies, as is the case in the Coma cluster (Caldwell et al. 1993, Caldwell et al. 1996)

At $z = 0.3$, a $\sim$ 10 arc-minute field of view, such as that available from many low dispersion survey spectrographs (i.e. LDSS2 on the William Herschel Telescope) corresponds to roughly $3h^{-1}Mpc$ ($h = H_0/50kms_{-1}Mpc^{-1}$). By using blocking filters designed for use at the redshift of each specific cluster, the multiplicity of such instruments can be tripled. The large area is needed because the lifetime of the starbursts responsible for the abnormal spectra ($\sim$ 0.5Gyr) is comparable to the crossing time in the core of the cluster. As we found in chapter 6, if we only sample the core, we would not be able to associate any X-ray substructure with a surfeit of starbursting galaxies. I have demonstrated the viability of this technique in a recent observing run. I was able to increase the multiplicity of the LDSS2 instrument on the WHT to 100 slits per mask (c.f. $\sim$ 30), and would have been able to increase it to $\sim$ 130 but for limitations in the mask manufacturing process. I propose to follow up the wide area surveys of these clusters with detailed spectroscopic analysis of the galaxies identified as starburst or post-starburst. Almost half of the high redshift active Butcher-Oemler galaxies appear to be involved in interactions or mergers (Couch et al. 1994, Smail et al. 1997, Couch et al. 1998). However this leaves just over half of the active population which do not, and given its large velocity dispersion, the cluster environment is probably the last place one would expect galaxy-galaxy interactions to occur in large numbers. The many integral field units (IFUs) being built on 8m class telescopes, such as the Gemini Multi Object Spectrographs (GMOS), will be ideal instruments for investigating these galaxies. The GMOS IFU will have 0.2 arcsec spatial sampling, and a field of view of 6×8.4 arcsec. This is ideally suited for galaxies at $0.2 < z < 0.4$ whose diameters are typically $2-4$ arcsec. By targeting bright 'old population' galaxies, and ongoing starburst galaxies, the IFU will not only be able to identify what part of the galaxy is undergoing or has undergone a starburst, but will also be able to probe for more subtle signs of past interactions in the 'non–interacting' population. An increased fraction of e.g. counter-rotating cores or counter-rotating discs in this population of galaxies would be a clear indication that in these galaxies too, galactic interactions are triggering the starbursts. By also targeting the 'interacting' population, where there are two galaxies with a modest separation ($> 1''$), we could use the IFUs to determine whether the pair is a cold bound pair, obviously interacting, or a hot bypass, at most harassing each other (Moore et al. 1996).

There is also a population of E+A galaxies in local clusters (Caldwell et al. 1993, Caldwell et al. 1996), but how do they relate to the high redshift Butcher-Oemler galaxies? The answer to the previous section will provide an important clue. Are the high redshift HDS galaxies preferentially associated with X-ray cluster substructure, as are the E+A galaxies in local clusters? The main difference between the low and high redshift E+A galaxies is in their luminosity. In the B band, a Coma E+A galaxy is on average a couple of magnitudes fainter than its high redshift counterpart (Caldwell et al. 1993). The new Coma data which I present chapter 2 shows no increase in scatter of the colour magnitude relation of early type galaxies in the outer regions of the dataset (~ 0.7 of the virial radius). This is contrary to what is observed by Van Dokkum et al. (1998) in the disky early type galaxies of the $z = 0.33$ cluster CL 1358+62, and to the predictions of hierarchical clustering models. Because we do not reach the virial radius of the cluster, it is still possible for the scatter in the CM relation to increase at larger radii than what we have so far probed. Follow up observations in the U and V bands on the outer parts of Coma would finally resolve this problem. By also targeting local compact groups, it will be possible to obtain a comparable number of galaxies in a much poorer environment to compare with the cluster results. While others have obtained large area photometry of clusters, no one has the wide area, deep U and V band CCD images of local clusters and groups needed for such detailed investigation of the CM relation.

References

Abraham R. G. et al., 1996, ApJ, 471, 694

Barger A. J., Aragon-Salamanca A., Ellis R. S., Couch W. J., Smail I., Sharples R. M., 1996, MNRAS, 279, 1

Bower R. G., Lucey J. R., Ellis R. S., 1992, MNRAS, 254, 601

Bressan A., Chiosi C., Tantalo R., 1996, A&A, 311, 425

Caldwell N., Rose J. A., Franx M., Leonardi A. J., 1996, AJ, 111, 78

Caldwell N., Rose J. A., Sharples R. M., Ellis R. S., Bower R. G., 1993, AJ, 106, 473

Couch W. J., Barger A. J., Smail I., Ellis R. S., Sharples R. M., 1998, ApJ, 497, 188

Couch W. J., Ellis R. S., Sharples R. M., Smail I., 1994, ApJ, 430, 121

Couch W. J., Sharples R. M., 1987, MNRAS, 229, 423

Dressler A. et al., 1997, ApJ, 490, 577

Guzman R., Lucey J. R., Carter D., Terlevich R. J., 1992, MNRAS, 257, 187

Kauffmann G., 1996, MNRAS, 281, 487

Moore B., Katz N., Lake G., Dressler A., Oemler J., A., 1996, Nature, 379, 613

Smail I., Dressler A., Couch W. J., Ellis R. S., Oemler J., Augustus, Butcher H., Sharples R. M., 1997, ApJS, 110, 213

Smail I., Edge A. C., Ellis R. S., Blandford R. D., 1998, MNRAS, 293, 124, Provided by the NASA Astrophysics Data System

Van Dokkum P. G., Franx M., Kelson D. D., Illingworth G. D., 1998, ApJ, 504, L17

Worthey G., 1994, ApJS, 95, 107

Appendix A

Tables of Photometry

A.1 Tables of photometry

Table A.1 gives the positions and name of all the objects observed. Where an object has a Godwin, Metcalfe, & Peach (1983) number (GMP), or a Dressler (1980) number D80, that is shown. One other name a galaxy may have, as reported by the NASA/IPAC extragalactic database (NED) is also reported. The morphology is taken from Andreon et al. (1996) and Andreon, Davoust, & Poulain (1997). The class star column shows the CLASS_STAR parameters from SExtractor (Bertin & Arnouts 1996). An point like object is represented by a CLASS_STAR of around 1, while an extended object has a CLASS_STAR close to zero. To be included in the sample, all objects must have a CLASS_STAR ≤ 0.2.

Tables A.2 and A.3 contain the actual U and V band photometry respectively. They simply state the object i.d., the GMP number (where an object has one) and the aperture magnitudes in 8.8,13,16,20.2 and 26 arcsec diameter apertures.

Positions for all the objects identified as galaxies. This table gives not just the positions, but the GMP number from (Godwin, Metcalfe, & Peach 1983), and the id from (Dressler 1980) (D80). The CStar column shows the CLASS STAR parameter from sextractor (Bertin & Arnouts 1996)

Object	GMP	D80	Other	RA	DEC	Morphology	CStar
				(J2000)			
coma10-4	1714	-	-	13:01:57.4	27:46:08.6	-	0.01
coma10-50	1724	-	-	13:01:56.3	27:54:29.0	-	0.03
comane7-26	1730	-	-	13:01:55.8	28:17:21.4	-	0.03
coma10-29	1745	-	-	13:01:54.7	27:51:02.0	-	0.01
comane3-69	1751	-	-	13:01:54.1	28:11:37.8	-	0.03
comane3-50	1757	-	-	13:01:53.7	28:09:47.0	-	0.00
comane7-37	1758	-	-	13:01:53.7	28:20:40.6	-	0.06
coma10-1	1764	-	-	13:01:53.3	27:45:58.1	-	0.02
comane3-51	1765	-	-	13:01:53.4	28:10:27.8	-	0.02
coma10-43	1767	-	-	13:01:52.8	27:52:15.2	-	0.01
coma10-36	1772	-	-	13:01:52.7	27:51:46.7	-	0.02
comane3-80	1777	-	-	13:01:52.5	28:13:07.2	-	0.04
coma10-61	1780	-	-	13:01:52.0	27:56:00.8	-	0.00
comane3-36	1781	-	-	13:01:51.8	28:08:20.0	-	0.03
comane7-34	1800	-	-	13:01:50.7	28:20:10.3	-	0.18
comane7-15	1805	-	-	13:01:50.6	28:13:51.9	-	0.03
comane7-23	1806	-	-	13:01:50.4	28:16:04.0	-	0.04
coma10-45	1807	96	-	13:01:50.2	27:53:36.2	diE/SAB0	0.03
coma17-30	1819	-	-	13:01:49.6	27:58:05.2	-	0.01
coma10-17	1828	-	-	13:01:48.6	27:48:19.8	-	0.01
comane3-47	1841	-	-	13:01:47.8	28:09:39.5	-	0.01
coma10-6	1844	-	-	13:01:47.5	27:46:13.7	-	0.01
comane3-17	1853	190	-	13:01:47.0	28:05:41.5	SA0	0.03
coma10-34	1856	-	-	13:01:46.8	27:51:29.8	-	0.01
coma10-23	1876	-	-	13:01:45.2	27:49:28.0	-	0.01
comane3-43	1882	-	-	13:01:44.7	28:09:10.4	-	0.01
comane3-76	1885	-	-	13:01:44.1	28:12:51.4	-	0.03
comane3-41	1887	-	-	13:01:43.9	28:09:01.2	-	0.00
comane3-72	1888	-	-	13:01:43.8	28:12:22.4	-	0.02
comane7-21	1889	-	-	13:01:43.9	28:15:03.4	-	0.11
comane7-27	1897	-	-	13:01:43.0	28:17:27.4	-	0.04
comane7-29	1898	-	-	13:01:43.0	28:17:53.8	-	0.03
comane3-61	1907	-	-	13:01:42.4	28:11:13.6	-	0.05

contiuned from previous page

Object	GMP	D80	Other	RA	DEC	Morphology	CStar
				(J2000)			
comane3-75	1918	-	-	13:01:41.5	28:12:39.7	-	0.02
comane3-10	1921	-	-	13:01:41.1	28:04:19.3	-	0.04
comane3-77	1926	-	-	13:01:40.1	28:13:00.0	-	0.03
comane7-18	1931	-	-	13:01:38.9	28:14:45.9	-	0.03
coma17-39	1941	-	-	13:01:38.1	27:59:21.6	-	0.02
coma17-50	1953	-	-	13:01:37.3	28:00:56.5	-	0.03
coma10-60	1958	-	-	13:01:36.8	27:56:03.3	-	0.03
coma17-72	1960	-	-	13:01:36.8	28:03:27.8	-	0.03
comane3-40	1966	-	-	13:01:36.0	28:09:03.4	-	0.02
comane3-38	1975	-	-	13:01:35.2	28:08:48.5	-	0.03
comane3-46	1977	-	-	13:01:34.9	28:09:41.4	-	0.02
coma10-53	1986	-	-	13:01:33.9	27:54:40.2	-	0.00
coma10-38	1993	-	-	13:01:32.4	27:51:55.4	-	0.01
coma17-41	1995	-	-	13:01:32.3	27:59:29.7	-	0.02
coma17-55	1996	-	-	13:01:32.2	28:01:47.4	-	0.03
coma17-31	1998	-	-	13:01:32.1	27:58:09.3	-	0.01
coma10-33	2000	78	NGC4923	13:01:31.8	27:50:50.9	unE	0.03
comane7-38	2002	-	-	13:01:31.5	28:20:54.1	-	0.03
comane3-63	2016	-	-	13:01:30.6	28:11:24.8	-	0.02
comane7-22	2019	-	-	13:01:30.0	28:15:39.5	-	0.03
coma17-71	2020	-	-	13:01:30.0	28:03:09.0	-	0.01
comane3-78	2027	-	-	13:01:29.0	28:13:05.2	-	0.01
coma10-56	2033	-	-	13:01:28.5	27:55:36.2	-	0.03
coma10-32	2035	-	-	13:01:28.2	27:51:06.6	-	0.03
comane3-57	2036	-	-	13:01:28.2	28:10:40.6	-	0.04
coma17-74	2040	-	-	13:01:27.9	28:03:34.4	-	0.00
comane7-17	2044	-	-	13:01:27.6	28:14:08.1	-	0.03
comane3-59	2047	-	-	13:01:27.3	28:10:55.3	-	0.03
coma17-45	2048	142	-	13:01:27.2	27:59:56.8	-	0.03
comane3-67	2052	-	-	13:01:26.9	28:11:39.8	-	0.01
comane7-20	2053	-	-	13:01:26.7	28:15:00.4	-	0.03
coma10-49	2059	97	-	13:01:26.2	27:53:09.9	Sp	0.03
comane3-81	2060	-	-	13:01:26.3	28:13:14.4	-	0.03
comane3-29	2063	-	-	13:01:26.0	28:07:32.4	-	0.08
comane3-48	2064	-	-	13:01:25.8	28:09:52.1	-	0.06
coma17-66	2068	-	-	13:01:25.4	28:02:20.0	-	0.01
comane3-70	2091	204	-	13:01:22.8	28:11:45.4	Epec	0.03
coma17-67	2103	-	-	13:01:22.3	28:02:22.8	-	0.01

contiuned from previous page

Object	GMP	D80	Other	RA	DEC	Morphology	CStar
				(J2000)			
coma17-54	2109	-	-	13:01:21.9	28:01:47.5	-	0.02
coma17-59	2110	-	-	13:01:21.9	28:02:02.1	-	0.02
coma17-76	2113	-	-	13:01:21.7	28:03:54.8	-	0.01
coma17-27	2129	-	-	13:01:20.0	27:57:39.6	-	0.03
coma22-63	2135	-	-	13:01:19.6	28:10:04.6	-	0.01
coma10-35	2141	-	-	13:01:19.4	27:51:38.2	-	0.03
coma22-45	2145	-	-	13:01:19.1	28:07:41.0	-	0.03
coma5-8	2148	-	-	13:01:18.4	27:37:46.6	-	0.03
coma22-64	2151	-	-	13:01:18.4	28:10:20.5	-	0.03
comane6-47	2155	-	-	13:01:17.7	28:19:20.5	-	0.05
coma10-22	2157	79	NGC4919	13:01:17.6	27:48:32.9	SA0	0.03
coma22-32	2158	-	-	13:01:17.8	28:05:49.0	-	0.03
coma5-52	2166	-	-	13:01:16.7	27:43:40.7	-	0.03
coma5-53	2170	-	-	13:01:16.3	27:43:45.1	-	0.03
coma16-53	2178	-	-	13:01:15.8	27:58:54.9	-	0.01
coma10-57	2183	-	-	13:01:15.4	27:55:45.7	-	0.00
coma5-25	2185	-	-	13:01:15.2	27:40:08.9	-	0.03
coma16-88	2190	-	-	13:01:15.3	28:02:20.0	-	0.00
coma16-72	2192	-	-	13:01:14.9	28:00:58.4	-	0.01
comane6-17	2193	-	-	13:01:14.7	28:14:43.0	-	0.02
coma16-40	2197	-	-	13:01:14.4	27:58:37.2	-	0.02
coma10-54	2201	-	RB129	13:01:13.7	27:54:52.5	unE	0.03
coma22-27	2205	-	-	13:01:13.7	28:04:58.8	-	0.03
comane3-82	2212	-	-	13:01:12.9	28:13:22.7	-	0.01
comane6-51	2213	-	-	13:01:12.6	28:19:47.5	-	0.12
comane6-52	2214	-	-	13:01:12.6	28:19:54.7	-	0.02
coma22-65	2215	-	-	13:01:12.9	28:10:21.2	-	0.01
comane3-83	2222	-	-	13:01:12.1	28:13:28.8	-	0.01
coma16-32	2226	-	-	13:01:11.6	27:57:14.3	-	0.00
coma5-56	2232	-	-	13:01:11.2	27:44:32.8	-	0.03
comane6-53	2233	-	-	13:01:11.1	28:20:18.6	-	0.01
coma10-19	2237	80	-	13:01:10.7	27:48:10.8	SA0	0.03
coma16-71	2239	-	-	13:01:10.7	28:00:15.4	-	0.01
coma5-30	2248	-	-	13:01:09.6	27:40:45.5	-	0.02
coma16-86	2251	-	-	13:01:09.4	28:01:58.8	-	0.03
coma9-30	2252	81	-	13:01:09.3	27:49:05.8	diE	0.03
coma9-58	2253	-	-	13:01:09.3	27:53:11.2	-	0.01
comane6-18	2257	-	-	13:01:08.9	28:14:26.1	-	0.01

contiuned from previous page

Object	GMP	D80	Other	RA	DEC	Morphology	CStar
				(J2000)			
comane6-65	2259	229	-	13:01:08.7	28:21:37.4	diE	0.03
coma9-57	2262	-	-	13:01:08.9	27:53:06.3	-	0.01
coma9-46	2263	-	-	13:01:08.5	27:50:47.9	-	0.00
coma5-67	2265	-	-	13:01:07.7	27:46:28.1	-	0.03
coma16-63	2267	-	-	13:01:07.6	27:59:52.6	-	0.01
coma16-24	2268	-	-	13:01:07.5	27:56:02.9	-	0.01
coma22-23	2269	-	-	13:01:07.6	28:04:27.2	-	0.01
coma22-42	2270	-	-	13:01:07.3	28:07:17.4	-	0.03
coma16-55	2273	-	-	13:01:07.2	27:58:58.8	-	0.00
coma9-20	2276	-	-	13:01:06.8	27:48:19.4	-	0.02
comane6-37	2281	-	-	13:01:06.1	28:18:15.5	-	0.01
coma5-43	2285	-	-	13:01:05.8	27:42:31.8	-	0.02
coma16-54	2287	-	-	13:01:05.6	27:58:55.3	-	0.01
coma16-45	2288	-	-	13:01:05.7	27:58:15.1	-	0.02
coma16-104	2289	-	-	13:01:05.6	28:03:43.0	-	0.03
coma22-74	2293	-	-	13:01:05.0	28:11:48.6	-	0.02
coma16-2	2295	-	-	13:01:04.8	27:53:30.1	-	0.03
coma16-89	2297	-	-	13:01:04.6	28:02:20.1	-	0.01
coma16-82	2311	-	-	13:01:03.1	28:01:34.2	-	0.01
coma5-68	2316	-	-	13:01:02.4	27:46:31.0	-	0.03
comane6-33	2321	-	-	13:01:02.1	28:17:35.3	-	0.01
coma22-59	2322	-	-	13:01:02.1	28:09:38.1	-	0.02
coma16-64	2323	-	-	13:01:02.0	27:59:48.7	-	0.12
coma16-13	2333	-	-	13:01:00.6	27:54:22.0	-	0.01
coma9-24	2335	-	-	13:01:00.1	27:48:27.4	-	0.00
coma5-45	2342	-	-	13:00:59.5	27:42:46.5	-	0.02
coma22-48	2343	-	-	13:00:59.5	28:08:07.7	-	0.02
coma16-12	2347	98	-	13:00:59.3	27:53:59.3	Sp	0.03
coma22-44	2349	-	-	13:00:59.4	28:07:45.1	-	0.01
coma5-49	2352	-	-	13:00:58.8	27:43:26.6	-	0.03
coma16-83	2353	-	-	13:00:58.8	28:01:36.2	-	0.01
coma5-18	2355	50	-	13:00:58.4	27:39:07.2	-	0.03
coma22-49	2359	-	-	13:00:58.3	28:08:16.6	-	0.02
comane6-62	2361	-	-	13:00:58.0	28:21:42.4	-	0.03
coma5-61	2364	-	-	13:00:57.7	27:45:42.2	-	0.03
coma22-38	2366	-	-	13:00:57.7	28:06:49.9	-	0.01
coma9-9	2374	82	-	13:00:56.1	27:47:26.6	Sp	0.03
coma16-9	2376	-	-	13:00:55.9	27:53:54.5	-	0.02

contiuned from previous page

Object	GMP	D80	Other	RA	DEC	Morphology	CStar
				(J2000)			
coma16-58	2382	-	-	13:00:55.2	27:59:25.9	-	0.13
comane6-28	2383	-	-	13:00:55.0	28:16:28.0	-	0.05
coma9-42	2385	-	-	13:00:54.8	27:50:30.9	-	0.03
coma16-74	2390	143	IC4051	13:00:54.5	28:00:27.1	unE	0.03
coma5-72	2393	62	-	13:00:54.1	27:47:01.3	-	0.03
coma16-43	2399	-	-	13:00:53.8	27:58:05.4	-	0.02
coma5-12	2407	-	-	13:00:52.7	27:38:14.1	-	0.03
coma9-34	2408	-	-	13:00:52.7	27:49:32.0	-	0.00
coma9-21	2411	-	-	13:00:52.5	27:48:17.4	-	0.02
coma5-11	2412	-	-	13:00:51.9	27:38:01.9	-	0.01
comane6-67	2413	230	-	13:00:51.9	28:21:59.6	SB0	0.03
coma22-37	2415	-	-	13:00:51.8	28:07:02.4	-	0.03
coma16-94	2417	167	NGC4908	13:00:51.5	28:02:33.8	unE	0.03
coma5-35	2420	-	-	13:00:51.3	27:41:20.8	-	0.03
coma5-57	2421	-	-	13:00:51.1	27:44:34.6	-	0.03
coma9-26	2427	-	-	13:00:50.5	27:48:36.9	-	0.02
comane6-27	2428	-	-	13:00:50.3	28:16:12.9	-	0.16
coma16-3	2430	-	-	13:00:50.2	27:53:40.9	-	0.02
coma22-54	2432	-	-	13:00:50.0	28:08:53.7	-	0.01
coma5-32	2438	-	-	13:00:49.0	27:41:00.7	-	0.03
coma22-31	2440	168	IC4045	13:00:48.7	28:05:26.2	diE/SA0	0.03
coma22-61	2441	205	-	13:00:48.8	28:09:29.6	Sp	0.03
coma16-84	2442	-	-	13:00:48.7	28:01:40.8	-	0.01
comane6-23	2443	-	-	13:00:48.5	28:15:16.7	-	0.01
coma9-38	2445	-	-	13:00:48.3	27:50:07.4	-	0.00
coma16-62	2448	-	-	13:00:48.0	28:00:03.3	-	0.01
coma22-33	2449	-	-	13:00:48.1	28:05:57.1	-	0.01
coma22-26	2452	-	-	13:00:48.0	28:04:58.2	-	0.01
coma16-60	2454	-	-	13:00:47.7	27:59:36.7	-	0.01
coma16-70	2455	-	-	13:00:47.6	28:00:42.1	-	0.12
coma16-17	2457	117	-	13:00:47.4	27:55:19.6	-	0.03
coma22-67	2464	-	-	13:00:46.9	28:10:42.2	-	0.03
coma5-26	2466	-	-	13:00:46.7	27:40:25.0	-	0.03
coma5-22	2469	-	-	13:00:46.3	27:40:04.9	-	0.00
coma16-61	2470	-	-	13:00:46.4	27:59:39.9	-	0.01
comane6-41	2475	-	-	13:00:45.7	28:18:50.0	-	0.19
coma5-55	2477	-	-	13:00:45.6	27:44:10.3	-	0.00
coma9-39	2478	-	-	13:00:45.4	27:50:07.3	-	0.03

contiuned from previous page

Object	GMP	D80	Other	RA	DEC	Morphology	CStar
				(J2000)			
coma5-58	2480	-	-	13:00:45.3	27:44:49.0	-	0.03
coma5-33	2485	-	-	13:00:45.0	27:41:10.3	-	0.03
coma22-69	2487	-	-	13:00:44.7	28:11:00.7	-	0.03
coma16-6	2488	-	-	13:00:44.6	27:53:47.8	-	0.00
coma22-34	2489	191	-	13:00:44.7	28:06:01.9	-	0.03
coma16-30	2490	-	-	13:00:44.6	27:56:33.3	-	0.04
coma5-71	2491	-	-	13:00:44.3	27:47:19.5	-	0.03
coma22-22	2492	-	-	13:00:44.4	28:04:26.4	-	0.02
coma5-65	2493	-	-	13:00:44.2	27:46:17.6	-	0.02
coma9-50	2494	-	-	13:00:44.3	27:51:29.3	-	0.01
comane6-54	2495	231	-	13:00:44.1	28:20:15.4	SA0	0.03
coma22-72	2501	-	-	13:00:43.9	28:11:32.0	-	0.03
coma16-51	2504	-	-	13:00:43.6	27:58:36.3	-	0.03
comane6-3	2505	-	-	13:00:43.4	28:12:12.5	-	0.02
coma15-63	2507	-	-	13:00:43.3	27:59:09.0	-	0.02
coma15-101	2508	-	-	13:00:43.1	28:02:57.7	-	0.03
coma15-55	2510	116	-	13:00:42.8	27:57:46.9	SB0	0.03
coma15-114	2511	-	-	13:00:42.9	28:03:13.8	-	0.00
comane6-36	2513	-	-	13:00:42.7	28:18:11.7	-	0.03
coma15-53	2516	144	-	13:00:42.8	27:58:16.3	Sp	0.03
coma15-116	2518	-	-	13:00:42.6	28:03:25.3	-	0.01
coma22-40	2519	-	-	13:00:42.6	28:06:58.3	-	0.00
coma15-109	2529	-	-	13:00:41.2	28:02:42.4	-	0.03
coma15-3	2531	-	-	13:00:41.2	27:53:41.4	-	0.03
coma15-75	2535	145	IC4041	13:00:40.9	27:59:47.4	SA0	0.03
coma4-55	2537	-	-	13:00:40.4	27:49:32.0	-	0.03
coma15-27	2541	118	NGC4906	13:00:39.8	27:55:25.9	unE	0.03
coma16-78	2550	-	-	13:00:39.1	28:00:35.1	-	0.00
coma15-89	2551	146	-	13:00:38.8	28:00:52.0	-	0.03
coma5-34	2553	-	-	13:00:38.3	27:41:13.4	-	0.00
coma15-62	2555	-	-	13:00:38.1	27:59:21.1	-	0.03
coma15-121	2559	169	IC4040	13:00:37.9	28:03:28.9	S..	0.05
coma25-53	2566	-	-	13:00:37.1	28:16:02.2	-	0.03
coma15-11	2570	-	-	13:00:36.7	27:54:27.1	-	0.02
coma15-29	2571	-	-	13:00:36.6	27:55:52.0	-	0.01
coma15-86	2577	-	-	13:00:36.3	28:00:54.8	-	0.03
coma21-72	2584	192	-	13:00:35.6	28:08:46.4	SA0	0.03
coma15-41	2585	-	-	13:00:35.4	27:56:33.6	-	0.03

contiuned from previous page

Object	GMP	D80	Other	RA	DEC	Morphology	CStar
				(J2000)			
coma8-30	2587	-	-	13:00:34.9	27:49:54.6	-	0.02
coma15-33	2591	-	-	13:00:34.4	27:56:04.7	-	0.02
coma15-112	2593	-	-	13:00:34.4	28:03:12.8	-	0.02
coma5-14	2599	51	-	13:00:33.7	27:38:15.6	Sp	0.03
coma4-57	2603	-	-	13:00:33.4	27:49:26.7	-	0.03
coma15-59	2605	-	-	13:00:33.3	27:58:49.1	-	0.01
coma4-49	2606	-	-	13:00:33.2	27:48:12.7	-	0.01
coma4-50	2613	-	-	13:00:32.7	27:48:19.1	-	0.02
coma15-118	2614	-	-	13:00:32.7	28:03:31.3	-	0.00
coma4-31	2615	63	-	13:00:32.6	27:45:57.3	-	0.03
coma25-48	2619	-	-	13:00:32.4	28:15:22.5	-	0.01
coma21-49	2626	-	-	13:00:31.0	28:06:30.3	-	0.02
coma21-80	2631	-	-	13:00:30.5	28:09:46.8	-	0.01
coma21-79	2633	-	-	13:00:30.2	28:09:36.8	-	0.02
coma4-32	2635	-	-	13:00:30.0	27:46:12.3	-	0.02
coma4-52	2644	-	-	13:00:29.0	27:48:35.5	-	0.04
coma21-77	2647	-	-	13:00:28.8	28:09:38.5	-	0.02
coma15-58	2651	147	RB100	13:00:28.4	27:58:20.4	SA0	0.03
coma15-51	2654	119	RB099	13:00:28.0	27:57:21.3	SB0	0.03
coma15-67	2655	-	-	13:00:27.9	27:59:16.3	-	0.01
coma15-115	2660	-	-	13:00:27.6	28:03:24.3	-	0.00
coma15-80	2663	-	-	13:00:27.3	28:00:33.2	-	0.04
coma15-26	2665	-	-	13:00:27.2	27:55:41.7	-	0.02
coma15-117	2667	-	-	13:00:27.0	28:03:47.1	-	0.04
coma15-81	2676	-	-	13:00:26.2	28:00:31.7	-	0.02
coma15-100	2677	-	-	13:00:26.2	28:02:56.5	-	0.01
coma15-113	2679	-	-	13:00:26.0	28:03:44.5	-	0.01
coma15-35	2683	-	-	13:00:25.5	27:56:14.9	-	0.03
coma15-45	2684	-	-	13:00:25.4	27:56:56.6	-	0.01
coma25-27	2685	-	-	13:00:25.3	28:13:46.0	-	0.01
coma21-76	2687	-	-	13:00:25.2	28:10:19.9	-	0.01
coma15-24	2692	-	-	13:00:24.8	27:55:35.7	-	0.03
coma15-30	2694	-	-	13:00:24.6	27:55:54.4	-	0.01
coma4-28	2698	-	-	13:00:24.1	27:44:54.9	-	0.01
coma25-21	2711	-	-	13:00:23.1	28:12:28.1	-	0.16
coma25-54	2712	-	-	13:00:23.0	28:16:17.5	-	0.08
coma8-36	2716	-	-	13:00:22.9	27:50:52.0	-	0.01
coma15-54	2718	-	-	13:00:22.7	27:57:54.6	-	0.01

contiuned from previous page

Object	GMP	D80	Other	RA	DEC	Morphology	CStar
				(J2000)			
coma15-110	2727	170	IC4026	13:00:22.2	28:02:48.9	SB0	0.03
coma25-44	2728	-	-	13:00:22.1	28:14:50.1	-	0.03
coma8-33	2735	-	-	13:00:21.8	27:50:41.4	-	0.01
coma15-5	2736	-	-	13:00:21.7	27:53:54.4	-	0.03
coma4-35	2738	-	-	13:00:21.5	27:48:52.3	-	0.01
coma4-51	2749	-	-	13:00:20.5	27:48:16.5	-	0.01
coma25-51	2750	-	-	13:00:20.4	28:15:41.0	-	0.01
coma21-26	2752	-	-	13:00:20.4	28:04:14.3	-	0.03
coma8-34	2753	-	-	13:00:20.2	27:50:36.3	-	0.03
coma15-72	2755	-	-	13:00:20.2	27:59:37.5	-	0.01
coma15-8	2763	-	-	13:00:19.8	27:54:13.0	-	0.01
coma21-55	2764	-	-	13:00:19.7	28:07:17.6	-	0.02
coma15-82	2777	-	-	13:00:18.9	28:00:33.2	-	0.03
coma15-37	2778	-	RB094	13:00:18.8	27:56:13.2	SB0/a	0.03
coma15-17	2780	-	-	13:00:18.7	27:55:12.4	-	0.01
coma4-53	2783	-	-	13:00:18.6	27:48:55.6	-	0.03
coma21-42	2784	-	-	13:00:18.6	28:05:49.8	-	0.02
coma15-119	2787	-	-	13:00:18.4	28:03:33.3	-	0.03
coma21-30	2790	-	-	13:00:18.0	28:04:44.0	-	0.01
coma21-96	2795	206	NGC4895	13:00:17.9	28:12:09.2	SA0	0.03
coma15-52	2798	121	NGC4898	13:00:17.7	27:57:18.7	???	0.03
coma15-68	2799	-	-	13:00:17.7	27:59:14.9	-	0.03
coma4-40	2800	-	-	13:00:17.6	27:47:03.6	-	0.01
coma4-14	2801	-	-	13:00:17.5	27:42:41.2	-	0.02
coma15-123	2805	171	RB091	13:00:17.0	28:03:49.9	SB0	0.03
coma15-9	2808	-	-	13:00:16.9	27:54:15.8	-	0.01
coma15-56	2815	122	NGC4894	13:00:16.5	27:58:02.9	SA0	0.03
coma15-39	2819	-	-	13:00:16.3	27:56:30.0	-	0.00
coma21-83	2825	-	-	13:00:15.8	28:10:14.7	-	0.13
coma15-2	2835	-	-	13:00:15.2	27:53:34.3	-	0.02
coma15-94	2838	-	-	13:00:14.8	28:01:32.8	-	0.01
coma15-107	2839	172	IC4021	13:00:14.8	28:02:28.3	SA0	0.03
coma25-28	2849	-	-	13:00:13.9	28:13:57.6	-	0.02
coma15-108	2851	-	-	13:00:13.8	28:02:43.3	-	0.01
coma8-45	2852	-	-	13:00:13.6	27:52:01.7	-	0.02
coma15-111	2856	-	-	13:00:13.4	28:03:11.6	-	0.02
coma15-96	2858	-	-	13:00:13.3	28:01:52.9	-	0.01
coma21-38	2860	-	-	13:00:13.2	28:05:24.6	-	0.01

contiuned from previous page

Object	GMP	D80	Other	RA	DEC	Morphology	CStar
				(J2000)			
coma21-29	2861	173	RB087	13:00:12.9	28:04:31.8	SA0/a	0.03
coma4-20	2863	-	-	13:00:12.8	27:43:10.4	-	0.02
coma4-39	2866	64	-	13:00:12.7	27:46:54.1	-	0.03
coma15-13	2877	-	-	13:00:11.4	27:54:35.9	-	0.01
coma4-34	2878	-	-	13:00:11.3	27:46:29.6	-	0.09
coma15-122	2879	-	-	13:00:11.2	28:03:54.7	-	0.03
coma15-70	2895	-	-	13:00:10.3	27:57:32.3	-	0.03
coma8-41	2897	99	RB083	13:00:10.2	27:51:50.2	SB0	0.03
coma25-10	2899	-	-	13:00:10.0	28:10:33.9	-	0.14
coma25-66	2906	-	-	13:00:09.3	28:19:11.8	-	0.02
coma21-81	2907	-	-	13:00:09.2	28:09:17.6	-	0.01
coma8-42	2910	100	RB082	13:00:09.1	27:51:59.2	SABa	0.03
coma8-32	2911	-	-	13:00:09.2	27:50:22.2	-	0.01
coma21-78	2912	207	RB167	13:00:09.1	28:10:13.6	SAB0	0.03
coma8-43	2913	-	-	13:00:09.0	27:51:39.8	-	0.01
coma21-84	2914	-	-	13:00:08.7	28:09:35.5	-	0.03
coma15-47	2917	-	-	13:00:08.4	27:57:16.6	-	0.03
coma25-69	2918	-	-	13:00:08.3	28:19:25.2	-	0.02
coma15-66	2921	148	NGC4889	13:00:08.1	27:58:36.7	boE	0.03
coma21-32	2922	174	IC4012	13:00:08.0	28:04:42.8	diE	0.02
coma3-39	2923	-	-	13:00:08.1	27:46:24.8	-	0.03
coma25-61	2928	-	-	13:00:07.4	28:18:25.6	-	0.01
coma15-50	2929	-	-	13:00:07.5	27:57:28.7	-	0.02
coma15-28	2931	-	-	13:00:07.1	27:55:51.2	-	0.03
coma3-18	2938	-	-	13:00:06.7	27:43:16.6	-	0.04
coma15-77	2940	150	IC4011	13:00:06.4	28:00:14.4	boE	0.03
coma3-6	2942	-	-	13:00:06.3	27:41:07.8	-	0.03
coma25-36	2943	-	-	13:00:06.1	28:15:07.0	-	0.00
coma3-41	2945	65	-	13:00:06.3	27:46:33.4	SA0	0.03
coma15-25	2952	-	-	13:00:05.7	27:55:35.0	-	0.02
coma21-31	2955	-	-	13:00:05.5	28:04:49.2	-	0.01
coma15-95	2960	-	RB074	13:00:05.4	28:01:27.7	SA0	0.03
coma15-38	2963	-	-	13:00:05.3	27:56:28.9	-	0.01
coma21-87	2973	-	-	13:00:04.4	28:11:04.0	-	0.00
coma15-69	2975	151	NGC4886	13:00:04.5	27:59:15.0	unE	0.03
coma21-75	2976	-	-	13:00:04.3	28:09:18.6	-	0.02
coma25-49	2981	-	-	13:00:04.2	28:15:35.6	-	0.01
coma15-79	2983	-	-	13:00:04.1	28:00:30.3	-	0.01

contiuned from previous page

Object	GMP	D80	Other	RA	DEC	Morphology	CStar
				(J2000)			
coma25-38	2989	216	RB160	13:00:03.0	28:14:25.5	Sa	0.03
coma15-92	2991	-	-	13:00:03.0	28:01:22.9	-	0.03
coma25-70	2994	-	-	13:00:02.7	28:19:35.9	-	0.02
coma3-10	2996	-	-	13:00:02.7	27:42:41.5	-	0.02
coma25-24	2997	-	-	13:00:02.6	28:13:01.9	-	0.03
coma3-17	3003	-	-	13:00:02.3	27:43:11.2	-	0.01
coma25-64	3004	-	-	13:00:01.9	28:19:00.4	-	0.01
coma3-31	3005	-	-	13:00:02.0	27:44:46.1	-	0.01
coma21-85	3006	-	-	13:00:01.9	28:10:27.5	-	0.07
coma3-25	3012	-	-	13:00:01.5	27:43:53.0	-	0.03
coma21-33	3016	-	-	13:00:01.1	28:04:55.3	-	0.01
coma14-86	3017	-	-	13:00:01.0	27:56:43.4	-	0.03
coma14-123	3018	-	-	13:00:01.0	27:59:29.4	-	0.01
coma14-17	3021	-	-	13:00:00.8	27:51:44.4	-	0.01
coma21-91	3024	-	-	13:00:00.0	28:11:47.1	-	0.03
coma14-12	3033	-	-	12:59:59.6	27:51:32.8	-	0.02
coma14-78	3034	-	-	12:59:59.5	27:56:25.8	-	0.02
coma3-51	3037	-	-	12:59:59.4	27:47:56.2	-	0.03
coma21-43	3043	-	-	12:59:58.8	28:05:51.6	-	0.02
coma7-2	3049	-	-	12:59:58.3	27:46:36.8	-	0.00
coma14-9	3050	-	-	12:59:58.3	27:51:18.7	-	0.01
coma14-48	3051	-	-	12:59:58.2	27:54:10.3	-	0.00
coma14-21	3052	-	-	12:59:58.2	27:51:57.7	-	0.00
coma25-46	3055	217	NGC4881	12:59:57.7	28:14:48.3	boE	0.03
coma21-64	3057	-	-	12:59:57.7	28:08:15.0	-	0.04
coma15-124	3058	-	-	12:59:57.6	28:03:54.2	-	0.03
coma21-47	3066	-	-	12:59:56.9	28:06:31.6	-	0.03
coma14-68	3068	123	RB064	12:59:56.7	27:55:48.0	Sa	0.03
coma3-34	3071	-	-	12:59:56.2	27:44:47.6	-	0.03
coma15-98	3073	175	NGC4883	12:59:56.0	28:02:04.7	SB0	0.03
coma14-76	3075	-	-	12:59:56.0	27:57:48.5	-	0.00
coma25-50	3076	-	-	12:59:56.0	28:15:37.0	-	0.06
coma7-29	3079	-	-	12:59:56.0	27:49:11.6	-	0.01
coma14-61	3080	-	-	12:59:55.7	27:55:03.6	-	0.02
coma21-58	3084	193	RB155	12:59:55.1	28:07:42.2	SB0	0.03
coma3-50	3092	-	-	12:59:54.9	27:47:46.0	-	0.03
coma14-5	3095	-	-	12:59:54.4	27:50:59.9	-	0.03
coma14-97	3098	-	-	12:59:54.0	27:58:13.5	-	0.02

contiuned from previous page

Object	GMP	D80	Other	RA	DEC	Morphology	CStar
				(J2000)			
coma21-44	3113	-	-	12:59:51.8	28:05:54.5	-	0.03
coma7-14	3116	-	-	12:59:51.6	27:48:03.0	-	0.01
coma21-28	3121	-	-	12:59:51.5	28:04:24.3	-	0.03
coma7-34	3122	-	-	12:59:51.6	27:49:45.7	-	0.00
coma7-37	3126	-	-	12:59:51.0	27:49:57.9	-	0.03
coma3-33	3127	-	-	12:59:50.8	27:44:51.9	-	0.11
coma21-68	3129	-	-	12:59:50.3	28:08:40.1	-	0.03
coma14-55	3131	-	-	12:59:50.2	27:54:45.3	-	0.02
coma14-65	3133	-	-	12:59:50.1	27:55:29.2	-	0.03
coma14-54	3134	-	-	12:59:50.0	27:54:33.0	-	0.01
coma14-94	3142	-	-	12:59:49.1	27:57:17.8	-	0.00
coma14-112	3146	-	-	12:59:48.6	27:58:57.5	-	0.01
coma14-3	3149	-	-	12:59:48.6	27:50:51.4	-	0.03
coma14-47	3150	-	-	12:59:48.4	27:54:09.9	-	0.02
coma3-16	3165	57	-	12:59:47.2	27:42:37.4	SA0	0.03
coma14-121	3166	-	-	12:59:47.0	27:59:30.8	-	0.02
coma14-108	3170	152	IC3998	12:59:46.8	27:58:25.6	SB0	0.03
coma14-81	3171	-	-	12:59:46.7	28:00:00.1	-	0.01
coma3-58	3174	-	-	12:59:46.5	27:48:41.3	-	0.08
coma3-32	3176	-	-	12:59:46.3	27:44:46.3	-	0.02
coma3-57	3177	-	-	12:59:46.2	27:48:25.2	-	0.01
coma14-15	3178	101	RB049	12:59:46.1	27:51:25.8	SA0	0.03
coma7-48	3180	-	-	12:59:46.0	27:51:07.3	-	0.00
coma3-28	3192	-	-	12:59:44.9	27:44:14.0	-	0.02
coma3-36	3195	-	-	12:59:45.0	27:45:49.2	-	0.01
coma14-39	3196	-	-	12:59:44.7	27:53:22.9	-	0.03
coma14-57	3201	124	NGC4876	12:59:44.4	27:54:44.7	diE	0.03
coma14-24	3205	-	-	12:59:44.2	27:52:03.5	-	0.03
coma14-99	3206	126	RB046	12:59:44.2	27:57:30.0	SA0	0.03
coma14-134	3209	-	-	12:59:44.2	28:00:46.7	-	0.02
coma14-122	3213	153	RB045	12:59:43.7	27:59:40.5	diE	0.03
coma14-71	3215	-	-	12:59:43.5	27:56:20.1	-	0.00
coma7-115	3222	125	RB043	12:59:42.3	27:55:28.7	boE	0.03
coma14-63	3222	125	-	12:59:42.3	27:55:28.9	-	0.03
coma14-11	3225	-	-	12:59:42.3	27:51:31.7	-	0.03
coma14-79	3229	-	-	12:59:42.1	27:56:34.3	-	0.00
coma14-35	3230	-	-	12:59:42.0	27:53:03.9	-	0.02
coma3-22	3231	-	-	12:59:41.9	27:43:24.8	-	0.01

contiuned from previous page

Object	GMP	D80	Other	RA	DEC	Morphology	CStar
				(J2000)			
coma7-39	3237	-	-	12:59:41.4	27:50:14.0	-	0.00
coma3-2	3238	52	-	12:59:41.3	27:39:35.3	-	0.03
comasw17-92	3243	-	-	12:59:41.1	27:44:12.5	-	0.01
coma14-32	3244	-	-	12:59:41.0	27:52:40.0	-	0.02
coma3-54	3247	-	-	12:59:40.9	27:48:24.8	-	0.01
coma14-104	3254	127	RB042	12:59:40.3	27:58:05.2	SA0	0.03
coma7-15	3257	-	-	12:59:40.4	27:48:10.3	-	0.01
coma14-10	3262	102	RB041	12:59:40.1	27:51:17.6	diE	0.03
coma14-102	3269	128	RB040	12:59:39.7	27:57:13.8	SA0	0.03
comasw17-5	3271	41	-	12:59:39.9	27:34:35.2	Sp	0.03
coma7-51	3275	-	RB039	12:59:39.5	27:51:16.3	SB0	0.01
coma14-28	3284	-	-	12:59:38.9	27:52:17.9	-	0.03
coma14-120	3291	154	RB038	12:59:38.3	27:59:13.5	SA0/a	0.03
coma14-98	3292	-	-	12:59:38.0	28:00:03.3	-	0.03
coma14-51	3296	104	NGC4875	12:59:37.9	27:54:26.1	SAB0	0.03
coma3-38	3298	-	-	12:59:37.8	27:46:36.4	-	0.03
coma3-7	3299	-	-	12:59:37.8	27:42:09.2	-	0.04
coma14-29	3301	-	-	12:59:37.6	27:52:23.0	-	0.03
coma14-27	3311	-	-	12:59:37.2	27:52:13.2	-	0.02
coma14-136	3312	-	-	12:59:37.0	28:01:06.8	-	0.03
coma3-64	3313	-	-	12:59:37.0	27:49:32.7	-	0.03
coma3-53	3324	-	-	12:59:36.0	27:48:14.9	-	0.01
coma14-49	3325	-	-	12:59:36.0	27:54:21.9	-	0.03
coma14-100	3329	129	NGC4874	12:59:35.7	27:57:33.0	unE	0.03
comasw17-21	3332	-	-	12:59:36.0	27:36:13.1	-	0.02
comasw17-15	3335	-	-	12:59:35.7	27:35:43.1	-	0.00
coma14-50	3336	-	-	12:59:35.5	27:54:21.4	-	0.03
coma14-18	3339	-	-	12:59:35.3	27:51:48.9	-	0.03
coma14-69	3340	-	-	12:59:35.2	27:56:04.8	-	0.02
comasw17-45	3343	-	-	12:59:35.1	27:38:28.9	-	0.00
coma14-80	3352	130	NGC4872	12:59:34.1	27:56:48.3	SB0	0.03
coma3-52	3356	-	-	12:59:33.8	27:48:10.6	-	0.01
coma14-119	3367	155	NGC4873	12:59:32.8	27:59:00.6	SA0	0.03
coma3-42	3371	-	-	12:59:32.5	27:46:29.0	-	0.01
coma14-62	3376	-	-	12:59:32.1	27:55:15.7	-	0.02
coma3-19	3381	-	-	12:59:32.1	27:43:13.5	-	0.01
coma14-14	3383	-	-	12:59:31.9	27:51:40.5	-	0.03
coma3-15	3391	-	-	12:59:31.4	27:42:58.0	-	0.03

contiuned from previous page

Object	GMP	D80	Other	RA	DEC	Morphology	CStar
				(J2000)			
coma3-8	3399	-	-	12:59:31.0	27:42:29.9	-	0.04
coma14-38	3400	103	IC3973	12:59:30.8	27:53:02.9	S..	0.03
coma3-47	3403	87	RB234	12:59:30.6	27:47:28.7	diE	0.03
comasw17-19	3410	-	-	12:59:30.2	27:35:59.3	-	0.02
coma3-63	3411	-	-	12:59:30.1	27:49:33.1	-	0.01
coma14-103	3414	131	NGC4871	12:59:30.0	27:57:22.7	SAB0/a	0.03
coma14-128	3420	-	-	12:59:29.6	28:00:22.3	-	0.00
coma14-7	3423	88	IC3976	12:59:29.4	27:51:00.2	SA0	0.03
coma3-56	3425	-	-	12:59:29.3	27:48:24.6	-	0.02
coma3-24	3435	-	-	12:59:28.7	27:43:34.0	-	0.02
coma14-137	3438	-	-	12:59:28.5	28:01:09.2	-	0.02
coma7-38	3449	-	-	12:59:28.1	27:50:12.2	-	0.05
coma3-43	3463	-	-	12:59:27.3	27:47:05.7	-	0.03
coma14-8	3473	-	-	12:59:26.5	27:51:24.5	-	0.02
coma13-82	3474	-	-	12:59:26.4	27:59:18.3	-	0.03
coma13-64	3480	-	-	12:59:26.0	27:57:49.7	-	0.00
coma13-48	3484	157	RB014	12:59:25.5	27:58:23.5	SA0	0.03
coma13-35	3486	-	-	12:59:25.4	27:56:04.0	-	0.03
coma13-58	3487	132	RB013	12:59:25.4	27:58:04.5	SA0	0.03
coma14-117	3489	-	-	12:59:25.1	27:59:48.0	-	0.03
coma3-30	3493	67	RB230	12:59:24.9	27:44:19.4	SA0	0.03
coma13-5	3501	-	-	12:59:24.0	27:53:50.5	-	0.02
coma3-9	3508	-	-	12:59:23.5	27:42:33.6	-	0.01
coma13-23	3510	105	NGC4869	12:59:23.4	27:54:41.4	unE	0.03
coma13-25	3511	-	-	12:59:23.5	27:55:10.2	-	0.16
coma13-72	3515	-	-	12:59:23.3	27:58:55.0	-	0.00
coma13-54	3516	-	-	12:59:23.3	27:58:07.9	-	0.02
coma7-25	3517	-	-	12:59:23.1	27:48:50.8	-	0.01
coma3-20	3519	-	-	12:59:22.9	27:43:24.0	-	0.01
coma13-6	3522	106	RB008	12:59:22.7	27:53:48.3	SB0	0.03
coma3-60	3531	-	-	12:59:21.8	27:49:05.9	-	0.05
coma13-106	3533	-	-	12:59:21.7	28:01:02.6	-	0.00
coma13-61	3534	158	RB007	12:59:21.5	27:58:24.7	SA0	0.03
coma14-25	3536	-	-	12:59:21.7	27:52:13.2	-	0.13
coma14-26	3536	-	-	12:59:21.3	27:52:17.3	-	0.01
coma13-129	3546	-	-	12:59:20.7	28:03:59.5	-	0.10
coma7-8	3548	-	-	12:59:20.6	27:47:30.7	-	0.01
coma23-31	3553	208	RB136	12:59:20.0	28:11:51.2	SA0	0.03

contiuned from previous page

Object	GMP	D80	Other	RA	DEC	Morphology	CStar
				(J2000)			
coma14-37	3557	107	RB006	12:59:20.2	27:53:09.2	diE/SA0	0.03
coma13-60	3565	-	-	12:59:19.7	27:58:24.5	-	0.03
coma13-55	3567	-	-	12:59:19.7	27:58:05.1	-	0.03
comasw17-88	3571	-	-	12:59:19.5	27:43:54.9	-	0.02
coma23-75	3573	-	-	12:59:18.5	28:16:55.7	-	0.00
coma23-30	3580	-	-	12:59:18.0	28:11:56.3	-	0.02
comasw17-13	3585	-	-	12:59:18.6	27:35:36.8	-	0.03
comasw17-76	3586	-	-	12:59:18.4	27:42:56.2	-	0.03
coma23-25	3592	-	-	12:59:17.4	28:11:03.4	-	0.06
coma13-42	3595	-	-	12:59:17.5	27:57:17.2	-	0.01
comasw17-40	3598	-	-	12:59:17.2	27:38:02.7	-	0.02
coma13-73	3602	-	-	12:59:16.7	27:58:57.2	-	0.03
coma19-72	3603	-	-	12:59:16.7	28:07:54.5	-	0.00
coma13-3	3606	-	-	12:59:16.8	27:53:45.7	-	0.12
coma19-97	3608	-	-	12:59:16.4	28:10:12.6	-	0.03
coma23-74	3609	-	-	12:59:16.3	28:16:37.6	-	0.00
coma13-79	3615	-	-	12:59:16.3	27:59:10.7	-	0.03
comasw22-29	3616	-	-	12:59:16.4	27:46:17.9	-	0.02
coma14-4	3621	-	-	12:59:16.0	27:51:06.4	-	0.01
coma13-92	3623	-	-	12:59:15.8	27:59:49.4	-	0.03
coma14-36	3625	-	-	12:59:15.8	27:53:09.3	-	0.01
coma13-7	3629	-	-	12:59:15.6	27:53:56.4	-	0.01
coma13-122	3630	-	-	12:59:15.6	28:02:45.1	-	0.04
coma7-22	3633	-	-	12:59:15.7	27:48:30.9	-	0.01
coma13-67	3639	133	NGC4867	12:59:15.3	27:58:14.3	diE	0.03
coma23-62	3640	-	-	12:59:14.9	28:15:03.6	-	0.03
comasw17-10	3643	-	-	12:59:15.1	27:35:35.3	-	0.01
coma13-2	3645	-	-	12:59:14.7	27:53:43.7	-	0.03
coma13-30	3648	-	-	12:59:14.4	27:55:58.2	-	0.03
coma13-46	3649	-	-	12:59:14.3	27:57:46.6	-	0.01
coma13-111	3650	-	-	12:59:14.2	28:01:58.2	-	0.01
coma19-47	3656	180	RB268	12:59:13.9	28:04:34.1	unE/SA0	0.03
comasw22-40	3660	68	IC3963	12:59:13.5	27:46:28.2	SA0	0.03
coma13-65	3664	159	NGC4864	12:59:13.1	27:58:37.0	unE	0.03
coma23-77	3665	-	-	12:59:12.8	28:17:10.4	-	0.03
coma13-113	3668	-	-	12:59:12.7	28:02:05.5	-	0.02
comasw17-51	3672	-	-	12:59:12.4	27:39:25.4	-	0.00
coma13-93	3675	-	-	12:59:12.0	27:59:52.2	-	0.02

contiuned from previous page

Object	GMP	D80	Other	RA	DEC	Morphology	CStar
				(J2000)			
comasw17-90	3676	-	-	12:59:12.1	27:44:03.8	-	0.02
comasw17-72	3677	-	-	12:59:12.0	27:42:32.2	-	0.04
coma23-34	3678	-	-	12:59:11.5	28:12:26.0	-	0.01
comasw22-66	3679	-	-	12:59:11.9	27:49:00.3	-	0.01
coma13-102	3681	-	-	12:59:11.6	28:00:33.2	-	0.03
coma19-74	3683	-	-	12:59:11.1	28:08:08.6	-	0.03
coma13-117	3685	-	-	12:59:11.0	28:02:17.7	-	0.02
comasw6-1	3688	-	-	12:59:11.2	27:18:16.1	-	0.01
comasw6-35	3691	-	-	12:59:11.1	27:21:57.1	-	0.01
comasw17-22	3696	-	-	12:59:10.5	27:36:18.5	-	0.03
comasw17-31	3697	53	-	12:59:10.3	27:37:11.3	-	0.03
coma13-62	3698	-	-	12:59:10.1	27:58:31.8	-	0.00
coma19-96	3699	-	-	12:59:09.9	28:09:51.6	-	0.03
comasw17-81	3700	-	-	12:59:10.1	27:43:28.5	-	0.01
comasw6-3	3703	-	-	12:59:10.3	27:18:20.8	-	0.01
coma23-78	3704	-	-	12:59:09.5	28:17:13.1	-	0.00
comasw22-100	3706	-	-	12:59:09.7	27:52:01.8	-	0.03
coma13-120	3707	-	-	12:59:09.5	28:02:27.2	-	0.03
coma19-43	3708	-	-	12:59:09.5	28:04:43.3	-	0.03
comasw17-41	3710	-	-	12:59:09.8	27:38:08.5	-	0.01
coma23-61	3712	-	-	12:59:09.0	28:15:07.3	-	0.11
comasw6-65	3716	-	-	12:59:09.6	27:26:07.4	-	0.01
coma13-4	3719	-	-	12:59:09.1	27:53:50.8	-	0.03
comasw17-62	3726	-	-	12:59:08.7	27:40:41.8	-	0.01
coma23-67	3727	-	-	12:59:07.9	28:15:38.2	-	0.03
comasw6-25	3728	-	-	12:59:08.6	27:20:58.8	-	0.03
comasw6-37	3729	-	-	12:59:08.6	27:22:01.7	-	0.03
comasw22-43	3730	69	IC3959	12:59:08.2	27:47:02.5	unE	0.03
comasw22-60	3731	-	-	12:59:08.2	27:48:37.7	-	0.02
comasw22-94	3733	109	IC3960	12:59:08.0	27:51:17.1	SB0	0.03
comasw17-46	3735	-	-	12:59:08.1	27:38:35.9	-	0.00
coma13-131	3736	-	-	12:59:07.6	28:04:16.1	-	0.00
comasw22-36	3739	70	IC3957	12:59:07.5	27:46:03.8	unE	0.03
comasw22-37	3750	-	-	12:59:06.9	27:46:20.5	-	0.03
coma19-59	3753	-	-	12:59:06.4	28:05:40.4	-	0.03
comasw22-78	3756	-	-	12:59:06.5	27:49:32.0	-	0.02
coma13-94	3761	160	IC3955	12:59:06.0	27:59:47.8	SB0/a	0.03
coma19-23	3762	-	-	12:59:06.0	28:02:28.6	-	0.00

contiuned from previous page

Object	GMP	D80	Other	RA	DEC	Morphology	CStar
				(J2000)			
comasw17-35	3766	-	-	12:59:06.2	27:37:37.0	-	0.02
coma13-130	3768	-	-	12:59:05.8	28:04:14.0	-	0.03
comasw22-24	3770	-	-	12:59:06.2	27:44:44.5	-	0.01
comasw22-23	3770	-	-	12:59:05.9	27:44:40.7	-	0.17
comasw21-81	3772	-	-	12:59:05.6	27:50:57.0	-	0.03
comasw21-44	3777	-	-	12:59:05.4	27:47:47.6	-	0.02
comasw17-48	3779	54	-	12:59:05.3	27:38:39.4	Sp	0.03
coma13-124	3780	-	-	12:59:04.8	28:03:01.1	-	0.03
coma23-89	3781	-	-	12:59:04.5	28:18:17.6	-	0.03
coma13-19	3782	108	RB262	12:59:04.7	27:54:39.1	SA0	0.03
comasw21-75	3785	-	-	12:59:04.7	27:50:27.6	-	0.01
comasw17-23	3787	-	-	12:59:04.8	27:36:26.9	-	0.01
comasw21-39	3788	-	-	12:59:04.7	27:47:30.1	-	0.03
coma19-70	3792	194	NGC4860	12:59:03.9	28:07:24.8	diE	0.03
coma13-38	3793	-	-	12:59:04.0	27:56:43.5	-	0.01
coma13-44	3794	134	RB261	12:59:04.2	27:57:32.6	diE/SA0	0.03
comasw21-65	3797	-	-	12:59:03.9	27:49:29.2	-	0.01
coma13-78	3804	-	-	12:59:03.2	27:59:09.3	-	0.01
comasw16-72	3805	-	-	12:59:03.2	27:43:41.8	-	0.03
coma13-57	3806	-	-	12:59:03.0	27:58:28.9	-	0.01
comasw21-62	3808	-	-	12:59:03.1	27:49:23.5	-	0.01
coma19-93	3809	-	-	12:59:02.4	28:09:48.1	-	0.03
coma13-96	3811	-	-	12:59:02.5	28:00:20.9	-	0.01
coma13-39	3815	-	-	12:59:02.4	27:56:59.4	-	0.06
coma19-66	3816	195	NGC4858	12:59:02.1	28:06:56.0	S..	0.03
coma23-46	3818	218	-	12:59:01.7	28:13:33.2	S..	0.03
comasw21-25	3820	-	-	12:59:02.0	27:46:03.6	-	0.01
comasw21-90	3821	-	-	12:59:01.9	27:51:54.5	-	0.01
coma13-34	3826	-	-	12:59:01.4	27:56:17.1	-	0.02
comasw21-99	3830	-	-	12:59:01.2	27:52:38.7	-	0.01
comasw16-19	3833	-	-	12:59:01.3	27:36:59.8	-	0.01
comasw16-56	3834	-	-	12:59:01.1	27:41:04.1	-	0.02
comasw21-96	3835	-	-	12:59:00.9	27:52:22.7	-	0.01
comasw16-25	3840	-	-	12:59:00.8	27:37:45.0	-	0.00
comasw21-17	3843	-	-	12:59:00.7	27:45:26.1	-	0.03
coma23-27	3844	-	-	12:59:00.1	28:11:16.0	-	0.01
comasw21-27	3845	-	-	12:59:00.6	27:46:02.1	-	0.02
comasw6-27	3847	-	-	12:59:00.9	27:21:19.3	-	0.03

contiuned from previous page

Object	GMP	D80	Other	RA	DEC	Morphology	CStar
				(J2000)			
comasw16-31	3848	-	-	12:59:00.4	27:38:38.2	-	0.03
comasw21-57	3849	-	-	12:59:00.3	27:49:07.9	-	0.01
comasw6-22	3850	-	-	12:59:00.6	27:20:13.7	-	0.03
coma13-56	3851	135	RB260	12:59:00.1	27:58:02.6	diE	0.03
comasw11-30	3853	-	-	12:59:00.0	27:31:45.0	-	0.02
coma13-32	3855	-	-	12:58:59.5	27:56:03.9	-	0.03
coma13-86	3856	-	-	12:58:59.5	27:59:35.8	-	0.00
coma19-63	3857	-	-	12:58:59.4	28:06:21.4	-	0.02
coma13-8	3859	-	-	12:58:59.3	27:54:02.4	-	0.03
comasw6-57	3863	-	-	12:58:59.4	27:24:49.5	-	0.03
comasw6-39	3864	-	-	12:58:59.3	27:22:10.0	-	0.03
comasw11-58	3865	-	-	12:58:59.1	27:35:59.8	-	0.00
coma19-90	3866	-	-	12:58:58.5	28:09:24.3	-	0.00
comasw16-60	3872	-	-	12:58:58.4	27:41:22.7	-	0.00
comasw11-55	3879	42	-	12:58:58.1	27:35:40.8	SAB0	0.03
comasw16-55	3880	-	-	12:58:57.9	27:41:01.8	-	0.01
coma23-38	3881	-	-	12:58:57.2	28:12:55.9	-	0.03
comasw21-36	3882	71	RB214	12:58:57.7	27:47:07.0	SA0	0.03
coma13-99	3883	-	-	12:58:57.4	28:00:29.0	-	0.02
coma19-52	3884	-	-	12:58:57.3	28:05:06.1	-	0.00
comasw16-36	3885	-	-	12:58:57.4	27:39:15.6	-	0.02
comasw21-13	3886	-	-	12:58:57.3	27:45:06.9	-	0.01
comasw11-56	3890	-	-	12:58:57.2	27:36:00.8	-	0.01
comasw21-63	3895	-	-	12:58:56.6	27:49:19.0	-	0.03
coma13-1	3897	-	-	12:58:56.4	27:53:45.1	-	0.01
comasw21-48	3898	-	-	12:58:56.4	27:48:12.5	-	0.02
coma13-14	3899	-	-	12:58:56.3	27:54:28.7	-	0.03
comasw6-40	3901	-	-	12:58:56.6	27:22:33.0	-	0.01
coma23-42	3904	-	-	12:58:55.7	28:13:34.9	-	0.03
comasw21-66	3907	-	-	12:58:55.8	27:49:28.3	-	0.01
comasw21-109	3911	-	-	12:58:55.5	27:53:15.2	-	0.01
comasw6-8	3913	-	-	12:58:55.8	27:18:57.0	-	0.02
coma13-50	3914	136	RB257	12:58:55.3	27:57:52.5	diE/SA0	0.03
comasw21-67	3916	-	-	12:58:55.1	27:49:30.4	-	0.03
coma23-29	3917	-	-	12:58:54.7	28:11:39.1	-	0.01
coma23-88	3918	-	-	12:58:54.6	28:18:12.0	-	0.05
coma13-51	3920	-	-	12:58:54.8	27:58:04.1	-	0.05
coma23-41	3921	-	-	12:58:54.3	28:13:25.8	-	0.02

contiuned from previous page

Object	GMP	D80	Other	RA	DEC	Morphology	CStar
				(J2000)			
coma19-83	3922	-	-	12:58:54.5	28:08:43.9	-	0.06
comasw21-105	3923	-	-	12:58:54.7	27:53:06.8	-	0.04
comasw21-46	3925	-	-	12:58:54.7	27:47:43.7	-	0.03
comasw22-26	3926	-	-	12:58:54.6	27:45:11.7	-	0.00
coma23-63	3927	-	-	12:58:54.0	28:15:22.3	-	0.02
coma23-82	3930	-	-	12:58:53.5	28:17:24.5	-	0.00
coma19-64	3935	196	-	12:58:53.4	28:07:33.3	SA0/a	0.03
coma13-128	3937	-	-	12:58:53.5	28:03:59.7	-	0.01
comasw6-46	3939	-	-	12:58:53.8	27:23:18.9	-	0.03
coma23-51	3940	-	-	12:58:52.9	28:14:05.1	-	0.03
comasw21-53	3943	90	RB209	12:58:53.1	27:48:48.0	SA0	0.03
comasw21-107	3946	-	-	12:58:53.0	27:53:09.8	-	0.02
coma13-17	3951	-	-	12:58:52.8	27:54:35.5	-	0.02
coma19-42	3953	-	-	12:58:52.2	28:04:23.1	-	0.02
coma23-68	3954	-	-	12:58:52.0	28:15:50.9	-	0.01
comasw21-37	3958	72	IC3947	12:58:52.1	27:47:05.7	SA0	0.03
coma13-116	3963	-	-	12:58:51.4	28:02:15.3	-	0.03
coma23-59	3964	-	-	12:58:51.1	28:14:57.6	-	0.03
coma13-11	3966	-	-	12:58:51.4	27:54:14.9	-	0.03
coma13-100	3969	-	-	12:58:50.8	28:00:24.7	-	0.03
coma19-57	3972	181	RB252	12:58:50.8	28:05:02.1	SA0	0.03
coma13-91	3973	-	-	12:58:50.8	27:59:43.7	-	0.03
comasw6-48	3977	-	-	12:58:50.8	27:23:36.6	-	0.02
coma13-101	3978	-	-	12:58:50.3	28:00:34.3	-	0.01
comasw21-58	3980	-	-	12:58:50.2	27:49:07.6	-	0.03
coma13-125	3982	-	-	12:58:50.1	28:03:13.9	-	0.03
coma23-43	3984	-	-	12:58:49.5	28:13:36.7	-	0.03
comasw11-18	3986	-	-	12:58:50.3	27:28:28.7	-	0.00
coma13-15	3987	-	-	12:58:49.8	27:55:10.9	-	0.02
coma23-71	3990	-	-	12:58:49.1	28:16:38.1	-	0.12
coma13-18	3993	-	-	12:58:49.4	27:54:38.1	-	0.03
comasw21-51	3997	91	IC3946	12:58:48.8	27:48:37.2	SAB0/a	0.03
coma13-12	3998	-	-	12:58:48.6	27:54:25.5	-	0.04
coma13-47	3999	-	-	12:58:48.4	27:57:49.4	-	0.01
comasw16-62	4001	-	-	12:58:48.6	27:41:59.5	-	0.01
coma23-70	4002	-	-	12:58:47.9	28:16:36.3	-	0.02
coma13-107	4003	-	-	12:58:48.2	28:01:06.9	-	0.02
comasw21-74	4005	-	-	12:58:48.1	27:50:24.4	-	0.03

contiuned from previous page

Object	GMP	D80	Other	RA	DEC	Morphology	CStar
				(J2000)			
coma13-16	4011	-	-	12:58:47.6	27:54:36.5	-	0.04
coma13-9	4016	-	-	12:58:47.3	27:54:06.4	-	0.02
comasw16-54	4017	58	NGC4854	12:58:47.4	27:40:28.8	SAB0	0.03
coma12-23	4020	-	-	12:58:46.6	27:58:52.6	-	0.00
coma18-68	4022	-	-	12:58:46.2	28:08:30.4	-	0.02
coma13-10	4024	-	-	12:58:46.5	27:54:05.8	-	0.03
comasw6-77	4026	-	-	12:58:46.7	27:28:02.5	-	0.00
comasw6-28	4028	-	-	12:58:46.6	27:21:23.7	-	0.02
comasw21-86	4029	-	-	12:58:46.1	27:51:39.0	-	0.02
comasw11-6	4032	-	-	12:58:46.1	27:30:08.8	-	0.01
comasw21-77	4033	-	-	12:58:45.6	27:50:45.4	-	0.01
comasw21-102	4034	-	-	12:58:45.5	27:52:47.9	-	0.03
comasw21-14	4035	-	-	12:58:45.6	27:45:13.0	-	0.02
comasw21-35	4037	-	-	12:58:45.3	27:46:54.5	-	0.03
comasw11-4	4039	-	-	12:58:45.6	27:26:48.5	-	0.00
coma12-68	4040	-	-	12:58:44.6	28:05:34.9	-	0.01
coma12-49	4042	-	-	12:58:44.2	28:02:56.3	-	0.02
coma23-76	4043	-	-	12:58:43.9	28:17:02.8	-	0.03
comasw21-10	4046	-	-	12:58:44.7	27:44:57.3	-	0.01
comasw21-11	4046	-	-	12:58:44.4	27:44:59.9	-	0.01
comasw21-42	4047	-	-	12:58:44.4	27:47:40.5	-	0.01
comasw16-66	4049	-	-	12:58:44.4	27:42:51.4	-	0.01
comasw21-43	4051	-	-	12:58:44.2	27:47:47.8	-	0.02
coma23-85	4052	-	-	12:58:43.5	28:17:56.1	-	0.02
comasw21-20	4060	-	-	12:58:42.7	27:45:37.0	-	0.00
coma12-16	4062	-	-	12:58:42.3	27:58:19.7	-	0.01
coma13-27	4063	-	-	12:58:41.9	27:55:19.1	-	0.03
coma23-26	4065	-	-	12:58:41.5	28:11:12.4	-	0.02
comasw16-52	4066	-	-	12:58:42.1	27:40:36.0	-	0.03
coma12-44	4068	-	-	12:58:41.5	28:02:43.5	-	0.01
coma23-81	4069	-	-	12:58:41.3	28:17:21.9	-	0.05
comasw21-19	4072	-	-	12:58:41.7	27:45:29.7	-	0.18
coma23-44	4073	-	-	12:58:41.1	28:13:49.7	-	0.03
coma12-45	4075	-	-	12:58:41.2	28:02:45.4	-	0.03
comasw11-43	4078	-	-	12:58:41.3	27:33:35.1	-	0.00
comasw16-51	4080	-	-	12:58:41.2	27:40:56.3	-	0.00
coma13-26	4081	-	-	12:58:40.7	27:55:12.6	-	0.03
comasw21-69	4083	-	RB198	12:58:40.8	27:49:36.4	SA0	0.03

contiuned from previous page

Object	GMP	D80	Other	RA	DEC	Morphology	CStar
				(J2000)			
comasw21-70	4087	-	-	12:58:40.4	27:49:54.4	-	0.15
comasw16-41	4090	-	-	12:58:40.4	27:39:53.8	-	0.03
comasw6-23	4093	-	-	12:58:40.5	27:20:28.0	-	0.03
comasw11-36	4098	-	-	12:58:39.7	27:32:30.2	-	0.00
comasw11-48	4101	-	-	12:58:39.5	27:34:00.4	-	0.01
comasw21-82	4102	-	-	12:58:39.2	27:51:05.9	-	0.04
coma12-15	4103	-	-	12:58:39.0	27:57:13.6	-	0.03
coma12-10	4108	-	-	12:58:38.6	27:56:35.2	-	0.03
coma18-65	4109	-	-	12:58:38.2	28:08:14.5	-	0.01
coma23-1	4109	-	-	12:58:38.0	28:08:19.5	-	0.02
coma12-12	4114	-	-	12:58:38.3	27:56:45.2	-	0.02
comasw21-71	4116	-	-	12:58:38.3	27:49:55.2	-	0.01
comasw11-38	4117	28	-	12:58:38.5	27:32:38.4	-	0.03
comasw21-64	4118	-	-	12:58:38.2	27:49:20.4	-	0.01
coma18-62	4126	-	-	12:58:37.0	28:07:54.5	-	0.00
comasw21-79	4129	-	-	12:58:36.8	27:50:57.7	-	0.03
coma18-51	4130	197	IC3943	12:58:36.4	28:06:48.9	Sa	0.03
comasw11-3	4137	-	-	12:58:36.7	27:26:17.1	-	0.01
coma12-55	4138	-	-	12:58:36.0	28:03:51.3	-	0.01
comasw6-73	4140	-	-	12:58:36.6	27:27:13.6	-	0.14
comasw21-93	4141	-	-	12:58:36.1	27:52:22.4	-	0.00
comasw6-21	4143	-	-	12:58:36.6	27:20:15.2	-	0.08
comasw16-24	4146	-	-	12:58:36.0	27:37:39.8	-	0.03
coma12-47	4148	-	-	12:58:35.3	28:02:55.0	-	0.01
comasw21-31	4150	-	-	12:58:35.5	27:46:29.4	-	0.01
coma12-67	4153	-	-	12:58:35.0	28:05:19.0	-	0.01
comasw11-29	4154	-	-	12:58:35.6	27:31:51.9	-	0.06
comasw11-59	4156	43	NGC4853	12:58:35.2	27:35:46.8	SAB0p	0.03
comasw16-27	4157	-	-	12:58:35.2	27:37:52.8	-	0.01
comasw6-42	4161	-	-	12:58:35.2	27:22:49.5	-	0.02
comasw11-10	4162	-	-	12:58:35.1	27:30:22.6	-	0.01
coma12-32	4163	-	-	12:58:34.4	28:00:35.3	-	0.00
coma12-8	4165	-	-	12:58:34.3	27:56:22.5	-	0.00
comasw11-17	4169	-	-	12:58:34.6	27:28:09.9	-	0.03
comasw21-72	4175	-	-	12:58:33.8	27:50:11.8	-	0.03
comasw16-49	4179	-	-	12:58:33.8	27:40:28.4	-	0.03
comasw16-67	4190	-	-	12:58:32.9	27:43:14.8	-	0.00
comasw6-38	4192	-	-	12:58:33.2	27:21:51.6	Sp	0.03

contiuned from previous page

Object	GMP	D80	Other	RA	DEC	Morphology	CStar
				(J2000)			
comasw21-80	4193	-	-	12:58:32.6	27:50:58.6	-	0.03
coma12-51	4200	182	RB243	12:58:31.9	28:02:58.3	SAB0	0.03
comasw21-83	4205	-	-	12:58:31.7	27:51:09.9	-	0.03
comasw11-11	4206	20	-	12:58:32.1	27:27:22.5	SA0	0.03
comasw21-103	4207	-	-	12:58:31.5	27:53:02.0	-	0.13
coma18-84	4208	-	-	12:58:31.2	28:10:07.6	-	0.02
comasw16-50	4209	59	RB188	12:58:31.7	27:40:24.3	diE	0.03
comasw6-11	4211	-	-	12:58:31.9	27:18:53.1	-	0.01
comasw6-10	4211	-	-	12:58:32.1	27:18:48.4	-	0.02
comasw21-34	4212	-	-	12:58:31.4	27:46:54.1	-	0.15
comasw6-50	4215	-	-	12:58:31.7	27:23:41.9	-	0.02
comasw21-84	4216	-	-	12:58:31.3	27:51:19.3	-	0.00
comasw21-115	4217	-	-	12:58:31.1	27:53:43.8	-	0.02
comasw6-14	4220	-	-	12:58:31.6	27:19:05.0	-	0.02
comasw21-41	4221	-	-	12:58:31.0	27:47:47.2	-	0.04
comasw6-13	4226	-	-	12:58:31.4	27:18:58.2	-	0.04
coma12-36	4230	161	RB241	12:58:30.2	28:00:52.8	boE	0.03
comasw10-79	4232	-	-	12:58:30.7	27:33:51.5	-	0.00
coma12-65	4238	-	-	12:58:29.4	28:05:16.2	-	0.02
comasw6-33	4240	-	-	12:58:30.0	27:21:37.6	-	0.07
comasw21-40	4245	-	-	12:58:29.2	27:47:42.4	-	0.02
comasw21-54	4246	-	-	12:58:29.0	27:48:52.4	-	0.03
comasw21-101	4247	-	-	12:58:28.8	27:52:50.4	-	0.01
coma12-71	4251	-	-	12:58:28.1	28:05:50.5	-	0.03
comasw10-24	4253	-	-	12:58:28.7	27:27:36.5	-	0.03
comasw10-78	4255	44	-	12:58:28.4	27:33:33.3	-	0.03
comasw20-96	4264	-	-	12:58:27.3	27:52:06.1	-	0.01
comasw16-33	4266	-	-	12:58:27.6	27:39:49.4	-	0.02
comasw16-63	4268	-	-	12:58:27.1	27:42:23.3	-	0.03
comasw10-59	4270	-	-	12:58:27.2	27:31:26.6	-	0.01
comasw20-33	4271	-	-	12:58:26.9	27:45:28.7	-	0.02
coma12-60	4275	-	-	12:58:26.5	28:04:54.6	-	0.00
coma12-29	4277	-	-	12:58:26.0	27:59:54.7	-	0.02
coma18-61	4281	-	-	12:58:25.5	28:07:43.6	-	0.03
comasw16-18	4285	-	-	12:58:25.9	27:37:02.7	-	0.00
coma18-69	4287	-	-	12:58:25.1	28:08:47.6	-	0.03
comasw10-101	4291	-	-	12:58:25.5	27:36:14.2	-	0.02
coma12-46	4295	-	-	12:58:24.0	28:02:48.5	-	0.00

contiuned from previous page

Object	GMP	D80	Other	RA (J2000)	DEC (J2000)	Morphology	CStar
comasw15-49	4303	-	-	12:58:23.4	27:38:57.7	-	0.01
comasw20-77	4304	-	-	12:58:22.8	27:50:37.4	-	0.02
coma18-75	4308	198	-	12:58:22.2	28:09:07.1	SA0	0.03
comasw21-104	4310	-	-	12:58:22.3	27:53:05.1	-	0.03
comasw10-63	4312	-	-	12:58:22.5	27:31:56.1	-	0.00
coma18-74	4313	199	NGC4851	12:58:21.7	28:08:54.9	SBa	0.03
comasw21-114	4314	-	-	12:58:22.0	27:53:32.1	-	0.03
coma12-17	4315	137	NGC4850	12:58:21.8	27:58:03.7	SB0	0.03
comasw15-26	4317	-	-	12:58:22.0	27:37:14.0	-	0.00
comasw16-83	4320	-	-	12:58:21.5	27:44:47.9	-	0.01
comasw15-76	4323	-	-	12:58:21.0	27:42:53.5	-	0.02
comasw21-120	4326	-	-	12:58:20.5	27:54:19.1	-	0.01
comasw10-77	4329	-	-	12:58:20.5	27:33:40.6	-	0.01
comasw10-4	4330	-	-	12:58:20.5	27:25:45.3	-	0.03
comasw20-35	4332	-	-	12:58:19.9	27:45:43.5	-	0.03
coma12-69	4333	-	-	12:58:19.8	28:05:41.7	-	0.00
comasw10-45	4339	-	-	12:58:19.8	27:29:43.5	-	0.02
comasw20-36	4341	73	RB183	12:58:19.1	27:45:41.5	SA0	0.03
coma12-56	4345	-	-	12:58:18.1	28:04:13.5	-	0.03
comasw20-83	4348	-	-	12:58:18.3	27:50:54.1	-	0.03
coma12-22	4350	-	-	12:58:17.8	27:58:51.9	-	0.01
comasw5-4	4351	9	-	12:58:18.7	27:18:37.5	-	0.03
coma12-59	4352	-	-	12:58:17.6	28:04:50.4	-	0.02
coma12-40	4355	-	-	12:58:17.4	28:02:24.0	-	0.03
comasw24-47	4361	-	-	12:58:17.0	27:54:01.2	-	0.05
comasw10-72	4363	-	-	12:58:17.0	27:32:56.0	-	0.00
comasw15-90	4364	-	RB182	12:58:16.9	27:43:46.4	S..	0.03
comasw20-54	4366	-	-	12:58:16.5	27:48:08.0	-	0.03
comasw20-68	4367	-	-	12:58:16.4	27:49:36.4	-	0.03
coma12-66	4376	-	-	12:58:15.5	28:05:16.2	-	0.03
coma18-56	4379	200	-	12:58:15.1	28:07:32.8	SA0	0.03
comasw10-75	4380	-	-	12:58:15.4	27:33:10.4	-	0.02
comasw10-28	4381	-	-	12:58:15.3	27:27:52.7	-	0.03
comasw10-29	4384	-	-	12:58:15.0	27:27:44.8	-	0.02
comasw24-51	4386	-	-	12:58:14.5	27:54:41.8	-	0.02
comasw15-67	4390	-	-	12:58:14.5	27:41:26.8	-	0.00
coma18-91	4391	209	-	12:58:13.8	28:10:56.8	SA0	0.03
comasw5-6	4394	-	-	12:58:14.6	27:19:07.7	-	0.03

contiuned from previous page

Object	GMP	D80	Other	RA (J2000)	DEC (J2000)	Morphology	CStar
comasw24-42	4395	-	-	12:58:13.7	27:53:36.9	-	0.01
coma12-54	4396	-	-	12:58:13.5	28:03:46.0	-	0.01
comasw24-50	4397	-	-	12:58:13.6	27:54:18.6	-	0.01
comasw5-39	4402	-	-	12:58:13.9	27:24:12.4	-	0.02
comasw10-12	4403	-	-	12:58:13.7	27:26:35.5	-	0.00
comasw24-52	4404	-	-	12:58:13.1	27:54:45.3	-	0.00
comasw5-38	4411	-	-	12:58:13.0	27:24:07.5	-	0.04
coma18-80	4412	-	-	12:58:12.1	28:09:32.3	-	0.02
comasw24-43	4419	-	-	12:58:11.7	27:53:36.9	-	0.02
coma12-9	4420	-	-	12:58:11.4	27:56:23.4	-	0.03
comasw10-67	4421	-	-	12:58:11.7	27:32:32.7	-	0.02
comasw15-96	4423	-	-	12:58:11.4	27:44:31.7	-	0.02
comasw20-91	4424	-	-	12:58:11.2	27:51:37.1	-	0.03
comasw15-66	4428	-	-	12:58:11.2	27:41:23.5	-	0.00
comasw20-47	4431	-	-	12:58:10.7	27:47:23.7	-	0.03
comasw10-46	4436	-	-	12:58:10.8	27:30:02.3	-	0.02
comasw20-63	4438	-	-	12:58:10.2	27:48:49.6	-	0.03
coma18-50	4441	-	-	12:58:09.6	28:06:58.3	-	0.01
coma18-89	4442	-	-	12:58:09.5	28:11:05.5	-	0.03
comasw24-41	4445	-	-	12:58:09.5	27:53:30.1	-	0.05
comasw10-73	4447	29	-	12:58:09.7	27:32:57.4	-	0.03
comasw5-34	4448	-	-	12:58:09.9	27:23:50.1	-	0.02
comasw24-53	4450	-	-	12:58:08.8	27:55:04.3	-	0.00
coma12-43	4451	-	-	12:58:08.8	28:02:40.3	-	0.02
comasw10-18	4452	-	-	12:58:09.2	27:27:16.9	-	0.00
coma18-70	4455	-	-	12:58:08.0	28:08:49.9	-	0.03
coma12-14	4458	-	-	12:58:08.0	27:56:52.9	-	0.01
comasw10-87	4469	-	-	12:58:06.9	27:34:36.4	-	0.03
comasw5-52	4479	-	-	12:58:06.1	27:25:08.0	-	0.03
coma18-77	4480	-	-	12:58:05.2	28:09:27.2	-	0.03
coma12-34	4481	-	-	12:58:05.4	28:00:38.9	-	0.03
comasw20-64	4483	-	-	12:58:05.1	27:49:00.6	-	0.01
comasw5-28	4484	-	-	12:58:05.8	27:22:57.4	-	0.00
comasw20-45	4485	-	-	12:58:05.1	27:47:20.6	-	0.03
comasw10-35	4490	-	-	12:58:04.9	27:29:04.3	-	0.04
comasw10-99	4491	-	-	12:58:04.5	27:35:58.8	-	0.00
coma12-2	4493	-	-	12:58:03.8	27:56:01.1	-	0.02
comasw20-65	4499	92	-	12:58:03.5	27:48:53.3	SA0	0.03

contiuned from previous page

Object	GMP	D80	Other	RA	DEC	Morphology	CStar
				(J2000)			
comasw20-67	4500	-	-	12:58:03.6	27:49:20.6	-	0.01
comasw15-63	4502	-	-	12:58:03.6	27:40:56.3	-	0.03
coma12-18	4503	138	-	12:58:03.1	27:58:13.6	S..	0.03
coma18-82	4504	-	-	12:58:03.0	28:09:51.5	-	0.01
comasw15-38	4506	-	-	12:58:03.5	27:37:59.5	-	0.03
comasw15-41	4508	-	-	12:58:03.4	27:38:30.9	-	0.03
comasw15-47	4509	-	-	12:58:03.3	27:38:45.0	-	0.02
coma12-20	4510	-	-	12:58:02.9	27:58:41.6	-	0.03
comasw20-58	4515	-	-	12:58:02.5	27:48:25.6	-	0.03
comasw20-87	4516	-	-	12:58:02.5	27:51:01.9	-	0.03
comasw20-88	4519	-	-	12:58:01.8	27:51:13.2	-	0.03
comasw10-44	4522	21	-	12:58:01.6	27:29:22.5	Sp	0.03
comasw10-47	4524	-	-	12:58:01.5	27:30:06.2	-	0.00
comasw20-71	4529	-	-	12:58:01.0	27:49:54.8	-	0.03
comasw5-53	4530	-	-	12:58:01.4	27:25:14.9	-	0.02
comasw20-55	4531	-	-	12:58:00.7	27:48:11.5	-	0.03
comasw10-19	4535	-	-	12:58:00.8	27:27:14.3	-	0.03
comasw10-97	4538	-	-	12:58:00.3	27:35:56.5	-	0.02
comasw20-86	4539	-	-	12:58:00.0	27:51:09.6	-	0.02
comasw15-74	4541	-	-	12:57:59.9	27:42:33.0	-	0.00
comasw5-32	4545	-	-	12:57:59.8	27:23:30.7	-	0.00
comasw23-46	4553	-	-	12:57:58.6	27:54:42.9	-	0.03
comasw5-16	4554	-	-	12:57:59.2	27:21:13.2	-	0.03
comasw26-27	4555	183	-	12:57:57.8	28:03:42.4	???	0.03
comasw15-60	4557	-	-	12:57:58.3	27:40:29.8	-	0.02
comasw26-40	4558	-	-	12:57:57.7	28:05:47.8	-	0.04
comasw10-98	4559	-	-	12:57:58.4	27:35:57.9	-	0.03
comasw23-50	4561	-	-	12:57:57.6	27:55:28.8	-	0.01
comasw15-95	4562	-	-	12:57:57.8	27:44:29.7	-	0.01
comasw23-58	4563	-	-	12:57:57.4	27:56:16.6	-	0.03
comasw5-15	4565	-	-	12:57:58.0	27:21:02.0	-	0.03
comasw19-40	4566	-	-	12:57:57.3	27:48:33.5	-	0.03
comasw10-11	4568	-	-	12:57:57.7	27:26:35.8	-	0.03
comasw23-47	4569	-	-	12:57:57.0	27:55:06.1	-	0.00
comasw23-82	4570	-	-	12:57:56.9	27:59:29.5	-	0.03
comasw5-47	4572	-	-	12:57:57.6	27:24:48.8	-	0.01
comasw15-22	4573	-	-	12:57:57.3	27:36:30.9	-	0.02
comasw10-10	4577	-	-	12:57:56.7	27:26:33.0	-	0.03

contiuned from previous page

Object	GMP	D80	Other	RA	DEC	Morphology	CStar
				(J2000)			
comasw4-28	4578	-	-	12:57:56.5	27:22:55.8	-	0.03
comasw10-92	4579	45	-	12:57:56.3	27:34:52.4	-	0.03
comasw15-29	4580	-	-	12:57:56.2	27:37:25.5	-	0.00
comasw15-25	4592	55	-	12:57:54.8	27:36:56.9	-	0.03
comasw15-33	4593	-	-	12:57:54.3	27:37:40.5	-	0.03
comasw10-34	4597	22	-	12:57:54.4	27:29:26.1	Sp	0.03
comasw26-22	4600	-	-	12:57:52.6	28:03:01.2	-	0.01
comasw15-73	4602	-	-	12:57:53.2	27:42:25.8	-	0.03
comasw23-66	4606	-	-	12:57:52.6	27:57:35.7	-	0.02
comasw19-33	4608	-	-	12:57:52.7	27:47:24.7	-	0.01
comasw10-86	4609	-	-	12:57:52.8	27:34:40.8	-	0.01
comasw15-93	4612	-	-	12:57:52.4	27:44:22.2	-	0.03
comasw23-88	4614	-	-	12:57:51.9	28:00:16.1	-	0.03
comasw15-70	4615	-	-	12:57:52.2	27:41:51.4	-	0.01
comasw10-9	4618	-	-	12:57:52.1	27:26:37.3	-	0.01
comasw15-34	4619	-	-	12:57:51.7	27:37:49.2	-	0.03
comasw23-33	4620	-	-	12:57:51.2	27:53:21.5	-	0.03
comasw23-87	4622	-	-	12:57:51.0	28:00:12.0	-	0.10
comasw19-50	4624	-	-	12:57:51.0	27:50:45.8	-	0.02
comasw19-61	4626	110	-	12:57:50.7	27:52:46.9	SA0/a	0.03
comasw10-62	4628	-	-	12:57:51.0	27:32:04.9	-	0.00
comasw10-42	4630	-	-	12:57:50.8	27:29:26.8	-	0.03
comasw15-44	4632	-	-	12:57:50.7	27:38:37.1	-	0.03
comasw10-53	4636	-	-	12:57:50.3	27:31:15.3	-	0.02
comasw15-36	4642	-	-	12:57:49.7	27:37:58.2	-	0.07
comasw10-54	4643	-	-	12:57:49.6	27:31:09.1	-	0.00
comasw4-27	4645	-	-	12:57:49.9	27:22:59.9	-	0.02
comasw10-33	4646	-	-	12:57:49.8	27:28:35.9	-	0.01
comasw10-32	4646	-	-	12:57:49.6	27:28:35.2	-	0.03
comasw23-80	4647	-	-	12:57:49.0	27:59:17.4	-	0.03
comasw23-31	4653	111	-	12:57:48.1	27:52:58.6	SA0	0.03
comasw15-87	4655	-	-	12:57:48.1	27:43:35.2	-	0.03
comasw19-25	4656	74	-	12:57:47.9	27:46:09.6	-	0.03
comasw19-57	4657	-	-	12:57:47.8	27:51:38.6	-	0.02
comasw19-51	4659	-	-	12:57:47.6	27:50:52.5	-	0.02
comasw26-38	4660	-	-	12:57:47.2	28:05:26.8	-	0.02
comasw10-36	4662	-	-	12:57:47.9	27:29:39.7	-	0.03
comasw19-45	4664	93	-	12:57:47.3	27:50:00.0	SA0	0.03

contiuned from previous page

Object	GMP	D80	Other	RA	DEC	Morphology	CStar
				(J2000)			
comasw26-69	4666	201	-	12:57:46.7	28:08:26.8	SAB0/a	0.03
comasw10-5	4667	-	-	12:57:47.8	27:26:04.8	-	0.01
comasw4-16	4669	-	-	12:57:47.7	27:21:59.7	-	0.08
comasw15-77	4670	-	-	12:57:47.2	27:43:28.4	-	0.01
comasw4-1	4675	-	-	12:57:47.1	27:18:29.6	-	0.07
comasw23-59	4676	-	-	12:57:46.0	27:56:26.7	-	0.00
comasw19-20	4679	75	-	12:57:46.2	27:45:24.7	SA0	0.03
comasw4-45	4682	-	-	12:57:46.3	27:24:58.4	-	0.00
comasw26-24	4686	-	-	12:57:45.0	28:03:44.6	-	0.01
comasw23-42	4689	-	-	12:57:45.3	27:54:20.8	-	0.03
comasw19-24	4690	-	-	12:57:45.4	27:46:16.8	-	0.00
comasw4-51	4692	14	-	12:57:45.7	27:25:45.1	-	0.03
comasw10-84	4696	-	-	12:57:45.0	27:34:33.8	-	0.03
comasw14-54	4699	-	-	12:57:44.5	27:40:03.0	-	0.03
comasw23-57	4706	-	-	12:57:43.8	27:56:13.4	-	0.01
comasw10-13	4709	-	-	12:57:44.1	27:26:58.6	-	0.01
comasw26-48	4711	-	-	12:57:42.9	28:06:52.5	-	0.01
comasw4-73	4712	-	-	12:57:43.8	27:27:40.6	-	0.01
comasw14-1	4714	-	-	12:57:43.2	27:34:39.9	-	0.03
comasw14-19	4715	-	-	12:57:43.0	27:36:28.8	-	0.03
comasw19-35	4718	-	-	12:57:42.7	27:47:46.3	-	0.00
comasw14-26	4719	-	-	12:57:42.8	27:37:17.2	-	0.03
comasw14-34	4725	-	-	12:57:42.1	27:37:57.3	-	0.01
comasw19-34	4727	-	-	12:57:41.8	27:47:43.9	-	0.04
comasw26-66	4733	-	-	12:57:40.7	28:08:21.0	-	0.01
comasw14-37	4735	-	-	12:57:41.3	27:38:12.8	-	0.02
comasw9-63	4739	-	-	12:57:41.1	27:32:03.4	-	0.02
comasw9-54	4740	-	-	12:57:40.9	27:30:54.3	-	0.03
comasw23-35	4742	-	-	12:57:40.1	27:53:38.9	-	0.01
comasw26-23	4745	-	-	12:57:39.5	28:03:31.1	-	0.01
comasw9-69	4749	-	-	12:57:40.2	27:32:27.2	-	0.03
comasw27-61	4752	-	-	12:57:38.9	28:09:11.0	-	0.02
comasw14-41	4753	-	-	12:57:39.6	27:38:46.4	-	0.01
comasw14-13	4757	-	-	12:57:39.4	27:36:22.4	-	0.03
comasw26-70	4758	-	-	12:57:38.3	28:08:45.8	-	0.02
comasw23-86	4759	-	-	12:57:38.5	28:00:08.9	-	0.01
comasw19-59	4761	-	-	12:57:38.4	27:51:49.9	-	0.10
comasw26-71	4762	-	-	12:57:37.7	28:08:45.0	-	0.03

contiuned from previous page

Object	GMP	D80	Other	RA	DEC	Morphology	CStar
				(J2000)			
comasw14-10	4763	-	-	12:57:38.5	27:36:01.4	-	0.01
comasw19-18	4766	-	-	12:57:38.1	27:44:55.8	-	0.01
comasw4-68	4768	-	-	12:57:38.8	27:27:18.2	-	0.02
comasw23-25	4773	-	-	12:57:37.6	27:52:18.8	-	0.02
comasw26-19	4774	-	-	12:57:37.2	28:02:25.8	-	0.02
comasw23-55	4775	-	-	12:57:37.2	27:55:59.0	-	0.00
comasw26-34	4779	184	-	12:57:36.4	28:04:37.8	SA0/a	0.03
comasw14-35	4780	-	-	12:57:37.1	27:38:04.4	-	0.03
comasw26-77	4782	-	-	12:57:36.1	28:09:35.3	-	0.04
comasw26-15	4783	-	-	12:57:36.0	28:01:17.7	-	0.02
comasw9-28	4784	-	-	12:57:36.8	27:27:46.2	-	0.04
comasw9-42	4792	23	NGC4842	12:57:36.2	27:29:04.8	SA0	0.03
comasw9-37	4794	30	NGC4842	12:57:35.9	27:29:35.1	unE/SA0	0.03
comasw9-46	4795	-	-	12:57:35.9	27:30:09.1	-	0.01
comasw4-55	4797	-	-	12:57:36.0	27:25:58.4	-	0.20
comasw4-8	4800	-	-	12:57:36.1	27:20:23.6	-	0.02
comasw23-53	4801	-	-	12:57:35.1	27:55:42.1	-	0.00
comasw26-43	4805	-	-	12:57:34.5	28:06:19.9	-	0.00
comasw9-77	4808	-	-	12:57:35.2	27:34:04.5	-	0.01
comasw14-42	4809	-	-	12:57:34.9	27:38:46.9	-	0.01
comasw23-51	4811	-	-	12:57:34.5	27:55:38.0	-	0.15
comasw9-45	4813	-	-	12:57:34.9	27:30:05.2	-	0.03
comasw19-21	4814	-	-	12:57:34.3	27:45:42.7	-	0.01
comasw4-3	4815	-	-	12:57:34.7	27:18:37.1	-	0.03
comasw23-3	4821	-	-	12:57:33.0	27:50:20.3	-	0.01
comasw9-41	4825	-	-	12:57:33.3	27:29:47.0	-	0.03
comasw14-20	4829	46	NGC4840	12:57:32.8	27:36:37.6	SAB0	0.03
comasw26-49	4833	-	-	12:57:31.4	28:07:03.6	-	0.17
comasw27-45	4833	-	-	12:57:31.7	28:06:58.2	-	0.02
comasw19-56	4835	-	-	12:57:31.8	27:51:34.5	-	0.20
comasw26-10	4837	-	-	12:57:31.2	28:01:07.2	-	0.02
comasw26-13	4838	-	-	12:57:31.2	28:00:52.8	-	0.03
comasw4-12	4845	-	-	12:57:31.6	27:21:23.9	-	0.00
comasw4-59	4846	-	-	12:57:31.5	27:26:02.9	-	0.03
comasw4-29	4848	-	-	12:57:31.5	27:23:04.3	-	0.03
comasw4-44	4851	-	-	12:57:31.0	27:25:02.9	-	0.02
comasw9-70	4852	-	-	12:57:30.6	27:32:34.5	-	0.03
comasw4-22	4855	-	-	12:57:30.7	27:22:17.0	-	0.02

contiuned from previous page

Object	GMP	D80	Other	RA	DEC	Morphology	CStar
				(J2000)			
comasw4-72	4858	-	-	12:57:30.4	27:28:08.6	-	0.03
comasw27-25	4865	-	-	12:57:28.8	28:03:44.4	-	0.01
comasw14-66	4867	-	-	12:57:29.2	27:41:44.2	-	0.01
comasw14-16	4868	-	-	12:57:29.1	27:36:31.4	-	0.01
comasw27-16	4869	-	-	12:57:28.5	28:01:52.4	-	0.01
comasw4-41	4870	-	-	12:57:29.4	27:24:48.6	-	0.01
comasw23-73	4871	-	-	12:57:28.4	27:58:30.0	-	0.03
comasw9-75	4878	-	-	12:57:28.6	27:33:38.4	-	0.04
comasw14-67	4879	-	-	12:57:28.1	27:42:02.2	-	0.03
comasw27-36	4880	-	-	12:57:27.5	28:05:59.1	-	0.01
comasw27-32	4882	-	-	12:57:27.4	28:05:03.2	-	0.02
comasw9-67	4887	-	-	12:57:27.7	27:32:13.1	-	0.03
comasw14-38	4888	-	-	12:57:27.5	27:38:10.7	-	0.03
comasw4-13	4893	-	-	12:57:27.6	27:21:25.7	-	0.01
comasw14-79	4896	-	-	12:57:26.9	27:44:04.9	-	0.01
comasw18-56	4897	-	-	12:57:26.7	27:50:27.8	-	0.00
comasw14-51	4905	-	-	12:57:26.1	27:39:33.8	-	0.03
comasw8-50	4907	33	-	12:57:25.9	27:32:45.7	SA0	0.03
comasw14-53	4911	-	-	12:57:25.4	27:40:04.7	-	0.05
comasw18-66	4913	-	-	12:57:24.9	27:51:28.5	-	0.01
comasw23-37	4916	-	-	12:57:24.7	27:54:02.9	-	0.02
comasw3-87	4918	15	-	12:57:25.3	27:24:16.0	SB0	0.03
comasw3-65	4919	-	-	12:57:25.2	27:26:21.9	-	0.06
comasw3-19	4926	-	-	12:57:24.7	27:21:18.3	-	0.03
comasw18-55	4927	-	-	12:57:23.9	27:50:27.7	-	0.01
comasw8-38	4928	31	NGC4839	12:57:24.4	27:29:51.6	SA0	0.03
comasw3-39	4930	-	-	12:57:24.4	27:23:18.3	-	0.19
comasw3-53	4931	-	-	12:57:24.2	27:25:04.1	-	0.03
comasw18-24	4933	76	-	12:57:23.5	27:45:57.6	SA0/a	0.03
comasw27-38	4934	-	-	12:57:23.0	28:06:03.8	-	0.02
comasw18-52	4935	-	-	12:57:23.3	27:49:41.9	-	0.02
comasw8-51	4937	-	-	12:57:23.6	27:32:59.5	-	0.02
comasw18-18	4940	-	-	12:57:22.6	27:45:01.8	-	0.00
comasw19-60	4945	112	-	12:57:21.8	27:52:49.9	SB0	0.03
comasw18-48	4948	-	-	12:57:21.5	27:49:13.2	-	0.00
comasw18-68	4953	-	-	12:57:21.2	27:51:30.2	-	0.03
comasw3-68	4954	-	-	12:57:21.8	27:26:47.2	-	0.16
comasw3-91	4956	-	-	12:57:21.7	27:28:28.9	-	0.03

contiuned from previous page

Object	GMP	D80	Other	RA	DEC	Morphology	CStar
				(J2000)			
comasw14-17	4960	-	-	12:57:20.7	27:36:32.5	-	0.03
comasw3-73	4962	-	-	12:57:20.6	27:27:22.3	-	0.05
comasw14-15	4967	-	-	12:57:19.5	27:36:50.0	-	0.03
comasw27-51	4968	-	-	12:57:18.7	28:08:00.2	-	0.02
comasw18-46	4974	94	-	12:57:17.8	27:48:38.9	SA0	0.03
comasw3-41	4978	-	-	12:57:18.2	27:23:37.3	-	0.01
comasw23-68	4981	-	-	12:57:16.8	27:58:07.4	-	0.01
comasw23-30	4986	-	-	12:57:16.5	27:53:10.3	-	0.02
comasw14-22	4987	56	-	12:57:16.7	27:37:06.8	-	0.03
comasw23-72	4988	-	-	12:57:16.0	27:58:28.8	-	0.08
comasw3-7	4992	-	-	12:57:16.5	27:19:18.5	-	0.02
comasw23-40	4993	-	-	12:57:15.4	27:54:29.5	-	0.03
comasw14-77	4995	-	-	12:57:15.3	27:43:46.6	-	0.02
comasw23-76	4997	-	-	12:57:14.7	27:59:03.9	-	0.03
comasw9-48	5004	-	-	12:57:14.6	27:30:35.6	-	0.02
comasw25-70	5007	-	-	12:57:13.2	27:58:50.0	-	0.02
comasw14-39	5009	-	-	12:57:13.8	27:38:22.3	-	0.03
comasw27-52	5010	-	-	12:57:12.7	28:07:59.6	-	0.01
comasw3-47	5017	-	-	12:57:13.7	27:24:31.0	-	0.09
comasw27-34	5018	-	-	12:57:12.3	28:05:41.9	-	0.01
comasw3-48	5020	-	-	12:57:13.3	27:24:36.9	-	0.01
comasw3-38	5026	-	-	12:57:12.3	27:23:13.6	-	0.00
comasw25-66	5029	-	-	12:57:10.8	27:58:38.5	-	0.02
comasw18-58	5030	-	-	12:57:11.2	27:50:56.8	-	0.01
comasw8-33	5031	-	-	12:57:11.5	27:29:30.0	-	0.01
comasw8-55	5033	-	-	12:57:11.0	27:33:38.2	-	0.00
comasw8-45	5034	-	-	12:57:11.0	27:31:41.6	-	0.00
comasw3-45	5038	16	-	12:57:10.8	27:24:17.4	SA0	0.03
comasw25-20	5039	-	-	12:57:09.7	27:52:34.4	-	0.00
comasw18-63	5040	-	-	12:57:09.7	27:51:26.1	-	0.02
comasw14-44	5042	-	-	12:57:09.8	27:39:06.1	-	0.03
comasw3-70	5050	-	-	12:57:09.6	27:27:00.6	-	0.01
comasw3-86	5051	24	-	12:57:09.5	27:27:58.5	SB0	0.03
comasw3-14	5054	-	-	12:57:09.6	27:21:03.0	-	0.02
comasw18-44	5058	-	-	12:57:08.3	27:48:07.7	-	0.02
comasw25-26	5059	-	-	12:57:08.1	27:52:51.8	-	0.16
comasw18-40	5060	-	-	12:57:08.1	27:47:37.8	-	0.04
comasw27-19	5063	-	-	12:57:07.5	28:03:06.3	-	0.04

contiuned from previous page

Object	GMP	D80	Other	RA	DEC	Morphology	CStar
				(J2000)			
comasw3-72	5066	-	-	12:57:08.3	27:27:21.3	-	0.03
comasw18-62	5075	-	-	12:57:07.0	27:51:25.0	-	0.01
comasw3-12	5076	-	-	12:57:07.7	27:20:25.9	-	0.03
comasw18-54	5083	-	-	12:57:06.0	27:50:21.7	-	0.00
comasw14-24	5090	-	-	12:57:05.6	27:37:17.1	-	0.02
comasw3-25	5091	-	-	12:57:06.1	27:22:07.6	-	0.13
comasw14-59	5095	-	-	12:57:04.9	27:40:38.1	-	0.03
comasw18-27	5096	77	-	12:57:04.6	27:46:23.3	-	0.03
comasw25-30	5098	-	-	12:57:04.3	27:52:59.2	-	0.03
comasw14-78	5100	-	-	12:57:04.3	27:43:47.4	-	0.03
comasw8-43	5102	34	-	12:57:04.3	27:31:32.8	-	0.03
comasw3-6	5103	-	-	12:57:04.8	27:18:54.7	-	0.06
comasw18-35	5104	-	-	12:57:04.0	27:47:08.5	-	0.01
comasw18-33	5110	-	-	12:57:03.5	27:46:45.9	-	0.02
comasw3-81	5118	-	-	12:57:03.1	27:27:54.3	-	0.04
comasw18-53	5119	-	-	12:57:02.5	27:50:15.0	-	0.03
comasw14-49	5120	-	-	12:57:02.5	27:39:23.9	-	0.03
comasw3-49	5129	-	-	12:57:02.7	27:24:44.9	-	0.01
comasw3-8	5133	-	-	12:57:02.4	27:19:21.0	-	0.03
comasw3-29	5136	-	-	12:57:01.8	27:22:19.3	-	0.03
comasw27-37	5138	-	-	12:56:59.9	28:06:04.2	-	0.00
comasw25-28	5142	-	-	12:57:00.0	27:52:56.5	-	0.02
comasw13-48	5144	-	-	12:56:59.8	27:41:35.3	-	0.02
comasw13-39	5146	-	-	12:56:59.8	27:40:42.8	-	0.03
comasw3-71	5154	-	-	12:56:59.7	27:27:18.4	-	0.01
comasw3-10	5155	-	-	12:57:00.0	27:20:01.2	-	0.03
comasw25-78	5158	-	-	12:56:58.2	28:00:16.9	-	0.01
comasw13-32	5159	-	-	12:56:58.7	27:39:30.0	-	0.02
comasw18-70	5163	-	-	12:56:58.2	27:51:51.7	-	0.19
comasw3-52	5164	-	-	12:56:58.8	27:25:03.8	-	0.03
comasw25-77	5166	-	-	12:56:57.0	27:59:40.7	-	0.06
comasw27-49	5169	-	-	12:56:56.6	28:07:52.7	-	0.10
comasw8-54	5172	-	-	12:56:56.7	27:33:35.1	-	0.00
comasw3-93	5176	-	-	12:56:56.2	27:28:45.6	-	0.03
comasw3-79	5178	-	-	12:56:56.0	27:27:44.1	-	0.03
comasw13-38	5179	-	-	12:56:55.5	27:40:33.8	-	0.02
comasw3-44	5190	-	-	12:56:54.4	27:24:24.1	-	0.04
comasw25-49	5191	139	-	12:56:53.2	27:55:45.9	diE/SA0	0.12

contiuned from previous page

Object	GMP	D80	Other	RA	DEC	Morphology	CStar
				(J2000)			
comasw18-23	5200	-	-	12:56:52.9	27:46:17.0	-	0.03
comasw13-53	5202	-	-	12:56:52.5	27:42:15.3	-	0.03
comasw18-28	5204	-	-	12:56:51.9	27:46:30.7	-	0.02
comasw25-57	5207	-	-	12:56:51.1	27:57:42.9	-	0.03
comasw18-25	5211	-	-	12:56:51.1	27:46:22.9	-	0.00
comasw18-59	5212	-	-	12:56:50.9	27:51:11.4	-	0.03
comasw28-26	5214	-	-	12:56:50.3	28:03:03.0	-	0.02
comasw13-22	5217	-	-	12:56:50.8	27:37:39.8	-	0.03
comasw28-21	5218	-	-	12:56:49.9	28:02:39.6	-	0.04
comasw25-25	5219	-	-	12:56:50.1	27:52:55.4	-	0.01
comasw3-63	5221	-	-	12:56:50.7	27:26:11.0	-	0.01
comasw28-51	5232	-	-	12:56:47.9	28:05:57.9	-	0.00
comasw28-64	5239	-	-	12:56:47.0	28:08:21.5	-	0.07
comasw3-1	5244	-	-	12:56:48.5	27:18:19.6	-	0.01
comasw13-8	5245	-	-	12:56:47.7	27:34:52.3	-	0.01
comasw3-56	5250	-	-	12:56:47.9	27:25:15.3	-	0.03
comasw28-14	5251	-	-	12:56:46.2	28:01:05.0	-	0.01
comasw8-44	5253	-	-	12:56:46.8	27:31:47.1	-	0.02
comasw3-74	5255	-	-	12:56:47.1	27:27:26.0	-	0.01
comasw28-28	5256	185	-	12:56:45.9	28:03:05.3	SB0	0.03
comasw28-62	5258	-	-	12:56:45.6	28:07:52.9	-	0.03
comasw18-30	5260	-	-	12:56:45.6	27:46:39.9	-	0.01
comasw28-27	5261	-	-	12:56:44.9	28:02:48.9	-	0.03
comasw13-46	5262	-	-	12:56:45.3	27:41:30.2	-	0.05
comasw28-17	5272	163	NGC4828	12:56:43.0	28:01:13.4	unE	0.03
comasw3-4	5274	-	-	12:56:44.2	27:18:36.2	-	0.03
comasw3-89	5276	-	-	12:56:43.4	27:28:25.0	-	0.01
comasw3-20	5277	-	-	12:56:43.5	27:21:32.0	-	0.03
comasw8-47	5278	-	-	12:56:42.7	27:32:13.5	-	0.01
comasw8-49	5284	-	-	12:56:42.3	27:32:53.1	-	0.03
comasw3-69	5296	-	-	12:56:41.0	27:26:51.6	-	0.03
comasw28-43	5304	186	-	12:56:38.9	28:04:51.3	SAB0	0.03
comasw13-63	5307	-	-	12:56:39.1	27:44:04.9	-	0.02
comasw28-48	5308	-	-	12:56:38.5	28:06:21.6	-	0.03
comasw13-4	5320	-	-	12:56:38.5	27:34:15.1	-	0.03
comasw25-31	5329	-	-	12:56:37.0	27:53:05.1	-	0.02
comasw13-18	5333	-	-	12:56:37.3	27:36:59.7	-	0.04
comasw25-14	5334	-	-	12:56:36.8	27:51:51.0	-	0.11

contiuned from previous page

Object	GMP	D80	Other	RA (J2000)	DEC (J2000)	Morphology	CStar
comasw13-5	5344	-	-	12:56:36.3	27:34:39.5	-	0.03
comasw13-57	5345	-	-	12:56:36.0	27:43:07.1	-	0.03
comasw28-19	5353	-	-	12:56:34.3	28:02:18.1	-	0.02
comasw28-40	5354	-	-	12:56:34.2	28:04:52.1	-	0.02
comasw13-21	5357	-	-	12:56:34.9	27:37:38.3	-	0.00
comasw13-43	5362	60	-	12:56:34.2	27:41:13.9	-	0.03
comasw13-66	5370	-	-	12:56:33.0	27:44:33.8	-	0.11
comasw13-65	5370	-	-	12:56:33.2	27:44:30.1	-	0.13
comasw25-29	5373	-	-	12:56:32.4	27:53:02.8	-	0.06
comasw13-42	5375	-	-	12:56:32.7	27:41:14.9	-	0.01
comasw25-7	5381	-	-	12:56:31.9	27:51:16.8	-	0.01
comasw28-34	5400	-	-	12:56:29.4	28:04:06.4	-	0.02
comasw28-41	5407	-	-	12:56:28.6	28:04:56.3	-	0.03
comasw13-25	5410	-	-	12:56:28.7	27:38:17.6	-	0.02
comasw13-62	5411	-	-	12:56:28.5	27:44:00.1	-	0.02
comasw13-36	5427	-	-	12:56:27.0	27:40:31.5	-	0.01
comasw13-60	5434	-	-	12:56:26.3	27:43:37.5	-	0.03
comasw28-33	5436	-	-	12:56:25.7	28:04:01.8	-	0.01
comasw13-50	5438	-	-	12:56:25.9	27:41:55.4	-	0.04
comasw13-20	5452	-	-	12:56:24.7	27:37:19.1	-	0.02
comasw28-9	5470	-	-	12:56:22.2	28:00:18.3	-	0.02
comasw13-29	5480	-	-	12:56:21.7	27:38:44.7	-	0.03
comasw28-25	5486	-	-	12:56:20.6	28:03:02.4	-	0.03
comasw13-28	5492	-	-	12:56:20.4	27:38:46.4	-	0.02
comasw13-23	5520	-	-	12:56:17.4	27:38:18.2	-	0.03
comasw13-58	5522	-	-	12:56:16.5	27:43:43.4	-	0.01
comasw13-2	5523	-	-	12:56:16.9	27:34:17.1	-	0.17
comasw20-89	-	-	-	12:58:11.0	27:51:45.1	-	0.04
comasw16-74	-	-	-	12:59:00.2	27:44:04.7	-	0.01
comasw20-85	-	-	-	12:57:45.8	27:51:15.1	-	0.02
comasw16-79	-	-	-	12:59:03.3	27:43:25.2	-	0.03
coma15-91	-	-	-	13:00:01.1	28:01:20.8	-	0.12
comasw20-76	-	-	-	12:57:46.2	27:50:32.9	-	0.01
comasw20-70	-	-	-	12:58:00.0	27:49:50.6	-	0.01
comasw20-93	-	-	-	12:58:15.2	27:51:44.5	-	0.11
comasw28-5	-	-	-	12:56:28.9	27:59:40.4	-	0.04
comasw20-59	-	-	-	12:58:03.5	27:48:30.5	-	0.04
comasw20-52	-	-	-	12:57:41.4	27:48:07.9	-	0.02

contiuned from previous page

Object	GMP	D80	Other	RA (J2000)	DEC (J2000)	Morphology	CStar
comasw28-8	-	-	-	12:56:18.4	28:00:19.1	-	0.01
coma23-56	-	-	-	12:58:59.9	28:14:31.5	-	0.01
comane6-46	-	-	-	13:01:19.2	28:19:07.9	-	0.04
comasw17-6	-	-	-	12:59:28.8	27:34:55.3	-	0.01
comasw22-106	-	-	-	12:59:28.6	27:52:32.6	-	0.00
comane6-32	-	-	-	13:00:56.3	28:16:51.5	-	0.04
coma15-15	-	-	-	13:00:12.3	27:54:43.3	-	0.02
comane6-21	-	-	-	13:01:13.9	28:14:53.2	-	0.13
comasw3-75	-	-	-	12:57:21.6	27:27:27.4	-	0.02
comasw3-66	-	-	-	12:57:02.5	27:26:43.9	-	0.00
comasw17-91	-	-	-	12:59:41.9	27:44:12.3	-	0.02
comasw20-30	-	-	-	12:58:27.0	27:45:04.1	-	0.01
comasw3-32	-	-	-	12:57:24.0	27:22:38.9	-	0.04
comasw16-81	-	-	-	12:58:44.0	27:44:29.7	-	0.01
comasw3-22	-	-	-	12:57:02.3	27:21:46.6	-	0.01
comasw17-59	-	-	-	12:59:21.0	27:40:08.5	-	0.03
comasw25-67	-	-	-	12:57:10.4	27:58:40.6	-	0.03
comasw17-44	-	-	-	12:59:15.4	27:38:17.2	-	0.02
comasw17-37	-	-	-	12:59:16.9	27:37:49.9	-	0.01
comasw17-34	-	-	-	12:59:36.0	27:37:31.8	-	0.02
coma12-3	-	-	-	12:58:03.1	27:56:04.7	-	0.12
coma19-46	-	-	-	12:58:48.3	28:05:12.6	-	0.02
comasw16-70	-	-	-	12:58:47.7	27:43:24.6	-	0.02
comasw17-26	-	-	-	12:59:10.3	27:36:32.4	-	0.10
comasw16-20	-	-	-	12:58:53.0	27:37:02.8	-	0.01
comasw16-22	-	-	-	12:58:35.4	27:37:11.1	-	0.01
coma16-101	-	-	-	13:00:44.4	28:03:33.5	-	0.05
coma10-11	-	-	-	13:01:30.3	27:47:01.7	-	0.02
comasw13-64	-	-	-	12:56:36.4	27:44:27.5	-	0.11
coma10-14	-	-	-	13:01:19.0	27:47:34.9	-	0.04
comasw13-61	-	-	-	12:56:47.8	27:43:50.4	-	0.16
comasw16-37	-	-	-	12:59:02.6	27:39:32.5	-	0.03
comasw28-20	-	-	-	12:56:14.7	28:02:44.1	-	0.01
coma16-90	-	-	-	13:01:18.0	28:02:27.4	-	0.04
comasw16-42	-	-	-	12:58:40.5	27:40:50.3	-	0.01
coma9-51	-	-	-	13:01:06.6	27:51:40.7	-	0.20
coma12-1	-	-	-	12:58:02.4	27:56:01.3	-	0.02
comasw21-73	-	-	-	12:58:55.9	27:49:59.6	-	0.05

contiuned from previous page

Object	GMP	D80	Other	RA	DEC	Morphology	CStar
				(J2000)			
coma13-108	-	-	-	12:58:58.0	28:01:24.1	-	0.03
coma13-104	-	-	-	12:59:03.1	28:00:54.6	-	0.20
comasw14-50	-	-	-	12:57:22.6	27:39:32.9	-	0.02
comasw14-45	-	-	-	12:57:09.7	27:39:13.0	-	0.01
coma17-70	-	-	-	13:01:31.2	28:03:06.2	-	0.19
comasw9-39	-	-	-	12:57:33.2	27:29:41.2	-	0.03
comasw22-44	-	-	-	12:59:09.6	27:47:27.5	-	0.03
coma17-57	-	-	-	13:01:43.2	28:02:00.0	-	0.05
comasw14-11	-	-	-	12:57:18.4	27:36:03.1	-	0.01
coma25-60	-	-	-	13:00:21.1	28:18:23.1	-	0.13
comasw9-19	-	-	-	12:57:37.4	27:27:11.5	-	0.02
coma17-40	-	-	-	13:01:21.0	27:59:24.6	-	0.02
coma22-71	-	-	-	13:00:56.5	28:11:31.9	-	0.07
coma25-41	-	-	-	13:00:19.6	28:14:41.8	-	0.07
coma25-37	-	-	-	13:00:15.3	28:14:37.6	-	0.13
coma5-9	-	-	-	13:01:02.0	27:37:56.1	-	0.03
coma5-3	-	-	-	13:00:36.0	27:37:12.4	-	0.02
comasw10-90	-	-	-	12:58:12.2	27:34:46.2	-	0.03
comasw10-89	-	-	-	12:58:20.8	27:34:41.6	-	0.01
comasw10-88	-	-	-	12:57:55.7	27:34:38.6	-	0.01
comasw10-83	-	-	-	12:58:29.6	27:34:23.0	-	0.01
coma7-28	-	-	-	12:59:17.9	27:49:08.4	-	0.01
comasw10-60	-	-	-	12:58:26.5	27:31:49.9	-	0.01
comasw6-31	-	-	-	12:58:46.0	27:21:31.8	-	0.01
coma13-90	-	-	-	12:59:03.2	27:59:59.5	-	0.11
comasw21-116	-	-	-	12:58:25.6	27:53:50.0	-	0.10
comasw10-57	-	-	-	12:58:19.2	27:31:29.1	-	0.02
comasw10-56	-	-	-	12:58:19.4	27:31:26.4	-	0.01
coma13-87	-	-	-	12:58:50.1	27:59:41.1	-	0.01
coma13-84	-	-	-	12:59:14.6	27:59:29.9	-	0.14
comasw10-50	-	-	-	12:58:13.6	27:30:19.5	-	0.13
comasw5-57	-	-	-	12:58:11.9	27:25:42.7	-	0.02
comasw21-108	-	-	-	12:58:19.3	27:53:18.4	-	0.10
comasw10-40	-	-	-	12:58:23.5	27:29:10.6	-	0.01
coma14-66	-	-	-	12:59:45.0	27:55:46.1	-	0.15
comasw5-41	-	-	-	12:58:26.6	27:24:14.0	-	0.00
comasw10-37	-	-	-	12:57:52.8	27:29:12.4	-	0.02
coma13-68	-	-	-	12:59:26.7	27:58:41.2	-	0.00

contiuned from previous page

Object	GMP	D80	Other	RA	DEC	Morphology	CStar
				(J2000)			
comasw10-26	-	-	-	12:58:25.7	27:27:40.3	-	0.01
comasw10-22	-	-	-	12:57:45.0	27:27:36.8	-	0.06
comasw10-20	-	-	-	12:58:25.9	27:27:21.3	-	0.01
coma13-52	-	-	-	12:58:54.3	27:58:04.6	-	0.01
comasw5-17	-	-	-	12:58:16.0	27:21:18.0	-	0.02
comasw27-62	-	-	-	12:57:01.5	28:09:30.5	-	0.08
comasw27-55	-	-	-	12:57:27.3	28:08:42.3	-	0.11
comasw27-50	-	-	-	12:57:20.9	28:07:54.0	-	0.03
comasw27-48	-	-	-	12:56:58.6	28:07:34.0	-	0.02
comasw27-33	-	-	-	12:57:29.5	28:05:38.1	-	0.04
comasw11-7	-	-	-	12:58:30.7	27:27:06.2	-	0.03
comasw15-79	-	-	-	12:57:46.3	27:43:40.9	-	0.01
comasw15-78	-	-	-	12:58:03.1	27:43:34.1	-	0.01
comasw15-62	-	-	-	12:57:53.4	27:40:36.8	-	0.18
comasw23-81	-	-	-	12:57:38.5	27:59:23.3	-	0.03
comasw23-79	-	-	-	12:57:17.7	27:59:27.4	-	0.05
comasw15-52	-	-	-	12:57:39.0	27:39:12.5	-	0.06
coma10-2	-	-	-	13:01:24.9	27:46:08.0	-	0.04
comasw15-48	-	-	-	12:57:47.9	27:39:04.8	-	0.09
comasw15-46	-	-	-	12:58:02.7	27:38:45.1	-	0.01
coma14-84	-	-	-	12:59:32.2	28:00:07.7	-	0.16
coma14-85	-	-	-	12:59:56.3	27:56:47.7	-	0.04
comasw23-65	-	-	-	12:57:30.6	27:57:42.7	-	0.02
comasw23-64	-	-	-	12:57:25.4	27:57:23.0	-	0.20
coma18-76	-	-	-	12:58:09.2	28:09:21.1	-	0.01
comasw23-61	-	-	-	12:57:36.1	27:56:51.3	-	0.12
comasw15-30	-	-	-	12:58:08.5	27:37:32.9	-	0.02
coma18-57	-	-	-	12:58:13.6	28:07:42.6	-	0.02
comasw15-23	-	-	-	12:57:55.8	27:37:01.2	-	0.03
comasw6-66	-	-	-	12:59:02.2	27:26:09.4	-	0.01
coma18-52	-	-	-	12:58:03.8	28:07:06.7	-	0.01
coma18-49	-	-	-	12:58:01.5	28:06:45.1	-	0.02
comasw23-32	-	-	-	12:57:59.4	27:53:18.0	-	0.13
comasw23-23	-	-	-	12:57:31.9	27:51:51.0	-	0.02
comasw6-72	-	-	-	12:59:01.4	27:27:02.0	-	0.01
coma18-22	-	-	-	12:58:02.0	28:03:10.9	-	0.01
comasw6-76	-	-	-	12:58:36.1	27:27:38.8	-	0.01
coma18-20	-	-	-	12:58:35.1	28:03:05.3	-	0.01

contiuned from previous page

Object	GMP	D80	Other	RA	DEC	Morphology	CStar
				(J2000)			
coma18-10	-	-	-	12:58:00.0	28:02:38.5	-	0.03

Raw U-band aperture magnitudes.

Object	GMP	Aperture Dia. (″)				
		8.8	13	16	20.2	26
coma10-4	1714	20.273 ± 0.056	20.297 ± 0.076	19.412 ± 0.051		
coma10-50	1724	21.120 ± 0.122	21.097 ± 0.174	20.983 ± 0.213	21.139 ± 0.332	
comane7-26	1730	18.740 ± 0.016	18.601 ± 0.017	18.409 ± 0.019	18.452 ± 0.023	
coma10-29	1745	20.707 ± 0.077	20.541 ± 0.086	20.358 ± 0.101	20.527 ± 0.141	20.582 ± 0.156
comane3-69	1751	18.122 ± 0.010	17.918 ± 0.010	17.716 ± 0.010	17.726 ± 0.012	
comane3-50	1757	19.998 ± 0.044	19.746 ± 0.043	19.505 ± 0.046	19.375 ± 0.049	
comane7-37	1758	20.595 ± 0.073	20.643 ± 0.103	20.691 ± 0.138	21.097 ± 0.258	
coma10-1	1764	19.652 ± 0.029	19.612 ± 0.036	19.511 ± 0.044	19.611 ± 0.058	19.834 ± 0.082
comane3-51	1765	19.508 ± 0.028	19.442 ± 0.032	19.308 ± 0.037	19.428 ± 0.049	
coma10-43	1767	20.109 ± 0.043	20.082 ± 0.055	19.792 ± 0.057	19.578 ± 0.057	19.581 ± 0.061
coma10-36	1772	21.145 ± 0.114	21.145 ± 0.159	21.131 ± 0.202	21.240 ± 0.290	20.935 ± 0.203
comane3-80	1777	19.299 ± 0.024	19.385 ± 0.030	19.249 ± 0.037	19.410 ± 0.048	
coma10-61	1780	19.968 ± 0.047	20.014 ± 0.065	19.972 ± 0.091	20.134 ± 0.134	20.589 ± 0.325
comane3-36	1781	18.467 ± 0.013	18.247 ± 0.012	18.042 ± 0.013	18.070 ± 0.015	
comane7-34	1800	20.495 ± 0.065	20.429 ± 0.082	20.301 ± 0.096	20.278 ± 0.118	
comane7-15	1805	19.381 ± 0.026	19.386 ± 0.033	19.274 ± 0.040	19.304 ± 0.049	
comane7-23	1806	19.977 ± 0.041	20.001 ± 0.055	19.933 ± 0.068	19.981 ± 0.089	
coma10-45	1807	16.851 ± 0.004	16.727 ± 0.004	16.570 ± 0.004	16.540 ± 0.004	16.414 ± 0.004
coma17-30	1819	20.488 ± 0.058	20.479 ± 0.078	20.352 ± 0.094	20.444 ± 0.126	20.648 ± 0.171
coma10-17	1828	19.998 ± 0.039	20.005 ± 0.050	19.872 ± 0.061	19.983 ± 0.080	20.072 ± 0.092
comane3-47	1841	20.997 ± 0.117	21.112 ± 0.163	21.542 ± 0.309	22.476 ± 0.910	
coma10-6	1844	20.481 ± 0.061	20.480 ± 0.078	20.396 ± 0.099	20.402 ± 0.120	20.657 ± 0.169
comane3-17	1853	16.466 ± 0.003	16.317 ± 0.003	16.167 ± 0.003	16.150 ± 0.003	
coma10-34	1856	21.475 ± 0.144	21.497 ± 0.204	21.544 ± 0.276	21.588 ± 0.371	21.061 ± 0.226
coma10-23	1876	19.808 ± 0.034	19.796 ± 0.042	19.669 ± 0.051	19.794 ± 0.069	19.690 ± 0.066
comane3-43	1882	20.373 ± 0.057	20.294 ± 0.067	20.180 ± 0.079	20.061 ± 0.086	
comane3-76	1885	18.024 ± 0.009	17.957 ± 0.010	17.845 ± 0.011	17.892 ± 0.014	
comane3-41	1887	20.039 ± 0.044	19.794 ± 0.043	19.529 ± 0.045	19.427 ± 0.049	
comane3-72	1888	20.742 ± 0.087	21.024 ± 0.143	21.114 ± 0.200	21.160 ± 0.261	
comane7-21	1889	19.327 ± 0.025	19.423 ± 0.033	19.362 ± 0.042	19.531 ± 0.059	
comane7-27	1897	20.127 ± 0.049	20.089 ± 0.062	19.969 ± 0.074	20.046 ± 0.098	
comane7-29	1898	18.931 ± 0.019	18.874 ± 0.022	18.762 ± 0.027	18.834 ± 0.034	
comane3-61	1907	20.269 ± 0.058	20.427 ± 0.081	20.314 ± 0.099	20.511 ± 0.139	
comane3-75	1918	19.815 ± 0.036	19.580 ± 0.037	19.397 ± 0.040	19.348 ± 0.048	
comane3-10	1921	20.340 ± 0.056	20.317 ± 0.069	20.193 ± 0.081	20.166 ± 0.095	
comane3-77	1926	20.906 ± 0.100	21.187 ± 0.147	21.520 ± 0.230	22.854 ± 0.428	
comane7-18	1931	18.585 ± 0.015	18.470 ± 0.016	18.287 ± 0.018	18.307 ± 0.022	
coma17-39	1941	20.120 ± 0.043	20.185 ± 0.058	20.086 ± 0.075	20.211 ± 0.099	20.721 ± 0.172
coma17-50	1953	19.028 ± 0.018	18.928 ± 0.020	18.802 ± 0.024	18.905 ± 0.032	18.831 ± 0.031
coma10-60	1958	20.009 ± 0.041	20.041 ± 0.058	19.883 ± 0.072	19.913 ± 0.094	19.981 ± 0.114
coma17-72	1960	19.261 ± 0.020	19.252 ± 0.026	19.218 ± 0.032	19.286 ± 0.043	19.203 ± 0.045
comane3-40	1966	19.567 ± 0.030	19.533 ± 0.035	19.391 ± 0.041	19.368 ± 0.047	
comane3-38	1975	18.507 ± 0.013	18.394 ± 0.014	18.233 ± 0.015	18.262 ± 0.018	
comane3-46	1977	19.665 ± 0.034	19.794 ± 0.045	19.693 ± 0.056	19.937 ± 0.081	
coma10-53	1986	18.857 ± 0.017	18.576 ± 0.017	18.340 ± 0.018	18.306 ± 0.021	18.169 ± 0.019
coma10-38	1993	20.747 ± 0.075	20.313 ± 0.067	19.810 ± 0.059	19.726 ± 0.065	22.847 ± 1.606
coma17-41	1995	20.748 ± 0.075	20.767 ± 0.102	20.545 ± 0.114	20.465 ± 0.131	20.613 ± 0.157
coma17-55	1996	19.120 ± 0.019	19.056 ± 0.023	18.887 ± 0.027	18.968 ± 0.034	19.062 ± 0.039
coma17-31	1998	20.799 ± 0.075	20.751 ± 0.096	20.736 ± 0.129	20.825 ± 0.173	21.184 ± 0.265
coma10-33	2000	16.289 ± 0.003	16.105 ± 0.003	15.924 ± 0.003	15.861 ± 0.003	15.681 ± 0.002
comane7-38	2002	20.212 ± 0.053	20.025 ± 0.060	19.899 ± 0.070	19.850 ± 0.084	
comane3-63	2016	20.226 ± 0.052	20.295 ± 0.067	20.250 ± 0.086	20.355 ± 0.112	
comane7-22	2019	20.331 ± 0.055	20.241 ± 0.067	20.113 ± 0.079	19.919 ± 0.083	

Raw U-band aperture magnitudes. *contiuned from previous page*

Object	GMP	Aperture Dia. (″) 8.8	13	16	20.2	26
coma17-71	2020	20.517 ± 0.060	20.408 ± 0.070	20.239 ± 0.085	20.408 ± 0.119	20.339 ± 0.124
comane3-78	2027	20.385 ± 0.058	20.297 ± 0.067	20.170 ± 0.079	20.148 ± 0.093	
coma10-56	2033	18.552 ± 0.012	18.491 ± 0.014	18.363 ± 0.016	18.425 ± 0.020	18.434 ± 0.023
coma10-32	2035	17.246 ± 0.006	17.435 ± 0.007	17.288 ± 0.008	17.480 ± 0.010	17.477 ± 0.011
comane3-57	2036	19.911 ± 0.042	19.952 ± 0.051	19.725 ± 0.058	19.785 ± 0.070	
coma17-74	2040	20.497 ± 0.062	20.361 ± 0.071	20.148 ± 0.078	20.192 ± 0.092	20.306 ± 0.122
comane7-17	2044	20.074 ± 0.044	20.146 ± 0.061	20.040 ± 0.073	20.062 ± 0.092	
comane3-59	2047	19.122 ± 0.020	19.078 ± 0.023	18.982 ± 0.027	18.997 ± 0.033	
coma17-45	2048	17.456 ± 0.006	17.435 ± 0.006	17.338 ± 0.007	17.362 ± 0.008	17.360 ± 0.009
comane3-67	2052	20.809 ± 0.083	20.762 ± 0.103	20.747 ± 0.129	20.747 ± 0.162	
comane7-20	2053	19.855 ± 0.037	19.730 ± 0.043	19.590 ± 0.050	19.548 ± 0.060	
coma10-49	2059	16.525 ± 0.004	16.288 ± 0.004	16.099 ± 0.004	16.038 ± 0.004	15.702 ± 0.003
comane3-81	2060	19.545 ± 0.028	19.371 ± 0.031	19.204 ± 0.035	19.177 ± 0.041	
comane3-29	2063	20.736 ± 0.083	20.842 ± 0.119	20.838 ± 0.151	20.970 ± 0.215	
comane3-48	2064	20.858 ± 0.088	20.991 ± 0.130	20.968 ± 0.161	20.998 ± 0.209	
coma17-66	2068	19.968 ± 0.040	20.039 ± 0.054	19.883 ± 0.066	19.926 ± 0.082	19.600 ± 0.063
comane3-70	2091	17.100 ± 0.005	16.952 ± 0.005	16.780 ± 0.005	16.747 ± 0.005	
coma17-67	2103	20.560 ± 0.063	20.596 ± 0.085	20.543 ± 0.111	20.584 ± 0.141	20.625 ± 0.157
coma17-54	2109	20.050 ± 0.040	20.104 ± 0.054	19.964 ± 0.065	19.884 ± 0.073	19.714 ± 0.069
coma17-59	2110	21.364 ± 0.121	21.132 ± 0.137	20.901 ± 0.148	20.662 ± 0.151	20.021 ± 0.090
coma17-76	2113	20.694 ± 0.078	20.664 ± 0.109	20.566 ± 0.134		
coma17-27	2129	19.118 ± 0.019	18.979 ± 0.021	18.826 ± 0.024	18.848 ± 0.030	18.759 ± 0.029
coma22-63	2135	20.693 ± 0.077	20.956 ± 0.127	21.031 ± 0.189	21.471 ± 0.345	20.610 ± 0.157
coma10-35	2141	18.074 ± 0.009	18.004 ± 0.010	17.828 ± 0.011	17.875 ± 0.013	17.821 ± 0.013
coma22-45	2145	18.355 ± 0.010	18.269 ± 0.012	18.128 ± 0.013	18.168 ± 0.016	18.107 ± 0.016
coma5-8	2148	20.040 ± 0.049	20.108 ± 0.071	19.988 ± 0.089	20.020 ± 0.114	
coma22-64	2151	19.047 ± 0.018	18.976 ± 0.021	18.835 ± 0.025	18.865 ± 0.031	18.952 ± 0.035
comane6-47	2155	20.924 ± 0.127	20.785 ± 0.154	20.649 ± 0.178	20.449 ± 0.190	
coma10-22	2157	16.285 ± 0.003	16.099 ± 0.003	15.919 ± 0.003	15.872 ± 0.003	15.755 ± 0.003
coma22-32	2158	19.085 ± 0.018	18.939 ± 0.020	18.755 ± 0.022	18.737 ± 0.025	18.628 ± 0.025
coma5-52	2166	19.685 ± 0.034	19.639 ± 0.041	19.333 ± 0.044	19.338 ± 0.052	19.166 ± 0.049
coma5-53	2170	20.053 ± 0.047	19.894 ± 0.053	19.526 ± 0.053	19.418 ± 0.057	19.237 ± 0.052
coma16-53	2178	20.132 ± 0.048	20.302 ± 0.070	20.276 ± 0.090	20.510 ± 0.129	20.359 ± 0.126
coma10-57	2183	20.330 ± 0.054	20.279 ± 0.067	20.113 ± 0.080	20.050 ± 0.092	20.176 ± 0.116
coma5-25	2185	18.236 ± 0.010	18.097 ± 0.011	17.934 ± 0.013	17.928 ± 0.015	17.845 ± 0.015
coma16-88	2190	20.645 ± 0.076	20.434 ± 0.079	20.236 ± 0.092	20.211 ± 0.109	20.212 ± 0.137
coma16-72	2192	20.226 ± 0.053	20.384 ± 0.075	20.256 ± 0.094	20.336 ± 0.118	20.397 ± 0.166
comane6-17	2193	20.219 ± 0.067	20.308 ± 0.092	20.210 ± 0.113	20.155 ± 0.130	
coma16-40	2197	20.091 ± 0.043	20.229 ± 0.061	20.101 ± 0.076	20.144 ± 0.093	20.081 ± 0.101
coma10-54	2201	17.632 ± 0.006	17.496 ± 0.007	17.313 ± 0.007	17.288 ± 0.008	17.178 ± 0.008
coma22-27	2205	18.726 ± 0.013	18.620 ± 0.015	18.466 ± 0.017	18.510 ± 0.021	18.499 ± 0.022
comane3-82	2212	19.421 ± 0.027	19.229 ± 0.030	19.021 ± 0.035	19.041 ± 0.043	
comane6-51	2213	21.494 ± 0.199	20.889 ± 0.160	20.462 ± 0.139	20.219 ± 0.143	
comane6-52	2214	20.435 ± 0.092	20.343 ± 0.123	20.261 ± 0.148	20.267 ± 0.183	
coma22-65	2215	19.843 ± 0.033	19.763 ± 0.039	19.620 ± 0.046	19.716 ± 0.060	19.710 ± 0.064
comane3-83	2222	20.275 ± 0.057	20.214 ± 0.067	19.991 ± 0.074	19.738 ± 0.072	
coma16-32	2226	20.103 ± 0.049	19.849 ± 0.050	19.575 ± 0.053	19.494 ± 0.059	19.464 ± 0.061
coma5-56	2232	19.468 ± 0.027	19.305 ± 0.031	19.102 ± 0.035	19.065 ± 0.041	19.005 ± 0.040
comane6-53	2233	19.696 ± 0.042	19.491 ± 0.044	19.381 ± 0.052	19.430 ± 0.064	
coma10-19	2237	17.285 ± 0.005	17.115 ± 0.005	16.926 ± 0.005	16.864 ± 0.006	16.739 ± 0.006
coma16-71	2239	20.583 ± 0.070	20.522 ± 0.085	20.418 ± 0.110	20.502 ± 0.151	20.748 ± 0.185
coma5-30	2248	20.271 ± 0.053	20.107 ± 0.061	19.921 ± 0.071	19.974 ± 0.090	20.027 ± 0.103
coma16-86	2251	17.876 ± 0.008	17.778 ± 0.009	17.629 ± 0.010	17.642 ± 0.012	17.564 ± 0.011

Raw U-band aperture magnitudes. *contiuned from previous page*

Object	GMP	Aperture Dia. (″) 8.8	13	16	20.2	26
coma9-30	2252	17.209 ± 0.005	17.046 ± 0.005	16.859 ± 0.005	16.822 ± 0.006	16.668 ± 0.005
coma9-58	2253	20.003 ± 0.039	19.849 ± 0.044	19.476 ± 0.043	19.443 ± 0.050	19.569 ± 0.063
comane6-18	2257	20.046 ± 0.060	20.023 ± 0.075	19.932 ± 0.093	20.061 ± 0.127	
comane6-65	2259	17.262 ± 0.006	17.094 ± 0.006	16.900 ± 0.006	16.854 ± 0.007	
coma9-57	2262	20.428 ± 0.059	20.239 ± 0.064	19.849 ± 0.062	19.699 ± 0.065	19.545 ± 0.062
coma9-46	2263	19.845 ± 0.033	19.657 ± 0.035	19.466 ± 0.040	19.471 ± 0.049	19.482 ± 0.055
coma5-67	2265	20.155 ± 0.049	20.147 ± 0.065	20.045 ± 0.081	20.128 ± 0.112	20.318 ± 0.116
coma16-63	2267	19.918 ± 0.037	19.819 ± 0.045	19.597 ± 0.050	19.549 ± 0.058	19.814 ± 0.081
coma16-24	2268	19.880 ± 0.036	19.727 ± 0.041	19.549 ± 0.048	19.581 ± 0.060	19.616 ± 0.067
coma22-23	2269	20.473 ± 0.058	20.452 ± 0.074	20.295 ± 0.087	20.284 ± 0.104	20.290 ± 0.114
coma22-42	2270	18.517 ± 0.012	18.495 ± 0.014	18.376 ± 0.016	18.489 ± 0.021	18.534 ± 0.023
coma16-55	2273	20.197 ± 0.049	20.172 ± 0.063	20.058 ± 0.078	20.066 ± 0.097	20.073 ± 0.103
coma9-20	2276	20.561 ± 0.065	20.508 ± 0.083	20.582 ± 0.117	20.853 ± 0.189	23.508 ± 2.496
comane6-37	2281	21.993 ± 0.309	21.774 ± 0.355	21.549 ± 0.371	21.459 ± 0.441	
coma5-43	2285	19.565 ± 0.029	19.343 ± 0.031	19.120 ± 0.035	19.110 ± 0.042	19.096 ± 0.044
coma16-54	2287	20.161 ± 0.047	20.047 ± 0.056	19.912 ± 0.067	19.984 ± 0.088	20.119 ± 0.107
coma16-45	2288	19.865 ± 0.038	19.971 ± 0.053	19.781 ± 0.063	19.937 ± 0.087	19.953 ± 0.092
coma16-104	2289	18.703 ± 0.015	18.625 ± 0.017	18.434 ± 0.020	18.433 ± 0.024	18.387 ± 0.023
coma22-74	2293	19.493 ± 0.026	19.433 ± 0.031	19.268 ± 0.036	19.301 ± 0.045	19.419 ± 0.055
coma16-2	2295	18.852 ± 0.017	18.673 ± 0.019	18.477 ± 0.021		
coma16-89	2297	20.627 ± 0.067	20.644 ± 0.091	20.538 ± 0.120	20.626 ± 0.167	21.331 ± 0.290
coma16-82	2311	20.222 ± 0.055	20.184 ± 0.074	19.918 ± 0.093	20.277 ± 0.118	20.445 ± 0.147
coma5-68	2316	19.273 ± 0.024	19.240 ± 0.029	19.068 ± 0.035	19.185 ± 0.046	19.575 ± 0.067
comane6-33	2321	19.894 ± 0.051	19.988 ± 0.070	19.813 ± 0.082	19.952 ± 0.110	
coma22-59	2322	19.347 ± 0.023	19.360 ± 0.029	19.269 ± 0.036	19.399 ± 0.048	19.380 ± 0.048
coma16-64	2323	19.967 ± 0.042	20.014 ± 0.056	19.837 ± 0.065	19.811 ± 0.077	19.783 ± 0.079
coma16-13	2333	19.659 ± 0.033	19.599 ± 0.041	19.442 ± 0.049	19.503 ± 0.064	19.354 ± 0.061
coma9-24	2335	19.834 ± 0.033	19.505 ± 0.032	19.256 ± 0.034	19.166 ± 0.038	19.198 ± 0.050
coma5-45	2342	20.070 ± 0.046	20.148 ± 0.064	20.074 ± 0.083	20.239 ± 0.117	20.677 ± 0.185
coma22-48	2343	19.937 ± 0.037	19.979 ± 0.048	19.890 ± 0.060	19.971 ± 0.077	19.716 ± 0.064
coma16-12	2347	16.878 ± 0.004	16.701 ± 0.004	16.525 ± 0.004	16.480 ± 0.005	16.356 ± 0.004
coma22-44	2349	20.004 ± 0.042	20.119 ± 0.058	20.083 ± 0.077	20.172 ± 0.099	19.896 ± 0.077
coma5-49	2352	19.624 ± 0.032	19.768 ± 0.047	19.695 ± 0.061	19.810 ± 0.081	19.609 ± 0.070
coma16-83	2353	19.610 ± 0.032	19.443 ± 0.039	19.197 ± 0.044	19.139 ± 0.056	19.607 ± 0.068
coma5-18	2355	18.135 ± 0.010	17.815 ± 0.009	17.510 ± 0.009	17.342 ± 0.009	17.089 ± 0.008
coma22-49	2359	21.006 ± 0.083	20.488 ± 0.071	20.187 ± 0.072	20.110 ± 0.083	19.869 ± 0.075
comane6-62	2361	18.986 ± 0.023	18.884 ± 0.026	18.759 ± 0.031	18.816 ± 0.039	
coma5-61	2364	18.992 ± 0.019	19.074 ± 0.026	18.962 ± 0.033	19.025 ± 0.042	19.032 ± 0.051
coma22-38	2366	20.612 ± 0.061	20.655 ± 0.083	20.588 ± 0.105	20.721 ± 0.145	20.888 ± 0.187
coma9-9	2374	16.581 ± 0.004	16.196 ± 0.003	15.819 ± 0.003	15.520 ± 0.003	14.990 ± 0.002
coma16-9	2376	19.092 ± 0.019	18.838 ± 0.020	18.612 ± 0.022	18.571 ± 0.025	18.458 ± 0.027
coma16-58	2382	22.156 ± 0.277	22.707 ± 0.671	25.258 ± 7.474		
comane6-28	2383	20.793 ± 0.108	20.816 ± 0.148	20.842 ± 0.196	21.628 ± 0.509	
coma9-42	2385	17.953 ± 0.008	17.911 ± 0.009	17.792 ± 0.010	17.834 ± 0.012	17.833 ± 0.013
coma16-74	2390	16.618 ± 0.004	16.294 ± 0.003	16.050 ± 0.003	15.916 ± 0.003	15.644 ± 0.002
coma5-72	2393	17.262 ± 0.006	17.094 ± 0.007	16.888 ± 0.007	16.828 ± 0.008	16.645 ± 0.007
coma16-43	2399	19.243 ± 0.022	19.111 ± 0.025	18.961 ± 0.029	18.982 ± 0.036	18.815 ± 0.032
coma5-12	2407	21.408 ± 0.139	21.320 ± 0.185	21.016 ± 0.184	20.637 ± 0.169	20.624 ± 0.175
coma9-34	2408	19.458 ± 0.024	19.218 ± 0.024	18.925 ± 0.025	18.835 ± 0.028	18.732 ± 0.028
coma9-21	2411	19.275 ± 0.023	19.144 ± 0.026	18.997 ± 0.030	19.029 ± 0.038	19.011 ± 0.043
coma5-11	2412	20.561 ± 0.071	20.465 ± 0.086	20.298 ± 0.102	20.368 ± 0.133	20.267 ± 0.130
comane6-67	2413	16.240 ± 0.003	16.052 ± 0.003	15.866 ± 0.003	15.799 ± 0.003	
coma22-37	2415	20.297 ± 0.047	20.287 ± 0.063	20.239 ± 0.078	20.382 ± 0.112	20.352 ± 0.115

Raw U-band aperture magnitudes. *continued from previous page*

Object	GMP	Aperture Dia. ('') 8.8	13	16	20.2	26
coma16-94	2417	16.281 ± 0.003	16.088 ± 0.003	15.906 ± 0.003	15.847 ± 0.003	15.686 ± 0.003
coma5-35	2420	19.425 ± 0.025	19.328 ± 0.030	19.169 ± 0.035	19.179 ± 0.042	19.265 ± 0.050
coma5-57	2421	18.592 ± 0.014	18.357 ± 0.014	18.134 ± 0.015	18.117 ± 0.017	18.042 ± 0.017
coma9-26	2427	20.207 ± 0.049	20.427 ± 0.075	20.246 ± 0.091	20.427 ± 0.125	
comane6-27	2428	20.250 ± 0.070	20.376 ± 0.098	20.305 ± 0.126	20.373 ± 0.161	
coma16-3	2430	19.920 ± 0.041	19.983 ± 0.057	19.816 ± 0.065	19.287 ± 0.045	18.580 ± 0.026
coma22-54	2432	20.214 ± 0.075	20.227 ± 0.101	20.218 ± 0.136	20.354 ± 0.192	19.614 ± 0.073
coma5-32	2438	20.100 ± 0.047	20.162 ± 0.062	19.945 ± 0.073	19.919 ± 0.084	20.209 ± 0.120
coma22-31	2440	16.338 ± 0.003	16.151 ± 0.003	15.989 ± 0.003	15.960 ± 0.003	15.852 ± 0.003
coma22-61	2441	16.878 ± 0.004	16.556 ± 0.003	16.282 ± 0.003	16.068 ± 0.003	15.628 ± 0.002
coma16-84	2442	19.602 ± 0.031	19.704 ± 0.042	19.521 ± 0.051	19.579 ± 0.063	18.890 ± 0.044
comane6-23	2443	20.311 ± 0.073	20.013 ± 0.073	19.852 ± 0.085	19.810 ± 0.099	
coma9-38	2445	20.341 ± 0.055	20.141 ± 0.060	19.969 ± 0.070	20.027 ± 0.089	20.046 ± 0.093
coma16-62	2448	21.321 ± 0.123	21.469 ± 0.199	21.507 ± 0.266	21.126 ± 0.247	22.305 ± 0.849
coma22-33	2449	20.175 ± 0.051	20.047 ± 0.059	19.890 ± 0.069	19.875 ± 0.084	19.653 ± 0.064
coma22-26	2452	19.494 ± 0.031	19.542 ± 0.040	19.381 ± 0.048	19.455 ± 0.061	19.041 ± 0.036
coma16-60	2454	20.914 ± 0.094	21.126 ± 0.154	21.040 ± 0.196	21.395 ± 0.333	21.257 ± 0.303
coma16-70	2455	22.153 ± 0.259	24.235 ± 2.477			
coma16-17	2457	17.442 ± 0.006	17.262 ± 0.006	17.081 ± 0.006	17.062 ± 0.007	16.976 ± 0.007
coma22-67	2464	20.468 ± 0.056	20.491 ± 0.076	20.521 ± 0.102	20.663 ± 0.147	21.151 ± 0.265
coma5-26	2466	20.970 ± 0.094	20.993 ± 0.134	20.916 ± 0.164	20.925 ± 0.214	21.418 ± 0.359
coma5-22	2469	20.564 ± 0.069	20.322 ± 0.073	20.053 ± 0.079	20.052 ± 0.096	19.914 ± 0.092
coma16-61	2470	19.959 ± 0.039	19.901 ± 0.049	19.702 ± 0.057	19.727 ± 0.069	20.147 ± 0.111
comane6-41	2475	21.140 ± 0.147	21.281 ± 0.222	21.124 ± 0.254	21.390 ± 0.406	
coma5-55	2477	20.720 ± 0.082	20.462 ± 0.087	20.163 ± 0.092	20.180 ± 0.113	19.974 ± 0.095
coma9-39	2478	18.506 ± 0.012	18.373 ± 0.013	18.217 ± 0.014	18.248 ± 0.018	18.222 ± 0.020
coma5-58	2480	19.211 ± 0.022	19.027 ± 0.024	18.773 ± 0.026	18.724 ± 0.029	18.702 ± 0.031
coma5-33	2485	20.415 ± 0.061	20.390 ± 0.079	20.225 ± 0.095	20.279 ± 0.120	20.494 ± 0.157
coma22-69	2487	20.534 ± 0.057	20.499 ± 0.075	20.335 ± 0.085	20.288 ± 0.102	20.236 ± 0.106
coma16-6	2488	20.518 ± 0.069	20.308 ± 0.080	20.157 ± 0.100	20.178 ± 0.131	20.047 ± 0.116
coma22-34	2489	17.382 ± 0.005	17.262 ± 0.005	17.112 ± 0.006	17.124 ± 0.007	17.108 ± 0.007
coma16-30	2490	20.210 ± 0.048	20.177 ± 0.063	20.029 ± 0.073	20.036 ± 0.092	20.541 ± 0.156
coma5-71	2491	19.685 ± 0.035	19.642 ± 0.043	19.505 ± 0.052	19.583 ± 0.067	19.747 ± 0.071
coma22-22	2492	21.462 ± 0.132	21.641 ± 0.213	21.483 ± 0.238	21.700 ± 0.374	
coma5-65	2493	20.596 ± 0.070	20.567 ± 0.082	20.461 ± 0.098	20.663 ± 0.146	20.992 ± 0.171
coma9-50	2494	20.474 ± 0.059	20.489 ± 0.078	20.375 ± 0.096	20.558 ± 0.137	21.145 ± 0.277
comane6-54	2495	16.615 ± 0.004	16.479 ± 0.004	16.324 ± 0.004	16.323 ± 0.005	
coma22-72	2501	20.012 ± 0.036	19.850 ± 0.041	19.782 ± 0.050	19.831 ± 0.066	19.766 ± 0.070
coma16-51	2504	20.596 ± 0.083	20.469 ± 0.105	20.225 ± 0.111	19.981 ± 0.115	18.875 ± 0.036
comane6-3	2505	20.012 ± 0.058	20.037 ± 0.078	19.914 ± 0.095	19.953 ± 0.123	
coma15-63	2507	20.019 ± 0.043	20.175 ± 0.067	20.043 ± 0.086		
coma15-101	2508	20.878 ± 0.106	21.028 ± 0.201	21.093 ± 0.313	20.044 ± 0.028	
coma15-55	2510	17.210 ± 0.005	17.022 ± 0.005	16.828 ± 0.006	16.767 ± 0.006	16.525 ± 0.004
coma15-114	2511	20.105 ± 0.043	19.982 ± 0.052	19.793 ± 0.060	19.716 ± 0.071	19.222 ± 0.021
comane6-36	2513	17.876 ± 0.010	17.841 ± 0.011	17.713 ± 0.013	17.807 ± 0.016	
coma15-53	2516	16.513 ± 0.003	16.357 ± 0.003	16.191 ± 0.004	16.145 ± 0.004	15.981 ± 0.003
coma15-116	2518	20.441 ± 0.062	20.291 ± 0.075	20.035 ± 0.080	19.949 ± 0.094	20.022 ± 0.158
coma22-40	2519	19.509 ± 0.026	19.242 ± 0.026	18.970 ± 0.027	18.858 ± 0.029	18.744 ± 0.028
coma15-109	2529	18.797 ± 0.014	18.748 ± 0.017	18.624 ± 0.020	18.670 ± 0.026	18.673 ± 0.030
coma15-3	2531	18.089 ± 0.009	17.810 ± 0.008	17.611 ± 0.009	17.660 ± 0.011	17.083 ± 0.011
coma15-75	2535	17.137 ± 0.004	16.934 ± 0.004	16.742 ± 0.004	16.675 ± 0.005	16.552 ± 0.005
coma4-55	2537	19.773 ± 0.056	19.763 ± 0.066	19.622 ± 0.078	19.765 ± 0.100	
coma15-27	2541	16.646 ± 0.003	16.419 ± 0.003	16.216 ± 0.003	16.148 ± 0.003	16.005 ± 0.003

Raw U-band aperture magnitudes. *continued from previous page*

Object	GMP	Aperture Dia. ('') 8.8	13	16	20.2	26
coma16-78	2550	19.440 ± 0.030	19.316 ± 0.036	19.081 ± 0.040	18.994 ± 0.045	18.294 ± 0.021
coma15-89	2551	17.165 ± 0.005	16.839 ± 0.004	16.456 ± 0.004		
coma5-34	2553	20.333 ± 0.055	20.152 ± 0.061	19.884 ± 0.067	19.974 ± 0.087	20.256 ± 0.123
coma15-62	2555	19.366 ± 0.023	19.437 ± 0.031	19.370 ± 0.040	19.514 ± 0.054	19.685 ± 0.073
coma15-121	2559	16.278 ± 0.003	16.021 ± 0.003	15.714 ± 0.002	15.677 ± 0.003	15.532 ± 0.002
coma25-53	2566	19.789 ± 0.034	19.686 ± 0.038	19.549 ± 0.044	19.577 ± 0.055	19.706 ± 0.064
coma15-11	2570	20.021 ± 0.042	19.891 ± 0.050	19.739 ± 0.062	19.805 ± 0.082	19.612 ± 0.080
coma15-29	2571	20.260 ± 0.052	20.350 ± 0.072	20.350 ± 0.097	20.463 ± 0.126	19.683 ± 0.061
coma15-86	2577	19.503 ± 0.027	19.552 ± 0.038	19.414 ± 0.046	19.431 ± 0.055	19.157 ± 0.043
coma21-72	2584	17.117 ± 0.005	16.918 ± 0.004	16.721 ± 0.004	16.671 ± 0.005	16.539 ± 0.004
coma15-41	2585	18.987 ± 0.017	18.815 ± 0.019	18.629 ± 0.022	18.662 ± 0.027	18.461 ± 0.025
coma8-30	2587	18.951 ± 0.022	19.058 ± 0.031	18.959 ± 0.039	19.157 ± 0.056	19.095 ± 0.051
coma15-33	2591	19.174 ± 0.020	18.991 ± 0.022	18.800 ± 0.025	18.793 ± 0.029	18.655 ± 0.027
coma15-112	2593	21.647 ± 0.129	21.114 ± 0.105	20.782 ± 0.110	20.722 ± 0.142	21.970 ± 0.236
coma5-14	2599	16.354 ± 0.003	16.161 ± 0.003	15.863 ± 0.003	15.853 ± 0.003	15.722 ± 0.003
coma4-57	2603	17.944 ± 0.014	17.797 ± 0.014	17.616 ± 0.015	17.619 ± 0.018	
coma15-59	2605	20.167 ± 0.042	20.014 ± 0.050	19.860 ± 0.060	19.916 ± 0.078	19.849 ± 0.091
coma4-49	2606	20.256 ± 0.085	20.087 ± 0.086	19.794 ± 0.089	19.591 ± 0.096	
coma4-50	2613	19.977 ± 0.069	19.984 ± 0.078	19.762 ± 0.088	19.749 ± 0.105	
coma15-118	2614	20.546 ± 0.063	20.363 ± 0.072	20.162 ± 0.080	20.154 ± 0.088	20.798 ± 0.263
coma4-31	2615	17.797 ± 0.012	17.601 ± 0.011	17.411 ± 0.012	17.380 ± 0.013	
coma25-48	2619	19.261 ± 0.022	19.021 ± 0.021	18.820 ± 0.023	18.773 ± 0.026	18.711 ± 0.029
coma21-49	2626	19.173 ± 0.019	19.064 ± 0.022	18.915 ± 0.025	18.917 ± 0.031	18.619 ± 0.024
coma21-80	2631	19.513 ± 0.026	19.441 ± 0.031	19.207 ± 0.034	19.026 ± 0.035	18.530 ± 0.023
coma21-79	2633	18.981 ± 0.017	18.801 ± 0.018	18.615 ± 0.020	18.562 ± 0.023	18.309 ± 0.019
coma4-32	2635	19.212 ± 0.035	19.108 ± 0.039	18.951 ± 0.044	18.961 ± 0.055	
coma4-52	2644	20.327 ± 0.089	20.175 ± 0.096	19.892 ± 0.099	19.923 ± 0.121	
coma21-77	2647	19.606 ± 0.027	19.747 ± 0.036	19.653 ± 0.045	19.779 ± 0.055	19.523 ± 0.053
coma15-58	2651	17.448 ± 0.005	17.243 ± 0.005	17.038 ± 0.005	16.962 ± 0.006	16.827 ± 0.006
coma15-51	2654	17.265 ± 0.005	17.127 ± 0.005	16.965 ± 0.005	16.948 ± 0.006	16.910 ± 0.006
coma15-67	2655	20.828 ± 0.073	20.940 ± 0.109	20.709 ± 0.120	20.820 ± 0.164	21.960 ± 0.537
coma15-115	2660	20.562 ± 0.062	20.399 ± 0.067	20.209 ± 0.077	20.299 ± 0.101	20.583 ± 0.156
coma15-80	2663	20.930 ± 0.081	20.898 ± 0.107	20.806 ± 0.134	20.756 ± 0.159	20.316 ± 0.112
coma15-26	2665	20.897 ± 0.080	20.937 ± 0.112	20.799 ± 0.134	20.807 ± 0.167	20.927 ± 0.201
coma15-117	2667	20.019 ± 0.043	20.021 ± 0.063	19.867 ± 0.078	19.754 ± 0.092	19.451 ± 0.066
coma15-81	2676	19.583 ± 0.026	19.500 ± 0.032	19.364 ± 0.038	19.446 ± 0.050	19.254 ± 0.044
coma15-100	2677	20.240 ± 0.048	20.418 ± 0.072	20.354 ± 0.095	20.461 ± 0.125	20.388 ± 0.135
coma15-113	2679	20.163 ± 0.050	20.017 ± 0.061	19.849 ± 0.074	19.868 ± 0.097	19.802 ± 0.099
coma15-35	2683	18.989 ± 0.017	19.017 ± 0.021	18.765 ± 0.023	18.852 ± 0.029	18.823 ± 0.032
coma15-45	2684	19.270 ± 0.021	19.282 ± 0.026	19.123 ± 0.031	19.286 ± 0.042	19.246 ± 0.045
coma25-27	2685	19.160 ± 0.022	19.147 ± 0.026	19.052 ± 0.031	19.219 ± 0.042	19.271 ± 0.043
coma21-76	2687	20.080 ± 0.042	19.871 ± 0.045	19.680 ± 0.050	19.658 ± 0.058	19.708 ± 0.060
coma15-24	2692	18.962 ± 0.016	18.797 ± 0.017	18.616 ± 0.019	18.607 ± 0.023	18.488 ± 0.022
coma15-30	2694	20.259 ± 0.050	20.290 ± 0.067	20.131 ± 0.080	20.190 ± 0.103	19.636 ± 0.062
coma4-28	2698	19.331 ± 0.037	19.307 ± 0.043	19.203 ± 0.052	19.353 ± 0.069	
coma25-21	2711	18.179 ± 0.010	18.309 ± 0.012	18.186 ± 0.014	18.346 ± 0.018	18.493 ± 0.025
coma25-54	2712	20.369 ± 0.057	20.477 ± 0.077	20.483 ± 0.104	20.784 ± 0.162	21.366 ± 0.292
coma8-36	2716	20.137 ± 0.059	20.027 ± 0.072	19.825 ± 0.082	20.015 ± 0.119	19.774 ± 0.097
coma15-54	2718	20.525 ± 0.059	20.349 ± 0.068	20.303 ± 0.088	20.377 ± 0.117	21.210 ± 0.284
coma15-110	2727	16.946 ± 0.004	16.737 ± 0.004	16.538 ± 0.004	16.478 ± 0.004	16.340 ± 0.004
coma25-44	2728	18.603 ± 0.013	18.461 ± 0.014	18.309 ± 0.015	18.349 ± 0.018	18.359 ± 0.020
coma8-33	2735	19.645 ± 0.041	19.760 ± 0.059	19.631 ± 0.073	19.746 ± 0.098	19.726 ± 0.093
coma15-5	2736	18.624 ± 0.012	18.519 ± 0.014	18.379 ± 0.016	18.436 ± 0.020	18.427 ± 0.020

Raw U-band aperture magnitudes. *continued from previous page*

Object	GMP	Aperture Dia. ('') 8.8	13	16	20.2	26
coma4-35	2738	19.741 ± 0.058	19.669 ± 0.063	19.529 ± 0.075	19.640 ± 0.104	
coma4-51	2749	19.788 ± 0.056	19.619 ± 0.055	19.440 ± 0.062	19.447 ± 0.070	
coma25-51	2750	19.601 ± 0.033	19.683 ± 0.043	19.587 ± 0.053	19.701 ± 0.070	19.450 ± 0.053
coma21-26	2752	20.483 ± 0.060	20.391 ± 0.072	20.293 ± 0.089	20.361 ± 0.115	20.661 ± 0.165
coma8-34	2753	18.571 ± 0.015	18.420 ± 0.017	18.243 ± 0.019	18.231 ± 0.023	18.191 ± 0.023
coma15-72	2755	20.414 ± 0.053	20.350 ± 0.066	20.194 ± 0.078	20.199 ± 0.097	20.133 ± 0.101
coma15-8	2763	20.255 ± 0.050	20.357 ± 0.072	20.262 ± 0.093	20.528 ± 0.142	20.900 ± 0.209
coma21-55	2764	19.336 ± 0.021	19.203 ± 0.023	19.023 ± 0.027	19.064 ± 0.033	19.129 ± 0.039
coma15-82	2777	18.586 ± 0.012	18.615 ± 0.015	18.524 ± 0.017	18.580 ± 0.022	18.697 ± 0.027
coma15-37	2778	17.826 ± 0.007	17.554 ± 0.007	17.316 ± 0.007	17.244 ± 0.007	17.145 ± 0.008
coma15-17	2780	20.457 ± 0.053	20.343 ± 0.064	20.105 ± 0.070	20.116 ± 0.087	20.786 ± 0.191
coma4-53	2783	18.257 ± 0.016	18.019 ± 0.015	17.807 ± 0.016	17.767 ± 0.018	
coma21-42	2784	19.012 ± 0.016	18.830 ± 0.017	18.632 ± 0.019	18.598 ± 0.022	18.654 ± 0.026
coma15-119	2787	18.885 ± 0.016	18.749 ± 0.018	18.588 ± 0.021	18.639 ± 0.026	18.842 ± 0.041
coma21-30	2790	20.304 ± 0.049	20.227 ± 0.061	20.162 ± 0.076	20.232 ± 0.101	22.551 ± 0.967
coma21-96	2795	15.992 ± 0.003	15.760 ± 0.003	15.568 ± 0.003	15.494 ± 0.003	15.327 ± 0.002
coma15-52	2798	16.111 ± 0.003	15.851 ± 0.002	15.585 ± 0.002	15.477 ± 0.002	15.355 ± 0.002
coma15-68	2799	19.366 ± 0.022	19.317 ± 0.028	19.152 ± 0.032	19.189 ± 0.040	19.241 ± 0.049
coma4-40	2800	19.334 ± 0.036	18.969 ± 0.033	18.660 ± 0.033	18.544 ± 0.036	
coma4-14	2801	19.631 ± 0.046	19.575 ± 0.053	19.428 ± 0.061	19.578 ± 0.084	
coma15-123	2805	17.369 ± 0.005	17.273 ± 0.006	17.133 ± 0.007	17.132 ± 0.008	17.076 ± 0.007
coma15-9	2808	20.710 ± 0.068	20.724 ± 0.092	20.540 ± 0.106	20.469 ± 0.122	21.852 ± 0.479
coma15-56	2815	17.019 ± 0.004	16.867 ± 0.004	16.683 ± 0.004	16.655 ± 0.005	16.582 ± 0.006
coma15-39	2819	20.491 ± 0.063	20.442 ± 0.080	20.306 ± 0.098	20.280 ± 0.115	20.047 ± 0.100
coma21-83	2825	19.471 ± 0.025	19.599 ± 0.035	19.455 ± 0.042	19.579 ± 0.055	19.871 ± 0.071
coma15-2	2835	19.610 ± 0.029	19.686 ± 0.040	19.565 ± 0.051	19.664 ± 0.068	19.783 ± 0.070
coma15-94	2838	20.429 ± 0.051	20.517 ± 0.072	20.339 ± 0.085	20.597 ± 0.130	21.851 ± 0.487
coma15-107	2839	16.810 ± 0.004	16.679 ± 0.004	16.525 ± 0.004	16.521 ± 0.004	16.482 ± 0.004
coma25-28	2849	19.856 ± 0.035	19.882 ± 0.044	19.780 ± 0.053	19.893 ± 0.070	20.006 ± 0.082
coma15-108	2851	20.590 ± 0.081	20.741 ± 0.146	20.814 ± 0.226	20.932 ± 0.338	19.485 ± 0.050
coma8-45	2852	18.816 ± 0.018	18.567 ± 0.019	18.346 ± 0.021	18.274 ± 0.024	18.177 ± 0.024
coma15-111	2856	19.099 ± 0.018	18.920 ± 0.019	18.695 ± 0.021	18.667 ± 0.024	18.791 ± 0.031
coma15-96	2858	20.100 ± 0.044	20.320 ± 0.068	20.218 ± 0.088	20.390 ± 0.121	20.410 ± 0.133
coma21-38	2860	19.644 ± 0.029	19.541 ± 0.034	19.406 ± 0.040	19.477 ± 0.052	19.439 ± 0.053
coma21-29	2861	17.123 ± 0.005	17.006 ± 0.005	16.855 ± 0.005	16.845 ± 0.005	16.780 ± 0.005
coma4-20	2863	19.207 ± 0.033	18.878 ± 0.030	18.673 ± 0.032	18.653 ± 0.038	
coma4-39	2866	17.693 ± 0.011	17.520 ± 0.010	17.328 ± 0.011	17.296 ± 0.012	
coma15-13	2877	20.091 ± 0.048	19.908 ± 0.052	19.645 ± 0.056	19.572 ± 0.062	18.989 ± 0.032
coma4-34	2878	20.660 ± 0.139	20.722 ± 0.172	20.859 ± 0.234	21.854 ± 0.408	
coma15-122	2879	18.602 ± 0.012	18.486 ± 0.014	18.319 ± 0.016	18.291 ± 0.018	
coma15-70	2895	18.985 ± 0.020	18.776 ± 0.022	18.512 ± 0.023	18.197 ± 0.021	17.822 ± 0.018
coma8-41	2897	17.697 ± 0.008	17.477 ± 0.008	17.257 ± 0.008	17.240 ± 0.010	17.094 ± 0.009
coma25-10	2899	20.159 ± 0.055	20.059 ± 0.061	19.948 ± 0.076	20.033 ± 0.096	19.646 ± 0.064
coma25-66	2906	20.310 ± 0.056	20.409 ± 0.075	20.334 ± 0.094	20.463 ± 0.126	20.606 ± 0.149
coma21-81	2907	19.990 ± 0.043	19.962 ± 0.054	19.774 ± 0.062	19.716 ± 0.071	19.351 ± 0.050
coma8-42	2910	16.619 ± 0.004	16.527 ± 0.004	16.355 ± 0.004	16.414 ± 0.005	16.367 ± 0.005
coma8-32	2911	20.086 ± 0.054	19.947 ± 0.064	19.770 ± 0.074	19.802 ± 0.094	19.890 ± 0.109
coma21-78	2912	17.046 ± 0.004	16.892 ± 0.004	16.740 ± 0.004	16.728 ± 0.005	16.639 ± 0.005
coma8-43	2913	19.370 ± 0.034	19.351 ± 0.043	19.178 ± 0.051	19.173 ± 0.061	18.467 ± 0.030
coma21-84	2914	18.264 ± 0.010	18.021 ± 0.010	17.804 ± 0.010	17.754 ± 0.012	17.572 ± 0.010
coma15-47	2917	19.600 ± 0.033	19.557 ± 0.042	19.421 ± 0.050	19.458 ± 0.064	19.005 ± 0.058
coma25-69	2918	20.701 ± 0.073	20.621 ± 0.087	20.528 ± 0.104	20.738 ± 0.154	21.276 ± 0.276
coma15-66	2921	15.637 ± 0.002	15.286 ± 0.002	15.045 ± 0.002	14.904 ± 0.002	14.609 ± 0.001

Raw U-band aperture magnitudes. *continued from previous page*

Object	GMP	Aperture Dia. ('') 8.8	13	16	20.2	26
coma21-32	2922	16.725 ± 0.004	16.615 ± 0.004	16.496 ± 0.004	16.513 ± 0.004	16.502 ± 0.004
coma3-39	2923	17.823 ± 0.010	17.755 ± 0.011	17.577 ± 0.012	17.649 ± 0.015	
coma25-61	2928	20.647 ± 0.070	20.734 ± 0.096	20.663 ± 0.117	20.765 ± 0.158	21.032 ± 0.213
coma15-50	2929	19.452 ± 0.029	19.231 ± 0.032	19.048 ± 0.036	19.027 ± 0.043	18.494 ± 0.040
coma15-28	2931	19.284 ± 0.021	19.302 ± 0.029	19.213 ± 0.036	19.304 ± 0.049	19.590 ± 0.080
coma3-18	2938	19.841 ± 0.037	19.787 ± 0.045	19.648 ± 0.052	19.671 ± 0.067	
coma15-77	2940	17.118 ± 0.004	16.926 ± 0.004	16.741 ± 0.004	16.713 ± 0.005	16.666 ± 0.006
coma3-6	2942	17.357 ± 0.006	17.250 ± 0.006	17.093 ± 0.006	17.045 ± 0.006	
coma25-36	2943	19.043 ± 0.019	18.565 ± 0.015	18.128 ± 0.014	17.928 ± 0.013	17.643 ± 0.011
coma3-41	2945	17.306 ± 0.006	17.106 ± 0.005	16.927 ± 0.005	16.892 ± 0.006	
coma15-25	2952	19.165 ± 0.021	19.038 ± 0.024	18.895 ± 0.027	18.955 ± 0.035	18.909 ± 0.033
coma21-31	2955	20.077 ± 0.043	20.003 ± 0.053	19.930 ± 0.066	19.929 ± 0.081	19.785 ± 0.073
coma15-95	2960	17.708 ± 0.006	17.505 ± 0.006	17.291 ± 0.007	17.248 ± 0.007	17.159 ± 0.007
coma15-38	2963	20.219 ± 0.047	20.262 ± 0.066	20.151 ± 0.083	20.239 ± 0.114	
coma21-87	2973	19.909 ± 0.034	19.755 ± 0.036	19.571 ± 0.042	19.676 ± 0.054	19.929 ± 0.076
coma15-69	2975	16.541 ± 0.004	16.307 ± 0.004	16.092 ± 0.004	16.016 ± 0.004	15.816 ± 0.004
coma21-75	2976	18.658 ± 0.012	18.423 ± 0.012	18.200 ± 0.013	18.159 ± 0.015	18.139 ± 0.017
coma25-49	2981	19.927 ± 0.046	20.002 ± 0.061	20.083 ± 0.087	20.495 ± 0.152	20.070 ± 0.093
coma15-79	2983	20.465 ± 0.060	20.535 ± 0.085	20.606 ± 0.123	20.891 ± 0.199	
coma25-38	2989	17.756 ± 0.007	17.638 ± 0.007	17.437 ± 0.008	17.423 ± 0.009	17.358 ± 0.011
coma15-92	2991	19.821 ± 0.033	19.921 ± 0.048	19.880 ± 0.062	20.028 ± 0.089	19.823 ± 0.072
coma25-70	2994	20.564 ± 0.072	20.606 ± 0.097	20.583 ± 0.122	20.712 ± 0.172	20.139 ± 0.100
coma3-10	2996	19.563 ± 0.031	19.498 ± 0.037	19.363 ± 0.044	19.450 ± 0.058	
coma25-24	2997	19.430 ± 0.026	19.366 ± 0.030	19.104 ± 0.030	18.738 ± 0.026	18.420 ± 0.020
coma3-17	3003	20.260 ± 0.059	20.171 ± 0.065	20.130 ± 0.083	20.272 ± 0.111	
coma25-64	3004	19.323 ± 0.024	19.356 ± 0.028	19.205 ± 0.033	19.329 ± 0.043	19.468 ± 0.053
coma3-31	3005	20.831 ± 0.089	20.725 ± 0.111	20.709 ± 0.129	20.809 ± 0.169	
coma21-85	3006	20.837 ± 0.074	20.927 ± 0.103	20.942 ± 0.138	21.052 ± 0.221	21.405 ± 0.253
coma3-25	3012	18.357 ± 0.011	18.099 ± 0.010	17.827 ± 0.010	17.726 ± 0.011	
coma21-33	3016	18.995 ± 0.017	18.823 ± 0.017	18.600 ± 0.019	18.599 ± 0.022	18.535 ± 0.023
coma14-86	3017	18.806 ± 0.027	18.627 ± 0.030	18.428 ± 0.034	18.442 ± 0.042	18.218 ± 0.038
coma14-123	3018	19.974 ± 0.073	19.927 ± 0.095	19.794 ± 0.108	19.893 ± 0.151	19.818 ± 0.151
coma14-17	3021	20.012 ± 0.073	20.071 ± 0.118	20.000 ± 0.164	20.183 ± 0.264	19.919 ± 0.147
coma21-91	3024	20.460 ± 0.056	20.396 ± 0.069	20.349 ± 0.090	20.472 ± 0.122	20.613 ± 0.150
coma14-12	3033	20.123 ± 0.092	20.153 ± 0.118	20.023 ± 0.144	20.160 ± 0.243	20.084 ± 0.264
coma14-78	3034	19.073 ± 0.035	18.811 ± 0.038	18.573 ± 0.042	18.512 ± 0.050	18.472 ± 0.058
coma3-51	3037	21.084 ± 0.102	21.266 ± 0.140	21.349 ± 0.156	21.462 ± 0.219	
coma21-43	3043	19.752 ± 0.029	19.745 ± 0.037	19.605 ± 0.044	19.731 ± 0.059	20.016 ± 0.087
coma7-2	3049	20.203 ± 0.126	20.138 ± 0.161	19.844 ± 0.180	19.861 ± 0.220	19.332 ± 0.137
coma14-9	3050	21.016 ± 0.104	20.591 ± 0.148	20.523 ± 0.191	20.727 ± 0.270	
coma14-48	3051	20.652 ± 0.152	20.576 ± 0.215	20.401 ± 0.254	20.437 ± 0.257	20.749 ± 0.567
coma14-21	3052	20.485 ± 0.114	20.512 ± 0.155	20.399 ± 0.199	20.469 ± 0.254	21.344 ± 0.610
coma25-46	3055	16.307 ± 0.003	16.114 ± 0.003	15.928 ± 0.003	15.867 ± 0.003	15.689 ± 0.002
coma21-64	3057	19.935 ± 0.040	20.009 ± 0.054	19.911 ± 0.069	20.035 ± 0.092	20.106 ± 0.101
coma15-124	3058	18.406 ± 0.011	18.213 ± 0.011	18.024 ± 0.013	18.016 ± 0.015	
coma21-47	3066	20.438 ± 0.052	20.557 ± 0.075	20.594 ± 0.103	20.578 ± 0.126	21.533 ± 0.360
coma14-68	3068	17.610 ± 0.009	17.355 ± 0.009	17.127 ± 0.010	17.060 ± 0.012	16.954 ± 0.012
coma3-34	3071	17.489 ± 0.007	17.447 ± 0.007	17.275 ± 0.007	17.331 ± 0.008	
coma15-98	3073	16.700 ± 0.003	16.478 ± 0.003	16.291 ± 0.003	16.231 ± 0.003	
coma14-76	3075	21.016 ± 0.181	20.981 ± 0.241	20.946 ± 0.316	20.913 ± 0.383	23.369 ± 3.892
coma25-50	3076	21.099 ± 0.105	21.155 ± 0.146	21.404 ± 0.228	21.875 ± 0.453	20.625 ± 0.184
coma7-29	3079	20.509 ± 0.148	20.359 ± 0.176	20.192 ± 0.211	20.221 ± 0.264	19.248 ± 0.118
coma14-61	3080	19.878 ± 0.071	19.874 ± 0.097	19.820 ± 0.134	19.929 ± 0.215	

Raw U-band aperture magnitudes. *contiuned from previous page*

Object	GMP	Aperture Dia. (″) 8.8	13	16	20.2	26
coma21-58	3084	17.301 ± 0.005	17.151 ± 0.005	16.998 ± 0.005	16.989 ± 0.006	16.907 ± 0.006
coma3-50	3092	18.009 ± 0.009	17.907 ± 0.009	17.777 ± 0.010	17.825 ± 0.012	
coma14-5	3095	20.564 ± 0.098	20.448 ± 0.147	20.517 ± 0.184	20.446 ± 0.194	20.355 ± 0.332
coma14-97	3098	19.369 ± 0.042	19.224 ± 0.049	19.043 ± 0.057	19.116 ± 0.075	19.073 ± 0.078
coma21-44	3113	18.535 ± 0.011	18.383 ± 0.012	18.201 ± 0.013	18.214 ± 0.016	18.083 ± 0.015
coma7-14	3116	20.066 ± 0.104	20.055 ± 0.137	19.777 ± 0.149	19.824 ± 0.188	19.870 ± 0.204
coma21-28	3121	18.567 ± 0.012	18.289 ± 0.011	18.077 ± 0.012	18.035 ± 0.014	17.796 ± 0.012
coma7-34	3122	20.686 ± 0.180	20.092 ± 0.143	19.575 ± 0.126	19.047 ± 0.094	18.198 ± 0.044
coma7-37	3126	18.189 ± 0.020	18.023 ± 0.022	17.836 ± 0.026	17.824 ± 0.031	17.691 ± 0.028
coma3-33	3127	19.873 ± 0.037	19.892 ± 0.044	19.762 ± 0.053	19.882 ± 0.070	
coma21-68	3129	18.488 ± 0.011	18.357 ± 0.012	18.199 ± 0.014	18.210 ± 0.017	
coma14-55	3131	19.234 ± 0.041	19.055 ± 0.047	18.858 ± 0.054	18.807 ± 0.067	18.516 ± 0.049
coma14-65	3133	18.099 ± 0.014	17.956 ± 0.016	17.779 ± 0.018	17.758 ± 0.021	17.685 ± 0.021
coma14-54	3134	19.723 ± 0.056	19.647 ± 0.071	19.463 ± 0.087	19.286 ± 0.092	19.016 ± 0.071
coma14-94	3142	20.344 ± 0.096	20.168 ± 0.110	20.009 ± 0.132	19.946 ± 0.152	20.455 ± 0.289
coma14-112	3146	19.353 ± 0.043	19.093 ± 0.046	18.843 ± 0.050	18.891 ± 0.064	18.836 ± 0.064
coma14-3	3149	20.195 ± 0.084	20.169 ± 0.122	20.058 ± 0.155	20.109 ± 0.258	20.448 ± 0.326
coma14-47	3150	21.054 ± 0.170	20.993 ± 0.288	21.118 ± 0.407	21.557 ± 1.323	
coma3-16	3165	16.302 ± 0.003	16.126 ± 0.003	15.950 ± 0.003	15.908 ± 0.003	
coma14-121	3166	19.209 ± 0.037	19.063 ± 0.044	18.939 ± 0.053	19.015 ± 0.070	19.251 ± 0.097
coma14-108	3170	17.081 ± 0.006	16.861 ± 0.006	16.660 ± 0.007	16.592 ± 0.008	16.470 ± 0.008
coma14-81	3171	19.806 ± 0.065	19.613 ± 0.074	19.421 ± 0.084	19.504 ± 0.112	19.392 ± 0.109
coma3-58	3174	19.276 ± 0.024	19.389 ± 0.031	19.339 ± 0.039	19.437 ± 0.052	
coma3-32	3176	18.671 ± 0.015	18.574 ± 0.016	18.415 ± 0.018	18.496 ± 0.022	
coma3-57	3177	19.411 ± 0.026	19.335 ± 0.028	19.185 ± 0.033	19.220 ± 0.041	
coma14-15	3178	17.022 ± 0.006	16.892 ± 0.006	16.746 ± 0.007	16.748 ± 0.009	16.687 ± 0.009
coma7-48	3180	20.470 ± 0.149	20.380 ± 0.187	20.104 ± 0.197	20.008 ± 0.226	19.001 ± 0.093
coma3-28	3192	18.870 ± 0.017	18.536 ± 0.015	18.246 ± 0.015	18.176 ± 0.016	
coma3-36	3195	20.245 ± 0.049	20.121 ± 0.055	19.948 ± 0.062	20.030 ± 0.080	
coma14-39	3196	18.924 ± 0.027	18.794 ± 0.032	18.628 ± 0.036	18.621 ± 0.044	18.545 ± 0.046
coma14-57	3201	16.582 ± 0.004	16.414 ± 0.005	16.249 ± 0.005	16.221 ± 0.006	16.163 ± 0.006
coma14-24	3205	18.261 ± 0.017	18.103 ± 0.019	17.935 ± 0.022	17.955 ± 0.027	17.883 ± 0.026
coma14-99	3206	17.495 ± 0.009	17.332 ± 0.009	17.157 ± 0.011	17.159 ± 0.013	17.149 ± 0.015
coma14-134	3209	19.965 ± 0.070	19.832 ± 0.084	19.591 ± 0.094	19.568 ± 0.112	20.573 ± 0.341
coma14-122	3213	17.201 ± 0.007	17.042 ± 0.007	16.873 ± 0.008	16.842 ± 0.010	16.791 ± 0.010
coma14-71	3215	21.086 ± 0.195	21.034 ± 0.256	20.899 ± 0.307	21.350 ± 0.579	
coma7-115	3222	17.115 ± 0.008	17.063 ± 0.009	16.940 ± 0.011	16.972 ± 0.014	17.000 ± 0.016
coma14-63	3222	18.805 ± 0.006	18.203 ± 0.008	17.682 ± 0.009	17.206 ± 0.011	17.034 ± 0.012
coma14-11	3225	18.626 ± 0.023	18.601 ± 0.028	18.484 ± 0.034	18.598 ± 0.047	18.812 ± 0.071
coma14-79	3229	20.482 ± 0.113	20.349 ± 0.136	20.195 ± 0.180	20.231 ± 0.250	
coma14-35	3230	20.119 ± 0.082	20.108 ± 0.110	19.984 ± 0.142	20.101 ± 0.197	20.404 ± 0.232
coma3-22	3231	19.647 ± 0.030	19.506 ± 0.033	19.323 ± 0.038	19.299 ± 0.046	
coma7-39	3237	20.241 ± 0.115	20.050 ± 0.130	19.922 ± 0.162		
coma3-2	3238	18.039 ± 0.009	17.766 ± 0.008	17.532 ± 0.009	17.433 ± 0.009	
comasw17-92	3243	20.511 ± 0.058	20.656 ± 0.087	20.547 ± 0.112	20.463 ± 0.127	
coma14-32	3244	21.487 ± 0.313	21.404 ± 0.406	21.594 ± 0.939		
coma3-54	3247	20.217 ± 0.053	20.116 ± 0.056	20.020 ± 0.069	20.080 ± 0.083	
coma14-104	3254	17.920 ± 0.013	17.793 ± 0.015	17.663 ± 0.018	17.681 ± 0.022	17.602 ± 0.029
coma7-15	3257	20.203 ± 0.114	20.168 ± 0.147	19.786 ± 0.150	20.001 ± 0.215	20.236 ± 0.287
coma14-10	3262	17.823 ± 0.011	17.625 ± 0.012	17.383 ± 0.013	17.263 ± 0.014	17.127 ± 0.013
coma14-102	3269	17.494 ± 0.010	17.393 ± 0.012	17.265 ± 0.014	17.293 ± 0.018	17.137 ± 0.020
comasw17-5	3271	16.721 ± 0.004	16.604 ± 0.004	16.388 ± 0.004	16.437 ± 0.004	
coma7-51	3275	18.701 ± 0.028	18.201 ± 0.024	17.675 ± 0.020	17.321 ± 0.018	17.138 ± 0.017

Raw U-band aperture magnitudes. *contiuned from previous page*

Object	GMP	Aperture Dia. (″) 8.8	13	16	20.2	26
coma14-28	3284	19.645 ± 0.053	19.644 ± 0.075	19.617 ± 0.093	19.724 ± 0.136	20.547 ± 0.243
coma14-120	3291	17.983 ± 0.013	17.745 ± 0.014	17.524 ± 0.015	17.466 ± 0.017	17.389 ± 0.018
coma14-98	3292	18.562 ± 0.020	18.414 ± 0.024	18.260 ± 0.028	18.255 ± 0.034	18.313 ± 0.040
coma14-51	3296	16.799 ± 0.005	16.675 ± 0.006	16.532 ± 0.006	16.525 ± 0.007	16.469 ± 0.008
coma3-38	3298	18.468 ± 0.012	18.202 ± 0.011	17.942 ± 0.011	17.844 ± 0.012	
coma3-7	3299	19.620 ± 0.028	19.537 ± 0.033	19.420 ± 0.038	19.402 ± 0.047	
coma14-29	3301	20.391 ± 0.104	20.357 ± 0.132	19.977 ± 0.132	19.583 ± 0.110	19.212 ± 0.087
coma14-27	3311	19.571 ± 0.056	19.462 ± 0.069	19.297 ± 0.079	19.265 ± 0.091	19.111 ± 0.084
coma14-136	3312	19.215 ± 0.038	19.131 ± 0.048	19.073 ± 0.063		
coma3-64	3313	17.886 ± 0.008	17.844 ± 0.009	17.702 ± 0.010	17.738 ± 0.012	
coma3-53	3324	19.860 ± 0.040	19.718 ± 0.043	19.586 ± 0.048	19.581 ± 0.058	
coma14-49	3325	19.355 ± 0.046	18.999 ± 0.043	18.745 ± 0.047	18.704 ± 0.058	18.420 ± 0.042
coma14-100	3329	16.337 ± 0.004	15.941 ± 0.003	15.679 ± 0.003	15.529 ± 0.003	15.174 ± 0.003
comasw17-21	3332	19.081 ± 0.018	19.154 ± 0.024	19.056 ± 0.029	19.177 ± 0.039	
comasw17-15	3335	20.392 ± 0.053	20.341 ± 0.067	20.226 ± 0.082	20.328 ± 0.110	
coma14-50	3336	19.262 ± 0.041	18.983 ± 0.043	18.752 ± 0.048	18.765 ± 0.060	18.497 ± 0.048
coma14-18	3339	18.147 ± 0.014	18.040 ± 0.017	17.886 ± 0.019	17.919 ± 0.025	17.976 ± 0.029
coma14-69	3340	19.185 ± 0.037	19.030 ± 0.044	18.861 ± 0.053	18.922 ± 0.068	19.356 ± 0.123
comasw17-45	3343	20.275 ± 0.046	20.043 ± 0.050	19.852 ± 0.057	19.831 ± 0.069	
coma14-80	3352	16.526 ± 0.005	16.391 ± 0.006	16.250 ± 0.007	16.227 ± 0.009	16.051 ± 0.008
coma3-52	3356	19.868 ± 0.039	19.659 ± 0.041	19.511 ± 0.046	19.607 ± 0.054	
coma14-119	3367	16.678 ± 0.005	16.453 ± 0.005	16.251 ± 0.005	16.182 ± 0.006	16.069 ± 0.006
coma3-42	3371	19.439 ± 0.027	19.296 ± 0.029	19.041 ± 0.032	19.241 ± 0.040	
coma14-62	3376	19.599 ± 0.046	19.341 ± 0.052	19.099 ± 0.060	19.099 ± 0.073	19.094 ± 0.083
coma3-19	3381	19.730 ± 0.032	19.447 ± 0.030	19.236 ± 0.032	19.186 ± 0.036	
coma14-14	3383	18.807 ± 0.025	18.733 ± 0.031	18.606 ± 0.036	18.659 ± 0.047	18.853 ± 0.061
coma3-15	3391	20.343 ± 0.054	20.244 ± 0.061	20.078 ± 0.067	20.147 ± 0.082	
coma3-8	3399	18.971 ± 0.019	19.071 ± 0.024	18.979 ± 0.028	19.093 ± 0.037	
coma14-38	3400	16.419 ± 0.004	16.311 ± 0.004	16.175 ± 0.004	16.156 ± 0.005	16.060 ± 0.005
coma3-47	3403	17.535 ± 0.006	17.422 ± 0.006	17.275 ± 0.007	17.290 ± 0.008	
comasw17-19	3410	19.451 ± 0.024	19.514 ± 0.031	19.373 ± 0.038	19.449 ± 0.048	
coma3-63	3411	19.717 ± 0.035	19.619 ± 0.039	19.457 ± 0.044	19.523 ± 0.053	
coma14-103	3414	16.762 ± 0.005	16.562 ± 0.005	16.371 ± 0.006	16.290 ± 0.006	16.142 ± 0.008
coma14-128	3420	20.043 ± 0.081	20.087 ± 0.110	19.906 ± 0.133	19.951 ± 0.165	20.584 ± 0.322
coma14-7	3423	16.715 ± 0.005	16.594 ± 0.005	16.454 ± 0.006	16.439 ± 0.007	16.363 ± 0.007
coma3-56	3425	19.466 ± 0.028	19.323 ± 0.030	19.120 ± 0.034	19.087 ± 0.041	
coma3-24	3435	19.491 ± 0.027	19.452 ± 0.031	19.356 ± 0.037	19.433 ± 0.048	
coma14-137	3438	19.531 ± 0.053	19.393 ± 0.065	19.237 ± 0.079		
coma7-38	3449	21.189 ± 0.238	20.919 ± 0.230	20.610 ± 0.238	20.703 ± 0.310	
coma3-43	3463	18.632 ± 0.014	18.449 ± 0.014	18.268 ± 0.015	18.260 ± 0.017	
coma14-8	3473	19.318 ± 0.041	19.264 ± 0.053	19.117 ± 0.065	19.136 ± 0.082	19.360 ± 0.121
coma13-82	3474	20.512 ± 0.065	20.759 ± 0.110	21.084 ± 0.165	21.234 ± 0.328	
coma13-64	3480	20.609 ± 0.071	20.496 ± 0.070	20.467 ± 0.078	20.696 ± 0.083	19.608 ± 0.028
coma13-48	3484	17.332 ± 0.006	17.213 ± 0.006	17.056 ± 0.007	17.035 ± 0.008	16.908 ± 0.006
coma13-35	3486	18.461 ± 0.011	18.340 ± 0.012	18.174 ± 0.014	18.173 ± 0.017	18.085 ± 0.015
coma13-58	3487	17.647 ± 0.007	17.487 ± 0.007	17.311 ± 0.008	17.265 ± 0.009	17.129 ± 0.008
coma14-117	3489	19.072 ± 0.034	18.907 ± 0.040	18.746 ± 0.046	18.745 ± 0.057	18.447 ± 0.043
coma3-30	3493	17.148 ± 0.005	17.059 ± 0.005	16.933 ± 0.005	16.941 ± 0.006	
coma13-5	3501	19.385 ± 0.029	19.370 ± 0.037	19.208 ± 0.047	19.229 ± 0.061	19.138 ± 0.077
coma3-9	3508	19.496 ± 0.031	19.482 ± 0.035	19.368 ± 0.044	19.484 ± 0.058	
coma13-23	3510	16.365 ± 0.003	16.129 ± 0.003	15.935 ± 0.003	15.864 ± 0.003	15.685 ± 0.003
coma13-25	3511	19.077 ± 0.020	19.098 ± 0.026	18.997 ± 0.031	18.960 ± 0.037	18.459 ± 0.024
coma13-72	3515	20.783 ± 0.082	20.953 ± 0.115	20.786 ± 0.141	20.762 ± 0.171	

Raw U-band aperture magnitudes. *contiuned from previous page*

Object	GMP	Aperture Dia. (″) 8.8	13	16	20.2	26
coma13-54	3516	20.361 ± 0.061	20.555 ± 0.089	20.825 ± 0.121	22.328 ± 0.189	20.633 ± 0.200
coma7-25	3517	20.364 ± 0.129	20.339 ± 0.174	20.181 ± 0.209	20.135 ± 0.254	20.198 ± 0.272
coma3-20	3519	20.216 ± 0.050	20.078 ± 0.053	19.932 ± 0.066	20.000 ± 0.080	
coma13-6	3522	17.152 ± 0.005	17.062 ± 0.005	16.930 ± 0.005	16.954 ± 0.007	
coma3-60	3531	19.112 ± 0.022	19.226 ± 0.028	19.126 ± 0.034	19.271 ± 0.046	
coma13-106	3533	20.469 ± 0.063	20.197 ± 0.066	20.009 ± 0.073	19.962 ± 0.083	20.255 ± 0.209
coma13-61	3534	18.076 ± 0.009	17.943 ± 0.009	17.793 ± 0.011	17.811 ± 0.013	17.746 ± 0.013
coma14-25	3536	20.864 ± 0.192	20.216 ± 0.152	19.751 ± 0.123	19.541 ± 0.127	19.552 ± 0.133
coma14-26	3536	19.746 ± 0.058	19.649 ± 0.074	19.441 ± 0.084	19.512 ± 0.114	19.705 ± 0.141
coma13-129	3546	21.749 ± 0.234	21.936 ± 0.399	21.857 ± 0.490	23.212 ± 2.196	22.754 ± 2.872
coma7-8	3548	20.228 ± 0.116	20.178 ± 0.146	19.938 ± 0.148	19.919 ± 0.175	20.255 ± 0.287
coma23-31	3553	17.735 ± 0.007	17.560 ± 0.007	17.387 ± 0.008	17.370 ± 0.009	
coma14-37	3557	17.331 ± 0.008	17.135 ± 0.008	16.939 ± 0.009	16.909 ± 0.010	16.852 ± 0.011
coma13-60	3565	19.101 ± 0.018	18.925 ± 0.020	18.733 ± 0.022	18.715 ± 0.026	18.681 ± 0.030
coma13-55	3567	19.324 ± 0.023	19.226 ± 0.028	19.066 ± 0.033	19.104 ± 0.041	19.040 ± 0.042
comasw17-88	3571	19.921 ± 0.035	20.054 ± 0.048	20.038 ± 0.062	20.244 ± 0.087	
coma23-75	3573	20.174 ± 0.046	19.994 ± 0.052	19.829 ± 0.062	19.774 ± 0.072	
coma23-30	3580	20.170 ± 0.049	20.062 ± 0.060	19.928 ± 0.074	20.082 ± 0.105	
comasw17-13	3585	18.210 ± 0.010	18.111 ± 0.011	17.902 ± 0.012	17.920 ± 0.014	
comasw17-76	3586	18.514 ± 0.011	18.449 ± 0.013	18.312 ± 0.015	18.356 ± 0.019	
coma23-25	3592	19.492 ± 0.026	19.272 ± 0.029	19.052 ± 0.031	19.034 ± 0.039	
coma13-42	3595	20.338 ± 0.056	20.453 ± 0.081	20.367 ± 0.107	20.393 ± 0.151	22.112 ± 0.914
comasw17-40	3598	19.764 ± 0.031	19.679 ± 0.038	19.535 ± 0.045	19.605 ± 0.059	
coma13-73	3602	20.886 ± 0.090	20.893 ± 0.153	21.011 ± 0.226	21.469 ± 0.459	
coma19-72	3603	19.769 ± 0.029	19.621 ± 0.033	19.444 ± 0.038	19.519 ± 0.049	19.291 ± 0.047
coma13-3	3606	18.253 ± 0.011	18.422 ± 0.015	18.245 ± 0.018		
coma19-97	3608	20.526 ± 0.057	20.475 ± 0.073	20.292 ± 0.089	20.253 ± 0.113	20.265 ± 0.111
coma23-74	3609	20.549 ± 0.065	20.118 ± 0.060	19.710 ± 0.058	19.636 ± 0.065	
coma13-79	3615	19.417 ± 0.025	19.332 ± 0.032	19.411 ± 0.040	19.516 ± 0.056	19.546 ± 0.073
comasw22-29	3616	20.138 ± 0.060	20.261 ± 0.090	20.219 ± 0.117	20.375 ± 0.169	
coma14-4	3621	21.836 ± 0.368	21.413 ± 0.363	21.381 ± 0.479	21.745 ± 0.862	20.313 ± 0.260
coma13-92	3623	19.773 ± 0.033	19.940 ± 0.048	19.811 ± 0.061	19.908 ± 0.079	20.833 ± 0.212
coma14-36	3625	20.475 ± 0.096	20.338 ± 0.103	20.357 ± 0.129		
coma13-7	3629	19.896 ± 0.038	19.746 ± 0.047	19.579 ± 0.056	19.662 ± 0.075	19.510 ± 0.052
coma13-122	3630	21.126 ± 0.094	21.245 ± 0.145	21.327 ± 0.201	21.481 ± 0.289	21.236 ± 0.430
coma7-22	3633	19.881 ± 0.069	19.788 ± 0.094	19.521 ± 0.101	19.419 ± 0.116	19.108 ± 0.103
coma13-67	3639	16.502 ± 0.003	16.361 ± 0.003	16.215 ± 0.003	16.197 ± 0.004	16.105 ± 0.004
coma23-62	3640	18.043 ± 0.009	17.859 ± 0.009	17.606 ± 0.009	17.597 ± 0.011	
comasw17-10	3643	20.543 ± 0.065	20.569 ± 0.088	20.463 ± 0.111	20.913 ± 0.203	
coma13-2	3645	19.163 ± 0.021				
coma13-30	3648	19.833 ± 0.032	19.901 ± 0.046	19.769 ± 0.058	19.936 ± 0.083	19.850 ± 0.076
coma13-46	3649	21.066 ± 0.113	21.310 ± 0.192	21.508 ± 0.306	21.779 ± 0.501	20.407 ± 0.147
coma13-111	3650	19.652 ± 0.030	19.698 ± 0.039	19.565 ± 0.048	19.482 ± 0.050	17.776 ± 0.013
coma19-47	3656	17.325 ± 0.005	17.058 ± 0.005	16.812 ± 0.005	16.701 ± 0.005	16.458 ± 0.005
comasw22-40	3660	17.020 ± 0.005	16.839 ± 0.005	16.657 ± 0.005	16.603 ± 0.006	
coma13-65	3664	16.372 ± 0.003	16.031 ± 0.003	15.801 ± 0.003	15.731 ± 0.003	15.576 ± 0.002
coma23-77	3665	19.945 ± 0.038	19.974 ± 0.052	19.846 ± 0.064	19.988 ± 0.089	
coma13-113	3668	20.939 ± 0.094	20.931 ± 0.138	20.730 ± 0.141	20.638 ± 0.157	19.854 ± 0.073
comasw17-51	3672	20.381 ± 0.049	20.293 ± 0.060	20.213 ± 0.076	20.191 ± 0.091	
coma13-93	3675	20.227 ± 0.045	20.081 ± 0.052	19.640 ± 0.048	18.356 ± 0.019	16.685 ± 0.005
comasw17-90	3676	20.550 ± 0.066	20.521 ± 0.084	20.457 ± 0.107	20.476 ± 0.139	
comasw17-72	3677	19.163 ± 0.019	19.343 ± 0.027	19.265 ± 0.034	19.494 ± 0.045	
coma23-34	3678	20.514 ± 0.060	20.274 ± 0.066	20.123 ± 0.079	20.113 ± 0.096	

Raw U-band aperture magnitudes. *contiuned from previous page*

Object	GMP	Aperture Dia. (″) 8.8	13	16	20.2	26
comasw22-66	3679	19.814 ± 0.041	19.729 ± 0.050	19.603 ± 0.061	19.592 ± 0.074	
coma13-102	3681	18.640 ± 0.013	18.529 ± 0.015	18.372 ± 0.017	18.397 ± 0.021	18.370 ± 0.021
coma19-74	3683	20.151 ± 0.039	20.350 ± 0.061	20.225 ± 0.076	20.285 ± 0.096	20.618 ± 0.144
coma13-117	3685	20.265 ± 0.055	20.451 ± 0.085	20.489 ± 0.122	20.920 ± 0.267	20.606 ± 0.184
comasw6-1	3688	20.027 ± 0.056	20.112 ± 0.085	20.027 ± 0.113	20.057 ± 0.149	
comasw6-35	3691	20.238 ± 0.059	20.329 ± 0.085	20.177 ± 0.107	20.365 ± 0.154	
comasw17-22	3696	20.858 ± 0.077	20.864 ± 0.109	20.829 ± 0.137	20.978 ± 0.205	
comasw17-31	3697	17.275 ± 0.005	17.155 ± 0.005	17.006 ± 0.005	16.995 ± 0.006	
coma13-62	3698	20.929 ± 0.107	20.902 ± 0.141	20.833 ± 0.180	20.866 ± 0.232	19.782 ± 0.093
coma19-96	3699	19.075 ± 0.016	18.919 ± 0.018	18.711 ± 0.020	18.686 ± 0.023	18.401 ± 0.019
comasw17-81	3700	20.531 ± 0.061	20.476 ± 0.081	20.389 ± 0.103	20.375 ± 0.135	
comasw6-3	3703	19.845 ± 0.049	19.791 ± 0.064	19.704 ± 0.084	19.764 ± 0.111	
coma23-78	3704	20.693 ± 0.071	20.372 ± 0.073	20.015 ± 0.073	19.876 ± 0.078	
comasw22-100	3706	17.978 ± 0.009	17.952 ± 0.011	17.844 ± 0.013	17.889 ± 0.016	
coma13-120	3707	18.517 ± 0.011	18.350 ± 0.012	18.188 ± 0.013	18.183 ± 0.016	18.160 ± 0.018
coma19-43	3708	21.442 ± 0.129	21.901 ± 0.270	22.536 ± 0.624		23.723 ± 3.045
comasw17-41	3710	20.040 ± 0.040	20.095 ± 0.054	20.055 ± 0.071	20.127 ± 0.093	
coma23-61	3712	20.140 ± 0.043	20.105 ± 0.058	19.967 ± 0.068	19.965 ± 0.086	
comasw6-65	3716	19.972 ± 0.050	20.111 ± 0.073	19.855 ± 0.083	19.951 ± 0.106	
coma13-4	3719	19.017 ± 0.018	18.839 ± 0.020	18.659 ± 0.023	18.633 ± 0.029	
comasw17-62	3726	19.839 ± 0.034	20.014 ± 0.049	19.865 ± 0.061	20.074 ± 0.087	
coma23-67	3727	20.144 ± 0.045	20.083 ± 0.058	19.989 ± 0.071	19.971 ± 0.089	
comasw6-25	3728	18.957 ± 0.019	19.058 ± 0.026	18.936 ± 0.032	19.020 ± 0.042	
comasw6-37	3729	19.314 ± 0.026	19.303 ± 0.034	19.228 ± 0.043	19.316 ± 0.058	
comasw22-43	3730	16.596 ± 0.004	16.417 ± 0.004	16.253 ± 0.004	16.210 ± 0.004	
comasw22-60	3731	21.295 ± 0.197	21.346 ± 0.297	21.348 ± 0.383	21.475 ± 0.567	
comasw22-94	3733	16.913 ± 0.005	16.718 ± 0.004	16.529 ± 0.005	16.475 ± 0.005	
comasw17-46	3735	20.694 ± 0.085	20.767 ± 0.123	20.712 ± 0.159	20.857 ± 0.228	
coma13-131	3736	20.679 ± 0.079	20.592 ± 0.103	20.378 ± 0.105		
comasw22-36	3739	16.935 ± 0.005	16.781 ± 0.005	16.619 ± 0.005	16.591 ± 0.006	
comasw22-37	3750	18.587 ± 0.018	18.463 ± 0.020	18.279 ± 0.023	18.209 ± 0.026	
coma19-59	3753	19.581 ± 0.024	19.562 ± 0.030	19.489 ± 0.038	19.547 ± 0.048	19.568 ± 0.057
comasw22-78	3756	19.940 ± 0.047	19.975 ± 0.063	19.747 ± 0.071	19.791 ± 0.089	
coma13-94	3761	16.868 ± 0.004	16.664 ± 0.004	16.469 ± 0.004	16.390 ± 0.004	16.237 ± 0.004
coma19-23	3762	20.733 ± 0.061	20.611 ± 0.074	20.351 ± 0.081	20.429 ± 0.105	20.793 ± 0.171
comasw17-35	3766	20.300 ± 0.048	20.280 ± 0.062	20.177 ± 0.077	20.258 ± 0.102	
coma13-130	3768	18.684 ± 0.014	18.700 ± 0.018	18.596 ± 0.022	18.738 ± 0.031	
comasw22-24	3770	20.981 ± 0.110	20.478 ± 0.097	20.206 ± 0.101	20.071 ± 0.112	
comasw22-23	3770	20.518 ± 0.079	20.116 ± 0.074	19.883 ± 0.081	19.830 ± 0.095	
comasw21-81	3772	18.079 ± 0.009	18.167 ± 0.011	18.006 ± 0.014	18.148 ± 0.017	
comasw21-44	3777	21.026 ± 0.133	21.038 ± 0.187	20.880 ± 0.217	20.214 ± 0.147	
comasw17-48	3779	15.859 ± 0.002	15.776 ± 0.002	15.547 ± 0.002	15.557 ± 0.002	
coma13-124	3780	18.650 ± 0.013	18.474 ± 0.014	18.287 ± 0.015	18.259 ± 0.018	18.186 ± 0.017
coma23-89	3781	19.315 ± 0.024	19.395 ± 0.033	19.259 ± 0.040	19.320 ± 0.051	
coma13-19	3782	17.434 ± 0.005	17.280 ± 0.005	17.112 ± 0.006	17.101 ± 0.006	17.035 ± 0.007
comasw21-75	3785	20.316 ± 0.054	20.377 ± 0.076	20.297 ± 0.101	20.415 ± 0.137	
comasw17-23	3787	20.061 ± 0.039	20.188 ± 0.057	19.974 ± 0.065	20.202 ± 0.096	
comasw21-39	3788	18.656 ± 0.013	18.759 ± 0.018	18.653 ± 0.021	18.734 ± 0.028	
coma19-70	3792	16.222 ± 0.003	15.995 ± 0.002	15.810 ± 0.002	15.733 ± 0.002	15.553 ± 0.002
coma13-38	3793	21.481 ± 0.135	21.278 ± 0.158	21.152 ± 0.186	21.174 ± 0.243	20.817 ± 0.183
coma13-44	3794	17.873 ± 0.007	17.804 ± 0.008	17.689 ± 0.009	17.720 ± 0.011	17.724 ± 0.012
comasw21-65	3797	20.305 ± 0.055	20.315 ± 0.076	20.235 ± 0.106	20.344 ± 0.152	
coma13-78	3804	20.327 ± 0.049	20.313 ± 0.063	20.205 ± 0.078	20.346 ± 0.109	20.369 ± 0.131

Raw U-band aperture magnitudes. *contiuned from previous page*

Object	GMP	Aperture Dia. (″) 8.8	13	16	20.2	26
comasw16-72	3805	20.663 ± 0.075	20.136 ± 0.025			
coma13-57	3806	20.418 ± 0.051	20.320 ± 0.062	19.885 ± 0.057	19.079 ± 0.034	18.984 ± 0.036
comasw21-62	3808	21.442 ± 0.090	20.833 ± 0.086	20.346 ± 0.090	20.069 ± 0.113	
coma19-93	3809	20.605 ± 0.053	20.589 ± 0.071	20.481 ± 0.082	20.368 ± 0.091	20.483 ± 0.125
coma13-96	3811	20.479 ± 0.055	20.511 ± 0.075	20.428 ± 0.102	20.545 ± 0.136	22.130 ± 0.665
coma13-39	3815	21.795 ± 0.177	21.610 ± 0.213	21.843 ± 0.346	22.093 ± 0.563	
coma19-66	3816	16.232 ± 0.003	15.989 ± 0.002	15.738 ± 0.002	15.773 ± 0.003	15.693 ± 0.003
coma23-46	3818	16.548 ± 0.003	16.368 ± 0.003	16.197 ± 0.003	16.153 ± 0.004	
comasw21-25	3820	20.787 ± 0.056	20.720 ± 0.084	20.603 ± 0.100	20.585 ± 0.119	
comasw21-90	3821	20.884 ± 0.089	20.996 ± 0.139	21.116 ± 0.255	21.316 ± 0.436	
coma13-34	3826	20.074 ± 0.044	20.225 ± 0.067	20.189 ± 0.088	20.316 ± 0.122	20.185 ± 0.102
comasw21-99	3830	20.519 ± 0.055	20.491 ± 0.072	20.290 ± 0.085	20.345 ± 0.114	
comasw16-19	3833	20.557 ± 0.067	20.507 ± 0.090	20.390 ± 0.114	20.621 ± 0.171	
comasw16-56	3834	20.240 ± 0.047	20.328 ± 0.071	20.227 ± 0.091	20.421 ± 0.131	
comasw21-96	3835	19.884 ± 0.033	19.699 ± 0.037	19.494 ± 0.042	19.450 ± 0.051	
comasw16-25	3840	20.705 ± 0.068	20.539 ± 0.078	20.328 ± 0.087	20.300 ± 0.106	
comasw21-17	3843	20.828 ± 0.066	20.873 ± 0.099	20.834 ± 0.122	20.660 ± 0.123	
coma23-27	3844	20.131 ± 0.047	20.260 ± 0.069	20.146 ± 0.087	20.361 ± 0.127	
comasw21-27	3845	19.434 ± 0.021	19.101 ± 0.021	18.824 ± 0.024	18.827 ± 0.030	
comasw6-27	3847	19.791 ± 0.038	19.808 ± 0.052	19.695 ± 0.063	19.711 ± 0.079	
comasw16-31	3848	18.818 ± 0.014	18.932 ± 0.019	18.811 ± 0.024	18.964 ± 0.032	
comasw21-57	3849	20.399 ± 0.053	20.539 ± 0.074	20.506 ± 0.097	20.846 ± 0.134	
comasw6-22	3850	20.005 ± 0.047	20.177 ± 0.073	20.078 ± 0.092	20.210 ± 0.127	
coma13-56	3851	17.776 ± 0.007	17.620 ± 0.007	17.465 ± 0.007	17.458 ± 0.008	17.421 ± 0.009
comasw11-30	3853	20.288 ± 0.053	20.226 ± 0.072	20.078 ± 0.083	20.107 ± 0.110	19.718 ± 0.073
coma13-32	3855	18.838 ± 0.014	18.663 ± 0.016	18.485 ± 0.017	18.478 ± 0.021	18.367 ± 0.020
coma13-86	3856	20.082 ± 0.043	19.933 ± 0.049	19.786 ± 0.059	19.925 ± 0.082	20.069 ± 0.094
coma19-63	3857	19.869 ± 0.032	19.968 ± 0.044	19.825 ± 0.054	19.850 ± 0.066	19.787 ± 0.071
coma13-8	3859	19.203 ± 0.021	19.320 ± 0.029	19.248 ± 0.037	19.459 ± 0.052	19.560 ± 0.062
comasw6-57	3863	19.968 ± 0.047	19.924 ± 0.061	19.836 ± 0.077	19.892 ± 0.100	
comasw6-39	3864	18.895 ± 0.019	18.971 ± 0.025	18.863 ± 0.032	19.017 ± 0.043	
comasw11-58	3865	20.432 ± 0.072	20.255 ± 0.083	19.973 ± 0.094	19.855 ± 0.108	19.273 ± 0.051
coma19-90	3866	20.090 ± 0.039	20.078 ± 0.050	19.961 ± 0.064	20.108 ± 0.084	20.351 ± 0.112
comasw16-60	3872	20.684 ± 0.065	20.453 ± 0.070	20.226 ± 0.077	20.270 ± 0.099	
comasw11-55	3879	17.026 ± 0.003	16.905 ± 0.004	16.765 ± 0.004	16.768 ± 0.005	16.679 ± 0.005
comasw16-55	3880	20.157 ± 0.046	20.219 ± 0.064	20.097 ± 0.080	20.300 ± 0.116	
coma23-38	3881	20.310 ± 0.052	20.505 ± 0.083	20.626 ± 0.125	20.768 ± 0.178	
comasw21-36	3882	17.831 ± 0.007	17.651 ± 0.007	17.459 ± 0.008	17.430 ± 0.009	
coma13-99	3883	19.945 ± 0.035	19.844 ± 0.043	19.709 ± 0.051	19.754 ± 0.066	19.665 ± 0.078
coma19-52	3884	20.483 ± 0.057	20.268 ± 0.064	20.076 ± 0.074	20.103 ± 0.093	19.670 ± 0.058
comasw16-36	3885	19.719 ± 0.030	19.629 ± 0.036	19.470 ± 0.044	19.565 ± 0.056	
comasw21-13	3886	20.530 ± 0.060	20.613 ± 0.084	20.563 ± 0.116	20.694 ± 0.143	
comasw11-56	3890	20.637 ± 0.088	20.798 ± 0.138	20.679 ± 0.176	19.472 ± 0.057	17.628 ± 0.011
comasw21-63	3895	18.024 ± 0.008	17.961 ± 0.009	17.820 ± 0.011	17.881 ± 0.013	
coma13-1	3897	20.346 ± 0.051	20.145 ± 0.053			
comasw21-48	3898	19.550 ± 0.026	19.417 ± 0.030	19.264 ± 0.035	19.307 ± 0.044	
coma13-14	3899	19.541 ± 0.024	19.465 ± 0.029	19.322 ± 0.033	19.302 ± 0.042	19.454 ± 0.055
comasw6-40	3901	20.238 ± 0.061	20.331 ± 0.087	20.363 ± 0.126	20.768 ± 0.218	
coma23-42	3904	20.488 ± 0.065	20.639 ± 0.098	20.608 ± 0.134	20.712 ± 0.178	
comasw21-66	3907	20.567 ± 0.067	20.407 ± 0.081	20.012 ± 0.082	19.392 ± 0.060	
comasw21-109	3911	19.918 ± 0.037	19.975 ± 0.050	19.818 ± 0.060	19.895 ± 0.078	
comasw6-8	3913	21.839 ± 0.229	21.712 ± 0.296	21.671 ± 0.368	21.352 ± 0.363	
coma13-50	3914	17.183 ± 0.005	17.127 ± 0.005	17.017 ± 0.005	17.044 ± 0.006	17.008 ± 0.006

Raw U-band aperture magnitudes. *contiuned from previous page*

Object	GMP	Aperture Dia. (″) 8.8	13	16	20.2	26
comasw21-67	3916	20.406 ± 0.063	20.153 ± 0.109	20.056 ± 0.154	20.015 ± 0.187	
coma23-29	3917	20.175 ± 0.048	20.008 ± 0.054	19.667 ± 0.056	19.586 ± 0.062	
coma23-88	3918	19.432 ± 0.027	19.602 ± 0.040	19.464 ± 0.050	19.623 ± 0.069	
coma13-51	3920	20.320 ± 0.047	19.938 ± 0.045	19.515 ± 0.041	19.108 ± 0.035	17.866 ± 0.013
coma23-41	3921	19.351 ± 0.023	19.189 ± 0.026	18.995 ± 0.030	18.973 ± 0.035	
coma19-83	3922	20.179 ± 0.037	20.137 ± 0.048	20.047 ± 0.057	20.088 ± 0.076	20.149 ± 0.088
comasw21-105	3923	20.914 ± 0.080	21.007 ± 0.122	20.997 ± 0.159	20.723 ± 0.160	
comasw21-46	3925	18.185 ± 0.009	17.836 ± 0.009	17.024 ± 0.006	16.287 ± 0.004	
comasw22-26	3926	21.322 ± 0.153	21.060 ± 0.166	20.936 ± 0.203	20.833 ± 0.229	
coma23-63	3927	20.383 ± 0.058	20.420 ± 0.079	20.264 ± 0.097	20.267 ± 0.117	
coma23-82	3930	19.356 ± 0.024	19.016 ± 0.024	18.728 ± 0.025	18.634 ± 0.028	
coma19-64	3935	17.361 ± 0.005	17.241 ± 0.005	17.088 ± 0.005	17.067 ± 0.006	16.994 ± 0.006
coma13-128	3937	19.322 ± 0.022	19.163 ± 0.024	18.960 ± 0.028	19.006 ± 0.035	19.090 ± 0.040
comasw6-46	3939	18.797 ± 0.017	18.804 ± 0.022	18.636 ± 0.026	18.719 ± 0.033	
coma23-51	3940	19.179 ± 0.020	18.941 ± 0.021	18.574 ± 0.020	18.553 ± 0.024	
comasw21-53	3943	17.814 ± 0.007	17.623 ± 0.007	17.418 ± 0.008	17.377 ± 0.009	
comasw21-107	3946	19.805 ± 0.033	19.774 ± 0.042	19.707 ± 0.053	19.769 ± 0.070	
coma13-17	3951	19.617 ± 0.028	19.448 ± 0.031	19.266 ± 0.036	19.326 ± 0.045	19.393 ± 0.052
coma19-42	3953	19.270 ± 0.020	19.380 ± 0.027	19.310 ± 0.035	19.499 ± 0.050	19.517 ± 0.051
coma23-68	3954	20.069 ± 0.044	19.931 ± 0.052	19.758 ± 0.062	19.792 ± 0.078	
comasw21-37	3958	16.770 ± 0.004	16.626 ± 0.004	16.475 ± 0.004	16.470 ± 0.004	
coma13-116	3963	20.133 ± 0.042	20.234 ± 0.060	20.162 ± 0.074	20.228 ± 0.095	20.347 ± 0.125
coma23-59	3964	18.514 ± 0.012	18.555 ± 0.016	18.463 ± 0.019	18.529 ± 0.024	
coma13-11	3966	19.771 ± 0.031	19.669 ± 0.037	19.538 ± 0.044	19.545 ± 0.055	19.579 ± 0.066
coma13-100	3969	19.188 ± 0.019	19.082 ± 0.022	18.914 ± 0.025	18.868 ± 0.029	18.694 ± 0.030
coma19-57	3972	17.222 ± 0.004	17.137 ± 0.005	16.997 ± 0.005	16.994 ± 0.006	16.929 ± 0.005
coma13-91	3973	19.216 ± 0.020	19.096 ± 0.024	18.917 ± 0.027	18.884 ± 0.032	18.732 ± 0.028
comasw6-48	3977	19.254 ± 0.025	19.188 ± 0.030	19.029 ± 0.036	19.090 ± 0.046	
coma13-101	3978	19.777 ± 0.030	19.610 ± 0.033	19.387 ± 0.037	19.218 ± 0.038	18.763 ± 0.033
comasw21-58	3980	19.931 ± 0.040	19.869 ± 0.052	19.781 ± 0.065	19.922 ± 0.090	
coma13-125	3982	19.548 ± 0.024	19.491 ± 0.030	19.414 ± 0.037	19.435 ± 0.047	19.359 ± 0.047
coma23-43	3984	20.654 ± 0.071	20.761 ± 0.104	20.798 ± 0.149	21.056 ± 0.231	
comasw11-18	3986	20.264 ± 0.055	20.152 ± 0.066	20.057 ± 0.079	20.284 ± 0.109	20.065 ± 0.184
coma13-15	3987	20.123 ± 0.044	20.372 ± 0.071	20.500 ± 0.110	20.958 ± 0.203	20.575 ± 0.150
coma23-71	3990	21.386 ± 0.138	21.448 ± 0.208	21.446 ± 0.274	21.518 ± 0.378	
coma13-18	3993	19.671 ± 0.027	19.580 ± 0.034	19.499 ± 0.041	19.524 ± 0.053	19.616 ± 0.065
comasw21-51	3997	16.368 ± 0.003	16.205 ± 0.003	16.048 ± 0.003	16.018 ± 0.003	
coma13-12	3998	20.965 ± 0.087	21.193 ± 0.140	21.212 ± 0.160	21.446 ± 0.231	20.665 ± 0.167
coma13-47	3999	20.612 ± 0.063	20.446 ± 0.072	20.267 ± 0.084	20.353 ± 0.111	20.619 ± 0.153
comasw16-62	4001	20.158 ± 0.044	19.880 ± 0.046	19.658 ± 0.051	19.710 ± 0.066	
coma23-70	4002	20.454 ± 0.064	20.567 ± 0.097	20.460 ± 0.119	20.450 ± 0.148	
coma13-107	4003	19.185 ± 0.018	18.929 ± 0.019	18.697 ± 0.020	18.644 ± 0.0[illegible]	18.665 ± 0.025
comasw21-74	4005	20.807 ± 0.042	20.309 ± 0.051	20.171 ± 0.063	20.174 ± 0.079	
coma13-16	4011	21.551 ± 0.155	22.213 ± 0.401	23.840 ± 2.076		21.367 ± 0.316
coma13-9	4016	19.979 ± 0.040	19.780 ± 0.044	19.449 ± 0.044	19.128 ± 0.041	18.391 ± 0.022
comasw16-54	4017	16.872 ± 0.004	16.622 ± 0.004	16.405 ± 0.004	16.304 ± 0.004	
coma12-23	4020	20.464 ± 0.064	20.272 ± 0.071	20.070 ± 0.081	19.980 ± 0.087	
coma18-68	4022	20.285 ± 0.046	20.326 ± 0.066	20.229 ± 0.080	20.331 ± 0.104	20.334 ± 0.121
coma13-10	4024	18.701 ± 0.013	18.492 ± 0.013	18.327 ± 0.015	18.263 ± 0.017	18.069 ± 0.016
comasw6-77	4026	20.990 ± 0.206	20.986 ± 0.282	21.006 ± 0.393	20.712 ± 0.376	
comasw6-28	4028	19.870 ± 0.044	19.917 ± 0.058	19.757 ± 0.070	19.655 ± 0.077	
comasw21-86	4029	19.240 ± 0.019	19.083 ± 0.021	18.867 ± 0.024	18.865 ± 0.028	
comasw11-6	4032	21.133 ± 0.114	20.959 ± 0.143	20.720 ± 0.149	20.663 ± 0.186	20.851 ± 0.336

Raw U-band aperture magnitudes. *contiuned from previous page*

Object	GMP	Aperture Dia. (″) 8.8	13	16	20.2	26
comasw21-77	4033	20.387 ± 0.052	20.555 ± 0.080	20.483 ± 0.104	20.537 ± 0.146	
comasw21-102	4034	19.203 ± 0.019	19.102 ± 0.022	18.938 ± 0.026	18.974 ± 0.033	
comasw21-14	4035	19.107 ± 0.018	18.889 ± 0.019	18.660 ± 0.021	18.631 ± 0.025	
comasw21-35	4037	20.268 ± 0.047	20.075 ± 0.054	19.896 ± 0.061	19.797 ± 0.071	
comasw11-4	4039	19.431 ± 0.031	19.137 ± 0.031	18.887 ± 0.035	18.905 ± 0.041	18.168 ± 0.029
coma12-68	4040	19.121 ± 0.020	19.149 ± 0.025	19.004 ± 0.030	19.117 ± 0.038	19.167 ± 0.049
coma12-49	4042	19.191 ± 0.021	19.008 ± 0.022	18.833 ± 0.025	18.849 ± 0.030	18.826 ± 0.032
coma23-76	4043	17.870 ± 0.009	17.726 ± 0.009	17.581 ± 0.011	17.611 ± 0.013	
comasw21-10	4046	21.360 ± 0.119	20.968 ± 0.121	21.005 ± 0.159	21.264 ± 0.268	
comasw21-11	4046	21.376 ± 0.118	21.084 ± 0.132	20.933 ± 0.147	20.721 ± 0.161	
comasw21-42	4047	20.301 ± 0.047	20.196 ± 0.058	19.951 ± 0.063	19.921 ± 0.075	
comasw16-66	4049	20.456 ± 0.056	20.367 ± 0.070	20.166 ± 0.080	20.223 ± 0.104	
comasw21-43	4051	21.302 ± 0.115	20.937 ± 0.114	20.546 ± 0.108	20.223 ± 0.101	
coma23-85	4052	21.000 ± 0.142	21.101 ± 0.217	21.197 ± 0.322	21.490 ± 0.532	
comasw21-20	4060	18.249 ± 0.010	18.007 ± 0.009	17.743 ± 0.010	17.711 ± 0.011	
coma12-16	4062	20.067 ± 0.042	19.945 ± 0.050	19.770 ± 0.057	19.790 ± 0.072	19.841 ± 0.085
coma13-27	4063	19.782 ± 0.030	19.665 ± 0.036	19.555 ± 0.042	19.510 ± 0.052	19.282 ± 0.045
coma23-26	4065	19.040 ± 0.018	18.828 ± 0.019	18.597 ± 0.021	18.544 ± 0.024	
comasw16-52	4066	21.386 ± 0.128	21.447 ± 0.195	21.487 ± 0.265	21.728 ± 0.431	
coma12-44	4068	20.306 ± 0.047	20.028 ± 0.049	19.870 ± 0.058	19.875 ± 0.075	19.832 ± 0.073
coma23-81	4069	20.510 ± 0.096	20.273 ± 0.112	20.068 ± 0.122	19.761 ± 0.119	
comasw21-19	4072	20.451 ± 0.058	20.215 ± 0.062	19.824 ± 0.060	19.413 ± 0.050	
coma23-44	4073	19.990 ± 0.039	19.926 ± 0.049	19.769 ± 0.059	19.845 ± 0.076	
coma12-45	4075	20.516 ± 0.058	20.147 ± 0.059	19.900 ± 0.061	19.826 ± 0.068	19.760 ± 0.069
comasw11-43	4078	19.438 ± 0.023	19.516 ± 0.032	19.358 ± 0.039	19.432 ± 0.051	19.561 ± 0.064
comasw16-51	4080	20.390 ± 0.053	20.399 ± 0.070	20.214 ± 0.082	20.055 ± 0.086	
coma13-26	4081	19.080 ± 0.017	18.856 ± 0.018	18.669 ± 0.021	18.701 ± 0.025	18.650 ± 0.026
comasw21-69	4083	18.464 ± 0.011	18.298 ± 0.012	18.097 ± 0.013	18.029 ± 0.014	
comasw21-70	4087	20.204 ± 0.045	20.389 ± 0.070	20.418 ± 0.085	20.774 ± 0.120	
comasw16-41	4090	20.433 ± 0.051	19.996 ± 0.049	19.877 ± 0.058	19.883 ± 0.074	
comasw6-23	4093	17.344 ± 0.006	17.328 ± 0.007	17.181 ± 0.008	17.221 ± 0.009	
comasw11-36	4098	20.115 ± 0.044	19.976 ± 0.053	19.820 ± 0.064	19.788 ± 0.076	19.157 ± 0.044
comasw11-48	4101	20.184 ± 0.045	20.046 ± 0.053	19.936 ± 0.067	19.963 ± 0.083	19.936 ± 0.088
comasw21-82	4102	20.569 ± 0.056	20.682 ± 0.079	20.678 ± 0.103	20.875 ± 0.141	
coma12-15	4103	18.322 ± 0.011	18.168 ± 0.011	17.998 ± 0.013	17.996 ± 0.015	17.912 ± 0.015
coma12-10	4108	19.983 ± 0.037	19.915 ± 0.046	19.861 ± 0.054	19.774 ± 0.062	19.426 ± 0.058
coma18-65	4109	20.134 ± 0.044	20.230 ± 0.061	20.148 ± 0.077	20.216 ± 0.098	19.093 ± 0.038
coma23-1	4109	19.866 ± 0.041	19.761 ± 0.052			
coma12-12	4114	20.657 ± 0.076	20.914 ± 0.116	20.737 ± 0.140	20.456 ± 0.135	19.735 ± 0.078
comasw21-71	4116	20.634 ± 0.065	20.681 ± 0.092	20.631 ± 0.125	20.845 ± 0.181	
comasw11-38	4117	17.383 ± 0.004	17.263 ± 0.004	17.126 ± 0.005	17.134 ± 0.006	17.048 ± 0.007
comasw21-64	4118	18.868 ± 0.015	18.635 ± 0.015	18.384 ± 0.016	18.351 ± 0.019	
coma18-62	4126	20.700 ± 0.077	20.558 ± 0.095	20.308 ± 0.102	20.117 ± 0.107	18.141 ± 0.018
comasw21-79	4129	18.967 ± 0.016	18.860 ± 0.019	18.755 ± 0.022	18.804 ± 0.028	
coma18-51	4130	16.614 ± 0.003	16.451 ± 0.003	16.285 ± 0.003	16.247 ± 0.003	16.154 ± 0.003
comasw11-3	4137	20.627 ± 0.137	20.889 ± 0.294	21.035 ± 0.601	21.201 ± 1.032	
coma12-55	4138	20.757 ± 0.080	20.765 ± 0.090	20.541 ± 0.098	20.329 ± 0.101	19.944 ± 0.079
comasw6-73	4140	22.095 ± 0.440	22.263 ± 0.746	22.184 ± 0.919	22.832 ± 2.158	
comasw21-93	4141	19.541 ± 0.025	19.226 ± 0.025	18.945 ± 0.026	18.878 ± 0.030	
comasw6-21	4143	20.092 ± 0.054	19.988 ± 0.064	19.856 ± 0.080	19.918 ± 0.100	
comasw16-24	4146	19.944 ± 0.038	19.980 ± 0.054	19.880 ± 0.066	19.941 ± 0.089	
coma12-47	4148	19.637 ± 0.033	19.680 ± 0.044	19.546 ± 0.053	19.519 ± 0.060	19.185 ± 0.047
comasw21-31	4150	20.212 ± 0.046	20.237 ± 0.063	20.104 ± 0.076	20.268 ± 0.109	

Raw U-band aperture magnitudes. *contiuned from previous page*

Object	GMP	Aperture Dia. (″) 8.8	13	16	20.2	26
coma12-67	4153	19.947 ± 0.039	20.006 ± 0.051	19.889 ± 0.061	20.007 ± 0.077	19.857 ± 0.074
comasw11-29	4154	20.308 ± 0.051	20.380 ± 0.072	20.326 ± 0.098	20.455 ± 0.131	21.233 ± 0.308
comasw11-59	4156	15.262 ± 0.001	15.061 ± 0.001	14.866 ± 0.001	14.877 ± 0.001	14.789 ± 0.001
comasw16-27	4157	19.928 ± 0.039	19.808 ± 0.046	19.613 ± 0.053	19.618 ± 0.065	
comasw6-42	4161	20.486 ± 0.070	20.100 ± 0.068	19.311 ± 0.044	19.082 ± 0.046	
comasw11-10	4162	20.576 ± 0.068	20.438 ± 0.084	20.355 ± 0.106	20.416 ± 0.140	20.652 ± 0.258
coma12-32	4163	20.251 ± 0.053	20.122 ± 0.061	19.944 ± 0.075	20.043 ± 0.102	20.015 ± 0.132
coma12-8	4165	19.952 ± 0.037	19.674 ± 0.038	19.475 ± 0.043	19.491 ± 0.052	19.546 ± 0.069
comasw11-17	4169	19.105 ± 0.037	19.070 ± 0.048	18.931 ± 0.056	18.994 ± 0.068	17.596 ± 0.028
comasw21-72	4175	18.884 ± 0.015	18.765 ± 0.017	18.601 ± 0.019	18.652 ± 0.024	
comasw16-49	4179	19.459 ± 0.025	19.432 ± 0.033	19.332 ± 0.040	19.299 ± 0.049	
comasw16-67	4190	20.279 ± 0.047	20.099 ± 0.054	19.952 ± 0.065	20.034 ± 0.085	
comasw6-38	4192	17.539 ± 0.006	17.236 ± 0.006	16.976 ± 0.006	16.885 ± 0.006	
comasw21-80	4193	19.901 ± 0.034	19.911 ± 0.048	19.897 ± 0.061	19.946 ± 0.085	
coma12-51	4200	17.406 ± 0.006	17.317 ± 0.006	17.184 ± 0.007	17.214 ± 0.008	17.167 ± 0.008
comasw21-83	4205	19.727 ± 0.028	19.579 ± 0.033	19.391 ± 0.037	19.241 ± 0.040	
comasw11-11	4206	17.262 ± 0.005	17.099 ± 0.005	16.930 ± 0.006	16.907 ± 0.007	16.713 ± 0.011
comasw21-103	4207	19.668 ± 0.030	19.745 ± 0.041	19.606 ± 0.051	19.772 ± 0.072	
coma18-84	4208	21.017 ± 0.086	20.660 ± 0.086	20.459 ± 0.098	20.463 ± 0.121	20.783 ± 0.177
comasw16-50	4209	17.493 ± 0.006	17.409 ± 0.006	17.269 ± 0.007	17.276 ± 0.008	
comasw6-11	4211	19.718 ± 0.036	19.525 ± 0.040	19.258 ± 0.043	19.129 ± 0.047	
comasw6-10	4211	20.038 ± 0.048	19.565 ± 0.042	19.306 ± 0.045	19.312 ± 0.056	
comasw21-34	4212	21.091 ± 0.091	21.294 ± 0.154	21.488 ± 0.239	21.622 ± 0.354	
comasw6-50	4215	19.013 ± 0.020	18.918 ± 0.024	18.712 ± 0.027	18.740 ± 0.033	
comasw21-84	4216	19.884 ± 0.033	19.643 ± 0.035	19.411 ± 0.037	19.307 ± 0.040	
comasw21-115	4217	19.605 ± 0.026	19.483 ± 0.030	19.313 ± 0.035	19.337 ± 0.044	
comasw6-14	4220	19.948 ± 0.043	19.860 ± 0.053	19.657 ± 0.060	19.687 ± 0.076	
comasw21-41	4221	20.891 ± 0.078	20.911 ± 0.113	20.993 ± 0.158	21.334 ± 0.282	
comasw6-13	4226	20.676 ± 0.080	19.954 ± 0.059	19.421 ± 0.049	19.114 ± 0.046	
coma12-36	4230	16.488 ± 0.003	16.273 ± 0.003	16.079 ± 0.003	16.013 ± 0.003	15.845 ± 0.003
comasw10-79	4232	18.945 ± 0.015	18.679 ± 0.015	18.411 ± 0.016	18.420 ± 0.019	18.338 ± 0.019
coma12-65	4238	19.560 ± 0.029	19.520 ± 0.036	19.405 ± 0.044	19.531 ± 0.059	19.628 ± 0.077
comasw6-33	4240	21.455 ± 0.162	21.428 ± 0.228	21.433 ± 0.298	21.312 ± 0.348	
comasw21-40	4245	20.869 ± 0.074	20.671 ± 0.089	20.557 ± 0.104	20.566 ± 0.136	
comasw21-54	4246	18.097 ± 0.009	18.050 ± 0.010	17.922 ± 0.011	18.032 ± 0.014	
comasw21-101	4247	19.960 ± 0.037	19.944 ± 0.049	19.736 ± 0.056	19.710 ± 0.067	
coma12-71	4251	20.260 ± 0.051	20.396 ± 0.079	20.340 ± 0.100	20.241 ± 0.122	20.238 ± 0.139
comasw10-24	4253	20.523 ± 0.059	20.705 ± 0.092	20.723 ± 0.132	21.035 ± 0.212	20.267 ± 0.119
comasw10-78	4255	17.108 ± 0.003	16.970 ± 0.003	16.798 ± 0.004	16.826 ± 0.005	16.748 ± 0.005
comasw20-96	4264	19.818 ± 0.501	19.834 ± 0.652	19.736 ± 0.795	19.876 ± 0.980	
comasw16-33	4266	20.546 ± 0.076	20.416 ± 0.092	20.166 ± 0.104	20.093 ± 0.119	
comasw16-63	4268	19.379 ± 0.022	19.235 ± 0.025	19.047 ± 0.029	19.043 ± 0.034	
comasw10-59	4270	21.811 ± 0.130	21.852 ± 0.182	22.067 ± 0.252	22.653 ± 0.290	22.296 ± 1.037
comasw20-33	4271	19.461 ± 0.027	19.619 ± 0.040	19.490 ± 0.050	19.625 ± 0.065	
coma12-60	4275	20.596 ± 0.076	20.540 ± 0.099	20.348 ± 0.112	20.447 ± 0.162	20.802 ± 0.236
coma12-29	4277	19.407 ± 0.023	19.446 ± 0.027	19.289 ± 0.032	19.492 ± 0.043	19.226 ± 0.048
coma18-61	4281	17.370 ± 0.005	17.260 ± 0.005	17.038 ± 0.005	17.054 ± 0.006	16.977 ± 0.006
comasw16-18	4285	20.721 ± 0.072	20.792 ± 0.104	20.728 ± 0.133	20.800 ± 0.178	
coma18-69	4287	19.929 ± 0.035	20.085 ± 0.051	19.991 ± 0.067	20.128 ± 0.089	20.597 ± 0.161
comasw10-101	4291	20.217 ± 0.045	20.276 ± 0.062	20.108 ± 0.074		
coma12-46	4295	20.635 ± 0.068	20.573 ± 0.082	20.447 ± 0.097	20.472 ± 0.122	19.934 ± 0.077
comasw15-49	4303	19.754 ± 0.041	19.572 ± 0.047	19.238 ± 0.051	19.123 ± 0.056	
comasw20-77	4304	20.395 ± 0.055	20.454 ± 0.071	20.338 ± 0.088	20.530 ± 0.117	

Raw U-band aperture magnitudes. *contiuned from previous page*

Object	GMP	Aperture Dia. ('') 8.8	13	16	20.2	26
coma18-75	4308	17.517 ± 0.006	17.275 ± 0.005	17.044 ± 0.006	16.921 ± 0.006	16.502 ± 0.004
comasw21-104	4310	18.863 ± 0.016	18.793 ± 0.019	18.647 ± 0.022	18.686 ± 0.027	
comasw10-63	4312	19.958 ± 0.032	19.803 ± 0.038	19.602 ± 0.044	19.570 ± 0.052	19.573 ± 0.048
coma18-74	4313	16.975 ± 0.004	16.760 ± 0.004	16.559 ± 0.004	16.483 ± 0.004	16.247 ± 0.003
comasw21-114	4314	18.387 ± 0.011	18.204 ± 0.012	18.027 ± 0.013	18.023 ± 0.015	
coma12-17	4315	16.435 ± 0.003	16.260 ± 0.003	16.097 ± 0.003	16.076 ± 0.003	15.971 ± 0.003
comasw15-26	4317	20.737 ± 0.074	20.697 ± 0.104	20.455 ± 0.125	20.393 ± 0.143	
comasw16-83	4320	20.848 ± 0.075	20.809 ± 0.100	20.817 ± 0.136	21.025 ± 0.179	
comasw15-76	4323	20.269 ± 0.048	20.257 ± 0.062	20.093 ± 0.074	20.084 ± 0.088	
comasw21-120	4326	20.465 ± 0.057	20.401 ± 0.078	20.309 ± 0.105	20.474 ± 0.154	
comasw10-77	4329	20.855 ± 0.044	20.371 ± 0.056	20.116 ± 0.064	20.086 ± 0.076	19.937 ± 0.068
comasw10-4	4330	18.291 ± 0.008	18.186 ± 0.010			
comasw20-35	4332	19.692 ± 0.032	19.451 ± 0.034	18.834 ± 0.027	18.061 ± 0.016	
coma12-69	4333	18.917 ± 0.019	18.493 ± 0.016	18.161 ± 0.016	18.119 ± 0.017	17.922 ± 0.013
comasw10-45	4339	19.938 ± 0.031	19.907 ± 0.041	19.785 ± 0.049	19.853 ± 0.064	19.953 ± 0.067
comasw20-36	4341	17.720 ± 0.007	17.629 ± 0.007	17.476 ± 0.008	17.461 ± 0.009	
coma12-56	4345	19.575 ± 0.027	19.509 ± 0.035	19.423 ± 0.040	19.440 ± 0.050	19.452 ± 0.053
comasw20-83	4348	18.222 ± 0.010	18.085 ± 0.011	17.875 ± 0.011	17.887 ± 0.013	
coma12-22	4350	19.368 ± 0.024	19.442 ± 0.032	19.363 ± 0.041	19.602 ± 0.057	19.715 ± 0.077
comasw5-4	4351	16.943 ± 0.005	16.800 ± 0.005	16.572 ± 0.005	16.626 ± 0.006	16.532 ± 0.005
coma12-59	4352	20.567 ± 0.071	20.655 ± 0.112	20.657 ± 0.171	20.601 ± 0.238	20.470 ± 0.189
coma12-40	4355	18.493 ± 0.012	18.377 ± 0.013	18.226 ± 0.015	18.244 ± 0.018	18.186 ± 0.019
comasw24-47	4361	20.564 ± 0.077	20.779 ± 0.129	20.896 ± 0.183	21.447 ± 0.393	
comasw10-72	4363	20.369 ± 0.048	20.223 ± 0.058	20.055 ± 0.069	20.250 ± 0.106	20.098 ± 0.091
comasw15-90	4364	18.355 ± 0.010	17.997 ± 0.010	17.697 ± 0.010	17.594 ± 0.010	
comasw20-54	4366	19.028 ± 0.018	18.904 ± 0.020	18.743 ± 0.023	18.739 ± 0.029	
comasw20-68	4367	18.333 ± 0.011	18.181 ± 0.012	18.023 ± 0.013	17.979 ± 0.015	
coma12-66	4376	19.982 ± 0.038	19.996 ± 0.046	19.878 ± 0.053	19.904 ± 0.062	20.090 ± 0.053
coma18-56	4379	16.629 ± 0.003	16.552 ± 0.003	16.428 ± 0.003	16.440 ± 0.004	16.401 ± 0.004
comasw10-75	4380	19.962 ± 0.033	19.999 ± 0.045	19.830 ± 0.055	19.943 ± 0.072	19.875 ± 0.078
comasw10-28	4381	19.429 ± 0.020	19.286 ± 0.024	19.050 ± 0.027	18.909 ± 0.030	18.738 ± 0.031
comasw10-29	4384	20.196 ± 0.041	20.069 ± 0.048	19.661 ± 0.046	19.243 ± 0.039	18.897 ± 0.035
comasw24-51	4386	20.699 ± 0.098	20.717 ± 0.132	20.677 ± 0.171	20.832 ± 0.245	
comasw15-67	4390	20.117 ± 0.043	19.951 ± 0.049	19.802 ± 0.058	19.885 ± 0.077	
coma18-91	4391	17.400 ± 0.005	17.120 ± 0.005	16.880 ± 0.005	16.791 ± 0.006	16.556 ± 0.005
comasw5-6	4394	18.758 ± 0.015	18.725 ± 0.018	18.619 ± 0.021	18.647 ± 0.027	18.664 ± 0.032
comasw24-42	4395	19.731 ± 0.043	19.805 ± 0.058	19.736 ± 0.077	19.941 ± 0.109	
coma12-54	4396	20.119 ± 0.046	20.171 ± 0.063	20.053 ± 0.080	20.175 ± 0.113	20.275 ± 0.122
comasw24-50	4397	19.963 ± 0.052	19.825 ± 0.060	19.695 ± 0.072	19.868 ± 0.103	
comasw5-39	4402	20.158 ± 0.049	20.202 ± 0.068	20.022 ± 0.079	19.928 ± 0.089	19.512 ± 0.067
comasw10-12	4403	20.633 ± 0.060	20.638 ± 0.083	20.567 ± 0.101	20.802 ± 0.137	20.588 ± 0.174
comasw24-52	4404	20.477 ± 0.082	20.478 ± 0.108	20.527 ± 0.151	20.558 ± 0.194	
comasw5-38	4411	20.201 ± 0.053	20.237 ± 0.072	20.204 ± 0.095	20.288 ± 0.126	19.612 ± 0.072
coma18-80	4412	20.014 ± 0.035	19.857 ± 0.042	19.128 ± 0.050	19.762 ± 0.063	19.695 ± 0.063
comasw24-43	4419	19.601 ± 0.035	19.463 ± 0.041	19.365 ± 0.050	19.424 ± 0.065	
coma12-9	4420	17.943 ± 0.008	17.839 ± 0.009	17.703 ± 0.010	17.738 ± 0.012	17.680 ± 0.013
comasw10-67	4421	19.572 ± 0.023	19.390 ± 0.026	19.193 ± 0.030	19.190 ± 0.037	18.831 ± 0.029
comasw15-96	4423	20.461 ± 0.062	20.616 ± 0.095	20.634 ± 0.138	20.880 ± 0.209	
comasw20-91	4424	19.149 ± 0.019	19.074 ± 0.023	18.859 ± 0.025	18.687 ± 0.026	
comasw15-66	4428	20.279 ± 0.050	20.054 ± 0.055	19.872 ± 0.063	19.860 ± 0.077	
comasw20-47	4431	20.166 ± 0.047	20.118 ± 0.061	20.021 ± 0.075	20.090 ± 0.099	
comasw10-46	4436	19.630 ± 0.027	19.731 ± 0.038	19.580 ± 0.048	19.756 ± 0.066	19.593 ± 0.066
comasw20-63	4438	18.835 ± 0.016	18.939 ± 0.022	18.828 ± 0.027	18.971 ± 0.037	

Raw U-band aperture magnitudes. *contiuned from previous page*

Object	GMP	Aperture Dia. ('') 8.8	13	16	20.2	26
coma18-50	4441	20.424 ± 0.050	20.418 ± 0.062	20.264 ± 0.072	20.417 ± 0.096	20.623 ± 0.142
coma18-89	4442	18.494 ± 0.011	18.507 ± 0.014	18.382 ± 0.016	18.513 ± 0.022	18.395 ± 0.023
comasw24-41	4445	19.942 ± 0.052	20.171 ± 0.081	20.154 ± 0.110	20.357 ± 0.159	
comasw10-73	4447	18.246 ± 0.007	18.128 ± 0.009	17.996 ± 0.010	18.029 ± 0.013	17.953 ± 0.013
comasw5-34	4448	20.210 ± 0.053	20.345 ± 0.078	20.341 ± 0.108	20.481 ± 0.148	20.703 ± 0.192
comasw24-53	4450	20.453 ± 0.076	20.318 ± 0.088	20.110 ± 0.099	20.020 ± 0.112	
coma12-43	4451	19.733 ± 0.033	19.771 ± 0.043	19.660 ± 0.055	19.763 ± 0.077	19.834 ± 0.090
comasw10-18	4452	20.399 ± 0.053	20.388 ± 0.070	20.335 ± 0.094	20.521 ± 0.135	20.082 ± 0.092
coma18-70	4455	19.917 ± 0.033	19.979 ± 0.047	19.856 ± 0.060	19.950 ± 0.086	19.968 ± 0.079
coma12-14	4458	20.266 ± 0.053	20.298 ± 0.070	20.124 ± 0.084	20.188 ± 0.106	20.976 ± 0.240
comasw10-87	4469	18.610 ± 0.010	18.289 ± 0.010	18.062 ± 0.010	18.021 ± 0.013	17.895 ± 0.012
comasw5-52	4479	18.271 ± 0.010	18.031 ± 0.010	17.835 ± 0.011	17.813 ± 0.013	17.700 ± 0.013
coma18-77	4480	19.144 ± 0.018	19.267 ± 0.024	19.146 ± 0.029	19.270 ± 0.038	19.187 ± 0.039
coma12-34	4481	18.033 ± 0.009	18.102 ± 0.011	17.965 ± 0.013	18.091 ± 0.017	18.037 ± 0.016
comasw20-64	4483	20.030 ± 0.048	20.128 ± 0.069	20.083 ± 0.092	20.215 ± 0.127	
comasw5-28	4484	20.670 ± 0.077	20.503 ± 0.089	20.328 ± 0.103	20.261 ± 0.120	20.363 ± 0.140
comasw20-45	4485	20.309 ± 0.049	20.216 ± 0.062	20.061 ± 0.071	19.984 ± 0.084	
comasw10-35	4490	20.770 ± 0.076	20.610 ± 0.089	20.526 ± 0.115	20.692 ± 0.165	20.185 ± 0.110
comasw10-99	4491	20.366 ± 0.047	20.331 ± 0.062	20.221 ± 0.078	20.333 ± 0.118	20.751 ± 0.175
coma12-2	4493	20.496 ± 0.062	20.329 ± 0.075	20.154 ± 0.082		
comasw20-65	4499	16.868 ± 0.004	16.722 ± 0.004	16.572 ± 0.004	16.562 ± 0.005	
comasw20-67	4500	19.954 ± 0.044	19.880 ± 0.055	19.768 ± 0.067	19.838 ± 0.090	
comasw15-63	4502	18.500 ± 0.011	18.352 ± 0.012	18.214 ± 0.014	18.250 ± 0.017	
coma12-18	4503	18.146 ± 0.010	17.847 ± 0.009	17.576 ± 0.009	17.453 ± 0.010	17.190 ± 0.008
coma18-82	4504	20.064 ± 0.036	20.006 ± 0.045	19.802 ± 0.052	19.809 ± 0.063	19.796 ± 0.067
comasw15-38	4506	17.890 ± 0.007	17.781 ± 0.008	17.674 ± 0.009	17.703 ± 0.012	
comasw15-41	4508	18.798 ± 0.016	18.943 ± 0.022	18.841 ± 0.029	18.985 ± 0.038	
comasw15-47	4509	20.350 ± 0.057	20.350 ± 0.074	20.060 ± 0.080	20.008 ± 0.091	
coma12-20	4510	18.734 ± 0.015	18.615 ± 0.017	18.460 ± 0.020	18.498 ± 0.024	18.270 ± 0.020
comasw20-58	4515	19.502 ± 0.030	19.500 ± 0.040	19.382 ± 0.049	19.465 ± 0.066	
comasw20-87	4516	18.422 ± 0.011	18.387 ± 0.014	18.267 ± 0.016	18.230 ± 0.019	
comasw20-88	4519	18.150 ± 0.009	17.998 ± 0.010	17.818 ± 0.011	17.801 ± 0.013	
comasw10-44	4522	17.290 ± 0.003	17.022 ± 0.003	16.779 ± 0.004	16.674 ± 0.004	16.470 ± 0.004
comasw10-47	4524	19.658 ± 0.026	19.448 ± 0.028	19.252 ± 0.033	19.351 ± 0.044	19.478 ± 0.058
comasw20-71	4529	20.401 ± 0.055	20.189 ± 0.064	19.987 ± 0.070	19.881 ± 0.078	
comasw5-53	4530	17.975 ± 0.009	17.836 ± 0.009	17.646 ± 0.010	17.738 ± 0.013	17.747 ± 0.014
comasw20-55	4531	19.332 ± 0.023	19.298 ± 0.029	19.238 ± 0.036	19.269 ± 0.047	
comasw10-19	4535	18.283 ± 0.007	18.198 ± 0.009	18.039 ± 0.010	18.070 ± 0.013	18.029 ± 0.014
comasw10-97	4538	20.099 ± 0.037	20.264 ± 0.054	20.168 ± 0.067	20.396 ± 0.091	20.339 ± 0.121
comasw20-86	4539	19.319 ± 0.026	19.221 ± 0.031	19.058 ± 0.036	19.086 ± 0.048	
comasw15-74	4541	20.788 ± 0.061	20.469 ± 0.067	20.186 ± 0.073	20.142 ± 0.088	
comasw5-32	4545	20.045 ± 0.044	19.793 ± 0.046	19.638 ± 0.054	19.589 ± 0.064	19.701 ± 0.080
comasw23-46	4553	19.408 ± 0.029	19.341 ± 0.036	19.256 ± 0.046	19.445 ± 0.066	
comasw5-16	4554	20.523 ± 0.065	20.413 ± 0.083	20.255 ± 0.094	20.237 ± 0.118	20.377 ± 0.151
comasw26-27	4555	16.785 ± 0.004	16.533 ± 0.004	16.256 ± 0.003	16.243 ± 0.004	
comasw15-60	4557	19.753 ± 0.031	19.774 ± 0.041	19.689 ± 0.051	19.807 ± 0.070	
comasw26-40	4558	19.705 ± 0.031	19.659 ± 0.037	19.462 ± 0.043	19.608 ± 0.057	
comasw10-98	4559	19.644 ± 0.027	19.730 ± 0.038	19.620 ± 0.050	19.760 ± 0.069	20.340 ± 0.115
comasw23-50	4561	20.138 ± 0.055	20.061 ± 0.068	19.923 ± 0.083	19.933 ± 0.103	
comasw15-95	4562	22.089 ± 0.221	21.743 ± 0.268	21.779 ± 0.316	21.863 ± 0.652	
comasw23-58	4563	19.401 ± 0.029	19.445 ± 0.039	19.310 ± 0.047	19.355 ± 0.060	
comasw5-15	4565	19.516 ± 0.029	19.544 ± 0.038	19.462 ± 0.048	19.535 ± 0.063	19.848 ± 0.093
comasw19-40	4566	18.910 ± 0.027	18.782 ± 0.033	18.644 ± 0.039	18.633 ± 0.048	18.447 ± 0.042

Raw U-band aperture magnitudes. *contiuned from previous page*

Object	GMP	Aperture Dia. ('') 8.8	13	16	20.2	26
comasw10-11	4568	18.262 ± 0.008	18.262 ± 0.010	18.092 ± 0.012	18.103 ± 0.014	17.800 ± 0.013
comasw23-47	4569	20.858 ± 0.112	20.861 ± 0.154	20.945 ± 0.225	21.609 ± 0.521	
comasw23-82	4570	17.169 ± 0.006	17.055 ± 0.006	16.775 ± 0.006	16.831 ± 0.007	
comasw5-47	4572	20.054 ± 0.048	20.046 ± 0.063	19.864 ± 0.073	19.925 ± 0.095	19.789 ± 0.084
comasw15-22	4573	20.562 ± 0.066	20.557 ± 0.088	20.430 ± 0.109	20.443 ± 0.134	
comasw10-10	4577	18.316 ± 0.008	18.285 ± 0.010	18.098 ± 0.012	18.116 ± 0.014	17.844 ± 0.013
comasw4-28	4578	18.599 ± 0.013	18.403 ± 0.013	18.202 ± 0.015	18.172 ± 0.018	18.168 ± 0.019
comasw10-92	4579	17.189 ± 0.003	17.074 ± 0.004	16.817 ± 0.004	16.819 ± 0.005	16.671 ± 0.004
comasw15-29	4580	21.015 ± 0.110	20.991 ± 0.147	21.074 ± 0.216	21.933 ± 0.595	
comasw15-25	4592	17.578 ± 0.006	17.368 ± 0.006	17.189 ± 0.006	17.104 ± 0.007	
comasw15-33	4593	19.115 ± 0.019	19.098 ± 0.024	18.957 ± 0.029	19.093 ± 0.039	
comasw10-34	4597	17.898 ± 0.006	17.624 ± 0.006	17.304 ± 0.006	17.116 ± 0.006	16.865 ± 0.005
comasw26-22	4600	19.684 ± 0.030	19.565 ± 0.034	19.372 ± 0.038	19.341 ± 0.044	
comasw15-73	4602	18.928 ± 0.016	18.673 ± 0.016	18.430 ± 0.017	18.365 ± 0.020	
comasw23-66	4606	19.622 ± 0.034	19.521 ± 0.041	19.420 ± 0.051	19.491 ± 0.068	
comasw19-33	4608	19.981 ± 0.066	19.953 ± 0.084	19.824 ± 0.106	19.893 ± 0.136	21.668 ± 0.782
comasw10-86	4609	20.781 ± 0.071	20.756 ± 0.093	20.640 ± 0.111	20.573 ± 0.127	20.792 ± 0.156
comasw15-93	4612	19.398 ± 0.025	19.289 ± 0.030	19.183 ± 0.037	19.235 ± 0.050	
comasw23-88	4614	20.017 ± 0.054				
comasw15-70	4615	20.244 ± 0.050	20.337 ± 0.071	20.150 ± 0.084	20.403 ± 0.127	
comasw10-9	4618	21.036 ± 0.085	20.908 ± 0.104	20.788 ± 0.129	20.834 ± 0.166	21.389 ± 0.323
comasw15-34	4619	19.964 ± 0.037	20.050 ± 0.053	20.026 ± 0.071	20.125 ± 0.096	
comasw23-33	4620	19.809 ± 0.044	19.952 ± 0.064	19.867 ± 0.085	20.282 ± 0.146	
comasw23-87	4622	21.111 ± 0.163	21.156 ± 0.277			
comasw19-50	4624	20.144 ± 0.077	19.970 ± 0.093	19.810 ± 0.105	19.698 ± 0.120	19.419 ± 0.104
comasw19-61	4626	17.537 ± 0.010	17.377 ± 0.011	17.206 ± 0.013	17.177 ± 0.015	17.067 ± 0.013
comasw10-62	4628	20.146 ± 0.039	19.990 ± 0.047	19.825 ± 0.056	19.898 ± 0.073	19.905 ± 0.078
comasw10-42	4630	19.235 ± 0.017	19.281 ± 0.025	19.221 ± 0.031	19.330 ± 0.042	19.291 ± 0.046
comasw15-44	4632	18.716 ± 0.013	18.587 ± 0.015	18.403 ± 0.017	18.397 ± 0.020	
comasw10-53	4636	19.813 ± 0.031	19.842 ± 0.042	19.590 ± 0.048	19.462 ± 0.053	19.189 ± 0.045
comasw15-36	4642	20.055 ± 0.040	20.110 ± 0.057	20.086 ± 0.075	20.259 ± 0.110	
comasw10-54	4643	19.976 ± 0.036	19.663 ± 0.037	19.368 ± 0.039	19.186 ± 0.041	18.913 ± 0.037
comasw4-27	4645	20.622 ± 0.072	20.663 ± 0.102	20.629 ± 0.139	20.800 ± 0.232	20.610 ± 0.164
comasw10-33	4646	19.800 ± 0.028	19.796 ± 0.039	19.605 ± 0.048	19.700 ± 0.061	19.782 ± 0.079
comasw10-32	4646	19.793 ± 0.028	19.810 ± 0.039	19.653 ± 0.048	19.773 ± 0.061	19.631 ± 0.079
comasw23-80	4647	19.422 ± 0.030	19.445 ± 0.040	19.389 ± 0.051	19.534 ± 0.070	
comasw23-31	4653	16.832 ± 0.004	16.642 ± 0.004	16.453 ± 0.004	16.397 ± 0.005	
comasw15-87	4655	18.690 ± 0.013	18.511 ± 0.015	18.315 ± 0.016	18.265 ± 0.019	
comasw19-25	4656	18.109 ± 0.014	17.973 ± 0.016	17.810 ± 0.018	17.826 ± 0.022	17.773 ± 0.025
comasw19-57	4657	20.615 ± 0.124	20.601 ± 0.138	20.496 ± 0.152	20.672 ± 0.209	19.707 ± 0.137
comasw19-51	4659	19.757 ± 0.060	19.637 ± 0.073	19.480 ± 0.082	19.521 ± 0.102	18.938 ± 0.070
comasw26-38	4660	19.664 ± 0.029	19.707 ± 0.037	19.590 ± 0.045	19.627 ± 0.056	
comasw10-36	4662	19.658 ± 0.025	19.716 ± 0.035	19.571 ± 0.043	19.663 ± 0.058	19.574 ± 0.065
comasw19-45	4664	16.876 ± 0.006	16.781 ± 0.006	16.640 ± 0.007	16.634 ± 0.008	16.538 ± 0.008
comasw26-69	4666	18.121 ± 0.009	17.928 ± 0.009	17.726 ± 0.009	17.696 ± 0.011	
comasw10-5	4667	20.477 ± 0.059	20.636 ± 0.093	20.647 ± 0.127	20.701 ± 0.164	20.113 ± 0.071
comasw4-16	4669	21.210 ± 0.114	21.114 ± 0.155	20.957 ± 0.187	21.129 ± 0.316	22.534 ± 1.505
comasw15-77	4670	20.350 ± 0.060	20.473 ± 0.088	20.365 ± 0.116	20.070 ± 0.121	
comasw4-1	4675	20.456 ± 0.071	20.599 ± 0.117	20.596 ± 0.179	20.852 ± 0.318	20.395 ± 0.176
comasw23-59	4676	20.475 ± 0.070	20.324 ± 0.083	20.175 ± 0.100	20.167 ± 0.121	
comasw19-20	4679	17.506 ± 0.009	17.235 ± 0.009	16.993 ± 0.009	16.898 ± 0.010	16.694 ± 0.009
comasw4-45	4682	19.397 ± 0.026	19.068 ± 0.025	18.771 ± 0.026	18.734 ± 0.030	18.718 ± 0.032
comasw26-24	4686	20.119 ± 0.043	20.137 ± 0.054	19.956 ± 0.063	20.047 ± 0.081	

Raw U-band aperture magnitudes. *contiuned from previous page*

Object	GMP	Aperture Dia. ('') 8.8	13	16	20.2	26
comasw23-42	4689	18.674 ± 0.016	18.640 ± 0.019	18.473 ± 0.023	18.529 ± 0.028	
comasw19-24	4690	20.252 ± 0.086	20.244 ± 0.122	20.134 ± 0.156	20.311 ± 0.239	19.498 ± 0.116
comasw4-51	4692	18.107 ± 0.009	17.905 ± 0.009	17.708 ± 0.010	17.696 ± 0.012	17.599 ± 0.011
comasw10-84	4696	19.287 ± 0.019				
comasw14-54	4699	19.813 ± 0.037	19.790 ± 0.051	19.671 ± 0.063	19.732 ± 0.086	
comasw23-57	4706	20.117 ± 0.054	20.361 ± 0.086	20.283 ± 0.115	20.434 ± 0.157	
comasw10-13	4709	20.362 ± 0.054				
comasw26-48	4711	20.649 ± 0.064	20.707 ± 0.088	20.616 ± 0.107	20.550 ± 0.125	
comasw4-73	4712	20.457 ± 0.064	20.326 ± 0.078	20.151 ± 0.088	20.224 ± 0.114	20.299 ± 0.134
comasw14-1	4714	18.055 ± 0.009	17.955 ± 0.010	17.803 ± 0.011	17.823 ± 0.014	
comasw14-19	4715	19.027 ± 0.018	18.877 ± 0.021	18.739 ± 0.025	18.769 ± 0.031	
comasw19-35	4718	18.789 ± 0.025	18.505 ± 0.025	18.264 ± 0.028	18.220 ± 0.032	18.005 ± 0.028
comasw14-26	4719	18.414 ± 0.011	18.299 ± 0.012	18.159 ± 0.014	18.136 ± 0.017	
comasw14-34	4725	20.091 ± 0.045	20.182 ± 0.061	20.078 ± 0.073	20.243 ± 0.097	
comasw19-34	4727	19.979 ± 0.074	19.735 ± 0.081	19.323 ± 0.075	18.989 ± 0.065	18.460 ± 0.043
comasw26-66	4733	20.342 ± 0.051	20.389 ± 0.068	20.327 ± 0.087	20.384 ± 0.111	
comasw14-37	4735	20.128 ± 0.045	20.089 ± 0.055	19.950 ± 0.064	19.942 ± 0.072	
comasw9-63	4739	20.698 ± 0.064	20.783 ± 0.096	20.875 ± 0.142	21.187 ± 0.239	20.588 ± 0.137
comasw9-54	4740	21.500 ± 0.120	21.727 ± 0.217	21.872 ± 0.313	22.137 ± 0.539	21.755 ± 0.388
comasw23-35	4742	20.920 ± 0.102				
comasw26-23	4745	19.998 ± 0.038	19.847 ± 0.041	19.692 ± 0.048	19.684 ± 0.058	
comasw9-69	4749	19.703 ± 0.025	19.610 ± 0.031	19.428 ± 0.036	19.424 ± 0.044	19.379 ± 0.044
comasw27-61	4752	20.799 ± 0.784	20.809 ± 1.081	20.695 ± 1.439	21.001 ± 2.305	
comasw14-41	4753	21.459 ± 0.129	21.420 ± 0.174	21.403 ± 0.260	21.666 ± 0.412	
comasw14-13	4757	18.691 ± 0.014	18.675 ± 0.017	18.594 ± 0.020	18.633 ± 0.026	
comasw26-70	4758	19.594 ± 0.027	19.369 ± 0.028	19.066 ± 0.027	18.880 ± 0.028	
comasw23-86	4759	21.188 ± 0.140	21.148 ± 0.179	21.027 ± 0.225	21.334 ± 0.496	
comasw19-59	4761	21.062 ± 0.168	20.934 ± 0.202	20.561 ± 0.197	20.348 ± 0.195	20.024 ± 0.175
comasw26-71	4762	19.601 ± 0.026	19.358 ± 0.027	19.071 ± 0.027	18.870 ± 0.028	
comasw14-10	4763	20.644 ± 0.069	20.773 ± 0.099	20.733 ± 0.122	20.896 ± 0.151	
comasw19-18	4766	18.288 ± 0.017	17.912 ± 0.016	17.600 ± 0.016	17.563 ± 0.018	17.497 ± 0.018
comasw4-68	4768	19.546 ± 0.027	19.410 ± 0.031	19.233 ± 0.036	19.205 ± 0.043	19.144 ± 0.045
comasw23-25	4773	21.279 ± 0.138	21.214 ± 0.183	20.929 ± 0.192	21.007 ± 0.258	
comasw26-19	4774	18.948 ± 0.017	18.668 ± 0.016	18.422 ± 0.017	18.349 ± 0.018	
comasw23-55	4775	20.429 ± 0.066	20.159 ± 0.070	19.902 ± 0.076	19.904 ± 0.094	
comasw26-34	4779	18.007 ± 0.008	17.744 ± 0.008	17.520 ± 0.008	17.461 ± 0.009	
comasw14-35	4780	18.959 ± 0.017	18.925 ± 0.021	18.849 ± 0.026	18.887 ± 0.033	
comasw26-77	4782	20.002 ± 0.040	20.049 ± 0.055	19.999 ± 0.072	20.124 ± 0.100	
comasw26-15	4783	19.187 ± 0.021	19.298 ± 0.027	19.136 ± 0.032	19.276 ± 0.043	
comasw9-28	4784	20.425 ± 0.046	20.623 ± 0.073	20.546 ± 0.096	20.828 ± 0.150	21.060 ± 0.207
comasw9-42	4792	17.240 ± 0.003	17.107 ± 0.004	16.974 ± 0.004	16.980 ± 0.005	16.904 ± 0.005
comasw9-37	4794	16.495 ± 0.002	16.312 ± 0.002	16.149 ± 0.002	16.105 ± 0.002	15.998 ± 0.002
comasw9-46	4795	22.330 ± 0.284	22.645 ± 0.560	22.428 ± 0.590	22.629 ± 0.953	20.592 ± 0.139
comasw4-55	4797	20.038 ± 0.038	20.083 ± 0.054	20.028 ± 0.068	20.076 ± 0.093	19.671 ± 0.070
comasw4-8	4800	18.367 ± 0.011	18.109 ± 0.010	17.895 ± 0.011	17.982 ± 0.014	17.969 ± 0.015
comasw23-53	4801	20.468 ± 0.071	20.255 ± 0.079	19.974 ± 0.084	19.752 ± 0.085	
comasw26-43	4805	20.295 ± 0.047	20.064 ± 0.050	19.834 ± 0.055	19.835 ± 0.064	
comasw9-77	4808	20.881 ± 0.072	20.972 ± 0.107	21.000 ± 0.150	21.125 ± 0.211	20.780 ± 0.159
comasw14-42	4809	20.591 ± 0.069	20.907 ± 0.121	20.973 ± 0.176	21.266 ± 0.286	
comasw23-51	4811	20.249 ± 0.060	20.110 ± 0.069	19.805 ± 0.073	19.627 ± 0.075	
comasw9-45	4813	20.095 ± 0.042	20.291 ± 0.069	20.388 ± 0.103	20.912 ± 0.208	20.235 ± 0.102
comasw19-21	4814	19.936 ± 0.078	20.102 ± 0.119	20.064 ± 0.162	20.261 ± 0.235	19.548 ± 0.118
comasw4-3	4815	18.773 ± 0.016	18.698 ± 0.019	18.591 ± 0.023	18.647 ± 0.030	18.397 ± 0.023

Raw U-band aperture magnitudes. *contiuned from previous page*

Object	GMP	Aperture Dia. (″) 8.8	13	16	20.2	26
comasw23-3	4821	20.268 ± 0.062	20.462 ± 0.097	20.329 ± 0.120	20.267 ± 0.137	
comasw9-41	4825	19.370 ± 0.022	19.365 ± 0.029	19.209 ± 0.035	18.938 ± 0.033	18.691 ± 0.027
comasw14-20	4829	16.272 ± 0.003	16.064 ± 0.003	15.884 ± 0.003	15.822 ± 0.003	
comasw26-49	4833	20.940 ± 0.082	21.120 ± 0.110	21.204 ± 0.157	21.624 ± 0.274	
comasw27-45	4833	21.129 ± 0.097	21.278 ± 0.151	21.440 ± 0.229	22.232 ± 0.601	
comasw19-56	4835	20.073 ± 0.077	20.142 ± 0.103	19.985 ± 0.122	20.048 ± 0.151	19.706 ± 0.129
comasw26-10	4837	19.101 ± 0.020	18.892 ± 0.021	18.672 ± 0.023	18.634 ± 0.027	
comasw26-13	4838	19.792 ± 0.035	19.675 ± 0.041	19.478 ± 0.046	19.341 ± 0.051	
comasw4-12	4845	20.504 ± 0.064	20.325 ± 0.073	20.160 ± 0.085	20.135 ± 0.103	19.919 ± 0.089
comasw4-59	4846	19.250 ± 0.020	19.194 ± 0.025	19.099 ± 0.030	19.145 ± 0.038	19.222 ± 0.043
comasw4-29	4848	19.979 ± 0.038	19.761 ± 0.043	19.610 ± 0.049	19.467 ± 0.055	19.385 ± 0.054
comasw4-44	4851	19.801 ± 0.034	19.877 ± 0.047	19.719 ± 0.056	19.601 ± 0.060	19.750 ± 0.073
comasw9-70	4852	18.656 ± 0.010	18.628 ± 0.013	18.532 ± 0.016	18.580 ± 0.021	18.614 ± 0.026
comasw4-22	4855	19.288 ± 0.021	19.022 ± 0.022	18.793 ± 0.024	18.690 ± 0.027	18.561 ± 0.026
comasw4-72	4858	19.165 ± 0.019	18.993 ± 0.022	18.838 ± 0.025	18.878 ± 0.032	18.944 ± 0.037
comasw27-25	4865	20.093 ± 0.040	20.019 ± 0.047	19.826 ± 0.055	19.900 ± 0.069	
comasw14-66	4867	21.043 ± 0.106	21.082 ± 0.151	21.073 ± 0.204	21.333 ± 0.323	
comasw14-16	4868	21.013 ± 0.104	21.313 ± 0.187	21.635 ± 0.332	22.769 ± 1.199	
comasw27-16	4869	19.780 ± 0.029	19.684 ± 0.033	19.550 ± 0.040	19.624 ± 0.051	
comasw4-41	4870	20.394 ± 0.056	20.299 ± 0.069	20.188 ± 0.084	20.319 ± 0.118	21.058 ± 0.250
comasw23-73	4871	18.544 ± 0.015	18.646 ± 0.020	18.518 ± 0.024	18.626 ± 0.031	
comasw9-75	4878	20.323 ± 0.043	20.372 ± 0.061	20.258 ± 0.077	20.428 ± 0.109	20.711 ± 0.154
comasw14-67	4879	18.738 ± 0.015	18.579 ± 0.017	18.409 ± 0.019	18.426 ± 0.024	
comasw27-36	4880	19.537 ± 0.025	19.451 ± 0.028	19.262 ± 0.033	19.340 ± 0.041	
comasw27-32	4882	20.418 ± 0.051	20.331 ± 0.063	20.295 ± 0.080	20.418 ± 0.113	
comasw9-67	4887	19.771 ± 0.026	19.779 ± 0.035	19.671 ± 0.044	19.774 ± 0.060	20.264 ± 0.117
comasw14-38	4888	18.568 ± 0.012	18.435 ± 0.014	18.255 ± 0.016	18.271 ± 0.019	
comasw4-13	4893	19.646 ± 0.030	19.661 ± 0.038	19.548 ± 0.048	19.700 ± 0.065	20.143 ± 0.113
comasw14-79	4896	20.317 ± 0.052	20.324 ± 0.073	20.227 ± 0.089	20.230 ± 0.125	
comasw18-56	4897	20.338 ± 0.050	20.198 ± 0.067	20.031 ± 0.080	20.167 ± 0.119	
comasw14-51	4905	18.335 ± 0.011	18.196 ± 0.012	17.994 ± 0.013	18.042 ± 0.016	
comasw8-50	4907	16.728 ± 0.003	16.605 ± 0.003	16.462 ± 0.004	16.458 ± 0.004	
comasw14-53	4911	21.376 ± 0.133	20.998 ± 0.136	20.917 ± 0.166	21.125 ± 0.260	
comasw18-66	4913	20.436 ± 0.056	20.501 ± 0.078	20.349 ± 0.097	20.488 ± 0.126	
comasw23-37	4916	20.258 ± 0.057	20.259 ± 0.076	20.133 ± 0.095	20.286 ± 0.132	
comasw3-87	4918	16.493 ± 0.003	16.378 ± 0.003	16.175 ± 0.003	16.186 ± 0.004	16.082 ± 0.003
comasw3-65	4919	20.599 ± 0.073	20.756 ± 0.128	20.771 ± 0.168	20.858 ± 0.214	20.533 ± 0.132
comasw3-19	4926	18.265 ± 0.010	18.131 ± 0.011	17.980 ± 0.013	17.940 ± 0.015	17.806 ± 0.013
comasw18-55	4927	21.064 ± 0.092	21.128 ± 0.134	20.976 ± 0.150	20.979 ± 0.171	
comasw8-38	4928	16.160 ± 0.003	15.836 ± 0.003	15.603 ± 0.002	15.474 ± 0.003	
comasw3-39	4930	19.760 ± 0.033	19.811 ± 0.045	19.658 ± 0.055	19.748 ± 0.070	19.787 ± 0.080
comasw3-53	4931	19.911 ± 0.036	19.927 ± 0.048	19.782 ± 0.058	19.892 ± 0.082	20.125 ± 0.097
comasw18-24	4933	17.642 ± 0.007	17.395 ± 0.006	17.154 ± 0.007	17.048 ± 0.007	
comasw27-38	4934	19.392 ± 0.022	19.449 ± 0.029	19.347 ± 0.036	19.413 ± 0.045	
comasw18-52	4935	20.192 ± 0.047	20.072 ± 0.053	19.991 ± 0.065	20.084 ± 0.083	
comasw8-51	4937	18.803 ± 0.014	18.676 ± 0.016	18.534 ± 0.018	18.573 ± 0.023	
comasw18-18	4940	20.321 ± 0.051	20.177 ± 0.058	19.920 ± 0.067	19.913 ± 0.083	
comasw19-60	4945	17.163 ± 0.007	17.056 ± 0.008	16.892 ± 0.009	16.899 ± 0.010	16.886 ± 0.011
comasw18-48	4948	20.806 ± 0.079	20.217 ± 0.063	19.965 ± 0.069	20.009 ± 0.088	
comasw18-68	4953	18.682 ± 0.013	18.483 ± 0.014	18.328 ± 0.016	18.311 ± 0.019	
comasw3-68	4954	21.170 ± 0.103	21.166 ± 0.155	21.108 ± 0.204	21.206 ± 0.338	22.371 ± 0.794
comasw3-91	4956	19.035 ± 0.019	18.974 ± 0.022	18.834 ± 0.026	18.899 ± 0.034	18.802 ± 0.029
comasw14-17	4960	20.223 ± 0.051	20.407 ± 0.082	20.330 ± 0.103	20.399 ± 0.139	

Raw U-band aperture magnitudes. *contiuned from previous page*

Object	GMP	Aperture Dia. (″) 8.8	13	16	20.2	26
comasw3-73	4962	19.623 ± 0.028	19.754 ± 0.039	19.625 ± 0.047	19.771 ± 0.062	19.933 ± 0.081
comasw14-15	4967	18.533 ± 0.012	18.416 ± 0.014	18.243 ± 0.015	18.268 ± 0.019	
comasw27-51	4968	19.849 ± 0.031	19.972 ± 0.043	19.801 ± 0.051	19.736 ± 0.057	
comasw18-46	4974	17.058 ± 0.005	16.901 ± 0.004	16.722 ± 0.005	16.742 ± 0.005	
comasw3-41	4978	20.318 ± 0.053	20.343 ± 0.072	20.122 ± 0.082	20.177 ± 0.104	20.178 ± 0.109
comasw23-68	4981	19.706 ± 0.037	19.619 ± 0.043	19.463 ± 0.051	19.596 ± 0.071	
comasw23-30	4986	19.960 ± 0.047	20.116 ± 0.070	20.089 ± 0.094	20.276 ± 0.129	
comasw14-22	4987	17.283 ± 0.005	17.239 ± 0.006	17.132 ± 0.006	17.162 ± 0.007	
comasw23-72	4988	20.629 ± 0.079	20.793 ± 0.125	20.806 ± 0.160	20.749 ± 0.182	
comasw3-7	4992	19.735 ± 0.031	19.859 ± 0.043	19.757 ± 0.056	19.907 ± 0.076	19.790 ± 0.075
comasw23-40	4993	19.408 ± 0.028	19.476 ± 0.039	19.341 ± 0.050	19.494 ± 0.069	
comasw14-77	4995	19.548 ± 0.026	19.308 ± 0.027	19.082 ± 0.030	19.001 ± 0.035	
comasw23-76	4997	19.374 ± 0.027	19.375 ± 0.037	19.280 ± 0.048	19.423 ± 0.063	
comasw9-48	5004	21.917 ± 0.169	21.956 ± 0.251	21.927 ± 0.326	21.906 ± 0.412	
comasw25-70	5007	19.900 ± 0.048	19.997 ± 0.068	19.993 ± 0.094	20.143 ± 0.131	
comasw14-39	5009	19.340 ± 0.022	19.289 ± 0.028	19.200 ± 0.034	19.261 ± 0.045	
comasw27-52	5010	19.368 ± 0.021	19.179 ± 0.023	18.964 ± 0.025	18.951 ± 0.029	
comasw3-47	5017	20.499 ± 0.066	20.360 ± 0.076	19.935 ± 0.072	19.740 ± 0.072	19.471 ± 0.058
comasw27-34	5018	19.392 ± 0.021	19.152 ± 0.021	18.935 ± 0.023	18.882 ± 0.026	
comasw3-48	5020	20.114 ± 0.047	19.966 ± 0.054	19.683 ± 0.057	19.779 ± 0.077	19.421 ± 0.053
comasw3-38	5026	20.582 ± 0.065	20.362 ± 0.071	20.189 ± 0.083	20.180 ± 0.101	20.668 ± 0.182
comasw25-66	5029	19.550 ± 0.034	19.549 ± 0.043	19.375 ± 0.051	19.398 ± 0.063	
comasw18-58	5030	20.526 ± 0.069	20.643 ± 0.099	20.561 ± 0.132	20.544 ± 0.171	
comasw8-33	5031	20.416 ± 0.052	20.189 ± 0.057	19.840 ± 0.057	19.527 ± 0.052	
comasw8-55	5033	19.794 ± 0.028	19.700 ± 0.034	19.578 ± 0.040	19.658 ± 0.054	
comasw8-45	5034	20.307 ± 0.047	20.137 ± 0.054	19.909 ± 0.059	19.836 ± 0.068	
comasw3-45	5038	17.213 ± 0.005	17.003 ± 0.005	16.776 ± 0.005	16.713 ± 0.005	16.596 ± 0.005
comasw25-20	5039	20.552 ± 0.085	20.292 ± 0.091	20.126 ± 0.107	20.164 ± 0.137	
comasw18-63	5040	21.058 ± 0.112	21.208 ± 0.199	21.157 ± 0.259	21.463 ± 0.557	
comasw14-44	5042	20.892 ± 0.082	20.572 ± 0.088	20.213 ± 0.084	20.138 ± 0.101	
comasw3-70	5050	20.085 ± 0.046	20.087 ± 0.058	19.943 ± 0.070	20.063 ± 0.092	20.137 ± 0.113
comasw3-86	5051	16.559 ± 0.003	16.410 ± 0.003	16.259 ± 0.003	16.223 ± 0.003	16.105 ± 0.003
comasw3-14	5054	19.011 ± 0.018	18.882 ± 0.020	18.743 ± 0.024	18.847 ± 0.031	18.873 ± 0.034
comasw18-44	5058	20.098 ± 0.043	19.989 ± 0.052	19.877 ± 0.064	19.886 ± 0.081	
comasw25-26	5059	20.893 ± 0.110	20.720 ± 0.134	20.686 ± 0.168	20.868 ± 0.261	
comasw18-40	5060	19.251 ± 0.023	19.368 ± 0.032	19.235 ± 0.040	19.325 ± 0.051	
comasw27-19	5063	20.990 ± 0.078	21.124 ± 0.120	21.038 ± 0.145	21.052 ± 0.188	
comasw3-72	5066	20.381 ± 0.061	20.495 ± 0.098	20.469 ± 0.129	20.680 ± 0.206	20.087 ± 0.107
comasw18-62	5075	19.860 ± 0.036	19.912 ± 0.048	19.782 ± 0.059	19.801 ± 0.071	
comasw3-12	5076	19.145 ± 0.018	19.026 ± 0.021	18.864 ± 0.025	18.895 ± 0.031	18.963 ± 0.036
comasw18-54	5083	19.546 ± 0.027	19.403 ± 0.031	19.183 ± 0.035	19.179 ± 0.041	
comasw14-24	5090	19.570 ± 0.029	19.530 ± 0.036	19.424 ± 0.045	19.594 ± 0.064	
comasw3-25	5091	20.932 ± 0.086	21.033 ± 0.130	20.868 ± 0.150		
comasw14-59	5095	19.207 ± 0.020	19.019 ± 0.022	18.815 ± 0.025	18.787 ± 0.030	
comasw18-27	5096	17.556 ± 0.006	17.328 ± 0.006	17.123 ± 0.006	17.121 ± 0.007	
comasw25-30	5098	21.048 ± 0.125	20.992 ± 0.166	20.891 ± 0.203	20.971 ± 0.278	
comasw14-78	5100	18.123 ± 0.009	17.870 ± 0.009	17.640 ± 0.009	17.570 ± 0.010	
comasw8-43	5102	18.285 ± 0.009	18.080 ± 0.009	17.892 ± 0.010	17.872 ± 0.012	
comasw3-6	5103	21.659 ± 0.164	21.409 ± 0.188	21.353 ± 0.233	21.596 ± 0.378	22.216 ± 0.739
comasw18-35	5104	20.490 ± 0.063	20.350 ± 0.078	20.246 ± 0.094	20.431 ± 0.137	
comasw18-33	5110	18.688 ± 0.015	18.342 ± 0.014	18.037 ± 0.014	18.008 ± 0.016	
comasw3-81	5118	20.178 ± 0.046	20.271 ± 0.062	20.120 ± 0.078	20.129 ± 0.088	20.014 ± 0.096
comasw18-53	5119	19.876 ± 0.036	20.017 ± 0.051	20.016 ± 0.067	20.257 ± 0.089	

Raw U-band aperture magnitudes. *contiuned from previous page*

Object	GMP	Aperture Dia. ('') 8.8	13	16	20.2	26
comasw14-49	5120	18.742 ± 0.014	18.541 ± 0.015	18.364 ± 0.016	18.353 ± 0.020	
comasw3-49	5129	20.698 ± 0.074	20.374 ± 0.074	20.113 ± 0.081	20.180 ± 0.104	20.080 ± 0.097
comasw3-8	5133	19.092 ± 0.019	19.224 ± 0.026	19.103 ± 0.033	19.210 ± 0.043	19.310 ± 0.050
comasw3-29	5136	17.607 ± 0.006	17.407 ± 0.006	17.224 ± 0.006	17.179 ± 0.007	17.093 ± 0.007
comasw27-37	5138	19.632 ± 0.027	19.418 ± 0.027	19.189 ± 0.030	19.254 ± 0.037	
comasw25-28	5142	20.619 ± 0.086	20.781 ± 0.136	20.760 ± 0.179	20.921 ± 0.261	
comasw13-48	5144	19.087 ± 0.019	18.796 ± 0.019	18.571 ± 0.020	18.639 ± 0.026	
comasw13-39	5146	21.311 ± 0.126	21.064 ± 0.142	20.902 ± 0.153	21.044 ± 0.214	
comasw3-71	5154	20.410 ± 0.049	20.336 ± 0.059	20.216 ± 0.072	20.345 ± 0.100	20.470 ± 0.149
comasw3-10	5155	19.838 ± 0.033	19.852 ± 0.045	19.775 ± 0.056	19.823 ± 0.074	19.616 ± 0.065
comasw25-78	5158	20.796 ± 0.111	20.852 ± 0.175	20.836 ± 0.255	21.067 ± 0.431	
comasw13-32	5159	20.483 ± 0.066	20.480 ± 0.088	20.317 ± 0.101	20.509 ± 0.141	
comasw18-70	5163	20.556 ± 0.071	20.476 ± 0.076	20.324 ± 0.087	20.430 ± 0.124	
comasw3-52	5164	20.230 ± 0.045	20.248 ± 0.062	20.184 ± 0.079	20.154 ± 0.095	20.074 ± 0.098
comasw25-77	5166	19.972 ± 0.049	20.114 ± 0.071	20.010 ± 0.087	20.134 ± 0.108	
comasw27-49	5169	19.989 ± 0.036	20.091 ± 0.047	20.028 ± 0.060	20.164 ± 0.078	
comasw8-54	5172	19.883 ± 0.033	19.822 ± 0.040	19.645 ± 0.047	19.692 ± 0.058	
comasw3-93	5176	18.809 ± 0.015	18.841 ± 0.019	18.658 ± 0.023	18.712 ± 0.029	18.584 ± 0.028
comasw3-79	5178	19.067 ± 0.018	18.911 ± 0.020	18.713 ± 0.022	18.662 ± 0.026	18.601 ± 0.026
comasw13-38	5179	19.332 ± 0.023	19.230 ± 0.027	19.111 ± 0.032	19.145 ± 0.041	
comasw3-44	5190	21.001 ± 0.087	20.953 ± 0.116	20.865 ± 0.142	20.924 ± 0.191	21.263 ± 0.284
comasw25-49	5191	17.081 ± 0.005	17.028 ± 0.006	16.927 ± 0.006	16.955 ± 0.008	
comasw18-23	5200	21.740 ± 0.173	21.530 ± 0.211	21.482 ± 0.260	21.424 ± 0.328	
comasw13-53	5202	19.454 ± 0.024	19.338 ± 0.029	19.215 ± 0.033	19.155 ± 0.040	
comasw18-28	5204	20.466 ± 0.062	20.576 ± 0.092	20.427 ± 0.110	20.383 ± 0.132	
comasw25-57	5207	18.917 ± 0.021	19.044 ± 0.029	18.937 ± 0.037	19.126 ± 0.052	
comasw18-25	5211	20.404 ± 0.059	20.261 ± 0.070	20.120 ± 0.085	20.103 ± 0.103	
comasw18-59	5212	20.447 ± 0.054	20.418 ± 0.071	20.250 ± 0.083	20.334 ± 0.108	
comasw28-26	5214	19.255 ± 0.020	19.338 ± 0.025	19.262 ± 0.032	19.441 ± 0.044	
comasw13-22	5217	18.631 ± 0.013	18.531 ± 0.015	18.379 ± 0.017	18.451 ± 0.022	
comasw28-21	5218	20.125 ± 0.041	20.265 ± 0.058	20.172 ± 0.074	20.180 ± 0.089	
comasw25-25	5219	20.121 ± 0.056	20.078 ± 0.073	19.942 ± 0.087	20.048 ± 0.119	
comasw3-63	5221	20.428 ± 0.052	20.527 ± 0.071	20.381 ± 0.084	20.457 ± 0.106	20.476 ± 0.142
comasw28-51	5232	19.605 ± 0.027	19.527 ± 0.030	19.340 ± 0.036	19.452 ± 0.045	
comasw28-64	5239	20.476 ± 0.055	20.554 ± 0.075	20.458 ± 0.095	20.531 ± 0.121	
comasw3-1	5244	20.184 ± 0.052				
comasw13-8	5245	19.214 ± 0.022	19.018 ± 0.023	18.770 ± 0.026	18.825 ± 0.031	
comasw3-56	5250	17.686 ± 0.006	17.527 ± 0.006	17.343 ± 0.007	17.327 ± 0.008	17.249 ± 0.008
comasw28-14	5251	20.978 ± 0.097	21.447 ± 0.199	21.961 ± 0.402	23.336 ± 1.850	
comasw8-44	5253	19.492 ± 0.023	19.538 ± 0.030	19.459 ± 0.038	19.574 ± 0.051	
comasw3-74	5255	20.368 ± 0.053	20.261 ± 0.061	20.053 ± 0.072	20.051 ± 0.087	19.963 ± 0.087
comasw28-28	5256	18.118 ± 0.009	17.909 ± 0.008	17.690 ± 0.009	17.617 ± 0.009	
comasw28-62	5258	19.612 ± 0.025	19.628 ± 0.032	19.519 ± 0.038	19.556 ± 0.048	
comasw18-30	5260	20.691 ± 0.071	20.524 ± 0.082	20.248 ± 0.090	20.388 ± 0.124	
comasw28-27	5261	18.710 ± 0.015	18.703 ± 0.018	18.588 ± 0.022	18.638 ± 0.027	
comasw13-46	5262	20.049 ± 0.041	20.071 ± 0.058	19.998 ± 0.071	20.051 ± 0.095	
comasw28-17	5272	16.544 ± 0.003	16.389 ± 0.003	16.228 ± 0.003	16.186 ± 0.003	
comasw3-4	5274	20.674 ± 0.064	20.517 ± 0.079	20.495 ± 0.100	20.507 ± 0.134	20.087 ± 0.103
comasw3-89	5276	20.438 ± 0.052	20.269 ± 0.062	20.066 ± 0.074	20.137 ± 0.101	19.966 ± 0.092
comasw3-20	5277	20.066 ± 0.042	20.182 ± 0.059	20.143 ± 0.081	20.324 ± 0.113	20.701 ± 0.206
comasw8-47	5278	20.153 ± 0.041	20.233 ± 0.057	20.068 ± 0.069	20.208 ± 0.093	
comasw8-49	5284	18.406 ± 0.010	18.296 ± 0.011	18.126 ± 0.012	18.148 ± 0.014	
comasw3-69	5296	19.118 ± 0.018	19.042 ± 0.021	18.893 ± 0.025	18.913 ± 0.031	18.906 ± 0.034

Raw U-band aperture magnitudes. *contiuned from previous page*

Object	GMP	Aperture Dia. ('') 8.8	13	16	20.2	26
comasw28-43	5304	18.206 ± 0.009	17.920 ± 0.008	17.680 ± 0.009	17.609 ± 0.009	
comasw13-63	5307	19.706 ± 0.031	19.612 ± 0.037	19.411 ± 0.042	19.428 ± 0.052	
comasw28-48	5308	18.703 ± 0.012	18.456 ± 0.012	18.217 ± 0.013	18.160 ± 0.014	
comasw13-4	5320	18.994 ± 0.019	18.893 ± 0.023	18.717 ± 0.026	18.741 ± 0.034	
comasw25-31	5329	19.155 ± 0.024	18.956 ± 0.027	18.756 ± 0.030	18.724 ± 0.036	
comasw13-18	5333	20.426 ± 0.058	20.539 ± 0.089	20.469 ± 0.110	20.579 ± 0.156	
comasw25-14	5334	20.370 ± 0.066	20.292 ± 0.086	20.158 ± 0.102	20.147 ± 0.127	
comasw13-5	5344	19.692 ± 0.031	19.697 ± 0.041	19.576 ± 0.050	19.664 ± 0.067	
comasw13-57	5345	18.579 ± 0.013	18.377 ± 0.013	18.171 ± 0.015	18.141 ± 0.017	
comasw28-19	5353	21.127 ± 0.092	20.937 ± 0.107	20.948 ± 0.138	20.873 ± 0.167	
comasw28-40	5354	19.695 ± 0.029	19.637 ± 0.034	19.422 ± 0.038	19.436 ± 0.046	
comasw13-21	5357	20.457 ± 0.060	20.169 ± 0.062	19.916 ± 0.068	19.861 ± 0.079	
comasw13-43	5362	18.308 ± 0.010	18.188 ± 0.011	18.040 ± 0.013	18.043 ± 0.015	
comasw13-66	5370	20.469 ± 0.063	20.312 ± 0.076	20.235 ± 0.096	20.361 ± 0.138	
comasw13-65	5370	20.632 ± 0.073	20.388 ± 0.082	20.369 ± 0.110	20.407 ± 0.145	
comasw25-29	5373	20.708 ± 0.093	20.767 ± 0.139	20.832 ± 0.197	20.847 ± 0.260	
comasw13-42	5375	20.190 ± 0.052	20.175 ± 0.067	20.090 ± 0.086	20.220 ± 0.118	
comasw25-7	5381	20.117 ± 0.058	20.110 ± 0.080	20.010 ± 0.101	20.198 ± 0.151	
comasw28-34	5400	21.120 ± 0.091	21.140 ± 0.127	21.223 ± 0.177	21.229 ± 0.228	
comasw28-41	5407	17.929 ± 0.007	17.800 ± 0.008	17.631 ± 0.008	17.633 ± 0.009	
comasw13-25	5410	19.256 ± 0.022	19.285 ± 0.028	19.205 ± 0.036	19.312 ± 0.047	
comasw13-62	5411	19.975 ± 0.040	20.025 ± 0.055	19.888 ± 0.067	20.025 ± 0.093	
comasw13-36	5427	20.643 ± 0.072	20.561 ± 0.091	20.308 ± 0.098	20.240 ± 0.115	
comasw13-60	5434	17.512 ± 0.006	17.444 ± 0.007	17.336 ± 0.007	17.360 ± 0.009	
comasw28-33	5436	19.603 ± 0.027	19.641 ± 0.034	19.549 ± 0.042	19.736 ± 0.059	
comasw13-50	5438	20.000 ± 0.041	20.105 ± 0.058	19.941 ± 0.070	19.878 ± 0.079	
comasw13-20	5452	19.420 ± 0.025	19.431 ± 0.032	19.285 ± 0.039	19.432 ± 0.052	
comasw28-9	5470	19.571 ± 0.025	19.512 ± 0.030	19.414 ± 0.036	19.535 ± 0.048	
comasw13-29	5480	19.648 ± 0.031	19.566 ± 0.038	19.399 ± 0.044	19.404 ± 0.054	
comasw28-25	5486	18.882 ± 0.014	18.728 ± 0.015	18.552 ± 0.016	18.571 ± 0.020	
comasw13-28	5492	20.258 ± 0.052	20.168 ± 0.062	20.030 ± 0.077	20.104 ± 0.098	
comasw13-23	5520	20.981 ± 0.089	20.790 ± 0.104	20.559 ± 0.115	20.668 ± 0.157	
comasw13-58	5522	20.761 ± 0.081	20.884 ± 0.122	20.869 ± 0.164	21.019 ± 0.234	
comasw13-2	5523	21.200 ± 0.122	20.936 ± 0.137	20.456 ± 0.127	19.808 ± 0.088	
comasw20-89	-	19.576 ± 0.029	19.573 ± 0.035	19.171 ± 0.033	18.879 ± 0.031	
comasw16-74	-	20.774 ± 0.059	20.667 ± 0.077	20.542 ± 0.099	20.664 ± 0.123	
comasw20-85	-	21.894 ± 0.204	21.850 ± 0.271	21.755 ± 0.379	21.497 ± 0.430	
comasw16-79	-	19.778 ± 0.032				
coma15-91	-	20.732 ± 0.066	20.851 ± 0.102	20.763 ± 0.125	20.796 ± 0.164	21.700 ± 0.423
comasw20-76	-	20.294 ± 0.057	20.573 ± 0.092	20.627 ± 0.125	21.112 ± 0.180	
comasw20-70	-	21.085 ± 0.107	21.113 ± 0.147	20.819 ± 0.160	20.580 ± 0.172	
comasw20-93	-	20.318 ± 0.051	20.375 ± 0.074	20.255 ± 0.089	20.401 ± 0.127	
comasw28-5	-	21.307 ± 0.106	21.116 ± 0.121	21.125 ± 0.159	21.226 ± 0.221	
comasw20-59	-	21.174 ± 0.129	21.112 ± 0.168	21.034 ± 0.212	20.670 ± 0.192	
comasw20-52	-	21.867 ± 0.238	21.353 ± 0.218	21.016 ± 0.222	21.221 ± 0.339	
comasw28-8	-	20.381 ± 0.051	20.554 ± 0.075	20.558 ± 0.102	20.737 ± 0.144	
coma23-56	-	21.447 ± 0.140	21.792 ± 0.269	22.086 ± 0.461	23.834 ± 2.954	
comane6-46	-	20.144 ± 0.070				
comasw17-6	-	20.474 ± 0.058	20.584 ± 0.083	20.483 ± 0.105	20.626 ± 0.144	
comasw22-106	-	22.635 ± 0.520				
comane6-32	-	21.603 ± 0.226	21.685 ± 0.333	21.787 ± 0.465	21.568 ± 0.497	
coma15-15	-	20.924 ± 0.106	20.895 ± 0.141	20.780 ± 0.176	20.744 ± 0.210	19.704 ± 0.080
comane6-21	-	21.253 ± 0.178	21.078 ± 0.201	20.917 ± 0.195	20.963 ± 0.284	

Raw U-band aperture magnitudes. *contiuned from previous page*

Object	GMP	Aperture Dia. (″) 8.8	13	16	20.2	26
comasw3-75	-	21.350 ± 0.140	21.139 ± 0.167	20.934 ± 0.160	20.809 ± 0.177	20.896 ± 0.224
comasw3-66	-	20.146 ± 0.046	19.836 ± 0.046	19.625 ± 0.053	19.683 ± 0.067	19.543 ± 0.060
comasw17-91	-	20.514 ± 0.062	20.673 ± 0.096	20.587 ± 0.125	20.507 ± 0.143	
comasw20-30	-	20.527 ± 0.071	20.587 ± 0.099	20.522 ± 0.133	20.631 ± 0.178	
comasw3-32	-	21.895 ± 0.202	21.747 ± 0.253	21.496 ± 0.267	21.547 ± 0.359	20.602 ± 0.167
comasw16-81	-	22.649 ± 0.466	23.317 ± 1.142	25.015 ± 5.578		
comasw3-22	-	21.425 ± 0.145	21.284 ± 0.177	21.187 ± 0.222	21.672 ± 0.430	21.388 ± 0.333
comasw17-59	-	19.706 ± 0.029	19.832 ± 0.042	19.783 ± 0.053	19.929 ± 0.077	
comasw25-67	-	20.775 ± 0.099	19.821 ± 0.059	19.331 ± 0.052	19.306 ± 0.062	
comasw17-44	-	21.899 ± 0.193	22.241 ± 0.375	22.588 ± 0.675	23.474 ± 1.976	
comasw17-37	-	20.742 ± 0.072	20.544 ± 0.080	20.413 ± 0.098	20.303 ± 0.108	
comasw17-34	-	20.482 ± 0.058	20.532 ± 0.078	20.380 ± 0.097	20.477 ± 0.125	
coma12-3	-	21.595 ± 0.175	21.069 ± 0.156	20.592 ± 0.136	20.016 ± 0.104	
coma19-46	-	22.345 ± 0.259	22.927 ± 0.655	25.225 ± 5.780		21.071 ± 0.205
comasw16-70	-	22.055 ± 0.224	21.542 ± 0.204	21.379 ± 0.236	21.221 ± 0.260	
comasw17-26	-	21.598 ± 0.143	21.578 ± 0.197	21.595 ± 0.263	22.057 ± 0.514	
comasw16-20	-	20.506 ± 0.059	20.458 ± 0.075	20.300 ± 0.092	20.444 ± 0.126	
comasw16-22	-	21.320 ± 0.130	21.168 ± 0.159	21.108 ± 0.205	21.541 ± 0.384	
coma16-101	-	21.215 ± 0.124	21.609 ± 0.243	21.987 ± 0.450	22.832 ± 1.256	22.821 ± 1.317
coma10-11	-	21.526 ± 0.140	21.329 ± 0.160	20.974 ± 0.156	20.791 ± 0.164	20.641 ± 0.158
comasw13-64	-	22.525 ± 0.394	22.472 ± 0.562	22.787 ± 0.957	24.895 ± 8.927	
coma10-14	-	18.218 ± 0.010	18.352 ± 0.013	18.233 ± 0.016	18.376 ± 0.020	18.403 ± 0.023
comasw13-61	-	21.904 ± 0.178	21.846 ± 0.215	21.655 ± 0.276	21.517 ± 0.280	
comasw16-37	-	20.438 ± 0.062	20.450 ± 0.087	20.257 ± 0.098	20.060 ± 0.098	
comasw28-20	-	20.457 ± 0.056	20.498 ± 0.077	20.394 ± 0.098		
coma16-90	-	22.404 ± 0.276	22.985 ± 0.586	22.198 ± 0.511	21.858 ± 0.495	21.073 ± 0.138
comasw16-42	-	21.233 ± 0.112	21.276 ± 0.162	21.221 ± 0.208	21.071 ± 0.229	
coma9-51	-	20.856 ± 0.081	20.798 ± 0.101	20.399 ± 0.098	19.955 ± 0.079	19.811 ± 0.075
coma12-1	-	20.325 ± 0.057	20.407 ± 0.073	20.194 ± 0.085		
comasw21-73	-	16.666 ± 0.004	16.329 ± 0.003	16.015 ± 0.003	15.862 ± 0.003	
coma19-78	-	19.760 ± 0.029	19.820 ± 0.042	19.709 ± 0.053	19.763 ± 0.070	20.039 ± 0.080
comasw16-44	-	22.082 ± 0.258	21.960 ± 0.364	22.113 ± 0.578	22.737 ± 2.019	
coma14-113	-	24.497 ± 3.874				
comasw8-53	-	21.024 ± 0.087	21.052 ± 0.121	20.930 ± 0.148	20.988 ± 0.193	
coma9-48	-	20.426 ± 0.052	20.544 ± 0.082	20.665 ± 0.115	20.804 ± 0.173	20.621 ± 0.150
comasw16-47	-	21.625 ± 0.146	21.424 ± 0.176	21.210 ± 0.194	21.604 ± 0.354	
comasw10-2	-	21.052 ± 0.092	20.938 ± 0.117			
coma9-35	-	21.651 ± 0.167	21.706 ± 0.245	21.995 ± 0.413	23.374 ± 1.880	
coma10-30	-	18.464 ± 0.014	18.633 ± 0.020	18.522 ± 0.025	18.629 ± 0.032	18.315 ± 0.022
coma14-124	-	18.944 ± 0.035				
comasw28-44	-	21.236 ± 0.099	21.280 ± 0.138	21.038 ± 0.148	20.982 ± 0.174	
comasw13-34	-	20.419 ± 0.059	20.546 ± 0.087	20.494 ± 0.118	20.593 ± 0.156	
comasw8-39	-	21.367 ± 0.113	21.371 ± 0.157	21.355 ± 0.209	21.472 ± 0.291	
coma22-30	-	22.113 ± 0.241	22.488 ± 0.477	22.968 ± 0.899		
coma14-133	-	22.526 ± 0.659				
coma14-125	-	20.781 ± 0.173	19.990 ± 0.123			
comasw16-58	-	20.785 ± 0.074	20.904 ± 0.110	20.780 ± 0.136	20.948 ± 0.196	
coma4-43	-	21.747 ± 0.222	21.893 ± 0.349	21.511 ± 0.509	20.557 ± 0.259	
comasw25-45	-	21.852 ± 0.242	22.221 ± 0.492	22.549 ± 0.825	23.186 ± 2.019	
coma19-102	-	20.683 ± 0.063	20.261 ± 0.059	19.870 ± 0.058	19.731 ± 0.062	19.190 ± 0.043
coma19-101	-	20.117 ± 0.042	19.890 ± 0.044	19.592 ± 0.047	19.427 ± 0.049	18.976 ± 0.035
comasw21-24	-	22.419 ± 0.297	22.490 ± 0.466	22.995 ± 0.922	22.945 ± 1.208	
comasw21-21	-	22.156 ± 0.225	21.504 ± 0.181	21.389 ± 0.219	21.270 ± 0.249	

Raw U-band aperture magnitudes. *contiuned from previous page*

Object	GMP	Aperture Dia. (″) 8.8	13	16	20.2	26
coma16-29	-	21.942 ± 0.211	22.125 ± 0.358	22.643 ± 0.717	22.877 ± 1.203	20.876 ± 0.212
comasw27-7	-	20.354 ± 0.049	20.492 ± 0.070	20.504 ± 0.100	20.674 ± 0.131	
coma5-69	-	22.019 ± 0.238	21.681 ± 0.252	21.480 ± 0.278	20.961 ± 0.222	20.294 ± 0.138
coma5-66	-	22.354 ± 0.375	22.594 ± 0.675	25.054 ± 50.690		21.709 ± 0.303
comasw16-5	-	20.631 ± 0.064	20.689 ± 0.088	20.496 ± 0.105	20.507 ± 0.127	
coma5-54	-	21.889 ± 0.211	21.808 ± 0.282	21.343 ± 0.246	21.142 ± 0.262	20.525 ± 0.156
coma14-22	-	21.138 ± 0.080	20.290 ± 0.117	20.142 ± 0.151	20.187 ± 0.195	20.366 ± 0.259
coma5-48	-	20.791 ± 0.084	20.918 ± 0.128	20.778 ± 0.153	20.586 ± 0.159	19.828 ± 0.085
coma14-23	-	19.611 ± 0.049	19.737 ± 0.070	19.714 ± 0.092	19.728 ± 0.116	19.181 ± 0.076
coma5-44	-	20.539 ± 0.069	20.686 ± 0.103	20.485 ± 0.122	20.434 ± 0.138	20.281 ± 0.131
coma5-40	-	21.547 ± 0.163	21.410 ± 0.201	21.590 ± 0.312	21.727 ± 0.455	21.744 ± 0.499
coma12-73	-	20.554 ± 0.071	20.709 ± 0.100	20.597 ± 0.121	20.748 ± 0.142	20.692 ± 0.083
coma5-27	-	20.519 ± 0.066	20.547 ± 0.089	20.385 ± 0.106	20.431 ± 0.135	20.317 ± 0.134
comasw18-72	-	22.603 ± 0.394	21.817 ± 0.288	20.983 ± 0.186	19.597 ± 0.066	
coma5-21	-	21.372 ± 0.136	21.302 ± 0.177	21.120 ± 0.204	20.716 ± 0.177	20.215 ± 0.122
coma5-20	-	21.205 ± 0.120	20.978 ± 0.136	20.878 ± 0.166	20.959 ± 0.226	20.910 ± 0.224
coma12-58	-	20.879 ± 0.094	21.261 ± 0.176	21.283 ± 0.245	21.728 ± 0.453	21.036 ± 0.251
coma19-92	-	20.258 ± 0.048	20.007 ± 0.050	19.635 ± 0.050	19.438 ± 0.050	18.901 ± 0.031
comasw5-2	-	22.262 ± 0.218	22.067 ± 0.456	22.218 ± 0.697	22.704 ± 1.510	20.953 ± 0.292
comane3-71	-	21.352 ± 0.134	21.517 ± 0.200	21.638 ± 0.286	21.692 ± 0.376	
coma5-16	-	21.323 ± 0.140	20.941 ± 0.139	20.759 ± 0.158	20.965 ± 0.240	20.481 ± 0.152
coma5-10	-	22.130 ± 0.277	21.631 ± 0.254	21.374 ± 0.268	21.535 ± 0.396	24.581 ± 6.923
coma12-48	-	21.664 ± 0.213	21.397 ± 0.257	21.065 ± 0.274	20.640 ± 0.245	19.446 ± 0.057
comasw18-57	-	21.027 ± 0.107	20.961 ± 0.125	20.965 ± 0.180	21.330 ± 0.307	
coma17-7	-	20.876 ± 0.134	20.120 ± 0.097	19.565 ± 0.078	19.056 ± 0.065	
coma14-31	-	21.694 ± 0.249	21.220 ± 0.251	21.020 ± 0.259	21.076 ± 0.308	
comasw26-76	-	19.567 ± 0.030	19.694 ± 0.042	19.533 ± 0.052	19.702 ± 0.072	
coma22-52	-	19.023 ± 0.017	19.160 ± 0.022	19.035 ± 0.028	19.176 ± 0.036	19.655 ± 0.068
comasw26-74	-	21.065 ± 0.105	21.069 ± 0.139	21.060 ± 0.188	21.084 ± 0.236	
comane3-58	-	20.713 ± 0.091	21.059 ± 0.157	21.331 ± 0.259	22.381 ± 0.842	
comasw26-67	-	20.959 ± 0.096	20.934 ± 0.125	20.773 ± 0.148	20.949 ± 0.219	
comasw18-45	-	20.585 ± 0.064	20.489 ± 0.082	20.426 ± 0.103	20.522 ± 0.144	
comasw18-43	-	21.967 ± 0.218	22.267 ± 0.414	21.804 ± 0.355	21.358 ± 0.311	
coma12-27	-	20.595 ± 0.069	20.815 ± 0.103	20.878 ± 0.140	21.243 ± 0.302	24.758 ± 7.863
comasw26-57	-	21.292 ± 0.115	21.173 ± 0.137	20.870 ± 0.141	21.045 ± 0.201	
comasw18-37	-	21.711 ± 0.170	21.666 ± 0.236	21.376 ± 0.239	21.174 ± 0.259	
comasw26-56	-	18.972 ± 0.017	19.099 ± 0.022	18.987 ± 0.027	19.142 ± 0.036	
comasw6-12	-	20.926 ± 0.107	20.362 ± 0.088	19.836 ± 0.074	19.581 ± 0.073	
comasw26-53	-	21.214 ± 0.113	21.489 ± 0.191	21.706 ± 0.304	22.589 ± 0.863	
coma15-120	-	20.764 ± 0.077	20.530 ± 0.085	20.339 ± 0.098	20.278 ± 0.105	20.059 ± 0.096
comasw6-16	-	22.031 ± 0.277	22.471 ± 0.600	23.240 ± 1.482	29.256 ± 493.620	
coma12-57	-	20.466 ± 0.062	20.556 ± 0.091	20.483 ± 0.113	20.504 ± 0.136	20.524 ± 0.172
coma12-19	-	19.619 ± 0.029	19.708 ± 0.040	19.579 ± 0.050	19.705 ± 0.069	19.890 ± 0.085
comane3-30	-	21.075 ± 0.108	21.210 ± 0.154	21.436 ± 0.247	21.829 ± 0.441	
comasw18-20	-	19.190 ± 0.021	19.298 ± 0.029	19.178 ± 0.035	19.249 ± 0.045	
comane3-28	-	21.533 ± 0.161	21.509 ± 0.208	21.565 ± 0.276	21.464 ± 0.321	
comasw26-28	-	22.500 ± 0.349	22.884 ± 0.703	26.965 ± 28.952		
comasw26-12	-	22.145 ± 0.244	22.250 ± 0.378	23.059 ± 0.948	23.353 ± 1.714	
comasw9-83	-	20.424 ± 0.046	20.223 ± 0.051	20.050 ± 0.059	20.111 ± 0.080	20.351 ± 0.110
comasw22-91	-	19.401 ± 0.032	19.435 ± 0.040	19.097 ± 0.042	18.059 ± 0.019	
coma13-114	-	21.724 ± 0.142	21.932 ± 0.237	22.007 ± 0.416	21.798 ± 0.510	20.713 ± 0.175
comasw14-61	-	20.468 ± 0.062	20.487 ± 0.084	20.286 ± 0.098	20.559 ± 0.151	
comasw22-80	-	21.410 ± 0.182	20.460 ± 0.105	19.787 ± 0.082	19.256 ± 0.059	

Raw U-band aperture magnitudes. *contiuned from previous page*

Object	GMP	Aperture Dia. ('') 8.8	13	16	20.2	26
coma13-108	-	20.418 ± 0.055	20.625 ± 0.079	20.561 ± 0.098	20.721 ± 0.124	21.879 ± 0.346
coma13-104	-	19.267 ± 0.021	19.357 ± 0.028	19.219 ± 0.034	19.330 ± 0.045	19.545 ± 0.057
comasw14-50	-	20.945 ± 0.091	21.105 ± 0.144	21.148 ± 0.201	21.382 ± 0.315	
comasw14-45	-	20.628 ± 0.071	20.604 ± 0.094	20.360 ± 0.099	20.243 ± 0.114	
coma17-70	-	21.722 ± 0.171	21.922 ± 0.287	21.752 ± 0.326	21.380 ± 0.297	20.932 ± 0.211
comasw9-39	-	21.257 ± 0.108	19.929 ± 0.046	19.413 ± 0.039	18.999 ± 0.033	18.693 ± 0.028
comasw22-44	-	21.016 ± 0.141	20.682 ± 0.141	20.611 ± 0.180	20.670 ± 0.235	
coma17-57	-	19.934 ± 0.042	20.046 ± 0.061	19.943 ± 0.076	19.656 ± 0.072	18.546 ± 0.026
comasw14-11	-	20.848 ± 0.074	20.970 ± 0.113	20.996 ± 0.150	21.421 ± 0.208	
coma25-60	-	20.781 ± 0.081	20.919 ± 0.115	20.700 ± 0.126	20.751 ± 0.158	20.740 ± 0.170
comasw9-19	-	20.816 ± 0.065	20.909 ± 0.096	20.754 ± 0.116	20.759 ± 0.143	20.231 ± 0.097
coma17-40	-	20.558 ± 0.065	20.700 ± 0.097	20.691 ± 0.132	20.790 ± 0.176	20.704 ± 0.167
coma22-71	-	20.958 ± 0.090	20.866 ± 0.111	20.796 ± 0.138	20.804 ± 0.175	20.830 ± 0.185
coma25-41	-	19.886 ± 0.042	20.007 ± 0.058	19.967 ± 0.076	20.133 ± 0.104	19.641 ± 0.061
coma25-37	-	19.333 ± 0.025	19.543 ± 0.033	19.432 ± 0.042	19.676 ± 0.058	19.945 ± 0.084
coma5-9	-	22.299 ± 0.342	23.313 ± 1.257			
coma5-3	-	20.388 ± 0.067	20.361 ± 0.086	20.153 ± 0.106	20.177 ± 0.129	
comasw10-90	-	21.009 ± 0.081	21.009 ± 0.113	20.936 ± 0.130	21.184 ± 0.165	21.000 ± 0.212
comasw10-89	-	20.465 ± 0.056	20.630 ± 0.087	20.593 ± 0.112	21.000 ± 0.162	20.179 ± 0.102
comasw10-88	-	20.512 ± 0.049	20.033 ± 0.035	19.520 ± 0.032	19.114 ± 0.026	18.069 ± 0.011
comasw10-83	-	20.601 ± 0.065	20.737 ± 0.107	20.870 ± 0.153	21.498 ± 0.334	20.820 ± 0.195
coma7-28	-	21.561 ± 0.378	21.649 ± 0.529	21.521 ± 0.492	21.553 ± 0.737	21.685 ± 1.051
comasw10-60	-	21.042 ± 0.080	21.048 ± 0.115	21.061 ± 0.165	21.257 ± 0.241	22.693 ± 2.049
comasw6-31	-	21.997 ± 0.262	21.704 ± 0.298	21.955 ± 0.473	21.486 ± 0.417	
coma13-90	-	21.073 ± 0.100	21.051 ± 0.138	20.947 ± 0.165	20.943 ± 0.210	20.588 ± 0.157
comasw21-116	-	21.574 ± 0.139	21.311 ± 0.159	21.331 ± 0.168	21.029 ± 0.202	
comasw10-57	-	20.531 ± 0.054	20.524 ± 0.073	20.379 ± 0.089	20.351 ± 0.106	20.173 ± 0.102
comasw10-56	-	20.703 ± 0.053	20.485 ± 0.070	20.362 ± 0.091	20.424 ± 0.116	20.248 ± 0.089
coma13-87	-	20.613 ± 0.064	20.209 ± 0.059	19.657 ± 0.049	19.201 ± 0.040	18.823 ± 0.030
coma13-84	-	19.914 ± 0.039	20.193 ± 0.065	20.241 ± 0.096	20.522 ± 0.148	21.116 ± 0.288
comasw10-50	-	20.956 ± 0.081	21.106 ± 0.127	20.876 ± 0.142	20.838 ± 0.170	
comasw5-57	-	22.071 ± 0.259	22.153 ± 0.406	22.941 ± 1.027		22.074 ± 0.691
comasw21-108	-	20.848 ± 0.078	20.993 ± 0.127	21.056 ± 0.171	21.247 ± 0.303	
comasw10-40	-	21.251 ± 0.107	20.806 ± 0.100	20.736 ± 0.128	20.992 ± 0.202	20.876 ± 0.193
coma14-66	-	22.302 ± 0.346	21.930 ± 0.461	21.715 ± 0.491	22.597 ± 0.637	
comasw5-41	-	22.218 ± 0.457	22.154 ± 0.658	22.125 ± 0.771	21.912 ± 0.944	
comasw10-37	-	21.119 ± 0.102	20.890 ± 0.115	20.568 ± 0.119	20.163 ± 0.102	19.152 ± 0.039
coma13-68	-	21.881 ± 0.140	21.485 ± 0.110			
comasw10-26	-	20.568 ± 0.059	20.731 ± 0.090	20.644 ± 0.120	20.777 ± 0.162	24.044 ± 3.429
comasw10-22	-	20.523 ± 0.054	20.573 ± 0.075	20.370 ± 0.090	20.391 ± 0.109	20.099 ± 0.088
comasw10-20	-	20.766 ± 0.070	20.937 ± 0.113	20.867 ± 0.158	21.016 ± 0.254	21.318 ± 2.740
coma13-52	-	20.800 ± 0.081	20.458 ± 0.079	20.112 ± 0.078	20.021 ± 0.089	19.303 ± 0.045
comasw5-17	-	22.743 ± 0.455	22.532 ± 0.565	22.249 ± 0.556	22.276 ± 0.761	22.126 ± 0.711
comasw27-62	-	20.381 ± 0.051	20.425 ± 0.073	20.360 ± 0.092	20.455 ± 0.129	
comasw27-55	-	20.251 ± 0.046	20.329 ± 0.062	20.239 ± 0.080	20.365 ± 0.106	
comasw27-50	-	21.939 ± 0.186	22.095 ± 0.302	21.770 ± 0.295	21.667 ± 0.344	
comasw27-48	-	19.593 ± 0.024	19.602 ± 0.030	19.497 ± 0.036	19.559 ± 0.044	
comasw27-33	-	19.658 ± 0.028	19.773 ± 0.037	19.640 ± 0.046	19.794 ± 0.061	
comasw11-7	-	17.813 ± 0.008	18.039 ± 0.012	17.831 ± 0.015	18.005 ± 0.019	17.780 ± 0.027
comasw15-79	-	20.691 ± 0.079	20.763 ± 0.111	20.609 ± 0.134	20.682 ± 0.167	
comasw15-78	-	21.156 ± 0.104	21.020 ± 0.121	20.845 ± 0.146	21.004 ± 0.213	
comasw15-62	-	21.428 ± 0.132	21.299 ± 0.163	21.052 ± 0.175	20.935 ± 0.198	
comasw23-81	-	20.915 ± 0.106	20.845 ± 0.135	20.620 ± 0.155	20.791 ± 0.219	

Raw U-band aperture magnitudes. *contiuned from previous page*

Object	GMP	Aperture Dia. ('') 8.8	13	16	20.2	26
comasw23-79	-	22.733 ± 0.566	23.000 ± 0.715	23.208 ± 1.346		
comasw15-52	-	20.490 ± 0.060	20.639 ± 0.089	20.591 ± 0.121	20.653 ± 0.153	
coma10-2	-	21.860 ± 0.197	22.104 ± 0.346	23.575 ± 1.559		22.551 ± 0.928
comasw15-48	-	19.766 ± 0.032	19.903 ± 0.047	19.768 ± 0.057	19.828 ± 0.073	
comasw15-46	-	20.565 ± 0.063	20.561 ± 0.083	20.149 ± 0.080	19.782 ± 0.069	
coma14-84	-	20.271 ± 0.096	20.400 ± 0.147	20.286 ± 0.179	20.523 ± 0.279	20.477 ± 0.290
coma14-85	-	22.972 ± 2.769	22.053 ± 0.806	22.210 ± 1.729		
comasw23-65	-	20.454 ± 0.073	20.762 ± 0.127	20.667 ± 0.163	20.839 ± 0.232	
comasw23-64	-	21.187 ± 0.125	21.331 ± 0.200	21.137 ± 0.229	21.239 ± 0.317	
coma18-76	-	20.982 ± 0.082	21.195 ± 0.134	21.016 ± 0.157	20.810 ± 0.161	20.842 ± 0.178
comasw23-61	-	22.674 ± 0.462	22.440 ± 0.564	22.711 ± 0.901	23.046 ± 1.677	
comasw15-30	-	21.064 ± 0.102	21.331 ± 0.179	21.385 ± 0.251	21.540 ± 0.370	
coma18-57	-	20.079 ± 0.041	20.191 ± 0.057	20.008 ± 0.066	20.081 ± 0.079	19.391 ± 0.046
comasw15-23	-	21.122 ± 0.110	20.270 ± 0.071	19.628 ± 0.053	18.933 ± 0.036	
comasw6-66	-	20.467 ± 0.072	20.573 ± 0.104	20.455 ± 0.130	20.275 ± 0.134	
coma18-52	-	20.496 ± 0.053	20.657 ± 0.079	20.607 ± 0.107	20.844 ± 0.175	21.145 ± 0.231
coma18-49	-	20.609 ± 0.062	20.651 ± 0.084	20.386 ± 0.095	20.391 ± 0.117	20.272 ± 0.105
comasw23-32	-	20.460 ± 0.075	20.413 ± 0.095	19.523 ± 0.060	19.070 ± 0.048	
comasw23-23	-	20.685 ± 0.083	20.814 ± 0.127	20.790 ± 0.171	21.078 ± 0.275	
comasw6-72	-	21.086 ± 0.122	21.210 ± 0.190	21.185 ± 0.248	20.963 ± 0.258	
coma18-22	-	20.983 ± 0.079	21.058 ± 0.114	20.935 ± 0.137	20.889 ± 0.166	20.743 ± 0.162
comasw6-76	-	21.109 ± 0.214	20.709 ± 0.208	20.244 ± 0.193	19.813 ± 0.159	
coma18-20	-	20.134 ± 0.040	20.219 ± 0.056	20.087 ± 0.071	19.918 ± 0.072	19.212 ± 0.039
coma18-10	-	21.850 ± 0.168	21.685 ± 0.211	21.532 ± 0.251	21.359 ± 0.279	

Raw V-band aperture magnitudes.

Object	GMP	Aperture Dia. (″) 8.8	13	16	20.2	26
coma10-4	1714	19.620 ± 0.044	19.657 ± 0.062	19.559 ± 0.079		
coma10-50	1724	19.247 ± 0.031	19.319 ± 0.046	19.218 ± 0.058	19.344 ± 0.086	
comane7-26	1730	18.085 ± 0.008	17.890 ± 0.008	17.702 ± 0.009	17.721 ± 0.010	
coma10-29	1745	19.891 ± 0.050	19.856 ± 0.063	19.774 ± 0.080	20.072 ± 0.128	20.220 ± 0.165
comane3-69	1751	17.115 ± 0.005	16.949 ± 0.005	16.770 ± 0.005	16.795 ± 0.007	
comane3-50	1757	19.016 ± 0.022	18.753 ± 0.023	18.506 ± 0.024	18.489 ± 0.029	
comane7-37	1758	18.630 ± 0.012	18.663 ± 0.015	18.574 ± 0.018	18.662 ± 0.023	
coma10-1	1764	18.658 ± 0.017	18.672 ± 0.022	18.585 ± 0.028	18.680 ± 0.037	18.848 ± 0.048
comane3-51	1765	18.409 ± 0.013	18.395 ± 0.017	18.311 ± 0.020	18.430 ± 0.028	
coma10-43	1767	19.157 ± 0.027	19.164 ± 0.036	18.958 ± 0.040	18.816 ± 0.043	18.756 ± 0.042
coma10-36	1772	19.093 ± 0.025	19.112 ± 0.033	19.031 ± 0.041	19.171 ± 0.057	19.229 ± 0.064
comane3-80	1777	19.162 ± 0.026	19.244 ± 0.036	19.200 ± 0.047	19.328 ± 0.064	
coma10-61	1780	19.407 ± 0.038	19.305 ± 0.046	19.230 ± 0.061	19.396 ± 0.089	19.876 ± 0.226
comane3-36	1781	17.621 ± 0.007	17.397 ± 0.007	17.215 ± 0.008	17.250 ± 0.010	
comane7-34	1800	18.700 ± 0.013	18.701 ± 0.015	18.587 ± 0.018	18.633 ± 0.023	
comane7-15	1805	18.493 ± 0.011	18.508 ± 0.013	18.394 ± 0.015	18.419 ± 0.018	
comane7-23	1806	18.444 ± 0.011	18.437 ± 0.012	18.310 ± 0.014	18.385 ± 0.018	
coma10-45	1807	15.398 ± 0.002	15.322 ± 0.002	15.161 ± 0.002	15.164 ± 0.002	15.051 ± 0.002
coma17-30	1819	19.299 ± 0.030	19.263 ± 0.039	19.170 ± 0.049	19.209 ± 0.063	19.168 ± 0.068
coma10-17	1828	19.424 ± 0.033	19.497 ± 0.046	19.461 ± 0.060	19.589 ± 0.082	19.592 ± 0.089
comane3-47	1841	19.821 ± 0.046	19.805 ± 0.060	19.742 ± 0.076	19.965 ± 0.115	
coma10-6	1844	19.677 ± 0.040	19.701 ± 0.055	19.614 ± 0.068	19.681 ± 0.089	19.948 ± 0.130
comane3-17	1853	14.971 ± 0.001	14.866 ± 0.001	14.704 ± 0.001	14.714 ± 0.001	
coma10-34	1856	19.582 ± 0.040	19.648 ± 0.056	19.578 ± 0.071	19.710 ± 0.099	19.399 ± 0.074
coma10-23	1876	18.830 ± 0.020	18.767 ± 0.025	18.642 ± 0.029	18.711 ± 0.038	18.705 ± 0.039
comane3-43	1882	18.970 ± 0.021	18.940 ± 0.026	18.804 ± 0.031	18.768 ± 0.036	
comane3-76	1885	16.784 ± 0.004	16.747 ± 0.004	16.630 ± 0.005	16.685 ± 0.007	
comane3-41	1887	19.146 ± 0.026	18.853 ± 0.026	18.586 ± 0.027	18.460 ± 0.029	
comane3-72	1888	19.265 ± 0.030	19.405 ± 0.045	19.393 ± 0.060	19.440 ± 0.077	
comane7-21	1889	18.745 ± 0.013	18.793 ± 0.016	18.698 ± 0.019	18.788 ± 0.024	
comane7-27	1897	18.771 ± 0.014	18.771 ± 0.016	18.683 ± 0.020	18.759 ± 0.026	
comane7-29	1898	17.797 ± 0.007	17.751 ± 0.008	17.624 ± 0.009	17.682 ± 0.010	
comane3-61	1907	19.692 ± 0.042	19.795 ± 0.060	19.774 ± 0.080	19.927 ± 0.112	
comane3-75	1918	18.055 ± 0.011	17.877 ± 0.012	17.680 ± 0.014	17.661 ± 0.016	
comane3-10	1921	19.040 ± 0.022	19.108 ± 0.030	19.028 ± 0.038	19.012 ± 0.045	
comane3-77	1926	18.960 ± 0.024	19.072 ± 0.035	19.037 ± 0.047	19.215 ± 0.069	
comane7-18	1931	17.556 ± 0.006	17.429 ± 0.006	17.259 ± 0.006	17.266 ± 0.007	
coma17-39	1941	19.805 ± 0.046	19.927 ± 0.070	19.855 ± 0.090	19.887 ± 0.114	20.219 ± 0.170
coma17-50	1953	17.881 ± 0.009	17.816 ± 0.011	17.682 ± 0.013	17.738 ± 0.017	17.680 ± 0.017
coma10-60	1958	18.871 ± 0.022	18.926 ± 0.031	18.832 ± 0.040	18.934 ± 0.055	18.997 ± 0.065
coma17-72	1960	17.676 ± 0.008	17.714 ± 0.010	17.632 ± 0.013	17.726 ± 0.016	17.715 ± 0.017
comane3-40	1966	18.668 ± 0.017	18.664 ± 0.022	18.568 ± 0.027	18.614 ± 0.034	
comane3-38	1975	17.488 ± 0.006	17.380 ± 0.007	17.233 ± 0.008	17.263 ± 0.009	
comane3-46	1977	19.260 ± 0.028	19.344 ± 0.040	19.290 ± 0.051	19.402 ± 0.069	
coma10-53	1986	17.879 ± 0.009	17.598 ± 0.009	17.361 ± 0.010	17.308 ± 0.011	17.178 ± 0.011
coma10-38	1993	19.660 ± 0.042	19.405 ± 0.044	19.076 ± 0.044	19.118 ± 0.056	20.865 ± 0.454
coma17-41	1995	19.619 ± 0.040	19.666 ± 0.057	19.542 ± 0.070	19.581 ± 0.089	19.866 ± 0.121
coma17-55	1996	18.317 ± 0.013	18.292 ± 0.017	18.177 ± 0.020	18.252 ± 0.027	18.298 ± 0.029
coma17-31	1998	19.678 ± 0.041	19.696 ± 0.056	19.584 ± 0.068	19.634 ± 0.089	20.081 ± 0.150
coma10-33	2000	14.770 ± 0.001	14.636 ± 0.001	14.456 ± 0.001	14.437 ± 0.001	14.282 ± 0.001
comane7-38	2002	18.604 ± 0.012	18.547 ± 0.014	18.414 ± 0.016	18.447 ± 0.019	
comane3-63	2016	19.556 ± 0.035	19.635 ± 0.049	19.555 ± 0.061	19.601 ± 0.078	
comane7-22	2019	18.623 ± 0.012	18.632 ± 0.014	18.527 ± 0.016	18.525 ± 0.020	

Raw V-band aperture magnitudes. *continued from previous page*

Object	GMP	Aperture Dia. (″) 8.8	13	16	20.2	26
coma17-71	2020	19.532 ± 0.036	19.477 ± 0.044	19.394 ± 0.056	19.479 ± 0.077	19.454 ± 0.084
comane3-78	2027	19.328 ± 0.030	19.272 ± 0.038	19.157 ± 0.046	19.224 ± 0.059	
coma10-56	2033	17.412 ± 0.006	17.360 ± 0.007	17.234 ± 0.008	17.291 ± 0.010	17.318 ± 0.012
coma10-32	2035	17.670 ± 0.010	17.754 ± 0.014	17.686 ± 0.018	17.802 ± 0.024	17.745 ± 0.021
comane3-57	2036	19.759 ± 0.042	19.786 ± 0.056	19.709 ± 0.071	19.737 ± 0.088	
coma17-74	2040	19.610 ± 0.041	19.485 ± 0.050	19.301 ± 0.058	19.358 ± 0.076	19.718 ± 0.110
comane7-17	2044	18.889 ± 0.014	18.921 ± 0.018	18.834 ± 0.022	18.912 ± 0.028	
comane3-59	2047	17.587 ± 0.007	17.564 ± 0.008	17.440 ± 0.010	17.490 ± 0.012	
coma17-45	2048	16.017 ± 0.002	16.039 ± 0.003	15.938 ± 0.003	16.004 ± 0.004	15.998 ± 0.004
comane3-67	2052	19.095 ± 0.025	19.073 ± 0.032	18.980 ± 0.039	19.058 ± 0.051	
comane7-20	2053	18.151 ± 0.008	18.036 ± 0.009	17.884 ± 0.010	17.916 ± 0.012	
coma10-49	2059	14.974 ± 0.001	14.774 ± 0.001	14.565 ± 0.002	14.531 ± 0.002	14.224 ± 0.001
comane3-81	2060	17.918 ± 0.009	17.830 ± 0.010	17.666 ± 0.012	17.678 ± 0.014	
comane3-29	2063	18.987 ± 0.023	19.030 ± 0.031	18.941 ± 0.039	18.951 ± 0.048	
comane3-48	2064	18.956 ± 0.021	19.000 ± 0.028	18.912 ± 0.034	18.973 ± 0.044	
coma17-66	2068	19.627 ± 0.042	19.534 ± 0.051	19.387 ± 0.062	19.381 ± 0.075	19.206 ± 0.068
comane3-70	2091	15.763 ± 0.002	15.648 ± 0.002	15.472 ± 0.002	15.456 ± 0.002	
coma17-67	2103	19.734 ± 0.045	19.736 ± 0.060	19.706 ± 0.080	19.736 ± 0.102	19.552 ± 0.092
coma17-54	2109	19.266 ± 0.029	19.268 ± 0.039	19.111 ± 0.046	19.093 ± 0.056	18.839 ± 0.049
coma17-59	2110	19.581 ± 0.038	19.535 ± 0.049	19.298 ± 0.054	19.198 ± 0.061	18.836 ± 0.048
coma17-76	2113	19.654 ± 0.045	19.625 ± 0.063	19.532 ± 0.083		
coma17-27	2129	18.031 ± 0.010	17.913 ± 0.012	17.755 ± 0.013	17.782 ± 0.017	17.718 ± 0.017
coma22-63	2135	19.972 ± 0.060	20.231 ± 0.100	20.256 ± 0.141	20.643 ± 0.249	20.110 ± 0.142
coma10-35	2141	17.418 ± 0.006	17.298 ± 0.007	17.133 ± 0.008	17.146 ± 0.009	17.117 ± 0.011
coma22-45	2145	17.246 ± 0.005	17.189 ± 0.006	17.057 ± 0.007	17.111 ± 0.008	17.085 ± 0.009
coma5-8	2148	19.093 ± 0.024	19.209 ± 0.036	19.140 ± 0.047	19.147 ± 0.060	
coma22-64	2151	17.940 ± 0.009	17.916 ± 0.011	17.797 ± 0.013	17.849 ± 0.016	17.834 ± 0.017
comane6-47	2155	19.035 ± 0.028	19.013 ± 0.035	18.881 ± 0.042	18.924 ± 0.054	
coma10-22	2157	14.797 ± 0.001	14.664 ± 0.001	14.479 ± 0.001	14.465 ± 0.001	14.357 ± 0.001
coma22-32	2158	17.963 ± 0.009	17.843 ± 0.010	17.678 ± 0.011	17.691 ± 0.013	17.663 ± 0.015
coma5-52	2166	19.215 ± 0.025	19.113 ± 0.031	18.803 ± 0.032	18.783 ± 0.039	18.709 ± 0.039
coma5-53	2170	19.529 ± 0.032	19.308 ± 0.036	18.887 ± 0.033	18.821 ± 0.039	18.743 ± 0.040
coma16-53	2178	19.620 ± 0.041	19.720 ± 0.060	19.672 ± 0.078	19.799 ± 0.108	19.728 ± 0.122
coma10-57	2183	19.438 ± 0.032	19.387 ± 0.041	19.259 ± 0.049	19.222 ± 0.055	19.345 ± 0.076
coma5-25	2185	17.051 ± 0.004	16.919 ± 0.005	16.748 ± 0.005	16.757 ± 0.006	16.696 ± 0.006
coma16-88	2190	19.705 ± 0.044	19.595 ± 0.056	19.420 ± 0.063	19.384 ± 0.075	19.406 ± 0.094
coma16-72	2192	19.855 ± 0.049	19.983 ± 0.074	19.851 ± 0.088	19.943 ± 0.113	20.086 ± 0.150
comane6-17	2193	19.382 ± 0.036	19.358 ± 0.046	19.239 ± 0.055	19.043 ± 0.057	
coma16-40	2197	19.514 ± 0.037	19.572 ± 0.053	19.496 ± 0.067	19.500 ± 0.079	19.447 ± 0.086
coma10-54	2201	16.384 ± 0.003	16.290 ± 0.003	16.119 ± 0.003	16.113 ± 0.004	16.013 ± 0.004
coma22-27	2205	17.667 ± 0.007	17.583 ± 0.008	17.440 ± 0.009	17.470 ± 0.012	17.423 ± 0.012
comane3-82	2212	18.632 ± 0.017	18.524 ± 0.019	18.380 ± 0.023	18.357 ± 0.027	
comane6-51	2213	19.215 ± 0.032	18.914 ± 0.032	18.474 ± 0.028	18.283 ± 0.029	
comane6-52	2214	18.636 ± 0.020	18.481 ± 0.022	18.235 ± 0.024	18.208 ± 0.029	
coma22-65	2215	18.859 ± 0.019	18.780 ± 0.023	18.656 ± 0.028	18.704 ± 0.036	18.691 ± 0.036
comane3-83	2222	19.201 ± 0.027	19.145 ± 0.034	18.914 ± 0.037	18.686 ± 0.038	
coma16-32	2226	19.159 ± 0.026	18.890 ± 0.027	18.659 ± 0.030	18.597 ± 0.034	18.491 ± 0.037
coma5-56	2232	18.429 ± 0.013	18.248 ± 0.014	18.067 ± 0.016	18.079 ± 0.020	18.008 ± 0.020
comane6-53	2233	18.329 ± 0.015	18.162 ± 0.017	18.003 ± 0.019	18.031 ± 0.024	
coma10-19	2237	15.916 ± 0.002	15.790 ± 0.002	15.600 ± 0.002	15.572 ± 0.003	15.454 ± 0.003
coma16-71	2239	19.853 ± 0.047	19.875 ± 0.066	19.845 ± 0.090	20.040 ± 0.131	20.076 ± 0.145
coma5-30	2248	19.341 ± 0.027	19.185 ± 0.032	19.047 ± 0.038	19.105 ± 0.050	18.995 ± 0.049
coma16-86	2251	16.643 ± 0.003	16.585 ± 0.004	16.442 ± 0.005	16.474 ± 0.006	16.412 ± 0.006

Raw V-band aperture magnitudes. *continued from previous page*

Object	GMP	Aperture Dia. (″) 8.8	13	16	20.2	26
coma9-30	2252	15.891 ± 0.002	15.784 ± 0.002	15.608 ± 0.002	15.595 ± 0.003	15.466 ± 0.002
coma9-58	2253	19.297 ± 0.031	19.162 ± 0.035	18.925 ± 0.038	18.868 ± 0.045	18.865 ± 0.049
comane6-18	2257	19.237 ± 0.035	19.117 ± 0.040	18.947 ± 0.046	18.927 ± 0.056	
comane6-65	2259	16.009 ± 0.002	15.868 ± 0.002	15.678 ± 0.002	15.656 ± 0.003	
coma9-57	2262	19.701 ± 0.044	19.503 ± 0.048	19.170 ± 0.048	19.043 ± 0.052	18.901 ± 0.052
coma9-46	2263	18.834 ± 0.020	18.658 ± 0.022	18.474 ± 0.025	18.472 ± 0.030	18.440 ± 0.031
coma5-67	2265	19.342 ± 0.028	19.323 ± 0.037	19.221 ± 0.046	19.260 ± 0.058	19.059 ± 0.049
coma16-63	2267	18.919 ± 0.022	18.823 ± 0.027	18.625 ± 0.031	18.635 ± 0.039	18.785 ± 0.047
coma16-24	2268	18.911 ± 0.021	18.790 ± 0.026	18.595 ± 0.029	18.625 ± 0.037	18.590 ± 0.039
coma22-23	2269	19.535 ± 0.033	19.445 ± 0.040	19.318 ± 0.048	19.334 ± 0.060	19.554 ± 0.084
coma22-42	2270	17.909 ± 0.008	17.902 ± 0.010	17.813 ± 0.013	17.909 ± 0.017	17.914 ± 0.018
coma16-55	2273	19.368 ± 0.032	19.261 ± 0.040	19.134 ± 0.049	19.264 ± 0.068	19.102 ± 0.063
coma9-20	2276	18.942 ± 0.023	19.001 ± 0.031	18.943 ± 0.039	19.080 ± 0.055	19.145 ± 0.068
comane6-37	2281	19.569 ± 0.043	19.578 ± 0.057	19.456 ± 0.068	19.570 ± 0.093	
coma5-43	2285	18.548 ± 0.013	18.331 ± 0.015	18.122 ± 0.017	18.095 ± 0.020	18.029 ± 0.020
coma16-54	2287	19.246 ± 0.030	19.185 ± 0.038	19.073 ± 0.047	19.213 ± 0.066	19.147 ± 0.065
coma16-45	2288	19.103 ± 0.026	19.172 ± 0.037	19.147 ± 0.050	19.223 ± 0.066	19.282 ± 0.073
coma16-104	2289	17.846 ± 0.009	17.783 ± 0.011	17.628 ± 0.014	17.641 ± 0.017	17.610 ± 0.017
coma22-74	2293	18.565 ± 0.015	18.508 ± 0.019	18.349 ± 0.022	18.366 ± 0.027	18.456 ± 0.032
coma16-2	2295	17.649 ± 0.008	17.494 ± 0.009	17.307 ± 0.011		
coma16-89	2297	19.532 ± 0.037	19.470 ± 0.049	19.311 ± 0.059	19.344 ± 0.078	19.356 ± 0.076
coma16-82	2311	19.413 ± 0.034	19.365 ± 0.044	19.240 ± 0.055	19.406 ± 0.076	19.571 ± 0.099
coma5-68	2316	18.817 ± 0.017	18.742 ± 0.021	18.609 ± 0.026	18.677 ± 0.033	19.067 ± 0.056
comane6-33	2321	19.339 ± 0.033	19.338 ± 0.043	19.195 ± 0.050	19.239 ± 0.064	
coma22-59	2322	18.406 ± 0.012	18.383 ± 0.016	18.296 ± 0.019	18.364 ± 0.025	18.353 ± 0.026
coma16-64	2323	19.430 ± 0.036	19.276 ± 0.042	18.996 ± 0.045	19.040 ± 0.057	19.223 ± 0.074
coma16-13	2333	19.057 ± 0.028	18.944 ± 0.034	18.793 ± 0.041	18.821 ± 0.052	18.515 ± 0.039
coma9-24	2335	18.897 ± 0.021	18.579 ± 0.020	18.304 ± 0.021	18.215 ± 0.024	18.207 ± 0.031
coma5-45	2342	19.491 ± 0.032	19.549 ± 0.046	19.465 ± 0.058	19.658 ± 0.086	19.625 ± 0.086
coma22-48	2343	19.156 ± 0.024	19.207 ± 0.033	19.089 ± 0.040	19.172 ± 0.053	19.124 ± 0.053
coma16-12	2347	15.458 ± 0.002	15.323 ± 0.002	15.143 ± 0.002	15.131 ± 0.002	15.027 ± 0.002
coma22-44	2349	19.579 ± 0.035	19.665 ± 0.050	19.633 ± 0.066	19.765 ± 0.091	19.588 ± 0.082
coma5-49	2352	19.030 ± 0.021	19.113 ± 0.030	19.026 ± 0.038	19.075 ± 0.049	18.750 ± 0.038
coma16-83	2353	18.660 ± 0.018	18.529 ± 0.022	18.360 ± 0.025	18.373 ± 0.032	18.598 ± 0.044
coma5-18	2355	16.933 ± 0.004	16.612 ± 0.004	16.296 ± 0.004	16.132 ± 0.004	15.886 ± 0.003
coma22-49	2359	19.210 ± 0.025	19.105 ± 0.030	18.907 ± 0.033	18.895 ± 0.040	18.881 ± 0.043
comane6-62	2361	17.834 ± 0.009	17.755 ± 0.011	17.613 ± 0.013	17.652 ± 0.016	
coma5-61	2364	18.339 ± 0.012	18.413 ± 0.016	18.336 ± 0.020	18.418 ± 0.027	18.540 ± 0.035
coma22-38	2366	19.492 ± 0.032	19.533 ± 0.044	19.502 ± 0.058	19.613 ± 0.078	19.613 ± 0.085
coma9-9	2374	15.130 ± 0.002	14.871 ± 0.002	14.574 ± 0.002	14.400 ± 0.002	13.996 ± 0.001
coma16-9	2376	17.982 ± 0.010	17.754 ± 0.011	17.534 ± 0.012	17.499 ± 0.014	17.403 ± 0.016
coma16-58	2382	19.608 ± 0.044	19.721 ± 0.067	19.747 ± 0.093		
comane6-28	2383	19.087 ± 0.028	19.116 ± 0.038	19.040 ± 0.047	19.115 ± 0.062	
coma9-42	2385	16.760 ± 0.004	16.752 ± 0.004	16.642 ± 0.005	16.706 ± 0.006	16.693 ± 0.006
coma16-74	2390	15.022 ± 0.001	14.757 ± 0.001	14.505 ± 0.001	14.417 ± 0.001	14.188 ± 0.001
coma5-72	2393	16.040 ± 0.003	15.903 ± 0.003	15.704 ± 0.003	15.665 ± 0.004	15.490 ± 0.003
coma16-43	2399	18.176 ± 0.012	17.942 ± 0.013	17.741 ± 0.015	17.764 ± 0.018	17.699 ± 0.017
coma5-12	2407	19.151 ± 0.022	19.143 ± 0.030	18.992 ± 0.036	18.948 ± 0.043	18.878 ± 0.044
coma9-34	2408	18.576 ± 0.016	18.331 ± 0.016	18.087 ± 0.017	18.011 ± 0.019	17.861 ± 0.019
coma9-21	2411	18.207 ± 0.014	18.126 ± 0.017	18.002 ± 0.020	18.085 ± 0.026	17.898 ± 0.025
coma5-11	2412	19.677 ± 0.036	19.532 ± 0.043	19.335 ± 0.049	19.270 ± 0.057	19.145 ± 0.056
comane6-67	2413	14.772 ± 0.001	14.626 ± 0.001	14.431 ± 0.001	14.398 ± 0.001	
coma22-37	2415	18.500 ± 0.014	18.540 ± 0.018	18.462 ± 0.023	18.576 ± 0.031	18.540 ± 0.031

Raw V-band aperture magnitudes. *continued from previous page*

Object	GMP	Aperture Dia. (″) 8.8	13	16	20.2	26
coma16-94	2417	14.778 ± 0.001	14.632 ± 0.001	14.438 ± 0.001	14.411 ± 0.001	14.270 ± 0.001
coma5-35	2420	18.489 ± 0.013	18.405 ± 0.015	18.249 ± 0.018	18.271 ± 0.023	18.300 ± 0.026
coma5-57	2421	17.533 ± 0.006	17.305 ± 0.006	17.086 ± 0.007	17.059 ± 0.008	16.972 ± 0.008
coma9-26	2427	19.906 ± 0.066	20.122 ± 0.105	20.191 ± 0.151	20.472 ± 0.239	
comane6-27	2428	19.575 ± 0.042	19.610 ± 0.056	19.501 ± 0.069	19.398 ± 0.076	
coma16-3	2430	19.242 ± 0.029	19.176 ± 0.038	18.712 ± 0.037	17.277 ± 0.011	16.431 ± 0.006
coma22-54	2432	19.173 ± 0.032	19.140 ± 0.042	18.983 ± 0.050	18.906 ± 0.058	18.517 ± 0.038
coma5-32	2438	19.939 ± 0.046	19.925 ± 0.062	19.778 ± 0.075	19.722 ± 0.088	19.953 ± 0.118
coma22-31	2440	14.811 ± 0.001	14.675 ± 0.001	14.505 ± 0.001	14.511 ± 0.001	14.421 ± 0.001
coma22-61	2441	15.305 ± 0.002	15.063 ± 0.001	14.812 ± 0.001	14.692 ± 0.001	14.366 ± 0.001
coma16-84	2442	19.652 ± 0.042	19.717 ± 0.062	19.631 ± 0.075	19.689 ± 0.098	18.722 ± 0.057
comane6-23	2443	19.160 ± 0.029	19.075 ± 0.034	18.921 ± 0.040	18.942 ± 0.050	
coma9-38	2445	19.365 ± 0.033	19.244 ± 0.039	19.100 ± 0.045	19.144 ± 0.058	19.345 ± 0.072
coma16-62	2448	19.412 ± 0.034	19.406 ± 0.046	19.325 ± 0.058	19.424 ± 0.079	19.563 ± 0.114
coma22-33	2449	19.023 ± 0.027	18.952 ± 0.033	18.773 ± 0.038	18.790 ± 0.048	18.578 ± 0.036
coma22-26	2452	19.101 ± 0.028	19.092 ± 0.036	18.921 ± 0.042	18.861 ± 0.050	18.433 ± 0.030
coma16-60	2454	19.847 ± 0.051	20.078 ± 0.085	20.080 ± 0.118	20.187 ± 0.161	21.144 ± 0.431
coma16-70	2455	19.968 ± 0.058	20.108 ± 0.090			
coma16-17	2457	16.094 ± 0.002	15.947 ± 0.003	15.768 ± 0.003	15.770 ± 0.003	15.697 ± 0.003
coma22-67	2464	18.790 ± 0.019	18.862 ± 0.026	18.796 ± 0.032	18.844 ± 0.042	18.965 ± 0.052
coma5-26	2466	19.122 ± 0.022	19.107 ± 0.029	18.978 ± 0.036	19.027 ± 0.046	18.961 ± 0.048
coma5-22	2469	19.739 ± 0.037	19.454 ± 0.039	19.191 ± 0.042	19.147 ± 0.050	19.029 ± 0.050
coma16-61	2470	19.284 ± 0.030	19.248 ± 0.039	19.173 ± 0.050	19.277 ± 0.068	19.899 ± 0.139
comane6-41	2475	19.638 ± 0.044	19.644 ± 0.058	19.567 ± 0.072	19.700 ± 0.100	
coma5-55	2477	19.851 ± 0.044	19.600 ± 0.048	19.361 ± 0.053	19.349 ± 0.065	19.243 ± 0.061
coma9-39	2478	17.388 ± 0.006	17.290 ± 0.007	17.137 ± 0.008	17.177 ± 0.010	17.175 ± 0.011
coma5-58	2480	18.379 ± 0.012	18.174 ± 0.013	17.950 ± 0.014	17.911 ± 0.017	17.851 ± 0.017
coma5-33	2485	19.670 ± 0.036	19.698 ± 0.051	19.650 ± 0.067	19.719 ± 0.089	20.078 ± 0.132
coma22-69	2487	18.730 ± 0.016	18.788 ± 0.022	18.716 ± 0.028	18.812 ± 0.038	18.784 ± 0.040
coma16-6	2488	19.423 ± 0.037	19.247 ± 0.043	19.087 ± 0.051	19.102 ± 0.065	19.056 ± 0.064
coma22-34	2489	16.039 ± 0.002	15.951 ± 0.002	15.805 ± 0.002	15.838 ± 0.003	15.816 ± 0.003
coma16-30	2490	18.769 ± 0.019	18.727 ± 0.025	18.597 ± 0.030	18.634 ± 0.038	18.683 ± 0.045
coma5-71	2491	19.019 ± 0.021	18.966 ± 0.028	18.849 ± 0.037	18.928 ± 0.051	19.235 ± 0.080
coma22-22	2492	19.452 ± 0.032	19.552 ± 0.046	19.436 ± 0.056	19.530 ± 0.074	
coma5-65	2493	19.616 ± 0.035	19.686 ± 0.051	19.624 ± 0.064	19.744 ± 0.083	19.931 ± 0.093
coma9-50	2494	19.526 ± 0.036	19.645 ± 0.053	19.645 ± 0.071	19.873 ± 0.106	20.243 ± 0.174
comane6-54	2495	15.273 ± 0.002	15.169 ± 0.001	15.016 ± 0.002	15.037 ± 0.002	
coma22-72	2501	18.196 ± 0.010	18.168 ± 0.013	18.040 ± 0.015	18.076 ± 0.019	18.080 ± 0.022
coma16-51	2504	18.764 ± 0.023	18.599 ± 0.027	18.285 ± 0.028	18.026 ± 0.028	17.364 ± 0.014
comane6-3	2505	18.853 ± 0.022	18.868 ± 0.030	18.746 ± 0.036	18.787 ± 0.046	
coma15-63	2507	19.999 ± 0.057	20.205 ± 0.097	20.246 ± 0.142		
coma15-101	2508	18.825 ± 0.022	18.884 ± 0.033	18.819 ± 0.043	18.935 ± 0.064	
coma15-55	2510	15.792 ± 0.002	15.637 ± 0.002	15.434 ± 0.002	15.399 ± 0.003	15.265 ± 0.002
coma15-114	2511	19.008 ± 0.022	18.864 ± 0.026	18.683 ± 0.030	18.645 ± 0.035	18.583 ± 0.044
comane6-36	2513	17.154 ± 0.005	17.090 ± 0.006	16.968 ± 0.007	17.049 ± 0.009	
coma15-53	2516	15.061 ± 0.001	14.932 ± 0.001	14.750 ± 0.001	14.725 ± 0.002	14.576 ± 0.001
coma15-116	2518	19.540 ± 0.035	19.372 ± 0.044	19.125 ± 0.050	19.017 ± 0.056	18.858 ± 0.071
coma22-40	2519	18.553 ± 0.014	18.285 ± 0.014	18.013 ± 0.015	17.905 ± 0.016	17.718 ± 0.015
coma15-109	2529	17.638 ± 0.007	17.611 ± 0.008	17.502 ± 0.010	17.573 ± 0.013	17.582 ± 0.015
coma15-3	2531	17.169 ± 0.005	16.932 ± 0.005	16.765 ± 0.005	16.807 ± 0.007	16.734 ± 0.007
coma15-75	2535	15.685 ± 0.002	15.515 ± 0.002	15.310 ± 0.002	15.269 ± 0.002	15.145 ± 0.002
coma4-55	2537	18.973 ± 0.025	19.027 ± 0.032	18.946 ± 0.040	19.076 ± 0.056	
coma15-27	2541	15.179 ± 0.001	15.006 ± 0.001	14.801 ± 0.001	14.766 ± 0.001	14.638 ± 0.001

Raw V-band aperture magnitudes. *contiuned from previous page*

Object	GMP	Aperture Dia. ('') 8.8	13	16	20.2	26
coma16-78	2550	18.646 ± 0.025	18.489 ± 0.030	18.257 ± 0.033	18.080 ± 0.035	17.262 ± 0.012
coma15-89	2551	15.890 ± 0.002	15.618 ± 0.002	15.306 ± 0.002		
coma5-34	2553	19.609 ± 0.034	19.450 ± 0.041	19.281 ± 0.048	19.344 ± 0.063	19.358 ± 0.066
coma15-62	2555	18.658 ± 0.017	18.736 ± 0.024	18.697 ± 0.031	18.859 ± 0.043	18.975 ± 0.051
coma15-121	2559	15.965 ± 0.002	15.631 ± 0.002	15.356 ± 0.002	15.279 ± 0.002	15.135 ± 0.002
coma25-53	2566	18.390 ± 0.013	18.306 ± 0.014	18.140 ± 0.016	18.193 ± 0.021	18.315 ± 0.025
coma15-11	2570	18.935 ± 0.021	18.817 ± 0.025	18.641 ± 0.029	18.578 ± 0.034	18.407 ± 0.034
coma15-29	2571	19.321 ± 0.036	19.395 ± 0.052	19.427 ± 0.069	19.723 ± 0.098	18.919 ± 0.041
coma15-86	2577	18.740 ± 0.020	18.757 ± 0.028	18.640 ± 0.035	18.683 ± 0.045	18.389 ± 0.030
coma21-72	2584	15.824 ± 0.002	15.654 ± 0.002	15.457 ± 0.002	15.428 ± 0.002	15.306 ± 0.002
coma15-41	2585	17.959 ± 0.009	17.809 ± 0.010	17.638 ± 0.012	17.650 ± 0.014	17.515 ± 0.013
coma8-30	2587	18.446 ± 0.018	18.500 ± 0.026	18.454 ± 0.033	18.593 ± 0.046	18.718 ± 0.052
coma15-33	2591	18.090 ± 0.011	17.895 ± 0.012	17.699 ± 0.013	17.696 ± 0.016	17.597 ± 0.014
coma15-112	2593	19.566 ± 0.035	19.383 ± 0.038	19.117 ± 0.041	19.115 ± 0.049	19.596 ± 0.078
coma5-14	2599	16.349 ± 0.003	16.062 ± 0.002	15.799 ± 0.002	15.711 ± 0.003	15.546 ± 0.002
coma4-57	2603	16.877 ± 0.005	16.731 ± 0.005	16.550 ± 0.005	16.555 ± 0.006	
coma15-59	2605	19.068 ± 0.022	18.888 ± 0.025	18.719 ± 0.029	18.746 ± 0.037	18.747 ± 0.046
coma4-49	2606	19.082 ± 0.024	18.959 ± 0.026	18.685 ± 0.026	18.503 ± 0.027	
coma4-50	2613	18.996 ± 0.022	18.998 ± 0.025	18.792 ± 0.027	18.634 ± 0.028	
coma15-118	2614	19.484 ± 0.033	19.289 ± 0.037	19.117 ± 0.043	19.164 ± 0.055	20.005 ± 0.101
coma4-31	2615	16.447 ± 0.004	16.272 ± 0.004	16.076 ± 0.004	16.060 ± 0.004	
coma25-48	2619	18.206 ± 0.011	17.983 ± 0.011	17.749 ± 0.012	17.689 ± 0.013	17.590 ± 0.014
coma21-49	2626	18.078 ± 0.011	17.977 ± 0.012	17.822 ± 0.013	17.847 ± 0.016	17.556 ± 0.013
coma21-80	2631	18.921 ± 0.022	18.821 ± 0.025	18.542 ± 0.026	18.247 ± 0.024	17.687 ± 0.014
coma21-79	2633	17.927 ± 0.009	17.769 ± 0.010	17.582 ± 0.011	17.553 ± 0.012	17.387 ± 0.011
coma4-32	2635	18.187 ± 0.013	18.105 ± 0.014	17.948 ± 0.015	18.006 ± 0.019	
coma4-52	2644	19.336 ± 0.032	19.186 ± 0.034	19.007 ± 0.039	19.063 ± 0.049	
coma21-77	2647	19.172 ± 0.028	19.285 ± 0.039	19.227 ± 0.050	19.314 ± 0.065	18.972 ± 0.046
coma15-58	2651	16.099 ± 0.002	15.916 ± 0.002	15.701 ± 0.002	15.643 ± 0.002	15.505 ± 0.002
coma15-51	2654	15.861 ± 0.002	15.754 ± 0.002	15.583 ± 0.002	15.590 ± 0.002	15.547 ± 0.003
coma15-67	2655	19.768 ± 0.040	19.719 ± 0.052	19.616 ± 0.065	19.739 ± 0.090	20.311 ± 0.170
coma15-115	2660	19.600 ± 0.041	19.405 ± 0.046	19.235 ± 0.053	19.330 ± 0.073	19.607 ± 0.110
coma15-80	2663	19.649 ± 0.036	19.643 ± 0.049	19.550 ± 0.061	19.599 ± 0.079	19.191 ± 0.058
coma15-26	2665	19.746 ± 0.041	19.907 ± 0.065	19.737 ± 0.076	19.740 ± 0.095	19.864 ± 0.109
coma15-117	2667	18.649 ± 0.017	18.676 ± 0.024	18.566 ± 0.031	18.515 ± 0.036	18.255 ± 0.029
coma15-81	2676	18.520 ± 0.014	18.427 ± 0.017	18.303 ± 0.020	18.346 ± 0.026	18.318 ± 0.027
coma15-100	2677	19.817 ± 0.045	20.008 ± 0.073	19.979 ± 0.098	20.169 ± 0.144	20.084 ± 0.147
coma15-113	2679	19.172 ± 0.027	19.027 ± 0.033	18.881 ± 0.041	18.892 ± 0.052	18.667 ± 0.049
coma15-35	2683	18.519 ± 0.014	18.554 ± 0.019	18.340 ± 0.021	18.395 ± 0.027	18.376 ± 0.030
coma15-45	2684	18.920 ± 0.019	18.898 ± 0.024	18.782 ± 0.030	18.902 ± 0.041	18.901 ± 0.047
coma25-27	2685	18.586 ± 0.016	18.552 ± 0.020	18.459 ± 0.024	18.577 ± 0.033	18.590 ± 0.033
coma21-76	2687	18.733 ± 0.017	18.589 ± 0.019	18.412 ± 0.022	18.416 ± 0.026	18.407 ± 0.027
coma15-24	2692	17.804 ± 0.007	17.634 ± 0.008	17.436 ± 0.009	17.428 ± 0.011	17.343 ± 0.011
coma15-30	2694	19.552 ± 0.038	19.580 ± 0.053	19.415 ± 0.062	19.339 ± 0.072	18.805 ± 0.041
coma4-28	2698	18.845 ± 0.020	18.782 ± 0.023	18.696 ± 0.028	18.793 ± 0.037	
coma25;21	2711	18.036 ± 0.010	18.114 ± 0.013	18.039 ± 0.016	18.129 ± 0.021	18.323 ± 0.031
coma25-54	2712	19.756 ± 0.043	19.795 ± 0.057	19.731 ± 0.072	19.883 ± 0.100	20.139 ± 0.132
coma8-36	2716	19.128 ± 0.034	19.046 ± 0.043	18.923 ± 0.053	18.990 ± 0.069	18.633 ± 0.050
coma15-54	2718	19.365 ± 0.030	19.271 ± 0.037	19.117 ± 0.044	19.183 ± 0.058	19.483 ± 0.093
coma15-110	2727	15.541 ± 0.002	15.375 ± 0.002	15.175 ± 0.002	15.145 ± 0.002	15.027 ± 0.002
coma25-44	2728	17.453 ± 0.006	17.334 ± 0.006	17.176 ± 0.007	17.216 ± 0.009	17.208 ± 0.010
coma8-33	2735	19.119 ± 0.035	19.169 ± 0.050	19.077 ± 0.063	19.167 ± 0.085	18.736 ± 0.055
coma15-5	2736	17.488 ± 0.006	17.392 ± 0.007	17.257 ± 0.008	17.311 ± 0.010	17.308 ± 0.011

Raw V-band aperture magnitudes. *contiuned from previous page*

Object	GMP	Aperture Dia. ('') 8.8	13	16	20.2	26
coma4-35	2738	18.738 ± 0.021	18.730 ± 0.025	18.617 ± 0.030	18.728 ± 0.039	
coma4-51	2749	18.934 ± 0.021	18.786 ± 0.023	18.603 ± 0.026	18.656 ± 0.032	
coma25-51	2750	18.909 ± 0.022	18.970 ± 0.029	18.927 ± 0.037	19.075 ± 0.052	18.870 ± 0.044
coma21-26	2752	19.540 ± 0.036	19.527 ± 0.045	19.385 ± 0.053	19.447 ± 0.068	19.882 ± 0.120
coma8-34	2753	17.455 ± 0.008	17.294 ± 0.009	17.111 ± 0.010	17.117 ± 0.012	17.028 ± 0.012
coma15-72	2755	19.504 ± 0.034	19.410 ± 0.042	19.223 ± 0.049	19.305 ± 0.065	19.210 ± 0.071
coma15-8	2763	19.633 ± 0.036	19.826 ± 0.058	19.762 ± 0.076	19.869 ± 0.103	19.699 ± 0.093
coma21-55	2764	18.326 ± 0.012	18.265 ± 0.014	18.124 ± 0.016	18.181 ± 0.021	18.205 ± 0.024
coma15-82	2777	17.361 ± 0.005	17.421 ± 0.007	17.325 ± 0.008	17.405 ± 0.011	17.455 ± 0.013
coma15-37	2778	16.634 ± 0.003	16.386 ± 0.003	16.160 ± 0.003	16.111 ± 0.003	16.000 ± 0.004
coma15-17	2780	19.521 ± 0.032	19.353 ± 0.037	19.189 ± 0.044	19.239 ± 0.057	19.436 ± 0.078
coma4-53	2783	17.061 ± 0.006	16.825 ± 0.005	16.599 ± 0.005	16.560 ± 0.005	
coma21-42	2784	17.861 ± 0.008	17.700 ± 0.009	17.503 ± 0.009	17.488 ± 0.011	17.499 ± 0.013
coma15-119	2787	17.948 ± 0.009	17.826 ± 0.011	17.671 ± 0.013	17.716 ± 0.017	17.787 ± 0.022
coma21-30	2790	18.791 ± 0.019	18.792 ± 0.023	18.693 ± 0.028	18.800 ± 0.038	19.451 ± 0.089
coma21-96	2795	14.491 ± 0.001	14.288 ± 0.001	14.078 ± 0.001	14.037 ± 0.001	13.903 ± 0.001
coma15-52	2798	14.690 ± 0.001	14.451 ± 0.001	14.172 ± 0.001	14.090 ± 0.001	13.976 ± 0.001
coma15-68	2799	18.377 ± 0.013	18.350 ± 0.016	18.235 ± 0.020	18.316 ± 0.027	18.138 ± 0.034
coma4-40	2800	18.176 ± 0.012	17.840 ± 0.011	17.502 ± 0.010	17.362 ± 0.011	
coma4-14	2801	18.591 ± 0.016	18.498 ± 0.018	18.391 ± 0.021	18.487 ± 0.027	
coma15-123	2805	15.982 ± 0.002	15.916 ± 0.002	15.766 ± 0.003	15.786 ± 0.003	15.732 ± 0.003
coma15-9	2808	19.830 ± 0.042	19.693 ± 0.050	19.455 ± 0.056	19.456 ± 0.069	19.811 ± 0.105
coma15-56	2815	15.746 ± 0.002	15.627 ± 0.002	15.446 ± 0.002	15.437 ± 0.002	15.350 ± 0.003
coma15-39	2819	19.819 ± 0.049	19.791 ± 0.065	19.608 ± 0.076	19.534 ± 0.088	19.096 ± 0.063
coma21-83	2825	19.162 ± 0.026	19.233 ± 0.034	19.163 ± 0.044	19.280 ± 0.059	19.546 ± 0.071
coma15-2	2835	19.231 ± 0.025	19.256 ± 0.034	19.146 ± 0.044	19.216 ± 0.057	19.380 ± 0.075
coma15-94	2838	19.669 ± 0.038	19.785 ± 0.057	19.713 ± 0.074	19.747 ± 0.094	20.084 ± 0.143
coma15-107	2839	15.410 ± 0.001	15.314 ± 0.001	15.158 ± 0.002	15.181 ± 0.002	15.143 ± 0.002
coma25-28	2849	18.776 ± 0.017	18.804 ± 0.022	18.714 ± 0.027	18.773 ± 0.035	18.887 ± 0.044
coma15-108	2851	19.505 ± 0.046	19.506 ± 0.064	19.386 ± 0.077	19.344 ± 0.094	18.264 ± 0.026
coma8-45	2852	17.547 ± 0.009	17.331 ± 0.009	17.093 ± 0.010	17.023 ± 0.011	16.917 ± 0.011
coma15-111	2856	18.286 ± 0.011	18.108 ± 0.013	17.895 ± 0.014	17.855 ± 0.016	17.917 ± 0.022
coma15-96	2858	20.031 ± 0.055	20.204 ± 0.088	20.103 ± 0.111	20.345 ± 0.171	20.500 ± 0.210
coma21-38	2860	18.441 ± 0.016	18.345 ± 0.018	18.215 ± 0.022	18.288 ± 0.028	18.164 ± 0.023
coma21-29	2861	15.723 ± 0.002	15.646 ± 0.002	15.493 ± 0.002	15.515 ± 0.002	15.460 ± 0.002
coma4-20	2863	17.875 ± 0.010	17.670 ± 0.010	17.437 ± 0.010	17.379 ± 0.011	
coma4-39	2866	16.549 ± 0.004	16.397 ± 0.004	16.203 ± 0.004	16.182 ± 0.004	
coma15-13	2877	19.233 ± 0.029	19.117 ± 0.035	18.934 ± 0.040	18.931 ± 0.048	18.517 ± 0.031
coma4-34	2878	18.904 ± 0.023	18.924 ± 0.029	18.869 ± 0.035	18.963 ± 0.045	
coma15-122	2879	17.490 ± 0.006	17.373 ± 0.007	17.217 ± 0.008	17.238 ± 0.010	
coma15-70	2895	17.909 ± 0.016	17.667 ± 0.018	17.343 ± 0.018	16.979 ± 0.016	16.523 ± 0.010
coma8-41	2897	16.650 ± 0.004	16.407 ± 0.004	16.155 ± 0.005	16.131 ± 0.005	15.992 ± 0.005
coma25-10	2899	19.778 ± 0.054	19.604 ± 0.059	19.448 ± 0.070	19.398 ± 0.082	18.916 ± 0.046
coma25-66	2906	19.570 ± 0.036	19.631 ± 0.049	19.577 ± 0.063	19.697 ± 0.085	19.831 ± 0.101
coma21-81	2907	19.156 ± 0.033	19.096 ± 0.040	18.941 ± 0.046	18.838 ± 0.051	18.161 ± 0.024
coma8-42	2910	15.990 ± 0.003	15.864 ± 0.003	15.707 ± 0.003	15.732 ± 0.004	15.641 ± 0.004
coma8-32	2911	19.012 ± 0.029	18.910 ± 0.036	18.765 ± 0.043	18.840 ± 0.057	18.930 ± 0.068
coma21-78	2912	15.623 ± 0.002	15.504 ± 0.002	15.340 ± 0.002	15.354 ± 0.002	15.277 ± 0.002
coma8-43	2913	18.790 ± 0.031	18.723 ± 0.040	18.549 ± 0.047	18.434 ± 0.052	17.689 ± 0.022
coma21-84	2914	16.968 ± 0.005	16.747 ± 0.004	16.522 ± 0.005	16.475 ± 0.005	16.339 ± 0.005
coma15-47	2917	18.492 ± 0.024	18.440 ± 0.032	18.276 ± 0.038	18.297 ± 0.048	17.539 ± 0.026
coma25-69	2918	19.137 ± 0.025	19.135 ± 0.032	19.076 ± 0.041	19.183 ± 0.054	19.265 ± 0.061
coma15-66	2921	13.966 ± 0.001	13.661 ± 0.001	13.397 ± 0.001	13.296 ± 0.001	13.032 ± 0.001

Raw V-band aperture magnitudes. *continued from previous page*

Object	GMP	Aperture Dia. (″) 8.8	13	16	20.2	26
coma21-32	2922	15.237 ± 0.001	15.170 ± 0.001	15.039 ± 0.001	15.088 ± 0.002	15.072 ± 0.002
coma3-39	2923	17.295 ± 0.008	17.162 ± 0.008	16.993 ± 0.009	17.001 ± 0.011	
coma25-61	2928	19.348 ± 0.029	19.339 ± 0.037	19.240 ± 0.045	19.298 ± 0.058	19.428 ± 0.070
coma15-50	2929	18.300 ± 0.023	18.101 ± 0.026	17.901 ± 0.030	17.880 ± 0.036	17.097 ± 0.021
coma15-28	2931	18.217 ± 0.011	18.245 ± 0.015	18.141 ± 0.018	18.229 ± 0.025	18.559 ± 0.043
coma3-18	2938	18.166 ± 0.013	18.129 ± 0.014	18.006 ± 0.017	18.056 ± 0.020	
coma15-77	2940	15.757 ± 0.002	15.602 ± 0.002	15.421 ± 0.002	15.423 ± 0.002	15.353 ± 0.003
coma3-6	2942	16.045 ± 0.003	15.974 ± 0.003	15.817 ± 0.003	15.814 ± 0.003	
coma25-36	2943	18.504 ± 0.014	18.031 ± 0.012	17.662 ± 0.011	17.479 ± 0.011	17.253 ± 0.010
coma3-41	2945	15.871 ± 0.003	15.700 ± 0.003	15.507 ± 0.003	15.489 ± 0.003	
coma15-25	2952	18.241 ± 0.012	18.111 ± 0.014	17.965 ± 0.017	18.035 ± 0.022	17.984 ± 0.021
coma21-31	2955	19.081 ± 0.027	18.980 ± 0.031	18.860 ± 0.037	18.861 ± 0.045	18.712 ± 0.037
coma15-95	2960	16.576 ± 0.003	16.392 ± 0.003	16.183 ± 0.003	16.158 ± 0.004	16.074 ± 0.004
coma15-38	2963	19.337 ± 0.029	19.348 ± 0.040	19.267 ± 0.052	19.407 ± 0.075	
coma21-87	2973	19.485 ± 0.036	19.299 ± 0.038	19.152 ± 0.043	19.242 ± 0.055	19.274 ± 0.062
coma15-69	2975	15.175 ± 0.002	14.978 ± 0.002	14.757 ± 0.002	14.700 ± 0.002	14.512 ± 0.002
coma21-75	2976	17.582 ± 0.007	17.384 ± 0.007	17.166 ± 0.007	17.147 ± 0.009	17.102 ± 0.009
coma25-49	2981	19.101 ± 0.026	19.169 ± 0.035	19.152 ± 0.046	19.375 ± 0.069	19.280 ± 0.066
coma15-79	2983	19.403 ± 0.033	19.419 ± 0.046	19.354 ± 0.059	19.537 ± 0.087	
coma25-38	2989	16.823 ± 0.004	16.729 ± 0.004	16.556 ± 0.005	16.544 ± 0.005	16.469 ± 0.007
coma15-92	2991	18.566 ± 0.015	18.659 ± 0.022	18.604 ± 0.028	18.750 ± 0.040	18.683 ± 0.037
coma25-70	2994	18.965 ± 0.022	18.981 ± 0.029	18.936 ± 0.037	19.065 ± 0.051	18.992 ± 0.049
coma3-10	2996	18.539 ± 0.017	18.471 ± 0.019	18.349 ± 0.023	18.433 ± 0.029	
coma25-24	2997	18.356 ± 0.013	18.219 ± 0.014	17.732 ± 0.012	16.914 ± 0.007	16.369 ± 0.005
coma3-17	3003	19.287 ± 0.034	19.158 ± 0.037	19.013 ± 0.043	19.095 ± 0.056	
coma25-64	3004	18.906 ± 0.019	18.904 ± 0.024	18.816 ± 0.029	18.960 ± 0.040	19.077 ± 0.051
coma3-31	3005	18.937 ± 0.023	18.940 ± 0.028	18.862 ± 0.034	18.964 ± 0.046	
coma21-85	3006	18.982 ± 0.022	19.015 ± 0.028	18.960 ± 0.035	19.055 ± 0.046	19.095 ± 0.051
coma3-25	3012	17.326 ± 0.007	17.067 ± 0.006	16.800 ± 0.006	16.690 ± 0.006	
coma21-33	3016	18.457 ± 0.014	18.242 ± 0.014	18.039 ± 0.015	18.021 ± 0.018	17.980 ± 0.019
coma14-86	3017	17.733 ± 0.009	17.573 ± 0.010	17.391 ± 0.011	17.403 ± 0.014	17.304 ± 0.018
coma14-123	3018	18.736 ± 0.026	18.697 ± 0.034	18.607 ± 0.043	18.686 ± 0.057	18.115 ± 0.040
coma14-17	3021	19.153 ± 0.025	19.194 ± 0.035	19.111 ± 0.043	19.208 ± 0.057	19.288 ± 0.063
coma21-91	3024	19.689 ± 0.039	19.727 ± 0.050	19.611 ± 0.061	19.810 ± 0.088	20.024 ± 0.121
coma14-12	3033	19.166 ± 0.026	19.239 ± 0.037	19.160 ± 0.046	19.327 ± 0.065	19.290 ± 0.066
coma14-78	3034	18.006 ± 0.010	17.771 ± 0.011	17.550 ± 0.012	17.511 ± 0.014	17.463 ± 0.018
coma3-51	3037	19.462 ± 0.034	19.521 ± 0.043	19.455 ± 0.052	19.535 ± 0.070	
coma21-43	3043	18.869 ± 0.020	18.875 ± 0.025	18.782 ± 0.030	18.865 ± 0.039	19.020 ± 0.049
coma7-2	3049	19.688 ± 0.066	19.656 ± 0.090	19.663 ± 0.128	19.694 ± 0.166	19.607 ± 0.162
coma14-9	3050	19.567 ± 0.036	19.542 ± 0.049	19.434 ± 0.062	19.519 ± 0.080	
coma14-48	3051	19.750 ± 0.046	19.691 ± 0.062	19.550 ± 0.074	19.623 ± 0.094	19.789 ± 0.115
coma14-21	3052	19.895 ± 0.049	20.018 ± 0.076	20.030 ± 0.105	20.382 ± 0.180	19.902 ± 0.121
coma25-46	3055	14.824 ± 0.001	14.654 ± 0.001	14.451 ± 0.001	14.409 ± 0.001	14.234 ± 0.001
coma21-64	3057	19.332 ± 0.032	19.394 ± 0.042	19.337 ± 0.054	19.496 ± 0.076	19.445 ± 0.079
coma15-124	3058	17.334 ± 0.005	17.150 ± 0.006	16.969 ± 0.006	16.974 ± 0.008	
coma21-47	3066	19.447 ± 0.033	19.429 ± 0.041	19.295 ± 0.049	19.229 ± 0.055	19.273 ± 0.065
coma14-68	3068	16.289 ± 0.003	16.048 ± 0.002	15.814 ± 0.003	15.767 ± 0.003	15.663 ± 0.003
coma3-34	3071	16.977 ± 0.006	16.879 ± 0.005	16.724 ± 0.006	16.743 ± 0.007	
coma15-98	3073	15.183 ± 0.001	15.004 ± 0.001	14.804 ± 0.001	14.774 ± 0.001	
coma14-76	3075	19.803 ± 0.047	19.792 ± 0.064	19.695 ± 0.081	19.677 ± 0.098	19.294 ± 0.084
coma25-50	3076	19.093 ± 0.031	19.166 ± 0.043	19.096 ± 0.054	19.198 ± 0.073	18.713 ± 0.050
coma7-29	3079	19.515 ± 0.056	19.532 ± 0.078	19.487 ± 0.104	19.461 ± 0.126	19.303 ± 0.113
coma14-61	3080	18.708 ± 0.018	18.668 ± 0.024	18.558 ± 0.030	18.670 ± 0.041	

Raw V-band aperture magnitudes. *continued from previous page*

Object	GMP	Aperture Dia. (″) 8.8	13	16	20.2	26
coma21-58	3084	15.898 ± 0.002	15.789 ± 0.002	15.627 ± 0.002	15.645 ± 0.002	15.587 ± 0.003
coma3-50	3092	16.800 ± 0.005	16.716 ± 0.005	16.580 ± 0.005	16.626 ± 0.006	
coma14-5	3095	18.544 ± 0.014	18.513 ± 0.019	18.385 ± 0.022	18.427 ± 0.029	18.460 ± 0.035
coma14-97	3098	18.273 ± 0.012	18.191 ± 0.014	18.061 ± 0.017	18.132 ± 0.022	18.195 ± 0.028
coma21-44	3113	17.364 ± 0.006	17.253 ± 0.006	17.088 ± 0.007	17.109 ± 0.008	17.035 ± 0.008
coma7-14	3116	19.547 ± 0.055	19.458 ± 0.070	19.220 ± 0.078	19.143 ± 0.090	18.974 ± 0.085
coma21-28	3121	17.298 ± 0.006	17.050 ± 0.005	16.828 ± 0.006	16.786 ± 0.006	16.671 ± 0.006
coma7-34	3122	19.590 ± 0.062	19.312 ± 0.066	18.946 ± 0.065	18.581 ± 0.058	17.532 ± 0.023
coma7-37	3126	17.010 ± 0.006	16.862 ± 0.007	16.690 ± 0.008	16.686 ± 0.010	16.583 ± 0.010
coma3-33	3127	19.251 ± 0.029	19.265 ± 0.035	19.165 ± 0.042	19.245 ± 0.054	
coma21-68	3129	17.384 ± 0.006	17.276 ± 0.007	17.107 ± 0.007	17.119 ± 0.009	
coma14-55	3131	18.091 ± 0.010	17.930 ± 0.012	17.751 ± 0.013	17.724 ± 0.016	17.513 ± 0.015
coma14-65	3133	16.748 ± 0.003	16.644 ± 0.004	16.466 ± 0.004	16.463 ± 0.005	16.410 ± 0.005
coma14-54	3134	18.671 ± 0.017	18.655 ± 0.022	18.520 ± 0.026	18.404 ± 0.029	17.897 ± 0.022
coma14-94	3142	19.533 ± 0.035	19.444 ± 0.044	19.203 ± 0.049	19.218 ± 0.061	19.476 ± 0.112
coma14-112	3146	18.510 ± 0.017	18.325 ± 0.019	18.143 ± 0.022	18.182 ± 0.028	18.178 ± 0.031
coma14-3	3149	18.272 ± 0.012	18.318 ± 0.017	18.229 ± 0.021	18.321 ± 0.029	18.247 ± 0.028
coma14-47	3150	19.136 ± 0.024	19.160 ± 0.034	19.079 ± 0.043	19.127 ± 0.058	
coma3-16	3165	14.908 ± 0.002	14.771 ± 0.002	14.589 ± 0.002	14.575 ± 0.002	
coma14-121	3166	18.113 ± 0.011	18.001 ± 0.013	17.873 ± 0.016	17.930 ± 0.021	18.035 ± 0.030
coma14-108	3170	15.607 ± 0.002	15.411 ± 0.002	15.193 ± 0.002	15.147 ± 0.002	15.037 ± 0.002
coma14-81	3171	18.638 ± 0.018	18.451 ± 0.020	18.282 ± 0.024	18.345 ± 0.031	18.343 ± 0.036
coma3-58	3174	18.354 ± 0.015	18.420 ± 0.019	18.342 ± 0.023	18.459 ± 0.031	
coma3-32	3176	17.960 ± 0.011	17.841 ± 0.012	17.678 ± 0.013	17.704 ± 0.015	
coma3-57	3177	18.683 ± 0.018	18.557 ± 0.020	18.423 ± 0.022	18.446 ± 0.027	
coma14-15	3178	15.631 ± 0.002	15.531 ± 0.002	15.375 ± 0.002	15.392 ± 0.002	15.326 ± 0.002
coma7-48	3180	19.458 ± 0.054	19.169 ± 0.058	18.813 ± 0.057	18.367 ± 0.047	17.591 ± 0.025
coma3-28	3192	18.026 ± 0.011	17.765 ± 0.011	17.521 ± 0.011	17.466 ± 0.012	
coma3-36	3195	19.291 ± 0.029	19.186 ± 0.032	19.054 ± 0.037	19.119 ± 0.047	
coma14-39	3196	17.832 ± 0.008	17.750 ± 0.010	17.587 ± 0.011	17.596 ± 0.014	17.559 ± 0.014
coma14-57	3201	15.153 ± 0.001	14.996 ± 0.001	14.810 ± 0.001	14.801 ± 0.001	14.720 ± 0.001
coma14-24	3205	17.062 ± 0.005	16.912 ± 0.005	16.734 ± 0.006	16.734 ± 0.007	16.652 ± 0.007
coma14-99	3206	16.225 ± 0.003	16.089 ± 0.003	15.922 ± 0.003	15.938 ± 0.004	15.866 ± 0.007
coma14-134	3209	19.001 ± 0.022	18.999 ± 0.029	18.886 ± 0.036	18.882 ± 0.044	19.523 ± 0.112
coma14-122	3213	15.761 ± 0.002	15.654 ± 0.002	15.495 ± 0.002	15.509 ± 0.003	15.459 ± 0.003
coma14-71	3215	19.773 ± 0.053	19.710 ± 0.069	19.594 ± 0.085	19.611 ± 0.107	
coma7-115	3222	15.752 ± 0.002	15.745 ± 0.003	15.629 ± 0.003	15.684 ± 0.004	15.680 ± 0.005
coma14-63	3222	15.782 ± 0.002	15.758 ± 0.002	15.641 ± 0.002	15.688 ± 0.003	15.679 ± 0.003
coma14-11	3225	17.580 ± 0.007	17.552 ± 0.009	17.447 ± 0.012	17.540 ± 0.015	17.568 ± 0.016
coma14-79	3229	19.608 ± 0.047	19.483 ± 0.056	19.410 ± 0.072	19.497 ± 0.097	
coma14-35	3230	19.244 ± 0.028	19.357 ± 0.041	19.258 ± 0.052	19.376 ± 0.073	19.452 ± 0.079
coma3-22	3231	18.612 ± 0.018	18.447 ± 0.019	18.270 ± 0.021	18.282 ± 0.025	
coma7-39	3237	19.476 ± 0.052	19.419 ± 0.068	19.239 ± 0.080		
coma3-2	3238	16.676 ± 0.004	16.433 ± 0.004	16.190 ± 0.004	16.116 ± 0.004	
comasw17-92	3243	19.828 ± 0.044	19.969 ± 0.067	19.875 ± 0.085	19.765 ± 0.097	
coma14-32	3244	19.232 ± 0.026	19.256 ± 0.037	19.206 ± 0.048		
coma3-54	3247	19.342 ± 0.031	19.262 ± 0.036	19.085 ± 0.042	18.989 ± 0.046	
coma14-104	3254	16.483 ± 0.005	16.386 ± 0.006	16.227 ± 0.007	16.234 ± 0.008	16.021 ± 0.007
coma7-15	3257	19.602 ± 0.061	19.707 ± 0.092	19.621 ± 0.117	19.596 ± 0.142	19.647 ± 0.156
coma14-10	3262	16.475 ± 0.003	16.323 ± 0.003	16.087 ± 0.003	16.000 ± 0.003	15.864 ± 0.003
coma14-102	3269	16.147 ± 0.004	16.051 ± 0.005	15.889 ± 0.005	15.894 ± 0.007	15.685 ± 0.007
comasw17-5	3271	16.444 ± 0.003	16.240 ± 0.003	16.035 ± 0.003	16.030 ± 0.003	
coma7-51	3275	17.620 ± 0.010	17.094 ± 0.008	16.484 ± 0.007	16.099 ± 0.006	15.887 ± 0.005

Raw V-band aperture magnitudes. *contiuned from previous page*

Object	GMP	Aperture Dia. (″) 8.8	13	16	20.2	26
coma14-28	3284	18.056 ± 0.010	18.031 ± 0.013	17.924 ± 0.016	17.999 ± 0.020	18.031 ± 0.023
coma14-120	3291	16.663 ± 0.004	16.450 ± 0.004	16.214 ± 0.004	16.154 ± 0.005	16.010 ± 0.006
coma14-98	3292	17.373 ± 0.006	17.238 ± 0.007	17.064 ± 0.008	17.074 ± 0.009	17.034 ± 0.012
coma14-51	3296	15.321 ± 0.001	15.222 ± 0.001	15.062 ± 0.002	15.074 ± 0.002	15.012 ± 0.002
coma3-38	3298	17.272 ± 0.007	17.021 ± 0.006	16.776 ± 0.006	16.701 ± 0.006	
coma3-7	3299	17.886 ± 0.010	17.870 ± 0.011	17.734 ± 0.012	17.754 ± 0.015	
coma14-29	3301	19.901 ± 0.049	19.801 ± 0.061	19.472 ± 0.062	18.925 ± 0.047	18.277 ± 0.029
coma14-27	3311	18.459 ± 0.014	18.372 ± 0.018	18.228 ± 0.021	18.254 ± 0.026	18.077 ± 0.023
coma14-136	3312	18.120 ± 0.011	18.108 ± 0.015	18.001 ± 0.018		
coma3-64	3313	16.682 ± 0.005	16.663 ± 0.005	16.546 ± 0.005	16.602 ± 0.006	
coma3-53	3324	18.906 ± 0.022	18.711 ± 0.023	18.521 ± 0.025	18.523 ± 0.029	
coma14-49	3325	18.290 ± 0.014	17.857 ± 0.013	17.530 ± 0.013	17.500 ± 0.015	17.305 ± 0.013
coma14-100	3329	14.707 ± 0.001	14.346 ± 0.001	14.062 ± 0.001	13.947 ± 0.001	13.615 ± 0.001
comasw17-21	3332	18.507 ± 0.013	18.568 ± 0.018	18.512 ± 0.024	18.628 ± 0.032	
comasw17-15	3335	19.416 ± 0.029	19.333 ± 0.036	19.247 ± 0.045	19.347 ± 0.061	
coma14-50	3336	17.959 ± 0.010	17.741 ± 0.011	17.498 ± 0.012	17.496 ± 0.014	17.380 ± 0.014
coma14-18	3339	16.922 ± 0.004	16.840 ± 0.005	16.680 ± 0.005	16.703 ± 0.006	16.712 ± 0.007
coma14-69	3340	18.270 ± 0.018	18.182 ± 0.023	18.047 ± 0.028	18.105 ± 0.036	17.644 ± 0.027
comasw17-45	3343	19.226 ± 0.024	19.012 ± 0.026	18.801 ± 0.029	18.787 ± 0.035	
coma14-80	3352	15.029 ± 0.002	14.927 ± 0.002	14.764 ± 0.002	14.761 ± 0.003	14.586 ± 0.003
coma3-52	3356	18.838 ± 0.022	18.689 ± 0.024	18.530 ± 0.027	18.538 ± 0.033	
coma14-119	3367	15.253 ± 0.001	15.053 ± 0.001	14.837 ± 0.002	14.796 ± 0.002	14.664 ± 0.002
coma3-42	3371	18.994 ± 0.023	18.822 ± 0.024	18.681 ± 0.027	18.770 ± 0.035	
coma14-62	3376	18.431 ± 0.014	18.272 ± 0.017	18.092 ± 0.019	18.118 ± 0.025	18.154 ± 0.033
coma3-19	3381	18.520 ± 0.016	18.271 ± 0.015	18.051 ± 0.016	18.017 ± 0.019	
coma14-14	3383	17.670 ± 0.007	17.615 ± 0.009	17.483 ± 0.010	17.536 ± 0.013	17.589 ± 0.016
coma3-15	3391	19.245 ± 0.031	19.163 ± 0.035	19.037 ± 0.041	19.039 ± 0.048	
coma3-8	3399	18.285 ± 0.014	18.348 ± 0.017	18.264 ± 0.020	18.329 ± 0.025	
coma14-38	3400	14.930 ± 0.001	14.852 ± 0.001	14.697 ± 0.001	14.706 ± 0.001	14.608 ± 0.001
coma3-47	3403	16.245 ± 0.004	16.166 ± 0.003	16.018 ± 0.004	16.051 ± 0.004	
comasw17-19	3410	18.904 ± 0.018	18.970 ± 0.026	18.883 ± 0.032	18.973 ± 0.043	
coma3-63	3411	18.782 ± 0.021	18.657 ± 0.023	18.512 ± 0.026	18.581 ± 0.033	
coma14-103	3414	15.221 ± 0.002	15.053 ± 0.002	14.836 ± 0.002	14.780 ± 0.002	14.594 ± 0.002
coma14-128	3420	19.698 ± 0.046	19.651 ± 0.060	19.540 ± 0.075	19.688 ± 0.106	19.733 ± 0.118
coma14-7	3423	15.175 ± 0.001	15.097 ± 0.001	14.944 ± 0.001	14.959 ± 0.002	14.895 ± 0.002
coma3-56	3425	18.465 ± 0.015	18.357 ± 0.016	18.176 ± 0.018	18.178 ± 0.022	
coma3-24	3435	18.541 ± 0.018	18.525 ± 0.022	18.414 ± 0.026	18.508 ± 0.034	
coma14-137	3438	18.604 ± 0.018	18.528 ± 0.023	18.366 ± 0.027		
coma7-38	3449	19.158 ± 0.038	19.217 ± 0.054	19.126 ± 0.067	19.252 ± 0.090	
coma3-43	3463	17.430 ± 0.007	17.275 ± 0.007	17.105 ± 0.007	17.125 ± 0.009	
coma14-8	3473	18.307 ± 0.012	18.240 ± 0.015	18.123 ± 0.018	18.170 ± 0.023	18.198 ± 0.028
coma13-82	3474	19.129 ± 0.034	19.319 ± 0.057	19.391 ± 0.086	19.812 ± 0.175	
coma13-64	3480	19.498 ± 0.050	19.421 ± 0.065	19.234 ± 0.077	19.146 ± 0.090	18.083 ± 0.021
coma13-48	3484	15.939 ± 0.002	15.839 ± 0.003	15.664 ± 0.003	15.654 ± 0.004	15.557 ± 0.003
coma13-35	3486	17.354 ± 0.006	17.271 ± 0.008	17.110 ± 0.009	17.127 ± 0.011	16.959 ± 0.009
coma13-58	3487	16.220 ± 0.003	16.106 ± 0.003	15.928 ± 0.003	15.911 ± 0.004	15.778 ± 0.003
coma14-117	3489	17.821 ± 0.009	17.674 ± 0.011	17.488 ± 0.012	17.474 ± 0.015	17.328 ± 0.012
coma3-30	3493	15.692 ± 0.003	15.642 ± 0.002	15.508 ± 0.002	15.545 ± 0.003	
coma13-5	3501	18.814 ± 0.024	18.776 ± 0.034	18.680 ± 0.045	18.709 ± 0.062	18.186 ± 0.067
coma3-9	3508	18.966 ± 0.025	18.949 ± 0.029	18.854 ± 0.034	18.943 ± 0.044	
coma13-23	3510	14.818 ± 0.001	14.629 ± 0.001	14.421 ± 0.001	14.384 ± 0.001	14.236 ± 0.001
coma13-25	3511	17.701 ± 0.009	17.713 ± 0.013	17.569 ± 0.015	17.532 ± 0.019	17.195 ± 0.013
coma13-72	3515	19.878 ± 0.050	19.854 ± 0.064	19.789 ± 0.087	19.979 ± 0.130	

Raw V-band aperture magnitudes. *contiuned from previous page*

Object	GMP	Aperture Dia. (″) 8.8	13	16	20.2	26
coma13-54	3516	19.505 ± 0.046	19.602 ± 0.072	19.534 ± 0.096	19.661 ± 0.136	19.686 ± 0.098
coma7-25	3517	19.593 ± 0.060	19.553 ± 0.079	19.442 ± 0.100	19.453 ± 0.131	19.532 ± 0.141
coma3-20	3519	19.363 ± 0.032	19.271 ± 0.036	19.119 ± 0.042	19.174 ± 0.054	
coma13-6	3522	15.801 ± 0.002	15.737 ± 0.002	15.600 ± 0.002	15.642 ± 0.003	
coma3-60	3531	18.820 ± 0.022	18.898 ± 0.030	18.860 ± 0.039	19.011 ± 0.060	
coma13-106	3533	19.544 ± 0.034	19.393 ± 0.041	19.215 ± 0.048	19.186 ± 0.058	19.139 ± 0.067
coma13-61	3534	16.860 ± 0.004	16.758 ± 0.005	16.604 ± 0.005	16.634 ± 0.007	16.556 ± 0.006
coma14-25	3536	18.876 ± 0.020	18.757 ± 0.025	18.523 ± 0.028	18.535 ± 0.034	18.403 ± 0.029
coma14-26	3536	19.150 ± 0.027	18.770 ± 0.025	18.408 ± 0.024	18.463 ± 0.031	18.460 ± 0.032
coma13-129	3546	19.804 ± 0.050	19.991 ± 0.082	19.977 ± 0.113	20.194 ± 0.172	20.792 ± 0.419
coma7-8	3548	19.449 ± 0.050	19.470 ± 0.069	19.433 ± 0.090	19.562 ± 0.119	19.498 ± 0.135
coma23-31	3553	16.415 ± 0.003	16.272 ± 0.003	16.093 ± 0.003	16.089 ± 0.004	
coma14-37	3557	16.057 ± 0.002	15.888 ± 0.002	15.697 ± 0.002	15.682 ± 0.003	15.610 ± 0.003
coma13-60	3565	17.930 ± 0.009	17.775 ± 0.011	17.583 ± 0.012	17.554 ± 0.015	17.492 ± 0.016
coma13-55	3567	18.206 ± 0.011	18.109 ± 0.014	17.957 ± 0.016	17.968 ± 0.020	17.863 ± 0.021
comasw17-88	3571	19.042 ± 0.022	19.114 ± 0.031	19.038 ± 0.039	19.161 ± 0.054	
coma23-75	3573	19.324 ± 0.028	19.096 ± 0.031	18.896 ± 0.035	18.896 ± 0.044	
coma23-30	3580	19.263 ± 0.028	19.182 ± 0.036	19.116 ± 0.047	19.204 ± 0.064	
comasw17-13	3585	17.699 ± 0.007	17.532 ± 0.008	17.334 ± 0.009	17.329 ± 0.011	
comasw17-76	3586	17.364 ± 0.006	17.317 ± 0.007	17.183 ± 0.008	17.221 ± 0.009	
coma23-25	3592	17.802 ± 0.008	17.724 ± 0.009	17.568 ± 0.011	17.599 ± 0.014	
coma13-42	3595	19.646 ± 0.039	19.686 ± 0.055	19.660 ± 0.073	19.769 ± 0.103	21.039 ± 0.390
comasw17-40	3598	18.657 ± 0.016	18.587 ± 0.020	18.467 ± 0.024	18.524 ± 0.031	
coma13-73	3602	19.570 ± 0.045	19.734 ± 0.076	19.697 ± 0.108	19.916 ± 0.183	
coma19-72	3603	19.109 ± 0.022	18.928 ± 0.025	18.769 ± 0.030	18.815 ± 0.039	18.768 ± 0.042
coma13-3	3606	18.707 ± 0.018	18.757 ± 0.026	18.650 ± 0.034		
coma19-97	3608	19.517 ± 0.031	19.554 ± 0.045	19.445 ± 0.056	19.569 ± 0.078	19.767 ± 0.104
coma23-74	3609	19.623 ± 0.037	19.384 ± 0.041	19.091 ± 0.043	18.883 ± 0.044	
coma13-79	3615	17.931 ± 0.010	17.880 ± 0.013	17.771 ± 0.016	17.918 ± 0.021	17.666 ± 0.019
comasw22-29	3616	18.907 ± 0.028	19.023 ± 0.041	18.994 ± 0.055	19.220 ± 0.084	
coma14-4	3621	19.972 ± 0.053	19.953 ± 0.073	19.846 ± 0.091	19.852 ± 0.116	19.664 ± 0.116
coma13-92	3623	19.342 ± 0.030	19.480 ± 0.047	19.415 ± 0.061	19.521 ± 0.083	22.841 ± 2.167
coma14-36	3625	19.332 ± 0.030	19.236 ± 0.036	19.084 ± 0.045		
coma13-7	3629	18.780 ± 0.020	18.670 ± 0.024	18.507 ± 0.029	18.527 ± 0.037	18.526 ± 0.036
coma13-122	3630	19.000 ± 0.022	19.031 ± 0.030	18.929 ± 0.037	18.983 ± 0.049	19.083 ± 0.056
coma7-22	3633	18.877 ± 0.031	18.785 ± 0.039	18.623 ± 0.047	18.606 ± 0.057	18.341 ± 0.048
coma13-67	3639	15.013 ± 0.001	14.910 ± 0.001	14.753 ± 0.001	14.766 ± 0.002	14.691 ± 0.002
coma23-62	3640	17.393 ± 0.006	17.192 ± 0.006	16.977 ± 0.007	16.941 ± 0.008	
comasw17-10	3643	19.655 ± 0.037	19.774 ± 0.055	19.697 ± 0.070	19.970 ± 0.111	
coma13-2	3645	17.816 ± 0.009				
coma13-30	3648	18.354 ± 0.012	18.403 ± 0.016	18.331 ± 0.020	18.364 ± 0.027	18.376 ± 0.029
coma13-46	3649	19.972 ± 0.068	19.970 ± 0.094	19.804 ± 0.112	19.642 ± 0.121	18.813 ± 0.054
coma13-111	3650	19.222 ± 0.027	19.205 ± 0.035	19.099 ± 0.044	19.055 ± 0.052	17.414 ± 0.014
coma19-47	3656	15.980 ± 0.002	15.749 ± 0.002	15.501 ± 0.002	15.411 ± 0.002	15.181 ± 0.002
comasw22-40	3660	15.614 ± 0.002	15.459 ± 0.002	15.264 ± 0.002	15.230 ± 0.002	
coma13-65	3664	14.819 ± 0.001	14.420 ± 0.001	14.128 ± 0.001	14.106 ± 0.001	13.993 ± 0.001
coma23-77	3665	19.067 ± 0.022	19.136 ± 0.032	19.057 ± 0.041	19.174 ± 0.056	
coma13-113	3668	19.248 ± 0.028	19.226 ± 0.038	19.136 ± 0.048	19.222 ± 0.066	18.948 ± 0.053
comasw17-51	3672	19.567 ± 0.033	19.480 ± 0.041	19.328 ± 0.048	19.365 ± 0.061	
coma13-93	3675	19.279 ± 0.027	19.169 ± 0.033	18.850 ± 0.034	17.754 ± 0.015	15.589 ± 0.003
comasw17-90	3676	19.486 ± 0.031	19.480 ± 0.040	19.382 ± 0.051	19.473 ± 0.066	
comasw17-72	3677	19.113 ± 0.022	19.232 ± 0.032	19.164 ± 0.040	19.263 ± 0.053	
coma23-34	3678	19.436 ± 0.031	19.347 ± 0.039	19.216 ± 0.047	19.279 ± 0.062	

Raw V-band aperture magnitudes. *contiuned from previous page*

Object	GMP	Aperture Dia. (″) 8.8	13	16	20.2	26
comasw22-66	3679	18.747 ± 0.020	18.694 ± 0.025	18.561 ± 0.030	18.534 ± 0.036	
coma13-102	3681	17.407 ± 0.006	17.308 ± 0.007	17.155 ± 0.008	17.184 ± 0.010	17.159 ± 0.010
coma19-74	3683	19.589 ± 0.035	19.724 ± 0.054	19.630 ± 0.068	19.726 ± 0.092	20.013 ± 0.122
coma13-117	3685	19.635 ± 0.041	19.791 ± 0.065	19.728 ± 0.085	19.872 ± 0.118	19.603 ± 0.085
comasw6-1	3688	19.313 ± 0.032	19.326 ± 0.046	19.211 ± 0.060	19.222 ± 0.078	
comasw6-35	3691	19.757 ± 0.047	19.867 ± 0.072	19.767 ± 0.092	19.965 ± 0.139	
comasw17-22	3696	18.770 ± 0.017	18.773 ± 0.023	18.672 ± 0.028	18.738 ± 0.037	
comasw17-31	3697	15.914 ± 0.002	15.839 ± 0.002	15.691 ± 0.002	15.714 ± 0.003	
coma13-62	3698	19.950 ± 0.067	19.805 ± 0.081	19.581 ± 0.092	19.388 ± 0.096	18.322 ± 0.034
coma19-96	3699	18.145 ± 0.009	17.985 ± 0.011	17.807 ± 0.012	17.775 ± 0.015	17.512 ± 0.013
comasw17-81	3700	19.610 ± 0.034	19.559 ± 0.044	19.370 ± 0.051	19.423 ± 0.063	
comasw6-3	3703	19.057 ± 0.026	19.079 ± 0.036	18.980 ± 0.046	19.097 ± 0.065	
coma23-78	3704	19.729 ± 0.041	19.587 ± 0.049	19.295 ± 0.052	19.139 ± 0.055	
comasw22-100	3706	16.666 ± 0.004	16.680 ± 0.004	16.579 ± 0.005	16.649 ± 0.007	
coma13-120	3707	17.149 ± 0.005	17.015 ± 0.005	16.845 ± 0.006	16.856 ± 0.007	16.820 ± 0.007
coma19-43	3708	20.137 ± 0.060	20.361 ± 0.102	20.397 ± 0.145		20.464 ± 0.233
comasw17-41	3710	19.276 ± 0.026	19.249 ± 0.033	19.117 ± 0.040	19.087 ± 0.048	
coma23-61	3712	18.548 ± 0.014	18.524 ± 0.019	18.434 ± 0.023	18.506 ± 0.031	
comasw6-65	3716	19.798 ± 0.045	19.911 ± 0.068	19.885 ± 0.091	20.120 ± 0.139	
coma13-4	3719	17.735 ± 0.008	17.606 ± 0.009	17.442 ± 0.011	17.473 ± 0.014	
comasw17-62	3726	19.660 ± 0.036	19.751 ± 0.052	19.687 ± 0.067	19.862 ± 0.096	
coma23-67	3727	18.559 ± 0.015	18.503 ± 0.019	18.360 ± 0.022	18.387 ± 0.028	
comasw6-25	3728	18.300 ± 0.012	18.323 ± 0.016	18.219 ± 0.020	18.304 ± 0.026	
comasw6-37	3729	17.884 ± 0.009	17.847 ± 0.011	17.746 ± 0.013	17.749 ± 0.017	
comasw22-43	3730	15.033 ± 0.001	14.894 ± 0.001	14.714 ± 0.001	14.706 ± 0.001	
comasw22-60	3731	19.114 ± 0.037	19.189 ± 0.053	19.091 ± 0.067	19.153 ± 0.087	
comasw22-94	3733	15.376 ± 0.002	15.224 ± 0.002	15.033 ± 0.002	15.019 ± 0.002	
comasw17-46	3735	19.671 ± 0.044	19.648 ± 0.058	19.488 ± 0.069	19.490 ± 0.086	
coma13-131	3736	19.568 ± 0.040	19.415 ± 0.049	19.282 ± 0.061		
comasw22-36	3739	15.455 ± 0.002	15.358 ± 0.002	15.193 ± 0.002	15.195 ± 0.002	
comasw22-37	3750	17.343 ± 0.008	17.242 ± 0.010	17.058 ± 0.011	17.003 ± 0.013	
coma19-59	3753	18.623 ± 0.014	18.604 ± 0.019	18.495 ± 0.023	18.553 ± 0.030	18.608 ± 0.034
comasw22-78	3756	19.039 ± 0.025	19.093 ± 0.035	18.944 ± 0.042	19.028 ± 0.056	
coma13-94	3761	15.366 ± 0.001	15.193 ± 0.001	14.987 ± 0.001	14.939 ± 0.002	14.798 ± 0.001
coma19-23	3762	19.804 ± 0.042	19.781 ± 0.057	19.689 ± 0.072	19.801 ± 0.099	19.878 ± 0.114
comasw17-35	3766	19.197 ± 0.023	19.235 ± 0.032	19.145 ± 0.039	19.253 ± 0.053	
coma13-130	3768	18.072 ± 0.011	18.069 ± 0.015	17.999 ± 0.019	18.108 ± 0.027	
comasw22-24	3770	19.228 ± 0.030	18.844 ± 0.029	18.652 ± 0.033	18.725 ± 0.043	
comasw22-23	3770	19.253 ± 0.031	18.964 ± 0.032	18.717 ± 0.035	18.733 ± 0.044	
comasw21-81	3772	18.055 ± 0.010	18.096 ± 0.013	17.999 ± 0.017	18.097 ± 0.022	
comasw21-44	3777	19.309 ± 0.037	19.316 ± 0.051	19.165 ± 0.061	19.139 ± 0.074	
comasw17-48	3779	15.597 ± 0.002	15.408 ± 0.002	15.188 ± 0.002	15.130 ± 0.002	
coma13-124	3780	17.401 ± 0.006	17.243 ± 0.006	17.055 ± 0.007	17.034 ± 0.008	16.950 ± 0.008
coma23-89	3781	18.699 ± 0.017	18.750 ± 0.024	18.656 ± 0.030	18.677 ± 0.037	
coma13-19	3782	16.017 ± 0.002	15.903 ± 0.002	15.737 ± 0.002	15.749 ± 0.003	15.694 ± 0.003
comasw21-75	3785	19.721 ± 0.046	19.797 ± 0.068	19.709 ± 0.090	19.924 ± 0.136	
comasw17-23	3787	19.497 ± 0.031	19.599 ± 0.045	19.517 ± 0.057	19.607 ± 0.076	
comasw21-39	3788	17.906 ± 0.009	18.000 ± 0.013	17.945 ± 0.017	18.066 ± 0.024	
coma19-70	3792	14.574 ± 0.001	14.402 ± 0.001	14.201 ± 0.001	14.166 ± 0.001	14.012 ± 0.001
coma13-38	3793	19.530 ± 0.034	19.463 ± 0.044	19.343 ± 0.054	19.357 ± 0.068	19.272 ± 0.068
coma13-44	3794	16.456 ± 0.003	16.432 ± 0.003	16.316 ± 0.004	16.378 ± 0.005	16.351 ± 0.005
comasw21-65	3797	19.628 ± 0.039	19.629 ± 0.053	19.506 ± 0.064	19.525 ± 0.081	
coma13-78	3804	19.375 ± 0.030	19.314 ± 0.039	19.248 ± 0.050	19.340 ± 0.068	19.203 ± 0.067

Raw V-band aperture magnitudes. *contiuned from previous page*

Object	GMP	Aperture Dia. (″) 8.8	13	16	20.2	26
comasw16-72	3805	19.521 ± 0.034	19.516 ± 0.047			
coma13-57	3806	19.399 ± 0.029	19.331 ± 0.037	18.998 ± 0.037	18.492 ± 0.029	18.630 ± 0.039
comasw21-62	3808	19.696 ± 0.044	19.538 ± 0.052	19.335 ± 0.057	19.302 ± 0.070	
coma19-93	3809	18.701 ± 0.015	18.720 ± 0.021	18.590 ± 0.026	18.619 ± 0.033	18.672 ± 0.037
coma13-96	3811	19.423 ± 0.032	19.469 ± 0.046	19.427 ± 0.061	19.579 ± 0.086	19.945 ± 0.135
coma13-39	3815	19.796 ± 0.045	19.967 ± 0.073	19.946 ± 0.098	20.162 ± 0.149	
coma19-66	3816	15.954 ± 0.002	15.659 ± 0.002	15.438 ± 0.002	15.426 ± 0.003	15.339 ± 0.003
coma23-46	3818	15.050 ± 0.001	14.905 ± 0.001	14.718 ± 0.001	14.700 ± 0.001	
comasw21-25	3820	19.473 ± 0.033	19.470 ± 0.043	19.333 ± 0.053	19.341 ± 0.065	
comasw21-90	3821	19.722 ± 0.049	19.779 ± 0.077	19.791 ± 0.117	20.009 ± 0.174	
coma13-34	3826	19.121 ± 0.025	19.242 ± 0.037	19.189 ± 0.049	19.283 ± 0.066	19.329 ± 0.069
comasw21-99	3830	19.552 ± 0.040	19.489 ± 0.051	19.478 ± 0.063	19.460 ± 0.077	
comasw16-19	3833	19.761 ± 0.038	19.715 ± 0.049	19.606 ± 0.063	19.770 ± 0.095	
comasw16-56	3834	19.488 ± 0.030	19.552 ± 0.043	19.427 ± 0.053	19.485 ± 0.066	
comasw21-96	3835	18.784 ± 0.018	18.536 ± 0.019	18.196 ± 0.019	18.107 ± 0.021	
comasw16-25	3840	19.738 ± 0.038	19.566 ± 0.044	19.378 ± 0.051	19.420 ± 0.066	
comasw21-17	3843	19.004 ± 0.022	19.019 ± 0.030	18.903 ± 0.036	18.843 ± 0.043	
coma23-27	3844	19.586 ± 0.037	19.665 ± 0.054	19.612 ± 0.071	19.713 ± 0.096	
comasw21-27	3845	18.474 ± 0.014	18.282 ± 0.015	18.095 ± 0.017	18.122 ± 0.022	
comasw6-27	3847	18.716 ± 0.017	18.670 ± 0.021	18.538 ± 0.026	18.493 ± 0.030	
comasw16-31	3848	18.612 ± 0.015	18.689 ± 0.021	18.614 ± 0.026	18.723 ± 0.035	
comasw21-57	3849	19.525 ± 0.033	19.553 ± 0.045	19.483 ± 0.058	19.648 ± 0.081	
comasw6-22	3850	19.108 ± 0.024	19.155 ± 0.033	19.099 ± 0.043	19.176 ± 0.057	
coma13-56	3851	16.394 ± 0.003	16.281 ± 0.003	16.115 ± 0.003	16.131 ± 0.004	16.087 ± 0.004
comasw11-30	3853	18.464 ± 0.015	18.420 ± 0.020	18.254 ± 0.023	18.211 ± 0.028	18.071 ± 0.023
coma13-32	3855	17.634 ± 0.007	17.470 ± 0.007	17.283 ± 0.008	17.280 ± 0.010	17.189 ± 0.010
coma13-86	3856	19.057 ± 0.024	18.945 ± 0.030	18.800 ± 0.036	18.892 ± 0.049	18.846 ± 0.048
coma19-63	3857	19.482 ± 0.030	19.598 ± 0.046	19.546 ± 0.060	19.576 ± 0.076	19.476 ± 0.082
coma13-8	3859	18.702 ± 0.016	18.778 ± 0.023	18.702 ± 0.030	18.805 ± 0.040	18.963 ± 0.052
comasw6-57	3863	18.694 ± 0.017	18.682 ± 0.022	18.575 ± 0.027	18.645 ± 0.035	
comasw6-39	3864	18.591 ± 0.016	18.669 ± 0.023	18.578 ± 0.028	18.674 ± 0.038	
comasw11-58	3865	19.481 ± 0.048	19.313 ± 0.059	19.040 ± 0.065	18.954 ± 0.077	18.451 ± 0.035
coma19-90	3866	19.558 ± 0.032	19.498 ± 0.041	19.440 ± 0.051	19.556 ± 0.069	19.931 ± 0.114
comasw16-60	3872	19.633 ± 0.034	19.397 ± 0.038	19.164 ± 0.043	19.145 ± 0.051	
comasw11-55	3879	15.571 ± 0.002	15.499 ± 0.002	15.356 ± 0.002	15.390 ± 0.002	15.333 ± 0.002
comasw16-55	3880	19.816 ± 0.039	19.899 ± 0.056	19.869 ± 0.078	19.984 ± 0.105	
coma23-38	3881	19.373 ± 0.029	19.456 ± 0.042	19.356 ± 0.053	19.422 ± 0.070	
comasw21-36	3882	16.603 ± 0.003	16.452 ± 0.003	16.259 ± 0.004	16.239 ± 0.004	
coma13-99	3883	18.896 ± 0.020	18.732 ± 0.023	18.599 ± 0.028	18.640 ± 0.036	18.650 ± 0.039
coma19-52	3884	19.427 ± 0.032	19.273 ± 0.038	19.071 ± 0.044	19.092 ± 0.056	18.796 ± 0.040
comasw16-36	3885	19.003 ± 0.019	18.967 ± 0.025	18.887 ± 0.031	18.986 ± 0.042	
comasw21-13	3886	19.681 ± 0.038	19.795 ± 0.055	19.769 ± 0.073	19.997 ± 0.101	
comasw11-56	3890	19.594 ± 0.053	19.634 ± 0.081	19.401 ± 0.090	18.008 ± 0.030	16.055 ± 0.004
comasw21-63	3895	17.163 ± 0.005	17.056 ± 0.006	16.920 ± 0.007	16.974 ± 0.009	
coma13-1	3897	19.667 ± 0.039	19.615 ± 0.053			
comasw21-48	3898	18.444 ± 0.014	18.337 ± 0.017	18.182 ± 0.021	18.209 ± 0.026	
coma13-14	3899	18.143 ± 0.009	18.092 ± 0.012	17.928 ± 0.014	17.944 ± 0.017	17.959 ± 0.020
comasw6-40	3901	19.949 ± 0.052	20.042 ± 0.077	20.015 ± 0.104	20.205 ± 0.153	
coma23-42	3904	19.931 ± 0.049	20.121 ± 0.080	20.077 ± 0.106	20.181 ± 0.144	
comasw21-66	3907	19.604 ± 0.044	19.445 ± 0.051	19.031 ± 0.047	18.365 ± 0.033	
comasw21-109	3911	19.229 ± 0.028	19.259 ± 0.038	19.169 ± 0.047	19.220 ± 0.061	
comasw6-8	3913	19.632 ± 0.038	19.580 ± 0.049	19.422 ± 0.058	19.424 ± 0.072	
coma13-50	3914	15.749 ± 0.002	15.739 ± 0.002	15.623 ± 0.002	15.675 ± 0.003	15.642 ± 0.003

Raw V-band aperture magnitudes. *contiuned from previous page*

Object	GMP	Aperture Dia. ('')				
		8.8	13	16	20.2	26
comasw21-67	3916	18.607 ± 0.022	18.658 ± 0.031	18.553 ± 0.038	18.532 ± 0.047	
coma23-29	3917	19.563 ± 0.035	19.455 ± 0.043	19.208 ± 0.048	19.135 ± 0.055	
coma23-88	3918	18.913 ± 0.020	19.003 ± 0.030	18.931 ± 0.038	18.987 ± 0.050	
coma13-51	3920	19.096 ± 0.023	18.786 ± 0.023	18.396 ± 0.023	17.918 ± 0.018	16.553 ± 0.006
coma23-41	3921	18.259 ± 0.011	18.098 ± 0.013	17.917 ± 0.015	17.930 ± 0.018	
coma19-83	3922	18.407 ± 0.012	18.464 ± 0.016	18.379 ± 0.020	18.459 ± 0.025	18.491 ± 0.031
comasw21-105	3923	19.160 ± 0.025	19.255 ± 0.037	19.201 ± 0.047	19.264 ± 0.062	
comasw21-46	3925	16.990 ± 0.004	16.754 ± 0.004	16.260 ± 0.004	15.790 ± 0.003	
comasw22-26	3926	19.837 ± 0.053	19.864 ± 0.073	19.844 ± 0.098	20.054 ± 0.147	
coma23-63	3927	19.746 ± 0.042	19.856 ± 0.064	19.832 ± 0.087	19.872 ± 0.112	
coma23-82	3930	18.373 ± 0.012	18.043 ± 0.012	17.774 ± 0.013	17.689 ± 0.015	
coma19-64	3935	15.901 ± 0.002	15.819 ± 0.002	15.657 ± 0.002	15.665 ± 0.002	15.598 ± 0.002
coma13-128	3937	18.770 ± 0.019	18.622 ± 0.023	18.457 ± 0.028	18.505 ± 0.036	18.542 ± 0.034
comasw6-46	3939	18.132 ± 0.010	18.108 ± 0.013	17.983 ± 0.015	18.053 ± 0.020	
coma23-51	3940	17.968 ± 0.009	17.418 ± 0.007	16.800 ± 0.006	16.788 ± 0.007	
comasw21-53	3943	16.469 ± 0.003	16.317 ± 0.003	16.120 ± 0.003	16.108 ± 0.004	
comasw21-107	3946	18.576 ± 0.015	18.521 ± 0.018	18.415 ± 0.022	18.515 ± 0.030	
coma13-17	3951	18.723 ± 0.017	18.576 ± 0.020	18.450 ± 0.024	18.529 ± 0.032	18.532 ± 0.034
coma19-42	3953	18.603 ± 0.014	18.688 ± 0.021	18.618 ± 0.027	18.751 ± 0.037	18.721 ± 0.038
coma23-68	3954	19.155 ± 0.025	19.027 ± 0.031	18.850 ± 0.036	18.902 ± 0.047	
comasw21-37	3958	15.345 ± 0.001	15.239 ± 0.001	15.081 ± 0.002	15.097 ± 0.002	
coma13-116	3963	19.253 ± 0.025	19.325 ± 0.036	19.216 ± 0.044	19.302 ± 0.059	19.542 ± 0.080
coma23-59	3964	17.637 ± 0.007	17.629 ± 0.009	17.533 ± 0.011	17.603 ± 0.014	
coma13-11	3966	18.370 ± 0.013	18.303 ± 0.016	18.146 ± 0.018	18.157 ± 0.022	18.163 ± 0.025
coma13-100	3969	18.080 ± 0.009	17.974 ± 0.011	17.802 ± 0.013	17.747 ± 0.015	17.554 ± 0.015
coma19-57	3972	15.845 ± 0.002	15.792 ± 0.002	15.645 ± 0.002	15.662 ± 0.002	15.586 ± 0.002
coma13-91	3973	18.044 ± 0.010	17.929 ± 0.012	17.756 ± 0.014	17.724 ± 0.016	17.615 ± 0.014
comasw6-48	3977	18.296 ± 0.012	18.217 ± 0.015	18.059 ± 0.017	17.974 ± 0.019	
coma13-101	3978	18.759 ± 0.016	18.570 ± 0.018	18.346 ± 0.020	18.158 ± 0.021	17.653 ± 0.016
comasw21-58	3980	18.381 ± 0.016	18.353 ± 0.020	18.232 ± 0.025	18.319 ± 0.034	
coma13-125	3982	17.856 ± 0.008	17.843 ± 0.010	17.724 ± 0.012	17.763 ± 0.015	17.752 ± 0.016
coma23-43	3984	19.975 ± 0.050	20.142 ± 0.080	19.929 ± 0.091	20.101 ± 0.132	
comasw11-18	3986	19.613 ± 0.044	19.629 ± 0.058	19.510 ± 0.071	19.655 ± 0.092	19.393 ± 0.132
coma13-15	3987	19.478 ± 0.034	19.693 ± 0.056	19.765 ± 0.083	20.025 ± 0.131	19.731 ± 0.103
coma23-71	3990	19.630 ± 0.039	19.684 ± 0.056	19.584 ± 0.070	19.631 ± 0.092	
coma13-18	3993	17.898 ± 0.008	17.844 ± 0.011	17.705 ± 0.012	17.726 ± 0.016	17.668 ± 0.016
comasw21-51	3997	14.848 ± 0.001	14.735 ± 0.001	14.566 ± 0.001	14.569 ± 0.001	
coma13-12	3998	19.670 ± 0.037	19.794 ± 0.057	19.733 ± 0.075	19.769 ± 0.096	18.901 ± 0.048
coma13-47	3999	19.632 ± 0.037	19.577 ± 0.048	19.479 ± 0.060	19.551 ± 0.080	19.559 ± 0.085
comasw16-62	4001	19.091 ± 0.021	18.689 ± 0.020	18.532 ± 0.024	18.607 ± 0.031	
coma23-70	4002	19.337 ± 0.028	19.329 ± 0.038	19.214 ± 0.047	19.286 ± 0.063	
coma13-107	4003	18.085 ± 0.009	17.852 ± 0.010	17.631 ± 0.011	17.596 ± 0.013	17.569 ± 0.014
comasw21-74	4005	18.404 ± 0.013	18.387 ± 0.017	18.277 ± 0.020	18.324 ± 0.026	
coma13-16	4011	19.638 ± 0.047	19.757 ± 0.073	19.826 ± 0.106		19.367 ± 0.072
coma13-9	4016	18.819 ± 0.018	18.474 ± 0.018	18.043 ± 0.017	17.581 ± 0.014	16.917 ± 0.008
comasw16-54	4017	15.356 ± 0.001	15.168 ± 0.001	14.948 ± 0.001	14.887 ± 0.002	
coma12-23	4020	19.632 ± 0.041	19.478 ± 0.049	19.290 ± 0.058	19.234 ± 0.073	
coma18-68	4022	19.027 ± 0.020	19.052 ± 0.028	18.973 ± 0.036	19.066 ± 0.050	19.063 ± 0.053
coma13-10	4024	17.085 ± 0.004	16.924 ± 0.005	16.742 ± 0.005	16.710 ± 0.006	16.565 ± 0.006
comasw6-77	4026	19.899 ± 0.092	19.930 ± 0.130	19.843 ± 0.165	19.989 ± 0.235	
comasw6-28	4028	19.724 ± 0.042	19.420 ± 0.043	19.094 ± 0.043	18.937 ± 0.046	
comasw21-86	4029	18.175 ± 0.011	18.042 ± 0.012	17.859 ± 0.014	17.852 ± 0.017	
comasw11-6	4032	18.825 ± 0.019	18.697 ± 0.024	18.494 ± 0.027	18.510 ± 0.034	18.566 ± 0.054

Raw V-band aperture magnitudes. *continued from previous page*

Object	GMP	Aperture Dia. ('')				
		8.8	13	16	20.2	26
comasw21-77	4033	19.385 ± 0.031	19.441 ± 0.044	19.395 ± 0.058	19.485 ± 0.078	
comasw21-102	4034	18.084 ± 0.010	17.995 ± 0.012	17.855 ± 0.014	17.893 ± 0.017	
comasw21-14	4035	18.011 ± 0.010	17.812 ± 0.010	17.600 ± 0.011	17.582 ± 0.014	
comasw21-35	4037	18.535 ± 0.014	18.403 ± 0.017	18.218 ± 0.019	18.194 ± 0.023	
comasw11-4	4039	18.823 ± 0.023	18.514 ± 0.023	18.312 ± 0.027	18.309 ± 0.034	17.810 ± 0.034
coma12-68	4040	18.880 ± 0.020	18.832 ± 0.026	18.717 ± 0.032	18.789 ± 0.042	18.800 ± 0.048
coma12-49	4042	18.137 ± 0.010	17.971 ± 0.011	17.798 ± 0.013	17.819 ± 0.016	17.780 ± 0.018
coma23-76	4043	16.629 ± 0.003	16.513 ± 0.004	16.372 ± 0.004	16.419 ± 0.006	
comasw21-10	4046	18.979 ± 0.023	18.708 ± 0.024	18.536 ± 0.027	18.553 ± 0.034	
comasw21-11	4046	18.922 ± 0.021	18.677 ± 0.023	18.482 ± 0.026	18.466 ± 0.032	
comasw21-42	4047	19.262 ± 0.028	19.158 ± 0.033	18.902 ± 0.036	18.880 ± 0.043	
comasw16-66	4049	19.439 ± 0.028	19.351 ± 0.035	19.217 ± 0.042	19.271 ± 0.055	
comasw21-43	4051	19.875 ± 0.046	19.632 ± 0.050	19.227 ± 0.047	18.992 ± 0.046	
coma23-85	4052	19.750 ± 0.051	19.867 ± 0.078	19.834 ± 0.105	19.992 ± 0.151	
comasw21-20	4060	17.761 ± 0.008	17.468 ± 0.008	17.211 ± 0.008	17.125 ± 0.009	
coma12-16	4062	19.133 ± 0.025	19.006 ± 0.031	18.845 ± 0.036	18.871 ± 0.046	18.881 ± 0.057
coma13-27	4063	17.974 ± 0.009	17.940 ± 0.011	17.801 ± 0.013	17.819 ± 0.016	17.691 ± 0.016
coma23-26	4065	17.940 ± 0.008	17.709 ± 0.009	17.489 ± 0.010	17.440 ± 0.011	
comasw16-52	4066	19.483 ± 0.031	19.534 ± 0.045	19.502 ± 0.059	19.613 ± 0.082	
coma12-44	4068	19.044 ± 0.022	18.692 ± 0.021	18.521 ± 0.025	18.575 ± 0.033	18.544 ± 0.034
coma23-81	4069	18.503 ± 0.017	18.386 ± 0.021	18.211 ± 0.024	18.066 ± 0.026	
comasw21-19	4072	19.649 ± 0.039	19.518 ± 0.046	19.136 ± 0.045	18.749 ± 0.038	
coma23-44	4073	19.275 ± 0.026	19.230 ± 0.034	19.089 ± 0.041	19.177 ± 0.055	
coma12-45	4075	18.940 ± 0.021	18.753 ± 0.024	18.575 ± 0.028	18.599 ± 0.036	18.547 ± 0.033
comasw11-43	4078	18.863 ± 0.019	18.905 ± 0.026	18.758 ± 0.031	18.843 ± 0.042	19.075 ± 0.059
comasw16-51	4080	19.715 ± 0.037	19.692 ± 0.050	19.526 ± 0.059	19.384 ± 0.064	
coma13-26	4081	17.924 ± 0.008	17.787 ± 0.010	17.633 ± 0.011	17.678 ± 0.014	17.593 ± 0.015
comasw21-69	4083	17.267 ± 0.005	17.123 ± 0.006	16.932 ± 0.006	16.895 ± 0.007	
comasw21-70	4087	19.507 ± 0.036	19.631 ± 0.055	19.606 ± 0.073	19.735 ± 0.105	
comasw16-41	4090	18.535 ± 0.013	18.366 ± 0.015	18.192 ± 0.018	18.219 ± 0.022	
comasw6-23	4093	16.571 ± 0.003	16.492 ± 0.003	16.347 ± 0.004	16.385 ± 0.005	
comasw11-36	4098	19.220 ± 0.031	19.172 ± 0.041	19.034 ± 0.050	19.095 ± 0.065	18.305 ± 0.030
comasw11-48	4101	19.554 ± 0.037	19.460 ± 0.047	19.378 ± 0.059	19.444 ± 0.078	19.210 ± 0.065
comasw21-82	4102	19.106 ± 0.023	19.194 ± 0.034	19.142 ± 0.045	19.268 ± 0.064	
coma12-15	4103	17.144 ± 0.005	17.003 ± 0.005	16.834 ± 0.006	16.849 ± 0.007	16.782 ± 0.007
coma12-10	4108	18.100 ± 0.010	18.061 ± 0.012	17.936 ± 0.015	17.956 ± 0.019	17.824 ± 0.019
coma18-65	4109	19.370 ± 0.032	19.477 ± 0.049	19.378 ± 0.061	19.304 ± 0.070	18.398 ± 0.030
coma23-1	4109	19.272 ± 0.030	19.304 ± 0.045			
coma12-12	4114	19.730 ± 0.048	19.665 ± 0.062	19.329 ± 0.062	18.775 ± 0.044	18.004 ± 0.023
comasw21-71	4116	19.720 ± 0.049	19.837 ± 0.072	19.797 ± 0.095	20.051 ± 0.156	
comasw11-38	4117	16.023 ± 0.002	15.925 ± 0.002	15.779 ± 0.002	15.809 ± 0.003	15.763 ± 0.003
comasw21-64	4118	18.125 ± 0.010	17.900 ± 0.011	17.679 ± 0.012	17.639 ± 0.014	
coma18-62	4126	19.788 ± 0.046	19.674 ± 0.054	19.465 ± 0.060	19.301 ± 0.066	17.250 ± 0.012
comasw21-79	4129	17.614 ± 0.007	17.546 ± 0.008	17.419 ± 0.009	17.474 ± 0.012	
coma18-51	4130	15.090 ± 0.001	14.962 ± 0.001	14.778 ± 0.001	14.767 ± 0.001	14.681 ± 0.001
comasw11-3	4137	19.716 ± 0.106	19.873 ± 0.170	19.822 ± 0.217	19.724 ± 0.233	
coma12-55	4138	19.886 ± 0.045	19.964 ± 0.066	19.815 ± 0.074	19.648 ± 0.079	19.240 ± 0.058
comasw6-73	4140	19.935 ± 0.082	20.209 ± 0.146	20.300 ± 0.218	20.820 ± 0.438	
comasw21-93	4141	18.514 ± 0.014	18.211 ± 0.014	17.940 ± 0.014	17.868 ± 0.016	
comasw6-21	4143	19.664 ± 0.040	19.574 ± 0.050	19.502 ± 0.064	19.578 ± 0.085	
comasw16-24	4146	18.545 ± 0.015	18.545 ± 0.020	18.444 ± 0.024	18.505 ± 0.032	
coma12-47	4148	19.025 ± 0.023	19.007 ± 0.030	18.898 ± 0.037	18.870 ± 0.044	18.619 ± 0.039
comasw21-31	4150	19.220 ± 0.028	19.201 ± 0.036	19.111 ± 0.046	19.262 ± 0.065	

Raw V-band aperture magnitudes. *continued from previous page*

Object	GMP	Aperture Dia. ('') 8.8	13	16	20.2	26
comal2-67	4153	19.488 ± 0.034	19.541 ± 0.048	19.459 ± 0.061	19.580 ± 0.078	19.422 ± 0.075
comasw11-29	4154	19.931 ± 0.051	20.019 ± 0.075	19.988 ± 0.101	19.976 ± 0.123	20.519 ± 0.227
comasw11-59	4156	14.295 ± 0.001	14.091 ± 0.001	13.904 ± 0.001	13.911 ± 0.001	13.837 ± 0.001
comasw16-27	4157	19.208 ± 0.024	19.067 ± 0.029	18.876 ± 0.033	18.875 ± 0.041	
comasw6-42	4161	18.985 ± 0.022	18.564 ± 0.020	17.581 ± 0.011	17.236 ± 0.010	
comasw11-10	4162	19.288 ± 0.030	19.233 ± 0.039	19.114 ± 0.048	19.187 ± 0.064	19.521 ± 0.120
comal2-32	4163	19.582 ± 0.037	19.525 ± 0.047	19.468 ± 0.061	19.569 ± 0.081	19.334 ± 0.085
comal2-8	4165	18.980 ± 0.022	18.706 ± 0.023	18.518 ± 0.026	18.507 ± 0.032	18.638 ± 0.044
comasw11-17	4169	18.138 ± 0.021	18.150 ± 0.029	18.053 ± 0.036	18.132 ± 0.047	17.000 ± 0.027
comasw21-72	4175	17.796 ± 0.008	17.703 ± 0.009	17.557 ± 0.010	17.598 ± 0.013	
comasw16-49	4179	17.824 ± 0.008	17.875 ± 0.011	17.779 ± 0.013	17.848 ± 0.018	
comasw16-67	4190	19.364 ± 0.026	19.266 ± 0.032	19.130 ± 0.039	19.228 ± 0.053	
comasw6-38	4192	16.229 ± 0.003	15.947 ± 0.002	15.685 ± 0.002	15.616 ± 0.003	
comasw21-80	4193	18.132 ± 0.011	18.140 ± 0.014	18.043 ± 0.017	18.104 ± 0.022	
comal2-51	4200	16.099 ± 0.002	16.048 ± 0.003	15.917 ± 0.003	15.964 ± 0.003	15.925 ± 0.003
comasw21-83	4205	17.948 ± 0.009	17.920 ± 0.011	17.764 ± 0.013	17.700 ± 0.015	
comasw11-11	4206	15.873 ± 0.002	15.749 ± 0.002	15.573 ± 0.003	15.576 ± 0.003	15.471 ± 0.005
comasw21-103	4207	19.192 ± 0.027	19.297 ± 0.039	19.240 ± 0.052	19.392 ± 0.076	
comal8-84	4208	19.666 ± 0.035	19.549 ± 0.043	19.445 ± 0.053	19.519 ± 0.070	19.566 ± 0.082
comasw16-50	4209	16.170 ± 0.002	16.127 ± 0.002	15.986 ± 0.003	16.009 ± 0.003	
comasw6-11	4211	18.836 ± 0.020	18.462 ± 0.019	18.060 ± 0.018	17.851 ± 0.018	
comasw6-10	4211	18.956 ± 0.022	18.554 ± 0.021	18.228 ± 0.021	18.169 ± 0.025	
comasw21-34	4212	19.254 ± 0.027	19.397 ± 0.042	19.393 ± 0.057	19.594 ± 0.084	
comasw6-50	4215	18.356 ± 0.012	18.192 ± 0.014	18.004 ± 0.016	18.021 ± 0.020	
comasw21-84	4216	18.847 ± 0.019	18.585 ± 0.020	18.331 ± 0.022	18.116 ± 0.022	
comasw21-115	4217	18.556 ± 0.015	18.447 ± 0.018	18.286 ± 0.021	18.304 ± 0.026	
comasw6-14	4220	18.963 ± 0.023	18.808 ± 0.026	18.430 ± 0.025	18.314 ± 0.028	
comasw21-41	4221	18.886 ± 0.021	18.896 ± 0.029	18.825 ± 0.036	18.967 ± 0.051	
comasw6-13	4226	18.924 ± 0.021	18.571 ± 0.021	18.118 ± 0.019	17.889 ± 0.019	
comal2-36	4230	15.020 ± 0.001	14.859 ± 0.001	14.663 ± 0.001	14.632 ± 0.001	14.482 ± 0.001
comasw10-79	4232	18.498 ± 0.015	18.190 ± 0.015	17.940 ± 0.016	17.943 ± 0.020	17.869 ± 0.020
comal2-65	4238	18.830 ± 0.019	18.803 ± 0.025	18.701 ± 0.031	18.789 ± 0.040	18.775 ± 0.046
comasw6-33	4240	19.374 ± 0.032	19.417 ± 0.045	19.348 ± 0.058	19.353 ± 0.072	
comasw21-40	4245	18.721 ± 0.017	18.648 ± 0.021	18.529 ± 0.026	18.568 ± 0.033	
comasw21-54	4246	17.378 ± 0.006	17.330 ± 0.007	17.220 ± 0.008	17.296 ± 0.010	
comasw21-101	4247	19.335 ± 0.029	19.298 ± 0.038	19.164 ± 0.048	19.220 ± 0.062	
comal2-71	4251	19.034 ± 0.022	19.096 ± 0.031	18.991 ± 0.039	18.977 ± 0.049	19.060 ± 0.062
comasw10-24	4253	20.159 ± 0.060	20.230 ± 0.088	20.242 ± 0.123	20.306 ± 0.162	19.636 ± 0.109
comasw10-78	4255	16.075 ± 0.002	15.946 ± 0.002	15.784 ± 0.002	15.815 ± 0.003	15.753 ± 0.003
comasw20-96	4264	19.118 ± 0.028	19.165 ± 0.042	19.112 ± 0.057	19.267 ± 0.089	
comasw16-33	4266	19.706 ± 0.046	19.697 ± 0.063	19.535 ± 0.075	19.458 ± 0.088	
comasw16-63	4268	18.351 ± 0.011	18.239 ± 0.014	18.079 ± 0.016	18.104 ± 0.020	
comasw10-59	4270	19.682 ± 0.037	19.623 ± 0.048	19.523 ± 0.059	19.586 ± 0.077	19.656 ± 0.080
comasw20-33	4271	19.128 ± 0.026	19.259 ± 0.040	19.216 ± 0.054	19.294 ± 0.072	
comal2-60	4275	19.723 ± 0.041	19.506 ± 0.045	19.294 ± 0.050	19.302 ± 0.063	19.331 ± 0.071
comal2-29	4277	19.432 ± 0.033	19.554 ± 0.047	19.434 ± 0.056	19.581 ± 0.079	19.645 ± 0.106
comal8-61	4281	17.030 ± 0.004	16.805 ± 0.004	16.577 ± 0.004	16.520 ± 0.005	16.418 ± 0.005
comasw16-18	4285	19.614 ± 0.036	19.590 ± 0.048	19.482 ± 0.060	19.630 ± 0.085	
comal8-69	4287	19.645 ± 0.037	19.833 ± 0.061	19.818 ± 0.083	19.998 ± 0.121	20.471 ± 0.209
comasw10-101	4291	19.681 ± 0.040	19.738 ± 0.059	19.681 ± 0.078		
comal2-46	4295	19.741 ± 0.043	19.705 ± 0.055	19.617 ± 0.071	19.706 ± 0.095	19.365 ± 0.073
comasw15-49	4303	19.130 ± 0.034	19.065 ± 0.046	18.907 ± 0.056	18.866 ± 0.069	
comasw20-77	4304	19.809 ± 0.046	19.885 ± 0.064	19.798 ± 0.079	19.922 ± 0.108	

Raw V-band aperture magnitudes. *continued from previous page*

Object	GMP	Aperture Dia. ('') 8.8	13	16	20.2	26
comal8-75	4308	16.207 ± 0.003	15.986 ± 0.003	15.746 ± 0.003	15.641 ± 0.003	15.206 ± 0.002
comasw21-104	4310	17.774 ± 0.008	17.716 ± 0.010	17.573 ± 0.012	17.611 ± 0.015	
comasw10-63	4312	19.034 ± 0.022	18.886 ± 0.025	18.699 ± 0.029	18.694 ± 0.036	18.797 ± 0.045
comal8-74	4313	15.569 ± 0.002	15.383 ± 0.002	15.173 ± 0.002	15.123 ± 0.002	14.902 ± 0.001
comasw21-114	4314	17.046 ± 0.005	16.898 ± 0.005	16.722 ± 0.005	16.728 ± 0.007	
comal2-17	4315	15.001 ± 0.001	14.860 ± 0.001	14.686 ± 0.001	14.692 ± 0.001	14.590 ± 0.001
comasw15-26	4317	19.815 ± 0.042	19.694 ± 0.053	19.546 ± 0.061	19.566 ± 0.073	
comasw16-83	4320	19.751 ± 0.039	19.706 ± 0.052	19.609 ± 0.065	19.633 ± 0.080	
comasw15-76	4323	19.357 ± 0.027	19.330 ± 0.036	19.165 ± 0.042	19.168 ± 0.052	
comasw21-120	4326	19.547 ± 0.036	19.551 ± 0.050	19.501 ± 0.065	19.690 ± 0.094	
comasw10-77	4329	19.376 ± 0.028	19.369 ± 0.039	19.217 ± 0.047	19.178 ± 0.054	19.130 ± 0.056
comasw10-4	4330	17.360 ± 0.005	17.257 ± 0.006			
comasw20-35	4332	18.927 ± 0.020	18.700 ± 0.024	18.130 ± 0.020	17.250 ± 0.011	
comal2-69	4333	18.303 ± 0.013	17.962 ± 0.012	17.691 ± 0.013	17.621 ± 0.015	17.465 ± 0.014
comasw10-45	4339	18.837 ± 0.018	18.793 ± 0.024	18.675 ± 0.029	18.733 ± 0.038	19.059 ± 0.044
comasw20-36	4341	16.539 ± 0.003	16.488 ± 0.004	16.351 ± 0.004	16.369 ± 0.005	
comal2-56	4345	17.809 ± 0.008	17.774 ± 0.010	17.647 ± 0.012	17.700 ± 0.015	17.646 ± 0.015
comasw20-83	4348	17.560 ± 0.007	17.399 ± 0.007	17.213 ± 0.008	17.209 ± 0.010	
comal2-22	4350	18.745 ± 0.018	18.759 ± 0.024	18.680 ± 0.030	18.763 ± 0.039	18.969 ± 0.056
comasw5-4	4351	16.660 ± 0.004	16.473 ± 0.004	16.288 ± 0.004	16.298 ± 0.005	16.244 ± 0.005
comal2-59	4352	19.124 ± 0.024	19.174 ± 0.033	19.080 ± 0.041	19.046 ± 0.049	19.037 ± 0.057
comal2-40	4355	17.381 ± 0.006	17.277 ± 0.007	17.125 ± 0.008	17.152 ± 0.009	17.098 ± 0.009
comasw24-47	4361	18.701 ± 0.020	18.776 ± 0.028	18.692 ± 0.035	18.800 ± 0.048	
comasw10-72	4363	19.614 ± 0.036	19.544 ± 0.046	19.424 ± 0.057	19.545 ± 0.079	19.337 ± 0.068
comasw15-90	4364	17.213 ± 0.005	16.953 ± 0.005	16.710 ± 0.005	16.654 ± 0.006	
comasw20-54	4366	17.804 ± 0.008	17.696 ± 0.009	17.536 ± 0.011	17.567 ± 0.014	
comasw20-68	4367	16.843 ± 0.004	16.720 ± 0.004	16.544 ± 0.005	16.533 ± 0.006	
comal2-66	4376	18.815 ± 0.019	18.838 ± 0.027	18.725 ± 0.033	18.818 ± 0.045	19.080 ± 0.059
comal8-56	4379	15.172 ± 0.001	15.135 ± 0.001	15.003 ± 0.001	15.043 ± 0.002	15.008 ± 0.002
comasw10-75	4380	19.353 ± 0.029	19.382 ± 0.041	19.263 ± 0.050	19.345 ± 0.065	19.283 ± 0.068
comasw10-28	4381	18.283 ± 0.011	18.208 ± 0.014	18.025 ± 0.016	17.972 ± 0.019	17.863 ± 0.019
comasw10-29	4384	19.584 ± 0.036	19.415 ± 0.043	18.901 ± 0.034	18.282 ± 0.024	17.973 ± 0.020
comasw24-51	4386	19.573 ± 0.048	19.469 ± 0.058	19.318 ± 0.069	19.381 ± 0.090	
comasw15-67	4390	19.016 ± 0.021	18.825 ± 0.024	18.644 ± 0.028	18.646 ± 0.035	
comal8-91	4391	16.133 ± 0.002	15.886 ± 0.002	15.646 ± 0.002	15.575 ± 0.003	15.385 ± 0.002
comasw5-6	4394	17.252 ± 0.006	17.262 ± 0.007	17.154 ± 0.008	17.220 ± 0.011	17.223 ± 0.012
comasw24-42	4395	19.309 ± 0.037	19.410 ± 0.054	19.354 ± 0.070	19.463 ± 0.094	
comal2-54	4396	19.611 ± 0.038	19.663 ± 0.056	19.588 ± 0.071	19.711 ± 0.095	19.740 ± 0.109
comasw24-50	4397	18.995 ± 0.028	18.905 ± 0.034	18.762 ± 0.041	18.827 ± 0.054	
comasw5-39	4402	18.995 ± 0.025	19.001 ± 0.033	18.892 ± 0.041	18.818 ± 0.047	18.453 ± 0.035
comasw10-12	4403	19.690 ± 0.039	19.654 ± 0.052	19.566 ± 0.066	19.672 ± 0.091	19.399 ± 0.078
comasw24-52	4404	19.412 ± 0.041	19.316 ± 0.050	19.150 ± 0.058	19.177 ± 0.074	
comasw5-38	4411	19.444 ± 0.038	19.300 ± 0.044	19.201 ± 0.055	19.195 ± 0.067	18.628 ± 0.041
comal8-80	4412	18.880 ± 0.017	18.782 ± 0.022	18.568 ± 0.027	18.708 ± 0.034	18.654 ± 0.035
comasw24-43	4419	18.251 ± 0.015	18.195 ± 0.018	18.071 ± 0.022	18.132 ± 0.028	
comal2-9	4420	16.732 ± 0.004	16.650 ± 0.004	16.510 ± 0.005	16.555 ± 0.006	16.516 ± 0.006
comasw10-67	4421	18.571 ± 0.014	18.399 ± 0.016	18.197 ± 0.019	18.169 ± 0.022	17.909 ± 0.019
comasw15-96	4423	19.217 ± 0.027	19.282 ± 0.039	19.217 ± 0.051	19.293 ± 0.069	
comasw20-91	4424	17.903 ± 0.008	17.883 ± 0.011	17.729 ± 0.013	17.691 ± 0.015	
comasw15-66	4428	19.219 ± 0.026	18.933 ± 0.027	18.719 ± 0.030	18.645 ± 0.035	
comasw20-47	4431	18.884 ± 0.020	18.886 ± 0.026	18.784 ± 0.033	18.818 ± 0.042	
comasw10-46	4436	19.493 ± 0.033	19.547 ± 0.047	19.518 ± 0.063	19.619 ± 0.085	19.465 ± 0.085
comasw20-63	4438	18.274 ± 0.012	18.324 ± 0.017	18.237 ± 0.021	18.357 ± 0.029	

Raw V-band aperture magnitudes. *contiuned from previous page*

Object	GMP	Aperture Dia. ('') 8.8	13	16	20.2	26
coma18-50	4441	19.790 ± 0.038	19.849 ± 0.054	19.765 ± 0.069	19.892 ± 0.093	19.863 ± 0.104
coma18-89	4442	17.931 ± 0.009	17.917 ± 0.011	17.827 ± 0.014	17.924 ± 0.019	17.814 ± 0.018
comasw24-41	4445	19.404 ± 0.042	19.595 ± 0.066	19.570 ± 0.087	19.715 ± 0.123	
comasw10-73	4447	16.906 ± 0.004	16.819 ± 0.004	16.676 ± 0.005	16.718 ± 0.006	16.681 ± 0.006
comasw5-34	4448	19.622 ± 0.043	19.759 ± 0.066	19.672 ± 0.083	19.725 ± 0.107	19.546 ± 0.094
comasw24-53	4450	19.501 ± 0.042	19.281 ± 0.046	19.098 ± 0.052	19.142 ± 0.067	
coma12-43	4451	19.043 ± 0.023	19.057 ± 0.031	18.956 ± 0.038	19.048 ± 0.050	19.081 ± 0.053
comasw10-18	4452	19.951 ± 0.050	19.903 ± 0.066	19.775 ± 0.081	19.822 ± 0.105	19.447 ± 0.077
coma18-70	4455	19.138 ± 0.021	19.166 ± 0.028	19.030 ± 0.034	19.078 ± 0.043	19.169 ± 0.055
coma12-14	4458	19.653 ± 0.039	19.748 ± 0.057	19.749 ± 0.079	19.917 ± 0.113	20.117 ± 0.153
comasw10-87	4469	17.321 ± 0.005	17.009 ± 0.005	16.771 ± 0.005	16.739 ± 0.006	16.651 ± 0.006
comasw5-52	4479	17.015 ± 0.005	16.819 ± 0.005	16.628 ± 0.005	16.626 ± 0.006	16.549 ± 0.006
coma18-77	4480	18.910 ± 0.019	18.938 ± 0.026	18.776 ± 0.030	18.806 ± 0.038	18.736 ± 0.037
coma12-34	4481	17.706 ± 0.008	17.692 ± 0.010	17.582 ± 0.012	17.665 ± 0.015	17.606 ± 0.015
comasw20-64	4483	19.325 ± 0.037	19.406 ± 0.055	19.278 ± 0.067	19.234 ± 0.081	
comasw5-28	4484	19.476 ± 0.037	19.337 ± 0.043	19.163 ± 0.050	19.151 ± 0.061	19.274 ± 0.074
comasw20-45	4485	18.660 ± 0.016	18.606 ± 0.021	18.454 ± 0.025	18.450 ± 0.031	
comasw10-35	4490	19.800 ± 0.049	19.688 ± 0.061	19.643 ± 0.081	19.854 ± 0.122	19.440 ± 0.080
comasw10-99	4491	19.332 ± 0.028	19.270 ± 0.037	19.149 ± 0.045	19.206 ± 0.059	19.485 ± 0.083
coma12-2	4493	18.718 ± 0.018	18.636 ± 0.023	18.460 ± 0.027		
comasw20-65	4499	15.426 ± 0.002	15.342 ± 0.002	15.189 ± 0.002	15.212 ± 0.002	
comasw20-67	4500	18.820 ± 0.022	18.692 ± 0.027	18.514 ± 0.032	18.501 ± 0.039	
comasw15-63	4502	17.101 ± 0.004	17.011 ± 0.005	16.874 ± 0.006	16.927 ± 0.008	
coma12-18	4503	16.614 ± 0.003	16.414 ± 0.003	16.184 ± 0.004	16.120 ± 0.004	15.941 ± 0.003
coma18-82	4504	19.191 ± 0.023	19.128 ± 0.029	18.910 ± 0.032	18.891 ± 0.039	18.844 ± 0.041
comasw15-38	4506	16.240 ± 0.002	16.183 ± 0.003	16.035 ± 0.003	16.048 ± 0.004	
comasw15-41	4508	18.659 ± 0.017	18.738 ± 0.025	18.645 ± 0.031	18.753 ± 0.043	
comasw15-47	4509	19.936 ± 0.048	19.931 ± 0.066	19.573 ± 0.066	19.351 ± 0.066	
coma12-20	4510	17.538 ± 0.007	17.443 ± 0.008	17.288 ± 0.010	17.314 ± 0.012	17.244 ± 0.011
comasw20-58	4515	18.400 ± 0.016	18.390 ± 0.022	18.294 ± 0.027	18.382 ± 0.037	
comasw20-87	4516	16.907 ± 0.004	16.915 ± 0.005	16.796 ± 0.006	16.810 ± 0.007	
comasw20-88	4519	16.874 ± 0.004	16.759 ± 0.005	16.591 ± 0.005	16.588 ± 0.006	
comasw10-44	4522	15.874 ± 0.002	15.637 ± 0.002	15.383 ± 0.002	15.305 ± 0.002	15.129 ± 0.002
comasw10-47	4524	18.754 ± 0.018	18.585 ± 0.021	18.455 ± 0.026	18.551 ± 0.035	18.604 ± 0.041
comasw20-71	4529	18.600 ± 0.016	18.515 ± 0.020	18.347 ± 0.023	18.312 ± 0.027	
comasw5-53	4530	17.708 ± 0.008	17.532 ± 0.009	17.378 ± 0.010	17.434 ± 0.013	17.428 ± 0.015
comasw20-55	4531	17.599 ± 0.007	17.605 ± 0.009	17.498 ± 0.011	17.517 ± 0.013	
comasw10-19	4535	16.966 ± 0.004	16.924 ± 0.005	16.793 ± 0.005	16.837 ± 0.007	16.828 ± 0.007
comasw10-97	4538	19.526 ± 0.034	19.630 ± 0.051	19.578 ± 0.069	19.752 ± 0.103	20.153 ± 0.155
comasw20-86	4539	18.316 ± 0.013	18.211 ± 0.016	18.062 ± 0.020	18.086 ± 0.025	
comasw15-74	4541	19.532 ± 0.033	19.307 ± 0.037	19.089 ± 0.042	19.100 ± 0.052	
comasw5-32	4545	19.093 ± 0.026	18.859 ± 0.028	18.651 ± 0.032	18.588 ± 0.037	18.401 ± 0.035
comasw23-46	4553	18.663 ± 0.017	18.629 ± 0.023	18.542 ± 0.029	18.651 ± 0.039	
comasw5-16	4554	18.557 ± 0.016	18.539 ± 0.021	18.433 ± 0.026	18.445 ± 0.032	18.356 ± 0.034
comasw26-27	4555	16.406 ± 0.003	16.096 ± 0.002	15.830 ± 0.002	15.757 ± 0.003	
comasw15-60	4557	18.678 ± 0.016	18.657 ± 0.021	18.549 ± 0.026	18.629 ± 0.034	
comasw26-40	4558	19.147 ± 0.022	19.160 ± 0.029	19.079 ± 0.036	19.177 ± 0.048	
comasw10-98	4559	19.161 ± 0.025	19.247 ± 0.038	19.202 ± 0.052	19.319 ± 0.074	20.364 ± 0.125
comasw23-50	4561	19.251 ± 0.030	19.235 ± 0.040	19.070 ± 0.048	19.177 ± 0.065	
comasw15-95	4562	19.593 ± 0.037	19.443 ± 0.045	19.284 ± 0.055	19.297 ± 0.071	
comasw23-58	4563	18.466 ± 0.013	18.438 ± 0.017	18.334 ± 0.020	18.373 ± 0.026	
comasw5-15	4565	18.515 ± 0.016	18.545 ± 0.022	18.424 ± 0.026	18.491 ± 0.034	18.484 ± 0.037
comasw19-40	4566	17.322 ± 0.009	17.258 ± 0.012	17.110 ± 0.014	17.125 ± 0.018	16.947 ± 0.016

Raw V-band aperture magnitudes. *contiuned from previous page*

Object	GMP	Aperture Dia. ('') 8.8	13	16	20.2	26
comasw10-11	4568	17.796 ± 0.008	17.764 ± 0.009	17.602 ± 0.011	17.550 ± 0.013	17.258 ± 0.011
comasw23-47	4569	19.766 ± 0.046	19.630 ± 0.057	19.496 ± 0.069	19.640 ± 0.098	
comasw23-82	4570	17.421 ± 0.006	17.195 ± 0.006	16.968 ± 0.007	16.942 ± 0.008	
comasw5-47	4572	19.067 ± 0.029	19.019 ± 0.037	18.891 ± 0.044	18.927 ± 0.057	18.807 ± 0.049
comasw15-22	4573	19.791 ± 0.050	19.818 ± 0.070	19.791 ± 0.095	19.884 ± 0.128	
comasw10-10	4577	17.931 ± 0.008	17:773 ± 0.009	17.579 ± 0.010	17.544 ± 0.012	17.252 ± 0.011
comasw4-28	4578	17.442 ± 0.006	17.267 ± 0.007	17.079 ± 0.008	17.081 ± 0.010	17.086 ± 0.012
comasw10-92	4579	17.013 ± 0.004	16.776 ± 0.004	16.532 ± 0.004	16.467 ± 0.005	16.306 ± 0.005
comasw15-29	4580	19.863 ± 0.057	19.840 ± 0.078	19.765 ± 0.101	19.883 ± 0.140	
comasw15-25	4592	15.917 ± 0.002	15.758 ± 0.002	15.557 ± 0.002	15.524 ± 0.002	
comasw15-33	4593	18.406 ± 0.013	18.408 ± 0.018	18.319 ± 0.022	18.475 ± 0.032	
comasw10-34	4597	16.749 ± 0.003	16.456 ± 0.003	16.120 ± 0.003	15.927 ± 0.003	15.687 ± 0.003
comasw26-22	4600	18.704 ± 0.015	18.593 ± 0.018	18.422 ± 0.020	18.459 ± 0.026	
comasw15-73	4602	17.695 ± 0.007	17.477 ± 0.008	17.244 ± 0.008	17.196 ± 0.010	
comasw23-66	4606	18.637 ± 0.016	18.511 ± 0.019	18.377 ± 0.023	18.464 ± 0.031	
comasw19-33	4608	19.143 ± 0.045	19.241 ± 0.070	19.153 ± 0.089	19.231 ± 0.115	19.350 ± 0.137
comasw10-86	4609	19.689 ± 0.038	19.626 ± 0.049	19.414 ± 0.056	19.355 ± 0.067	19.440 ± 0.083
comasw15-93	4612	18.256 ± 0.011	18.147 ± 0.014	17.998 ± 0.016	18.043 ± 0.021	
comasw23-88	4614	20.055 ± 0.215				
comasw15-70	4615	19.617 ± 0.038	19.671 ± 0.055	19.601 ± 0.071	19.761 ± 0.102	
comasw10-9	4618	19.880 ± 0.044	19.876 ± 0.060	19.794 ± 0.077	19.750 ± 0.092	20.082 ± 0.142
comasw15-34	4619	18.758 ± 0.018	18.844 ± 0.026	18.818 ± 0.034	18.985 ± 0.050	
comasw23-33	4620	19.596 ± 0.046	19.791 ± 0.077	19.860 ± 0.114	20.140 ± 0.183	
comasw23-87	4622	19.568 ± 0.036	19.539 ± 0.053			
comasw19-50	4624	18.235 ± 0.019	18.126 ± 0.023	17.961 ± 0.027	17.934 ± 0.032	17.740 ± 0.032
comasw19-61	4626	16.080 ± 0.004	15.942 ± 0.005	15.758 ± 0.005	15.748 ± 0.007	15.662 ± 0.005
comasw10-62	4628	19.243 ± 0.026	19.029 ± 0.029	18.844 ± 0.034	18.855 ± 0.042	18.878 ± 0.043
comasw10-42	4630	17.832 ± 0.008	17.891 ± 0.011	17.814 ± 0.014	17.905 ± 0.018	17.851 ± 0.019
comasw15-44	4632	17.622 ± 0.007	17.521 ± 0.008	17.364 ± 0.009	17.377 ± 0.011	
comasw10-53	4636	19.566 ± 0.033	19.479 ± 0.041	19.226 ± 0.045	19.031 ± 0.046	18.758 ± 0.043
comasw15-36	4642	18.721 ± 0.017	18.796 ± 0.025	18.745 ± 0.032	18.864 ± 0.044	
comasw10-54	4643	19.408 ± 0.031	19.114 ± 0.032	18.861 ± 0.036	18.771 ± 0.041	18.535 ± 0.036
comasw4-27	4645	19.159 ± 0.028	19.208 ± 0.041	19.145 ± 0.054	19.281 ± 0.081	19.243 ± 0.074
comasw10-33	4646	19.308 ± 0.025	19.288 ± 0.033	19.190 ± 0.041	19.206 ± 0.050	19.418 ± 0.069
comasw10-32	4646	19.361 ± 0.029	19.281 ± 0.034	19.200 ± 0.043	19.261 ± 0.057	19.225 ± 0.067
comasw23-80	4647	18.368 ± 0.012	18.388 ± 0.016	18.303 ± 0.020	18.388 ± 0.026	
comasw23-31	4653	15.406 ± 0.002	15.248 ± 0.002	15.046 ± 0.002	15.017 ± 0.002	
comasw15-87	4655	17.399 ± 0.006	17.272 ± 0.007	17.099 ± 0.008	17.092 ± 0.009	
comasw19-25	4656	16.907 ± 0.007	16.802 ± 0.008	16.648 ± 0.009	16.681 ± 0.011	16.676 ± 0.013
comasw19-57	4657	19.554 ± 0.062	19.623 ± 0.093	19.511 ± 0.100	19.565 ± 0.129	19.616 ± 0.176
comasw19-51	4659	18.618 ± 0.030	18.580 ± 0.039	18.446 ± 0.048	18.525 ± 0.067	18.592 ± 0.072
comasw26-38	4660	18.856 ± 0.017	18.895 ± 0.023	18.819 ± 0.029	18.910 ± 0.038	
comasw10-36	4662	19.116 ± 0.022	19.110 ± 0.029	18.970 ± 0.035	19.033 ± 0.047	19.123 ± 0.062
comasw19-45	4664	15.477 ± 0.002	15.410 ± 0.002	15.257 ± 0.003	15.271 ± 0.003	15.228 ± 0.003
comasw26-69	4666	16.937 ± 0.004	16.758 ± 0.004	16.555 ± 0.004	16.532 ± 0.005	
comasw10-5	4667	19.596 ± 0.039	19.728 ± 0.063	19.702 ± 0.089	19.818 ± 0.126	19.528 ± 0.086
comasw4-16	4669	19.372 ± 0.031	19.409 ± 0.044	19.339 ± 0.056	19.407 ± 0.076	19.363 ± 0.079
comasw15-77	4670	19.546 ± 0.034	19.605 ± 0.048	19.496 ± 0.059	19.238 ± 0.058	
comasw4-1	4675	19.700 ± 0.052	19.851 ± 0.086	19.814 ± 0.116	20.102 ± 0.199	19.772 ± 0.116
comasw23-59	4676	19.523 ± 0.032	19.451 ± 0.042	19.309 ± 0.051	19.334 ± 0.064	
comasw19-20	4679	16.172 ± 0.004	15.910 ± 0.004	15.662 ± 0.004	15.588 ± 0.005	15.430 ± 0.004
comasw4-45	4682	18.836 ± 0.020	18.517 ± 0.020	18.247 ± 0.021	18.196 ± 0.025	18.217 ± 0.028
comasw26-24	4686	19.622 ± 0.033	19.622 ± 0.044	19.448 ± 0.051	19.501 ± 0.065	

Raw V-band aperture magnitudes. *continued from previous page*

Object	GMP	Aperture Dia. ('') 8.8	13	16	20.2	26
comasw23-42	4689	18.033 ± 0.009	17.910 ± 0.011	17.754 ± 0.013	17.795 ± 0.016	
comasw19-24	4690	19.163 ± 0.047	19.076 ± 0.059	18.977 ± 0.075	19.082 ± 0.103	18.963 ± 0.099
comasw4-51	4692	17.011 ± 0.004	16.820 ± 0.005	16.625 ± 0.005	16.615 ± 0.006	16.545 ± 0.006
comasw10-84	4696	18.057 ± 0.009				
comasw14-54	4699	18.715 ± 0.018	18.704 ± 0.025	18.603 ± 0.031	18.677 ± 0.042	
comasw23-57	4706	19.899 ± 0.047	19.986 ± 0.070	19.956 ± 0.094	20.119 ± 0.136	
comasw10-13	4709	19.798 ± 0.041				
comasw26-48	4711	19.483 ± 0.031	19.454 ± 0.040	19.327 ± 0.048	19.381 ± 0.062	
comasw4-73	4712	19.487 ± 0.038	19.400 ± 0.049	19.232 ± 0.057	19.301 ± 0.078	19.316 ± 0.080
comasw14-1	4714	16.808 ± 0.004	16.744 ± 0.004	16.602 ± 0.005	16.637 ± 0.006	
comasw14-19	4715	17.521 ± 0.006	17.416 ± 0.007	17.277 ± 0.008	17.322 ± 0.011	
comasw19-35	4718	17.872 ± 0.015	17.643 ± 0.017	17.440 ± 0.019	17.415 ± 0.023	17.213 ± 0.019
comasw14-26	4719	16.828 ± 0.004	16.766 ± 0.004	16.620 ± 0.005	16.642 ± 0.006	
comasw14-34	4725	19.575 ± 0.035	19.658 ± 0.050	19.576 ± 0.065	19.686 ± 0.090	
comasw19-34	4727	18.994 ± 0.038	18.844 ± 0.046	18.482 ± 0.045	18.155 ± 0.041	17.578 ± 0.026
comasw26-66	4733	19.352 ± 0.026	19.398 ± 0.036	19.318 ± 0.046	19.385 ± 0.059	
comasw14-37	4735	19.229 ± 0.026	19.270 ± 0.038	19.148 ± 0.047	19.198 ± 0.062	
comasw9-63	4739	19.428 ± 0.030	19.456 ± 0.043	19.403 ± 0.056	19.524 ± 0.078	19.437 ± 0.073
comasw9-54	4740	19.294 ± 0.025	19.284 ± 0.034	19.171 ± 0.042	19.237 ± 0.055	19.194 ± 0.059
comasw23-35	4742	19.562 ± 0.035				
comasw26-23	4745	18.929 ± 0.018	18.772 ± 0.021	18.559 ± 0.023	18.541 ± 0.028	
comasw9-69	4749	18.600 ± 0.015	18.562 ± 0.019	18.366 ± 0.022	18.391 ± 0.027	18.292 ± 0.025
comasw27-61	4752	20.102 ± 0.094	20.410 ± 0.173	20.638 ± 0.299	21.276 ± 0.684	
comasw14-41	4753	19.958 ± 0.051	20.026 ± 0.070	20.003 ± 0.090	20.103 ± 0.121	
comasw14-13	4757	17.093 ± 0.004	17.117 ± 0.006	17.016 ± 0.007	17.081 ± 0.008	
comasw26-70	4758	18.635 ± 0.015	18.224 ± 0.013	17.762 ± 0.011	17.553 ± 0.011	
comasw23-86	4759	19.820 ± 0.043	19.888 ± 0.064	19.837 ± 0.087	19.996 ± 0.124	
comasw19-59	4761	18.855 ± 0.036	18.797 ± 0.045	18.512 ± 0.048	18.448 ± 0.057	18.177 ± 0.046
comasw26-71	4762	17.900 ± 0.008	17.782 ± 0.009	17.547 ± 0.010	17.489 ± 0.011	
comasw14-10	4763	19.895 ± 0.050	19.995 ± 0.079	19.989 ± 0.110	20.180 ± 0.182	
comasw19-18	4766	17.418 ± 0.010	17.123 ± 0.010	16.874 ± 0.011	16.858 ± 0.013	16.801 ± 0.013
comasw4-68	4768	18.488 ± 0.015	18.328 ± 0.017	18.140 ± 0.020	18.158 ± 0.024	18.050 ± 0.024
comasw23-25	4773	19.755 ± 0.041	19.852 ± 0.062	19.691 ± 0.074	19.738 ± 0.097	
comasw26-19	4774	17.892 ± 0.008	17.638 ± 0.008	17.405 ± 0.008	17.343 ± 0.009	
comasw23-55	4775	19.360 ± 0.027	19.117 ± 0.030	18.934 ± 0.035	18.943 ± 0.044	
comasw26-34	4779	16.772 ± 0.003	16.532 ± 0.003	16.310 ± 0.003	16.274 ± 0.004	
comasw14-35	4780	17.591 ± 0.006	17.589 ± 0.008	17.494 ± 0.010	17.582 ± 0.013	
comasw26-77	4782	18.991 ± 0.020	19.067 ± 0.029	18.986 ± 0.037	19.093 ± 0.052	
comasw26-15	4783	18.987 ± 0.019	19.091 ± 0.027	19.003 ± 0.034	19.132 ± 0.045	
comasw9-28	4784	20.143 ± 0.054	20.144 ± 0.075	20.087 ± 0.098	20.199 ± 0.135	20.382 ± 0.170
comasw9-42	4792	15.709 ± 0.002	15.614 ± 0.002	15.467 ± 0.002	15.498 ± 0.002	15.455 ± 0.002
comasw9-37	4794	14.858 ± 0.001	14.715 ± 0.001	14.530 ± 0.001	14.518 ± 0.001	14.430 ± 0.001
comasw9-46	4795	20.019 ± 0.059	20.001 ± 0.081	19.922 ± 0.105	19.982 ± 0.139	19.063 ± 0.062
comasw4-55	4797	18.360 ± 0.014	18.408 ± 0.020	18.317 ± 0.025	18.380 ± 0.033	18.186 ± 0.025
comasw4-8	4800	17.954 ± 0.009	17.658 ± 0.009	17.487 ± 0.011	17.541 ± 0.013	17.517 ± 0.014
comasw23-53	4801	19.438 ± 0.032	19.223 ± 0.036	18.934 ± 0.038	18.731 ± 0.039	
comasw26-43	4805	19.312 ± 0.026	19.066 ± 0.028	18.844 ± 0.031	18.815 ± 0.037	
comasw9-77	4808	19.827 ± 0.042	19.807 ± 0.056	19.714 ± 0.071	19.885 ± 0.104	19.840 ± 0.104
comasw14-42	4809	19.899 ± 0.046	20.029 ± 0.070	19.917 ± 0.087	20.024 ± 0.119	
comasw23-51	4811	19.916 ± 0.047	19.648 ± 0.050	19.304 ± 0.051	18.998 ± 0.048	
comasw9-45	4813	19.297 ± 0.033	19.393 ± 0.050	19.304 ± 0.063	19.408 ± 0.088	18.790 ± 0.052
comasw19-21	4814	19.467 ± 0.066	19.604 ± 0.103	19.542 ± 0.135	19.653 ± 0.186	19.662 ± 0.187
comasw4-3	4815	17.510 ± 0.007	17.422 ± 0.008	17.280 ± 0.009	17.321 ± 0.012	17.251 ± 0.012

Raw V-band aperture magnitudes. *continued from previous page*

Object	GMP	Aperture Dia. ('') 8.8	13	16	20.2	26
comasw23-3	4821	19.865 ± 0.046	19.900 ± 0.066	19.771 ± 0.081	19.766 ± 0.100	
comasw9-41	4825	18.795 ± 0.021	18.626 ± 0.025	18.381 ± 0.028	17.789 ± 0.020	17.576 ± 0.021
comasw14-20	4829	14.639 ± 0.001	14.488 ± 0.001	14.293 ± 0.001	14.269 ± 0.001	
comasw26-49	4833	19.725 ± 0.039	19.651 ± 0.049	19.583 ± 0.064	19.700 ± 0.085	
comasw27-45	4833	19.647 ± 0.036	19.699 ± 0.050	19.630 ± 0.064	19.792 ± 0.091	
comasw19-56	4835	19.529 ± 0.063	19.590 ± 0.092	19.479 ± 0.117	19.417 ± 0.133	19.204 ± 0.117
comasw26-10	4837	18.092 ± 0.011	17.873 ± 0.012	17.664 ± 0.013	17.639 ± 0.016	
comasw26-13	4838	18.440 ± 0.014	18.386 ± 0.018	18.205 ± 0.021	18.099 ± 0.023	
comasw4-12	4845	19.392 ± 0.033	19.156 ± 0.036	18.943 ± 0.041	18.928 ± 0.050	18.864 ± 0.049
comasw4-59	4846	17.708 ± 0.008	17.651 ± 0.009	17.512 ± 0.011	17.563 ± 0.014	17.606 ± 0.016
comasw4-29	4848	18.055 ± 0.010	17.926 ± 0.012	17.745 ± 0.014	17.680 ± 0.016	17.512 ± 0.014
comasw4-44	4851	19.090 ± 0.024	19.067 ± 0.032	18.954 ± 0.040	18.970 ± 0.050	18.958 ± 0.053
comasw9-70	4852	17.324 ± 0.005	17.304 ± 0.006	17.195 ± 0.007	17.265 ± 0.010	17.302 ± 0.013
comasw4-22	4855	17.856 ± 0.009	17.650 ± 0.010	17.426 ± 0.010	17.361 ± 0.012	17.254 ± 0.012
comasw4-72	4858	17.795 ± 0.008	17.703 ± 0.010	17.558 ± 0.011	17.611 ± 0.014	17.660 ± 0.017
comasw27-25	4865	19.617 ± 0.033	19.541 ± 0.040	19.463 ± 0.051	19.520 ± 0.065	
comasw14-66	4867	19.881 ± 0.050	19.935 ± 0.072	19.802 ± 0.088	19.811 ± 0.111	
comasw14-16	4868	19.834 ± 0.055	19.953 ± 0.085	19.923 ± 0.114	20.154 ± 0.175	
comasw27-16	4869	18.990 ± 0.019	18.958 ± 0.024	18.862 ± 0.030	18.946 ± 0.039	
comasw4-41	4870	19.112 ± 0.026	19.115 ± 0.035	19.003 ± 0.044	19.148 ± 0.062	19.284 ± 0.073
comasw23-73	4871	18.067 ± 0.009	18.117 ± 0.013	18.018 ± 0.016	18.087 ± 0.021	
comasw9-75	4878	19.627 ± 0.034	19.736 ± 0.051	19.723 ± 0.070	19.820 ± 0.095	20.181 ± 0.150
comasw14-67	4879	17.553 ± 0.007	17.418 ± 0.007	17.256 ± 0.009	17.291 ± 0.011	
comasw27-36	4880	19.067 ± 0.021	18.993 ± 0.026	18.855 ± 0.030	18.877 ± 0.038	
comasw27-32	4882	18.931 ± 0.019	18.855 ± 0.023	18.723 ± 0.027	18.800 ± 0.036	
comasw9-67	4887	18.639 ± 0.016	18.649 ± 0.021	18.559 ± 0.027	18.681 ± 0.037	18.991 ± 0.061
comasw14-38	4888	17.535 ± 0.006	17.409 ± 0.007	17.241 ± 0.008	17.266 ± 0.010	
comasw4-13	4893	19.225 ± 0.028	19.205 ± 0.037	19.087 ± 0.046	19.231 ± 0.064	19.478 ± 0.089
comasw14-79	4896	19.351 ± 0.028	19.445 ± 0.040	19.407 ± 0.053	19.429 ± 0.072	
comasw18-56	4897	19.349 ± 0.028	19.225 ± 0.034	19.063 ± 0.041	19.094 ± 0.053	
comasw14-51	4905	17.840 ± 0.008	17.639 ± 0.008	17.452 ± 0.009	17.450 ± 0.011	
comasw8-50	4907	15.273 ± 0.001	15.190 ± 0.001	15.039 ± 0.001	15.063 ± 0.002	
comasw14-53	4911	19.309 ± 0.028	19.103 ± 0.032	18.958 ± 0.039	18.972 ± 0.049	
comasw18-66	4913	19.822 ± 0.045	19.872 ± 0.064	19.796 ± 0.083	19.961 ± 0.125	
comasw23-37	4916	19.559 ± 0.034	19.531 ± 0.046	19.421 ± 0.057	19.515 ± 0.077	
comasw3-87	4918	15.934 ± 0.002	15.775 ± 0.002	15.581 ± 0.002	15.519 ± 0.002	15.380 ± 0.002
comasw3-65	4919	19.460 ± 0.034	19.549 ± 0.049	19.502 ± 0.066	19.586 ± 0.088	19.382 ± 0.074
comasw3-19	4926	16.614 ± 0.004	16.519 ± 0.004	16.346 ± 0.005	16.334 ± 0.006	16.208 ± 0.004
comasw18-55	4927	19.440 ± 0.029	19.484 ± 0.040	19.400 ± 0.050	19.485 ± 0.065	
comasw8-38	4928	14.530 ± 0.001	14.245 ± 0.001	13.988 ± 0.001	13.895 ± 0.002	
comasw3-39	4930	19.059 ± 0.023	19.102 ± 0.033	19.016 ± 0.042	19.120 ± 0.057	19.264 ± 0.072
comasw3-53	4931	19.017 ± 0.022	19.053 ± 0.030	18.968 ± 0.039	19.044 ± 0.054	19.186 ± 0.075
comasw18-24	4933	16.277 ± 0.002	16.058 ± 0.002	15.812 ± 0.003	15.728 ± 0.003	
comasw27-38	4934	18.757 ± 0.016	18.834 ± 0.022	18.752 ± 0.027	18.870 ± 0.037	
comasw18-52	4935	18.715 ± 0.016	18.630 ± 0.019	18.502 ± 0.023	18.548 ± 0.029	
comasw8-51	4937	17.635 ± 0.007	17.517 ± 0.008	17.363 ± 0.009	17.388 ± 0.012	
comasw18-18	4940	19.236 ± 0.025	19.041 ± 0.029	18.851 ± 0.034	18.876 ± 0.043	
comasw19-60	4945	16.055 ± 0.003	15.957 ± 0.004	15.798 ± 0.004	15.812 ± 0.005	15.777 ± 0.006
comasw18-48	4948	19.639 ± 0.039	19.345 ± 0.041	19.091 ± 0.044	19.075 ± 0.054	
comasw18-68	4953	17.158 ± 0.005	17.029 ± 0.005	16.873 ± 0.006	16.897 ± 0.007	
comasw3-68	4954	19.671 ± 0.042	19.755 ± 0.065	19.684 ± 0.082	19.785 ± 0.120	19.985 ± 0.150
comasw3-91	4956	17.748 ± 0.009	17.547 ± 0.011	17.225 ± 0.011	17.276 ± 0.014	17.138 ± 0.012
comasw14-17	4960	18.827 ± 0.018	18.921 ± 0.026	18.830 ± 0.033	18.934 ± 0.045	

Raw V-band aperture magnitudes. *contiuned from previous page*

Object	GMP	Aperture Dia. (″) 8.8	13	16	20.2	26
comasw3-73	4962	19.226 ± 0.025	19.318 ± 0.037	19.260 ± 0.051	19.333 ± 0.067	19.456 ± 0.087
comasw14-15	4967	17.542 ± 0.006	17.422 ± 0.007	17.256 ± 0.008	17.276 ± 0.010	
comasw27-51	4968	19.263 ± 0.026	19.312 ± 0.036	19.219 ± 0.044	19.246 ± 0.056	
comasw18-46	4974	16.092 ± 0.002	15.938 ± 0.002	15.771 ± 0.002	15.789 ± 0.003	
comasw3-41	4978	19.686 ± 0.040	19.773 ± 0.059	19.660 ± 0.073	19.748 ± 0.098	19.773 ± 0.106
comasw23-68	4981	19.023 ± 0.023	18.977 ± 0.030	18.870 ± 0.037	18.991 ± 0.051	
comasw23-30	4986	19.456 ± 0.030	19.499 ± 0.043	19.422 ± 0.054	19.531 ± 0.077	
comasw14-22	4987	15.803 ± 0.002	15.798 ± 0.002	15.681 ± 0.002	15.736 ± 0.003	
comasw23-72	4988	18.975 ± 0.021	19.022 ± 0.030	18.956 ± 0.039	19.002 ± 0.049	
comasw3-7	4992	19.122 ± 0.025	19.189 ± 0.035	19.127 ± 0.046	19.244 ± 0.064	19.164 ± 0.064
comasw23-40	4993	18.790 ± 0.018	18.851 ± 0.025	18.784 ± 0.032	18.891 ± 0.044	
comasw14-77	4995	18.500 ± 0.013	18.275 ± 0.015	18.044 ± 0.016	17.975 ± 0.019	
comasw23-76	4997	18.359 ± 0.013	18.346 ± 0.017	18.238 ± 0.021	18.270 ± 0.027	
comasw9-48	5004	20.154 ± 0.056	20.200 ± 0.081	20.237 ± 0.115	20.458 ± 0.176	
comasw25-70	5007	19.207 ± 0.027	19.277 ± 0.040	19.195 ± 0.050	19.295 ± 0.068	
comasw14-39	5009	18.022 ± 0.009	18.005 ± 0.012	17.901 ± 0.015	17.991 ± 0.019	
comasw27-52	5010	18.398 ± 0.012	18.191 ± 0.012	17.989 ± 0.014	17.964 ± 0.016	
comasw3-47	5017	20.005 ± 0.062	19.741 ± 0.067	19.226 ± 0.058	18.944 ± 0.055	18.611 ± 0.039
comasw27-34	5018	18.426 ± 0.012	18.197 ± 0.013	17.993 ± 0.014	17.962 ± 0.017	
comasw3-48	5020	19.081 ± 0.026	18.989 ± 0.031	18.734 ± 0.034	18.779 ± 0.043	18.538 ± 0.033
comasw3-38	5026	19.706 ± 0.041	19.539 ± 0.048	19.364 ± 0.056	19.414 ± 0.072	19.540 ± 0.092
comasw25-66	5029	18.981 ± 0.022	18.786 ± 0.025	18.493 ± 0.026	18.479 ± 0.032	
comasw18-58	5030	19.684 ± 0.038	19.757 ± 0.056	19.671 ± 0.074	19.758 ± 0.104	
comasw8-33	5031	19.466 ± 0.030	19.368 ± 0.037	19.146 ± 0.042	18.962 ± 0.044	
comasw8-55	5033	18.628 ± 0.015	18.522 ± 0.018	18.363 ± 0.021	18.410 ± 0.027	
comasw8-45	5034	19.228 ± 0.025	19.091 ± 0.030	18.884 ± 0.034	18.853 ± 0.041	
comasw3-45	5038	16.013 ± 0.002	15.798 ± 0.002	15.557 ± 0.002	15.506 ± 0.002	15.405 ± 0.002
comasw25-20	5039	19.549 ± 0.037	19.280 ± 0.039	19.026 ± 0.043	19.021 ± 0.053	
comasw18-63	5040	19.732 ± 0.039	19.796 ± 0.059	19.721 ± 0.075	19.804 ± 0.097	
comasw14-44	5042	18.799 ± 0.017	18.711 ± 0.022	18.477 ± 0.024	18.465 ± 0.029	
comasw3-70	5050	19.504 ± 0.036	19.564 ± 0.052	19.537 ± 0.071	19.768 ± 0.110	19.761 ± 0.115
comasw3-86	5051	14.963 ± 0.001	14.852 ± 0.001	14.680 ± 0.001	14.676 ± 0.001	14.591 ± 0.001
comasw3-14	5054	18.338 ± 0.012	18.210 ± 0.014	18.062 ± 0.017	18.081 ± 0.021	18.010 ± 0.022
comasw18-44	5058	18.822 ± 0.017	18.789 ± 0.022	18.679 ± 0.028	18.687 ± 0.035	
comasw25-26	5059	18.762 ± 0.018	18.577 ± 0.021	18.402 ± 0.024	18.446 ± 0.031	
comasw18-40	5060	19.102 ± 0.022	19.220 ± 0.034	19.050 ± 0.040	19.050 ± 0.049	
comasw27-19	5063	19.152 ± 0.022	19.198 ± 0.030	19.120 ± 0.038	19.181 ± 0.049	
comasw3-72	5066	18.918 ± 0.025	19.033 ± 0.038	18.978 ± 0.051	19.079 ± 0.069	18.895 ± 0.054
comasw18-62	5075	19.181 ± 0.025	19.221 ± 0.035	19.152 ± 0.044	19.178 ± 0.054	
comasw3-12	5076	17.927 ± 0.009	17.843 ± 0.010	17.703 ± 0.012	17.751 ± 0.016	17.779 ± 0.017
comasw18-54	5083	18.894 ± 0.018	18.683 ± 0.020	18.489 ± 0.023	18.435 ± 0.027	
comasw14-24	5090	18.791 ± 0.018	18.748 ± 0.024	18.642 ± 0.030	18.727 ± 0.039	
comasw3-25	5091	19.451 ± 0.032	19.502 ± 0.046	19.434 ± 0.059		
comasw14-59	5095	18.092 ± 0.009	17.926 ± 0.011	17.726 ± 0.012	17.718 ± 0.014	
comasw18-27	5096	16.558 ± 0.003	16.317 ± 0.003	16.122 ± 0.003	16.118 ± 0.004	
comasw25-30	5098	19.337 ± 0.029	19.341 ± 0.040	19.276 ± 0.052	19.339 ± 0.068	
comasw14-78	5100	16.999 ± 0.004	16.763 ± 0.004	16.545 ± 0.004	16.491 ± 0.005	
comasw8-43	5102	16.994 ± 0.004	16.799 ± 0.004	16.604 ± 0.004	16.605 ± 0.005	
comasw3-6	5103	19.561 ± 0.035	19.478 ± 0.044	19.387 ± 0.055	19.501 ± 0.076	19.453 ± 0.080
comasw18-35	5104	19.531 ± 0.034	19.450 ± 0.043	19.274 ± 0.051	19.359 ± 0.068	
comasw18-33	5110	17.989 ± 0.010	17.650 ± 0.010	17.402 ± 0.010	17.360 ± 0.012	
comasw3-81	5118	19.796 ± 0.042	19.841 ± 0.058	19.674 ± 0.068	19.533 ± 0.076	19.118 ± 0.060
comasw18-53	5119	19.076 ± 0.022	19.153 ± 0.031	19.086 ± 0.040	19.217 ± 0.055	

Raw V-band aperture magnitudes. *contiuned from previous page*

Object	GMP	Aperture Dia. (″) 8.8	13	16	20.2	26
comasw14-49	5120	17.536 ± 0.006	17.360 ± 0.007	17.186 ± 0.008	17.193 ± 0.009	
comasw3-49	5129	19.706 ± 0.041	19.541 ± 0.048	19.385 ± 0.057	19.406 ± 0.072	19.410 ± 0.077
comasw3-8	5133	18.505 ± 0.014	18.593 ± 0.020	18.506 ± 0.025	18.613 ± 0.034	18.671 ± 0.039
comasw3-29	5136	16.186 ± 0.002	16.008 ± 0.002	15.810 ± 0.003	15.793 ± 0.003	15.706 ± 0.003
comasw27-37	5138	19.158 ± 0.025	18.931 ± 0.028	18.723 ± 0.031	18.727 ± 0.039	
comasw25-28	5142	19.451 ± 0.032	19.415 ± 0.042	19.314 ± 0.053	19.401 ± 0.071	
comasw13-48	5144	18.129 ± 0.010	17.950 ± 0.012	17.804 ± 0.014	17.877 ± 0.018	
comasw13-39	5146	19.295 ± 0.027	19.201 ± 0.034	19.092 ± 0.042	19.170 ± 0.058	
comasw3-71	5154	19.379 ± 0.028	19.297 ± 0.035	19.155 ± 0.042	19.207 ± 0.052	19.406 ± 0.080
comasw3-10	5155	18.310 ± 0.012	18.290 ± 0.016	18.167 ± 0.019	18.229 ± 0.025	18.190 ± 0.025
comasw25-78	5158	19.849 ± 0.056	19.887 ± 0.080	19.830 ± 0.105	19.919 ± 0.140	
comasw13-32	5159	19.614 ± 0.036	19.621 ± 0.050	19.543 ± 0.064	19.631 ± 0.081	
comasw18-70	5163	19.561 ± 0.034	19.612 ± 0.048	19.497 ± 0.061	19.521 ± 0.076	
comasw3-52	5164	19.062 ± 0.022	19.069 ± 0.029	18.990 ± 0.037	19.037 ± 0.048	18.990 ± 0.052
comasw25-77	5166	19.615 ± 0.038	19.709 ± 0.057	19.629 ± 0.070	19.723 ± 0.091	
comasw27-49	5169	19.724 ± 0.036	19.818 ± 0.053	19.734 ± 0.067	19.708 ± 0.079	
comasw8-54	5172	19.374 ± 0.027	19.300 ± 0.034	19.212 ± 0.043	19.131 ± 0.049	
comasw3-93	5176	18.340 ± 0.013	18.357 ± 0.018	18.220 ± 0.022	18.252 ± 0.029	18.249 ± 0.028
comasw3-79	5178	17.924 ± 0.008	17.808 ± 0.010	17.629 ± 0.011	17.623 ± 0.014	17.586 ± 0.015
comasw13-38	5179	18.292 ± 0.011	18.172 ± 0.013	18.050 ± 0.016	18.111 ± 0.020	
comasw3-44	5190	19.218 ± 0.025	19.235 ± 0.035	19.133 ± 0.043	19.145 ± 0.054	19.383 ± 0.073
comasw25-49	5191	15.580 ± 0.002	15.570 ± 0.002	15.454 ± 0.002	15.511 ± 0.002	
comasw18-23	5200	19.295 ± 0.028	19.264 ± 0.037	19.128 ± 0.045	19.130 ± 0.056	
comasw13-53	5202	17.590 ± 0.006	17.529 ± 0.008	17.389 ± 0.009	17.409 ± 0.011	
comasw18-28	5204	19.285 ± 0.027	19.324 ± 0.039	19.178 ± 0.047	18.949 ± 0.047	
comasw25-57	5207	18.503 ± 0.014	18.570 ± 0.019	18.499 ± 0.025	18.581 ± 0.033	
comasw18-25	5211	19.396 ± 0.031	19.279 ± 0.039	19.110 ± 0.045	19.126 ± 0.057	
comasw18-59	5212	19.013 ± 0.020	18.988 ± 0.026	18.845 ± 0.031	18.877 ± 0.039	
comasw28-26	5214	18.625 ± 0.014	18.686 ± 0.019	18.617 ± 0.024	18.719 ± 0.032	
comasw13-22	5217	17.607 ± 0.006	17.526 ± 0.008	17.393 ± 0.009	17.446 ± 0.011	
comasw28-21	5218	19.615 ± 0.033	19.693 ± 0.047	19.569 ± 0.057	19.500 ± 0.066	
comasw25-25	5219	18.978 ± 0.021	18.922 ± 0.027	18.804 ± 0.033	18.813 ± 0.041	
comasw3-63	5221	19.703 ± 0.042	19.812 ± 0.060	19.759 ± 0.079	19.885 ± 0.111	20.293 ± 0.172
comasw28-51	5232	19.565 ± 0.031	19.342 ± 0.033	19.132 ± 0.037	19.091 ± 0.044	
comasw28-64	5239	19.653 ± 0.034	19.752 ± 0.049	19.750 ± 0.066	19.919 ± 0.095	
comasw3-1	5244	19.598 ± 0.041				
comasw13-8	5245	18.686 ± 0.016	18.510 ± 0.018	18.332 ± 0.021	18.382 ± 0.027	
comasw3-56	5250	16.545 ± 0.003	16.397 ± 0.003	16.216 ± 0.003	16.220 ± 0.004	16.147 ± 0.004
comasw28-14	5251	19.528 ± 0.037	19.612 ± 0.054	19.587 ± 0.071	19.771 ± 0.105	
comasw8-44	5253	18.690 ± 0.015	18.714 ± 0.021	18.637 ± 0.026	18.703 ± 0.035	
comasw3-74	5255	19.355 ± 0.029	19.300 ± 0.038	19.156 ± 0.045	19.212 ± 0.059	19.107 ± 0.057
comasw28-28	5256	16.856 ± 0.004	16.680 ± 0.004	16.468 ± 0.004	16.424 ± 0.004	
comasw28-62	5258	18.415 ± 0.011	18.459 ± 0.015	18.370 ± 0.018	18.444 ± 0.024	
comasw18-30	5260	19.683 ± 0.040	19.670 ± 0.054	19.561 ± 0.067	19.644 ± 0.090	
comasw28-27	5261	17.805 ± 0.008	17.785 ± 0.010	17.667 ± 0.012	17.685 ± 0.015	
comasw13-46	5262	18.449 ± 0.013	18.478 ± 0.018	18.387 ± 0.023	18.454 ± 0.030	
comasw28-17	5272	15.051 ± 0.001	14.933 ± 0.001	14.759 ± 0.001	14.744 ± 0.001	
comasw3-4	5274	18.529 ± 0.014	18.473 ± 0.018	18.325 ± 0.022	18.351 ± 0.028	18.340 ± 0.030
comasw3-89	5276	19.364 ± 0.029	19.279 ± 0.037	19.149 ± 0.043	19.201 ± 0.056	19.028 ± 0.056
comasw3-20	5277	19.738 ± 0.041	19.871 ± 0.063	19.834 ± 0.084	20.068 ± 0.129	20.321 ± 0.206
comasw8-47	5278	19.729 ± 0.038	19.831 ± 0.056	19.780 ± 0.074	19.890 ± 0.101	
comasw8-49	5284	17.376 ± 0.005	17.246 ± 0.006	17.079 ± 0.007	17.100 ± 0.008	
comasw3-69	5296	17.921 ± 0.009	17.865 ± 0.011	17.735 ± 0.013	17.768 ± 0.016	17.764 ± 0.018

Raw V-band aperture magnitudes. *contiuned from previous page*

Object	GMP	Aperture Dia. ('') 8.8	13	16	20.2	26
comasw28-43	5304	16.941 ± 0.004	16.652 ± 0.004	16.396 ± 0.004	16.337 ± 0.004	
comasw13-63	5307	18.716 ± 0.016	18.581 ± 0.019	18.397 ± 0.022	18.390 ± 0.027	
comasw28-48	5308	17.739 ± 0.007	17.500 ± 0.007	17.264 ± 0.007	17.198 ± 0.008	
comasw13-4	5320	17.902 ± 0.008	17.840 ± 0.011	17.699 ± 0.013	17.754 ± 0.017	
comasw25-31	5329	18.094 ± 0.010	17.873 ± 0.011	17.660 ± 0.012	17.638 ± 0.015	
comasw13-18	5333	18.680 ± 0.016	18.700 ± 0.022	18.606 ± 0.028	18.703 ± 0.037	
comasw25-14	5334	18.736 ± 0.017	18.821 ± 0.025	18.763 ± 0.032	18.862 ± 0.044	
comasw13-5	5344	18.633 ± 0.015	18.587 ± 0.020	18.453 ± 0.024	18.512 ± 0.031	
comasw13-57	5345	17.422 ± 0.006	17.227 ± 0.006	17.033 ± 0.007	17.020 ± 0.008	
comasw28-19	5353	19.074 ± 0.021	18.920 ± 0.025	18.782 ± 0.029	18.747 ± 0.035	
comasw28-40	5354	19.126 ± 0.023	19.047 ± 0.028	18.862 ± 0.032	18.895 ± 0.040	
comasw13-21	5357	19.485 ± 0.031	19.219 ± 0.034	18.996 ± 0.037	18.966 ± 0.045	
comasw13-43	5362	16.978 ± 0.004	16.880 ± 0.005	16.726 ± 0.005	16.742 ± 0.006	
comasw13-66	5370	19.263 ± 0.028	18.975 ± 0.030	18.878 ± 0.038	18.926 ± 0.051	
comasw13-65	5370	19.194 ± 0.026	18.988 ± 0.030	18.908 ± 0.038	18.996 ± 0.052	
comasw25-29	5373	19.127 ± 0.025	19.184 ± 0.037	19.101 ± 0.047	19.144 ± 0.062	
comasw13-42	5375	19.531 ± 0.036	19.449 ± 0.046	19.268 ± 0.054	19.269 ± 0.067	
comasw25-7	5381	19.070 ± 0.025	19.024 ± 0.033	18.938 ± 0.042	19.002 ± 0.057	
comasw28-34	5400	19.339 ± 0.026	19.422 ± 0.037	19.321 ± 0.046	19.408 ± 0.061	
comasw28-41	5407	16.819 ± 0.003	16.702 ± 0.004	16.535 ± 0.004	16.543 ± 0.005	
comasw13-25	5410	18.550 ± 0.015	18.564 ± 0.020	18.485 ± 0.025	18.601 ± 0.035	
comasw13-62	5411	18.981 ± 0.021	18.968 ± 0.028	18.867 ± 0.035	18.988 ± 0.049	
comasw13-36	5427	19.515 ± 0.031	19.386 ± 0.038	19.193 ± 0.044	19.297 ± 0.060	
comasw13-60	5434	16.030 ± 0.002	15.989 ± 0.002	15.863 ± 0.003	15.909 ± 0.003	
comasw28-33	5436	19.322 ± 0.025	19.272 ± 0.032	19.206 ± 0.041	19.326 ± 0.055	
comasw13-50	5438	19.661 ± 0.036	19.686 ± 0.050	19.568 ± 0.062	19.432 ± 0.068	
comasw13-20	5452	19.056 ± 0.022	19.014 ± 0.028	18.907 ± 0.035	18.991 ± 0.047	
comasw28-9	5470	18.595 ± 0.013	18.565 ± 0.017	18.453 ± 0.020	18.520 ± 0.027	
comasw13-29	5480	18.506 ± 0.013	18.412 ± 0.017	18.242 ± 0.019	18.243 ± 0.024	
comasw28-25	5486	17.776 ± 0.007	17.626 ± 0.008	17.457 ± 0.009	17.484 ± 0.010	
comasw13-28	5492	19.781 ± 0.042	19.733 ± 0.056	19.600 ± 0.068	19.627 ± 0.086	
comasw13-23	5520	19.493 ± 0.032	19.530 ± 0.045	19.464 ± 0.059	19.540 ± 0.078	
comasw13-58	5522	19.733 ± 0.044	19.845 ± 0.066	19.755 ± 0.084	19.747 ± 0.104	
comasw13-2	5523	19.806 ± 0.046	19.861 ± 0.069	19.768 ± 0.088	19.717 ± 0.108	
comasw20-89	-	19.448 ± 0.036	19.061 ± 0.036	18.426 ± 0.027	17.932 ± 0.020	
comasw16-74	-	19.881 ± 0.041	19.920 ± 0.056	19.835 ± 0.072	19.844 ± 0.089	
comasw20-85	-	19.838 ± 0.048	19.900 ± 0.068	19.841 ± 0.091	19.750 ± 0.097	
comasw16-79	-	17.676 ± 0.007				
coma15-91	-	19.006 ± 0.021	19.046 ± 0.029	18.961 ± 0.037	18.971 ± 0.046	19.304 ± 0.070
comasw20-76	-	20.179 ± 0.069	20.589 ± 0.122	20.852 ± 0.186	22.347 ± 0.360	
comasw20-70	-	19.983 ± 0.058	20.007 ± 0.082	19.742 ± 0.091	19.440 ± 0.083	
comasw20-93	-	19.133 ± 0.026	19.248 ± 0.038	19.205 ± 0.050	19.275 ± 0.067	
comasw28-5	-	19.672 ± 0.035	19.629 ± 0.045	19.461 ± 0.052	19.560 ± 0.070	
comasw20-59	-	19.866 ± 0.056	19.820 ± 0.074	19.617 ± 0.085	19.371 ± 0.085	
comasw20-52	-	19.885 ± 0.056	19.984 ± 0.087	19.783 ± 0.101	19.395 ± 0.090	
comasw28-8	-	19.842 ± 0.040	19.922 ± 0.057	19.816 ± 0.070	19.911 ± 0.094	
coma23-56	-	19.967 ± 0.049	20.089 ± 0.076	20.049 ± 0.100	20.170 ± 0.139	
comane6-46	-	19.678 ± 0.052				
comasw17-6	-	19.932 ± 0.044	19.998 ± 0.063	19.880 ± 0.077	19.945 ± 0.100	
comasw22-106	-	19.722 ± 0.059				
comane6-32	-	19.640 ± 0.044	19.633 ± 0.057	19.546 ± 0.071	19.645 ± 0.095	
coma15-15	-	19.841 ± 0.055	19.991 ± 0.087	19.945 ± 0.115	20.058 ± 0.158	19.214 ± 0.068
comane6-21	-	18.759 ± 0.021	18.637 ± 0.025	18.486 ± 0.029	18.535 ± 0.038	

Raw V-band aperture magnitudes. *contiuned from previous page*

Object	GMP	Aperture Dia. ('') 8.8	13	16	20.2	26
comasw3-75	-	19.614 ± 0.037	19.161 ± 0.033	18.992 ± 0.038	19.038 ± 0.047	19.047 ± 0.067
comasw3-66	-	19.248 ± 0.025	19.037 ± 0.028	18.849 ± 0.033	18.870 ± 0.041	18.832 ± 0.045
comasw17-91	-	19.879 ± 0.046	20.063 ± 0.074	19.915 ± 0.090	19.695 ± 0.092	
comasw20-30	-	19.960 ± 0.056	20.068 ± 0.086	19.991 ± 0.112	19.998 ± 0.142	
comasw3-32	-	19.814 ± 0.046	19.842 ± 0.064	19.707 ± 0.078	19.508 ± 0.080	19.456 ± 0.081
comasw16-81	-	19.887 ± 0.050	19.966 ± 0.074	19.895 ± 0.092		
comasw3-22	-	19.966 ± 0.054	20.037 ± 0.079	20.023 ± 0.108	20.156 ± 0.152	20.299 ± 0.173
comasw17-59	-	18.160 ± 0.009	18.237 ± 0.013	18.154 ± 0.016	18.235 ± 0.021	
comasw25-67	-	19.263 ± 0.027	18.811 ± 0.025	18.458 ± 0.024	18.440 ± 0.030	
comasw17-44	-	20.049 ± 0.058	20.385 ± 0.106	20.605 ± 0.177	21.097 ± 0.346	
comasw17-37	-	19.788 ± 0.042	19.782 ± 0.056	19.596 ± 0.064	19.433 ± 0.068	
comasw17-34	-	19.987 ± 0.048	20.174 ± 0.075	20.129 ± 0.099	20.299 ± 0.142	
coma12-3	-	19.713 ± 0.043	19.525 ± 0.051	19.007 ± 0.044	18.461 ± 0.034	
coma19-46	-	19.701 ± 0.042	19.728 ± 0.060	19.627 ± 0.074		19.239 ± 0.060
comasw16-70	-	20.037 ± 0.048	19.989 ± 0.063	19.836 ± 0.075	19.827 ± 0.092	
comasw17-26	-	19.931 ± 0.049	19.924 ± 0.066	19.790 ± 0.079	19.778 ± 0.096	
comasw16-20	-	19.844 ± 0.041	19.890 ± 0.058	19.810 ± 0.075	19.904 ± 0.101	
comasw16-22	-	19.946 ± 0.053	19.890 ± 0.070	19.824 ± 0.091	20.097 ± 0.146	
coma16-101	-	19.983 ± 0.062	20.149 ± 0.100	20.113 ± 0.132	20.199 ± 0.178	20.863 ± 0.327
coma10-11	-	19.823 ± 0.047	19.843 ± 0.063	19.674 ± 0.074	19.616 ± 0.085	19.695 ± 0.098
comasw13-64	-	19.993 ± 0.057	20.108 ± 0.088	20.076 ± 0.118	20.329 ± 0.188	
coma10-14	-	18.009 ± 0.011	18.121 ± 0.015	18.057 ± 0.020	18.163 ± 0.026	18.135 ± 0.025
comasw13-61	-	19.927 ± 0.047	19.880 ± 0.060	19.764 ± 0.069	19.783 ± 0.083	
comasw16-37	-	19.582 ± 0.034	19.654 ± 0.051	19.507 ± 0.060	19.461 ± 0.070	
comasw28-20	-	19.719 ± 0.039	19.744 ± 0.054	19.674 ± 0.071		
coma16-90	-	19.688 ± 0.045	19.747 ± 0.063	19.681 ± 0.076	19.829 ± 0.108	19.581 ± 0.072
comasw16-42	-	19.883 ± 0.041	19.997 ± 0.062	19.865 ± 0.076	19.759 ± 0.085	
coma9-51	-	19.905 ± 0.049	19.869 ± 0.062	19.651 ± 0.068	19.424 ± 0.068	19.308 ± 0.069
coma12-1	-	19.799 ± 0.051	19.956 ± 0.078	19.937 ± 0.103		
comasw21-73	-	15.539 ± 0.002	15.245 ± 0.002	14.949 ± 0.002	14.826 ± 0.002	
coma19-78	-	19.100 ± 0.021	19.202 ± 0.033	19.137 ± 0.042	19.250 ± 0.059	19.386 ± 0.067
comasw16-44	-	19.517 ± 0.029	19.562 ± 0.041	19.485 ± 0.053	19.612 ± 0.074	
coma14-113	-	19.794 ± 0.069				
comasw8-53	-	19.864 ± 0.044	19.954 ± 0.066	19.839 ± 0.081	19.837 ± 0.101	
coma9-48	-	17.945 ± 0.010	18.102 ± 0.014	18.070 ± 0.018	18.207 ± 0.024	18.148 ± 0.023
comasw16-47	-	19.645 ± 0.034	19.694 ± 0.049	19.586 ± 0.060	19.652 ± 0.080	
comasw10-2	-	20.029 ± 0.057	19.855 ± 0.069			
coma9-35	-	19.762 ± 0.047	19.943 ± 0.073	19.968 ± 0.100	20.116 ± 0.141	
coma10-30	-	18.240 ± 0.017	18.311 ± 0.023	18.200 ± 0.029	18.213 ± 0.036	17.810 ± 0.025
coma14-124	-	19.155 ± 0.054				
comasw28-44	-	19.928 ± 0.043	19.882 ± 0.055	19.785 ± 0.068	19.778 ± 0.083	
comasw13-34	-	20.066 ± 0.057	20.111 ± 0.083	20.043 ± 0.109	20.133 ± 0.149	
comasw8-39	-	19.955 ± 0.047	20.133 ± 0.076	20.092 ± 0.101	20.237 ± 0.143	
coma22-30	-	19.836 ± 0.046	19.889 ± 0.064	19.803 ± 0.079		
coma14-133	-	19.104 ± 0.024				
coma14-125	-	18.920 ± 0.052	18.125 ± 0.036			
comasw16-58	-	19.924 ± 0.043	19.975 ± 0.061	19.833 ± 0.074	20.000 ± 0.107	
coma4-43	-	19.236 ± 0.026	19.331 ± 0.035	19.163 ± 0.039	19.035 ± 0.043	
comasw25-45	-	19.600 ± 0.036	19.654 ± 0.051	19.569 ± 0.065	19.647 ± 0.087	
coma19-102	-	19.669 ± 0.038	19.458 ± 0.043	19.201 ± 0.048	19.097 ± 0.054	18.731 ± 0.042
coma19-101	-	19.700 ± 0.038	19.378 ± 0.039	19.070 ± 0.040	18.945 ± 0.045	18.610 ± 0.037
comasw21-24	-	20.023 ± 0.057	20.134 ± 0.085	20.081 ± 0.111	20.292 ± 0.167	
comasw21-21	-	19.904 ± 0.046	19.936 ± 0.064	19.844 ± 0.080	19.931 ± 0.107	

Raw V-band aperture magnitudes. *contiuned from previous page*

Object	GMP	Aperture Dia. ('') 8.8	13	16	20.2	26
coma16-29	-	19.803 ± 0.047	19.873 ± 0.068	19.791 ± 0.086	19.681 ± 0.096	18.886 ± 0.053
comasw27-7	-	19.881 ± 0.041	19.974 ± 0.063	19.937 ± 0.084	20.106 ± 0.120	
coma5-69	-	19.918 ± 0.045	19.899 ± 0.061	19.727 ± 0.072	19.504 ± 0.073	19.118 ± 0.059
coma5-66	-	19.942 ± 0.055	20.080 ± 0.088	20.055 ± 0.123		19.744 ± 0.088
comasw16-5	-	20.050 ± 0.051	20.145 ± 0.076	20.039 ± 0.095	19.993 ± 0.113	
coma5-54	-	19.809 ± 0.042	19.793 ± 0.056	19.656 ± 0.068	19.743 ± 0.092	19.477 ± 0.075
coma14-22	-	19.778 ± 0.044	19.796 ± 0.063	19.683 ± 0.079	19.677 ± 0.103	19.433 ± 0.089
coma5-48	-	19.650 ± 0.034	19.794 ± 0.054	19.650 ± 0.065	19.526 ± 0.072	18.846 ± 0.042
coma14-23	-	19.142 ± 0.029	19.236 ± 0.044	19.123 ± 0.053	19.077 ± 0.060	18.115 ± 0.024
coma5-44	-	20.129 ± 0.056	20.309 ± 0.090	20.146 ± 0.107	20.058 ± 0.122	19.416 ± 0.072
coma5-40	-	19.985 ± 0.047	19.897 ± 0.060	19.789 ± 0.074	19.809 ± 0.094	19.796 ± 0.102
coma12-73	-	20.068 ± 0.065	20.198 ± 0.102	20.215 ± 0.149	20.495 ± 0.262	20.431 ± 0.202
coma5-27	-	19.695 ± 0.037	19.729 ± 0.053	19.594 ± 0.064	19.656 ± 0.084	19.429 ± 0.073
comasw18-72	-	19.949 ± 0.049	19.913 ± 0.065	19.853 ± 0.085	19.822 ± 0.103	
coma5-21	-	19.895 ± 0.046	19.935 ± 0.066	19.916 ± 0.089	19.909 ± 0.110	19.320 ± 0.065
coma5-20	-	19.688 ± 0.036	19.558 ± 0.044	19.419 ± 0.053	19.475 ± 0.070	19.268 ± 0.062
coma12-58	-	20.062 ± 0.058	20.280 ± 0.095	20.288 ± 0.131	20.492 ± 0.196	20.507 ± 0.217
coma19-92	-	19.884 ± 0.045	19.591 ± 0.048	19.308 ± 0.051	19.167 ± 0.055	18.737 ± 0.040
comasw5-2	-	19.729 ± 0.053	19.857 ± 0.091	19.852 ± 0.141	20.062 ± 0.255	19.779 ± 0.139
comane3-71	-	19.830 ± 0.045	19.912 ± 0.064	19.909 ± 0.086	19.951 ± 0.109	
coma5-16	-	19.746 ± 0.040	19.500 ± 0.044	19.333 ± 0.052	19.360 ± 0.066	19.271 ± 0.062
coma5-10	-	20.008 ± 0.049	19.929 ± 0.063	19.730 ± 0.072	19.752 ± 0.092	19.972 ± 0.121
coma12-48	-	19.978 ± 0.065	19.950 ± 0.083	19.743 ± 0.096	19.456 ± 0.093	18.534 ± 0.035
comasw18-57	-	19.725 ± 0.039	19.785 ± 0.056	19.744 ± 0.074	19.876 ± 0.098	
coma17-7	-	19.001 ± 0.055	18.313 ± 0.041	17.774 ± 0.035	17.347 ± 0.030	
coma14-31	-	19.726 ± 0.037	19.802 ± 0.054	19.745 ± 0.070	19.789 ± 0.094	
comasw26-76	-	19.349 ± 0.027	19.497 ± 0.041	19.467 ± 0.055	19.700 ± 0.085	
coma22-52	-	18.773 ± 0.017	18.871 ± 0.024	18.815 ± 0.031	18.894 ± 0.040	19.204 ± 0.065
comasw26-74	-	19.913 ± 0.047	20.041 ± 0.070	20.052 ± 0.097	20.183 ± 0.135	
comane3-58	-	19.659 ± 0.043	19.665 ± 0.056	19.659 ± 0.076	19.884 ± 0.114	
comasw26-67	-	19.805 ± 0.040	19.913 ± 0.059	19.869 ± 0.078	19.985 ± 0.107	
comasw18-45	-	18.887 ± 0.019	18.935 ± 0.027	18.849 ± 0.034	18.941 ± 0.046	
comasw18-43	-	19.902 ± 0.045	19.882 ± 0.061	19.727 ± 0.072	19.764 ± 0.093	
coma12-27	-	19.821 ± 0.044	19.895 ± 0.065	19.854 ± 0.083	20.136 ± 0.119	20.404 ± 0.213
comasw26-57	-	19.862 ± 0.040	19.939 ± 0.057	19.864 ± 0.072	19.995 ± 0.099	
comasw18-37	-	19.509 ± 0.033	19.486 ± 0.044	19.372 ± 0.055	19.386 ± 0.069	
comasw26-56	-	18.690 ± 0.015	18.804 ± 0.021	18.714 ± 0.026	18.875 ± 0.037	
comasw6-12	-	19.715 ± 0.045	19.232 ± 0.039	18.642 ± 0.032	18.380 ± 0.031	
comasw26-53	-	19.893 ± 0.043	20.002 ± 0.063	19.972 ± 0.083	20.174 ± 0.123	
coma15-120	-	19.558 ± 0.035	19.559 ± 0.046	19.433 ± 0.057	19.448 ± 0.075	19.523 ± 0.100
comasw6-16	-	19.837 ± 0.049	19.931 ± 0.073	19.963 ± 0.102	20.124 ± 0.147	
coma12-57	-	19.848 ± 0.046	19.915 ± 0.068	19.824 ± 0.089	19.813 ± 0.105	19.833 ± 0.125
coma12-19	-	19.145 ± 0.024	19.224 ± 0.035	19.156 ± 0.044	19.260 ± 0.059	19.474 ± 0.086
comane3-30	-	19.971 ± 0.054	20.006 ± 0.074	19.941 ± 0.094	20.137 ± 0.140	
comasw18-20	-	19.103 ± 0.022	18.598 ± 0.019	18.457 ± 0.023	18.509 ± 0.029	
comane3-28	-	19.580 ± 0.037	19.606 ± 0.050	19.507 ± 0.062	19.551 ± 0.079	
comasw26-28	-	19.969 ± 0.049	20.109 ± 0.074	20.093 ± 0.097		
comasw26-12	-	19.715 ± 0.037	19.735 ± 0.050	19.661 ± 0.063	19.624 ± 0.075	
comasw9-83	-	19.714 ± 0.038	18.706 ± 0.021	18.525 ± 0.024	18.579 ± 0.032	18.613 ± 0.034
comasw22-91	-	19.220 ± 0.031	19.203 ± 0.040	18.874 ± 0.041	17.723 ± 0.018	
coma13-114	-	19.997 ± 0.051	20.122 ± 0.075	20.069 ± 0.101	20.095 ± 0.127	19.575 ± 0.097
comasw14-61	-	19.935 ± 0.048	20.042 ± 0.072	19.805 ± 0.080	19.902 ± 0.108	
comasw22-80	-	20.145 ± 0.076	19.904 ± 0.083	19.559 ± 0.083	19.054 ± 0.065	

Raw V-band aperture magnitudes. *contiuned from previous page*

Object	GMP	Aperture Dia. ('') 8.8	13	16	20.2	26
coma13-108	-	20.070 ± 0.054	20.201 ± 0.091	20.169 ± 0.124	20.358 ± 0.193	20.890 ± 0.242
coma13-104	-	19.070 ± 0.022	19.085 ± 0.030	18.988 ± 0.038	19.058 ± 0.051	19.258 ± 0.075
comasw14-50	-	19.695 ± 0.039	19.730 ± 0.055	19.643 ± 0.070	19.680 ± 0.090	
comasw14-45	-	19.556 ± 0.035	19.146 ± 0.033	18.600 ± 0.028	18.486 ± 0.031	
coma17-70	-	19.922 ± 0.051	20.066 ± 0.079	20.019 ± 0.104	19.715 ± 0.097	19.374 ± 0.077
comasw9-39	-	19.703 ± 0.046	18.959 ± 0.033	18.487 ± 0.030	17.744 ± 0.019	17.572 ± 0.021
comasw22-44	-	19.979 ± 0.074	19.754 ± 0.082	19.472 ± 0.087	19.277 ± 0.090	
coma17-57	-	19.026 ± 0.028	19.182 ± 0.043	19.110 ± 0.055	18.919 ± 0.057	17.815 ± 0.020
comasw14-11	-	19.907 ± 0.046	19.992 ± 0.066	19.968 ± 0.092	20.161 ± 0.133	
coma25-60	-	19.762 ± 0.044	19.855 ± 0.061	19.741 ± 0.074	19.673 ± 0.084	19.677 ± 0.088
comasw9-19	-	20.049 ± 0.052	20.077 ± 0.073	19.819 ± 0.079	19.495 ± 0.073	18.710 ± 0.036
coma17-40	-	19.831 ± 0.047	19.883 ± 0.067	19.807 ± 0.085	19.945 ± 0.120	19.792 ± 0.114
coma22-71	-	19.416 ± 0.032	19.393 ± 0.041	19.295 ± 0.051	19.442 ± 0.072	19.552 ± 0.082
coma25-41	-	19.299 ± 0.033	19.435 ± 0.048	19.436 ± 0.065	19.641 ± 0.095	19.148 ± 0.055
coma25-37	-	19.831 ± 0.046	19.887 ± 0.061	19.817 ± 0.077	19.961 ± 0.107	20.793 ± 0.255
coma5-9	-	20.013 ± 0.052	20.126 ± 0.080			
coma5-3	-	20.186 ± 0.058	20.343 ± 0.092	20.321 ± 0.126	20.754 ± 0.234	
comasw10-90	-	19.753 ± 0.040	19.861 ± 0.060	19.822 ± 0.078	20.043 ± 0.113	19.771 ± 0.103
comasw10-89	-	19.881 ± 0.041	20.022 ± 0.062	20.022 ± 0.079	20.193 ± 0.099	19.886 ± 0.113
comasw10-88	-	19.871 ± 0.049	19.571 ± 0.048	19.170 ± 0.047	18.815 ± 0.041	17.821 ± 0.017
comasw10-83	-	19.959 ± 0.056	19.970 ± 0.078	19.987 ± 0.104	20.397 ± 0.190	19.994 ± 0.135
coma7-28	-	19.956 ± 0.087	19.977 ± 0.121	19.913 ± 0.148	20.030 ± 0.196	19.882 ± 0.193
comasw10-60	-	19.651 ± 0.036	19.726 ± 0.052	19.638 ± 0.063	19.786 ± 0.088	19.841 ± 0.109
comasw6-31	-	19.391 ± 0.032	19.350 ± 0.042	19.257 ± 0.052	19.242 ± 0.064	
coma13-90	-	19.211 ± 0.032	19.272 ± 0.046	19.152 ± 0.057	19.227 ± 0.076	18.815 ± 0.049
comasw21-116	-	19.547 ± 0.033	19.561 ± 0.045	19.470 ± 0.055	19.568 ± 0.074	
comasw10-57	-	19.734 ± 0.039	19.731 ± 0.054	19.662 ± 0.070	19.792 ± 0.097	20.176 ± 0.151
comasw10-56	-	19.728 ± 0.042	19.732 ± 0.058	19.659 ± 0.077	19.802 ± 0.113	20.074 ± 0.136
coma13-87	-	19.733 ± 0.041	19.244 ± 0.036	18.617 ± 0.028	18.083 ± 0.021	17.744 ± 0.016
coma13-84	-	19.432 ± 0.036	19.714 ± 0.063	19.817 ± 0.096	20.277 ± 0.183	20.409 ± 0.231
comasw10-50	-	20.059 ± 0.052	20.131 ± 0.077	19.944 ± 0.090	20.133 ± 0.132	
comasw5-57	-	19.778 ± 0.051	19.910 ± 0.078	19.881 ± 0.103		19.989 ± 0.146
comasw21-108	-	19.218 ± 0.025	19.337 ± 0.039	19.337 ± 0.054	19.486 ± 0.081	
comasw10-40	-	19.887 ± 0.053	19.742 ± 0.064	19.575 ± 0.076	19.541 ± 0.092	19.279 ± 0.071
coma14-66	-	19.943 ± 0.055	20.106 ± 0.088	20.112 ± 0.113	20.184 ± 0.151	
comasw5-41	-	19.798 ± 0.046	19.760 ± 0.063	19.641 ± 0.075	19.650 ± 0.095	
comasw10-37	-	20.035 ± 0.061	19.920 ± 0.077	19.586 ± 0.078	19.288 ± 0.075	18.336 ± 0.028
coma13-68	-	19.741 ± 0.060	18.886 ± 0.039			
comasw10-26	-	20.154 ± 0.060	20.315 ± 0.096	20.354 ± 0.137	20.554 ± 0.205	21.306 ± 0.457
comasw10-22	-	19.892 ± 0.044	19.949 ± 0.063	19.803 ± 0.077	19.863 ± 0.100	19.572 ± 0.083
comasw10-20	-	19.874 ± 0.049	19.986 ± 0.078	19.906 ± 0.103	20.025 ± 0.143	20.156 ± 0.327
coma13-52	-	19.919 ± 0.053	19.340 ± 0.043	18.885 ± 0.039	18.776 ± 0.043	18.199 ± 0.025
comasw5-17	-	19.801 ± 0.050	19.798 ± 0.067	19.738 ± 0.086	19.815 ± 0.114	19.360 ± 0.081
comasw27-62	-	18.731 ± 0.016	18.805 ± 0.023	18.742 ± 0.030	18.829 ± 0.040	
comasw27-55	-	19.846 ± 0.042	19.960 ± 0.061	19.881 ± 0.078	19.962 ± 0.102	
comasw27-50	-	19.961 ± 0.045	20.046 ± 0.064	19.985 ± 0.082	20.022 ± 0.105	
comasw27-48	-	18.706 ± 0.015	18.694 ± 0.020	18.601 ± 0.024	18.689 ± 0.033	
comasw27-33	-	19.704 ± 0.037	19.735 ± 0.050	19.645 ± 0.063	19.781 ± 0.087	
comasw11-7	-	18.894 ± 0.027	18.922 ± 0.038	18.799 ± 0.047	18.745 ± 0.055	18.231 ± 0.051
comasw15-79	-	19.943 ± 0.050	20.087 ± 0.080	20.048 ± 0.104	20.151 ± 0.141	
comasw15-78	-	19.790 ± 0.042	19.761 ± 0.055	19.606 ± 0.070	19.817 ± 0.099	
comasw15-62	-	19.970 ± 0.049	19.934 ± 0.066	19.639 ± 0.069	19.341 ± 0.065	
comasw23-81	-	20.101 ± 0.055	20.169 ± 0.081	20.073 ± 0.103	20.135 ± 0.136	

Raw V-band aperture magnitudes. *contiuned from previous page*

Object	GMP	Aperture Dia. (″) 8.8	13	16	20.2	26
comasw23-79	-	19.907 ± 0.048	19.927 ± 0.072	19.840 ± 0.092		
comasw15-52	-	20.015 ± 0.055	20.084 ± 0.081	20.141 ± 0.118	20.409 ± 0.188	
coma10-2	-	19.715 ± 0.045	19.797 ± 0.064	19.763 ± 0.083		20.124 ± 0.149
comasw15-48	-	18.989 ± 0.021	19.064 ± 0.030	18.827 ± 0.033	18.764 ± 0.039	
comasw15-46	-	19.747 ± 0.040	19.733 ± 0.054	19.450 ± 0.058	19.207 ± 0.057	
coma14-84	-	19.023 ± 0.024	19.068 ± 0.034	18.947 ± 0.041	18.963 ± 0.052	18.456 ± 0.039
coma14-85	-	19.746 ± 0.047	19.878 ± 0.076	19.795 ± 0.103		
comasw23-65	-	20.006 ± 0.051	20.081 ± 0.076	19.983 ± 0.096	20.045 ± 0.126	
comasw23-64	-	19.840 ± 0.042	19.909 ± 0.063	19.806 ± 0.079	19.906 ± 0.109	
coma18-76	-	20.061 ± 0.049	20.130 ± 0.072	20.063 ± 0.094	20.062 ± 0.116	20.187 ± 0.141
comasw23-61	-	19.902 ± 0.046	19.850 ± 0.060	19.729 ± 0.074	19.689 ± 0.089	
comasw15-30	-	19.686 ± 0.040	19.755 ± 0.058	19.706 ± 0.077	19.809 ± 0.105	
coma18-57	-	19.990 ± 0.054	20.030 ± 0.076	19.833 ± 0.088	19.603 ± 0.087	18.624 ± 0.033
comasw15-23	-	19.595 ± 0.046	18.881 ± 0.033	18.251 ± 0.026	17.622 ± 0.018	
comasw6-66	-	19.907 ± 0.050	19.897 ± 0.067	19.744 ± 0.080	19.711 ± 0.096	
coma18-52	-	19.856 ± 0.039	19.951 ± 0.057	19.856 ± 0.074	20.019 ± 0.107	20.248 ± 0.148
coma18-49	-	19.861 ± 0.042	19.974 ± 0.063	19.856 ± 0.076	19.885 ± 0.090	19.631 ± 0.084
comasw23-32	-	19.911 ± 0.050	19.830 ± 0.065	19.060 ± 0.045	18.655 ± 0.039	
comasw23-23	-	19.678 ± 0.038	19.797 ± 0.058	19.711 ± 0.073	19.760 ± 0.096	
comasw6-72	-	19.583 ± 0.037	19.639 ± 0.053	19.556 ± 0.067	19.581 ± 0.086	
coma18-22	-	19.965 ± 0.045	19.897 ± 0.058	19.575 ± 0.059	19.528 ± 0.070	19.484 ± 0.075
comasw6-76	-	19.858 ± 0.083	19.782 ± 0.108	19.584 ± 0.125	19.424 ± 0.135	
coma18-20	-	20.009 ± 0.051	20.073 ± 0.077	20.037 ± 0.105	19.634 ± 0.088	18.730 ± 0.038
coma18-10	-	20.051 ± 0.050	20.149 ± 0.077	20.021 ± 0.095	20.066 ± 0.127	

References

Andreon S., Davoust E., Michard R., Nieto J. L., Poulain P., 1996, Astronomy and Astrophysics Supplement Series, 116, 429

Andreon S., Davoust E., Poulain P., 1997, Astronomy and Astrophysics Supplement Series, 126, 67

Bertin E., Arnouts S., 1996, Astronomy and Astrophysics Supplement Series, 117, 393

Dressler A., 1980, ApJS, 42, 565

Godwin J. G., Metcalfe N., Peach J. V., 1983, MNRAS, 202, 113

Appendix B

The Biweight Estimators

B.1 Resistance, robustness and efficiency

The notions of resistance and robustness in statistical indicators are central to our decision to use the biweight indicators, so we will briefly define them here. For a more complete definition of these terms, and also of the biweight indicators, see Beers, Flynn, & Gebhardt (1990) and references therein.

Resistance characterises how an indicator changes when a small part of the data is replaced with new and possibly very different data. A resistant indicator, such as the median will change only a little, while a nonresistant indicator such as the mean will possibly change by a large amount. A resistant indicator is therefore sensitive to the bulk of the data, and not sensitive to the occasional outlier.

Robustness characterises an estimator's insensitivity to the assumed probability distribution of the population from which the data are drawn, i.e. an estimator which assumes a Gaussian distribution at any stage is therefore not robust.

Of lesser importance to us, is efficiency. The efficiency of an indicator refers to the quality of information that can be derived by using it. In data-limited applications, an efficient indicator can produce the required information, where a less efficient indicator may require many times the number of data points to extract an equivalent result.

B.2 The biweight estimator

The biweight location and scale indicators require an auxiliary scale estimator. In line with Beers, Flynn, & Gebhardt we use the median absolute deviation (MAD).

$$MAD = median(|x_i - M|)$$

where M is the median of the sample.

B.2.1 The location indicator

The biweight location indicator is defined as

$$C_{BI} = M + \frac{\sum_{|u_i|<1}(x_i - M)(1 - u_i^2)^2}{\sum_{|u_i|<1}(1 - u_i^2)^2}$$

where again M is the sample median and u_i is defined by

$$u_i = \frac{(x_i - M)}{cMAD}$$

The c in the definition of u_i is the tuning constant. In keeping with Beers, Flynn, & Gebhardt, we use a value of $c = 6.0$, giving a high efficiency for a broad range of distributions, and effectively excluding all data further than 4 standard deviations from the central location.

B.2.2 The scale indicator

The biweight scale indicator is defined as

$$S_{BI} = n^{1/2} \frac{\left[\sum_{|u_i|<1}(x_i - M)^2(1 - u_i^2)^4\right]^{1/2}}{\left|\sum_{|u_i|<1}(1 - u_i^2)(1 - 5u_i^2)\right|}$$

where u_i is again defined as above, but with the tuning constant $c = 9.0$.

Both the scale and location indicator can be run iteratively by replacing M with C_{BI} after the first run, however we found that for our data, this made little difference.

B.3 Data fitting

In fitting a model to our data, we are ultimately interested in minimising the residuals of the data to our model. It therefore makes sense to define a set of x_i such that

$$x_i = Y_i - f(X_i)$$

where the (X_i, Y_i) are the data pairs, and $f(x)$ is our model. In this case, we are interested in fitting a straight line, so $f(x) = mx + c$. We therefore want to minimise both the scale and location of the x_i. This can be achieved in one simple step by defining a derivative of S_{BI} with effectively a zero median.

$$S_{BIFIT} = n^{1/2} \frac{\left[\sum_{|u_i|<1}(1-u_i^2)^4\right]^{1/2}}{\left|\sum_{|u_i|<1}(1-u_i^2)(1-5u_i^2)\right|}$$

where this time, $u_i = x_i/cMAD$. Again $c = 9.0$.

Setting $M = 0$ has the effect if increasing S_{BIFIT} if the location of the x_i differs from zero. If however, the location of the x_i is close to zero (what we require), then S_{BIFIT} behaves similarly to S_{BI}.

It is then relatively simple to minimise $S_{BIFIT}(m, c|x_i)$ by iteration in the (m, c) plane. To achieve this we use the multidimensional downhill simplex method (Press et al. 1992) with a limiting tolerance of 10^8. It is not very computationally efficient, but is easy to implement, and the S_{BIFIT} is computationally cheap. We have yet to encounter a situation where it could not find the minimum of the x_i, and therefore fit a function to the (X_i, Y_i).

References

Beers T. C., Flynn K., Gebhardt K., 1990, AJ, 100, 32

Press W. H., Teukolsky S. A., Vetterling W. T., Flannery B. P., 1992, in Cambridge: University Press, —c1992, 2nd ed.

Bibliography

References

Aaronson M., Persson S. E., Frogel J. A., 1981, ApJ, 245, 18

Aarseth S. J., Fall S. M., 1980, ApJ, 236, 43

Abraham R. G. et al., 1996, ApJ, 471, 694

Andreon S., Davoust E., Michard R., Nieto J. L., Poulain P., 1996, Astronomy and Astrophysics Supplement Series, 116, 429

Andreon S., Davoust E., Poulain P., 1997, Astronomy and Astrophysics Supplement Series, 126, 67

Arimoto N., Yoshii Y., 1987, A&A, 173, 23

Bahcall N. A., 1975, ApJ, 198, 249

Baier F. W., 1984, Astronomische Nachrichten, 305, 175

Balogh M. L., Schade D., Morris S. L., Yee H. K. C., Carlberg R. G., Ellingson E., 1998, ApJ, 504, L75

Barger A. J., Aragon-Salamanca A., Ellis R. S., Couch W. J., Smail I., Sharples R. M., 1995, American Astronomical Society Meeting, 187, 6306

Barger A. J., Aragon-Salamanca A., Ellis R. S., Couch W. J., Smail I., Sharples R. M., 1996, MNRAS, 279, 1

Barnes J. E., 1988, ApJ, 331, 699

Baugh C. M., Cole S., Frenk C. S., Lacey C. G., 1998, ApJ, 498, 504

Beers T. C., Flynn K., Gebhardt K., 1990, AJ, 100, 32

Bender R., Burstein D., Faber S. M., 1992, ApJ, 399, 462

Bender R., Burstein D., Faber S. M., 1993, ApJ, 411, 153

Bertin E., Arnouts S., 1996, Astronomy and Astrophysics Supplement Series, 117, 393

Biviano A., Durret F., Gerbal D., Le Fevre O., Lobo C., Mazure A., Slezak E., 1996, A&A, 311, 95

Bond J. R., Kaiser N., Cole S., Efstathiou G., 1991, ApJ, 379, 440

Bower R. G., 1991, MNRAS, 248, 332

Bower R. G., Kodama T., Terlevich A. I., 1998, MNRAS, 299, 1193, astro-ph/9805290

Bower R. G., Lucey J. R., Ellis R. S., 1992a, MNRAS, 254, 589

Bower R. G., Lucey J. R., Ellis R. S., 1992b, MNRAS, 254, 601

Bressan A., Chiosi C., Tantalo R., 1996, A&A, 311, 425

Briel U. G., Henry J. P., Boehringer H., 1992, A&A, 259, L31

Bruzual A. G., 1983, ApJ, 273, 105

Butcher H., Oemler J., A., 1978, ApJ, 226, 559

Butcher H., Oemler J., A., 1984, ApJ, 285, 426

Buzzoni A., Chincarini G., Molinari E., 1993, ApJ, 410, 499

Buzzoni A., Gariboldi G., Mantegazza L., 1992, AJ, 103, 1814

Caldwell N., Rose J. A., Franx M., Leonardi A. J., 1996, AJ, 111, 78

Caldwell N., Rose J. A., Sharples R. M., Ellis R. S., Bower R. G., 1993, AJ, 106, 473

Cash W., 1979, ApJ, 228, 939

Charlot S., Silk J., 1994, ApJ, 432, 453

Cole S., Aragon-Salamanca A., Frenk C. S., Navarro J. F., Zepf S. E., 1994, MNRAS, 271, 781

Colless M., Dunn A. M., 1996, ApJ, 458, 435

Couch W. J., Barger A. J., Smail I., Ellis R. S., Sharples R. M., 1998, ApJ, 497, 188

Couch W. J., Ellis R. S., Sharples R. M., Smail I., 1994, ApJ, 430, 121

Couch W. J., Newell E. B., 1984, ApJS, 56, 143

Couch W. J., Sharples R. M., 1987, MNRAS, 229, 423

Davies R. L., Sadler E. M., Peletier R. F., 1993, MNRAS, 262, 650

De Jong R. S., Davies R. L., 1997, MNRAS, 285, L1

Djorgovski S., Davis M., 1987, ApJ, 313, 59

Dressler A., 1980, ApJS, 42, 565

Dressler A., 1984, ApJ, 281, 512

Dressler A., Gunn J. E., 1983, ApJ, 270, 7

Dressler A., Gunn J. E., 1992, ApJS, 78, 1

Dressler A., Lynden-Bell D., Burstein D., Davies R. L., Faber S. M., Terlevich R., Wegner G., 1987, ApJ, 313, 42

Dressler A. et al., 1997, ApJ, 490, 577

Eggen O. J., Lynden-Bell D., Sandage A. R., 1962, ApJ, 136, 748

Ellis R. S., Smail I., Dressler A., Couch W. J., Oemler J., Augustus, Butcher H., Sharples R. M., 1997, ApJ, 483, 582

Escalera E., Mazure A., 1992, ApJ, 388, 23

Escalera E., Slezak E., Mazure A., 1992, A&A, 264, 379

Faber S. M., 1973, ApJ, 179, 731

Faber S. M., Jackson R. E., 1976, ApJ, 204, 668

Feigelson E. D., Babu G. J., 1992, ApJ, 397, 55

Ferguson H. C., 1993, MNRAS, 263, 343

Franx M., Illingworth G., 1990, ApJ, 359, L41

Fried D. L., 1966, J. Opt. Soc. Am., 56, 1372

Frogel J. A., Persson S. E., Matthews K., Aaronson M., 1978, ApJ, 220, 75

Godwin J. G., Metcalfe N., Peach J. V., 1983, MNRAS, 202, 113

González J. J., 1993, Ph.D. thesis, Univ. California, Santa Cruz

Grebenev S. A., Forman W., Jones C., Murray S., 1995, ApJ, 445, 607

Guzman R., Lucey J. R., Carter D., Terlevich R. J., 1992, MNRAS, 257, 187

Isobe T., Feigelson E. D., Akritas M. G., Babu G. J., 1990, ApJ, 364, 104

Johnson H. L., Morgan W. W., 1953, ApJ, 117, 313

Jorgensen I., Franx M., Kjaergaard P., 1993, ApJ, 411, 34

Kauffmann G., 1996, MNRAS, 281, 487

Kauffmann G., White S. D. M., Guiderdoni B., 1993, MNRAS, 264, 201

Kodama T., 1997, Ph.D. thesis, Institute of Astronomy, University of Tokyo

Kodama T., Arimoto N., 1997, A&A, 320, 41

Kodama T., Arimoto N., Barger A. J., Arag'On-Salamanca A., 1998, A&A, 334, 99

Kormendy J., Djorgovski S., 1989, ARA&A, 27, 235

Kuntschner H., 1998, Ph.D. thesis, Department of Physics, University of Durham

Kuntschner H., Davies R. L., 1998, MNRAS, 295, L29

Lacey C., Cole S., 1993, MNRAS, 262, 627

Landolt A. U., 1992, AJ, 104, 340

Larson R. B., 1974, MNRAS, 169, 229

Larson R. B., Tinsley B. M., Caldwell C. N., 1980, ApJ, 237, 692

Lega E., Scholl H., Alimi J.-M., Bijaoui A., Bury P., 1995, Parallel Computing, 21, 265

Lucey J. R., Guzman R., Steel J., Carter D., 1997, MNRAS, 287, 899L

Maddox S. J., Efstathiou G., Sutherland W. J., 1990, MNRAS, 246, 433

Mehlert D., Bender R., Saglia R. P., Wegner G., 1998, in Untangling Coma Berenices: A New Vision of an Old Cluster, p. 107

Moore B., Katz N., Lake G., Dressler A., Oemler J., A., 1996, Nature, 379, 613

Navarro J. F., Frenk C. S., White S. D. M., 1995, MNRAS, 275, 56

Osterbrock D. E., 1989, in Published by University Science Books, 648 Broadway, Suite 902, New York, NY 10012, 1989.

Ostriker J., 1980, Comments on Astrophysics, 8, 177

Pahre M. A., Djorgovski S. G., De Carvalho R. R., 1995, ApJ, 453, L17

Pei Y. C., Fall S. M., 1995, ApJ, 454, 69

Persson S. E., Frogel J. A., Aaronson M., 1979, ApJS, 39, 61

Poggianti B., Smail I. R., Dressler A., Couch W., Barger A., Butcher H., Ellis R. S., Oemler A., 1999, ApJ, in press, (astro-ph/9901264)

Press W. H., Schecter P., 1974, ApJ, 187, 425

Press W. H., Teukolsky S. A., Vetterling W. T., Flannery B. P., 1992, in Cambridge: University Press, —c1992, 2nd ed.

Renzini A., Buzzoni A., 1986, in Spectral Evolution of Galaxies, p. 195

Renzini A., Ciotti L., 1993, ApJ, 416, L49

Rosati P., Della Ceca R., Burg R., Norman C., Giacconi R., 1995, ApJ, 445, L11

Saglia R. P., Bender R., Dressler A., 1993, A&A, 279, 75

Saglia R. P., Bertschinger E., Baggley G., Burstein D., Colless M., Davies R. L., McMahan J., R. K., Wegner G., 1993, MNRAS, 264, 961

Saglia R. P., Burstein D., Baggley G., Bertschinger E., Colless M. M., Davies R. L., McMahan J., Robert K., Wegner G., 1997, MNRAS, 292, 499

Schweizer F., Seitzer P., 1992, AJ, 104, 1039

Schweizer F., Seitzer P., Faber S. M., Burstein D., Dalle Ore C. M., Gonzalez J. J., 1990, ApJ, 364, L33

Searle L., Sargent W. L. W., Bagnuolo W. G., 1973, ApJ, 179, 427

Secker J., Harris W. E., Plummer J. D., 1997, PASP, 109, 1377

Slezak E., Bijaoui A., Mars G., 1990, A&A, 227, 301

Slezak E., De Lapparent V., Bijaoui A., 1993, ApJ, 409, 517

Slezak E., Durret F., Gerbal D., 1994, AJ, 108, 1996

Smail I., Dressler A., Couch W. J., Ellis R. S., Oemler J., Augustus, Butcher H., Sharples R. M., 1997, ApJS, 110, 213

Smail I., Edge A. C., Ellis R. S., Blandford R. D., 1998, MNRAS, 293, 124, Provided by the NASA Astrophysics Data System

Stanford S. A., Eisenhardt P. R., Dickinson M., 1998, ApJ, 492, 461

Tinsley B. M., 1980, ApJ, 241, 41

Tinsley B. M., Gunn J. E., 1976, ApJ, 203, 52

Toomre A., Toomre J., 1972, ApJ, 178, 623

Trager S. C., 1997, Ph.D. thesis, Univ. California, Santa Cruz

Vader J. P., 1986, ApJ, 306, 390

Van Den Burgh S., 1991, PASP, 103, 390

Van Dokkum P. G., Franx M., Kelson D. D., Illingworth G. D., 1998, ApJ, 504, L17

Vazdekis A., Casuso E., Peletier R. F., Beckman J. E., 1996, ApJS, 106, 307

Vazdekis A., Peletier R. F., Beckman J. E., Casuso E., 1997, ApJS, 111, 203

Vikhlinin A., Forman W., Jones C., 1994, ApJ, 435, 162

Visvanathan N., Sandage A., 1977, ApJ, 216, 214

White S. D. M., 1976, MNRAS, 177, 717

White S. D. M., 1979, MNRAS, 189, 831

White S. D. M., Briel U. G., Henry J. P., 1993, MNRAS, 261, L8

White S. D. M., Frenk C. S., 1991, ApJ, 379, 52

Woolf N. J., 1982, ARA&A, 20, 367

Worthey G., 1994, ApJS, 95, 107

Worthey G., Ottaviani D. L., 1997, ApJS, 111, 377

Zabludoff A. I., Zaritsky D., Lin H., Tucker D., Hashimoto Y., Shectman S. A., Oemler A., Kirshner R. P., 1996, ApJ, 466, 104

Zepf S. E., Whitmore B. C., Levison H. F., 1991, ApJ, 383, 524